

SEDIMENTOLOGY, CYCLOSTRATIGRAPHY, SEQUENCE STRATIGRAPHY  
AND GEOCHEMISTRY OF THE MIDDLE EOCENE LACUSTRINE-MARINE  
OIL-SHALES TRANSITION, MUDURNU-GÖYNÜK BASIN, NW ANATOLIA,  
TURKEY.

A THESIS SUBMITTED TO  
THE GRADUATE SCHOOL OF NATURAL AND APPLIED SCIENCES  
OF  
MIDDLE EAST TECHNICAL UNIVERSITY

BY

BAKHT ZAMIR AFRIDI

IN PARTIAL FULFILLMENT OF THE REQUIREMENTS  
FOR  
THE DEGREE OF DOCTOR OF PHILOSOPHY  
IN  
GEOLOGICAL ENGINEERING

MAY 2019



Approval of the thesis:

**SEDIMENTOLOGY, CYCLOSTRATIGRAPHY, SEQUENCE  
STRATIGRAPHY AND GEOCHEMISTRY OF THE MIDDLE EOCENE  
LACUSTRINE-MARINE OIL-SHALES TRANSITION, MUDURNU-  
GÖYNÜK BASIN, NW ANATOLIA, TURKEY.**

submitted by **BAKHT ZAMIR AFRIDI** in partial fulfillment of the requirements for the degree of **Doctor of Philosophy in Geological Engineering Department, Middle East Technical University** by,

Prof. Dr. Halil Kalıpçılar  
Dean, Graduate School of **Natural and Applied Sciences**

\_\_\_\_\_

Prof. Dr. Erdin Bozkurt  
Head of Department, **Geological Engineering**

\_\_\_\_\_

Prof. Dr. İsmail Ömer Yılmaz  
Supervisor, **Geological Engineering, METU**

\_\_\_\_\_

**Examining Committee Members:**

Prof. Dr. Sevinç Özkan Altınar  
Geological Engineering, METU

\_\_\_\_\_

Prof. Dr. İsmail Ömer Yılmaz  
Geological Engineering, METU

\_\_\_\_\_

Prof. Dr. Cemal Tunoğlu  
Geological Engineering, Hacettepe University

\_\_\_\_\_

Assoc. Prof. Dr. Erman Özsayın  
Geological Engineering, Hacettepe University

\_\_\_\_\_

Assoc. Prof. Dr. Kaan Sayıt  
Geological Engineering, METU

\_\_\_\_\_

Date: 28.05.2019

**I hereby declare that all information in this document has been obtained and presented in accordance with academic rules and ethical conduct. I also declare that, as required by these rules and conduct, I have fully cited and referenced all material and results that are not original to this work.**

Name, Surname: BAKHT ZAMIR AFRIDI

Signature:

## ABSTRACT

### **SEDIMENTOLOGY, CYCLOSTRATIGRAPHY, SEQUENCE STRATIGRAPHY AND GEOCHEMISTRY OF THE MIDDLE EOCENE LACUSTRINE-MARINE OIL-SHALES TRANSITION, MUDURNU- GÖYNÜK BASIN, NW ANATOLIA, TURKEY.**

AFRIDI, BAKHT ZAMIR

Doctor of Philosophy, Geological Engineering

Supervisor: Prof. Dr. İsmail Ömer Yılmaz

May 2019, 435 pages

Continuous studied successions of the Middle Eocene, Mudurnu-Göynük basin, in the NW Anatolia indicate a transition from marine-influence lacustrine to marine environment due to the relative rise in sea-level, which was separated by barrier deposits. Different lithofacies are identified in the studied sections, including limestone, marl, oil-shale, calcareous sandstone, conglomeratic and bio-calcirudite. Number of fossil assemblages are recorded including ostracods, charophyte gyrogonites, gastropods, bivalve and benthic foraminifera, rare fish-teeth-scale, echinoderms, algal filamentous and plant fragments. The recorded ostracod interprets Oligo-Mesohaline lacustrine environment, which is overlain by marine environment. Based on the detailed facies analysis, the depositional environment is characterized as relatively marginal to deep lacustrine- marine deposits, floodplain to paralic-marine deposits, from south to north. The lacustrine deposits indicate balanced-fill type lake setting within the regime in foreland setting in relation to İzmir-Ankara suture. The centimeter-meter scale order cycles show symmetrical to asymmetrical transgressive-regressive cycles, which is due to repetitive change in the water-depth and/or fluctuating sediments influx. The cm-m scale cycles correspond to Milankovitch obliquity band and indicate climatic control linked with the earth`s orbital forces and

local tectonics. In the sequence framework, the successions indicate marine transgression onto lacustrine environment in the region. The studied sections indicate a change from TST to HST in lacustrine-marine deposits. Lacustrine and Marine oil-shales in the studied area are interpreted that they have a possible source rock potential in the central and north, and in the south of the basin.

Keywords: Middle Eocene, Facies Analysis, Lacustrine to Marine environment, Cyclostratigraphy, Sequence Stratigraphy, Geochemistry, Mudurnu-Göynük Basin

## ÖZ

### **ORTA EOSEN GÖLSEL-DENİZEL BİTÜMLÜ ŞEYLLERİN GEÇİŞİNİN SEDİMENTOLOJİSİ, DEVİRSEL STRATİGRAFİSİ, SEKANS STRATİGRAFİSİ VE JEOKİMYASI, MUDURNU-GÖYNÜK HAVZASI, KB ANADOLU, TÜRKİYE.**

AFRIDI, BAKHT ZAMİR  
Doktora, Jeoloji Mühendisliği  
Tez Danışmanı: Prof. Dr. İsmail Ömer Yılmaz

Mayıs 2019, 435 sayfa

Mudurnu-Göynük baseninde, Kuzeybatı Anadolu bölgesi, Orta Eosen yaşlı çalışılan gölssel istifler gölssel ortamdan denizel çökelim ortamına geçiş göstermektedir. Deniz seviyesi değişimleri ile etkili olduğu düşünülen bu geçiş bariyer kompleksi ile ayrılmıştır. Çalışma alanında incelenen kesitlerde kireçtaşı, marn, bitümlü-şeyl, kalkerli kumtaşı, konglomera ve biyo-kalsirüdit içeren farklı lithofasiyesler tanımlandı. Çalışılan istifte ostrakod, karofit, bivalv, bentik foraminifer, nadir balık dişi, ekinoderm, alg lifleri ve bitki parçaları dahil olmak üzere birçok fosil grubu tespit edilmiştir. İstif içerisinde tanımlanan ostrakodlar orta tuzlu gölssel ortamına ait birimlerin üzerine denizel ortam birimlerinin geldiğini gösterir. Detaylı fasiyes analizlerine göre, birimin kuzeyden güneye doğru göl kenarından derin gölssel, taşkın ovasından paralik denizel çökelim ortamlarında çökeldiği belirlenmiştir. Gölssel çökeller İzmir-Ankara kenet ön ülke kuşağında dolgu tipi gölssel çökel ortamını işaret etmektedir. Santimetre – metre skalasındaki transgresif – regresif birimler değişken deniz seviyesini ve/veya değişken sediman gelişini/birikimini göstermektedir. Santimetre-metre skalasındaki devirsel döngüler Milankovitch yörüngesel eğikliğe karşılık gelmekte olup, dünya dönüş hareketi ve yerel tektonik aktivite ile ilintilidir. Sekansiyel bakış açısı ile çalışılan gölssel birimlerin üzerine transgresif denizel

ökellerin geldiđi gözlemlenmiştir. alıřılan gölssel-denizel birim içerisinde TST den HST e geiş gözlemlenmiştir. alıřılan gölssel-denizel bitümlü şeyler basenin merkezinde, kuzeyinde ve güneyinde kaynak kaya özelliđini gösterebilme potansiyeli vardır.

Anahtar Kelimeler: Orta Eosen, Fasiyes Analizi, Gölssel-Denizel ökelim Ortamı, Devirsel Stratigrafisi, Sekans Stratigrafisi, Jeokimya, Mudurnu-Göynük Havzası

To my beloved FAMILY.....

## ACKNOWLEDGEMENTS

I would like to express my sincere gratitude to Prof. Dr. İsmail Ömer Yılmaz, my supervisor, for his patient guidance, enthusiastic encouragement, immense knowledge and useful critiques of this research work.

Besides my supervisor, I am thankful to my committee members: Prof. Dr. Sevinç Özkan Altın, Prof. Dr. Cemal Tunoğlu, Assoc. Prof. Dr. Erman Özsayın and Assoc. Prof. Dr. Kaan Sayıt, for their encouragement and insightful comments, but also for the hard question which incited me to widen my research from various perspectives. I am also thankful to Prof. Dr. Cemal Tunoğlu for the identification of the ostracod in the samples.

I am grateful to lab technicians of the Geological Engineering Department, Orhan Karaman, and Gonca Alptekin for their help in the laboratory work.

A special thanks to my family. Words cannot express how grateful I am to my Parents, Dr. Khalid Zamir Afridi, my elder sister (Mrs. Khalid Zamir Afridi) and my beloved wife Rahat Afridi for all the sacrifices that they have made on my behalf. Your prayer for me was what sustained me thus far. A bundle of thanks to my Brothers, Sisters, my -in-laws, Uncles, Aunts, Cousins, sweet nephews and nieces whose unconditional love and support always encouraged me in every movement of my life. To my beloved niece Sana Afridi, I would like to express my thanks for being such a good girl always cheering me up and for showing your overwhelming love.

I would like to extend my heartfelt thanks to Ishfaq Bashir, Özlem Yeter, Saeed Yousafzai, Saad Arshad, Abdul Qayyum, Nouman Ahmad, Ilir Sheraj, Tanvir Shah, Majid Akbar, Mohsin Ali and Rizwan Aziz for their good wishes, moral support, motivation and for all the fun we have had in the last five years.

## TABLE OF CONTENTS

ABSTRACT .....	v
ÖZ .....	vii
ACKNOWLEDGEMENTS .....	x
TABLE OF CONTENTS .....	xi
LIST OF TABLES .....	xx
LIST OF FIGURES .....	xxiii
CHAPTERS	
1. INTRODUCTION .....	1
1.1. Introduction .....	1
1.2. Oil-shales in the World and Turkey .....	4
1.3. Aim and Scope .....	7
1.4. Geographic and Geological Setting .....	8
1.5. Methodology .....	8
1.6. Analytic Method: Chemical process for removing of Organic matter content and minerals from the samples to estimate their weight percent.....	14
1.6.1. Chemical Procedure .....	16
1.7. Previous work.....	18
1.8. Regional Geological Setting.....	26
1.8.1. Mudurnu-Göynük Basin .....	31
2. GENERAL STRATIGRAPHY .....	35
2.1. General Geology of the Region.....	35
2.2. Stratigraphy of Mudurnu-Göynük Basin.....	37

2.2.1. Jurassic to Cretaceous Succession.....	39
2.2.2. Tertiary Succession .....	41
2.2.2.1. Kızılçay Group.....	42
2.2.2.2. Ağsaklar Formation .....	42
2.2.2.3. Kabalar Formation .....	43
2.2.2.4. Dağhacılar Formation .....	44
2.3. Lithostratigraphy of the Measured Sections .....	44
2.3.1. Dağhacılar Measured Section.....	46
2.3.2. Hasanlar Measured Stratigraphic Section .....	59
2.3.3. Kösüre Measured Section (Yenipazar).....	60
2.3.4. Karahisar Measured Stratigraphic Section .....	74
2.3.5. Sünnet Measured Stratigraphic Section .....	81
3. SEDIMENTOLOGY .....	93
3.1. Sedimentological Studies.....	93
3.2. Microfacies of Dağhacılar Section.....	96
3.2.1. Limestone Facies .....	96
3.2.1.1. Lime Mudstone Microfacies (DA1) .....	96
3.2.1.2. Interpretation (DA1) .....	100
3.2.1.3. Wackestone Microfacies (DA2a) .....	100
3.2.1.4. Packstone Microfacies (DA2b).....	102
3.2.1.5. Interpretation (DA2a; DA2b) .....	102
3.2.2. Marl Facies (DA3).....	105
3.2.2.1. Interpretation (DA3) .....	105
3.2.3. Oil-shale Facies (DA4).....	107

3.2.3.1. Interpretation (DA4) .....	110
3.2.4. Calcareous Sandstone Facies (DA5).....	114
3.2.4.1. Interpretation (DA5) .....	117
3.3. Microfacies of Hasanlar Section .....	120
3.3.1. Limestone Facies .....	121
3.3.1.1. Lime Mudstone Microfacies (HA1).....	122
3.3.1.2. Interpretation (HA1) .....	122
3.3.1.3. Wackestone Microfacies (HA2).....	122
3.3.1.4. Interpretation (HA3) .....	124
3.3.2. Marl Facies (HA3).....	124
3.3.2.1. Interpretation (HA3) .....	124
3.3.3. Oil-shale Facies (HA4) .....	125
3.3.3.1. Interpretation (HA4) .....	125
3.4. Microfacies of Kösüre Section .....	128
3.4.1. Limestone Facies .....	128
3.4.1.1. Wackestone Microfacies (KA1a).....	128
3.4.1.2. Packstone Microfacies (KA1b).....	129
3.4.1.3. Interpretation (KA1a; KA1b).....	129
3.4.2. Marl facies (KA2).....	135
3.4.2.1. Interpretation (KA2) .....	135
3.4.3. Oil-shale Facies (KA3) .....	137
3.4.3.1. Interpretation (KA3) .....	139
3.4.4. Calcareous Sandstone Facies (KA4).....	139
3.4.4.1. Interpretation (KA4) .....	141

3.5. Microfacies of Karahisar Section.....	144
3.5.1. Limestone Facies .....	144
3.5.1.1. Lime Mudstone Microfacies (TA1).....	144
3.5.1.2. Interpretation (TA1).....	146
3.5.2. Oil-shale Facies (TA2) .....	147
3.5.2.1. Interpretation (TA2).....	148
3.5.3. Calcareous Sandstone Facies (TA3).....	153
3.5.3.1. Interpretation (TA3).....	153
3.6. Microfacies of Sünnet Section .....	154
3.6.1. Limestone Facies .....	154
3.6.1.1. Lime Mudstone Microfacies (SA1) .....	154
3.6.1.2. Interpretation (SA1).....	155
3.6.1.3. Wackestone Microfacies (SA2a) .....	157
3.6.1.4. Packstone Microfacies (SA2b) .....	158
3.6.1.5. Interpretation (SA2a; SA2b).....	158
3.6.1.6. Rudstone microfacies (Bio-calcurudite) (SA3) .....	161
3.6.1.7. Interpretation (SA3).....	161
3.6.2. Oil-shale Facies (SA4) .....	163
3.6.2.1. Interpretation (SA4).....	163
3.6.3. Calcareous Sandstone Facies (SA5).....	164
3.6.3.1. Interpretation (SA5).....	166
3.6.4. Pebble-Conglomerate (SA6) .....	167
3.6.4.1. Interpretation (SA6).....	167
4. OSTRACODS AND CHAROPHYTE GYROGONITES .....	175

4.1. Introduction .....	175
4.2. Charophyte Gyrogonites.....	176
4.3. Ostracods .....	180
4.4. Interpretation: Paleoecology and Age Constraint for the Studied Sections ..	184
5. FACIES ASSOCIATION, LACUSTRINE ENVIRONMENT AND TRANSITION TO MARINE ENVIRONMENT SETTING.....	189
5.1. Introduction .....	189
5.2. Facies Association and Depositional Setting of the Studied Sections .....	203
5.2.1. Dağhacılar Section: Facies Association and Depositional Setting .....	203
5.2.1.1. Littoral-sublittoral Lacustrine (Relatively Shallow Lacustrine): Facies Association 1 .....	204
5.2.1.2. Sub-littoral-profundal lacustrine (Deep lacustrine): Facies Association 2.....	205
5.2.1.3. Marine offshore transition: Facies Association 3.....	206
5.2.2. Hasanlar Section: Facies Association and Depositional Setting .....	208
5.2.2.1. Upper sublittoral-profundal lacustrine (Deep lacustrine): Facies Association 2.....	208
5.2.3. Köşüre Section: Facies Association and Depositional Setting .....	209
5.2.3.1. Upper littoral-sublittoral lacustrine (Relatively shallow lacustrine): Facies Association 1 .....	210
5.2.3.2. Upper sublittoral-profundal lacustrine (Relatively deeper Lacustrine): Facies Association 2.....	210
5.2.3.3. Marine offshore transition: Facies Association 3.....	211
5.2.4. Karahisar Section: Facies Association and Depositional Setting .....	212

5.2.4.1. Upper sublittoral-profundal lacustrine (Relatively deeper lacustrine): Facies Association 2 .....	213
5.2.4.2. Marine offshore transition: Facies Association 3 .....	214
5.2.5. Sünnet Section: Facies Association and Depositional Setting .....	215
5.2.5.1. Marine Shelf Environment: Facies Association 4 .....	216
5.2.5.2. Floodplain Paleosols: Facies Association 5.....	218
5.3. Lacustrine Environment and Transition to Marine Environment in the Studied Basin.....	219
6. CYCLOSTRATIGRAPHY .....	229
6.1. Introduction.....	229
6.2. Cyclic Hierarchy in the Studied sections .....	233
6.3. Dağhacılar Section Depositional Cyclicity .....	233
6.4. Hasanlar Section Depositional Cyclicity .....	240
6.5. Köşüre Section Depositional Cyclicity .....	242
6.6. Karahisar Section Depositional Cyclicity .....	246
6.7. Sünnet Section Depositional Cyclicity .....	248
6.8. Interpretation.....	252
6.8.1. Milankovitch Periodicity Analysis .....	252
6.8.2. Fischer Plot Workflow .....	253
6.8.3. Carbonate and Organic Matter Content relationship with Cyclostratigraphy .....	255
7. SEQUENCE STRATIGRAPHY.....	267
7.1. Introduction.....	267
7.2. Sequence stratigraphy framework in the Dağhacılar section.....	271
7.3. Sequence stratigraphy framework in the Hasanlar section .....	273

7.4. Sequence stratigraphy framework in the Köşüre section .....	274
7.5. Sequence stratigraphy framework in the Karahisar section .....	274
7.6. Sequence stratigraphy framework in the Sünnet section.....	276
7.7. Sequence stratigraphic framework and correlation of the studied sections in the Basin.....	278
7.7.1. Lowstand Systems Tract (LST) .....	279
7.7.2. Flooding Surfaces (FS) .....	279
7.7.3. Transgressive Systems Tract (TST).....	279
7.7.4. Maximum Flooding Zones (MFZ).....	280
7.7.5. Highstand Systems Tract (HST).....	281
8. GEOCHEMICAL ANALYSES AND HYDROCARBON DEPOSITS .....	287
8.1. Introduction .....	287
8.2. Minerals and Organic Matter .....	288
8.2.1. Carbonate Content in the Studied Sections.....	289
8.2.2. Clay Content in the Studied Sections .....	304
8.2.3. Quartz/Feldspar Content in the Studied Sections .....	306
8.2.4. Organic Matter Content in the Studied Sections .....	307
8.3. Organic Matter and mineral associations .....	309
8.3.1. The relationship between CaCO <sub>3</sub> vs Organic matter .....	310
8.3.2. The relationship between clay content vs organic matter.....	310
8.3.3. The relationship between Quartz/Feldspar vs organic matter .....	311
8.3.4. Characterization and interpretation of the CaCO <sub>3</sub> , Clay, Quartz/ Feldspar contents vs Organic matter .....	315
8.4. Porosity Types and Visual Estimated Porosity .....	317

8.4.1. Intraparticle Pores Type .....	321
8.4.2. Interparticle Pores Type .....	321
8.4.3. Micro-Fracture Type Porosity .....	321
8.5. Source Rock Potential on the Petrographic and Geochemical Approaches in the Studied Sections.....	327
8.5.1. Source rock potential on the petrographic and geochemical approaches in the Dağhacılar section .....	330
8.5.2. Source rock potential on the petrographic and geochemical approaches in the Hasanlar section.....	330
8.5.3. Source rock potential on the petrographic and geochemical approaches in the Köşüre section .....	331
8.5.4. Source rock potential on the petrographic and geochemical approaches in the Karahisar section .....	331
8.5.5. Source rock potential on the petrographic and geochemical approaches in the Sünnet section.....	332
9. DISCUSSION .....	339
9.1. Facies Distribution in the Middle Eocene (Lutetian-Bartonian) studied sections .....	340
9.2. Paleoenvironment and Age; based on fossil assemblages .....	341
9.3. Variation in the relative lacustrine level and relative sea-level (Oligo-Mesohaline/Brackish-lacustrine and marine offshore transitional) .....	343
9.4. Type of Lacustrine Basin and Marine transgression.....	346
9.5. Cyclostratigraphic Framework.....	348
9.6. Sequence Stratigraphic Framework .....	350
9.7. Source rock potential on the petrographic and geochemical approaches .....	352
10. CONCLUSION .....	357

REFERENCES.....	363
APPENDICES .....	425
APPENDIX A. Geochemical Data of the Studied Sections .....	425
APPENDIX B. Extracted Ostracods and Charophyte gyrogonites statistical data..	431
CURRICULUM VITAE .....	435

## LIST OF TABLES

### TABLES

Table 1.1. Main oil-shale reserves in Turkey (Altun et al., 2006).....	6
Table 1.2. Characteristics of the major oil-shale deposits in Turkey (EGOS, on average basis) (Akkuş et al., 1982 and Altun et al., 2006). .....	6
Table 1.3. Brief descriptions of the pre-treatment methods studied (Vaasma, 2008). .....	16
Table 3.1. Folk`s (1965) texture classification of fine-grained sedimentary rock.*..	96
Table 3.2. Limestone, oil-shale and marl petrographic data and established/recognized facies in the Dağhacılar studied section.....	97
Table 3.3. Sandstone petrographic data and established/recognized facies in the Dağhacılar studied section.....	97
Table 3.4. Classifications of the limestone, oil-shale, marl and sandstone and established/recognized microfacies in the Dağhacılar studied section.....	98
Table 3.5. Mudstone and Shale Classification Schemes (Zou et al., 2010). .....	108
Table 3.6. Summary of Mudstone and Shale Classification Schemes of the Lacustrine environment. ....	108
Table 3.7. Limestone, oil-shale and marl petrographic data and established/recognized facies in the Hasanlar studied section.....	120
Table 3.8. Classifications of the limestone, oil-shale, marl and sandstone and established/recognized microfacies in the Hasanlar studied section. ....	121
Table 3.9. Limestone, oil-shale and marl petrographic data and established/recognized facies in the Köşüre studied section.....	132
Table 3.10. Sandstone petrographic data and established/recognized facies in the Köşüre studied section.....	132
Table 3.11. Sandstone petrographic data and established/recognized facies in the Köşüre studied section.....	133

Table 3.12. Limestone, oil-shale and marl petrographic data and established/recognized facies in the Karahisar section. ....	144
Table 3.13. Sandstone petrographic data and established/recognized facies in the Karahisar section. ....	145
Table 3.14. Classifications of the limestone, sandstone, oil-shale, marl and sandstone and established/ recognized microfacies in the Karahisar section. ....	145
Table 3.15. Limestone, oil-shale and marl petrographic data and established/recognized microfacies in the Sünnet studied section. ....	155
Table 3.16. Limestone, oil-shale and marl petrographic data and established/recognized microfacies in the Sünnet studied section. ....	156
Table 3.17. Classifications of the limestone, oil-shale, marl and sandstone and established/recognized microfacies in the Sünnet studied section. ....	156
Table 5.1. Formation and degree of pyrite related to redox depositional conditions (Lazar, 2007). ....	202
Table 5.2. Facies Associations from established lithofacies of the studied sections and interpreted their depositional setting. ....	203
Table 5.3. Representative Attributes of Three Major Lacustrine Facies Associations (Carrol and Bohacs, 1999; Bohacs et al., 2000). ....	221
Table 6.1. Number of Beds and Cycles and their thickness in the Middle Eocene (Lutetian-Bartonian) studied sections. ....	232
Table 6.2. Number of Beds and Cycles and their thickness in the Middle Eocene (Lutetian-Bartonian) studied sections. ....	232
Table 8.1. The minimum, maximum and average weight percent values of lithofacies from the Dağhacılar measured section. ....	291
Table 8.2. The minimum, maximum and average weight percent value of lithofacies from the Hasanlar section. ....	294
Table 8.3. The minimum, maximum and average weight percent data of lithofacies from the Köüre measured section. ....	296
Table 8.4. The minimum, maximum and average weight percent values of lithofacies from the Karahisar measured section. ....	298

Table 8.5. The minimum, maximum and average weight percent values of lithofacies from the Sünnet measured section.....	301
Table 8.6. Total porosity % and types of porosity in the Dağhacılar section.....	318
Table 8.7. Total porosity % and types of porosity in the Hasanlar section. ....	318
Table 8.8. Total porosity % and types of porosity in the Köşüre section.....	319
Table 8.9. Total porosity % and types of porosity in the Karahisar section.....	319
Table 8.10. Total porosity % and types of porosity in the Sünnet section. ....	319
Table 8.11. Geochemical parameters used to determine the oil potential (Quantity) of an immature source rock. (Tissot and Welte, 1984; Jarvie, 1991; Peters and Cass, 1994).....	331
Table 9.1. The obtained minimum, maximum and average weight percent of CaCO <sub>3</sub> , organic matter, clay content, quartz/feldspar content and visual porosity from the Middle Eocene (Lutetian-Bartonian) measured succession. ....	354

## LIST OF FIGURES

### FIGURES

Figure 1.1. General scheme of the oil-shale components (Yen and Chilingarian, 1976). .....	2
Figure 1.2. Classification of oil-shales from Hutton (1987, 1991). ....	3
Figure 1.3. Oil-shale classification based on maceral composition and environment of deposition (after Hutton et al., 1980; Hutton, 1982). ....	4
Figure 1.4. Main oil-shale reserves in Turkey (Şengüler, 2001). ....	5
Figure 1.5. Representing the studied area (Studied measured section shown by yellow pin). ....	9
Figure 1.6. Showing regional tectonic of the Turkey and adjacent areas (modified from Okay and Tüysüz, 1999). (Red Arrow-North). ....	9
Figure 1.7. A) Crushed sample, B) soaked in diluted H <sub>2</sub> O <sub>2</sub> and diluted CH <sub>3</sub> COOH, C) washed with distilled water and sieve through 500um, 250um, 125um and 63um, D) Dry in oven at 60°C, E) Collected samples and store it in the 15ml bottle, F) Picked the extracted fossils from store samples under reflected microscope and placed on microfossils slide. ....	12
Figure 1.8. a) Lab oven to dry the samples; b) 10% diluted Hydrochloric acid used to remove carbonate and placed it in the fume chamber. c) 30% Hydrogen peroxide (H <sub>2</sub> O <sub>2</sub> ) acid used to remove the organic matter and d) placed it in the water bath. ...	17
Figure 1.9. Showing Tectonic evaluation of Turkey during Late Triassic to Early Jurassic. (Şengör et al. 1984; Robertson et al., 1991; Szary, 2014). ....	28
Figure 2.1. Composites stratigraphic section of the Mudurnu-Göynük Basin (Modified from Altınar et al., 1991; Şener and Şengüler 1998 and Gedik and Aksay, 2002). Red line shows studied interval. ....	36
Figure 2.2. Generalized stratigraphic Hatıldığ oil field (Şener and Şengüler, 1998). Red line shows studied interval. ....	38

Figure 2.3. Satellite image showing the measured Dağhacılar Section in the Mudurnu-Göynük Basin (Dağhacılar Section represented by yellow icon).....	47
Figure 2.4. The field photograph showing lime mudstone and marl, the starting point of the Dağhacılar section. (D1-D6). .....	47
Figure 2.5. The field photograph of Lutetian-Bartonian measured stratigraphic section near Dağhacılar village, Bolu. N dip direction (white lines).....	48
Figure 2.6. The field photograph of Lutetian-Bartonian measured stratigraphic section near Dağhacılar village, Bolu. N dip direction (green lines). (from D37 to D76).....	48
Figure 2.7. Measured stratigraphic section near Dağhacılar Village (0m-31.5m). ...	49
Figure 2.8. The field photographs of Dağhacılar measured stratigraphic section showing; (A) wackestone bedding (D7), overlain by high fossiliferous unit Packstone (D8) and then followed by wackestone (D9); B) Close view of Packstone limestone of sample D8; C and D) Close view of Gastropod in the sample D8 beddings. ....	54
Figure 2.9. The field photographs of Dağhacılar measured stratigraphic section showing; (A) wackestone bedding (D7), overlain by high fossiliferous unit Packstone (D8) and then followed by wackestone (D9); B) Close view of Packstone limestone of sample D8; C and D) Close view of Gastropod in the sample D8 beddings. ....	54
Figure 2.10. Figure 2.10. The field photograph of Dağhacılar studied section showing, A) Siliceous concretion; B) marl (D34) with nodularity feature and above planar very thin bedded to algal laminated oil-shale (D35, D36).....	55
Figure 2.11. The field photograph of Dağhacılar measured stratigraphic section illustrating A) algal laminated oil-shales; B) Thin preparation cutting algal laminated D40 sample; C) Algal Laminated Oil-shale and marl alternation with occasional thin bedded sandstone. ....	55
Figure 2.12. The field photograph of Dağhacılar measured stratigraphic section illustrating A) laminated to thin planar bedded oil-shale; B) Cross cutting section of sample D52 for thin section preparation.....	56
Figure 2.13. The field photograph of Dağhacılar measured stratigraphic section illustrating Thin to laminated oil-shale with interbedded sandstone. ....	56

Figure 2.14. The field photograph of Dağhacılar measured stratigraphic section illustrating dominated up section sandstone; A) Sandstone beds are low angle wavy rippled bedded sandstone with interbedded oil-shale; B) wavy rippled bedded sandstone (Sample D65). .....	57
Figure 2.15. The field photograph of Dağhacılar measured stratigraphic section presenting thin to thick bedded sandstone and marl, Oil-shale deposited above section. ....	57
Figure 2.16. The field photograph of Dağhacılar measured stratigraphic section presenting oil-shale followed by marl with interbedded very thin wavy rippled sandstone to very thin to medium bedded planar bedded sandstone (shown by B). B) Marl and sandstone intercalation at the top portion of the measured section. ....	58
Figure 2.17. Satellite image showing the Hasanlar measured section in the Mudurnu-Göynük Basin, in the vicinity of Hasanlar village (Hasanlar studied section represented by yellow icon). ....	60
Figure 2.18. The field photograph of Hasanlar measured section presenting base of the section, started with limestone of wackestone feature, then followed by planar thin bedded Oil-shale; B) Thin section preparation rock-cutting Oil-shale sample H0b. .	61
Figure 2.19. The field photograph of Hasanlar measured section presenting intercalation of lime mudstone and fragile laminated oil-shale. ....	61
Figure 2.20. Measured stratigraphic section near Hasanlar Village. ....	62
Figure 2.21. The field photograph of Hasanlar studied section presenting intercalation of A) lime mudstone and marl; B) representing intercalation of lime mudstone and laminated oil-shale. ....	63
Figure 2.22. The field photograph of Hasanlar measured section presenting; A) Wackestone and Laminated Oil-shale; B) Lab cutting sample H14; C) representing intercalation of lime Mudstone and Laminated Oil-shale. ....	64
Figure 2.23. Satellite image showing the measured Köşüre studied section in the Mudurnu-Göynük Basin, Köşüre village (yellow icon represents the studied section). ....	66

Figure 2.24. The field photograph of 82-meter Lutetian-Bartonian measured stratigraphic section near Kösüre village, Bolu. N dip direction (white lines).....	66
Figure 2.25. Measured stratigraphic section in the vicinity of Kösüre Village (0-31.5m).....	67
Figure 2.26. The field photograph of Lutetian-Bartonian Kösüre studied section presenting; A) marl and medium bedded sandstone; B) thin to thick to massive bedded limestone with thin to medium intervals of marls. ....	70
Figure 2.27. The field photograph of Lutetian-Bartonian Kösüre studied section presenting; A) marl and medium bedded sandstone; B) thin to thick to massive bedded limestone with thin to medium intervals of marls. ....	71
Figure 2.28. The field photograph of Lutetian-Bartonian Kösüre studied section presenting; A) marl and medium bedded sandstone; B) thin-thick to massive bedded limestone with thin to medium intervals of marls. ....	71
Figure 2.29. The field photograph of Kösüre studied section presenting A) close view of nodularity in Sandstone with marl interbeds (sample K18); B) close view of laminated oil-shale (sample K24).....	72
Figure 2.30. The field photograph of Kösüre studied section presenting marl and limestone intervals (sample K31-K34).....	72
Figure 2.31. The field photograph of Kösüre studied section presenting Sandstone, marl and oil-shale interbeds; B) Close view of oil-shale (sample K40); C); Close view of thin planar bedded sandstone (sample K43).....	73
Figure 2.32. The field photograph of Kösüre studied section presenting A) Fish tooth in Sandstone sample (K39); B) Oil-shale with thin bedded sandstone (Sample K46-K49).....	73
Figure 2.33. Satellite image showing the measured Karahisar studied section in the Mudurnu-Göynük Basin, near Karahisar village (yellow icon represents the studied section).....	74
Figure 2.34. Satellite image showing the measured Karahisar studied section in the Mudurnu-Göynük Basin, near Karahisar village (yellow icon represents the studied section).....	75

Figure 2.35. Karahisar Measured stratigraphic section, near Karahisar Village (0-31.5m). .....	76
Figure 2.36. The field photograph of Karahisar studied section presenting laminated oil-shale and thin to thin-medium bedded limestone (Sample T6 to T7). (White arrow indicates SW bedding dip direction). .....	78
Figure 2.37. The field photograph of Karahisar studied section presenting A) thin planar bedded limestone (Sample T8 and T9); B) Close view of Sample T8 with concretion bedding surface and oxidation.....	79
Figure 2.38. The field photographs of Karahisar studied section representing A) Thin planar bedded limestone with abundant manganese spherical nodules (0.1mm to 2cm) (Sample T12 and T13); B) Close view of Sample T13 and marble size manganese ball; C) Thin section preparation cutting sample T13 and manganese spherical ball are indicated by black arrow. ....	79
Figure 2.39. The field photographs of Karahisar studied section representing A) Thin planar bedded limestone with abundant manganese spherical nodules (0.1mm to 2cm) (Sample T12 and T13); B) Close view of Sample T13 and marble size manganese ball; C) Thin section preparation cutting sample T13 and manganese spherical ball are indicated by black arrow. ....	80
Figure 2.40. Satellite image showing the measured Sünnet studied section in the Mudurnu-Göynük Basin, Sünnet village (yellow icon represents the studied section). .....	83
Figure 2.41. The field photograph of 70-meter Lutetian-Bartonian Sünnet measured stratigraphic section, Sünnet village, Bolu. (Sample S1-S36). .....	83
Figure 2.42. Sünnet Measured stratigraphic section, Sünnet Village (0-31.5m). .....	84
Figure 2.43. The field photograph of Sünnet studied section presenting thick bedded Coarser and Finer Sandstone and sharp contact with pebble conglomerate and above red bedded fragile Sandstone, black arrow indicates lensoidal conglomeratic bed (Sample S1-S5). .....	86
Figure 2.44. The field photograph of Sünnet studied section presenting fragile red sandstone with occasional grayish silty oil-shale (Sample S7-S11). .....	87

Figure 2.45. The field photograph of Sünnet studied section presenting Sandstone and oil-shale intercalation. The sandstone shows load structure contact with Oil-shale lithofacies (Sample S20-S23). ..... 87

Figure 2.46. The field photograph of Sünnet studied section presenting; A) 4cm thin yellowish orange abundant charophytes bearing packstone interval with plant materials/charcoal (Sample 24); B) Close view of the collected sample. .... 88

Figure 2.47. The field photograph of Sünnet studied section presenting; A) thick bedded bioclastic limestone (Rudstone/ calcirudite) (Sample S28); B) Close view of the collected sample. (black arrows indicate fossil clasts and pink arrows indicate siliciclastic grains). ..... 88

Figure 2.48. The field photograph of Sünnet studied section presenting; A) red line indicates sharp contact between oil-shale and sandstone, the black arrows indicate load structures; B) Large scale low angle rippled fine sandstone overlain by coarser sandstone. (black arrows indicate flute structure). ..... 89

Figure 2.49. The field photograph of Sünnet studied section presenting sandstone with sandstone concretion (shown by red lines) and pebble conglomerate..... 90

Figure 2.50. The field photograph of Sünnet studied section presenting; A) Fossiliferous oil-shale (black arrows show bivalve clast and yellow shows gastropod clast) (Sample S13); B) Fossiliferous packstone interval with charcoal fragment, shown by yellow arrows and white dots in the yellow rectangle indicates Charophytes (Sample S17). ..... 90

Figure 2.51. The field photograph of Sünnet studied section presenting; A) Fossiliferous oil-shale (black arrows show bivalve clast) (Sample S20); B) Fossiliferous wackestone interval with a charcoal fragment, shown by white arrows (Sample S26). ..... 91

Figure 3.1. A) Diaz et al. (2012) and B) the Allix et al. (2010) ternary mudstone compositional classification diagrams (for unconventional); the studied samples are plotted, and their comparison with known unconventional reservoirs from the USA. .... 94

Figure 3.2. Stow`s compositional classification (2005) ternary diagram based on biogenic (carbonate and silica) and mud/clays: the representative symbol of the studied sections are shown in the red box.....	95
Figure 3.3. The Folk`s (1974) Sandstone classification ternary diagram based on relative proportions of grains size and presence of matrix. The representative symbol of the studied samples are shown in the red box.....	95
Figure 3.4. The field photograph of Lime Mudstone microfacies in the Dağhacılar measured stratigraphic section; a) Sample D3 and b) Sample D18 (Scale: Hammer). .....	99
Figure 3.5. Photomicrographs of Lime Mudstone microfacies (a, b, c, d) and wackestone (e, f) presenting charophyta (Ch), ostracods (Os), gastropod (G), quartz (Q), pyrite (P), euhedral pyrite (Ep), organic matter (Om), sparite (Sp) and fracture (Fc). (Sample no. a) D3, PPI x4; b) D8, PPI x4; c) D20, PPI x100; d) D33, XPI x10; e) D4, PPI x4; f) D14, PPI x4. ....	101
Figure 3.6. The field photograph of wackestone microfacies of Dağhacılar measured stratigraphic section; a) Sample D4; b) D6 having gastropods; c) D14 and d) D30 (Scale: Hammer and pencil).....	104
Figure 3.7. Photomicrographs of wackestone (a, b, c) and Packstone microfacies (d) presenting ostracod (Os), framboidal pyrite (Fp), organic matter (Om) and phytoclast (Pc). (Sample no. a) D14, PPI x100; b) D15, PPI x4; c) D30, PPI x4 and d) D11, XPI x4.....	104
Figure 3.8. The field photograph of gastropods bearing packstone microfacies of Dağhacılar measured stratigraphic section; a) Packstone bedding between D12 and D13; b) D19 (Scale: Hammer). ....	105
Figure 3.9. Photomicrographs of gastropods bearing Packstone microfacies (a, b, c) and marl (d, e) presenting ostracod (Os), gastropod (G), gastropod valve (Gw; dotted line indicates gastropod wall shell) bivalve (Bi), quartz (Q), microsparite (Ms) and organic matter (Om). (Sample no. a) D19, PPI x4; b) D19, PPI x4; c) D19 hand specimen photography; d) D21, XPI x10; e) D21, field photography. ....	106

Figure 3.10. Photomicrographs of marl microfacies presenting ostracod (Os), glauconite (Gt), bioturbation (Bt; dotted yellow line), organic matter (Om), quartz (Q) and fracture (Fc). (Sample no. a) D25, PPI x4; b) D73, PPI x4..... 107

Figure 3.11. The field photograph of Oil-shale of Dağhacılar measured stratigraphic section; a) Non-laminated fossiliferous oil-shale (Sample D10); b) Laminated oil-shale with intercalated marl (Sample D36); c) Laminated oil-shale with interbedded marl (Sample D44). ..... 109

Figure 3.12. Photomicrographs of oil-shale facies presenting ostracod (Os), quartz (Q), nummulite (N), pyrite (P) and organic matter (Om). (Sample no. a, b) fossiliferous oil-shale, D10, PPI x4; c) Lenticular laminated oil-shale, D36, PPI x4; d) D36, Euhedral pyrite, PPI, x100. .... 112

Figure 3.13. Photomicrographs of oil-shale presenting quartz (Q) and organic matter (Om). (Sample no. a) Laminated oil-shale, D40, PPI x4; b) field photography, D40, indicates convolute laminae (white arrow) and micro-fault (red arrow); c) D40, PPI, x100; d) D40, XPI, x100; e) Lenticular lamination, D69, PPI, x100; f) field photography of sample D69; g) Cut sample for thin section and show alternating dark and light laminae. (yellow arrow indicates organic-rich laminae-dark laminae) (Scale; Hammer and Pencil). ..... 113

Figure 3.14. a) The field photograph of alternating shale and sandstone and showing bedding sandstone geometry planar to hummocky cross-stratification to wave ripple symmetry (Note; Close view hummocky cross-stratification in figure 3.14b). ..... 115

Figure 3.15. Pie graphs of the sandstone lithofacies in the Dağhacılar section..... 116

Figure 3.16. The field photograph of interbedded marl and sandstone interbeds (arrow indicates planar sandstone bedding). ..... 117

Figure 3.17. Photomicrographs of sandstone presenting quartz (Q), polyquartz (Qp), bioclasts (Bc,marine Bioclast), Nummulites (N), limestone fragment (Lf), shale fragment (Sf), microquartz (Qc), muscovite (Mu), sericitization (Sc), chlorite (Cr), sparite (Sp), feldspar (F), bioturbation (Bt, indicated by yellow line) and organic matter (Om). (Sample no. a) sandstone, D42, PPI x4; b) field photography of low angle wavy laminated sandstone, D42, indicates deformed features (white arrow); c) a-XPI

x4; d) Sandstone, D53, XPl, x10; e) sandstone with vertical bioturbation, D76, XPl, X4.....	118
Figure 3.18. Photomicrographs of sandstone presenting quartz (Q), polycrystalline quartz (Qp), limestone fragment (Lf), shale fragment (Sf), cryptoquartz (Qc), muscovite (Mu), sericitization (Sc), chlorite (Cr), calcite fragment (Ct), and organic matter (Om). (Sample no. a) sandstone, D76, XPl, x4; b) sandstone, D76, PPl, x4; c) sandstone, charcoal, PPl, x100; d) Close view of hummocky cross-stratification, D64. ....	119
Figure 3.19. Photomicrographs of Lime Mudstone microfacies (a, b, c, d) and wackestone (e, f) presenting ostracod (Os), quartz (Q), pyrite (P), framboidal pyrite (Fp), organic matter (Om), rare dolomitic patches(D), phytoclast (Py), cuticles (Cu) and stylolite (Su). (Sample no. a) H4, PPl x4; b) H5, PPl x4; c) H5, PPl x100; d) H19, PPl x10; e) H10, PPl x4; f) H10, PPl x10. ....	123
Figure 3.20. Photomicrographs of wackestone and oil-shale presenting quartz (Q), phytoclast (Py), Bioclast (Bc, dissolved fragment), ostracod (Os), micro dolomitic (D) and organic matter (Om). (Sample no. a) Wackestone, H10, PPl x100; b) Wackestone, H12, PPl, x4; c) organic-rich laminae oil-shale, H13, PPl, x4; d) close view, OIL stain lenses in organic-rich laminae, H13, PPl, x10; e) laminated organic-rich oil-shale (Yellow arrow indicates organic-rich laminae), H13, PPl, x4; f) lenticular/convolute laminated oil-shale, PPl, x4 (yellow arrow indicates organic-rich laminae-dark laminae and white represent organic-poor lenses). ....	126
Figure 3.21. Photomicrographs of oil-shale presenting quartz (Q), ostracod (Os) and organic matter (Om). (Sample no. a) H20, PPl x4; b) H20, XPl, x4 (yellow arrow indicates organic-rich laminae-dark laminae). ....	127
Figure 3.22. The field photograph of wackestone and marl microfacies of Kösure measured stratigraphic section; a) Sample wackestone K6, K7, K8 with intercalated marl; b) Wackestone K25, K27 with intercalated marl (Sample K26). ....	130
Figure 3.23. The field photograph of a) intercalating wackestone and marl microfacies; b) Packstone microfacies of Kösure measured stratigraphic section; a) Sample K31, K32, K33; b) packstone K11, K12. ....	131

Figure 3.24. Photomicrographs of wackestone microfacies presenting charophyta (Ch), ostracod (Os), quartz (Q), plagioclase (Pg), bioclasts (Bc), calcite (Ct), peloid (Pl), clay (Cy), sparite (Sp), euhedral pyrite (Ep), Bivalve (Bi), organic matter (Om), sparite (Sp) and fracture (Fc). (Sample no. a) K6, PPl x4; b) K9, PPl x4; c) K16, XPl x4; d) K25, PPl x4; e) K25, x4; f) K34, x4..... 134

Figure 3.25. Photomicrographs of a) wackestone microfacies; b) packstone microfacies; c, d, e) marl facies and f) oil-shale facies presenting ostracod (Os), quartz (Q), bioclasts (Bc), peloid (Pl), biotite (Be), organic matter (Om), sparite (Sp) and porosity (Po). (Sample no. a) K38, Echinoderm, x4; b) K11, PPl x4; c) K2, PPl x4; d) K20, fish-tooth, x4; e) K28, fish-tooth, x4; f) K13, PPl, x4..... 136

Figure 3.26. Photomicrographs of a, b, c, d, e) oil-shale facies; and f) sandstone facies presenting quartz (Q), plagioclase (Pg), calcite (Ct), polycrystalline quartz (Pq), chlorite (Cr), biotite (Be), organic matter (Om), and sparite (Sp) (Sample no. a) K13, Xpl, x4; b) K19, PPl, x4; c) K19, XPl, x4; d) K40, laminated oil-shale, PPl, x4; e) K40, hand specimen ; f) K18, PPl, x10. .... 138

Figure 3.27. Photomicrographs of sandstone facies presenting quartz (Q), plagioclase (Pg), chert (Ce), polycrystalline quartz (Pq), chlorite (Cr), organic matter (Om), and sparite (Sp) (Sample no. a) K18, Xpl, x10; b) K39, PPl, x4; c) K39, XPl, x4; d) K43, long angle wavy very thin planar bedding, hand specimen; e) K43, PPl, x10 ; f) K43, XPl, x10. .... 140

Figure 3.28. Pie graphs of the sandstone lithofacies in the Kösüre section..... 142

Figure 3.29. Photomicrographs of sandstone facies presenting quartz (Q), feldspar (Fd) and sparrite (Sp). (Sample no. a) K47, hand specimen, showing wavy rippled bedding (indicated by red line); b) K47, XPl x10; c) field photograph of interbedded sandstone and shale (K48, K49). .... 143

Figure 3.30. Photomicrographs of lime mudstone microfacies presenting quartz (Q), pyrite (P), phytoclast (Py), organic matter (Om), charcoal fragment (Cc) and cuticle (Cu). (Sample no. a) T7, PPl, x10; b) T8, hand specimen, yellow outline indicates calcareous concretion on the bedding plane; c) T8, PPl x4; d) T8, representing close

view of phytoclast, PPl, x100; e) T11, hand specimen showing coaly wood fragment; f) T12, PPl, x10. ....	149
Figure 3.31. Photomicrographs of lime mudstone microfacies presenting ferrous-manganese (FM), oxidation of Fe-Mn nodules (Ox) and organic matter (Om). (Sample no. a) T12, organic matter (charcoal fragment), x2.5; b) T13, hand specimen showing Fe-Mn nodules; c) T13, cross cut hand specimen showing Fe-Mn nodules; d) T16, organic matter (plant fragment), x2.5; e) T13, PPl x4; f) T13, Fe-Mn nodule, PPl, x4. ....	150
Figure 3.32. Photomicrographs of lime mudstone (a, b) and oil-shale (c, d, e, f) facies presenting organic-rich dark laminae (yellow arrow) and organic poor light laminae (white arrow), quartz (Q), and pyrite (P). (Sample no. a) T23, field photograph showing Fe-Mn nodules with outline oxidation; b) T12, PPl, x10; c) T1, parallel laminated, PPl, x4; d) T1, graded to thick laminae, PPl, x4; e) T4, hand specimen showing alternating organic-rich dark laminae (yellow) and organic-poor laminae (white arrow); f) T4, PPl, x4. ....	151
Figure 3.33. Photomicrographs of oil-shale (a, b, c) and sandstone (d, e, f) facies presenting quartz (Q), cuticle (Cu), euhedral pyrite (Ep), silica (Si), organic matter (Om), chlorite (Cr), blue tourmaline (T) and sparite cement (Sp). (Sample no. a) T4, XPl, x10; b) T5, PPl, x4; c) T17, non-laminated, PPl, x4; d) T27, PPl, x10; e) T27, XPl, x10; f) T27, PPl, x10. ....	152
Figure 3.34. Pie graphs of sandstone lithofacies in the Karahisar section. ....	154
Figure 3.35. Photomicrographs of Lime Mudstone microfacies (a, b), wackestone (c, d, e) and packstone (f) presenting charophyta (Ch), ostracod (Os), plagioclase (Pg), quartz (Q), bivalve (Bi), phytoclast (Py), cuticle (Cu), algal filament (Ag) and organic matter (Om), pore (Po). (Sample no. a) S12, PPl, x4; b) S12, PPl, x100; c) S16, PPl, x4; d) S26, PPl, x4; e) S26, PPl, x4; f) S17, PPl, x4. ....	159
Figure 3.36. Photomicrographs of Packstone (a, b, c) and rudstone (d, e) presenting bivalve (Bi), quartz (Q), ostracod (Os), polycrystalline quartz (Qp), feldspar (F) and organic matter (Om). (Sample no. a) S17, PPl, x4; b) S17, XPl, x4; c) S17, Hand specimen, yellow dotted line showing leaf outline and red arrow pointing the plant	

fragments; d) S28, yellow outline indicates the intraclast, PPI, x4; e) S28, PPI, x4. .....	160
Figure 3.37. Photomicrographs of rudstone (a, b, c) presenting quartz (Q), polycrystalline quartz (Qp) and Nummulites (N). (Sample no. a) S33, PPI, x4; b) S33, XPI, x4; c) S33, hand specimen, red arrow pointing the bivalve. ....	162
Figure 3.38. Photomicrographs of oil-shale (a, b, c, d) and sandstone (e, f) presenting quartz (Q), bioclast (Bc), foraminifera (Fr), tourmaline (T), feldspar (F), chert (Ce), polycrystalline quartz (Qp), chlorite (Cr), glauconite (Gt) and organic matter (Om). (Sample no. a) S11, PPI x4; b) S13, PPI, x4; c) S13, PPI, x10; d) S20, PPI, x4; e) S1, PPI, x4; f) S1, XPI, x4.....	165
Figure 3.39. Pie graphs of the sandstone lithofacies of floodplain depositional environment in the Sünnet section.....	167
Figure 3.40. Pie graphs of the marine deposited sandstone lithofacies in the Sünnet section. ....	168
Figure 3.41. Photomicrographs of sandstone (a, b, c, d) and pebble-conglomerate (e, f) presenting quartz (Q), polycrystalline quartz (Qp), bioclasts (Bc), limestone fragment (Lf), feldspar (F) and organic matter (Om). (Sample no. a) S18, PPI x4; b) S18, XPI, x4; c) S29, PPI x4; d) S29, XPI, x4; e) field photography of S3 sample of pebble conglomerate; f) S3, Hand specimen. ....	169
Figure 3.42. Photomicrographs of extracted fossils from Dağhacılar section presenting wackestone, packstone and marl facies. (Sample no. a) D6 wackestone, micro-tooth, x2.5; b) D6 wackestone, ostracods, x2.5; c) D14 wackestone, ostracods, x2; d) D17 wackestone, ostracods, x2; e) D11 packstone, ostracods, charophyta (yellow arrow), x2; f) D20 marl, ostracods, x2.5. ....	170
Figure 3.43. Photomicrographs of extracted fossils from Dağhacılar section (a), Hasanlar (b) and Kösüre sections (c, d, e, f) presenting wackestone, oil-shale and marl facies. (Sample no. a) D10 oil-shale, ostracods, x2.5; b) H13 oil-shale, ostracods, x2.5; c) K33 wackestone, ostracods and charophyte gyrogonites (yellow arrow), x3; d) K38 wackestone, crinoid, x1.5; e) K20 marl, ostracods, x2.5; f) K20 marl, micro-tooth, x2.5. ....	171

Figure 3.44. Photomicrographs of extracted fossils from Köüre (a) and Sünnet sections (b, c, d, e, f) presenting wackestone, oil-shale and marl facies. (Sample no. a) K28 marl, ostracods, x2.5; b) S16 wackestone, ostracods, x2.5; c) S26 wackestone, ostracods, bivalve (white arrow) and charophyte gyrogonites (yellow arrow), x2.5; d) S26 wackestone, ostracods, perforated ostracods (pink arrow), x2.5; e) S26 wackestone, fish scales, x3; f) S13 oil-shale, bivalve fragment, x2.5.....	172
Figure 3.45. Photomicrographs of extracted fossils from Sünnet sections. (Sample no. a) S17 packstone, charophyte gyrogonites, x2.5; b) S32 rudstone, bivalve.....	173
Figure 4.1. General evolutionary trend in Charophyte fructifications (Grambast, 1974). .....	177
Figure 4.2. Photomicrographs of extracted fossils Charophyte gyrogonites from Dağhacılar section (a, b), Köüre sections (c) and Sünnet section (d, e). (Sample no. a) D11 packstone, ostracods, charophyta (white arrow), x2; b) D17 wackestone, ostracods, x2; c) K33 wackestone, ostracods and charophyta (white arrow), x3; d) S17 packstone, charophytes, x2.5. e) S26 wackestone, ostracods, bivalve and charophyta (white arrow), x2.5; Charophyte Gyrogonites (1, 2, 3, 4, 5, 6, 7, 8, 9, 10, 11, Figure d) .....	179
Figure 4.3. Scanning electron photomicrographs of the Dağhacılar ostracods genera. (D= Dağhacılar sample) .....	181
Figure 4.4. Scanning electron photomicrographs of the Dağhacılar and Köüre ostracods genera. Note: Charophyte gyrogonites genera from Köüre section. (D= Dağhacılar sample; K= Köüre sample) .....	183
Figure 4.5. Scanning electron photomicrographs of the Sünnet ostracods genera. (S= Sünnet sample) .....	184
Figure 4.6. The identified ostracods and charophyte gyrogonites genera along the measured Dağhacılar section, Hasanlar section, Köüre sections, Karahisar section and Sünnet section.....	188
Figure 5.1. Generalized model for laminated mudrocks/shale type and their depositional setting (O'Brien, 1990).....	193

Figure 5.2. Graphic presentation of petrographic percent data of quartz along measured stratigraphic sections; Dağhacılar, Köşüre, Karahisar and Sünnet sections and their correlation. ....	194
Figure 5.3. Graphic presentation of petrographic percent data of feldspar along measured stratigraphic sections; Dağhacılar, Köşüre, Karahisar and Sünnet sections and their correlation. ....	195
Figure 5.4. Graphic presentation of petrographic percent data of plagioclase along measured stratigraphic sections; Dağhacılar, Köşüre, Karahisar and Sünnet sections and their correlation. ....	196
Figure 5.5. Graphic presentation of petrographic percent data of rock fragments along measured stratigraphic sections; Dağhacılar, Köşüre, Karahisar and Sünnet sections and their correlation. ....	197
Figure 5.6. Graphic presentation of petrographic percent data of bioclasts along measured stratigraphic sections; Dağhacılar, Köşüre, Karahisar and Sünnet sections and their correlation. ....	198
Figure 5.7. Graphic presentation of petrographic percent data of matrix along measured stratigraphic sections; Dağhacılar, Köşüre, Karahisar and Sünnet sections and their correlation. ....	199
Figure 5.8. Graphic presentation of sandstone pie diagram (Chapter 3) along measured stratigraphic sections; Dağhacılar, Köşüre, Karahisar and Sünnet sections and their correlation. ....	200
Figure 5.9. Depositional setting and correlation of the studied sections. ....	220
Figure 5.10. The paleogeographic position of studied area related with the Neo-Tethys (Studied regime is represented by green rectangle) (Şengör and Yilmaz, 1983). ...	224
Figure 5.11. A) Satellite image of studied sections; B) Depositional setting stage of the studied sections during Middle Eocene. The first stage of lacustrine setting development in the studied regime after the marine regression. According to Saner (1978), development of lacustrine due to marine regression in the studied regime. (White block represents studied sections and transparent blue represent water level; arrow shows north direction). ....	225

Figure 5.12. 1/100000 Geological map of the Northwestern Anatolia, Turkey (Adapazarı-H25 and Adapazarı-H26) (Timur and Aksay, 2002; Gedik and Aksay, 2002) and studied stratigraphic sections in the area. (red arrow-North direction)...	226
Figure 5.13. Generalized depositional model of the studied sections from south to central to north. A) Representing the next stages of the lacustrine environment with sub-environment and overlain by marine environment setting in the studied section during Middle Eocene time. B) Simple display of lacustrine evolving into the marine environmental setting. Gray color represents an early stage of the lacustrine layer, the green layer representing the next stage of the lacustrine; blue layer representing marine overlying on the lacustrine environment setting. (Red arrow pointing the first phase of lacustrine water; black arrow pointing the second phase of lacustrine water; pink arrow pointing marine water phase; N-North direction). .....	228
Figure 6.1. Facies distribution depositional diagram as interpreted from sedimentological analysis and stacking pattern. (Not to the scale) (Abouelresh et al., 2017; Platt & Wright 1991).....	235
Figure 6.2. Types of cycle determined in the Dağhacılar Section. ....	235
Figure 6.3. Types of cycle along the Dağhacılar Section. Triangles indicate centimeter to meter scale cycles. (for legend; Figure 6.2). ....	236
Figure 6.4. Types of cycle determined in the Hasanlar Section.....	240
Figure 6.5. Types of cycle along the Hasanlar Section. Triangles indicate centimeter to meter scale cycles. (For legend; Figure 6.4) .....	241
Figure 6.6. Types of cycle determined in the Kösüre Section. ....	243
Figure 6.7. Types of cycle along the Kösüre Section. Triangles indicate centimeter to meter scale cycles. (For legend: Figure 6.6) .....	244
Figure 6.8. Types of cycle determined in the Karahisar Section. ....	246
Figure 6.9. Types of cycle along the Karahisar Section. Triangles indicate centimeter to meter scale cycles. (For legend; Figure 6.8) .....	247
Figure 6.10. Types of cycle determined in the Sünnet Section.....	250
Figure 6.11. Types of cycle along the Sünnet Section. Triangles indicate centimeter to meter scale cycles. (For legend; Figure 6.10) .....	251

Figure 6.12. Fischer plot of the Middle Eocene (Lutetian-Bartonian) studied sections. Blue arrow indicates increase in accommodation space and red arrow indicates decrease in accommodation spaces. Red rectangle indicates marine successions in the upper portion of the studied sections. .... 256

Figure 6.13. Correlation of Fischer plot of the Middle Eocene (Lutetian-Bartonian) studied sections, A) Hasanlar Section and B) Kösüre Section with the Dağhacılar Section. Rectangle indicates marine depositional cycles in the studied sections.... 257

Figure 6.14. Correlation of Fischer plot of the Middle Eocene (Lutetian-Bartonian) studied sections, A) Karahisar Section and B) Sünnet Section with the Dağhacılar Section. Rectangle indicates marine depositional cycles in the studied sections .... 258

Figure 6.15. Correlation of Fischer plot of the Middle Eocene (Lutetian-Bartonian) studied sections. Solid arrows indicate increase in accommodation space and Dotted arrows indicate decrease in accommodation spaces. Solid line rectangle indicates marine depositional cycles in the upper portion of the studied sections. Dotted brown rectangle shows overall deepening trend and Dotted light blue shows overall shallowing trend..... 259

Figure 6.16. Relationship between organic matter content, carbonate content and centimeter to meter scale order cycles of the Dağhacılar section..... 260

Figure 6.17. Relationship between organic matter content, carbonate content and centimeter to meter scale order cycles of the Hasanlar section. .... 261

Figure 6.18. Relationship between organic matter content, carbonate content and centimeter to meter scale order cycles of the Kösüre section..... 262

Figure 6.19. Relationship between organic matter content, carbonate content and centimeter to meter scale order cycles of the Karahisar section..... 263

Figure 6.20. Relationship between organic matter content, carbonate content and centimeter to meter scale order cycles of the Sünnet section. .... 264

Figure 6.21. Relationship between carbonate content and centimeter to meter scale order cycles within the studied sections. .... 265

Figure 6.22. Relationship between organic matter content and centimeter to meter scale order cycles within the studied sections. .... 266

Figure 7.1. Sequence stratigraphic interpretation of the Dağhacılar section. (OS-oil-shale; M-marl; LL-Lime mudstone; Wp-wackestone-packstone; SS-sandstone; Cc-conglomeratic).....	272
Figure 7.2. Sequence stratigraphic interpretation of the Hasanlar section. (OS-oil-shale; M-marl; LL-Lime mudstone; Wp-wackestone-packstone; SS-sandstone; Cc-conglomeratic).....	273
Figure 7.3. Sequence stratigraphic interpretation of the Kösüre section. (OS-oil-shale; M-marl; LL-Lime mudstone; Wp-wackestone-packstone; SS-sandstone; Cc-conglomeratic).....	275
Figure 7.4. Sequence stratigraphic interpretation of the Karahisar section. (OS-oil-shale; M-marl; LL-Lime mudstone; Wp-wackestone-packstone; SS-sandstone; Cc-conglomeratic).....	276
Figure 7.5. Sequence stratigraphic interpretation of the Sünnet section. (OS-oil-shale; M-marl; LL-Lime mudstone; Wp-wackestone-packstone; SS-sandstone; Cc-conglomeratic).....	278
Figure 7.6. Correlation of the sequence stratigraphic interpretation of the studied sections and relative change of the sea-level/lacustrine level in the studied sections. (FS-flooding surface; MFZ-maximum flooding zones; OS-oil-shale; M-marl; LL-Lime mudstone; Wp-wackestone-packstone; SS-sandstone; Cc-conglomeratic)....	283
Figure 7.7. Correlation of Sequences and maximum flooding zones between the studied sections and with Eustatic Sea-level Curve chart (Haq et al., 1987).....	285
Figure 8.1. Photomicrographs of the Dağhacılar lithofacies, examined for chemical analysis (PPI, x4).....	290
Figure 8.2. The pie chart of average weight percent values of lithofacies from the Dağhacılar measured section. ....	292
Figure 8.3. Representing the Dağhacılar measured stratigraphic log and graphical representation of geochemical analysis data of weight percent CaCO <sub>3</sub> , organic matter, clay and quartz/feldspar and their comparison along the measured stratigraphic log. ....	293

Figure 8.4. Photomicrographs of the Hasanlar lithofacies, examined for chemical analysis (PPI, x4). .....	294
Figure 8.5. The pie chart of average weight percent values of lithofacies from the Hasanlar measured section. ....	295
Figure 8.6. Representing the Hasanlar measured stratigraphic log and graphical representation of geochemical analysis data of weight percent CaCO <sub>3</sub> , Organic Matter, Clay and Quartz/feldspar and their comparison along the measured stratigraphic log. ....	295
Figure 8.7. Photomicrographs of the Kösüre lithofacies, examined for chemical analysis (PPI, x4). ....	296
Figure 8.8. The pie chart of average weight percent data of lithofacies from the Kösüre measured section.....	297
Figure 8.9. Representing the Kösüre measured stratigraphic log and graphical representation of geochemical analysis data of weight percent CaCO <sub>3</sub> , Organic Matter, Clay and quartz/feldspar and their comparison along the measured stratigraphic log. ....	297
Figure 8.10. Photomicrographs of the Karahisar lithofacies, examined for chemical analysis (PPI, x4). ....	298
Figure 8.11. The pie chart of average weight percent values of lithofacies from the Karahisar section. ....	299
Figure 8.12. Representing the Karahisar measured stratigraphic log and graphical representation of geochemical analysis data of weight percent CaCO <sub>3</sub> , Organic Matter, Clay and Quartz/feldspar and their comparison along the measured stratigraphic log. ....	299
Figure 8.13. Photomicrographs of the Sünnet lithofacies, examined for chemical analysis (PPI, x4). ....	300
Figure 8.14. The pie chart of average weight percent values of lithofacies from the Sünnet measured section.....	301
Figure 8.15. Representing the Sünnet measured stratigraphic log and graphical representation of geochemical analysis data of weight percent CaCO <sub>3</sub> , organic matter,	

Clay and quartz/feldspar and their comparison along the measured stratigraphic log. .....	302
Figure 8.16. Cross-Plot of wt.% Organic matter vs wt.% CaCO <sub>3</sub> , wt.% organic matter vs wt.% clay content and wt.% organic matter vs wt.% quartz/feldspar content of the Dağhacılar geochemical studied samples data. CaCO <sub>3</sub> represent a negative linear trend to organic matter, Clay and quartz /feldspar show a positive linear trend to organic matter (Solid line shows a linear trend of the minerals component).....	312
Figure 8.17. Cross-Plot of wt.% Organic matter vs wt.% CaCO <sub>3</sub> , wt.% organic matter vs wt.% clay content and wt.% organic matter vs wt.% quartz/feldspar content of the Hasanlar geochemical studied samples data. CaCO <sub>3</sub> represent a negative linear trend to organic matter, Clay and quartz /feldspar show a positive linear trend to organic matter (Solid line shows a linear trend of the mineral component). ....	313
Figure 8.18. Cross-Plot of wt.% Organic matter vs wt.% CaCO <sub>3</sub> , wt.% organic matter vs wt.% clay content and wt.% organic matter vs wt.% quartz/feldspar content of the Köşüre geochemical studied samples data. CaCO <sub>3</sub> represent a negative linear trend to organic matter, Clay and quartz /feldspar show a positive linear trend to organic matter (Solid line shows a linear trend of the mineral component). ....	313
Figure 8.19. Cross-Plot of wt.% Organic matter vs wt.% CaCO <sub>3</sub> , wt.% organic matter vs wt.% clay content and wt.% organic matter vs wt.% quartz/feldspar content of the Karahisar geochemical studied samples data. CaCO <sub>3</sub> represent a negative linear trend to organic matter, Clay and quartz /feldspar show a positive linear trend to organic matter (Solid line shows a linear trend of the mineral component). ....	314
Figure 8.20. Cross-Plot of wt.% Organic matter vs wt.% CaCO <sub>3</sub> , wt.% organic matter vs wt.% clay content and wt.% organic matter vs wt.% quartz/feldspar content of the Sünnet geochemical studied samples data. CaCO <sub>3</sub> represent a negative linear trend to organic matter, Clay and quartz /feldspar show a positive linear trend to organic matter (Solid line shows a linear trend of the minerals component).....	314
Figure 8.21. The pie chart of average weight percent values of the CaCO <sub>3</sub> , organic matter, clay content and quartz/feldspar in the Dağhacılar, Hasanlar, Köşüre, Karahisar and Sünnet measured sections. ....	315

Figure 8.22. Graphic presentation of total porosity% along measured stratigraphic section of the Dağhacılar, Köşüre, Karahisar and Sünnet sections and their correlation. .... 320

Figure 8.23. Photomicrographs and porosity sketch of the Dağhacılar section (D) samples. The red color indicates pore spaces in the photomicrographs. Black patches within the white square background indicates pore spaces sketch in the photomicrographic image. (PPI, x04). .... 322

Figure 8.24. Photomicrographs and porosity sketch of the Dağhacılar section (D) and Hasanlar section (H) samples. The red color indicates pore spaces in the photomicrographs. Black patches within the white square background indicates pore spaces sketch in the photomicrographic image. (PPI, x04). .... 323

Figure 8.25. Photomicrographs and porosity sketch of the Hasanlar section (H) and Köşüre section (K) samples. The red color indicates pore spaces in the photomicrographs. Black patches within the white square background indicates pore spaces sketch in the photomicrographic image. (PPI, x04). .... 324

Figure 8.26. Photomicrographs and porosity sketch of the Köşüre section (K) and Karahisar section (T) samples. The red color indicates pore spaces in the photomicrographs. Black patches within the white square background indicates pore spaces sketch in the photomicrographic image. (PPI, x04) ..... 325

Figure 8.27. Photomicrographs and porosity sketch of the Karahisar section (T) and Sünnet section (S) samples. The red color indicates pore spaces in the photomicrographs. Black patches within the white square background indicates pore spaces sketch in the photomicrographic image. (PPI, x04). .... 326

Figure 8.28. Graphic presentation of the CaCO<sub>3</sub> wt.% along measured stratigraphic sections of the Dağhacılar, Köşüre, Karahisar and Sünnet sections and their correlation. .... 333

Figure 8.29. Graphic presentation of the organic matter content wt.% along measured stratigraphic sections of the Dağhacılar, Köşüre, Karahisar and Sünnet sections and their correlation. .... 334

Figure 8.30. Graphic presentation of the clay content wt.% along measured stratigraphic sections of the Dağhacılar, Köşüre, Karahisar and Sünnet sections and their correlation. ....	335
Figure 8.31. Graphic presentation of the quartz/feldspar content wt.% along measured stratigraphic sections of the Dağhacılar, Köşüre, Karahisar and Sünnet sections and their correlation. ....	336
Figure 8.32. Representing photomicrographs of oil stained shale and sandstone from the A) Dağhacılar (sample D40, x4, PPI), B) Hasanlar (sample H13, x10, PPI), C) Karahisar (sample T1, x4, PPI) and D-E) Sünnet sections (S1 and S29, x4, PPI)...	337
Figure 8.33. Graphic presentation of the source rock, porosity and brittle character composition along measured stratigraphic section of the Dağhacılar, Köşüre, Karahisar and Sünnet sections. ....	338
Figure 9.1. Correlation of the sequence stratigraphic interpretation, centimeter-meter scale cycles, relative lake level/sea-level, organic matter content, CaCO <sub>3</sub> , and charophytes and ostracods within the studied sections from south to central to north. (FS-flooding surface; MFZ-maximum flooding zones; OS-oil-shale; M-marl; LL-Lime mudstone; Wp-wackestone-packstone; SS-sandstone; Cc-conglomeratic)....	355



## CHAPTER 1

### INTRODUCTION

#### 1.1. Introduction

Several lacustrine basins have been documented from central and western Anatolia during the Paleocene to Upper Miocene. Some of the lacustrine basins are important resources of oil-shale and coal (Şener, et al., 1995; Şener and Gündoğdu, 1996). The Paleocene-Eocene and Middle-Upper Miocene age strata are generally well documented for oil-shale in Turkey. The oil-shale deposits are reported from the Seyitömer-Kütahya, Beypazarı-Ankara, Himmetoğlu, Bolu and Hatıldağ-Bolu, Mengen-Bolu regions (Şener & Şengüler, 1998). The Paleocene-Eocene oil-shales deposits of Turkey are early to intermediate maturity in general (Sarı and Sonel, 2000; Sonel et al., 1987a, 1987b; Sarı et al., 2007).

Oil-Shale is defined as the kerogen-rich sediments, which is one of the most important energy alternatives. These deposits are in enormous quantity and widely distributed around the world which makes them one of promising option as an oil source and solid fuel supplement. Lithologically, the term “Oil-Shale” is not only restricted to shales. It also includes marl and carbonate lithofacies, which forms a mixture of tightly bound organic and inorganic materials. Simply, oil-shale can be defined as tightly-bound organic and inorganic composites (Figure 1.1). 1:4 ratio of organic to inorganic are rarely exceeding (Yen and Chilingarian, 1976; Cestari, 2015). Generally, the mineral composition of carbonate-rich oil-shales comprise of calcite, dolomite and siderite with lesser amount of aluminosilicates. In silicate-rich oil-shales, the oil-shales are dominated by quartz, feldspar and clay mineral and lesser components of carbonates (Yen and Chilingarian, 1976; Şengüler, 1999 and Altun et al., 2006; Dyni, 2006). The other minerals in the oil-shales are sulfide minerals such as pyrite and marcasite but

in small quantity and indicates that facies deposited in dysoxic to anoxic conditions (Figure 1.1). The nature and organic materials extent mostly depend on the depositional environment and host rock character. In the oil-shales, organic matter is predominantly composed of kerogen, with also some existence of bitumen and/or prebitumen (Altun et al., 2006).

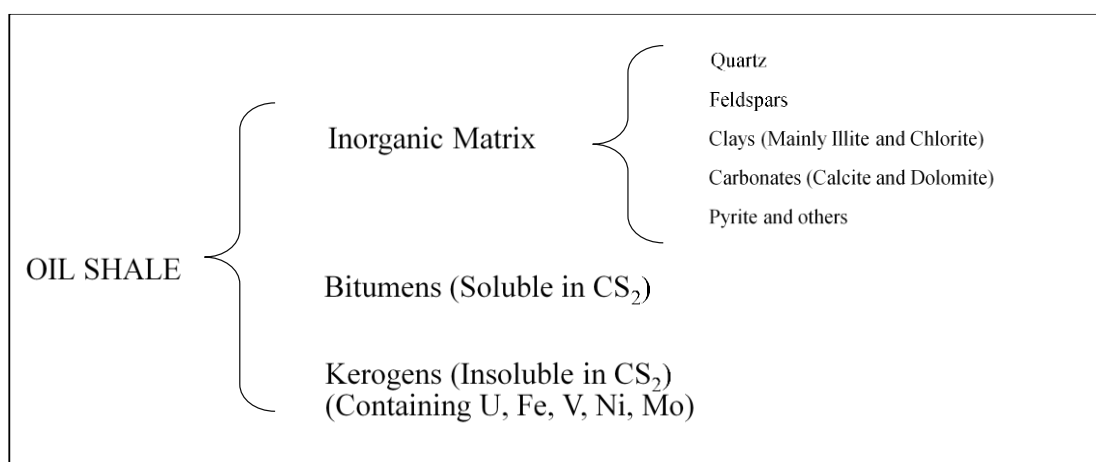


Figure 1.1. General scheme of the oil-shale components (Yen and Chilingarian, 1976).

The oil-shales are different in many ways from coal in terms of mineral and elemental contents. The large amount of inert minerals (60 to 90 %) is present in the oil-shales, while coal contains less than 40 % mineral matters. The higher content of hydrogen and lower content of oxygen are observed in organic matter of oil-shales, which is the source of typically liquid and gaseous hydrocarbon. These contents are lesser than those of lignite and bitumen coal. The origin of organic matter in oil-shales are of algal source with presences of some vascular land plants remains, which predominantly occurs in the coal organic matter. Sometime, the origin of organic matter in oil-shales are difficult to characterize because of the lack of biological structures as biological structures are helpful in the identification of precursor organisms. Such material may be of bacterial origin or product of bacterial degradation of algae or other organic

matter. Most of the organic matter in oil-shales are derived from various types of marine and lacustrine algae (Dyini, 2006).

Recently, many different types of oil-shale have been classified on the basis of the depositional environment, the petrographic character of the organic matter, and the precursor organisms from which the organic matter was derived. In 1991, Hutton divided the organic-rich sedimentary rocks into three major groups, which are humic coal and carbonaceous shale, bitumen-impregnated rock, and oil-shale. Hutton (1987, 1991) further classified the oil-shale into three groups on the basis their environment of deposition, such as terrestrial, lacustrine, and marine (Figure 1.2).

Oil-shales are found in both fresh water and marine settings, i.e large fresh-water to saline lacustrine, continental platforms and continental shelves, epicontinental marine basins, and related subtidal shelves as well as shallow ponds or lakes associated with coal-forming peat in limnic and coastal swamp depositional environments. Organic matter in oil-shales is mostly hosted by various types of marine and lacustrine algae, with some debris from spores, pollen, plant cuticle, corky fragments of herbaceous and woody plants, plant resins, and plant waxes, and other cellular remains of lacustrine, marine, and land plants (Dyini, 2003, 2006; Scouten, 1990), depending on the depositional environment and sediment sources (Figure 1.3).

<b>Organic-rich sedimentary Rocks</b>	<b>Bitumen- impregnated Rocks</b>	
	<b>Oil Shales</b>	<b>Terrestrial oil shale</b>
		<b>Lacustrine Oil shale</b>
		<b>Marine Oil shale</b>
<b>Humic Coals</b>		
	<b>Cannel Coal</b>	
	<b>Lamosite Torbanite</b>	
	<b>Kukersite Tasmanite Marinite</b>	

Figure 1.2. Classification of oil-shales from Hutton (1987, 1991).

## 1.2. Oil-shales in the World and Turkey

Recently, oil-shales are one of the substantial and focusing unconventional fossil resource in the world, which can be converted into liquid hydrocarbons via different processes. Oil-shales have been deposited across the globe in variety of lacustrine and marine setting. Oil-shales are recorded from Pre-Cambrian to Tertiary age and occur as giant deposits or minor accumulation of little or no economic values. As a need for the alternative energy and worldwide distribution, these deposits have received much attention in recent years. Within this scope, the unconventional oil exploration takes important place in the agenda of big countries such as the USA and China. Turkey has also accelerated investigations in the unconventional oil exploration. Although oil-shales exist in the form of extensive deposits in many countries, in the USA, Estonia, China, Jordan, Australia, Canada, Israel and Brazil have been very important over the past hundred years. The Eocene age Oil-shale extends mainly over Piceance Creek basin (Colorado), Uinta basin (Utah), Green River basin, Washakie basins (Wyoming) and Middle Western Anatolian Turkey (Altun et al., 2006; Dyni, 2006 and Zeng et al., 2015).

	CHLOROPHYCEAE (green algae)				Mixed	CYANOPHYCEAE (blue-green algae)	
<b>Parent Genus</b>	<i>Gloeocapsomorpha prisca</i>	<i>Reinschia</i>	<i>Pila</i>	<i>Tasminites punctatus</i>	Dinoflagellates acritarchs algae ( <i>Nostocopsis</i> )	Blue-green algae	<i>Pediastrum</i> species
<b>Modern-Day Equivalent</b>		<i>Botryococcus braunii</i>		<i>Pachysphaera</i>			
<b>Life Form</b>	Colonial	Colonial	Colonial	Unicellular			
<b>Dominant Liptinite</b>	Telalginite	telalginite	Telalginite	Telalginite	Bituminite Micrinite	Lamalginite	Lamalginite
<b>Oil Shale</b>	Kukersite	Torbanite	Torbanite	Tasminite	Marinite	Lamosite	Lamosite
<b>Non-Algal Organic Compounds</b>	?	vitrinite inertinite sporinite resinite	vitrinite inertinite sporinite	vitrinite lamalginite	liptodetrinite telalginite inertinite sporinite	corpohuminite sporinite vitrinite bitumen	vitrinite telalginite sporinite bitumen corpohuminite resinite
<b>Deposit</b>	Estonia, Nawabi Kas (Pakistan)	Joadja, N.S.W. Newnes Glen Davis Alpha, Qld Carnarvon Creek, Qld Lacustrine freshwater lake in a lake peat mire (swamp)	Westfield Torbane Hill, N.S.W.	Mersey River, Tas	Toolebuc Formation, Qld. Posidonia Shale, Toarcian, Paris Basin.	Green River Formation, U.S.A.	Stuart Rundle Condor
<b>Environment</b>	marine		lacustrine	Marine (shallow sea)	shallow marine	Stratified (saline) lacustrine	shallow freshwater lacustrine

Figure 1.3. Oil-shale classification based on maceral composition and environment of deposition (after Hutton et al., 1980; Hutton, 1982).

After lignite coal, oil-shale includes the second largest potential fossil fuel in Turkey. These oil-shales are documented from Paleocene to late Miocene age and their main resources are located in the middle and western regions of Anatolia (Figure 1.4; Altun et al., 2006). The general lithologies of the organic rich sedimentary rocks are marl, clay and carbonates. The main potential resources of oil-shale deposits in Turkey are in Beypazarı (Ankara), Seyitömer (Kütahya), Himmetoğlu (Bolu) and Hatıladağ (Bolu) which are of major importance in terms of quality, amount and exploitability (Tables 1.1, 1.2). Other reported potentially important resources are in Mengen (Bolu), Ulukışla (Niğde), Bahçecik (İzmit), Burhaniye (Balıkesir), Beydili (Ankara), Dodurga (Çorum) and Demirci (Manisa), Sarıcakaya and Celtik (Table 1.1; Altun et al., 2006).

The geological studies and oil possibilities of the area between Göynük, Nallıhan and Beypazarı have been studied by several workers (Stepinsky, 1940; Akarsu, 1974; Granit and Şener, 1987; Sonel et al., 1987a, 1987b; Şeker and Kesgin, 1991; Sarı and Sonel, 2000; Sarı et al., 2004a, b; Sarı et al., 2007).

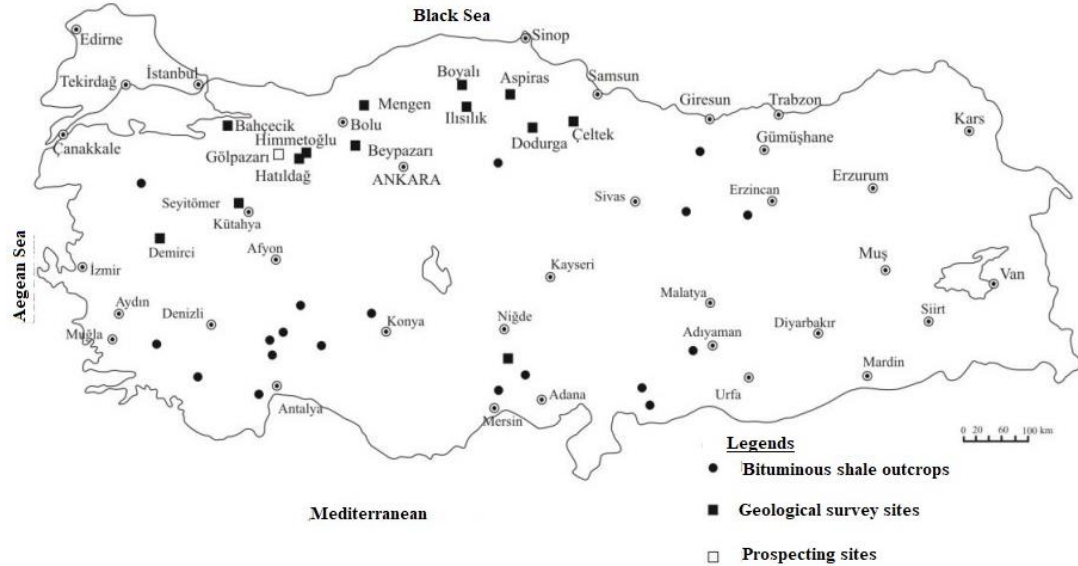


Figure 1.4. Main oil-shale reserves in Turkey (Şengüler, 2001).

Table 1.1. Main oil-shale reserves in Turkey (Altun et al., 2006).

Name of the deposit	Geological reserve (x10 <sup>6</sup> tones)	Possible reserve (x10 <sup>6</sup> tones)	Total reserve (x10 <sup>6</sup> tones)
Beypazarı	327.68	–	327.68
Seyitömer	83.32	38.85	122.17
Himmetoğlu	65.97	–	65.97
Hatıldağ	78.37	389.20	467.57
Mengen	–	50.00	50.00
Ulukışla	–	130.00	130.00
Bahçecik	–	42.00	42.00
Burhaniye	–	15.60	15.60
Beydili	–	300.00	300.00
Dodurga	–	138.00	138.00
Demirci	–	172.00	172.00
Sarıcakaya	–	300.00	300.00
Çeltik	–	90.00	90.00
<b>TOTAL</b>	<b>555.34</b>	<b>1665.65</b>	<b>2220.99</b>

Table 1.2. Characteristics of the major oil-shale deposits in Turkey (EGOS, on average basis) (Akkuş et al., 1982 and Altun et al., 2006).

Deposit	Upper calorific value, kcal/kg	Total organic carbon, %	Oil content, %	Oil content, I	Total sulphur, %
Beypazarı	812.07	4.8	5.4	60.0	1.4
Seyitömer	847.90	6.9	5.0	54.3	0.9
Himmetoğlu	4991.88	30.9	43.0	482.0	2.5
Hatıldağ	773.86	5.6	5.3	58.0	1.3

In this study, the research area related to the Middle Eocene oil-shales is lying in the Mudurnu-Göynük basin, in the Bolu province, Turkey. The Eocene formations with oil-shales units are well exposed in Mudurnu-Göynük basin, i.e. Yunuslar Formation, Güvenç Formation, Gemiciköy Formation, Kabalar Formation, Çaycuma Formation, Kızılçay Formation, Kislakoy Formation, Calatepe Formation, Halidiye Formation (Saner, 1978b; Meriçand Şengüler, 1986) and Hacili Formation (Gedik and Aksay, 2002). In previous studies, these are identified as oil-shales of lacustrine and marine transitional depositional units. The Eocene oil host rocks are settled in high sulfurous, anoxic condition, which occurs due to high organic productivity developing in the basin and lead to high accumulation of dead organism at the bottom (Sarı et al., 2015).

### **1.3. Aim and Scope**

In this study, the detailed work on the middle Eocene marine-influenced lacustrine deposits in the Mudurnu-Göynük Basin will be reviewed in terms of sedimentology, cyclostratigraphy, sequence stratigraphic relationships and geochemical studies. It is also intended to interpret the basin correlation, lateral distribution, change in the depositional environment and source rock character in the studied sections. One of the main objectives of this study is to identify the lateral continuity of oil-shale within the basin, marine influence in the lacustrine system and transgression to marine transitional environment in the regime during Middle Eocene. The Eocene successions are particularly important and likely favorable for the oil-shale deposits in the studied region. Therefore, more recent aspects of sedimentology, cyclostratigraphy and sequence stratigraphy are applied to study marine influence in the lacustrine setting and overlying marine environment, architecture and structure of sedimentary packages and their organic-rich character within the basin. Another objective is to understand the process controlling their evolution in the basin and modelling with the best correlation of the studied sections by employing this methodology. In addition, this study incorporates to document the vertical and lateral variation in the facies and facies recognition in the Mudurnu-Göynük Basin. This research also intended to study the nature and origin of cyclic succession in the Middle Eocene in order to determine the factors involved in Milankovitch climatic signals changing responses in the Eocene sedimentary record in the studied area. These interpretations will show the generation of oil-shale cycles in lacustrine in response of the orbital mode and tectonic forces in the continental to marginal marine setting. Finally, possible depositional setting model, relative sea-level/water level curve, vertical and lateral distribution of the Middle Eocene oil-shale deposits in the basin will be interpreted based on sedimentology, cyclostratigraphy, sequence stratigraphy and geochemical analysis. The interpreted data will be useful for future oil-shale exploration in the studied region.

#### **1.4. Geographic and Geological Setting**

The geographic coordinates of the Middle Eocene studied sections are present in Bolu province, in the Northwestern Anatolia of Turkey, and geologically in the Mudurnu-Göynük Basin (Figures 1.5). The studied sections were measured near the Dağhacılar village, Hasanlar village (east of the Dağhacılar village), Köşüre village (southwest of the Dağhacılar village), in the vicinity of Karahisar village (southeast of the Dağhacılar village) and Sünnet village (north of the Dağhacılar village) as shown in the figure 1.5. In the geological map of Turkey, the Dağhacılar section, Hasanlar section, Köşüre section, and Sünnet section are positioning in the Adapazarı H25, 1:100000 scaled topographic map (Gedik and Aksay, 2002). The Karahisar section lays in the Adapazarı H26, 1:100000 scaled topographic map (Timur and Aksay, 2002). Geographically, Mudurnu-Göynük Basin are lying between the Istanbul in the north and Ankara in the southeast. Geologically, the Intra-Pontide suture zone is present in the north and İzmir-Ankara-Erzincan suture zone in the south of the studied sections. The development of these sutures was occurred as result of closing of the Neo-Tethyan ocean during the Eocene period (Koçyiğit et al., 1991; Figures 1.6; 1.9).

#### **1.5. Methodology**

Oil-shales are experiential in a diverse range of sedimentary environment such as marine, fluvial and lacustrine settings (Demaison and Moore, 1980; Katz, 1990). In worldwide, oil-shale bearing lacustrine and marine deposits represent promising proportion of hydrocarbon resources. Organic rich bearing shale of lacustrine environment is almost entirely composed of algal remains. In a lacustrine setting, there is high frequency fluctuation in lake level and sediment invasion which gives a characteristic cyclic sequence of newly deposited organic matter and/or other lithology (Ocakoglu et al., 2012).

In the field studies, five stratigraphic sections are measured in the well exposed Middle-Eocene sedimentary sequence in the Mudurnu-Göynük basin and named as Dağhacılar, Hasanlar, Köşüre, Karahisar and Sünnet sections. The measured

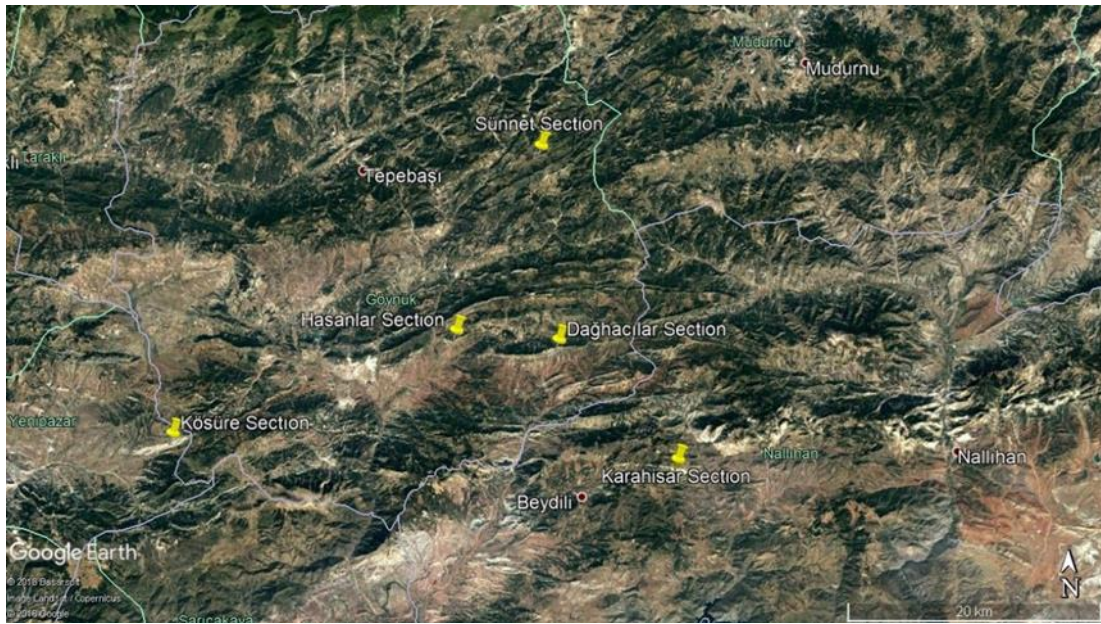


Figure 1.5. Representing the studied area (Studied measured section shown by yellow pin).

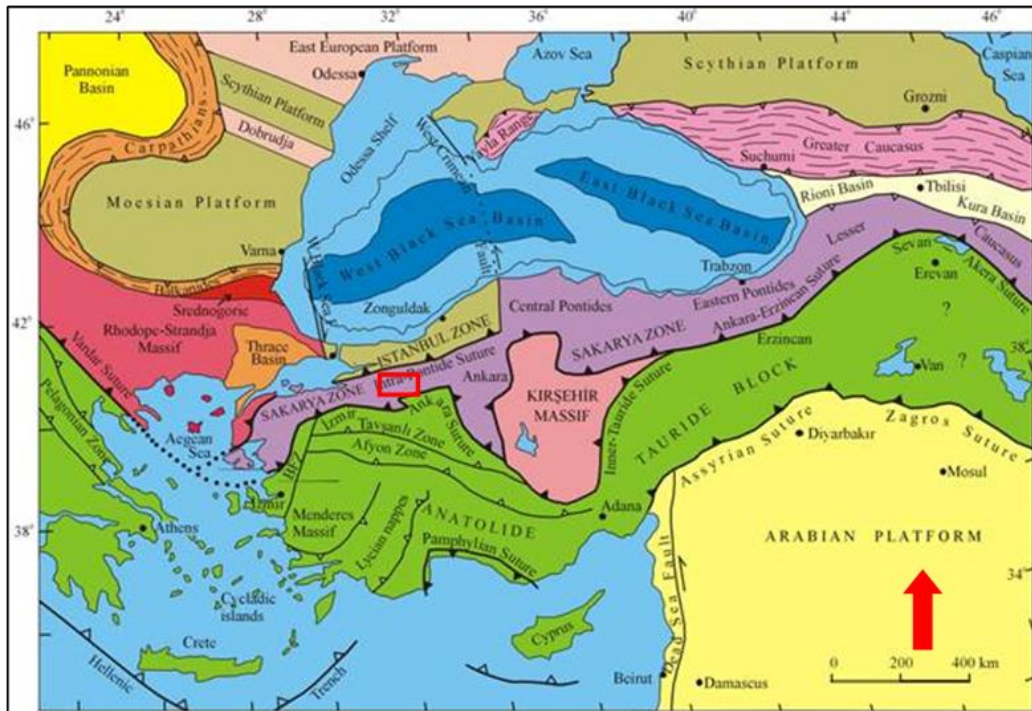


Figure 1.6. Showing regional tectonic of the Turkey and adjacent areas (modified from Okay and Tüysüz, 1999). (Red Arrow-North).

thicknesses of the studied stratigraphic sections are 159.50m, 25.20m, 81.80m, 71.80m and 69.30m, respectively. A total of 76, 21, 49, 29 and 36 orientated and unorientated samples are collected in the field from the Dağhacılar, Hasanlar, Kösüre, Karahisar and Sünnet sections, respectively. The samples are collected at random interval and their collection is based on change in biofacies, variation in lithofacies, sedimentary structures and change in color. The stratigraphic log is drawn on the notebook along with description of field observation and observed sedimentary features. In the field, the rock colors are described by using colour codes of the geological rock color chart of Geological Society of USA (GSA), 2009.

In the laboratory studies, the collected samples are separated for further detailed analyses such as microscopic studies, sedimentology, geochemical analysis, microfossils observation and source rock potential. The thin sections for detailed studies of the selected samples are prepared in the rock cutting lab at METU and then studied under the polarized microscope. The microscopic studies of the samples led to defining and recognizing the microfacies, their composition and depositional setting interpretation in the studied regime. The identified mineralogical compositions of the studied samples are classified by using different classification models, depending on the types of the rock unit, such as Diaz et al. (2012) mudstone classification, Allix's et al. (2010) shale classification and Stow's (2005) classification for shale, mudstone and marl, Embry and Klovan's classification (1971) and Folk's (1962) classification for limestone, Folk's (1974) and Pettijohn et al. (1987) triangular classifications for sandstone and Folk's (1965) texture classification of fine sedimentary rocks. In this study, calcirudite lithofacies is recorded in the Sünnet section. Therefore, the Embry and Klovan's classification (1971) is preferred over the Dunham's limestone classification (1962). The study is then followed by cyclostratigraphic analyses and sequence stratigraphy studies, which are interpreted by field studies and by using microscopic observation and geochemical analyses.

A number of chemical methods and techniques were explained in the previous literatures to extract microfossils from the sedimentary rocks. The selected chemical

method and technique for the extraction of microfossils from samples depend on the lithofacies chemical composition and hardness. During this study, 50% diluted acetic acid (CH<sub>3</sub>COOH) and 15% diluted Hydrogen peroxide (H<sub>2</sub>O<sub>2</sub>) chemical solvents are used to extract desired fossils from selected samples, which are soaked for a duration of 10 minutes to 30 minutes, depending on the hardness of the lithofacies. The diluted CH<sub>3</sub>COOH and diluted H<sub>2</sub>O<sub>2</sub> methods are used by a number of researchers to extract the different types of microfossils from the lithofacies (Lirer, 2000; Petrizzo, 2000; Luciani, 2002; Esmeray, 2006; Şafak et al., 2015).

For the extraction of ostracods and charophytes, 50g of sample is collected from each studied sample for the extraction of desired fossils. The 50g sample is crushed to the size of 1-5 mm in diameter in order to obtain more fragmented residue and less than that size is removed from the samples (Lirer, 2000). Then the sample is placed in the oven at 80°C for an hour to dry (Figure 1.7). After drying, the sample was immersed in a 1:3 ratio solvent of diluted CH<sub>3</sub>COOH and diluted H<sub>2</sub>O<sub>2</sub> in the beaker for 10 minutes to 30 minutes, depending on the type of lithofacies and hardness character (Appendices B1, B2, B3, B4, B 5). After the immersing the samples in diluted solvent, the sample is washed with distilled water through 500um, 250um, and 125um sieves (Figure 1.7).

After the chemical disintegration technique and distilled water washing and sieving, the samples of 250um, and 125um are placed in the oven at 60°C to dry. Then the 250um, and 125um collected samples are preserved for microscopic analysis (Figure 1.7). The ostracods and charophyte gyrogonites are picked out under reflected microscope. The extracted ostracods and charophyte gyrogonites are studied by using a scanning electron microscope (Figures 4.3, 4.4, 4.5, 4.6).

The cycles in the studied successions are established on the basis of centimeter to meter scale sediment interval (Einsele et al., 1991; Schwarzacher, 1993; Matthews

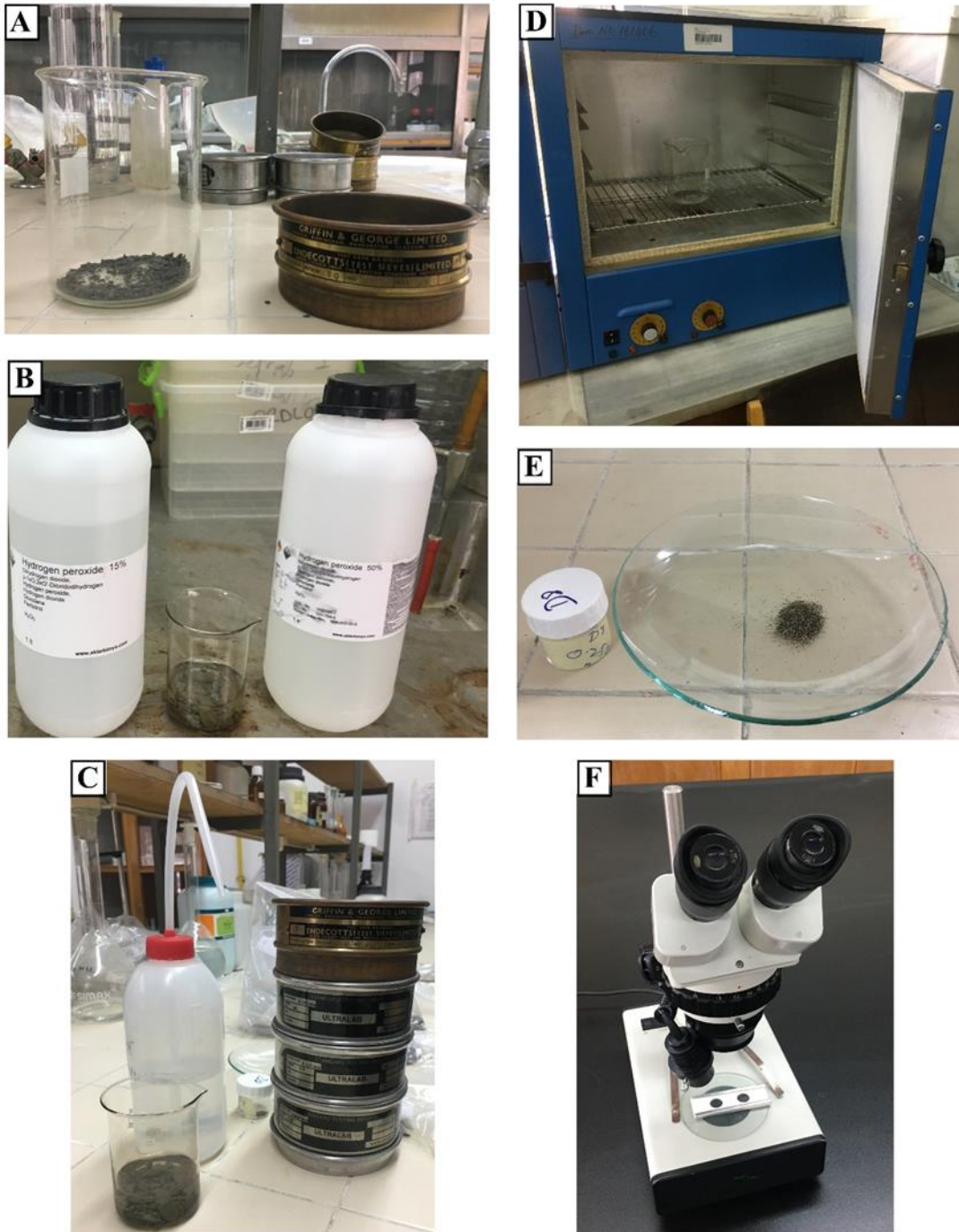


Figure 1.7. A) Crushed sample, B) soaked in diluted  $H_2O_2$  and diluted  $CH_3COOH$ , C) washed with distilled water and sieve through 500 $\mu m$ , 250 $\mu m$ , 125 $\mu m$  and 63 $\mu m$ , D) Dry in oven at 60°C, E) Collected samples and store it in the 15ml bottle, F) Picked the extracted fossils from store samples under reflected microscope and placed on microfossils slide.

and Perlmutter, 1994; Einsele, 2000; Strasser et al., 2006; Machlus et al., 2008). The determined cycles are also examined by using sedimentological, petrographically (both siliciclastic and carbonate), vertical and lateral facies association, within and along the sections. In Fischer plots, we constructed a plot of cumulative departure from mean cycle thickness as a function of cycle number and thickness. To generate the Fischer plots for studied sections, cycle thicknesses data are entered to the Fischer plot excel spreadsheet program, which constructed a Fischer plots for the studied sections (Sadler et al., 1993; Husinec et al., 2008)

Later, geochemical analyses and microscopic studies of the selected samples data are interpreted and are used to evaluate the source rock capability and geochemical character. In geochemical analyses, microscopic data and values obtained using chemical method from the powder samples are used to determine organic matter content and inorganic matter content in the studied samples. In this study, 10% dilute hydrochloric acid (HCl) solution is used to remove the carbonate component from samples and 30% diluted hydrogen peroxide is used to remove organic matter from samples (Saxby, 1970; Lewis and McConchie, 1994; Vaasma, 2008; Wang et al., 2009; Zeng et al., 2018). Later, the obtained data in the geochemical analyses is examined from different aspects. The visual porosity of the studied samples is estimated by using imageJ software™, which processes microscopic image and the percent porosity value is obtained from the studied samples processes image (Widiatmoko et al., 2010; Loucks et al., 2012; Schieber, 2013; Datta et al., 2016). The types of the existing porosity are determined by carrying out microscopic studies and imageJ software™ processed microscopic image (Widiatmoko et al., 2010; Loucks et al., 2012; Schieber, 2013; Datta et al., 2016).

This study also examines the relationships between the Middle Eocene oil-shale of lacustrine and marine transition, the cyclic changes related with Milankovitch forces and other factors. The analysis also proved to be helpful in the framework to understand the cyclicity transition, driving mechanism related with oil-shale and in understanding the processes controlling their evolution (Schwarzacher, 1993; Einsele,

2000; Strasser et al., 2006). In addition, detailed work is carried out on the Middle Eocene marine influenced lacustrine oil-shale, to establish sequence stratigraphic models. The Fischer plot is used to describe the accommodation and sea level fluctuation (Fischer and Roberts, 1991; Matthews and Perlmutter, 1994; Machlus et al., 2008).

The detailed analysis of the sedimentary record such as stacking patterns of beds, disconformities, facies changes, facies thickness, fluctuations in biological composition, organic matter and color changes are studied to recognize the cycles with high confidence in lacustrine and marine influence fluctuated environment. Depositional sequences are established due to the interaction of eustatic sea-level fluctuation, tectonic activities, sediment supply, accommodation and paleogeography (Posamentier and Allen, 1999). In the sedimentary record, these variable interactions are observed as a change in relative sea-level that controls the facies distribution and stratal architecture. Small-scale sequences and the large sequences of kilo-year scale in the facies evolution is interpreted in terms of sequence stratigraphy (Strasser, 1998). The sequence stratigraphy and cyclostratigraphy studies help to reconstruct the depositional history of marine-influence lacustrine system in the Middle-Eocene time within the Mudurnu-Göynük basin.

#### **1.6. Analytic Method: Chemical process for removing of Organic matter content and minerals from the samples to estimate their weight percent**

Different compounds in an aquatic environment are consolidated within or fascinated on minerals matter which depends on the physical, chemical, and biological processes and may significantly change the sediment texture. During the fine-grained sediments analysis, there are extra complications arise. In an aquatic condition, the fine-grained sediments may form as an aggregate and known as flocs. By characterization, these sediments are cohesive and temporally changeable their composition and structure (Paterson, 1997 and Kim et al., 2005). In the aquatic condition, different micro and macro-component, as well as organic matter, will be closely associated with

suspended mineral particles and deposited in a favorable depositional environment. Different techniques are used to describe sediment texture and composition, depending on the area of interest. Such as an electron microscopic research enables to analyze the three-dimensional structure of the particles and their aggregates (Roberts et al., 1998; Kim et al., 2005; Vaasma, 2008). Another example, Light microscopic studies which are used to determine the sediment composition and texture and selection of appropriate pretreatment methods.

In the previous research, it has been revealed that a majority of sedimentary non-reservoir rocks contain organic matter from few hundredth to 25 percent or more (Forsman & Hunt, 1958). In the sedimentary rocks, two types of organic matter are identified. These are described as soluble organic matter and insoluble organic matter (Kerogen). The soluble organic matter is extracted from the rock by using organic solvent, i.e paraffin-naphthene hydrocarbons, benzene-acetone-methanol (3:1:1), benzene-methanol (4:1), benzene-ethanol-acetone (3:1:1), benzene-methanol (3:1), chloroform, ether, methanol-acetone-chloroform and Soxhlet extraction method (Saxby, 1970; Durand, 1980; Lewis and McConchie, 1994; Shrivastava and Ahmad 2004; Linye et al., 2006; Alnawafleh and Fraige, 2015). In case of insoluble organic matter, a number of researches have been carried out on the chemical studies of kerogen in shales, carbonate and siliciclastic lithologies. In this prospect, Lewis and McConchie (1994) worked on the kerogen or insoluble organic matter in sedimentary rock and carried out to determine the chemical and physical properties of the kerogen and their extraction from the host rocks. The extraction or removal of the organic matter from the sedimentary rock were treated by different types of acid solution and chemical procedures, depending on the lithological composition of the rock (Lewis and McConchie, 1994 and Wang et al., 2009). The organic matter and minerals in the sedimentary rocks are removed by using different chemical groups such as 30% diluted hydrogen peroxide to remove organic matter, 0.5N-10N hydrochloric acid to dissolve carbonate, 50% hydrofluoric acid to remove quartz and clay minerals, dilute

Nitric acid or lithium aluminum hydride used to eliminate pyrite (Table 1.3; Saxby, 1970; Lewis and McConchie, 1994; Vaasma, 2008).

Table 1.3. Brief descriptions of the pre-treatment methods studied (Vaasma, 2008).

Chemical	Description of method
LOI550	Organic matter removal by thermal combustion at 550 °C for 3.5 hours
H <sub>2</sub> O <sub>2</sub>	Elimination of organic matter by 30 % H <sub>2</sub> O <sub>2</sub>
LOI950	Removal of carbonate at 950 °C thermal combustion for 2.5 hours
HCl+ H <sub>2</sub> O <sub>2</sub>	Removal of carbonate by 10% HCl and thereafter removal of organic matter by 30% H <sub>2</sub> O <sub>2</sub>
HCl+H <sub>2</sub> O <sub>2</sub> + KOH	Carbonate dissolution by 10% HCl and thereafter removal of organic matter by 30% H <sub>2</sub> O <sub>2</sub> ; 10% KOH to remove silica
HCl+Zinc	Removal of pyrite

### 1.6.1. Chemical Procedure

In this study, different chemical and/or physical techniques are used to determine the organic matter and mineral weight percent in the studied samples (Table 1.3). For this purpose, randomly samples are selected along the five-measured stratigraphic section to calculate the weight percent of the organic matter, carbonate, clay and quartz/feldspar in studied lithofacies (Appendices A1; A2; A3; A4; A5; A6; A7; A8; A9; A10; Figures 8.3; 8.7; 8.11; 8.15; 8.19). A total of 43, 12, 25, 21 and 14 samples are selected for geochemical analysis along the Dağhacılar, Hasanlar, Köşüre, Karahisar, and Sünnet measured sections, respectively. Firstly, each sample is crushed to the size of less than 0.250 mm and about 10g are separated in the beaker. The sample weight is noted. Then the samples are placed in the oven at 100 °C for an hour to remove the moisture from the samples (Figure 1.8a). After an hour, the samples are again measured and noted the dry weight and water loss weight. In the next step, the dry samples are treated to determine the carbonate and organic matter content in the samples, which are described as below.

To remove the carbonate component from the selected studied samples, the dry samples are treated with 10% dilute hydrochloric acid (HCl) solution and leave it for

5 hours or more, till the reaction ceased out (Saxby 1970; Vaasma, 2008; Wang et al., 2009) (Figure 1.8b). The samples are shaken after every 15 to 30 mins during the experiment. After the completion, the HCl treated samples are washed three times with deionized water and then dry it in the oven. The weight loss of the samples after the diluted HCl treatment are weighed of carbonate content in the studied sample (Appendices A1; A2; A3; A4; A5; A6; A7; A8; A9; A10).

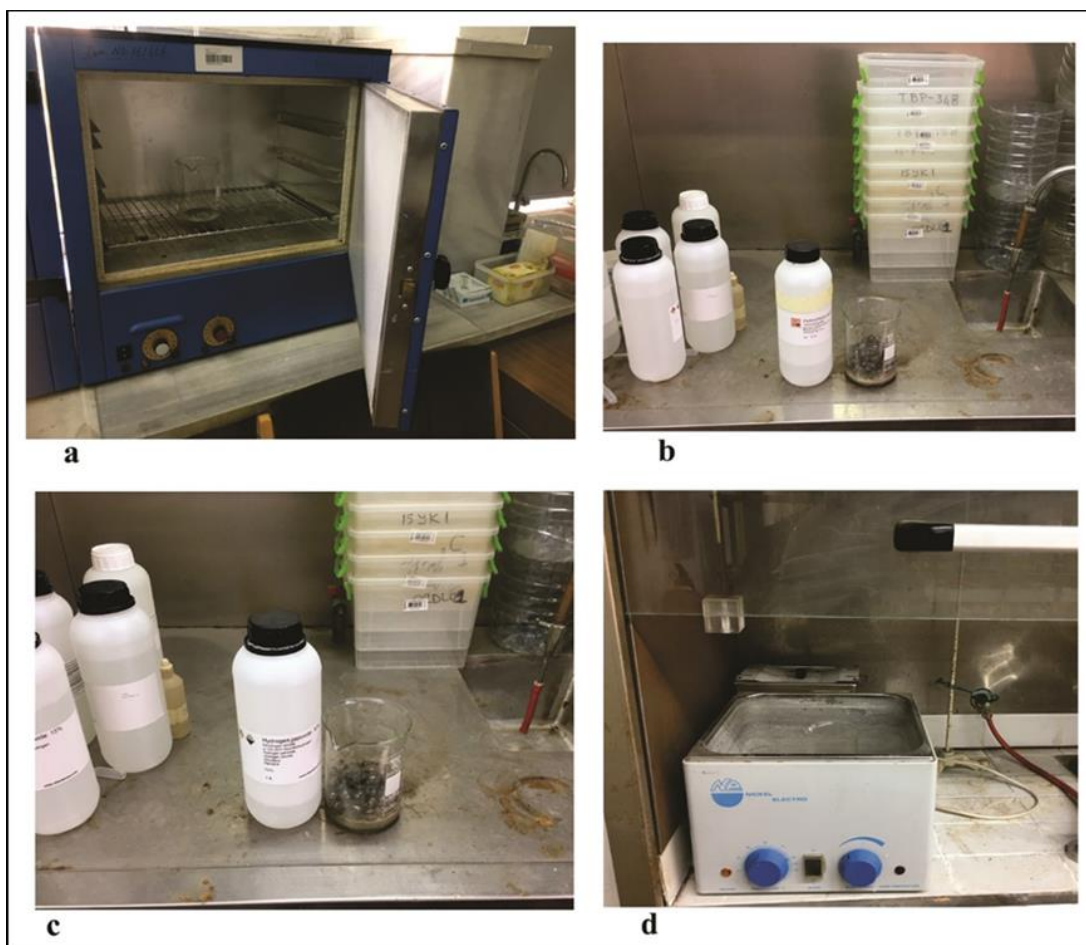


*Figure 1.8. a) Lab oven to dry the samples; b) 10% diluted Hydrochloric acid used to remove carbonate and placed it in the fume chamber. c) 30% Hydrogen peroxide ( $H_2O_2$ ) acid used to remove the organic matter and d) placed it in the water bath.*

After the removal of carbonate from the sediments, the next step is to remove organic matter from studied samples by using 30% diluted hydrogen peroxide (H<sub>2</sub>O<sub>2</sub>) (Saxby 1970; Vaasma, 2008; Wang et al., 2009) (Figure 1.8b). The H<sub>2</sub>O<sub>2</sub> is added to the samples after every 30 mins until the sample solution turns white in color and cease of frothing. The samples are left for several hours in H<sub>2</sub>O<sub>2</sub> solution at around 80°C in a water bath to completely digest organic matter. The samples are stirred from time to time (Vaasma 2008). After the ending of active reaction, the samples are washed three times with deionized water and dry it in the oven. At the end, the calculated weight loss in the samples are the weighed of the organic matter in the samples (Appendices A1; A2; A3; A4; A5; A6; A7; A8; A9; A10). The clay content and quartz-feldspar content are calculated from petrographic data and geochemical analyses (Using 50% diluted Hydrofluoric acid).

### **1.7. Previous work**

The Mudurnu-Göynük Basin having the studied sections is located in the Sakarya-Pontide zone of the Northwestern Anatolian block, Turkey. In the beginning of 1900`s, number of articles has been published on the east west trending Sakarya-Pontide belt of Anatolia from different point of view. This region has greater prospect for the geoscientists in terms of hydrocarbon and coal exploration and tectonic history related to the Tethyan Oceans. Biostratigraphy and biozonation studies are also conducted in the Northwestern Anatolian block by number of researcher (Altiner, 1991; Altiner et al., 1991; Altiner and Özkan, 1991; Özkan, 1993a and 1993b; Özkan-Altiner, 1996 and 1999; Rojay and Altiner, 1998, Oçakoğlu et al., 2007, 2012; Şafak et al., 2015; Şafak, 2018). The oil-shales of Tertiary age in the northwestern Anatolian region has been investigated by Yanılmaz et al., 1980; Sonel et al., 1987a and 1987b; Şener and Şengüler, 1992; Görür and Tüysüz, 2001; Sarı and Aliyev, 2006; Gülbay and Korkmaz, 2008; Sarı and Geze, 2008; Aliyev et al., 2009; Çimen et al., 2013; and assessed their source potential, thermal maturity and type of organic matter.

In 1928, Lucius (1928) conducted the study on the bituminous schist beds in the Çağa Çay valley in Bolu Basin. The research is based on the general characteristics of the bituminous schist deposits and oil-bearing bituminous schists.

In Bolu-Mengen basin adjacent to Mudurnu-Göynük Basin, 0.15-2.0 m intervals of oil-shale are identified by Lokman (1929) and estimated around 91.250 tons oil-shale reserve from 1 m interval at 10 km depth. Later, Blumenthal (1937) has conducted a geological survey of the region and calculated 37 million tons of bituminous shale reserves at the depth of 300 m.

In 1960`s, Mudurnu-Göynük basin has been analyzed for stratigraphic studies and basin analyses by Abdüsselamoğlu (1959) and Türkünel (1957). The Pre-Devonian to recent stratigraphic sequences is documented and illustrated on 1:100,000 scale geological map. According to Abdüsselamoğlu (1959), Lower Cretaceous are composed of carbonates and Upper Cretaceous are comprised of alternating carbonate-turbidite facies in the southern Mudurnu region. Türkünel (1957) investigated the Nallıhan, Mudurnu and Seben region and describe the developed ENE to WSW trending orogenic succession in the northwestern Anatolian block and are known as the Cretaceous Sillon and Cordilleres zones. The Cretaceous Sillon zone is comprised of clay, planktonic Foraminifera bearing variegated carbonate, volcanic and flyschoidal deposits. The Sillon zone restricted to Mudurnu basin, Vaccinates basin, Şıhlar village basin and Köstebekçayı basin. The Cretaceous Cordilleres zone is composed of marly limestone. The Tavgat Mountain, Nallıhan Mountain, Sariçal Mountain and Çal Mountain are defined in Cretaceous Cordilleres zone. These sedimentary sequence zones were examined and correlated to determine the paleogeography and tectonics evolution of the Northwestern Anatolia, Turkey.

The higher hydrocarbon potentials and coal bearing interval in the Northwestern Anatolian block has greater impact in the field of geological researches. Since 1960`s, the Northwestern Anatolian block has been greatly focused for the nature of hydrocarbon, their depositional history and potential, cyclostratigraphy studies,

stratigraphy, biostratigraphy, geochemical analyses and tectonic history (Rigo de Righi and Cortesini, 1959; Reckamp and Özbey, 1960; Schmidt, 1960; Akarsu, 1971; Arıkan, 1975; Şenalp and Gökçen, 1978; Ünalın and Yüksel, 1985; Görür and Tüysüz, 2001; Gülbay and Kormaz, 2008; Sarı and Geze, 2008; Yılmaz, 2008; Yılmaz et al., 2010, 2012 and 2012; Aliyev et al., 2009; Çimen et al., 2013; Ocakođlu et al., 2007, 2012; Şafak et al., 2015; and Şafak, 2018).

In 1969, Beseme (1969) calculated the bitumen content in the Kabalar syncline in the vicinity of Göynük (Bolu) village and determine the possibility of oil-shale reserve in the region.

The general stratigraphy and tectono-stratigraphy of the Northwestern Anatolia was described by Altınlı (1973a, 1973b, 1975, 1976 and 1977), Fourquin (1975), Toker (1975), Saner (1980a and 1980b) and Ocakođlu et al. (2007, 2008, and 2012). The geophysical survey was conducted by Saner (1980a) in the western Pontide and represented the geological structure and geotectonic character in the Upper Cretaceous regime. In his studies, he demonstrates the tectonic proceeding in the northwestern limit and formation of basin in nearby western Pontide. Later in 1980b, Saner also established the Jurassic-Quaternary stratigraphic succession in the Mudurnu-Göynük Basin and also known as Mudurnu Trough (Altınler et al., 1989). In terms of lithostratigraphy, the Mudurnu Trough of the former Sakarya Continent was first investigated by Arabu (1934/1935), Erk (1942) and Aygen (1956).

Görmüş (1980) studied the detail geological characteristic of Yıđılca (KB Bolu) region and interpret the paleogeographic and geological evolution of the region. He determines the main tectonic directions which is effective in the deformation of the region. During his studies, the last active orogenic movements in the region were occurred in the north-east direction. Stratigraphic and paleontological data revealed that the Yıđılca (KB Bolu) region succession is composed of the Upper Devonian-Upper Cretaceous age. The transgression in Upper Cretaceous sedimentation continued until the Lower Eocene in this region.

Yanılmaz et al. (1980) identified possible bituminous shale reserves in the Hasanlar-Dağşeyhleri villages, 27 km southwest of Göynük village. They determined the quality of bituminous shale and stated that the bituminous shale in this area could be obtained by open pit mine. This bituminous shale could be used as crude oil after distillation.

Yılmaz (1981) studied the tectonic evolution history of the southern margin of the Sakarya Continent and observed that it is composed of different rock groups, which were deposited in a wide range of tectonic setting, time and conditions. The basement granite and metabasic rocks are overlain by northern autochthonous strata. The southern ophiolite successions are characterized as Upper Cretaceous units in the area. A Liassic to Late Cretaceous aged shallow carbonate platform are underlain by the northern granitic units. During this time flysch-like sediments were deposited against the continent margin. Three tectonic successions are defined in the region such as 1) granitic rocks, metabasic rock and overlying rocks, 2) ophiolite complex and its equivalent metaophiolite and 3) dynamic metamorphosed rocks. According to Yılmaz (1981), the rock units in the north of the Sakarya river were deposited in different times, environmental setting and conditions than the rock units deposited in the south of the Sakarya river.

The Upper Jurassic/Lower Cretaceous limestones in the Seben-Nallıhan-Atça region has been studied by Varol and Kazancı (1981) and identified as Soğukçam Limestone. The Soğukçam Limestone are consisting of flysch deposits of pelagic and reworked limestones and deposited in the slope to basin condition. They identified *Calpionella* biozones in the pelagic limestones, and *Dasycladaean* algae in the massive biocalcarenes which define the Jurassic-Cretaceous boundary in the region.

Görür et al. (1983) describe the development of Mudurnu basin at the end of the Liassic in the Mudurnu region. His research was based on sedimentological analysis of various Liassic sequences in the Pontides. During his research, he identified the geomorphological, depositional and tectonic characteristics of the region.

In the eastern part of Göynük coal basin, Sonel et al. (1987a) examined the structural and stratigraphic characteristics near the Ahmetbeyler village. Their study interprets the depositional setting of the stratigraphic successions and revealed the tectonic of the region. The studied stratigraphic successions in the region are Yenipazar formation, Selvipınar limestone, Denizli, Kızılçay Group, Himmetoğlu and Ahmetbeyler formations. These studied stratigraphic successions are interpreted as deposited in the marine to terrestrial environments.

Sonel et al. (1987b) studied geology and bituminous shales of Himmetoğlu-Göynük-Bolu region. They studied the geological characteristic of coal deposits and their formation in the region. The coal and bituminous shales were investigated and determine the volatile matter content, moisture content, relative carbon, calorie value and total sulfur content in the coal and bituminous shales.

The Northwestern Anatolia has also been explored for tectono-stratigraphy and regional tectonic geology by Koçyiğit et al. (1988 and 1991). Koçyiğit et al. (1988 and 1991) developed structural geological model in the northern margin of the Sakarya Continent. On the basis of this development structural model of Sakarya Continent, it was interpreted that northern margin of the Sakarya Continent was a divergent margin in late Triassic-Aptian period interval.

Şener and Şengüler (1992) carried out the work on the bituminous shale in the Hatıldağ (Bolu-Göynük) region. They reported 26 to 120 m ranging thick bituminous shale intervals and rated as poor-quality deposits in terms of organic matter. They identified the 30.5m thick intervals of bituminous shale in the lower part with good economic potential. This bituminous shale interval indicates 5.3% oil content and 1.34% sulfur content.

In 1996, Göncüoğlu et al. (1996) has studied and mapped the western, northern and southern sections of Central Sakarya. This study covering the Sarıcakaya east, Beydili, Sarıyar and Gökçekaya regions and revealed that the Tertiary basin deposits covering the tectonic units which was found to contain three main tectono-stratigraphic

associations that came together during closing of the İzmir-Ankara Ocean in the Late Cretaceous.

Sarı (1999) studied the bituminous shale samples from Himmetoğlu formation (Göynük-Bolu Basin) by using organic geochemical analysis and organic petrographic methods. The determined data indicate that organic matter is of type II kerogen which can produce oil and gas. By determining the thermal maturity, spore color index, Tmax and production index of the bituminous shale of Himmetoğlu formation, he interprets that Himmetoğlu formation has excellent source rock potential but low thermal maturity.

Okay and Tüysüz (1999) explained the closing of Tethyan Oceans of Turkey and established the stratigraphy of the western central part of the Sakarya zone. They concluded that these sequences were deposited in continental to shallow marine condition. The successions are composed of clastic sediments of lower Jurassic to lower Cretaceous with association of interbedded Rosso-Ammonitico facies horizons (Altner et al., 1991), pelagic carbonates of Upper Jurassic-Lower Cretaceous and volcanogenic-turbiditic sedimentary succession of Upper Cretaceous-Paleocene.

Sarı and Sonel (2000) collected bituminous shales samples from Himmetoğlu/Bolu (Miocene), Seyitömer/Kütahya (Miocene), Ulukışla/Niğde (Miocene) and Kabalar / Bolu (Paleocene-Eocene) of lacustrine basins. These shales were studied for organic geochemical, organic petrographic, gas chromatographic analysis and combustion experiments, in terms of defining their economic value. The bituminous shales of Kabalar Formation of lake basin indicates excellent oil source rock potential. Himmetoğlu, Seyitömer, Ulukışla bituminous shales illustrate that these are suitable to oil production.

The Tethyan tectonic evolution of western Turkey has been discussed by Okay et al. (2001), on the basis of Upper Cretaceous-Early Eocene sedimentary sequences. These sedimentary records reflect various event in the Northwestern Anatolia, Turkey. According to Okay et al. (2001), the Northwestern Anatolia was subjected to four

main tectonic events from late Cretaceous-Early Eocene. The four main tectonic events were subduction, ophiolitic obduction, high pressure/low temperature metamorphic and continent-continent collision. These Tethyan tectonic evolution lead to the formation of foreland basin in the Central Sakarya continent and then followed by closing of Tethyan ocean (Yiğitbaş and Elmas, 1997 and Ocakoğlu et al., 2007)

Sarı and Aliyev (2005) carried out detail studies on lacustrine oil-shale bearing deposits in the Göynük-Bolu region. The Oil-shales of Paleocene-Eocene Kabalar Formation (Göynük, Bolu/Turkey) has been studied in order to evaluate the hydrocarbon source potential and lacustrine shale intervals in the formation by using organic geochemical methods (LECO/Rock-Eval, gas chromatography), microscopic studies and geochemical analyses. Type I kerogen is determined in these bituminous shales and indicates oil rich character. The organic carbon content in the shale were more than 10% and having more than 900mg HC/g Corg hydrogen index values. Pyrolysis yield and organic petrographic studies indicate excellent source rock potential with type I kerogen. Spore color index and Tmax value indicate that the Paleocene-Eocene Kabalar Formation oil-shale are immature to early mature and are at the early stages of oil-generation.

Yeşiladalı-Bulkan et.al., (2005) investigated the paleo-environmental conditions of Neogene coal and bituminous shale in Himmetoğlu basin (Göynük-Bolu), which characterized two different depositional conditions. It is indicated that lower 8.5m interval is humic coals and above 12.5m is oil-shale dominance. In between these two intervals are defined by rapid and periodical changes in the environmental conditions. The lithofacies, bio-geochemical parameters and properties of water column (salinity, redox) were carried out to determine the paleo-environmental conditions. The concluded studied data indicates that lower 8.5m interval are of terrestrial OM rich deposits in an over-filled, open, fresh-water lake with an oxic water column. The above 12.5m thick interval are identified as sapropelic OM rich and deposited in a balanced-filled, closed lake, which had a dominantly brackish/salty water column. The

interval between the 8.5m and 12.5m was documented as transitional period from an open lake to a closed lake and represent alternating sequence.

The Paleocene–Eocene Kızılçay Group in Nallıhan region has been carried out to determine organic geochemical characteristic of the oil-shale by Sarı and Aliyev (2006). In the studied region, Paleocene–Eocene Kızılçay Group is defined by Beyköy, Çamalan and Laçın Formations. It is concluded in their studied that Paleocene-Eocene oil-shale Çamalan formation has high total carbon content (1.32-40.72wt%) and categorized as good to excellent source rock potential. Pyrolysis analyze data of the Çamalan formation, oil-shale indicates excellent source rock. Hydrogen index and oxygen index result shows type I kerogen organic matter. Spore Color Index and Tmax evaluations data indicates early to intermediate maturity.

Ocakoğlu et al. (2007) conducted the detail studies in relation to sequence stratigraphy of the Late Cretaceous-Paleogene deposits in the Central Sakarya Region. According to their study, at the end of the Late Cretaceous, occurrence of basin scale uplift in the region and sustained until the end of Lutetian age. It results in the deposition of continental-shallow marine successions in the south and deposition of deep marine clastic sediments and carbonaceous in the north. Later, Şafak et al. (2015) worked on the Eocene Ostracoda assemblages of Halidiye formation in Central Sakarya region. In their studies, they determine biozonation and correlated with adjacent basin and predicate paleo-environmental condition and age. The observed Ostracoda assemblages in Halidiye Formation define Lutetian-Priabonian age and reflects transitional lagoonal to deep marine environmental setting.

Paleocene-Eocene terrestrial deposited in the former foreland setting related to southern situated İzmir-Ankara suture zone. Ocakoğlu et al. (2012) carried out detailed work on the Middle Eocene oil-shale lacustrine deposits in the Mudurnu-Göynük basin to determine the orbital forcing control and cyclic pattern in the oil-shale bearing lacustrine successions. In this study, meter-scale symmetric to asymmetric transgressive-regressive cycles are document in the Middle Eocene lacustrine units. It

is proposed that short duration cyclic pattern in the lacustrine oil-shale successions develop in the response of abrupt changes in the climatic condition and long duration cycles define the tectonic loading activity.

In the Bolu basin, number of Eocene sections are considered for organic geochemical analysis by Koralay (2009). The purpose of the study is to evaluate the organic matter quantity, hydrocarbon potential, organic matter type and their maturity. In this study, it is identified that Eocene bituminous shale in the basin possess good to excellent source potential character and categorized as suboxic to anoxic environmental deposits, type I and type II kerogen with immature to early mature phase.

Sarı et al. (2015) investigated the element enrichments in bituminous lithofacies (bituminous shale, bituminous claystone and bituminous marl) of the Kabalar formation in the Hatıldağ field in the Göynük basin. In this study, the economic potential of the bituminous rocks was discussed in terms of mineral occurrence and their concentration. 0.40-8.25 wt% of Corg have been recorded from studied samples. According to Sarı et al. (2015), the presence of higher concentrations of Ca, Mg and Ba elements in the bituminous rocks leads to information of more carbonaceous and suboxic depositional setting of Hatıldağ field bituminous rocks.

### **1.8. Regional Geological Setting**

The Eocene measured sections are in the southern margin of the Sakarya zone and are surrounded by the branches of North Anatolian Fault. The Sakarya zone was a separated block of the Cimmeridian continent during the anti-clockwise rotation and resulted in the closing of Paleo-Tethys ocean (Figure 1.8; Şengör, 1987; Şengör and Yılmaz, 1981).

The current tectonic evolution of Turkey is associated with the closure of multibranch Neo-Tethys oceans in the Late Mesozoic and Cenozoic era (Şengör and Yılmaz, 1981). Turkey is an amalgamation of several continental blocks and oceanic crust with lateral Alpine-Himalayan tectonic setting (Ketin, 1966; Şengör and Yılmaz, 1981; Görür and Tüysüz, 2001; Lefebvre et al., 2013; Figure 1.6).

The Middle Eocene studied sections tectonically lie in the Northwestern Anatolian block, Turkey. The northwestern Anatolian block is described by the Istanbul zone, Strandja zone and Sakarya zone (Figure 1.6). The zones were separated from each other by the Intra-Pontide and the İzmir-Ankara oceans in the most of Mesozoic period (Şengör and Yılmaz, 1981; Okay and Tüysüz, 1999). The Istanbul and Strandja zones define the part of southern margin of Eurasia block. The Sakarya zone is considered as independent continental block. The Istanbul zone, Strandja zone and Sakarya zone along with Armutlu-Almacık zone are known as western Pontide blocks (Yılmaz et al., 1997). In the south, the İzmir-Ankara-Erzincan suture separates the Sakarya zone from Anatolide-Tauride block (Okay et al., 2001).

The Sakarya zone forms the east-west extending crustal terrane from the Biga Peninsula in west and from the Eastern Pontide in the east. The basement of Sakarya Continent is described by three units; (1) Carboniferous high grade metamorphic units of gneiss, amphibolite and marble (Topuz et al., 2004, 2006; Okay et al., 2006a); (2) Paleozoic granitoids (Devonian, Carboniferous, and early Permian periods) (Okay et al., 2002, 2006a; Topuz et al., 2006; Aysal et al., 2012); and (3) Karakaya complex of Permian-Triassic subduction-accretion assemblages (Şengör and Yılmaz, 1981; Şengör et al., 1984; Okay and Göncüoğlu, 2004).

During the Early Jurassic period, the continue subduction of the Karakaya basin lead to formation of Neo-Tethys (İzmir-Ankara ocean) (Figure 1.9). The Lower Jurassic rifting event has been described by Yılmaz (1971) and Görür et al., (1983). The Lower Jurassic deposits are composed of coarser clastic rocks with association of alkaline and tholeiitic basaltic lavas and are overlain by Middle-Upper Jurassic shelf deposits, known as the Bilecik limestone (Altınlı, 1973a). The upper contact of the Bilecik limestone is transitional with pelagic deposits of the Soğukçam formation (Yılmaz et al., 1997).

During Middle Jurassic, steady demise of the Paleo-Tethyan ocean and results in the formation of south facing continental margin units (Şengör and Yılmaz, 1981).

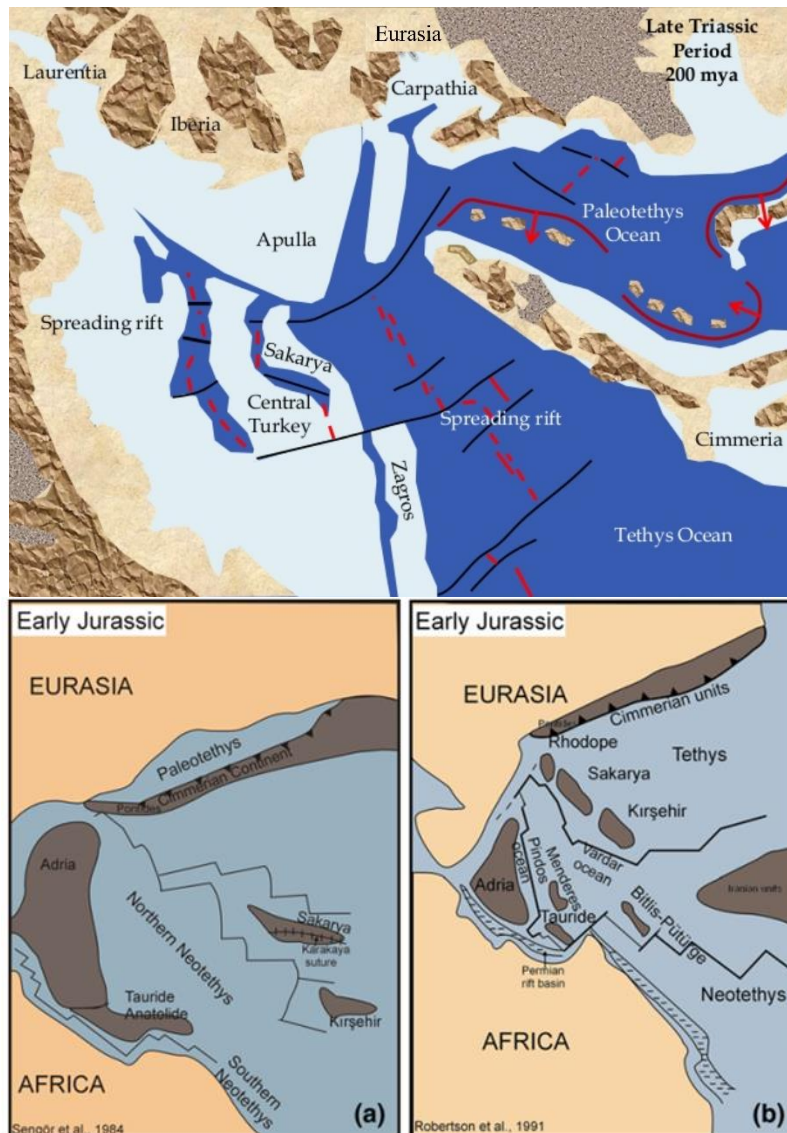


Figure 1.9. Showing Tectonic evaluation of Turkey during Late Triassic to Early Jurassic. (Şengör et al. 1984; Robertson et al., 1991; Szary, 2014).

According to Deveciler et al. (1989) and Aydın et al. (1995), the Paleo-Tethyan ocean was closed in the eastern Pontide during the Middle-Late Mesozoic period. Though, the region lying in the west of Kastamonu indicates continuous deposition in the marine units. In the Late Jurassic, the north-south extension occurred in the Pontide in relation to collision-related convergent regime and continued until Early Cretaceous. During this period, the region was characterized by horst and graben structures and

the marine invasion to the successive deposits (Yılmaz et al., 1997). In Early Cretaceous, gradual subsidence occurred in the Pontide and development of Neo-Tethys ocean with passive continental margin. Pelagic units were deposited in the Neo-Tethyan basin during the Cenomanian-Turonian stage. Through Late Cretaceous, Neo-Tethyan ocean began to subduct under the Pontide in the north. This subduction generated active continental margin with volcanic activity in north of the Pontide and flysch deposits and accumulation of mélangé at continental edge during Turonian (Yılmaz et al., 1997). In Campanian-Maastrichtian, volcanic arc-front shifted to south with regional transgression. This resulted with development of Black Sea basin in the north and clockwise moment in the western Pontide. The clockwise movements in the western region led to the closing of Paleo-Tethys relic, which was remained open in this region (Şengör and Yılmaz, 1981 and Yılmaz et al., 1997). This clockwise movement occurred in the Sakarya zone. Due to the clockwise rotational movement of continental fragment, the convergence in the region became oblique and development of North Anatolian transform fault zone. This transform fault zone resulted in the western drifting of Sakarya zone from eastern Pontide (Yılmaz et al., 1997).

Late Cretaceous timing, ophiolitic mélangé in the southern margin of the Sakarya zone was overlain by back thrusting nappes (Çoğulu, 1967). The shallow marine regressive facies were deposited on the top of the Sakarya zone in the Maastrichtian to Early Eocene epoch. The northern margin of the Sakarya zone was composed of Coniacian-Santonian pelagic and flysch deposits (Saner, 1977; Yılmaz, 1981; Yılmaz et al., 1995). Upper Campanian deposits in the northern region of the Sakarya zone are defined by transgressive clastic deposits (Yılmaz, 1981). In the Maastrichtian-Paleocene transition, the northern region of the Sakarya zone is defined by changing from deep marine to shallow-marine deposits and then followed by continental red bed deposits (Altınlı, 1973a; Saner, 1977; Yılmaz, 1981; Yılmaz et al., 1995). According to Göncüoğlu et al. (2000), during the Middle Paleocene to Middle Miocene, the Central Sakarya zone was subjected to tensional-transtensional tectonic

setting, which was concluded from post-collision andesitic magmatism and fault-controlled continental-shallow marine deposits.

During Early to Middle Eocene, new stage of north-south shortening begins in the region. As a result, Mesozoic carbonate platform units was detached from its basement and moved toward the north direction as a decollement tectonic movement (Yılmaz et al., 1997). In the beginning of the Middle Eocene, the compression regime is replaced by north-south extension and incursion of marine environment to the basin. Therefore, the continental clastic were replaced by the marine deposits (Yılmaz et al., 1993). In the Lutetian, the marine sediments were deposited in region along with volcanic activity associated strata in some region. Late Eocene-Oligocene transition is described by the initiation of transpressional tectonic in the region. This transpressional resulted in the uplift of the Pontide and retreat the previously existed marine environment in Early-Middle Eocene time. The marine sediments were progressively replaced by continental clastics. This tectonic activity resulted in the development of peripheral basins. These basins are extended from the Sivas region in the east to the Eskisehir region in the west. The basins are characterized by lagoonal to marine shelf depositional setting in the Mudurnu-Göynük Basin (Saner, 1977, 1980b; Ocakoğlu et al., 2007), fluvio-lacustrine and carbonate marine shelf depositional setting in the Orhaniye and Haymana basins (Kazancı and Gökten, 1986; Koçyiğit, 1991; Ocakoğlu and Çiner, 1995; Çiner et al., 1996a, 1996b), deltaic to evaporitic marginal marine deposits in the Çankırı-Çorum basin (Hakyemez et al., 1986; Ocakoğlu, 1997; Kaymakci et al., 2003) and shelf to evaporitic marginal marine setting in the Sivas basin in the east (Cater et al., 1991; Sümengen et al., 1987). The Pontides and its adjacent areas were exposed to extensive erosion at the end of Oligocene (Yılmaz et al., 1993 and Yılmaz et al., 1997).

The Early Miocene period was documented as another new phase of north-south extension in the Pontide and Sakarya zone. The marine incursions were introduced to fault associated basins in this period. The adjacent plain regimes were occupied by interrelated lacustrine environment and associated fluvial deposits (Benda et al., 1977

and Yılmaz et al., 1997). At the end of the Early Miocene, the region was subjected to regressive event and then is followed by the Pontide mountain orogeny uplift and continue in the Quaternary (Yılmaz et al., 1997).

### **1.8.1. Mudurnu-Göynük Basin**

Geologically, the Middle Eocene studied sections are present in the Mudurnu-Göynük basin, Northwestern Anatolian block. The Mudurnu-Göynük basin is lying in the north of the Sakarya zone. The Mudurnu-Göynük basin is also known as Mudurnu Trough and is defined as rift basin along Sakarya Continental margin (Koçyiğit et al., 1991). The Upper Jurassic to Cretaceous successions in the Sakarya Continent is comprised of alternative marine shelf and pelagic carbonates, volcanic and pyroclastic deposits and then are overlain by upper Cretaceous slope to basinal deposits (Altiner, 1991; Altiner et al., 1991). From Late Cretaceous to the end of Lutetian, there was continuous basin-scale tectonic uplift in the Sakarya Continent. As a result, the Late Cretaceous deep marine sediments with association of organic rich deposits were deposited in the south and Middle Eocene continental to shallow marine deposits were deposited in the north, respectively (Ocakoglu et al., 2007, 2012; Şafak et al., 2015). The Late Cretaceous deep marine clasts are represented by the Taraklı and Selvipınar Formations and Middle Eocene continental to shallow marine are defined by the Kızılcay, Halidiye and Ciciler Formations (Saner, 1980b and Ocakoglu et al., 2007).

During Toarcian-Bathonian, the rifting was initiated and continued until Late Cretaceous and development of Mudurnu-Göynük Basin (Saner, 1980b; Şengör and Yılmaz, 1981 and Koçyiğit et al., 1991). The deposits in the rifting are characterized by Callovian-Tithonian carbonate sedimentation with association of rift volcanics. Later, the Mudurnu trough were further extend in the Valanginian-Early Hauterivian and development of broad Biga-Bilecik carbonate platform (Koçyiğit et al., 1991). The deposited sequence to the Late Cretaceous are of shelf and pelagic carbonate deposits with occasional silicic-clasts and are followed by slope and basinal deposits with low preserved organic carbon quantity successions (Wagreich and Krenmayr,

2005; Yılmaz, 2008; Wagreich et al., 2009 and Yılmaz et al., 2010). The slope to basinal deposits with low preserved organic carbon quantity are defined by the red pelagic carbonate that were deposited in the Early Campanian and are identified as Cretaceous oceanic red beds (CORB) (Değirmenözü member of Yenipazar formation). These carbonate sedimentations are overlain by lower Paleocene hemipelagic marls and then are followed by shallow marine deposits, the Selvipınar reefal limestone and the Ağsaklar formation (deltaic, lagoonal and fluvial deposits) till Eocene period (Gedik and Aksay, 2002). The sediments of Lower Miocene in the region are composed of coal and bituminous shale of lacustrine environment and are overlain by rivers and terrestrial deposits of Late Miocene (Taka and Şener 1988).

In the Dağhacılar village and adjacent regime, Mudurnu-Göynük Basin, the Selvipınar Formation and Kızılçay Group are determined as Paleocene and Paleocene-Eocene successions, respectively. The Selvipınar formation are composed of reefal limestone of the Early Paleocene age and having transitional contact with the Upper Cretaceous Taraklı Formation. The Upper Cretaceous Taraklı formation is comprised of marl, shale and sandstone units (Figure 2.2). Lower Paleocene unit has conformable contact with the Kızılçay Group. The Kızılçay Group consists of the Middle Paleocene Ağsaklar Formation, Upper Paleocene Kabalar Formation and Eocene Dağhacılar Formation. The Ağsaklar Formation is represented by reddish brown gray conglomerate, siltstone, sandstone and mudstone intercalation. The shallow marine units of Kabalar Formation is reported as oil-shale, shale, marls, mudstone, siltstone and limestone with occasional claystone. The Eocene Dağhacılar Formation is consisting of reddish-brownish, gray to greenish mudstone, sandstone, siltstone and marls (Altınır et al., 1991; Şener and Şengüler, 1998 and Çimen et al., 2013).

In the Himmetoğlu and Seyitömer field, Mudurnu-Göynük basin, the Eocene units are conformably overlain by the Miocene formations. The Himmetoğlu formation represents lignite, oil-shale, limestone, marl and alternated conglomerate, claystone and tuffs deposits of Miocene age. The overlain succession is composed of oil-shale, marls, tuffs and occasional conglomerate, siltstone and identified as the Gölpararı

successions of Oligocene age. The Pliocene Seyitömer succession are characterized by occasional limestone, tuffs, sandstone and siltstone. These successions are covered by the Quaternary deposits (Ünalın et al., 1976, Altınır et al., 1991; Şener and Şengüler 1998, Gülbay and Korkmaz, 2008).



## CHAPTER 2

### GENERAL STRATIGRAPHY

#### 2.1. General Geology of the Region

In the Northwestern Anatolia, the documented stratigraphic sequences are ranging from Paleozoic to Quaternary age (Figure 2.1). In the studied region, the Upper Triassic Karakaya Complex is the older rock reported in the Sakarya zone. The younger reported succession is the Pliocene units which are roofed by Quaternary alluvial and talus breccias sediments (Ünalán et al., 1976; Koçyiğit et al., 1988, 1991; Koçyiğit, 1991).

In the Anatolian block, the basement of Sakarya zone is comprised of volcanic-volcano-clastic sedimentary units and low to high grade metamorphosed units, associated with subduction-accretion complexes (Tekeli, 1981; Şengör et al., 1984; Tüysüz and Yiğitbaş, 1994). The Sakarya basement is described by three units; 1) Variscan high grade metamorphic successions of gneiss, amphibolite and marble and characterized as Carboniferous (Topuz et al., 2004, 2006; Okay et al., 2006a); (2) Paleozoic granitoids (Devonian, Carboniferous, and Early Permian periods) (Okay et al., 2002, 2006a; Topuz et al., 2006; Aysal et al., 2012); and (3) Permian-Triassic subduction-accretion assemblages of the Karakaya complex (Şengör and Yılmaz, 1981; Şengör et al., 1984; Okay and Göncüoğlu, 2004). In the east, the Sakarya basement Variscan unit is overlain by molasses of the Upper Carboniferous deposits (Göncüoğlu, 2010). The pitches of Paleozoic granitoids are randomly bared at the different locality in the Sakarya Continent. The Jurassic-Eocene successions are unconformably resting over these pre-Jurassic crystalline basements in the Sakarya Continent (Delaloye and Bingöl, 2000; Okay et al., 2002, 2006a; Topuz et al., 2007). The lower portion of the Karakaya complex is characterized by green schist facies

Period	Epoch	Age	Lithology	Descriptions	Formations		
TERTIARY	Quaternary	Recent		Alluvial Sediments	Alluvium Cover		
		Pliocene		Conglomerate, marls with occasional limestone, tuffs, sandstone and siltstone. Lower and upper boundaries display unconformity.	Reported from Beypazarı, Bahçecik and Seyitömer localities in Mudurnu-Göynük Basin		
		Miocene		Lignite and oil bearing shale in middle portion, limestone, marl and occasional interbedded conglomerate, claystone and tuffs.	Reported from Himmetođlu (Unconformable over paleocene), Beypazarı and Seyitömer localities in Mudurnu-Göynük Basin		
		Oligocene		Oil bearing shale in middle portion, marl, tuffs and occasional interbedded conglomerate and siltstone. (Represented by Oligocene Gölpaźarı Oil shale deposits)	Reported from Gölpaźarı and Bahçecik localities and Mudurnu-Göynük Basin		
		Eocene		Reddish to brownish, grayey to greenish mudstone, sandstone, siltstone and marls interbedding.	Dađhacılar Formation		
				Intercalation of marl, oil bearing shale, siltstone, limestone with occasional claystone.	Kabalar Formation		
				Reddish brown, sandstone, siltstone and mudstone intercalation, and occasional conglomerate.	Ađsaklar Formation		
		Paleocene		Reefal Limestone	Selvişınar Formation		
		CRETACEOUS	Late	Campanian-Maastrichtian		Turbiditic sequence (Fine clastic sedimentation) Marl, Shale and limestone Alternation	Taraklı Formation
				Santonian-Early Campanian		Red-pink-grayish pelagic carbonates and marls/shales	Deđirmenözü Member
Albian-Cenomanian				Volcano sedimentary sequence (Siltstones, Sandstones and Conglomerates) including pelagic micritic carbonates	Üzümlü Member		
Early	Valanginian-Aptian			Alternation of micritic limestones with planktonic foraminifera, marls and blackshales	Şođukçam Limestone		
	Tithonian-Valanginian			Volcano sedimentary sequence with olistromes, diabase dikes and detritic pelagic limestones	Yosunlukbayırı Formation		
	Callovian-Kimmeridgian			Limestone with radiolaria, tuffs and olistrostromes	Kurucalıkdere Formation		
JURASSIC	Middle	Bajocian-Callovian?		Tuffs, volcanogenic sandstones and spillitic basalts Equivalent to Dogger Formation	Mudurnu Formation		
	Early	Hettangian-Plensbachian		Shallow marine clastics with Rosso-Ammonitico facies	?		
TRIASSIC	Late	Norian		Metamorphic Basement	Karakaya Complex		
				Granitoids			

KIZILÇAY GROUP

Yenişar Formation

Not to Scale

Figure 2.1. Composites stratigraphic section of the Mudurnu-Göynük Basin (Modified from Altuner et al., 1991; Şener and Şengüler 1998 and Gedik and Aksay, 2002). Red line shows studied interval.

metabasites along with some association of marble and phyllite (Okay and Göncüoğlu, 2004). The upper portion of the Karakaya complex is tectonically overlying the lower Karakaya complex. The upper portion of the Karakaya complex is composed of deformed arkosic sandstone, graywackes with Carboniferous and Permian blocks (Okay et al., 2002; and Okay and Göncüoğlu, 2004). It is also known as Nilüfer meta-volcanic sequences. The lower Karakaya complex is identified as lower Middle Triassic age and upper Karakaya complex is reported as Upper Triassic age (Okay et al., 2001).

At the different localities, the Karakaya complex is overlain by varying successions in the Sakarya Continent. In the western margin, the Karakaya complex is unconformably covered by sandstone, shale and conglomerate of Lower Jurassic fluvial to shallow marine deposits with Ammonitic Rosso interval (Altınler et al., 1991). The eastern zone of the Sakarya Continent is defined by unconformably overlying volcanoclastic with sandstone intercalation (Koçyiğit, 1991; Koçyiğit et al., 1991; Okay and Tüysüz, 1999; Okay and Altınler, 2004; Okay, 2008; Göncüoğlu, 2010). In Mudurnu-Göynük Basin, the Karakaya complex is unconformably covered by Liassic successions. The Middle Jurassic-Lower Cretaceous ophiolitic mélangé of the Ankara group having tectonic contact with underneath Karakaya complex in the Ankara region (Ünalán et al., 1976; Koçyiğit, 1991; Okay and Altınler, 2004).

In the Mudurnu-Göynük region, Paleozoic to Quaternary stratigraphic framework has been illustrated by number of researchers; i.e Fourquin (1975), Toker (1975), Altınlı (1977), Saner (1980a), Altınler et al. (1991), Koçyiğit et al. (1991), Okay and Tüysüz (1999), Okay et al. (2001); Okay and Altınler, 2004; Okay (2008), Özcan et al. (2012, 2018), Ocakoğlu et al. (2007, 2012) and Şafak et al. (2015).

## **2.2. Stratigraphy of Mudurnu-Göynük Basin**

In the Mudurnu-Göynük Basin, the Mesozoic-Cenozoic sedimentary sequences are unconformably overlying the Pre-Jurassic basement units (Figures 2.1 and 2.2). These 5 km thick sedimentary successions are studied by Altınlı (1975), Saner (1978a and

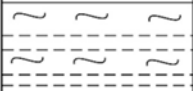
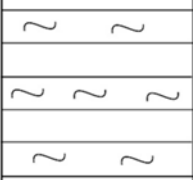
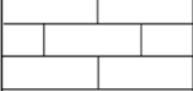
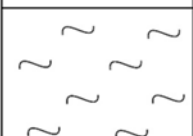
Age	Group	Lithology	Thickness	Descriptions	Formations		
Quaternary			50m	Alluvium			
Paleocene-Eocene	Kızılcay		300m	Mudstone	Daghacılar Formation		
			75m	Siltstone-Sandstone	Siltstone Member	Kabalar Formation	
			75m	Bituminous Marl and Shale	Oil Shale Member		
			100m	Marl-Mudstone	Marl Member		
			300m	Mudstone	Ağsaklar Formation		
		Paleocene			100m	Limestone	Selvişınar Formation
		Upper Cretaceous	BASEMENT		150m	Sandstone	Taraklı Formation
	200m			Marl	Seben Formation		

Figure 2.2. Generalized stratigraphic Hatıldağ oil field (Şener and Şengüler, 1998). Red line shows studied interval.

1978b) and Altiner et al. (1991). The Mesozoic to Early Eocene successions can be divided into two sedimentary packages; 1) transgressive packages during Early Jurassic to Late Cretaceous, and 2) regressive packages in the Maastrichtian to Early

Eocene. The initial transgressive sandstone-conglomerate deposits of lower Jurassic age in the Mudurnu-Göynük Basin has unconformably contact with underlying Sakarya basements (Altınlı, 1975; Yılmaz, 1977 and Saner, 1978a and 1978b).

### **2.2.1. Jurassic to Cretaceous Succession**

In the Mudurnu-Göynük Basin, Jurassic to Lower Cretaceous successions are identified as the Mudurnu Formation, Kurucalıkdere Formation, Yosunlukbayırı Formation and Soğukçam Limestones by Altıner et al. (1991) (Figure 2.1). The Mudurnu Formation is composed of volcanogenic deposits and the Middle Jurassic age has been assigned to the formation (Saner, 1980b). According to Altıner et al. (1991), the Mudurnu Formation is composed of marine deposits and equivalent to the Dogger Formation. The Bajocian-Callovian age has been allotted to the Mudurnu Formation. The overlying formation on the Mudurnu Formation is known as the Kurucalıkdere Formation of Callovian-Kimmeridgian age and having a transitional character with the underlying Mudurnu Formation. The Kurucalıkdere Formation represents olistostromes of reefal fragments, tuffaceous, siliceous and basaltic level and pelagic mudstones lithofacies. It has conformable contact with the Tithonian-Valanginian Yosunlukbayırı Formation, which is composed of calciturbiditic limestone and packstone with interbeds of mudstone. The upper contact is transitional with the Soğukçam Limestones (Altıner et al., 1991).

During the Berriasian-Aptian, the Mudurnu Trough was subjected to the transgressive conditions. These are indicated by the Soğukçam Limestones, which are composed of the slope to basin pelagic limestone with interbedded black shale and mudstone (Altıner, 1991; Altıner et al., 1991; Yılmaz, 2008; Yılmaz et al., 2012). The base of the formation is defined by cherty limestone and then are followed by pelagic fauna mudstone/wackestone. The upper portion is composed of black shale/marl with alternating limestone. The Soğukçam Limestones are covered by Üzümlü member of the Yenipazar Formation of Late Cretaceous (Altınlı, 1977 and Altıner et al., 1991).

The unconformable overlain Üzümlü member is known as Albian-Cenomanian member of the Yenipazar Formation. This member is represented by volcanic clastics, pelagic limestone with interbedded gray-black shale deposits. It has unconformable upper contact with the Santonian-Campanian Değirmenözü member of Yenipazar Formation (Timur and Aksay, 2002; Yılmaz, 2008). The Değirmenözü member is described by red-pink pelagic marls, mudstone, claystone with occasional siltstone and sandstone deposits (Timur and Aksay, 2002; Yılmaz, 2008 and Afridi, 2014). In the Mudurnu-Göynük region, the upper contact of the Soğukçam limestone and Yenipazar Formation is described as disconformable contact with Neptunian Dykes (Yılmaz, 2008)

In some region in the Mudurnu-Göynük basin, the overlying formation on the Yenipazar formation is described by the Seben Formation of Late Cretaceous (Şener and Şengüler, 1998). The Seben Formation is identified by Beseme (1967). It has been reported from the Gölpazarı, Mudurnu, near Nallıhan and north of Göynük village (Saner, 1980b). It has flyschoidal character deposits with occasional micro-faunal marls and neritic horizons and increases in the shales lithofacies toward the top (Saner, 1980b). The observed fauna in the lower portion of Seben Formation are *Ananchytes (Echinocorys) ovatu* LAMARCK, *Neithea (Janire) seacostate* LAMARCK, *Gryohea (Pycnodonta) veskularis* LAMARCK, *Ostrea lunata* NiLLSON, *Alectryonia trons* PARKINSIN, *Micraster costestudinarium* GOLDFUSS, *Belemnitella macronuta* SCHLOTHEM. The fauna documented in the upper portion of the Seben Formation are *Globotruncana contusa* CUSHMAN, *Globotruncana arca*, *Globotruncana stuarti* Gt. *Stuartiformis* DALBiEZ, *Globotruncana falsostuarti* SIGAL and define Santonian-Early Campanian age (Şener and Şengüler, 1998; Taka and Şener 1988). It is interpreted that the formation is deposited in the marine shelf environment (Saner, 1980b). The Taraklı Formation overlies the Seben Formation. The Taraklı Formation appears as marl, shale, sandstone and pebbly sandstone and having shallow marine fauna (Saner, 1980b). The Campanian-Maastrichtian age has been assigned to the Taraklı Formation by Saner (1977), based on *Orbitoides*

*gruenbachensis* PAPY, *Orbitoides apiculatus* SCHLUMBERGER and *Siderolites* sp. According to Saner (1980b) and Göncüoğlu et al. (1996), towards the top, the Taraklı Formation sandstone indicate the regressive marine condition and interpreted as deltaic, coastal control depositional setting. The overlain Paleocene Selvipınar reefal limestone has progressively transitional contact with the Taraklı Formation (Figures 2.1 and 2.2; Saner, 1980b).

### **2.2.2. Tertiary Succession**

Marine depositional environment continued during the Paleocene-Eocene periods. The Lower Paleocene hemipelagic marls are gradually replaced by shallow marine and reefal limestones. They are followed by deltaic, lagoonal and fluvial deposits, in the Mudurnu-Göynük Basin (Gedik and Aksay, 2002). According to Saner (1978a), during the Paleocene-Eocene, the region demonstrates transgressive marine packages. It is illustrated by deposition of the reefal Selvipınar Limestone in the Paleocene period and also documentation of meandering river channels. The Tertiary succession is characterized by the Paleocene Selvipınar and Eocene Kızıldağ Group, which includes Ağsaklar Formation, Kabalar Formation, Dağhacılar Formation and then followed by Miocene-Quaternary succession (Ünalın et al., 1976; Altınler et al., 1991; Şener and Şengüler, 1998 and Çimen et al., 2013).

The Lower Paleocene Selvipınar Formation is composed of pinkish, yellow and gray reefal limestone at the base and sandstone and marl at the top. The macro-fossils recorded in the Selvipınar Formation are algae, gastropods, bivalve and coral. The Early Paleocene age has been assigned by determining *Laffitteina* cf. *bibensis* MARIE, *Laffitteina* aff. *monodis* MARIE, *Cymopolia* cf. MOROLET, *Solenomeris couvillei* PREFENDER and *Pseudolithamnium album* PREFENDER (Altınlı, 1973b and Saner, 1977). After the marine regression, the upper portion of Selvipınar formation was replaced by lacustrine setting. Therefore, the upper portion of Selvipınar Formation represents the transitional character and documented as red colored shoreline deposits (Saner, 1978b).

### **2.2.2.1. Kızılçay Group**

The red-colored terrestrial sediments were first named as Kızılçay Formation by Eroskay (1965) and Altınlı (1973b). Later Altınlı (1973a, 1973b) and Saner (1977 and 1980b) described it as Kızılçay Group. The Kızılçay Group is well exposed in the Gölpazarı, Hatıldağ mountain in the Göynük and the Sarıcakaya-Nallıhan region. Generally, the Kızılçay Group deposits are composed of red, variegated colored, poorly sorted conglomerate, sandstone, shale, claystone, marl, limestone, bituminous shale and mudstone. In some places, there is rarely observed coal and gypsum horizons. Overall, the Kızılçay Group defines terrestrial deposits until the Bartonian period (Sarı et al., 2015). As, at the end of Cretaceous, the Sakarya Continent is subjected to the regressive phase of marine environment until Eocene. Thereafter, during the Middle Eocene, the basin indicates the onset of marine transgression in the region (Saner, 1978b; Altıner et al., 1991; Şener and Şengüler, 1998 and Çimen et al., 2013).

The Kızılçay Group is divided into the Ağsaklar Formation, Kabalar Formation and Dağhacılar Formation (Figure 2.2; Şener and Şengüler, 1998).

### **2.2.2.2. Ağsaklar Formation**

The formation was firstly named as “Lower red series” by Beseme (1967). Later, it was named as Ağsaklar Formation by Yanılmaz et al. (1980). It describes the lower portion of Kızılçay Group. The type locality of Ağsaklar Formation is in the Ağsaklar village. The formation is also exposed near the Hasanlar village, Hatıldağ village and Turgutlar village.

The Ağsaklar Formation is mainly composed of green-gray sandstone, mudstone and marl intercalation. The recorded fauna in the Ağsaklar Formation is *STCHEPINSKY*, *Ostrea rariamella* MELLEVILLA muf. *Prisca* DONCIEUK, *Amgullina* cf. *forbesi* DESHAYES, *Tympanotonus futanus* MANTELL, *Cyrena cuneiformis* FERRUSAC, *Batillaria subacuta* D’ORBIGNY, *Viviperusaff suesson’iensis* DESHAYES (Taka and Şener, 1988; Koralay, 2009). Near the Ahmetbeyler and Hasanlar village, the base

of the formation is defined by a conglomerate and then is followed by red sandstone, marl and mudstone. The red sandstone identified as fluvial channel filled deposits. The Ağsaklar Formation has conformable lower contact with the Selvipınar Formation. The Late Paleocene-Middle Eocene age has been assigned to the formation (Şener and Şengüler, 1998 and Koralay, 2009).

### **2.2.2.3. Kabalar Formation**

In the type locality, near the Kabalar village, it is composed of clay limestone, bituminous shale, marl, claystone and sandstone with occasional coal and named as Kabalar formation by Saner (1978b). It is also reported in the proximity of Dağhacılar, Dağşeyhleri, Köşüre, Kürnüç, Kuyupınar, Himmetoğlu village, Hatıldağ mountain and Çapar village (Koralay, 2009). The sandstone in the formation is appeared as green color beds and coarser grained sandstone. The bituminous shales are gray colored, laminated and usually interbedded with marl and sandstone. Some limestone units within the formation contain plant fragments and gastropods at different intervals.

Şener and Şengüler (1998) divided the Kabalar Formation into three members, includes marl member, oil-shale member and siltstone member (Figure 2.2). The marl member unit is identified as the first lacustrine deposit in the Kabalar Formation in Paleocene-Eocene periods. The marl member is consisting of marl and claystone with underlying red mudstone and then is followed by oil-shale member. Oil-shale member is composed of varve-structured light and dark gray laminated shale. The observed average organic matter content in the oil-shale member is around 10% oil yielded organic matter. The upper portion of the formation is restricted to siltstone member and consist of siltstone with interbedded fine to coarser sandstone and mudstone. Overall, the Kabalar Formation is described as a meandering river to lacustrine depositional environment with occasionally marine incursion character (Şener and Şengüler, 1998).

The Kabalar Formation is devoid of fossils, though Upper Paleocene-Lower Eocene age is confined, based on its stratigraphic position. It has conformable contact with underlying the Ağsaklar Formation and overlying the Eocene Dağhacılar Formation (Granit and Şener, 1987).

#### **2.2.2.4. Dağhacılar Formation**

Şener and Şengüler (1992) identified the Dağhacılar Formation near the Dağhacılar and Hasanlar village in the Kabalar syncline. It is composed of predominantly marl with limestone, siltstone and sandstone. In some places, there is the presence of iron oxide reddish-orange color sandstone. According to the stratigraphic position, Beseme (1967) referred Eocene age to the formation. Şener and Şengüler (1992) regarded the Eocene-Oligocene age to the formation. It also describes the new phase of marine transgression in the region during the Eocene period. Thus, the Paleocene-Eocene terrestrial deposits are overlain by new phase marine transgression. It has unconformable contact with overlain Quaternary deposits (Şener and Şengüler, 1992).

In the Himmetoğlu and Seyitömer village, the Eocene units are overlain by the Oligocene Gölpazarı successions and Miocene Himmetoğlu Formation. The Miocene Himmetoğlu Formation consists of lignite, oil-shale, limestone, marl and alternated conglomerate, claystone and tuffs. The Pliocene Seyitömer succession is composed limestone, tuffs, sandstone and siltstone. Quaternary deposits topple these successions in the region (Ünalın et al., 1976, Altın et al., 1991; Şener and Şengüler 1998, Gülbay and Korkmaz, 2008).

### **2.3. Lithostratigraphy of the Measured Sections**

The five stratigraphic sections forming Middle Eocene (Lutetian-Bartonian) age have been measured and studied in the southwest, in the southeast and in the northeast of Göynük town near the Dağhacılar village, Hasanlar village, Köşüre village, Karahisar village, and Sünnet village in the Mudurnu-Göynük Basin. The measured stratigraphic sections are identified as Middle Eocene (Lutetian-Bartonian) age; Upper Kızılçay Formation and Halidiye Formation (Ocakoğlu et al., 2007, 2012 and Şafak et al.,

2015). The formations are composed of continental (lacustrine- brackish lacustrine) to marine deposits. The deposits are consisting of limestone, marl, oil-shale and fine to coarser sandstone-oil-shale intercalation. Near the Sünnet village, in the Middle Eocene (Lutetian-Bartonian) measured succession, there is also documentation of occasional conglomerate and calcirudite lithofacies at different horizons. The recorded fauna in the formation include ostracods, charophytes, gastropods, bivalve and occasionally benthic foraminifera, rare fish-teeth and scale, echinoderms, algal filamentous and plant fragments.

According to Saner (1978a, 1978b), the Halidiye Formation is confined to Sparnacian (Ypresian)-Lutetian, based on the observed fossil assemblage, includes molluscs (*Tympanotonus*, *Ampullina*, *Dentalium*, *Trochus*, *Lucina* aff. *L. corbarica*, *Ostrea*, *Natica*), benthic foraminifers (*Nummulites*, *Alveolina*), and Ostracoda. Planktonic foraminifera (*Acarinina bulbrooki*, *A. densa*, *A. nitida*, *Subbotina eocaena*, *Turborotalia cerroazulensis frontosa*, *Globigerapsis subconglobata*), nannoplankton assemblage (*Coccolithus pelagicus*, *Reticulofenestra dictyoda*, *R. hillae*) and microfossils assemblages (*Cerithium sismondai*, *Nerinea*, *Ampullaria canalifera*, *Glycymeris*, *Exogyra lateralis*, *Pycnodonte vesicularis*, *Micraster* cf. *cortestudinarium*) are observed by the Ocakoğlu et al. (2007) and assigned Middle Eocene age to the formation. Therefore, based on the fossil assemblages, it is interpreted that the Kızılcay Formation and Halidiye Formation was deposited during Lutetian-Priabonian periods (Ocakoğlu et al., 2007, 2012; Şafak et al., 2015). According to Saner (1977), the Kızılcay Formation is terrestrial river-lake deposited and overlain by marine Halidiye Formation.

In this study, a total of 76, 21, 49, 29 and 36 samples have been collected in the field from the measured Dağhacılar, Hasanlar, Köşüre, Karahisar and Sünnet sections in order to determine the lithofacies and depositional environment, respectively. The field studies and microscopic analysis are used to designate the lateral and vertical changes in the facies and environmental condition changes. During the field and laboratory studies, the recorded lithologies along the studied sections are medium gray

to dark gray laminated and non-laminated oil-shale, limestone, marl and sandstone. The pebble conglomerate and calcirudite are only recorded along the Sünnet studied section.

### **2.3.1. Dağhacılar Measured Section**

The locality of the Dağhacılar studied section lies near the Dağhacılar village, Bolu Province (GPS: 40°15' 37.10N, 30° 58' 46.77"E with 1101 meter at base and 40° 15' 43.64"N, 30° 58' 48.59"E with 1175 meter at top) (Figure 2.3). A total of 76 samples were collected from 159.50m measured stratigraphic section (Figures 2.5 and 2.7).

The Dağhacılar measured section is documented as brownish black to dark gray to medium gray to medium dark gray to greenish gray to dark greenish gray to pale yellowish brown to very pale orange to yellowish gray to grayish orange, very thick to very thin bedded high fossiliferous limestone, limestone, marl, laminated and non-laminated oil-shale and very fine to coarser sandstone (Figures 2.4, 2.8, 2.9, 2.10, 2.11, 2.13, 2.14, 2.15 and 2.16). The measured stratigraphic section is starting with medium bedded gray dominated limestone with subordinate gastropod and ostracod fossils and interbedded marl. As move up in the measured section, the limestone intervals show an increase in the gastropod fossils content at certain level in the measured section (Figures 2.8 and 2.9). Highly abundant gastropod fossil bearing intervals are observed between 6m to 44m of the measured stratigraphic section with occasional interbedded marl and oil-shale units (Figures 2.8 and 2.9). The marl beds are present dominantly in the lower portion and upper portion of the measured section. In the lower portion and upper portion, the marl beds are interbedded with limestone units and sandstone units, respectively. The oil-shale lithofacies are prominent in the middle to upper portion of the studied section with occasional marls and sandstone beds. The oil-shale is characterized by thin to laminated intervals. The lamina in oil-shale is composed of organic-rich lamina and carbonate-rich lamina (Figures 2.10, 2.11, 2.12, 2.13, 2.15). The oil-shale interval in the lower portion of the stratigraphic unit is defined by highly

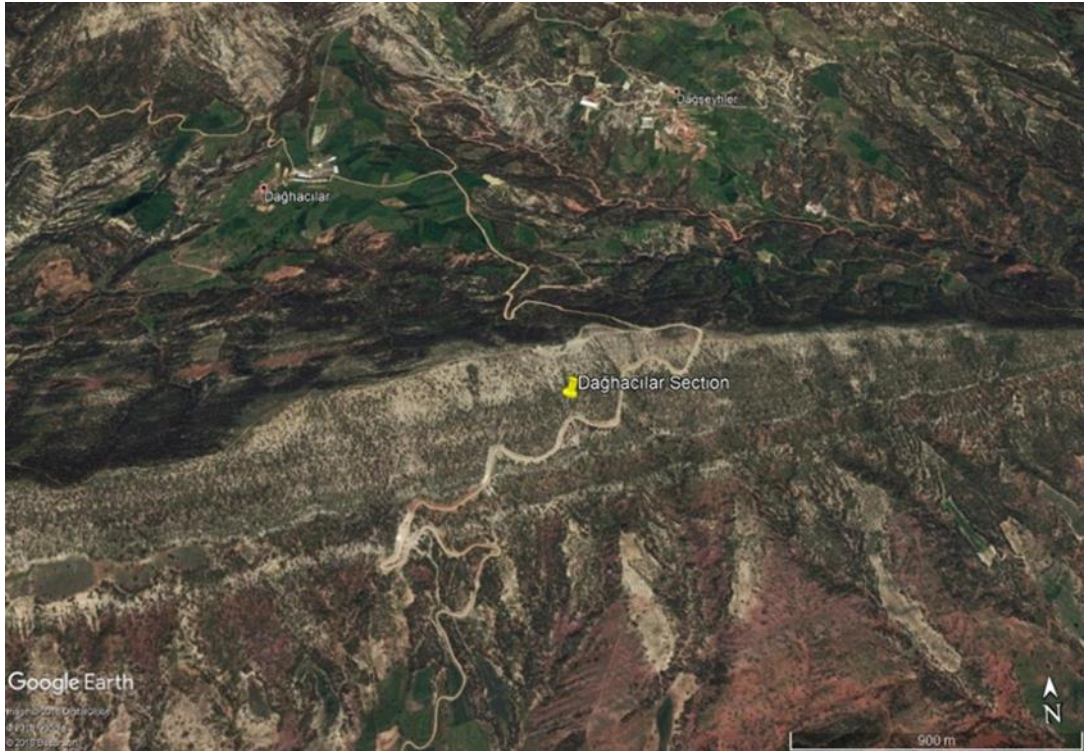


Figure 2.3. Satellite image showing the measured Dağhacılar Section in the Mudurnu-Göynük Basin (Dağhacılar Section represented by yellow icon).

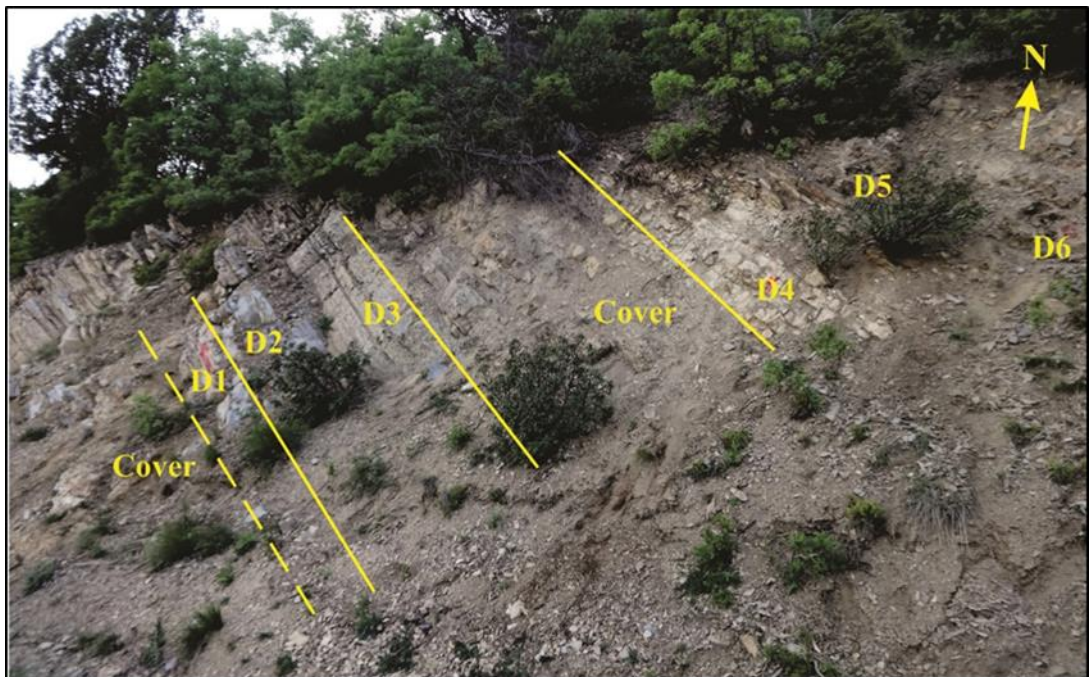


Figure 2.4. The field photograph showing lime mudstone and marl, the starting point of the Dağhacılar section. (D1-D6).

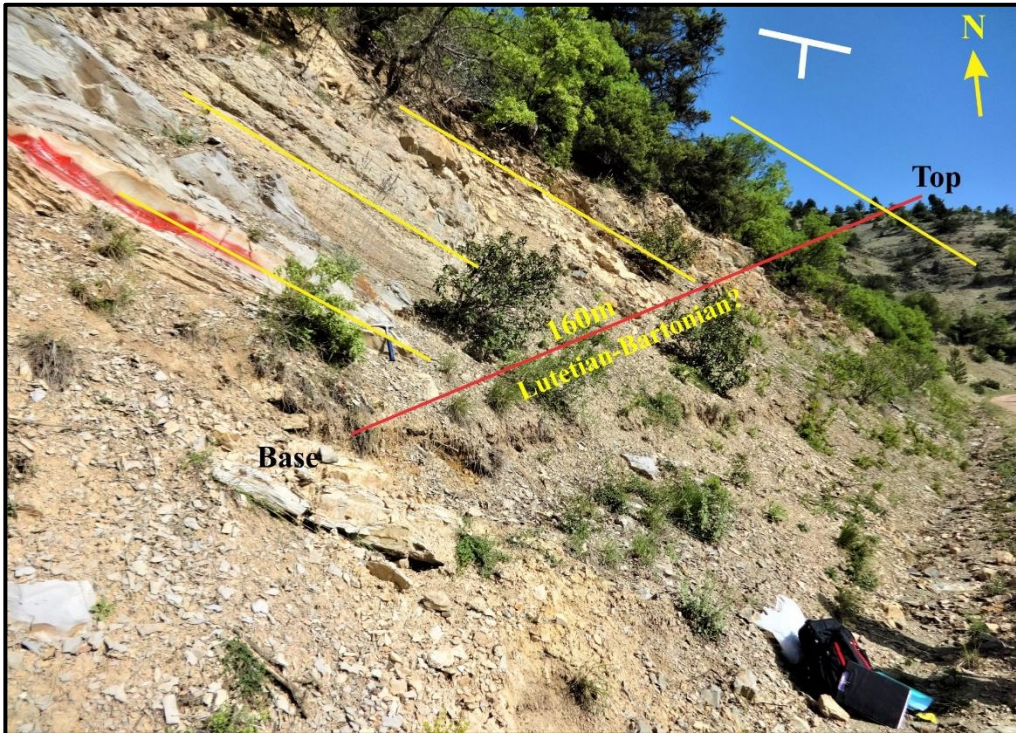


Figure 2.5. The field photograph of Lutetian-Bartonian measured stratigraphic section near Dağhacılar village, Bolu. N dip direction (white lines).

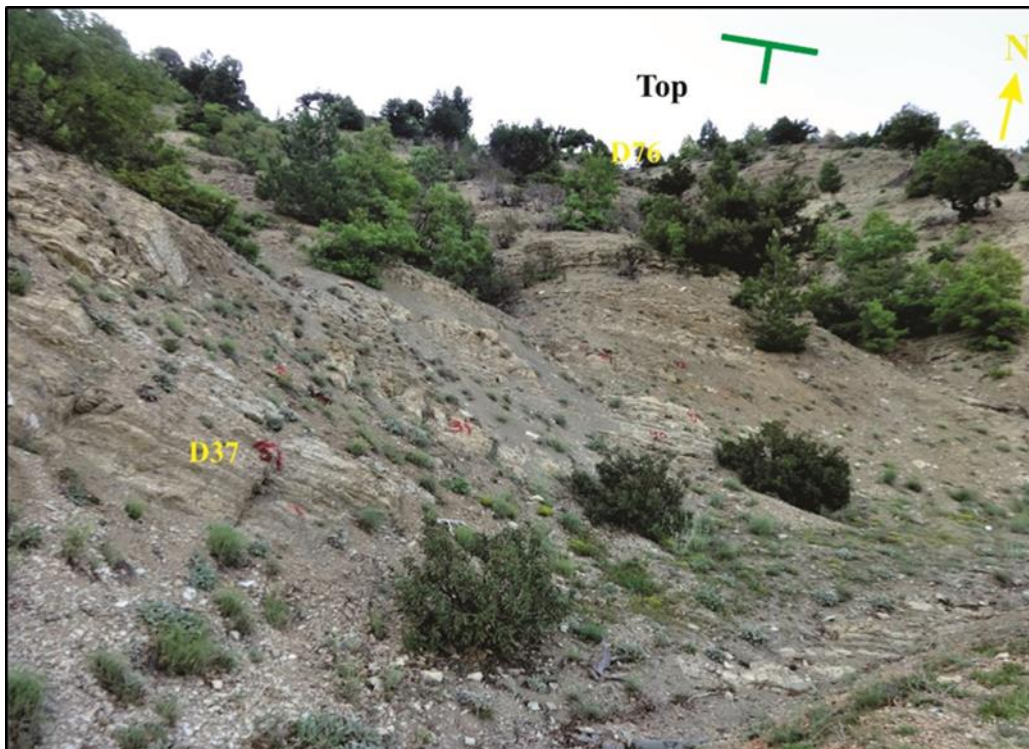


Figure 2.6. The field photograph of Lutetian-Bartonian measured stratigraphic section near Dağhacılar village, Bolu. N dip direction (green lines). (from D37 to D76).

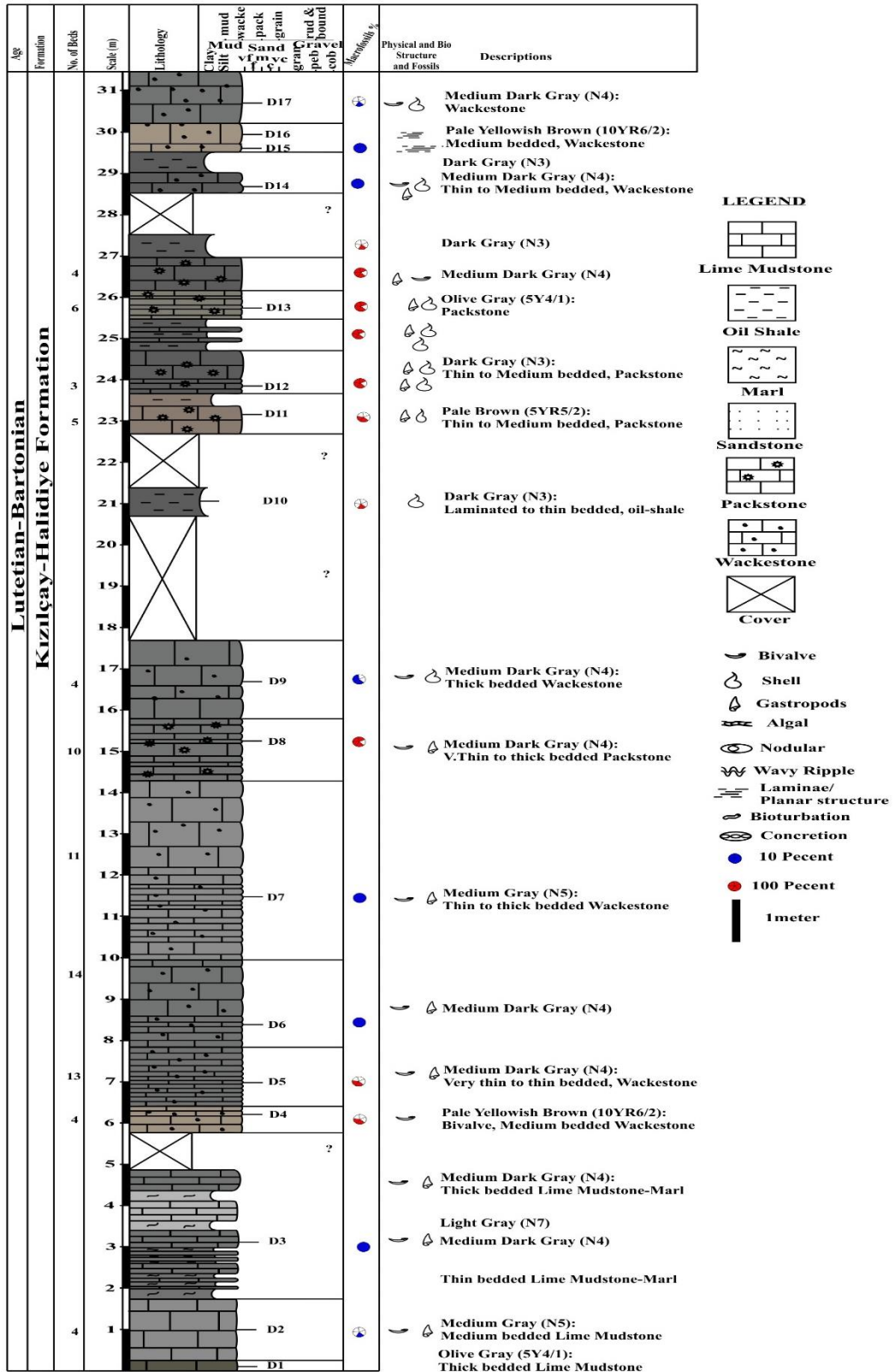


Figure 2.7. Measured stratigraphic section near Dağhacılar Village (0m-31.5m).

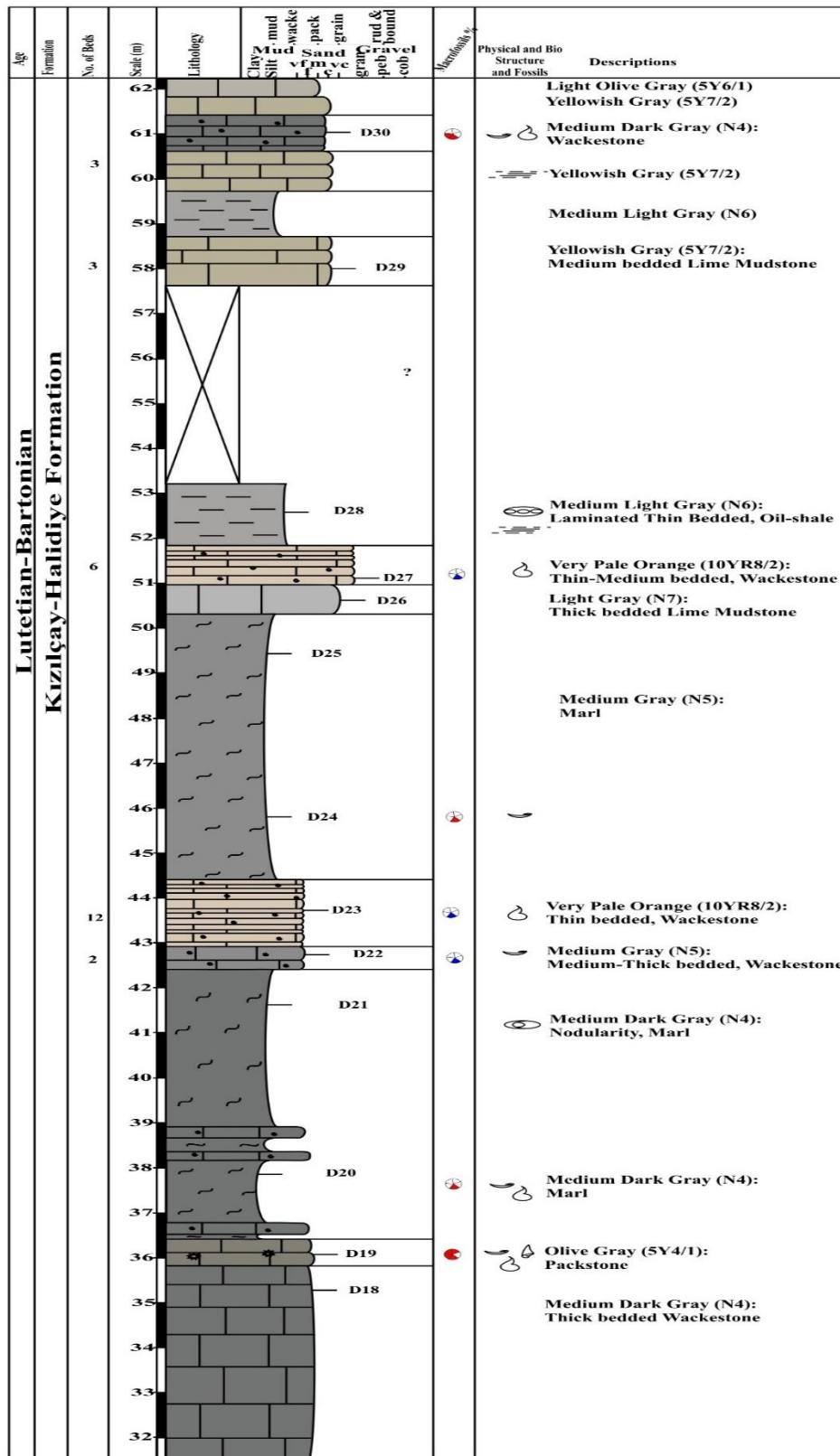


Figure 2.7: Continued (31.5m-62.3m).

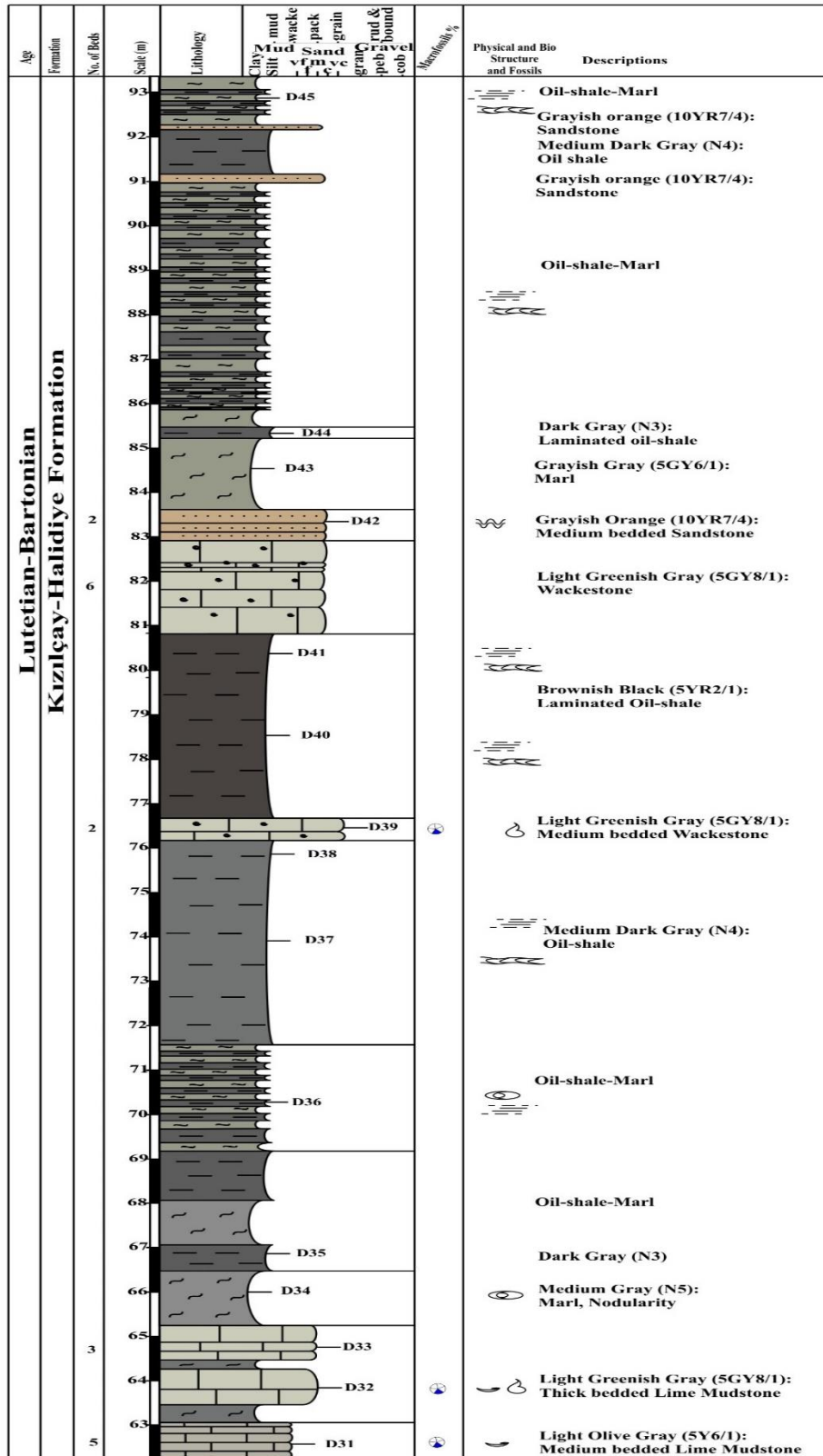


Figure 2.7: Continued (63.3m-93.5m).

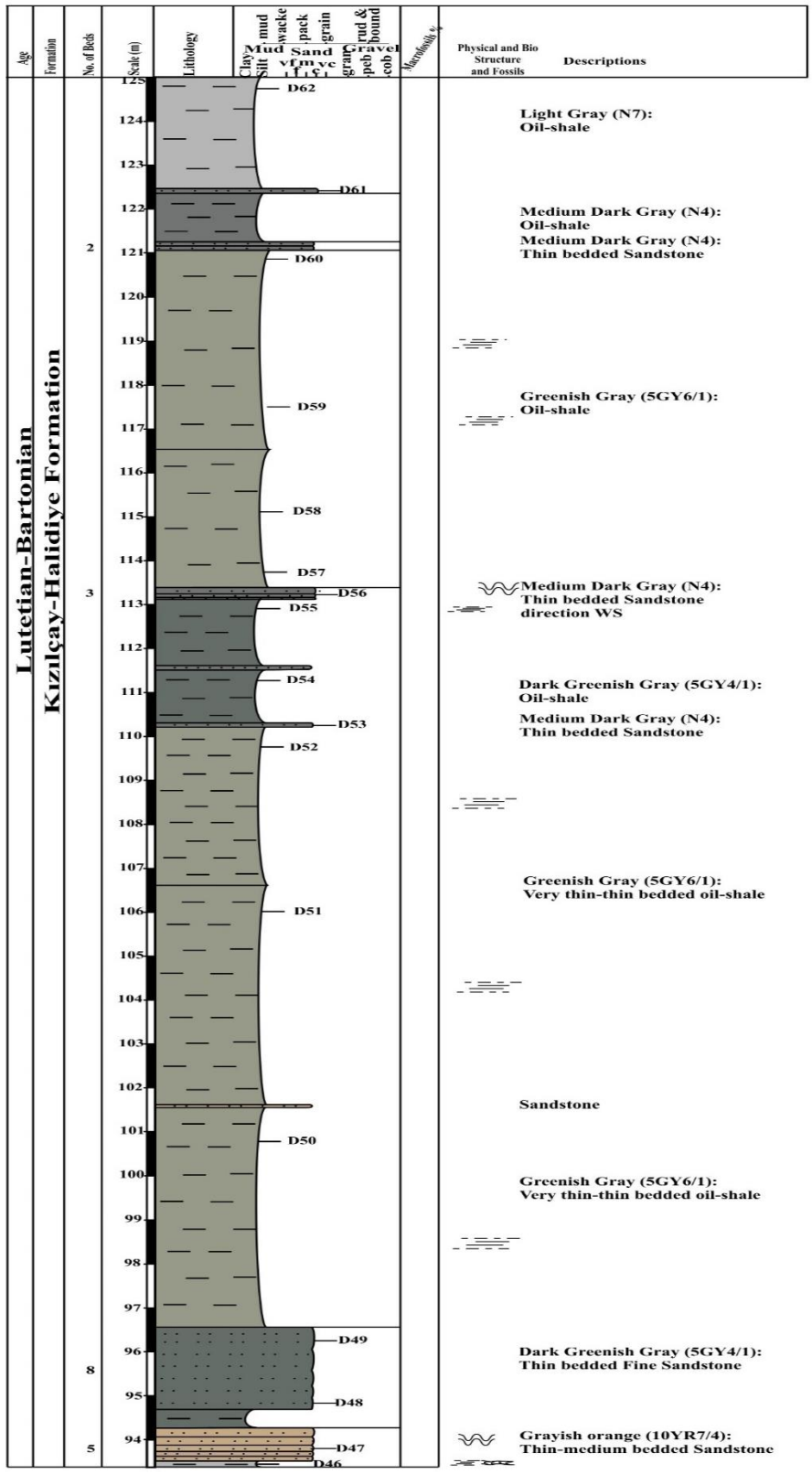


Figure 2.7: Continued (93.5m-125m).

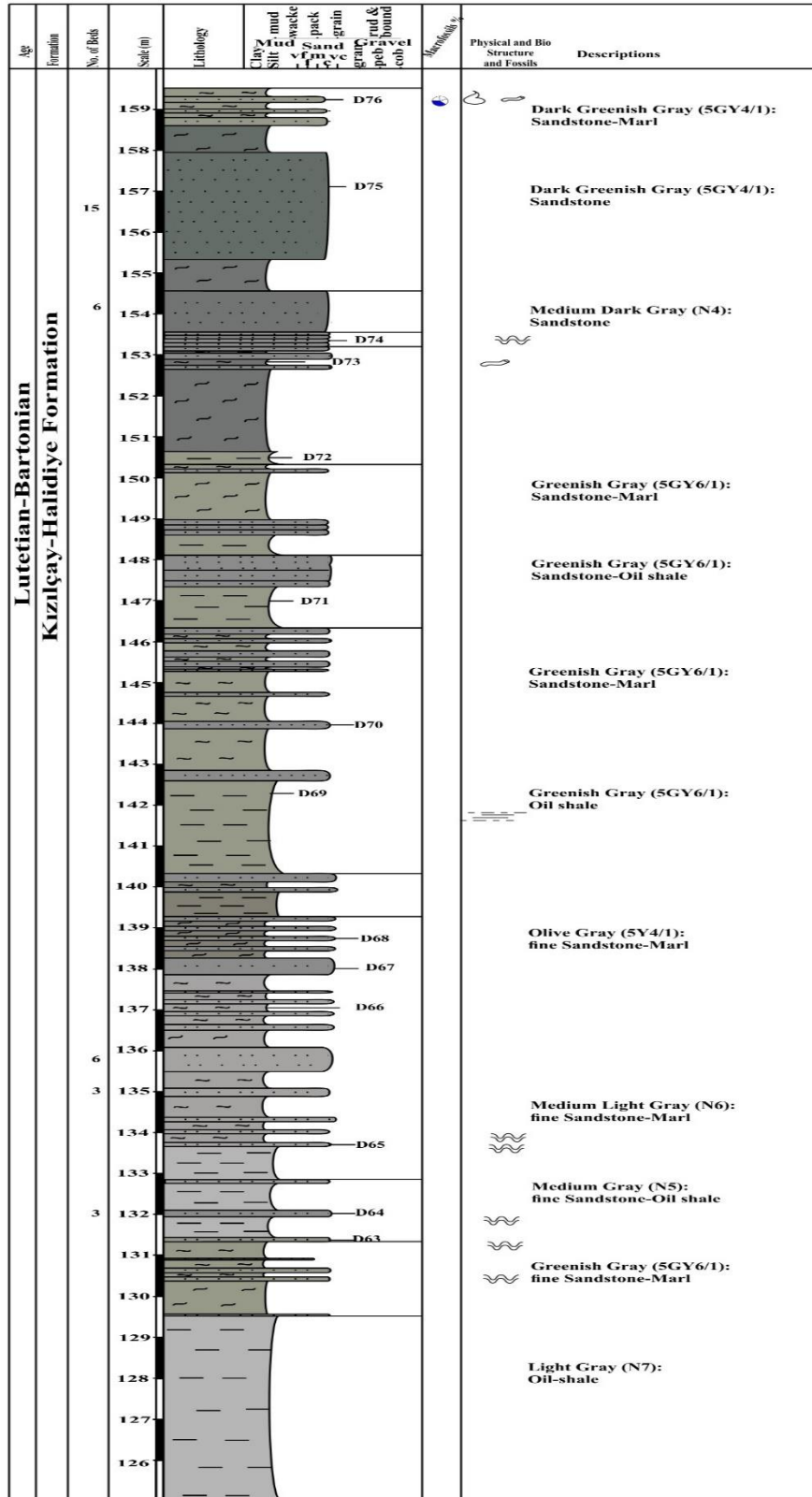


Figure 2.7: Continued (125m-160m).

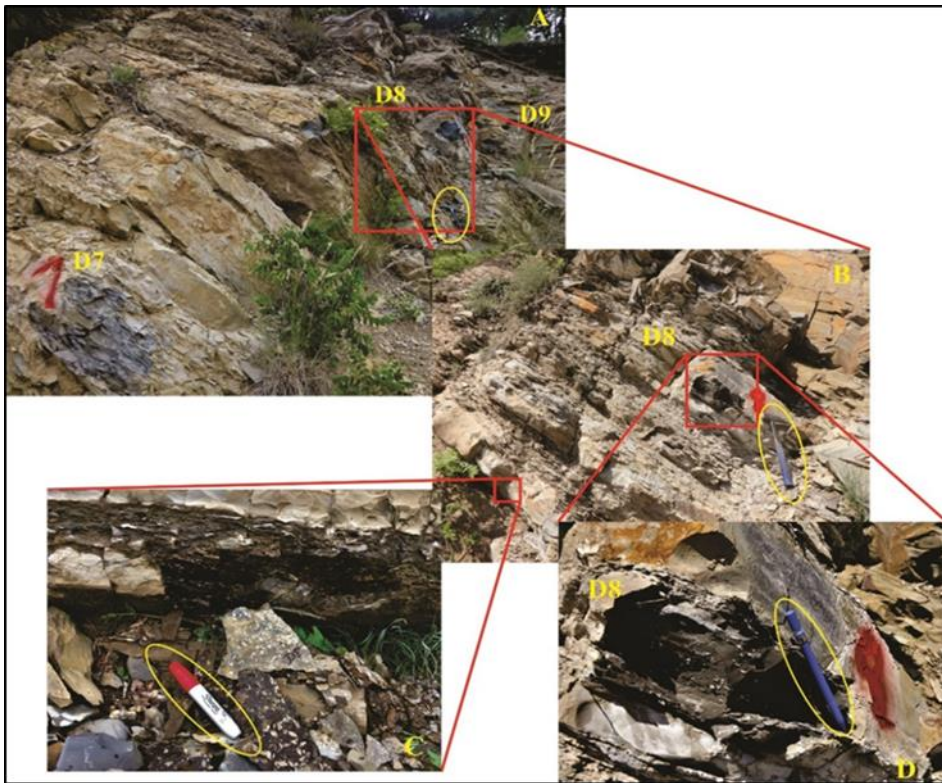


Figure 2.8. The field photographs of Dağhacılar measured stratigraphic section showing; (A) wackestone bedding (D7), overlain by high fossiliferous unit Packstone (D8) and then followed by wackestone (D9); B) Close view of Packstone limestone of sample D8; C and D) Close view of Gastropod in the sample D8 beddings.

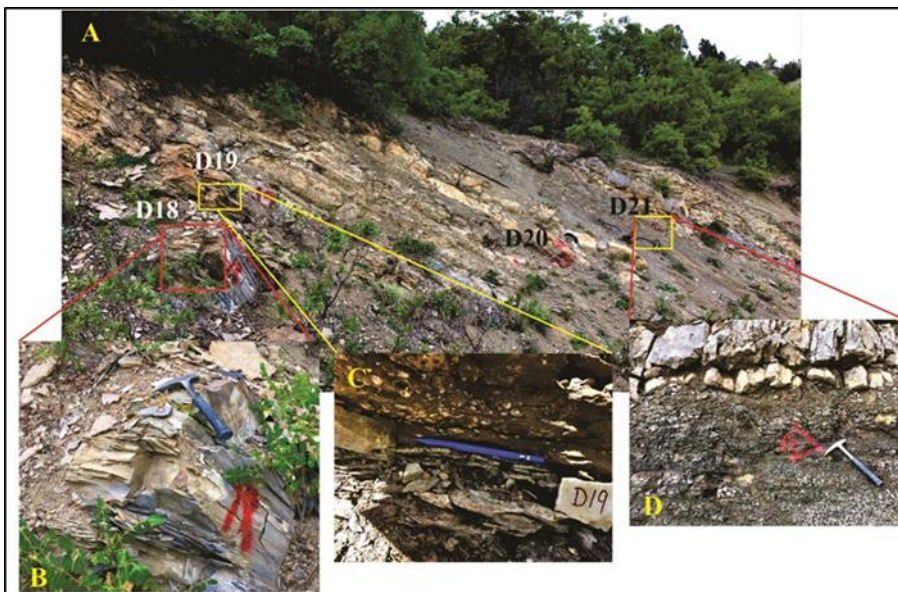


Figure 2.9. The field photographs of Dağhacılar measured stratigraphic section showing; (A) wackestone bedding (D7), overlain by high fossiliferous unit Packstone (D8) and then followed by wackestone (D9); B) Close view of Packstone limestone of sample D8; C and D) Close view of Gastropod in the sample D8 beddings.

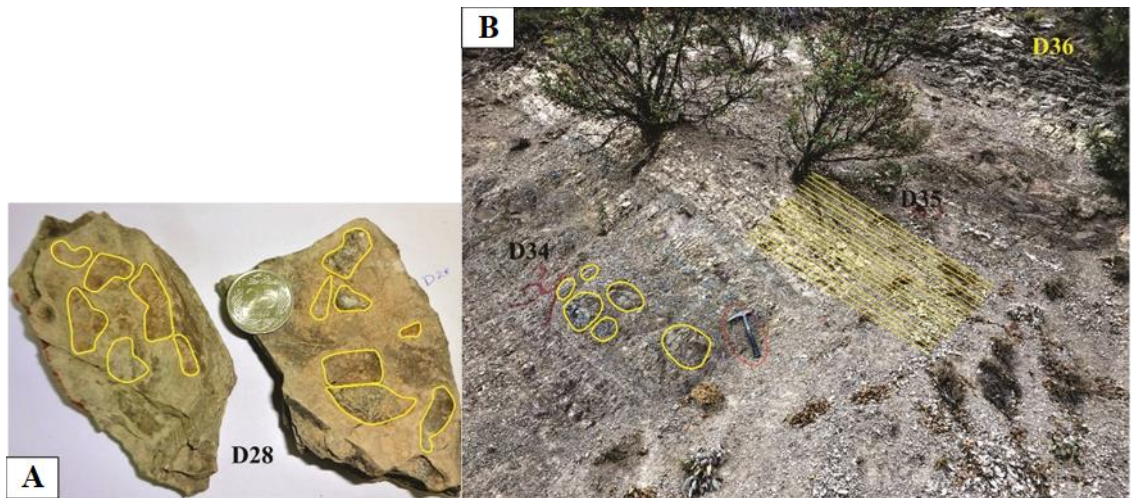


Figure 2.10. Figure 2.10. The field photograph of Dağhacılar studied section showing, A) Siliceous concretion; B) marl (D34) with nodularity feature and above planar very thin bedded to algal laminated oil-shale (D35, D36).

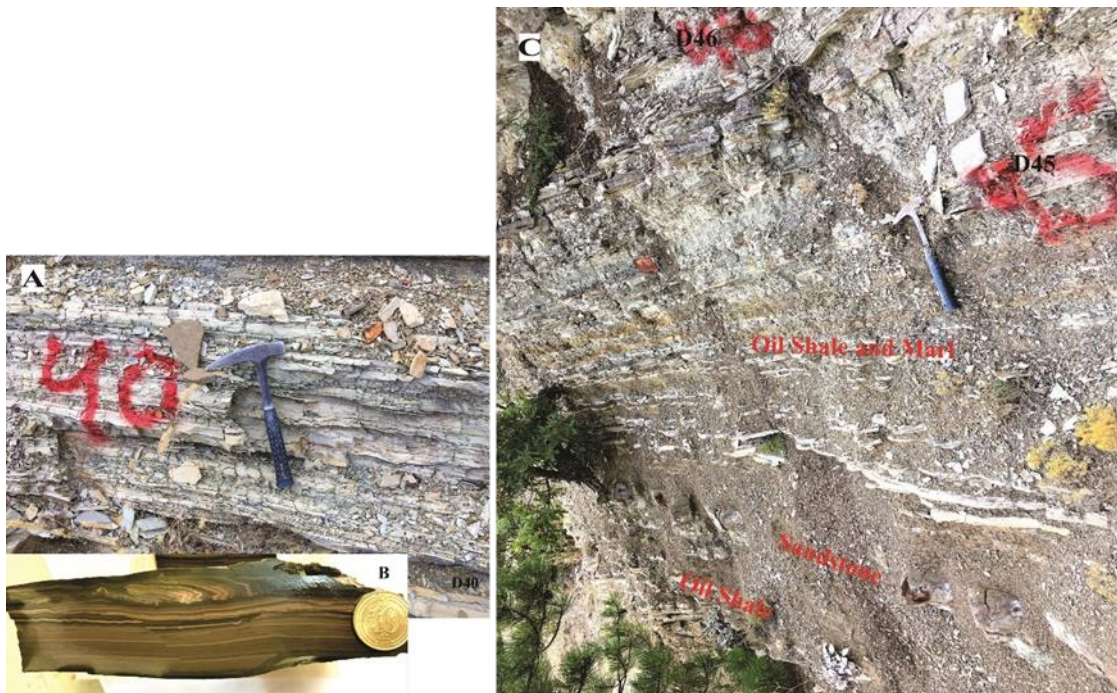


Figure 2.11. The field photograph of Dağhacılar measured stratigraphic section illustrating A) algal laminated oil-shales; B) Thin preparation cutting algal laminated D40 sample; C) Algal Laminated Oil-shale and marl alternation with occasional thin bedded sandstone.



Figure 2.12. The field photograph of Dağhacılar measured stratigraphic section illustrating A) laminated to thin planar bedded oil-shale; B) Cross cutting section of sample D52 for thin section preparation.

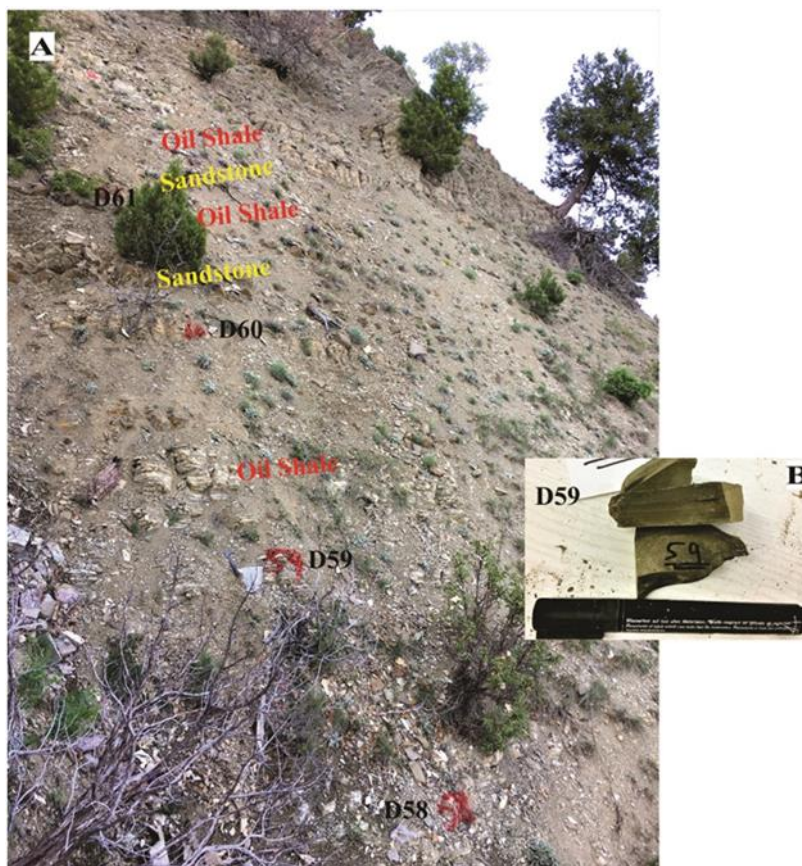


Figure 2.13. The field photograph of Dağhacılar measured stratigraphic section illustrating Thin to laminated oil-shale with interbedded sandstone.



Figure 2.14. The field photograph of Dağhacılar measured stratigraphic section illustrating dominated up section sandstone; A) Sandstone beds are low angle wavy rippled bedded sandstone with interbedded oil-shale; B) wavy rippled bedded sandstone (Sample D65).

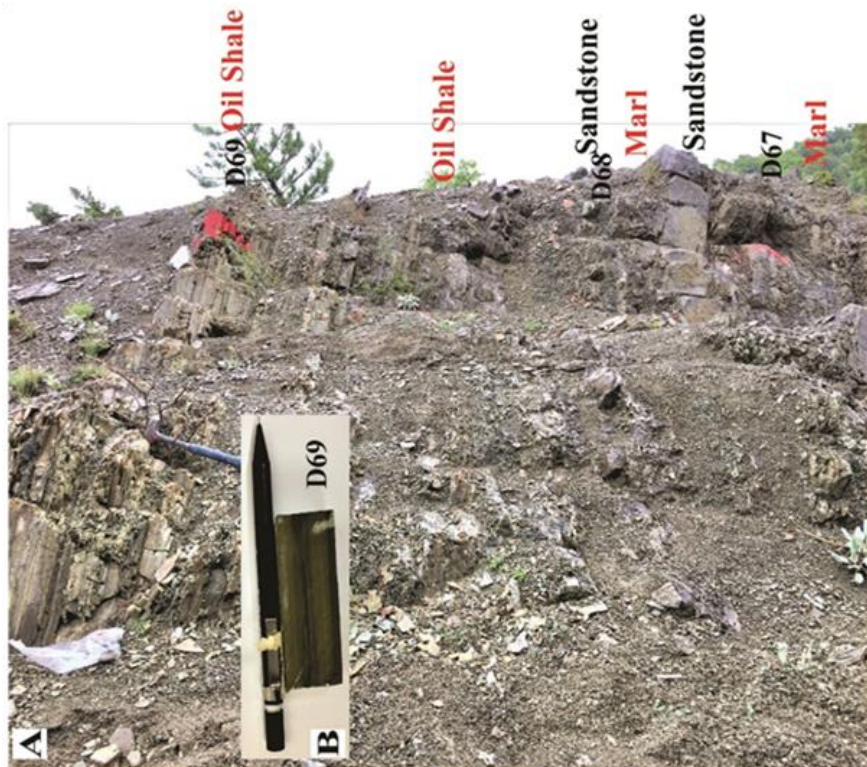


Figure 2.15. The field photograph of Dağhacılar measured stratigraphic section presenting thin to thick bedded sandstone and marl, Oil-shale deposited above section.

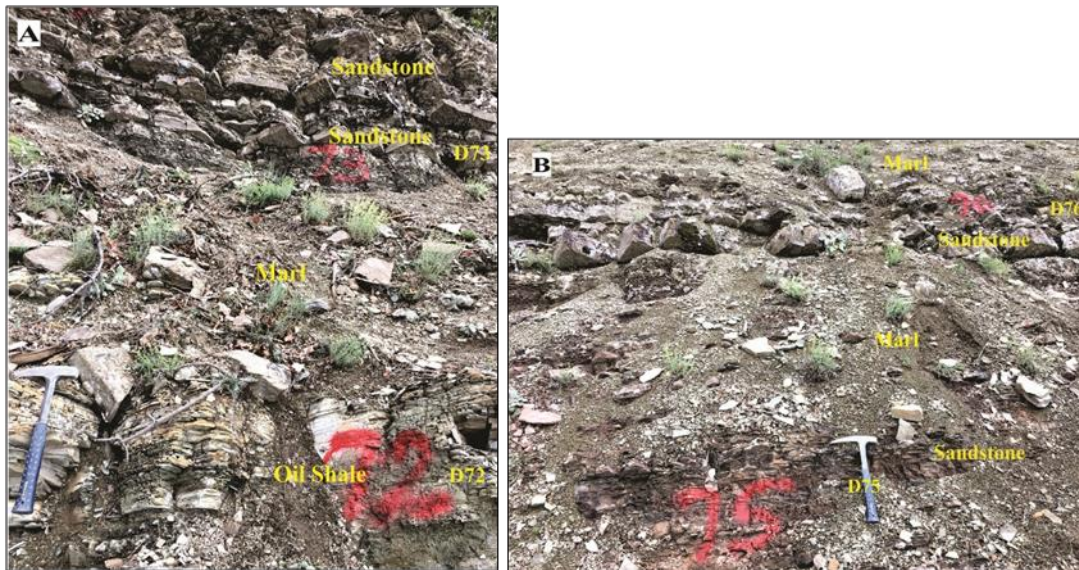


Figure 2.16. The field photograph of Dağhacılar measured stratigraphic section presenting oil-shale followed by marl with interbedded very thin wavy rippled sandstone to very thin to medium bedded planar bedded sandstone (shown by B). B) Marl and sandstone intercalation at the top portion of the measured section.

bearing ostracod shells. The thin to very thin bedded sandstone intervals increase in the upper portion and intercalated with marl and oil-shale.

In the field, the recorded fauna in the studied section are gastropods, ostracod and algal laminated features at different intervals (Figures 2.8, 2.9 and 2.11). The sedimentary structure in the measured stratigraphic bedding is algal lamina, laminated to thick bedded, planar laminated bedding, very thin- to medium-bedded planar bedding, wavy rippled feature bedding and rare nodularity and siliceous concretion (Figures 2.4, 2.5, 2.8, 2.9). The very thin planar bedding, algal lamination and non-algal lamination are sedimentary features in the oil-shale (Figures 2.11, 2.12, 2.13 and 2.15). The oil-shale also appeared as shaly to flaggy features at certain horizons. The sandstones are characterized by planar to wavy laminated to planar thin bedding to wavy rippled bedding sedimentary features (Figures 2.14 and 2.16).

The age of the Dağhacılar measured section is defined as Lutetian-Bartonian on their chronostratigraphic position and previous paleontological studies (Şener and

Şengüler, 1997; Gedik and Aksay, 2002). The recorded ostracods in the middle portion of Hatıl section (lacustrine) near Dağhacılar village are *Cyamocytheridea hebertiana* (Bosquet), *Cytheridea (Clithrocytheridea) faboides* (Bosquet), *Cytheridea (Haplocytheridea) sp.*, *Vetustocytheridea sp.* and indicates Late Lutetian age (Ocakoglu et al., 2012). These are overlain by marine succession during late Middle Eocene in the Mudurnu-Göynük basin (Ocakoglu et al., 2007, 2012; Şafak et al., 2015).

### **2.3.2. Hasanlar Measured Stratigraphic Section**

The GPS coordinate of the Hasanlar stratigraphic section lies in the 40°16' 3.26" N, 30° 53' 6.20" E with 842 meters and 40°16' 6.36" N, 30° 53' 4.36" E with 855 meters at the base and top, respectively (Figure 2.17). The studied section is measured near the Hasanlar and Kabalar village, which is around 8km approx. away from the Dağhacılar measured section in the northwest direction. The collected samples along the measured succession are 21, which are collected at random interval. The samples were selected on the basis of change in lithologies, color and sedimentary features (Figure 2.20). 14 samples were selected for the microscopic and petrographic analysis of the studied section.

In the field, the identified lithologies in the Hasanlar measured stratigraphic section are the light brown, pale green, very pale orange, medium light gray to medium gray to dark gray, very thin to thin to medium planar bedded limestone and algal laminated to laminated to thin planar bedded oil-shale and occasional marl (Figures 2.18, 2.19, 2.21 and 2.22) The studied region shows high tensional tectonic regime. The oil-shale in the field appeared as thin planar bedding, laminated and occasionally shaly to flaggy and fragile character (Figures 2.18, 2.19, 2.21 and 2.22). The recorded fauna in the middle portion of studied section are ostracods.

The Hasanlar measured section is identified and correlatable with bituminous oil-shale member of the Kabalar Formation of Şener and Şengüler (1998) in the vicinity of Hasanlar village. Therefore, it can be characterized as Late Lutetian age and can

correlatable with the middle portion of the Dağhacılar measured section and bituminous oil-shale member of the Kabalar Formation. In this study, it is described as a portion of the Kızılcay Formation (Gedik and Aksay,2002; Oçakoğlu et al., 2007 and 2012).

### 2.3.3. Köşüre Measured Section (Yenipazar)

The other measured section, stratigraphically equivalent to the Dağhacılar Section, is exposed near the Köşüre village, Yenipazar, Bolu Province (Figure 2.23). The measured section is started from with GSP coordinates of 40° 11' 39.49" N; 30° 37' 22.37" E with 844meter and end at 40° 11' 43.83" N; 30° 37' 19.59" E with 863meter. Total of 49 numbers of samples was collected along the stratigraphic section and vertical changes were recorded along the measured section in the field (Figures 2.24 and 2.25).

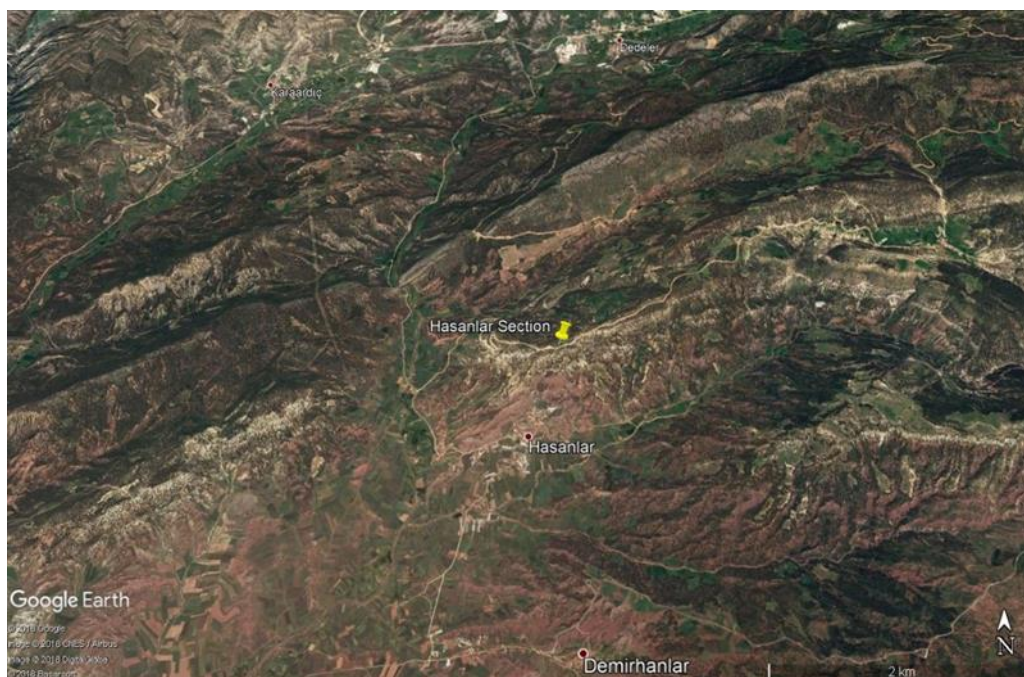


Figure 2.17. Satellite image showing the Hasanlar measured section in the Mudurnu-Göynük Basin, in the vicinity of Hasanlar village (Hasanlar studied section represented by yellow icon).

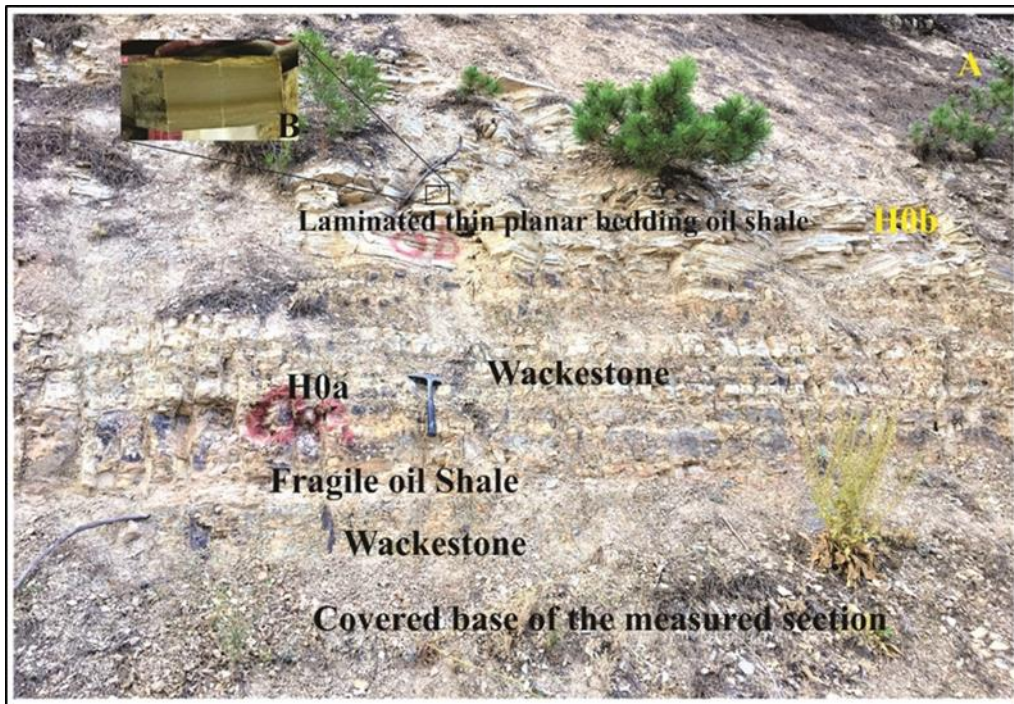


Figure 2.18. The field photograph of Hasanlar measured section presenting base of the section, started with limestone of wackestone feature, then followed by planar thin bedded Oil-shale; B) Thin section preparation rock-cutting Oil-shale sample H0b.

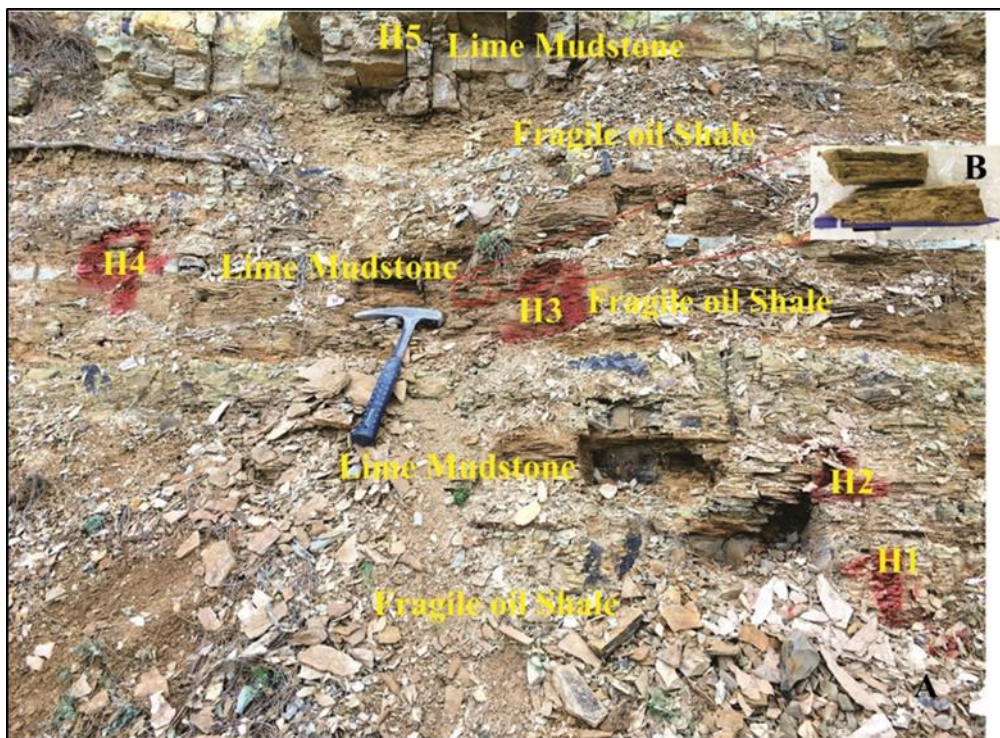


Figure 2.19. The field photograph of Hasanlar measured section presenting intercalation of lime mudstone and fragile laminated oil-shale.



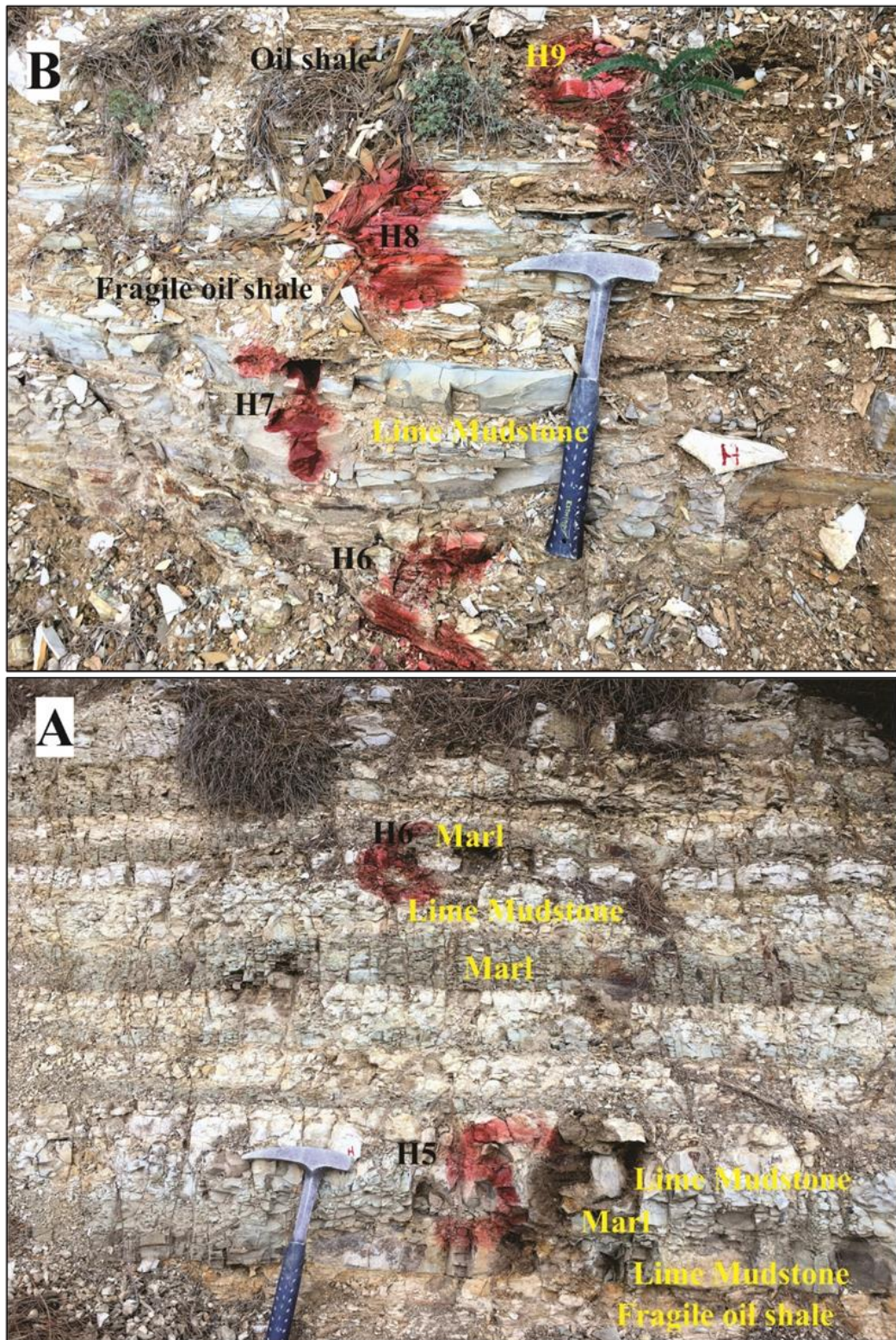


Figure 2.21. The field photograph of Hasanlar studied section presenting intercalation of A) lime mudstone and marl; B) representing intercalation of lime mudstone and laminated oil-shale.

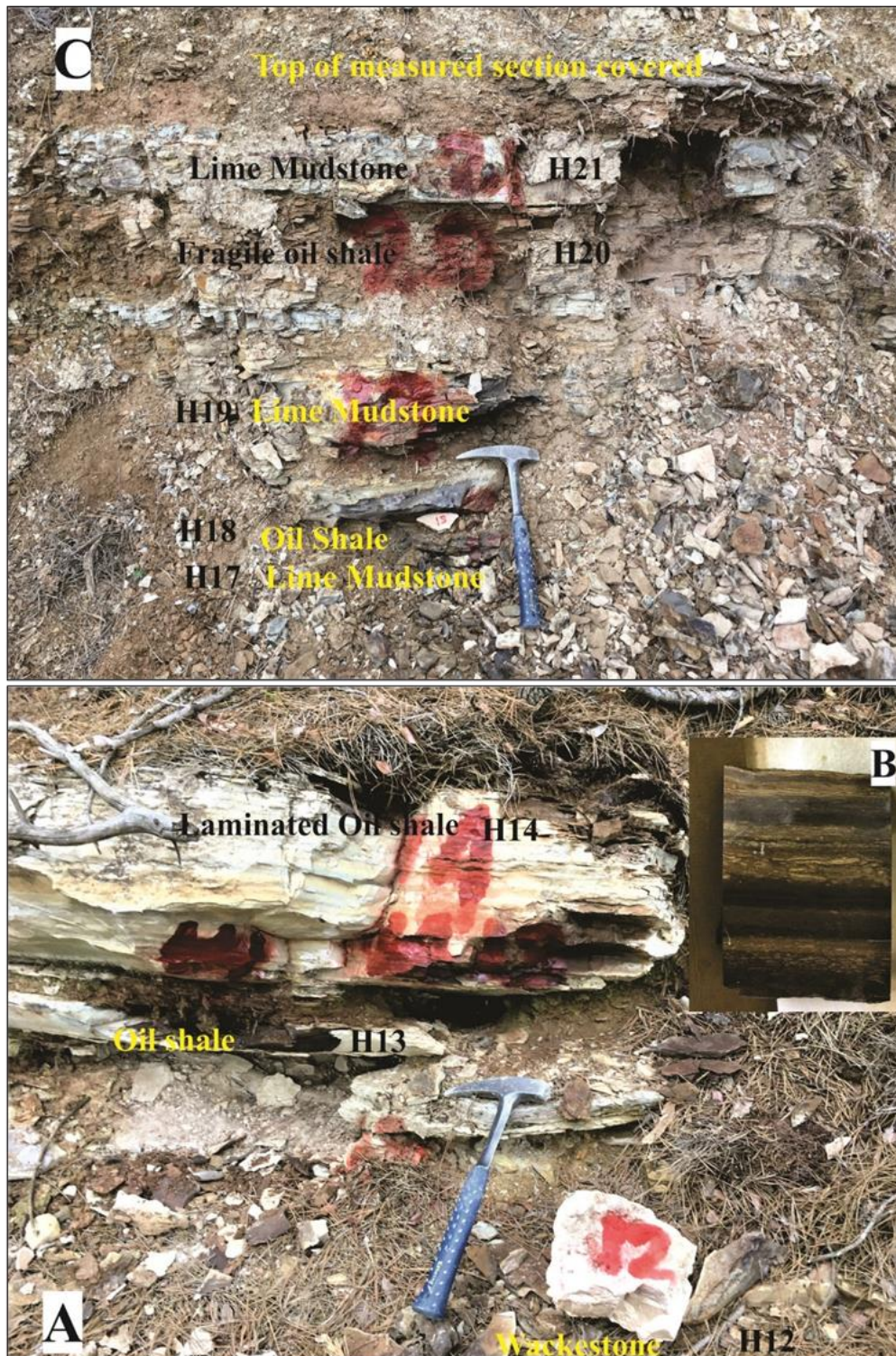


Figure 2.22. The field photograph of Hasanlar measured section presenting; A) Wackestone and Laminated Oil-shale; B) Lab cutting sample H14; C) representing intercalation of lime Mudstone and Laminated Oil-shale.

The lithological sequence in the Köşüre measured section is composed of marls and limestone intercalation with occasional sandstone and oil-shale (Figure 2.26). The sandstone is dominated in the upper portion of the measured section (Figures 2.30; 2.31 and 2.32). In the field, the lower portion of the studied section is dominantly composed of light gray to pinkish gray to whitish, medium to very thick bedded limestone with grayish to dark green-gray marl and occasional greenish gray thin to thick bedded sandstone intervals (Figures 2.26 and 2.27). The middle unit is defined by the high occurrence of greenish gray marl beds with thin to thick bedded, light gray to pinkish limestone and occasional nodular sandstone and oil-shale horizons in the places (Figures 2.28; 2.29; 2.30 and 2.31). Then the units switch to dominate, very thin to thin planar and low angle wavy bedding sandstone with interbedded oil-shale (Figures 2.30; 2.31 and 2.32). The oil-shale units are observed at different horizon and are documented as dark gray to grayish black laminated to shaly feature appearance (fissility character). The limestone intervals contain bioclasts include charophytes, ostracods and bivalve and rare gastropod fragment and fish teeth (Figures 2.27A; 2.32A).

On the basis of the stratigraphic position and fauna, the lower limestone with marls units and occasional oil-shale are defined as Upper Kızılçay Formation and Upper portion of limestone, interbedded oil-shale and sandstone are characterized as Halidiye Formation. According to Ocakoğlu et al. (2007), in the Yenipazar region, the Middle Eocene succession interprets brackish-lacustrine succession, that are overlain by marine successions. The *Turborotalia cerroazulensis frontosa*, *Acarinina bullbrooki*, *Acarinina medizai*, *Pseudohastigerina micra*, *Truncorotaloides collactea*, *Subbotina eocaena*, *Subbotina officinalis*, *Subbotina praeturritilina*, *Turborotalia cerroazulensis pomeroli*, *Globoquadrina pseudovenezuelana* were recorded fauna in the overlying marine succession by Ocakoğlu et al. (2007), Koralay (2009) and assigned a Bartonian age. Therefore, the stratigraphic position and fauna in the studied section, the Lutetian-Bartonian age is assigned to the Köşüre

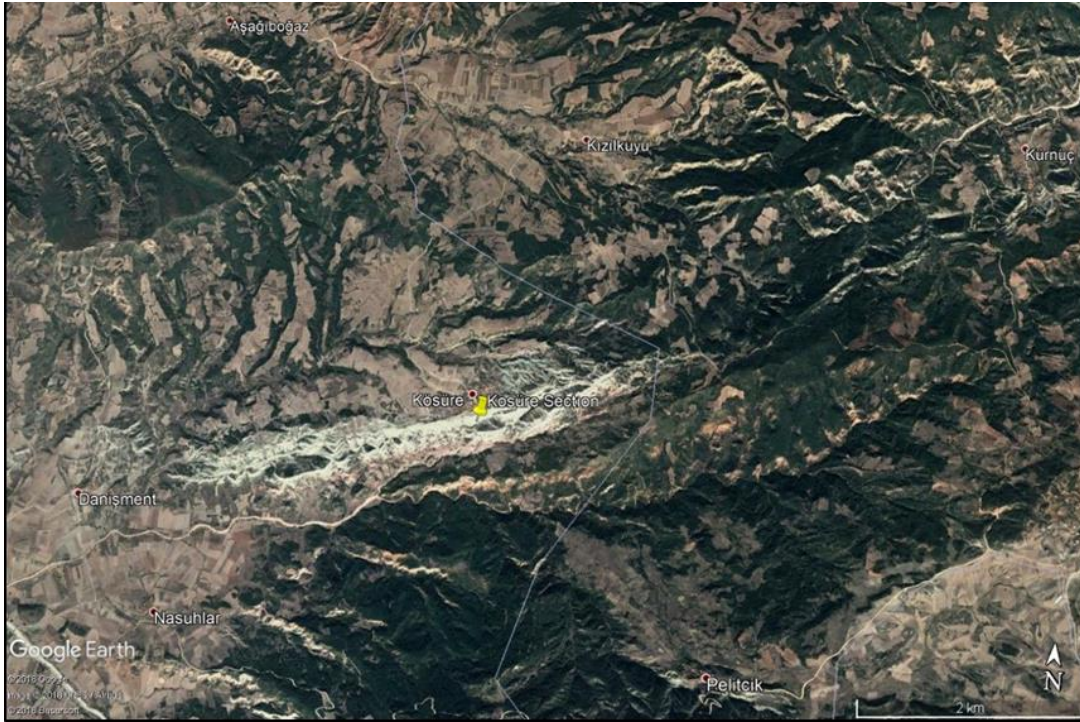


Figure 2.23. Satellite image showing the measured Kösüre studied section in the Mudurnu-Göynük Basin, Kösüre village (yellow icon represents the studied section).

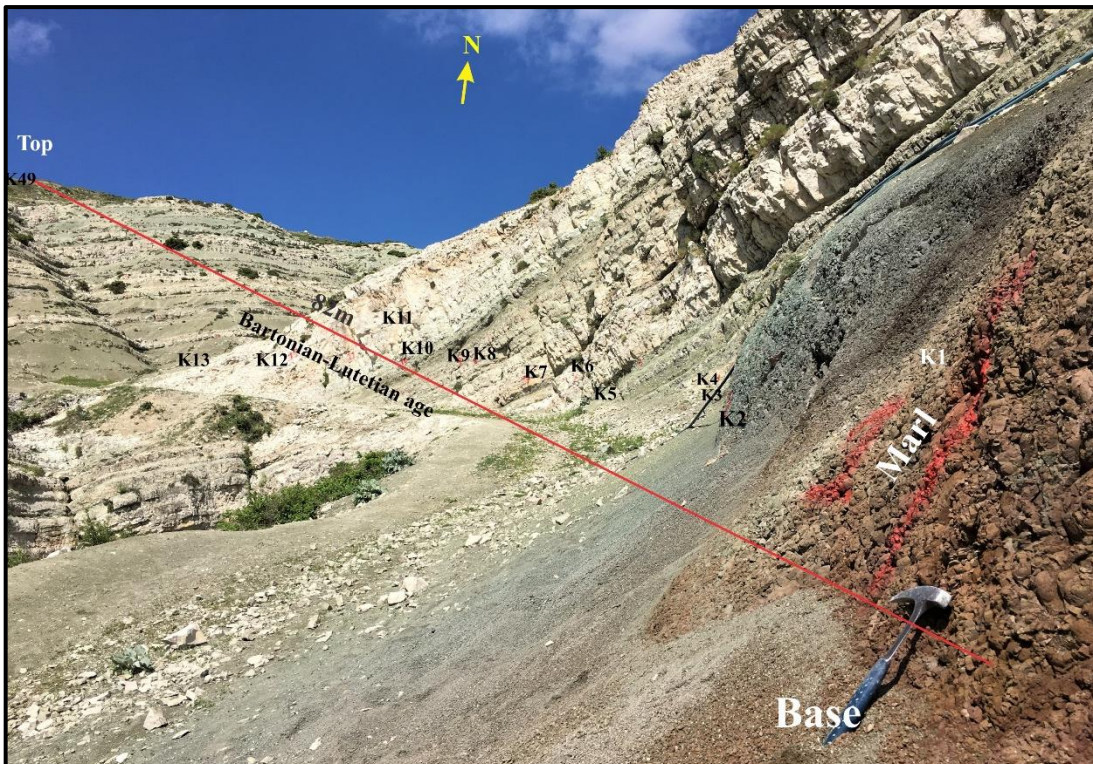


Figure 2.24. The field photograph of 82-meter Lutetian-Bartonian measured stratigraphic section near Kösüre village, Bolu. N dip direction (white lines).

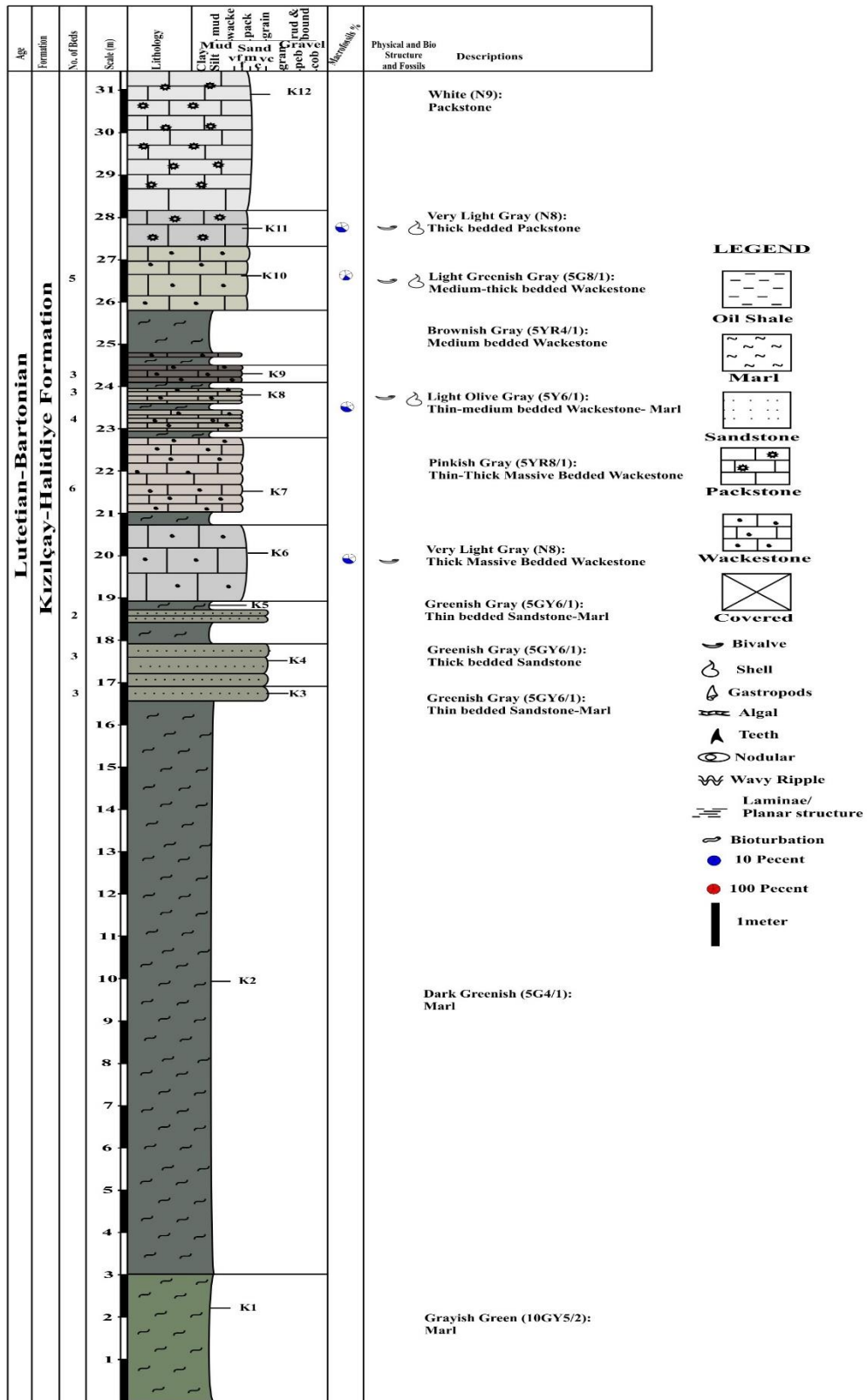


Figure 2.25. Measured stratigraphic section in the vicinity of Köşüre Village (0-31.5m).





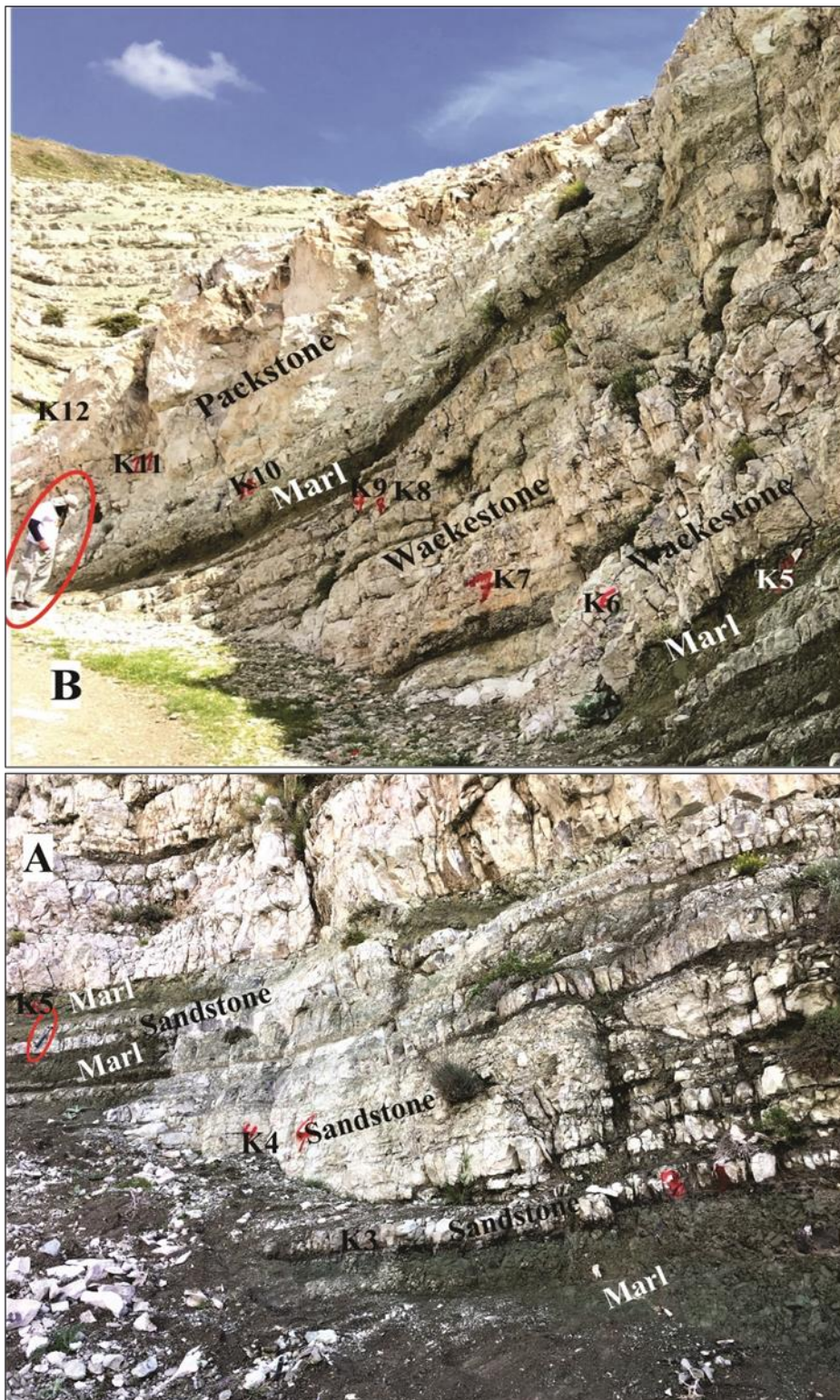


Figure 2.26. The field photograph of Lutetian-Bartonian Kösiüre studied section presenting; A) marl and medium bedded sandstone; B) thin to thick to massive bedded limestone with thin to medium intervals of marls.

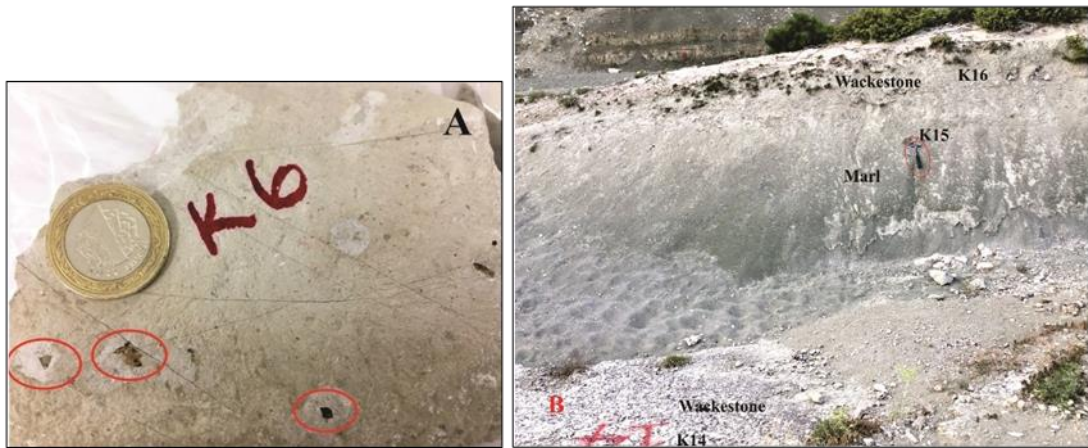


Figure 2.27. The field photograph of Lutetian-Bartonian Kösüre studied section presenting; A) marl and medium bedded sandstone; B) thin to thick to massive bedded limestone with thin to medium intervals of marls.



Figure 2.28. The field photograph of Lutetian-Bartonian Kösüre studied section presenting; A) marl and medium bedded sandstone; B) thin-thick to massive bedded limestone with thin to medium intervals of marls.

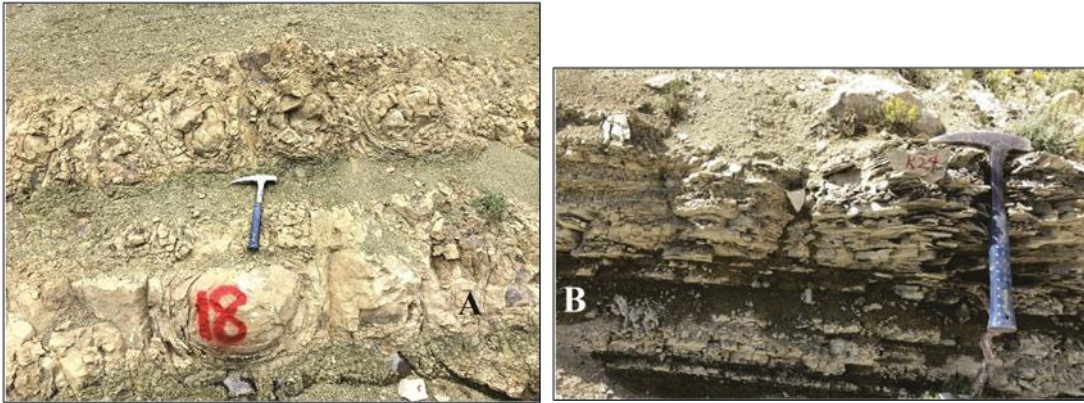


Figure 2.29. The field photograph of Kösiire studied section presenting A) close view of nodularity in Sandstone with marl interbeds (sample K18); B) close view of laminated oil-shale (sample K24).

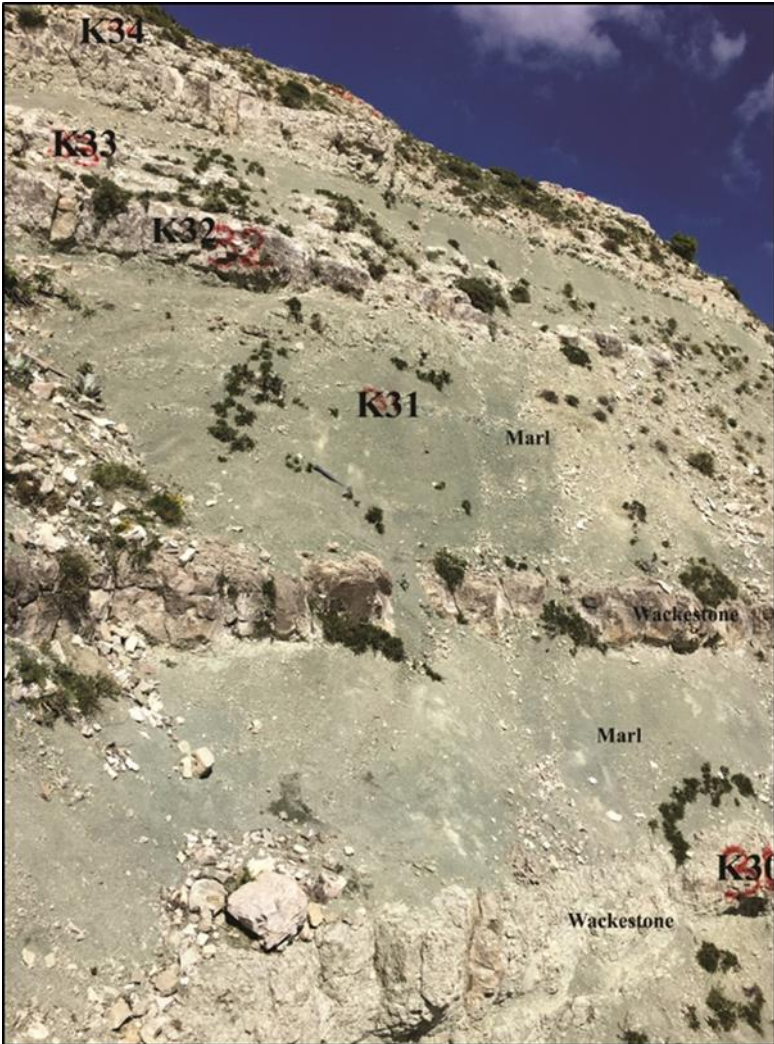


Figure 2.30. The field photograph of Kösiire studied section presenting marl and limestone intervals (sample K31-K34).

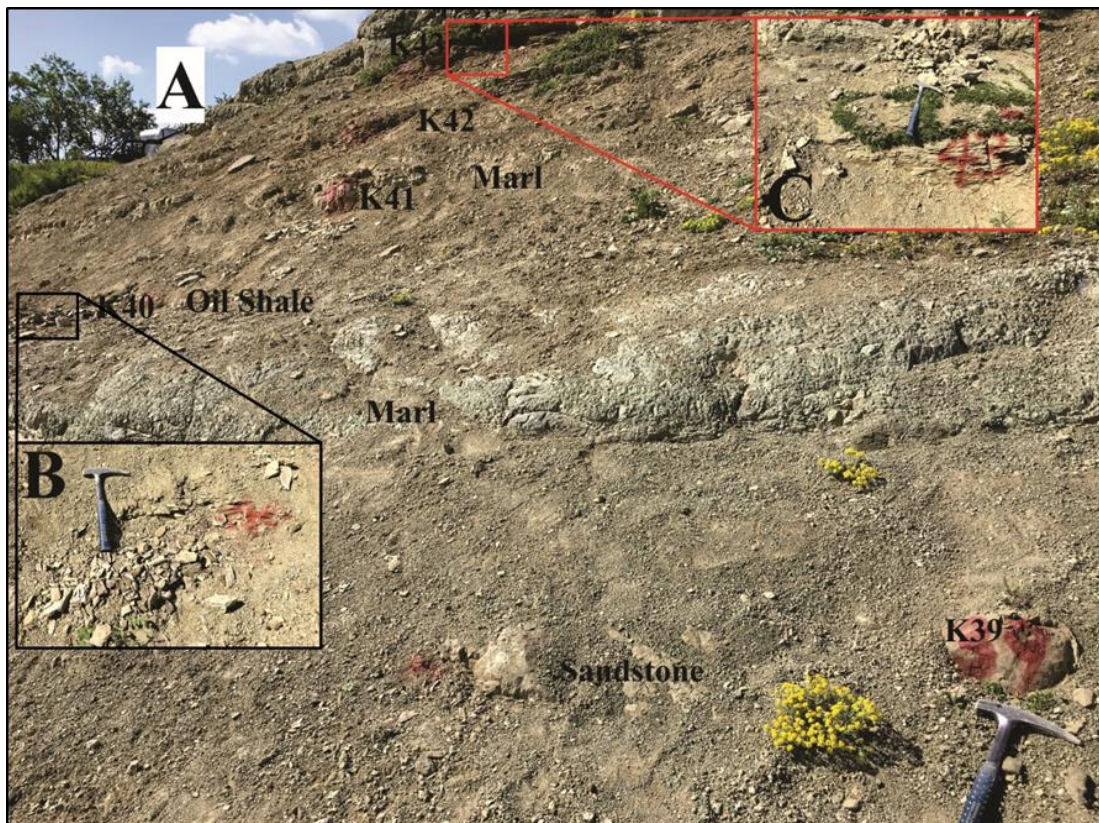


Figure 2.31. The field photograph of Kösiire studied section presenting Sandstone, marl and oil-shale interbeds; B) Close view of oil-shale (sample K40); C); Close view of thin planar bedded sandstone (sample K43).



Figure 2.32. The field photograph of Kösiire studied section presenting A) Fish tooth in Sandstone sample (K39); B) Oil-shale with thin bedded sandstone (Sample K46-K49).

measured section (Gedik and Aksay, 2002; Ocakoğlu et al., 2007 and 2012; Koralay, 2009 and Şafak et al., 2015).

#### 2.3.4. Karahisar Measured Stratigraphic Section

The type locality of the Karahisar measured section is in the vicinity of Karahisar village, Nallıhan. This measured section lies 15km in the southeast of the Dağhacılar measured section. The starting and ending points GPS coordinate of the Karahisar studied section are 40°10' 38.43" N, 31° 5' 22.74" E with 945 meters and 40° 10' 34.15" N, 31° 5' 21.57" E with 929 meters, respectively (Figure 2.33). In the field, a total of 29 samples were selected from the studied section (Figure 2.35).

Three types of lithofacies are observed in the Karahisar measured section which includes lime mudstone, thin to laminated oil-shale and rare sandstone intervals (Figure 2.35). The studied section is predominantly composed of the oil-shale beds (Figures 2.34, 2.35, 2.36 and 2.37). The starting lithology in the measured Karahisar

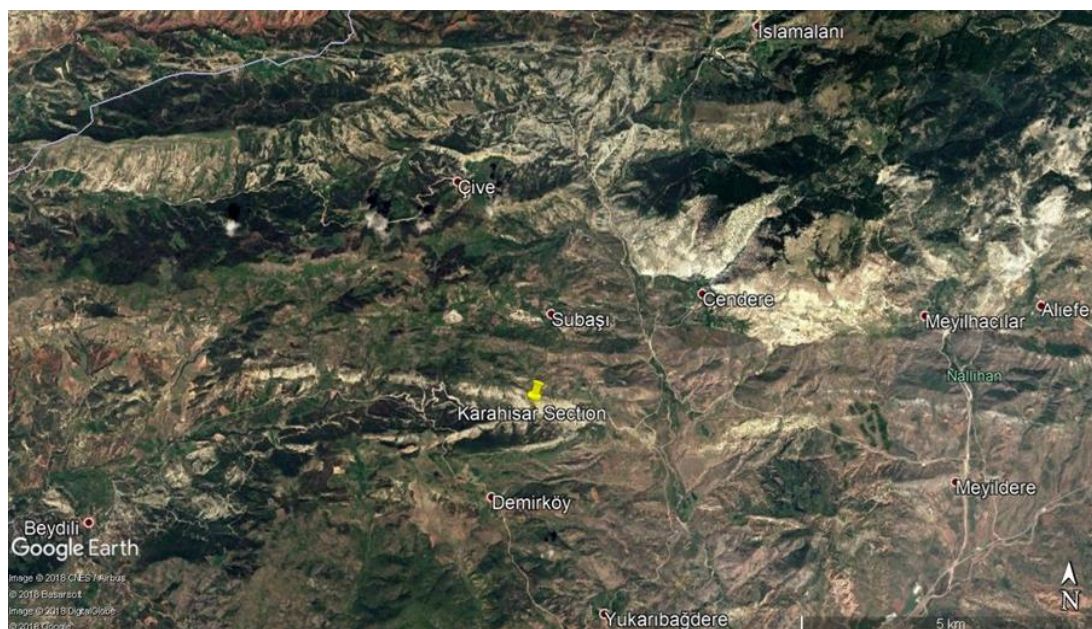


Figure 2.33. Satellite image showing the measured Karahisar studied section in the Mudurnu-Göynük Basin, near Karahisar village (yellow icon represents the studied section).

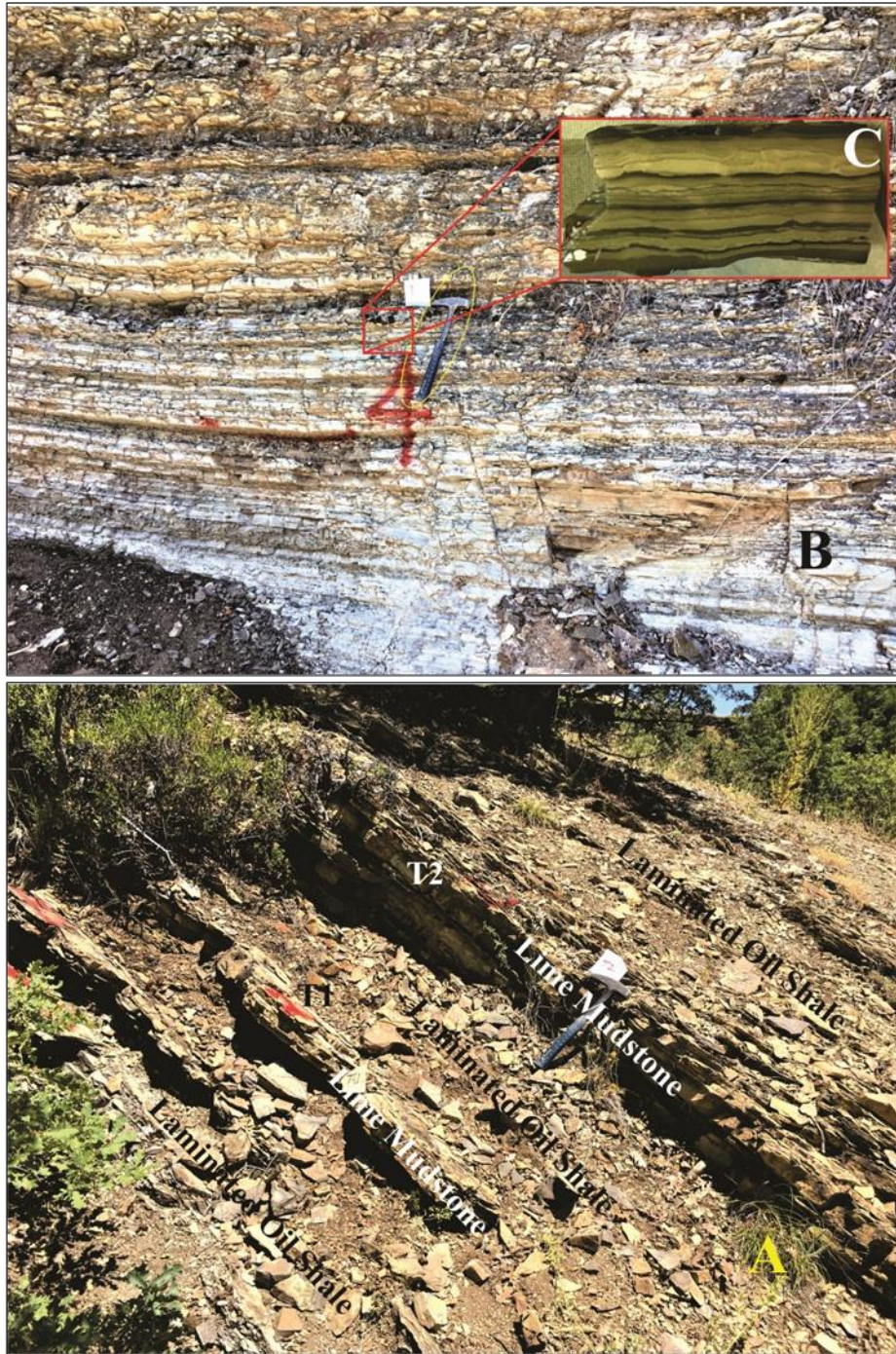


Figure 2.34. Satellite image showing the measured Karahisar studied section in the Mudurnu-Göynük Basin, near Karahisar village (yellow icon represents the studied section).

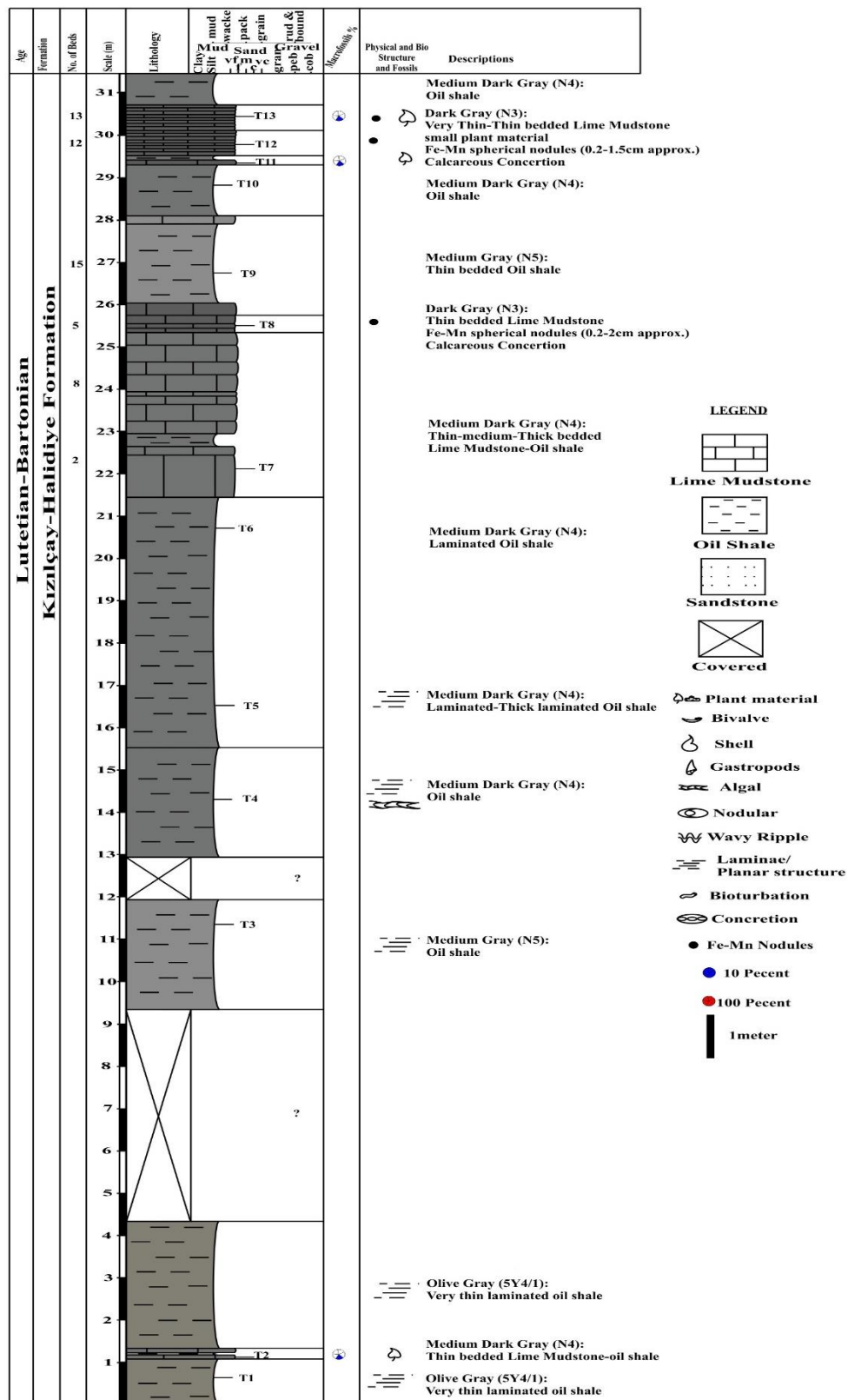


Figure 2.35. Karahisar Measured stratigraphic section, near Karahisar Village (0-31.5m).

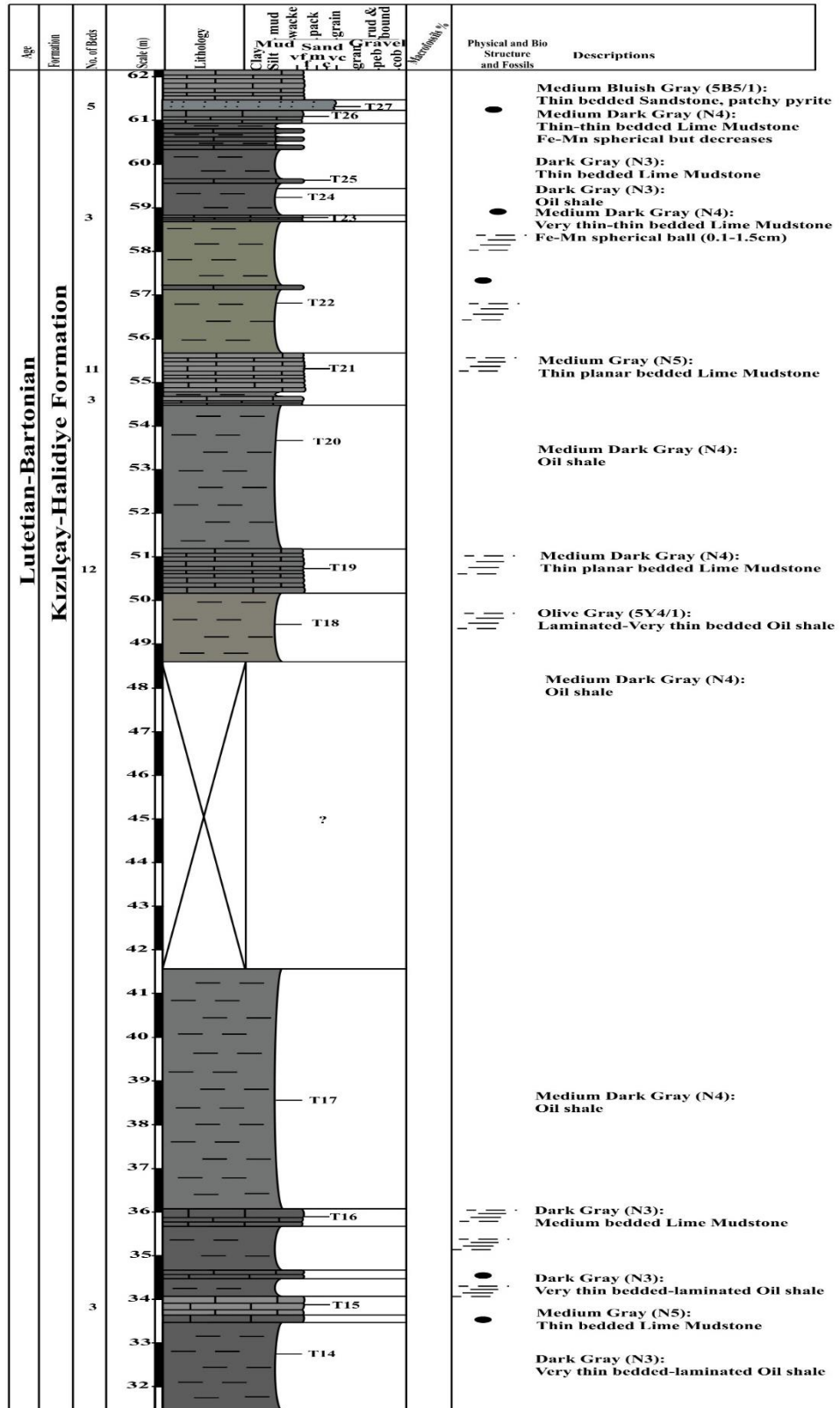


Figure 2.35: Continued (31.5m-62.2m).

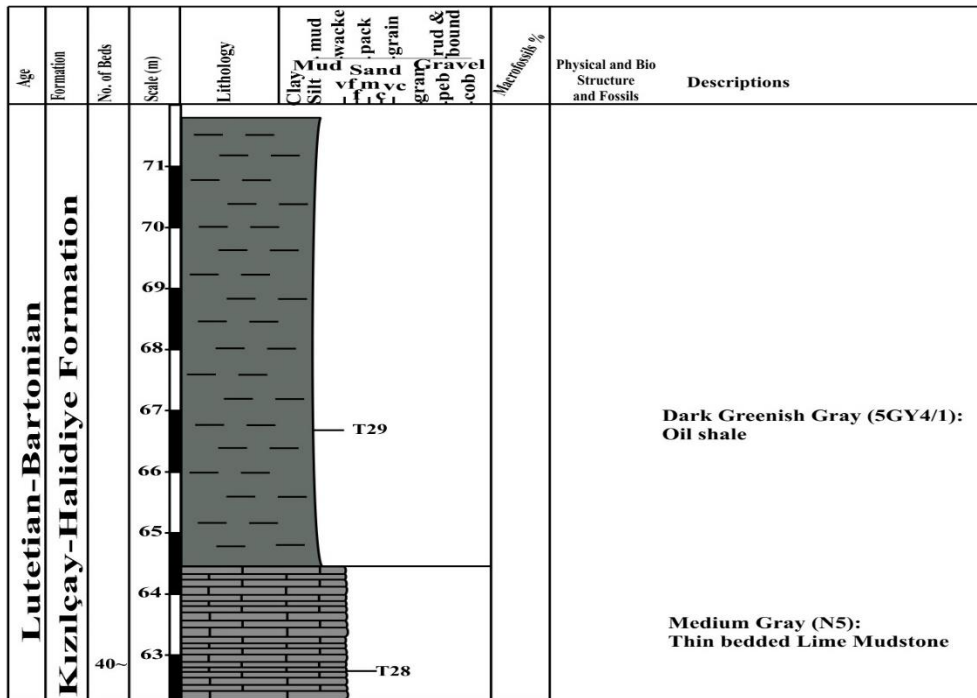


Figure 2.35: Continued (62.2m-72m).

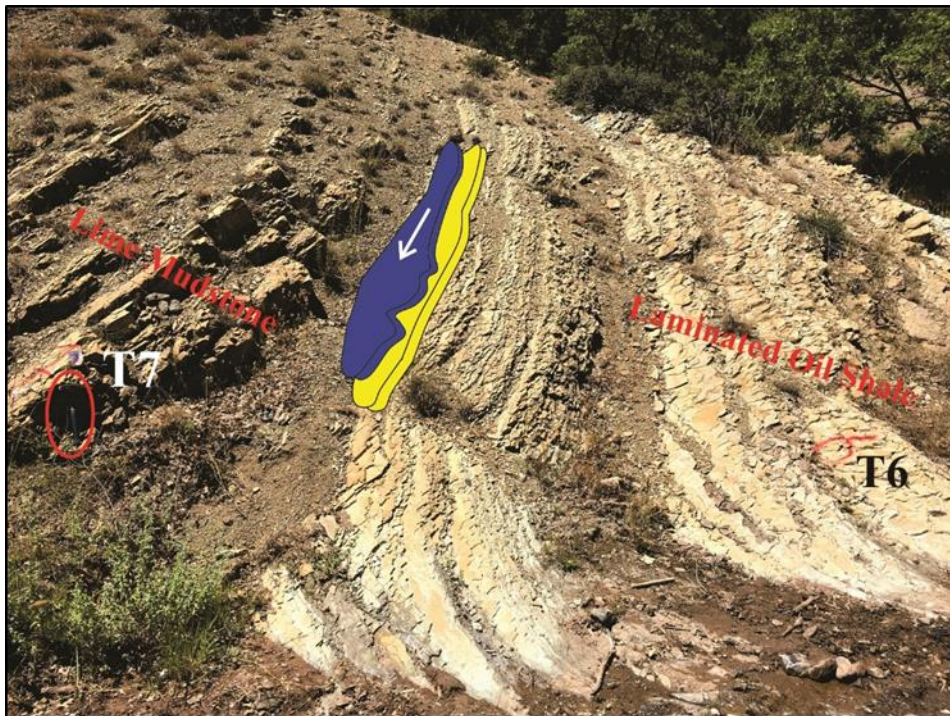


Figure 2.36. The field photograph of Karahisar studied section presenting laminated oil-shale and thin to thin-medium bedded limestone (Sample T6 to T7). (White arrow indicates SW bedding dip direction).

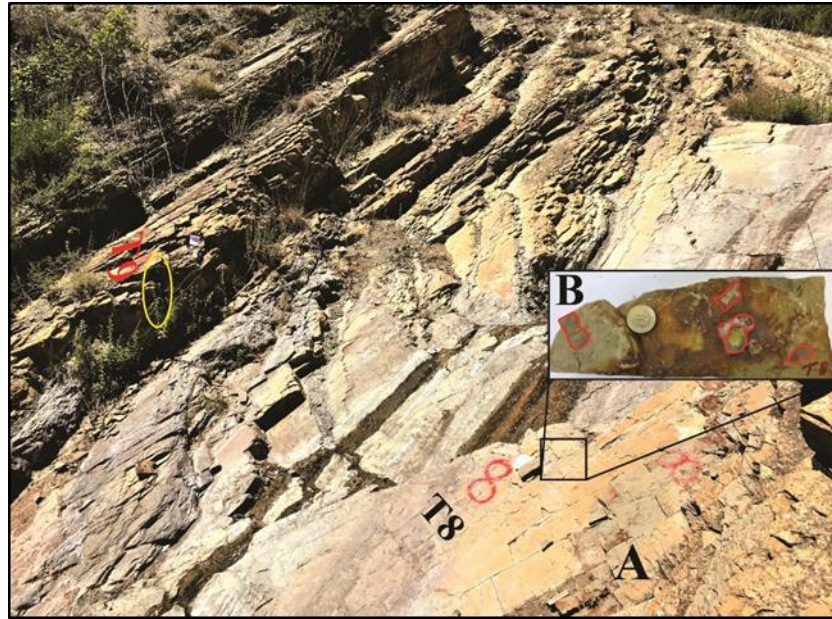


Figure 2.37. The field photograph of Karahisar studied section presenting A) thin planar bedded limestone (Sample T8 and T9); B) Close view of Sample T8 with concretion bedding surface and oxidation.



Figure 2.38. The field photographs of Karahisar studied section representing A) Thin planar bedded limestone with abundant manganese spherical nodules (0.1mm to 2cm) (Sample T12 and T13); B) Close view of Sample T13 and marble size manganese ball; C) Thin section preparation cutting sample T13 and manganese spherical ball are indicated by black arrow.



Figure 2.39. The field photographs of Karahisar studied section representing A) Thin planar bedded limestone with abundant manganese spherical nodules (0.1mm to 2cm) (Sample T12 and T13); B) Close view of Sample T13 and marble size manganese ball; C) Thin section preparation cutting sample T13 and manganese spherical ball are indicated by black arrow.

section is olive gray to medium dark gray thin to laminated to algal laminated bedded oil-shale with rare limestone. These deposits are followed by thin to medium bedded limestone which is dominating with thin bedded oil-shale intervals. The limestone units are characterized by medium dark gray to dark gray, thin to medium planar bedded units with occasional marble-size manganese nodules bearing beds at different intervals. The occurrence of spherical manganese nodules is 0.1mm to 2cm in size (Figures 2.38). At place, the flatten concretion nodules documented on the lime mudstone units in the field (Figure 2.37). In some places, there is an observation of some small size unidentified plant material. Thin bedded medium bluish gray sandstone is observed in the upper portion of the studied section (Figure 2.39B).

The studied Karahisar stratigraphic section deposits are identified as the Middle Eocene. The Lutetian-Bartonian age is confirmed by stratigraphic position of the studied section (Gedik and Aksay, 2002; Ocakoğlu et al., 2007). The assigned age to studied section is support by the Ocakoğlu et al. (2007) and Şafak et al. (2015) recorded *Paleomonsmirabilia nodulosa*, rare *Cyprinotus* sp. and *Heterocypris* sp. of ostracods and *Chara* sp in the studied regime near the Nallıhan and Karahisar village.

### **2.3.5. Sünnet Measured Stratigraphic Section**

Toward the north of the Dağhacılar measured section, another Middle Eocene stratigraphic outcrop is measured for detailed studies. This succession is exposed near the Sünnet village. 40° 23' 49.26" N, 30° 57' 49.47" E with 1143 meter and 40° 23' 50.88" N, 30° 57' 46.44" E with 1155 meter are the GPS coordinate at base and top of the measured column, respectively (Figure 2.40). For detailed studies, 36 samples were collected at different intervals along the measured stratigraphic column (Figures 2.41; 2.42 and 2.43).

The exposed Middle Eocene measured section is comprised of grayish yellow, light brownish gray, pale brown to grayish red, greenish gray to medium dark gray, medium to thick to massive bedded coarser to fine sandstone, greenish gray bioclasts bearing limestone, yellowish gray pebble conglomerate, and grayish red, olive gray, medium

dark gray to dark gray, oil-shale intervals with fossils contain in places and occasional fossiliferous limestone intervals (Figures 2.42; 2.43, 2.44, 2.45, 2.46, 2.47, 2.48, 2.49, 2.50, 2.51). The base of the studied section is introduced by coarse sandstone with sharp contacted conglomeratic interval and then is followed by 18m thick reddish fine sandstone intervals (Figures 2.42; 2.43 and 2.44). The fine sandstone units are overlain by dark gray oil-shale with occasional limestone and thin fossiliferous limestone. The fossiliferous limestone contains bivalve, charophyte algae and gastropods and charcoal fragment (Figures 2.45, 2.50 and 2.51). In the places, the oil-shale units are characterized by fossils such as bivalve and gastropod. Towards the top, after 44 m, the studied section is characterized by sandstone successions with the periodic incursion of approximately 1m massive beds of pebble conglomeratic and calcirudite limestone units (Figures 2.42, 2.47). The measured section is topped by coarser sandstone with pebble-conglomeratic bed intervals (Figure 2.49).

The recorded macrofauna and flora in the studied section are gastropod, bivalve, ostracods, plant materials, charcoal and charophyte gyrogonites (Figures 2.46, 2.47, 2.50 and 2.51). The observed sedimentary structures are sandstone concretion, large scale wavy low angle rippled in sandstone units and load cast at the contact between oil-shale and sandstone units (Figures 2.45, 2.48 and 2.49). Based on the Gedik and Aksay (2002), Ocakoğlu et al. (2007 and 2012) stratigraphic and paleontological studies near the Sünnet village, the measured Sünnet stratigraphic succession is identified as Middle Eocene (Lutetian-Bartonian).

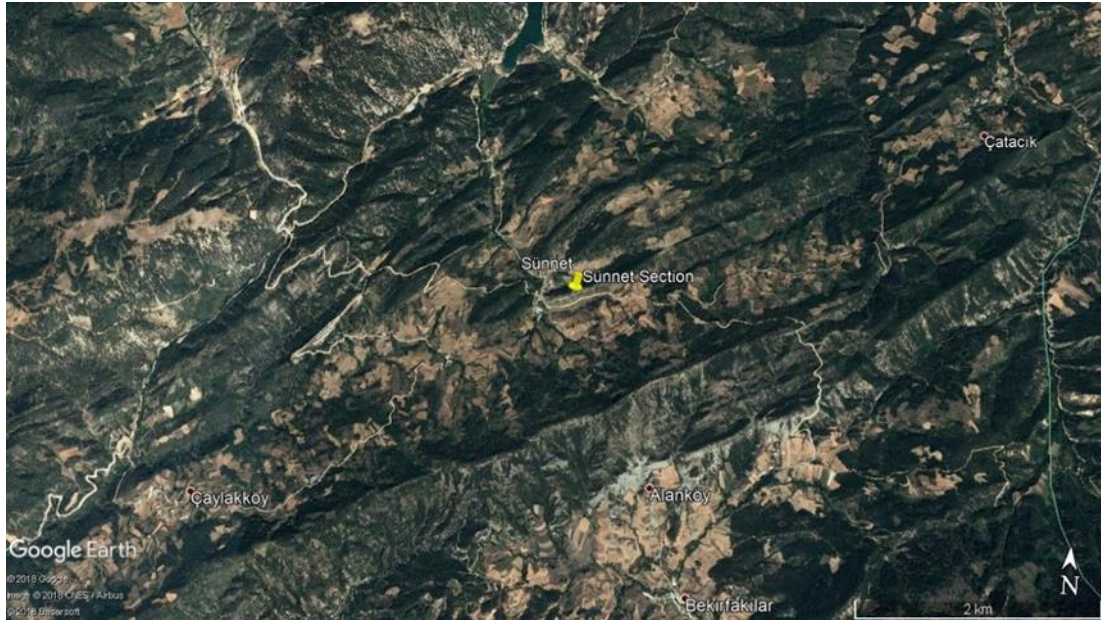


Figure 2.40. Satellite image showing the measured Sünnet studied section in the Mudurnu-Göynük Basin, Sünnet village (yellow icon represents the studied section).

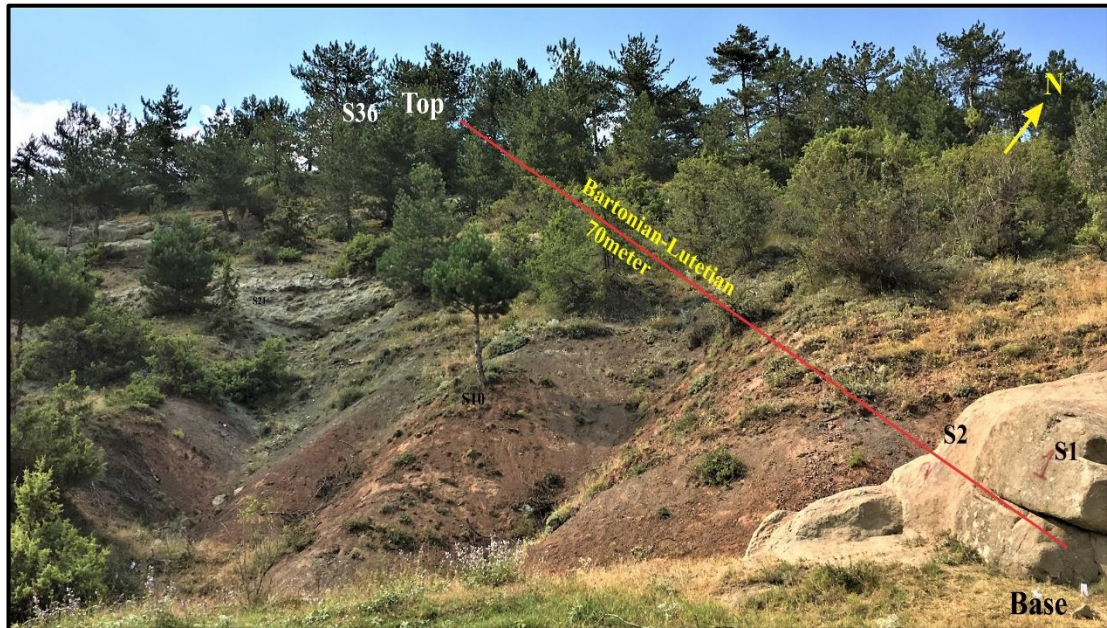


Figure 2.41. The field photograph of 70-meter Lutetian-Bartonian Sünnet measured stratigraphic section, Sünnet village, Bolu. (Sample S1-S36).

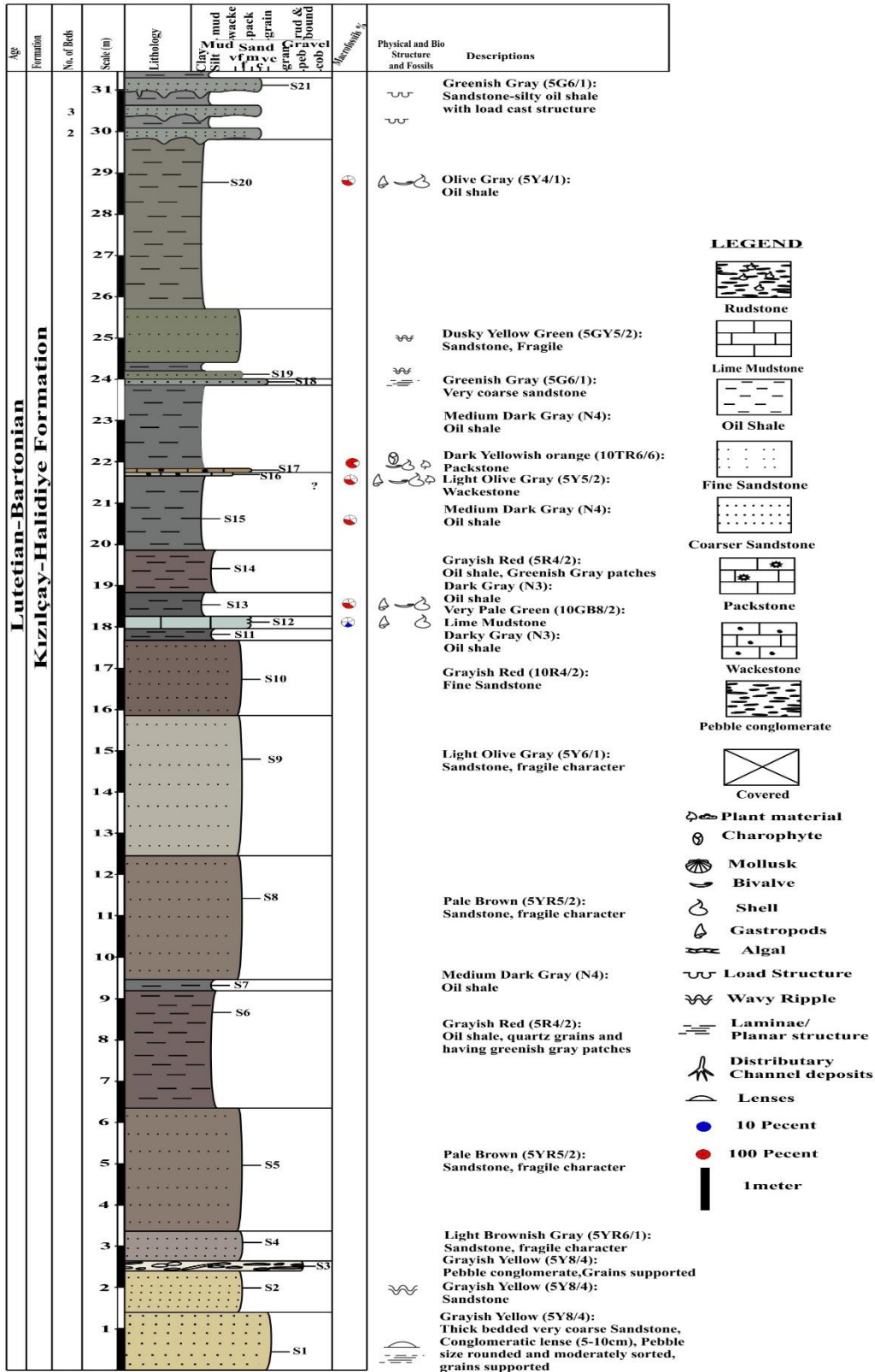


Figure 2.42. Sünnet Measured stratigraphic section, Sünnet Village (0-31.5m).

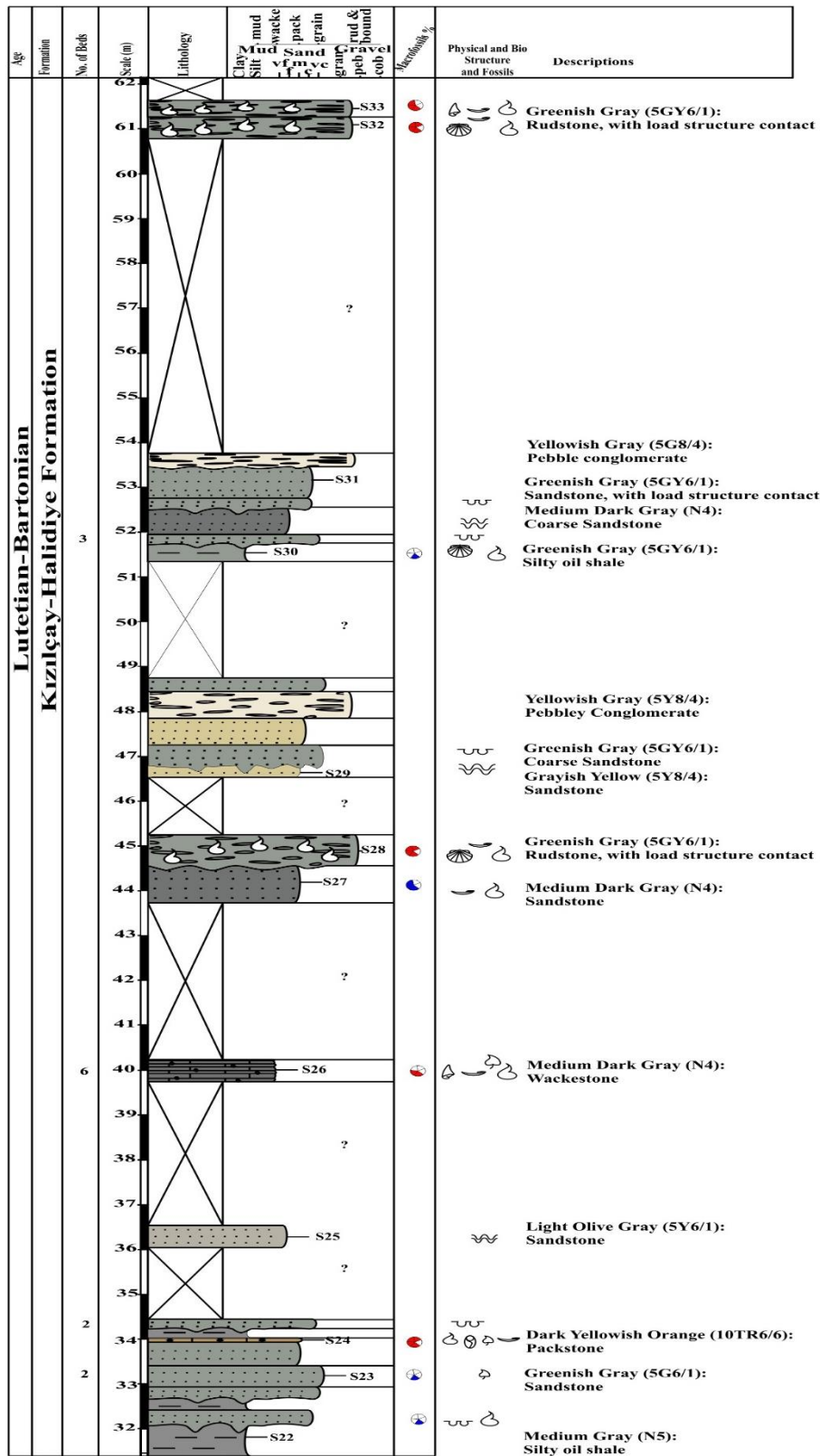


Figure 2.42: Continued (31.5m-62.2m).

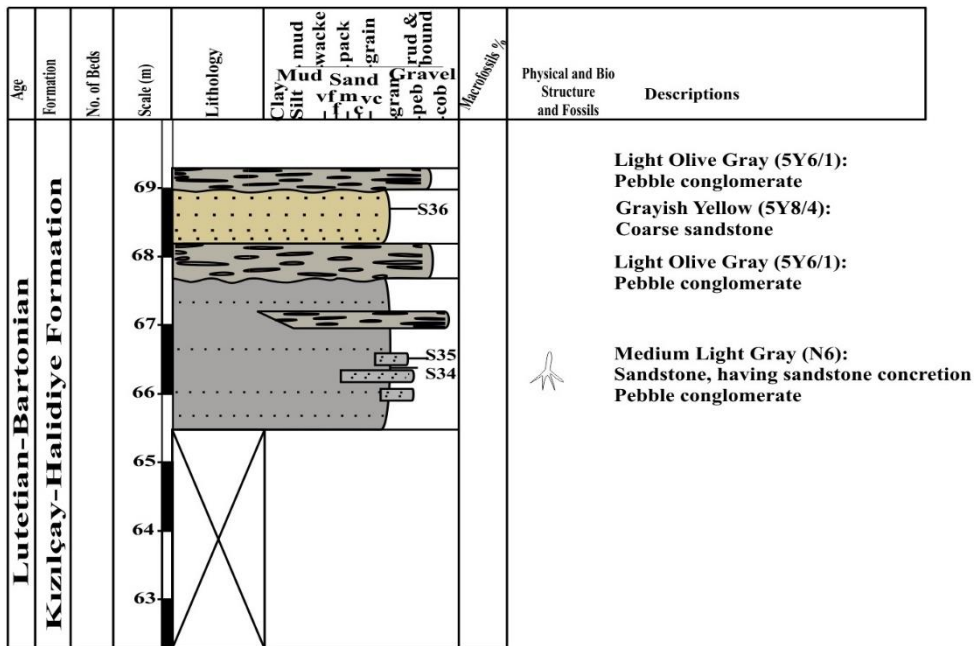


Figure 2.42: Continued (62.2m-70m).



Figure 2.43. The field photograph of Sünnet studied section presenting thick bedded Coarser and Finer Sandstone and sharp contact with pebble conglomerate and above red bedded fragile Sandstone, black arrow indicates lensoidal conglomeratic bed (Sample S1-S5).

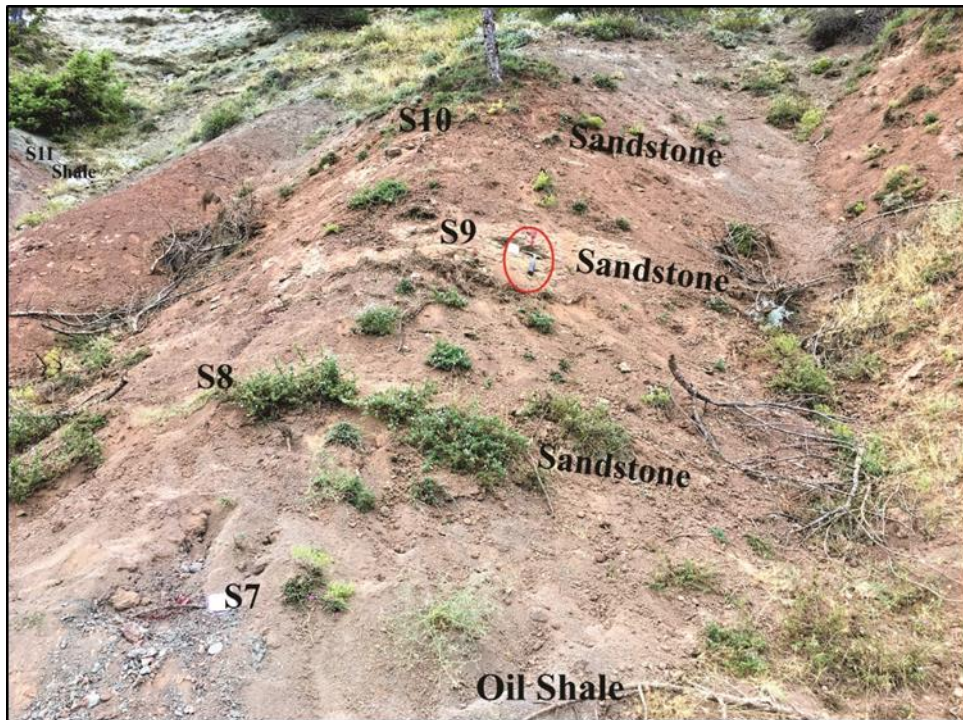


Figure 2.44. The field photograph of Sünnet studied section presenting fragile red sandstone with occasional grayish silty oil-shale (Sample S7-S11).

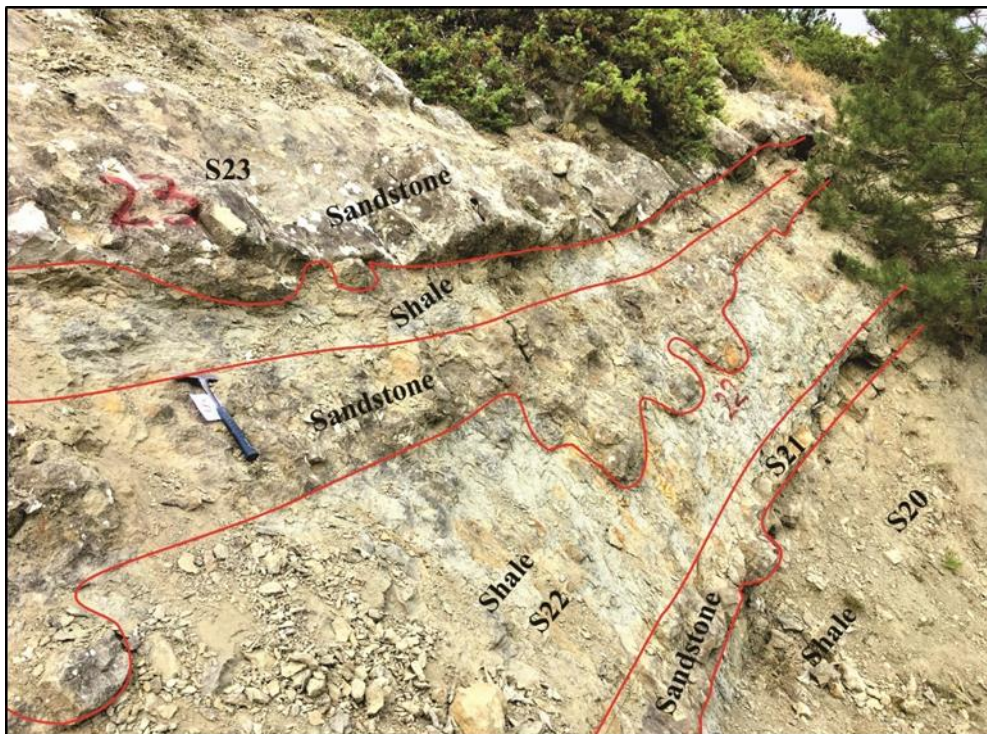


Figure 2.45. The field photograph of Sünnet studied section presenting Sandstone and oil-shale intercalation. The sandstone shows load structure contact with Oil-shale lithofacies (Sample S20-S23).

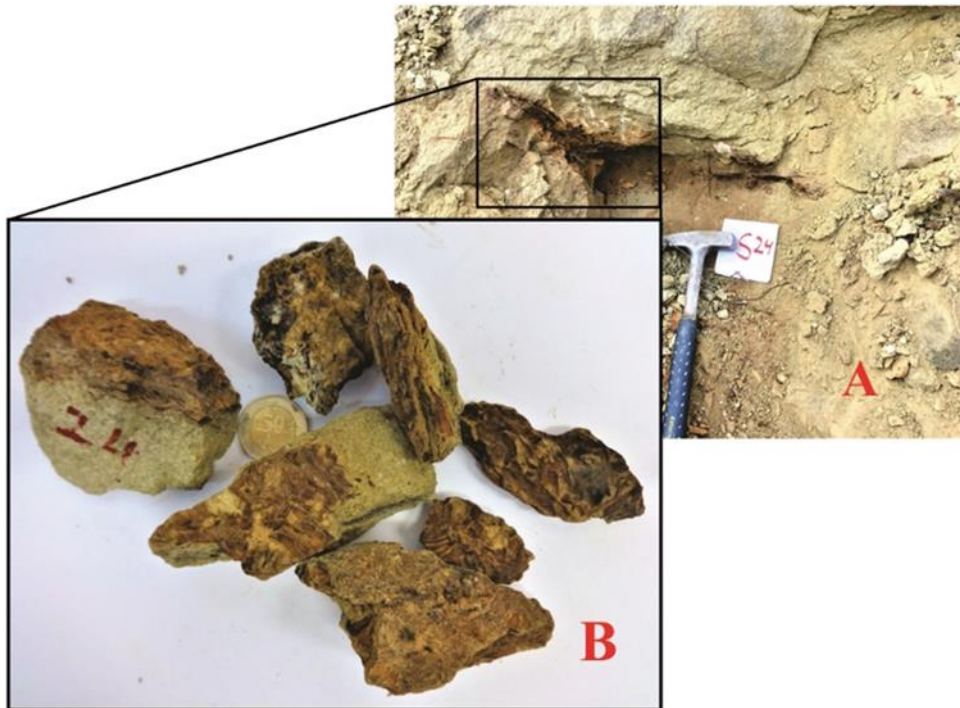


Figure 2.46. The field photograph of Sünnet studied section presenting; A) 4cm thin yellowish orange abundant charophytes bearing packstone interval with plant materials/charcoal (Sample 24); B) Close view of the collected sample.

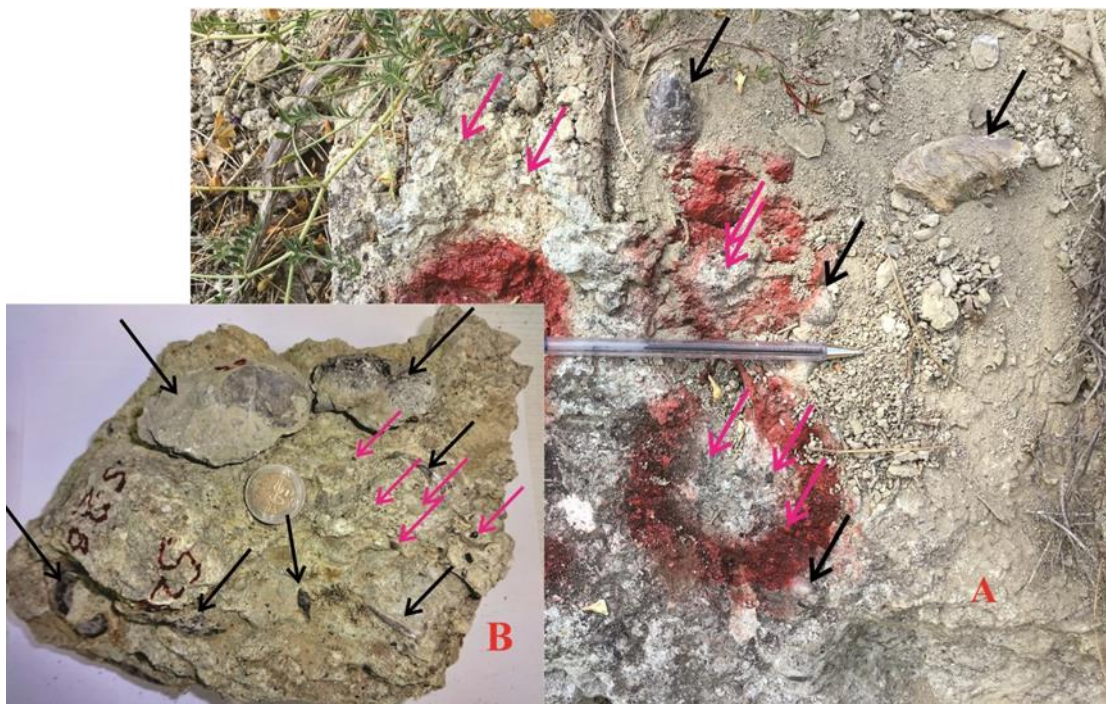


Figure 2.47. The field photograph of Sünnet studied section presenting; A) thick bedded bioclastic limestone (Rudstone/ calcirudite) (Sample S28); B) Close view of the collected sample. (black arrows indicate fossil clasts and pink arrows indicate siliciclastic grains).

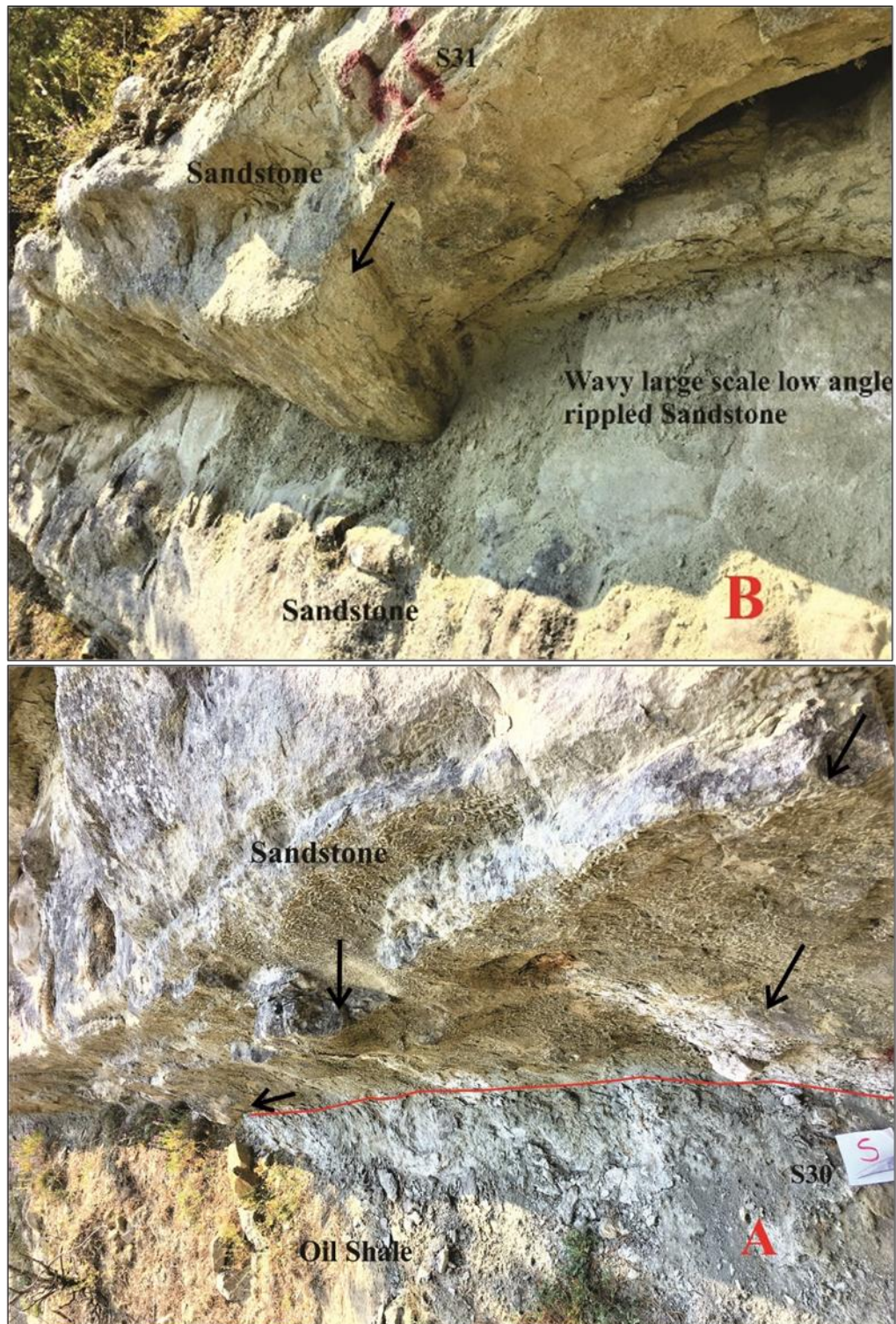


Figure 2.48. The field photograph of Sünnet studied section presenting; A) red line indicates sharp contact between oil-shale and sandstone, the black arrows indicate load structures; B) Large scale low angle rippled fine sandstone overlain by coarser sandstone. (black arrows indicate flute structure).

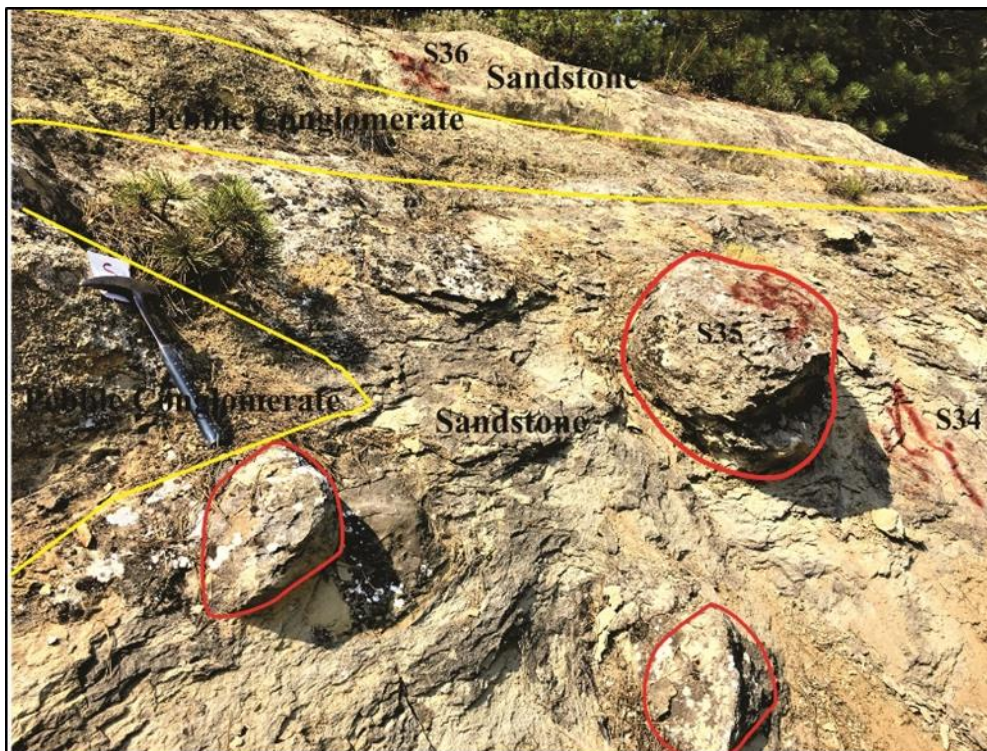
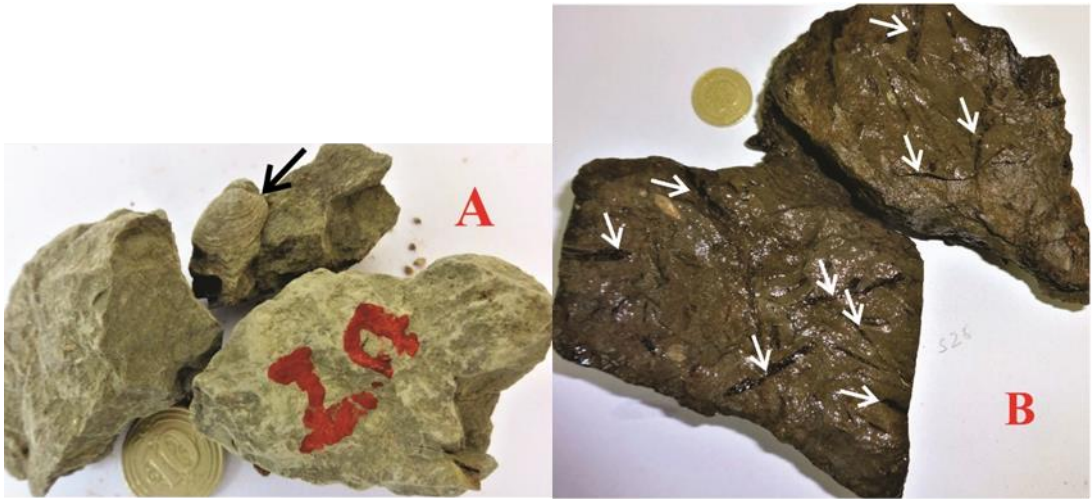


Figure 2.49. The field photograph of Sünnet studied section presenting sandstone with sandstone concretion (shown by red lines) and pebble conglomerate.



Figure 2.50. The field photograph of Sünnet studied section presenting; A) Fossiliferous oil-shale (black arrows show bivalve clast and yellow shows gastropod clast) (Sample S13); B) Fossiliferous packstone interval with charcoal fragment, shown by yellow arrows and white dots in the yellow rectangle indicates Charophytes (Sample S17).



*Figure 2.51. The field photograph of Sünnet studied section presenting; A) Fossiliferous oil-shale (black arrows show bivalve clast) (Sample S20); B) Fossiliferous wackestone interval with a charcoal fragment, shown by white arrows (Sample S26).*



## CHAPTER 3

### SEDIMENTOLOGY

#### 3.1. Sedimentological Studies

The five stratigraphic sections from the Middle Eocene (Lutetian-Bartonian age) successions have been measured in the Bolu province at different localities. The measured stratigraphic sections are the Dağhacılar, Hasanlar, Köşüre, Karahisar and Sünnet sections, and are identified as the Kızılçay Formation and Halidiye Formation. The sedimentological analysis is carried out to identify microfacies and their depositional environment in the Mudurnu-Göynük basin, based on the field observation and microscopic studies.

Based on textural and grain-size studied in the field, mineralogical composition, fabrics and petrographic analyses, various facies are identified in the five measured studied sections. The identified facies are limestone, oil-shale, marl and sandstone in the studied sections. The other facies, pebble conglomerate and bio-calcirudite (rudstone) facies, are only observed in the Sünnet Section. The petrographic analyses of the studied sections allow the identification of microfacies in the measured stratigraphic sections which are described below.

The division and identification of lithofacies are mainly based on the grain-size, mineral composition, organic matter content and physical sedimentary structures. Different types of classification are used to describe and classify lithofacies in the studied sections, based on the lithofacies type, which are Folk's classification (1965), Embry and Klovan's classification (1971), Pettijohn et al.'s classification (1987), Stow's classification (2005), Allix et al.'s (2010) and Diaz et al.'s (2012) classifications (Figures 3.1, 3.2 and 3.3; Table 3.1).



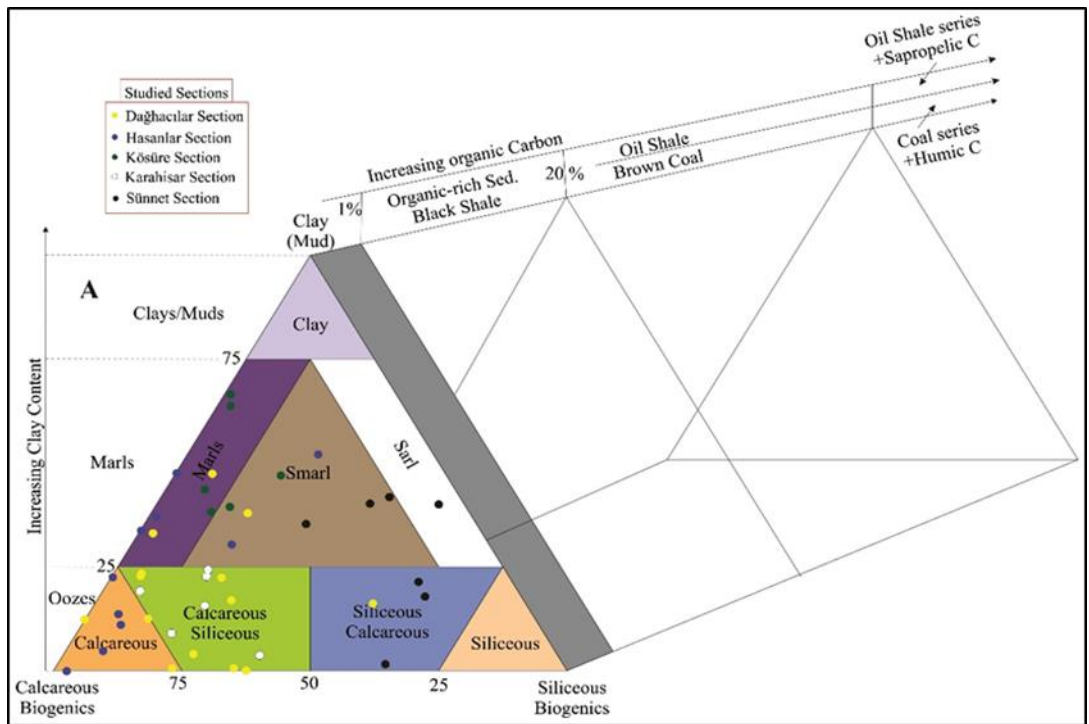


Figure 3.2. Stow's compositional classification (2005) ternary diagram based on biogenic (carbonate and silica) and mud/clays: the representative symbol of the studied sections are shown in the red box.

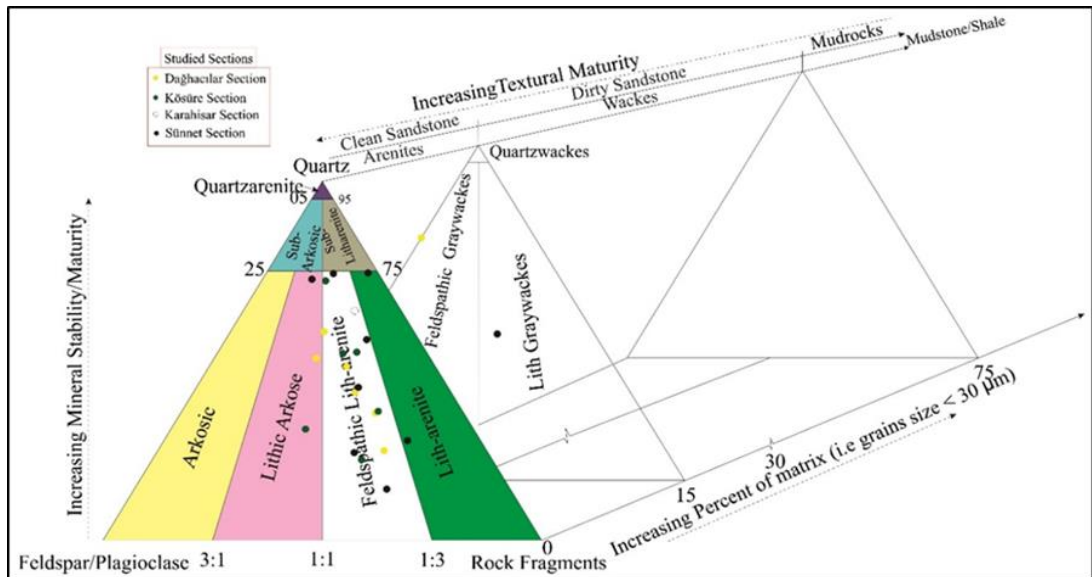


Figure 3.3. The Folk's (1974) Sandstone classification ternary diagram based on relative proportions of grains size and presence of matrix. The representative symbol of the studied samples are shown in the red box.

Table 3.1. Folk's (1965) texture classification of fine-grained sedimentary rock.\*

<b>Mud-rock division based upon texture and structure</b>			
<b>Grain size of mud fraction</b>	<b>Soft</b>	<b>Indurated, Non-fissile</b>	<b>Indurated, Fissile</b>
>66 % Silt	Silt	Siltstone	Silt-Shale
33-66 % (Sub-equal silt and clay)	Mud	Mudstone	Mud-Shale
>66 % Clay	Clay	Claystone	Clay-Shale

### **3.2. Microfacies of Dağhacılar Section**

A total of 4 microfacies are identified in the Dağhacılar Section along the measured sections (Tables 3.2, 3.3 and 3.4: Figure 2.7).

#### **3.2.1. Limestone Facies**

In the Dağhacılar studied section, the limestone facies is present dominantly in the lower portion of the stratigraphic section (Figure 2.7). The facies is examined in the field and analyzed under microscope in order to recognize microfacies and paleontological character in the facies. Limestone facies is further divided into three sub-microfacies based on microscopic features. The limestone facies are identified and classified by using Embry and Klovan's (1971) classification. The sub-facies are described as below (Tables 3.2 and 3.4);

##### **3.2.1.1. Lime Mudstone Microfacies (DA1)**

In the field, the lime mudstone appeared as olive gray to yellowish gray to medium dark gray, light greenish gray, thin to thick bedded limestone units (Figures 2.7 and 3.4). Microscopically, it is composed of allochem less than 10 percent includes bioclasts, quartz which are embedded in the predominantly micrite matrix (Tables 3.2 and 3.4; Figure 3.5a, b, c and d). The documented bioclasts in the samples are ostracods, gastropods and hardly charophytes (Figure 3.5a). The other identified grains in the microfacies are pyrite in the form of euhedral within the matrix and randomly

Table 3.2. Limestone, oil-shale and marl petrographic data and established/recognized facies in the Dağhacılar studied section.

Sample No.	Q	F	Pg	Om	Pl	Pi	In	Bioclasts (Os/Ch/GUb/Al/Da/N/Br)	Other (P/He/Ph/Cr/Ce/Ct)	Matrix (Mi/Cl/Sp/Or D/Cr)	Field Nomenclature
D3	2	-	-	2	-	-	-	20s/1Ch=3	5P	88Mi	Limestone
D4	-	-	-	-	-	-	-	39Os/2G=41	-	59Mi	Bio- Limestone
D6	5	-	-	-	-	-	-	200s	5P/1Ph=6	69Mi	Bio- Limestone
D10	-	-	-	5	-	-	-	53Os/1N=54	6P	35Mi+Or	Oil-shale
D11	3	-	-	4	-	-	-	53Os/3G/2Bi=58	3P/1Ph=4	31Mi+sp	Bio- Limestone
D14	-	-	-	10	-	5	-	35Os/5Bi=40	10P	35Mi	Bio- Limestone
D15	-	-	-	2	-	-	-	35Os/5Bi/2Ch=42	5P	51Mi+D	Bio- Limestone
D17	-	-	-	4	-	-	-	50s/10Ub/5Ch=20	20P	56Mi+Or	Bio- Limestone
D18	-	-	-	-	-	-	-	20s	20P	78Mi	Limestone
D19	-	-	-	2	-	-	-	40G/10Os/5Ub=55	3P	40Mi+Sp	Bio- Limestone
D21	2	-	-	-	-	-	-	-	15P/1Ph=16	82Mi	Marl
D23	2	-	-	-	-	-	-	15Bi	3P	80Mi+D	Bio- Limestone
D25	5	-	-	-	-	-	-	30s	2P	90Mi+Sp	Marl
D27	-	-	-	3	-	14	10	20s/4Ub=6	3P	64Mi	Bio- Limestone
D28	3	-	-	-	-	35	-	-	3Ce	59Mi+Or	Oil-shale
D29	10	-	1	-	-	-	-	-	3P	86Mi	Limestone
D30	2	-	-	3	1	-	-	50Os/3Ub=53	3P	38Mi	Bio- Limestone
D33	5	-	-	1	-	3	-	4Ub=4	2P	85Mi	Limestone
D35	15	-	-	3	-	-	-	-	15P	67Cl+Or	Oil-shale
D36	30	-	-	5	-	-	-	50s	25P	35Mi+Or	Oil-shale
D38	20	-	-	-	-	-	-	-	10P	70Mi+sp+Or	Oil-shale
D40	30	-	-	5	-	-	-	-	6Ct	59Mi+Or	Oil-shale
D41	17	-	1	-	-	-	-	-	2P	80Mi+Or	Oil-shale
D42											Sandstone
D45	15	-	-	1	-	-	-	-	6P	78Mi	Marl
D49											Sandstone
D52	5	-	-	2		-	-	-	-	93Mi+Or	Oil-shale
D53											Sandstone
D59	10	-	1	4		15	-	-	-	70Mi+Or	Oil-shale
D63											Sandstone
D68											Sandstone
D69	25	-	1	3		-	-	-	-	71Mi+Or	Oil-shale
D73	40	-	-	2		-	-	-	5P/3Cr=8	35Mi+15Cr	Marl
D74											Sandstone
D76											Sandstone

Os-Ostracoda, Ch-Charopyta, G-Gastropod, Al-Algal, Da-Diatoms, N-Nummulite, Pl-Plant, Fr-Foraminifera, Py-Palynofacies, Ub-Unidentified Bioclasts, Q-Quartz, Qp-Polyquartz, Cr-Chlorite, Ct-Calcite, Mu-Muscovite, Mn-Manganese, P-Pyrite, Ce-Chert, F-Feldspar, Pg-Plagioclase, Sf-Shale fragment, Srf-Siltstone Fragment, Lf-Limestone fragment, Bo-Biotite, T-Tourmaline, Pi-Peloid, In-Intraclasts, R-Rutile, Z-Zircon, Sp-Sparite, Mi-Micrite, D-Dolomite, Cl-Clay, Or-Organic Rich, Om-Organic matter/Bitumen, He-Hematite, Ph-Phosphate, Se-Sphene, Si-silica

Table 3.3. Sandstone petrographic data and established/recognized facies in the Dağhacılar studied section.

Sample No.	Q	F	Pg	Om	Accessory Minerals	Rock Fragment	Bioclasts (Os/Ch/G/Ub/Al/Da/N/Br)	Other (P/He/Ph/Cr/Ce/Ct)	Matrix (Mi/Cl/Sp/Or D/Cr)	Field Nomenclature
D42	28	13	3	5	4.7Cr/0.2Bo/0.1T=5	5Pq/5Ce/5Srf/5Sl/15Lf=35	-	5He	6Sp	Fine Sandstone
D49	28	15	-	3	1.8Cr/0.1T/0.1R=2	2Pq/3Ce/2Be/10L/6Sf/2Srf=25	-	-	24sp+3Cr	Very Fine Sandstone
D53	31	10	3	-	4.8Cr/1Bo/0.1T/1Mu/0.1R=7	5Pq/13L/2Ce=20	2Ub	-	20Sp+7Cr	Medium Sandstone
D63	32	10	2	3	3.9Cr/0.1Bo=4	-	-	5P	40Mi+4Cr	Fine Sandstone
D68	40	10	5	3	0.1T/0.2Bo/4.6Cr/0.1R/1Mu=6	7L/5Sf=12	0.5Fr/0.5N=1	5P	13Mi+5Cr	Fine Sandstone
D74	32	15	3	6	7Cr/1Bo/1Mu=9	5Ce/4Pq/10Sf=19	0.5Fr/0.5N=1	2P	13Sp	Very Fine Sandstone
D76	17	15	1	7	4.8Cr/0.2T/0.5Bo/0.5Mu=6	11Pq/5Sf/10Ce/10L=36	2N/0.5Fr/0.5Be/2Ub=5	2P	11Sp	Coarse Sandstone

Os-Ostracoda, Ch-Charopyta, G-Gastropod, Br-Brachiopod, Al-Algal, Da-Diatoms, N-Nummulite, Pl-Plant, Fr-Foraminifera, Py-Palynofacies, Ub-Unidentified Bioclasts, Q-Quartz, Qp-Polyquartz, Cr-Chlorite, Ct-Calcite, Mu-Muscovite, Mn-Manganese, P-Pyrite, Ce-Chert, F-Feldspar, Pg-Plagioclase, Sf-Shale fragment, Srf-Siltstone Fragment, Lf-Limestone fragment, Bo-Biotite, T-Tourmaline, Pi-Peloid, In-Intraclasts, R-Rutile, Z-Zircon, Sp-Sparite, Mi-Micrite, D-Dolomite, Cl-Clay, Or-Organic Rich, Om-Organic matter/Bitumen, He-Hematite, Ph-Phosphate, Se-Sphene

Table 3.4. Classifications of the limestone, oil-shale, marl and sandstone and established/recognized microfacies in the Dağhacılar studied section.

Sample No.	Compositional Classification of shale and marl			Texture Classification*	Limestone Classification (Embry and Klovan's 1971)	Sandstone Classification (Folk's 1974)	Defined Facies in Studied Section
	Diaz's (2012) Mudstone (Unconventional)	Stow's (2005)	Allix's (2010) Shale	Fine Grained Rock Folk's (1965)			
D3					Lime Mudstone		Lime Mudstone
D4					Bio-Wackestone		Wackestone
D6					Bio-Wackestone		Wackestone
D10	Carbonate-Dominated Lithotype	Calcareous	Calcareous Mudstone	Silt-Shale			Oil-shale
D11					Bio-Packstone		Packstone
D14					Bio-Wackestone		Wackestone
D15					Bio-Wackestone		Wackestone
D17					Bio-Wackestone		Wackestone
D18					Pyritic Lime Mudstone		Lime Mudstone
D19					Bio-Packstone		Packstone
D21	Clay-rich Carbonate Mudstone	Marl	Argillaceous Marlstone	Mud-Shale			Marl
D23					Bio-Wackestone,		Wackestone
D25	Clay-rich Carbonate Mudstone	Calcareous-Siliceous	Calcareous Mudstone	Clay-Shale			Marl
D27							Wackestone
D28	Argillaceous/Carbonate Mudstone (Marl)	Marl	Argillaceous Marlstone	Mud-Shale			Oil-shale
D29					Extra- Lime Mudstone		Lime Mudstone
D30					Bio-Wackestone		Wackestone
D33					Lime Mudstone		Lime Mudstone
D35	Silica-rich dominated Mudstone	Calcareous	Calcareous Mudstone	Clay-Shale			Oil-shale
D36	Silica-rich dominated Mudstone	Calcareous-Siliceous	Siliceous Marlstone	Silt-Shale			Oil-shale
D38	Silica-rich dominated Mudstone	Calcareous-Siliceous	Calcareous Mudstone	Clay-Shale			Oil-shale
D40	Silica-rich dominated Mudstone	Calcareous-Siliceous	Siliceous Marlstone	Mud-Shale			Oil-shale
D41	Mixed Carbonate Mudstone	Calcareous-Siliceous	Argillaceous Marlstone	Clay-Shale			Oil-shale
D42						Feldspathic litharenite	Sandstone
D45	Argillaceous/Carbonate Mudstone (Marl)	Smarl	Argillaceous Marlstone	Mud-Shale			Marl
D49						Feldspathic litharenite	Sandstone
D52	Clay-rich Carbonate Mudstone	Calcareous	Calcareous Mudstone	Clay-Shale			Oil-shale
D53						Feldspathic litharenite	Sandstone
D59	Mixed Carbonate Mudstone	Calcareous-Siliceous	Calcareous Mudstone	Clay-Shale			Oil-shale
D63						Feldspathic graywackes	Sandstone
D68						Lithic arkose	Sandstone
D69	Mixed Carbonate Mudstone	Calcareous-Siliceous	Siliceous Marlstone	Mud-Shale			Oil-shale
D73	Mixed Siliceous Mudstone	Siliceous-Calcareous	Siliceous Mudstone	Silt-Shale			Marl
D74						Feldspathic litharenite	Sandstone
D76						Feldspathic litharenite	Sandstone

\* Based on grains size of mud fraction, non-fissile/fissile and soft.

Table 3. 4: Continue....

Sample No.	(Texture and/or Compositional)	Defined Facies in Studied Section
D3	More than 90% Matrix	Lime Mudstone
D4	Bioclastic and Matrix	Wackestone
D6	Bioclastic and Matrix, Pyrite in the matrix as well as in Bioclast	Wackestone
D10	Bioclastic and Organic-rich, Calcareous-rich	Oil-shale
D11	Bioclastic-rich (>60%) and Matrix	Packstone
D14	Bioclastic and Matrix, Organic-rich matrix	Wackestone
D15	Bioclastic and Matrix, and Patchy dolomitic appearance	Wackestone
D17	Bioclastic and Matrix, Organic-rich matrix	Wackestone
D18	Pyritic-rich matrix	Lime Mudstone
D19	Bioclastic-rich (>60%) and Matrix	Packstone
D21	Lime Mud	Marl
D23	Bioclastic and Matrix, Patchy dolomite	Wackestone
D25	Patchy sparite	Marl
D27	Intra-clasts, Peloidal and Matrix, Patchy dolomite, Organic-rich staining	Wackestone
D28	Thick Laminated, Organic-rich laminae, Fecal pellet-rich and Chert Nodules, Calcareous-rich	Oil-shale
D29	Silt-size quartz, subangular	Lime Mudstone
D30	Bioclastic and Matrix, Plant fossil	Wackestone
D33	Silt to sand-size quartz, subangular, Matrix (>90%)	Lime Mudstone
D35	Algal Laminated, Organic-rich and Calcareous-rich	Oil-shale
D36	Laminated, Organic-rich and Calcareous-rich, Pyrite in matrix and bioclasts	Oil-shale
D38	Laminated, Calcareous-rich and silt-size Quartz	Oil-shale
D40	Laminated, silt-size Quartz bearing Organic-rich and Calcareous-rich laminae	Oil-shale
D41	Laminated, silt-size quartz-bearing Organic-rich and Calcareous-rich laminae	Oil-shale
D42	Fine Sand-size, well sorted, closely packed	Sandstone
D45	Silt-size Quartz and Lime Mud	Marl
D49	Very fine sand-size moderated sorted, loosely packed,	Sandstone
D52	Laminated, organic-rich and calcareous rich laminae with silt-size quartz	Oil-shale
D53	Medium sand-size, well sorted, loosely packed	Sandstone
D59	Laminated, Organic-rich and Calcareous-rich with fecal pellet and silt-size quartz	Oil-shale
D63	Fine sand-size, well sorted, Loosely Packed	Sandstone
D68	Fine sand-size, Moderated sorted, Loosely packed,	Sandstone
D69	Laminated, Organic-rich and Calcareous rich laminae with silt to very fine sand-size quartz	Oil-shale
D73	Silt-size quartz and Lime Mud	Marl
D74	Very Fine Sand, Charcoal, Oil Stained, closely packed, moderately sorted	Sandstone
D76	Coarse sand-size, Marine fossil, poorly sorted, closely packed, Charcoal	Sandstone



Figure 3.4. The field photograph of Lime Mudstone microfacies in the Dağhacılar measured stratigraphic section; a) Sample D3 and b) Sample D18 (Scale: Hammer).

distributed (Figure 3.5c). The quartz grains are silt to very fine sand-size with sub-angular to rounded in the matrix (Figure 3.5a and d). According to the Embry and Klovan's classification (1971), this facies is identified as lime mudstone facies. The lime mudstone microfacies is categorized as LMF 6 of Flügel's (2004) LMF model.

### **3.2.1.2. Interpretation (DA1)**

The Lime Mudstone Microfacies is characterized by the predominance of lime mud as a matrix with less than 10% bioclastic debris. This microfacies reflects low energy environmental condition. In the studied section, lime mudstone texture and having few ostracods, gastropods and charophytes indicate low energy, relatively deeper lacustrine deposits (Willmann, 1985; Czaja et al, 2014). The lack of clastic particles in the lithofacies suggests clastic influx restricted during deposition of lime mudstone. The high organic content, the presence of few biota and the absence of bioturbation indicate dysoxic to the anoxic sublittoral lacustrine depositional environment (Gingras et al., 2011 and Amezcua, 2012). The low diversity of biota with the association of abundant micritic texture also indicates relatively deeper lacustrine environments (Anan, 2014).

### **3.2.1.3. Wackestone Microfacies (DA2a)**

The wackestone microfacies observed in the outcrop as pale yellowish gray to very pale orange, medium gray to a medium dark gray color with thin to thick bedded intervals (Figures 2.7 and 3.6). The wackestone microfacies name is given on basis of Embry and Klovan's classification (1971). As it is composed of >10 % and <60% percent allochem in the microfacies (Tables 3.2 and 3.4). The observed allochems in the wackestone microfacies are microfossils, macrofossils with subordinate quartz, randomly distributed framboidal pyrite and solid organic matter (Figures 3.5e, f; 3.6b; 3.7a, b, c). In some samples, there is the presence of intra-clasts and peloids allochems. The identified fossils in the microfacies are ostracods, gastropods, charophytes, phytoclasts and unidentified bioclasts (Figures 3.5e, f; 3.6b; 3.7b, c). There is also documentation of organic matter and sparite development within the matrix.

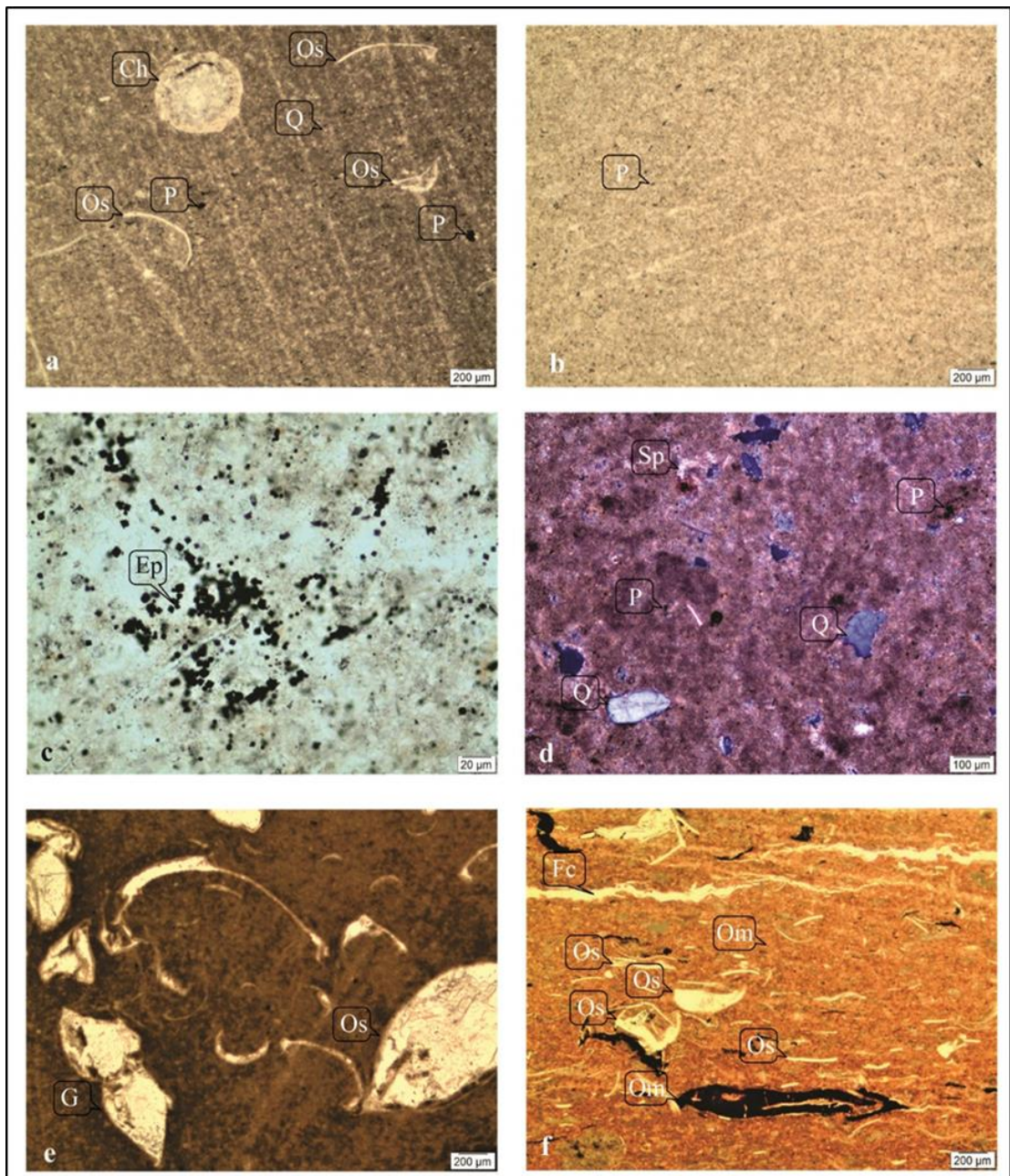


Figure 3.5. Photomicrographs of Lime Mudstone microfacies (a, b, c, d) and wackestone (e, f) presenting charophyta (Ch), ostracods (Os), gastropod (G), quartz (Q), pyrite (P), euhedral pyrite (Ep), organic matter (Om), sparite (Sp) and fracture (Fc). (Sample no. a) D3, PPI x4; b) D8, PPI x4; c) D20, PPI x100; d) D33, XPI x10; e) D4, PPI x4; f) D14, PPI x4.

According to Flügel's (2004) LMF model, this microfacies resembles LMF 6. The microfacies is dominated in the lower portion and occasionally in the middle portion of the studied section (Figure 2.7).

#### **3.2.1.4. Packstone Microfacies (DA2b)**

In the outcrop, the packstone microfacies demonstrate olive gray to pale brown, medium dark gray to dark gray color and very thin bedded to medium bedded limestone units with highly fossiliferous character, mostly gastropods (Figures 2.7; 2.8B, C, D; 2.9C; 3.8a, b; 3.9c). Based on microscopic analysis, this microfacies is composed of abundant bioclastic allochems, which is embedded in the micrite matrix (Figure 3.9a, b). The recorded fossils in the field and microscopically in this microfacies are abundant gastropods, ostracods, bivalves, charophytes and other unidentified fauna (Figures 3.7d; 3.9a, b). The framboidal pyrite is randomly distributed in the thin section and show oxidation effects. This microfacies is observed in the lower portion of the studied stratigraphic column (Figure 2.7). This microfacies indicate the LMF 8 of Flügel's (2004) LMF model.

#### **3.2.1.5. Interpretation (DA2a; DA2b)**

In the Dağhacılar measured section, wackestone-packstone facies displays abundant ostracod and gastropod assemblages. The observation of abundant ostracod and gastropod in the facies support the moderate energy depositional setting in the shallow lake (Sanjuan and Martín-Closas, 2012). The limestone microfacies with gastropod bearing wackestone-packstone, ostracod wackestone and subordinately the charophyta bearing wackestone in the studied section indicate the shallow slightly brackish-lacustrine depositional environment (Amezcuca, 2012).

Based on presence of ostracods with association of rare freshwater gastropods and charophytes, the lower part of the studied section interprets freshwater lacustrine depositional condition. Then evolved to brackish water with episodic marine incursion. It is recognized by abundant gastropods with occasional ostracods at certain the intervals. The abundant gastropods bearing microfacies interval in the studied

section indicate brackish environmental condition (Willmann, 1985; Pierce, 1993). According to Keighley et al. (2003), the association of ostracods and mollusks bearing limestone indicate shallow-water lacustrine with at least seasonally oxygenated and destratified basin setting.

Generally, Charophytes occurred in freshwater but can also be found locally in the brackish and saline environment, in a water depth of less than 10m. The microfacies is characterized by having well-preserved gastropods and charophytes. Therefore, it is indicating relatively low energy, slightly brackish lacustrine environment (Owen et al., 2015). In contrast, the occurrence of charophytes with ostracods and rare gastropods in the microfacies indicate freshwater environmental deposits (Grosjean & Pittet, 2013). Kadolsky (2015) studied the upper Rhine Graben and Paris basin, where he records the similar gastropods in the upper Rhine Graben and Paris basin. The gastropods in the upper Rhine Graben and Paris basin describe the middle Eocene age and indicates brackish water condition. In this study, similar gastropod fauna is noticed in the middle Eocene Dağhacılar section. Based on the Kadolsky (2015) studies, gastropod bearing middle Eocene intervals in the Dağhacılar section are characterized as brackish water habitat with relatively low salinity environmental condition i.e shoreline lake deposits. In contrast, the underneath rare gastropods with charophytes bearing lithofacies intervals (lime mudstone-wackestone) in the studied stratigraphic succession are categorized as relatively freshwater lacustrine deposits. In the underlying lime mudstone-wackestone intervals, gastropods are identical to the freshwater gastropod of Aksenova et al. (2018).

The observed couplet of wackestone-packstone microfacies in the studied section suggest that the deposition occurs in the sublittoral lacustrine zone (inner lacustrine zones) (Freytet and Plaziat, 1982; Sanjuan and Martín-Closas, 2012). The coquina character packstone intervals in the studied section are interpreted as deposition in the relatively low energy, littoral-sublittoral environmental condition (Tucker and Wright, 1990; McGlue et al., 2010; Yang et al., 2018).



Figure 3.6. The field photograph of wackestone microfacies of Dağhacılar measured stratigraphic section; a) Sample D4; b) D6 having gastropods; c) D14 and d) D30 (Scale: Hammer and pencil).

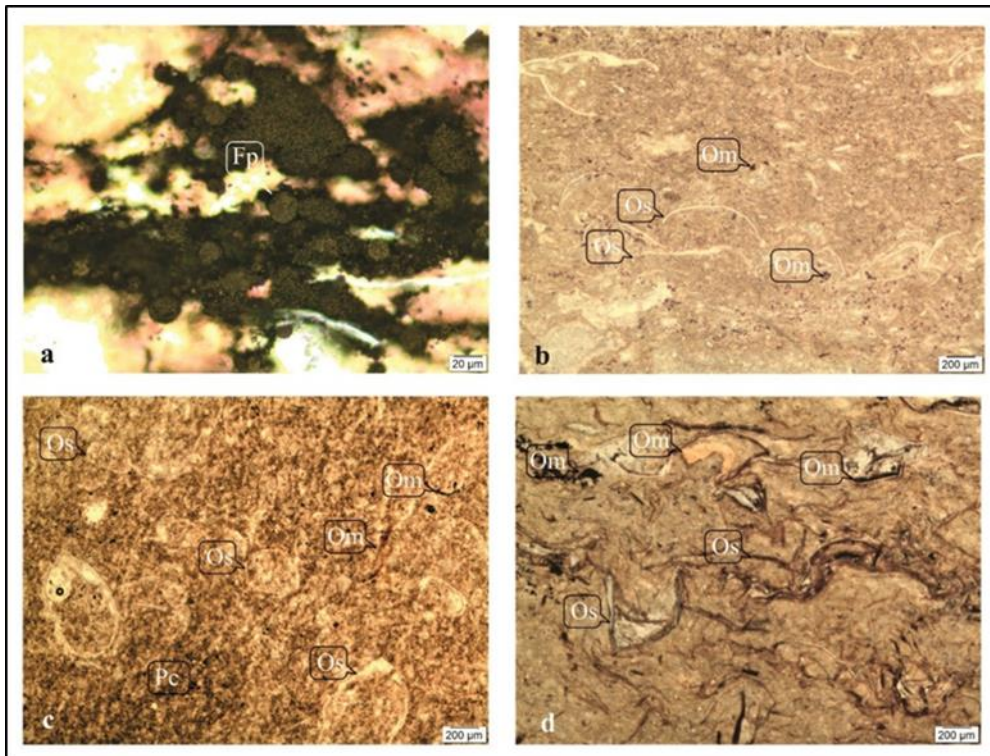
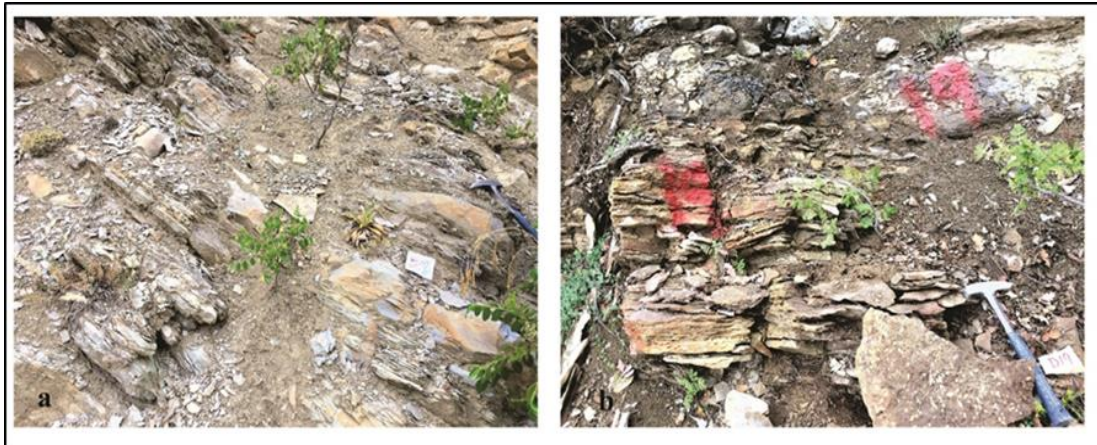


Figure 3.7. Photomicrographs of wackestone (a, b, c) and Packstone microfacies (d) presenting ostracod (Os), framboidal pyrite (Fp), organic matter (Om) and phytoclast (Pc). (Sample no. a) D14, PPI x100; b) D15, PPI x4; c) D30, PPI x4 and d) D11, XPI x4.



*Figure 3.8. The field photograph of gastropods bearing packstone microfacies of Dağhacılar measured stratigraphic section; a) Packstone bedding between D12 and D13; b) D19 (Scale: Hammer).*

### **3.2.2. Marl Facies (DA3)**

Marl is defined as a fine-grained carbonate rock type which has relatively soft/loose sediment with a high proportion of calcareous character and non-fissile feature (Pettijohn, 1975; Potter et al., 2005 and Stow, 2005). In the studied section, the distinguished marl facies is appeared as medium gray to medium dark gray to greenish gray color and alternating with limestone, oil-shale and sandstone in the measured stratigraphic section at different intervals and show occasional nodularity at places (Figures 2.7; 2.9D; 2.10B; 2.11C; 2.15; 2.16; 3.9e). Microscopically, it is composed of predominantly lime mud with subordinate silt-size quartz, ostracods shell and randomly distributed pyrite and organic matter (Tables 3.2; 3.4; Figure 3.9a; 3.10a, b). In the upper portion, there is an observation of micro-bioturbation under microscopic studies in the marl facies (Figure 3.10b). The marl facies is dominant in the lower middle portion and the upper portion of the studied section (Figure 2.7).

#### **3.2.2.1. Interpretation (DA3)**

In the studied section, marl facies interpret deposition from decantation of mud in the alkaline lacustrine and in the marine environment. Occasionally, the marls facies are characterized by ostracod in the lower portion of the studied section.

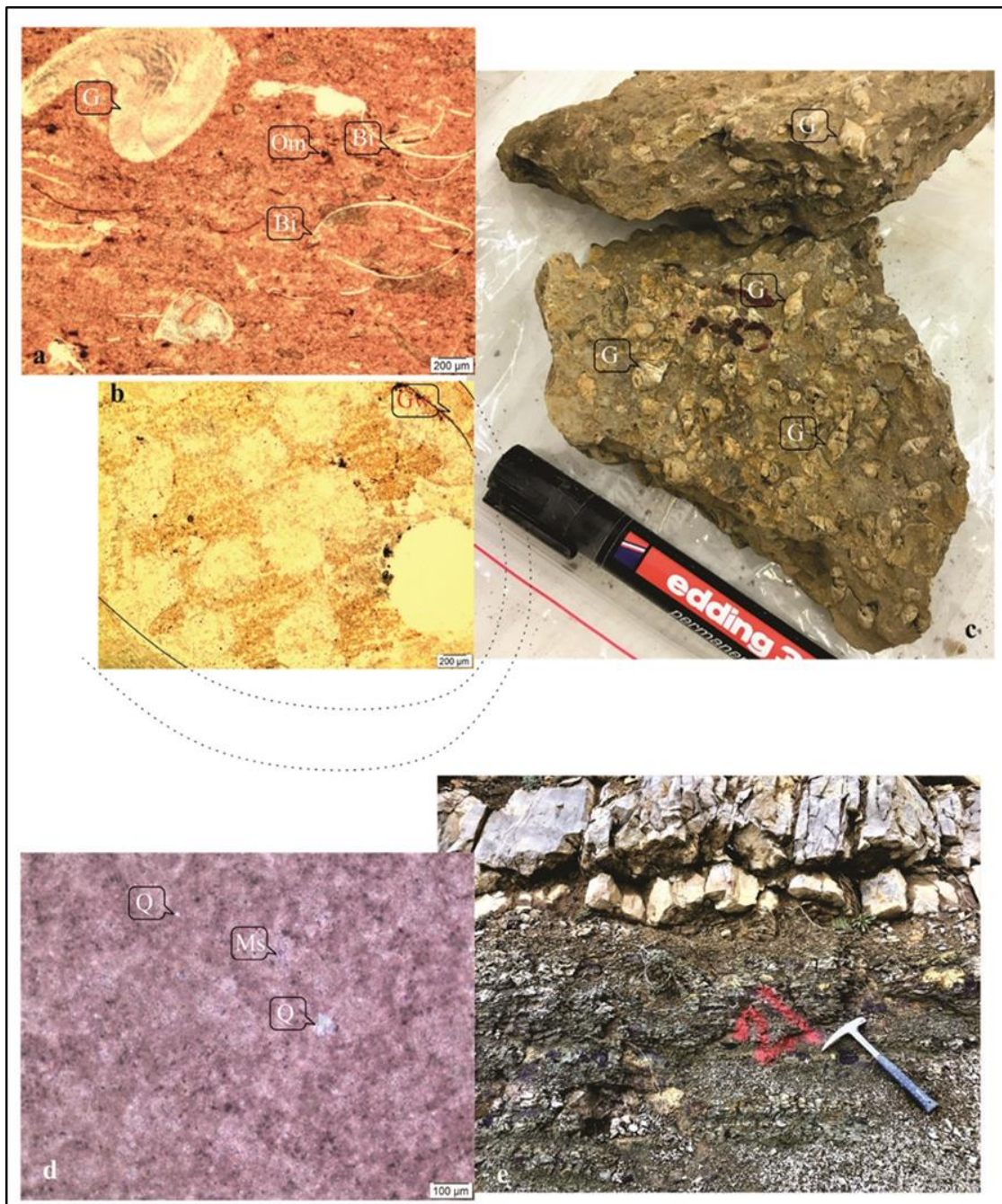


Figure 3.9. Photomicrographs of gastropods bearing Packstone microfacies (a, b, c) and marl (d, e) presenting ostracod (Os), gastropod (G), gastropod valve (Gw; dotted line indicates gastropod wall shell) bivalve (Bi), quartz (Q), microsparite (Ms) and organic matter (Om). (Sample no. a) D19, PPL x4; b) D19, PPL x4; c) D19 hand specimen photography; d) D21, XPL x10; e) D21, field photography.

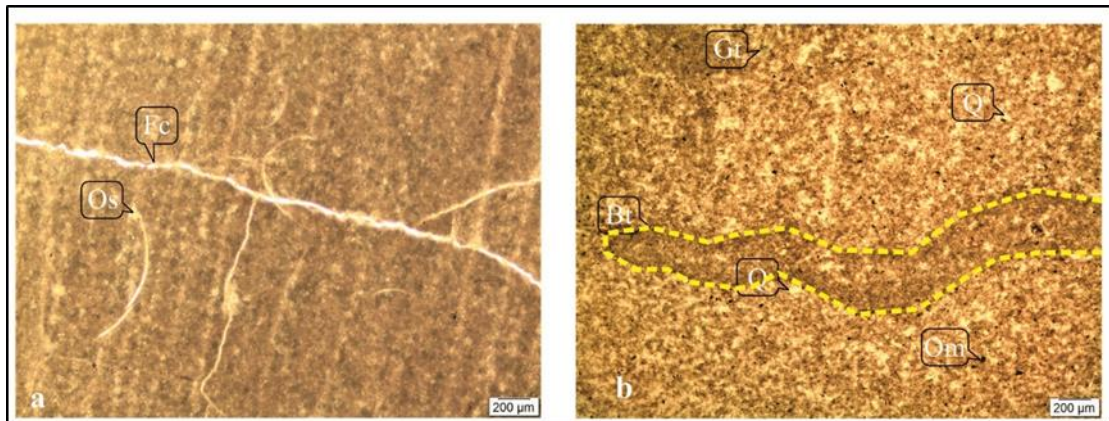


Figure 3.10. Photomicrographs of marl microfacies presenting ostracod (Os), glauconite (Gt), bioturbation (Bt; dotted yellow line), organic matter (Om), quartz (Q) and fracture (Fc). (Sample no. a) D25, PPI x4; b) D73, PPI x4.

In the studied section, Marls facies in the lower portion are deposited in relatively deeper lacustrine environment with the dysoxic condition. The marl facies is overlain by limestone facies, which indicates lacustrine margins deposits with increasing lime-producing organisms' activity (Gierlowski-Kordesch, 2010; Sanjuan & Martín-Closas, 2012). The thick intervals and massive appearance of the marls indicate deposition from suspension in a calm environmental condition (Pavelić et al., 1998). The occasionally observed ostracod in the marl facies also indicate the quiet environmental condition.

In the upper portion of the Dağhacılar section, the marl with occasionally interbedded fine sandstone reflect deposition in relatively shallow water as compared with the lower portion marly intervals. The documentation of rare *cruziana* ichnofossil and silty appearance of facies suggest deposition in relatively low energy condition in offshore transitional marine setting under dysoxic environmental condition (Figure 3.10b) (Pemberton et al., 1992; Ranson, 2012).

### 3.2.3. Oil-shale Facies (DA4)

The shale or mudstone or claystone or mudrock are the numbers of terms used to described fine-grained sedimentary rocks. The fine-grained sedimentary rocks are

classified on basis of composition, sedimentary structure and organic matter content by number of researchers (as shown in the tables 3.1; 3.2; 3.4; 3.5; 3.6; Figures 3.1; 3.2) (Deng and Qian, 1990; Stow, 2005; Allix et al., 2010; Diaz et al., 2012; Wang, 2012; Jiang et al., 2013; Zou et al., 2010). In this study, the oil-shale is described on basis of composition, sedimentary structure and organic matter content by using the above mention classification studies.

In the Dağhacılar measured section, the oil-shale facies are characterized as very thin laminated shale and non-laminated fossiliferous shale. This facies is classified on the basis of Stow`s (2005), Wang`s (2012) and Zou et al., (2010) shale classifications. In the field, the shale units are the most common lithofacies in the middle and upper portion of the measured section (Figure 2.7). It is usually dark gray, medium light

Table 3.5. *Mudstone and Shale Classification Schemes (Zou et al., 2010).*

Category	Main Features
Calcareous mudstone/shale	Claystone with CaCO content not exceeding 50%
Ferrous mudstone/shale	Fe <sub>3</sub> -bearing oxides, F <sub>2</sub> -bearing silicates, and mudstone containing significant amounts of sulfides
Siliceous mudstone/shale	Argillite containing significant autogenous free SiO <sub>2</sub> but not exceeding 50%
Silty mudstone/shale	Argillite containing 50-25% terrestrial silty clasts
Silt-bearing mudstone/shale	Argillite containing 5-25% terrestrial silty clasts
Caceous shale	Shale containing a significant amount of uniformly distributed, carbonized, fine, dispersed organic matter; contaminates the hand when touched
Dark Shale	Shale looking black due to the presence of significant amount of organic matter and fine, dispersed FeS; looks like Caceous shale but does not contaminate the hand when touched
Oil-shale	Brown-to-black laminoid shale containing 4-20% (30% max) of hydrocarbon compounds

Table 3.6. *Summary of Mudstone and Shale Classification Schemes of the Lacustrine environment.*

Author	Principles for Classification	Main Types of Rock
Deng and Qian (1990)	Sedimentary structure	Black shale, horizontal lamina silty shale, graded lamina silty mudstone, calcareous black shale, calcareous lamina shale
Guo et al. (2009a, b)	Organic matter types	Sapropelic oil-shale, mixed oil-shale, humus-liptobiolith oil-shale
Liu et al. (2009a, b)	Type of lake/basin	Depression lake oil-shale, fault depression oil-shale, fault depression lake/swamp oil-shale
	Water body salinity	Freshwater oil-shale and brackish water oil-shale
Wang (2012)	Laminae composition	Black shale, calcareous lamina shale, oil-shale, laminoid shale, laminoid limestone, calcareous shale, mud shale
Jiang et al. (2013)	Organic and mineral contents	High-organic limestone, high-organic claystone, medium-organic claystone, medium-organic limestone, low-organic limestone, low-organic claystone



*Figure 3.11. The field photograph of Oil-shale of Dağhacılar measured stratigraphic section; a) Non-laminated fossiliferous oil-shale (Sample D10); b) Laminated oil-shale with intercalated marl (Sample D36); c) Laminated oil-shale with interbedded marl (Sample D44).*

gray, medium dark gray to brownish black, greenish to dark greenish gray, non-laminated/poorly laminated to well-laminated organic-rich units (Figures 2.10; 2.11a, b, c; 2.12a, b; 2.13; 2.14a; 2.15; 3.11). The laminae in the fields are identified as massive, thin to wavy laminae and thick parallel laminae (Figure 2.11 and 2.12). At a single interval, there is an observation of siliceous concretion within this facies (Figure 2.10). In general, the laminated shale units are dominantly observed in the measured stratigraphic section (Figure 2.7). Under microscopic studies, laminated oil-shales facies composed of alternating light and dark laminae. The lighter laminae indicate organic poor laminae and the darker laminae characterize organic-rich laminae, and occasionally variable detrital content, and presence of ostracods at certain thin sections (Figures 3.12c; 3.13). The microscopically observed particles in the shale lithofacies are quartz, pyrite, ostracods, unidentified fossils and rare plagioclase, nummulite (Figures 3.13). In the microscopic studies, the laminae in the laminated shales are documented in the form of very thin to medium parallel laminae, wavy laminae, lenticular laminae and deformed soft sediment structure/ convolute laminae (O'Brien, 1990, 1996; Wilkins, 2003) (Figure 3.13). Non-laminated oil-shales are composed of the organic-rich matrix along with ostracods, bivalves and hardly nummulite (Figure 3.13a, b). The shale units show no sign of bioturbation in the studied section. Chemically, the oil-shale facies are identified as a calcareous character in the studied section.

#### **3.2.3.1. Interpretation (DA4)**

Generally, the massive organic-rich calcareous mudstone was interpreted to have deposited in shallow, brackish lacustrine environment with dysoxic-anoxic, cool and arid climatic condition. In contrast, the laminated organic-rich calcareous mudstone is generally documented in the relatively high saline bottom water, deep stratified lacustrine with oxic to anoxic conditions, and also represent more humid and warmer climatic environment (Ma et al., 2016).

In the Dağhacılar studied section, massive fossiliferous oil-shale is interpreted to have deposited in anoxic condition, relatively deeper brackish lacustrine environment. The presence of abundant ostracods and rare nummulite fragment in the oil-shale indicate marine incursion to the depositional setting, and probably fauna is transported by density current to relatively deeper brackish lacustrine condition (Sunardi, 2015).

In the lacustrine environment, the deposition of shale is generally controlled by a complex set of factors which includes basin setting, sediment supply, climatic, changes salinity and redox condition of the depositional setting (Xu et al., 2015; Liang et al., 2018). The middle portion of the Dağhacılar section is defined by laminated oil-shale with intercalating marls. The intercalating oil-shale and marls are recognized as lacustrine deposits with occasional observation of ostracod and abundant framboidal pyrite in the some of the oil-shale thin section. In the algal laminated oil-shale, the occurrence of calcification is a common phenomenon in the microbial mats which are controlled by a micro-organism (cyano-bacteria). The well-preserved laminae in the oil-shale indicate a low hydrodynamic condition in the subaqueous environment. The occurrence of ostracod suggests relatively shallow water depth (Lettéron et al., 2018). The observation of heterogeneous grains in the algal laminated and laminated oil-shale are transported by aeolian and/or from water suspension sediments to deep environmental setting (Rios et al., 2004). Generally, the oil-shales are deposited in the extensive deep lakes (Carroll and Bohacs, 2001). The Oil-shale of this section is defining the profundal lacustrine environment. The lack of bioturbation and high organic content in laminated and non-laminated shale lithofacies indicate low energy environment and interpreted as center lacustrine setting with anoxic environmental condition (Zeller et al., 2015). In the basinal portion, carbonate content is controlled by transportation of carbonate and siliciclastic components (Zeller et al., 2015).

The upper portion oil-shale intervals in the Dağhacılar measured section are recognized as marine offshore transitional deposits. The transition of thin-wavy laminated oil-shale to thick laminated oil-shale with increasing fine sandstone

interbeds and having marine fauna suggest oil-shale deposits under marine environmental condition.

The documentation of thick horizontal laminae in oil-shale indicate bottom flowing current influence, that is most possibly related to storm condition on the marine offshore-transitional zone (O'Brien, 1990; Esteban, 2003). The introduction of the saline environment to the lacustrine also lead to the demise of intolerance brackish and freshwater fauna and flora in oil-shale lithofacies (Esteban, 2003). In this interval, the absence of ostracod, freshwater gastropod and algal structure indicate salinity increase in the depositional environment, but not saline adequate to precipitate saline

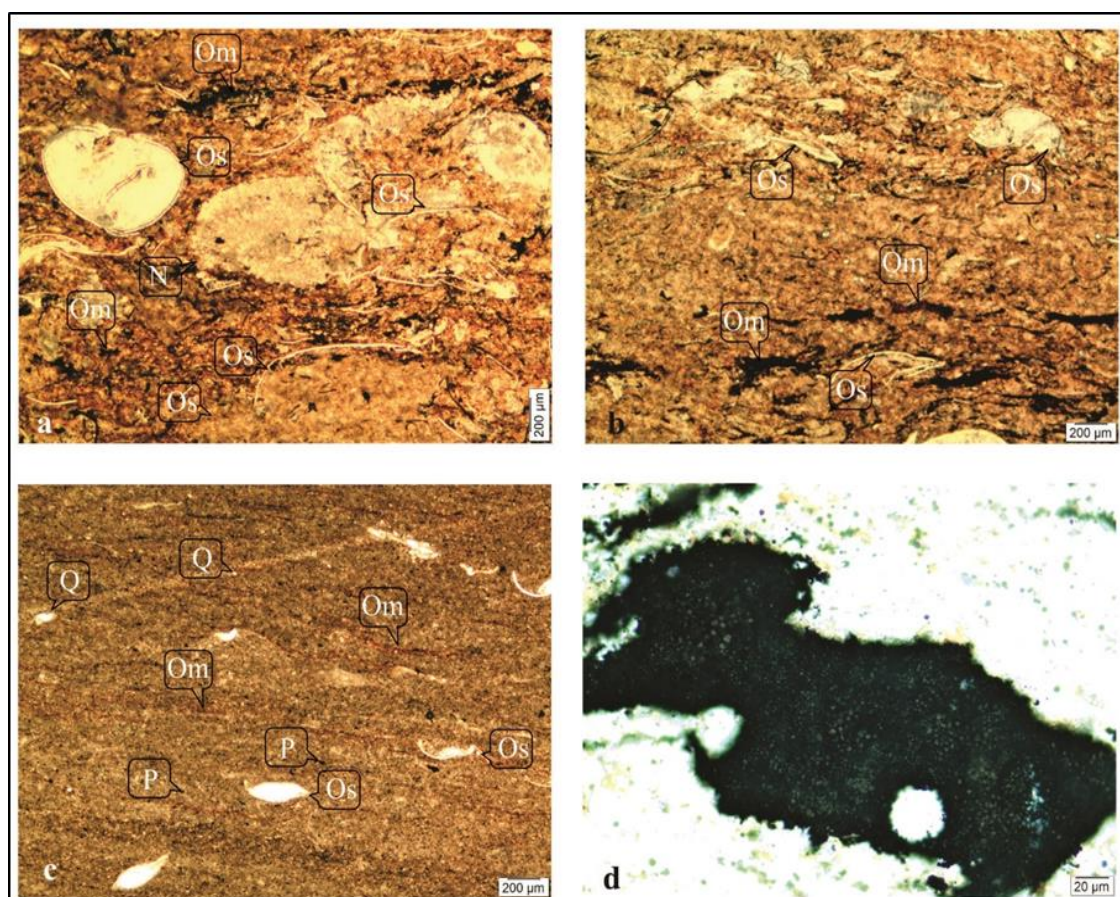


Figure 3.12. Photomicrographs of oil-shale facies presenting ostracod (Os), quartz (Q), nummulite (N), pyrite (P) and organic matter (Om). (Sample no. a, b) fossiliferous oil-shale, D10, PPI x4; c) Lenticular laminated oil-shale, D36, PPI x4; d) D36, Euhedral pyrite, PPI, x100.

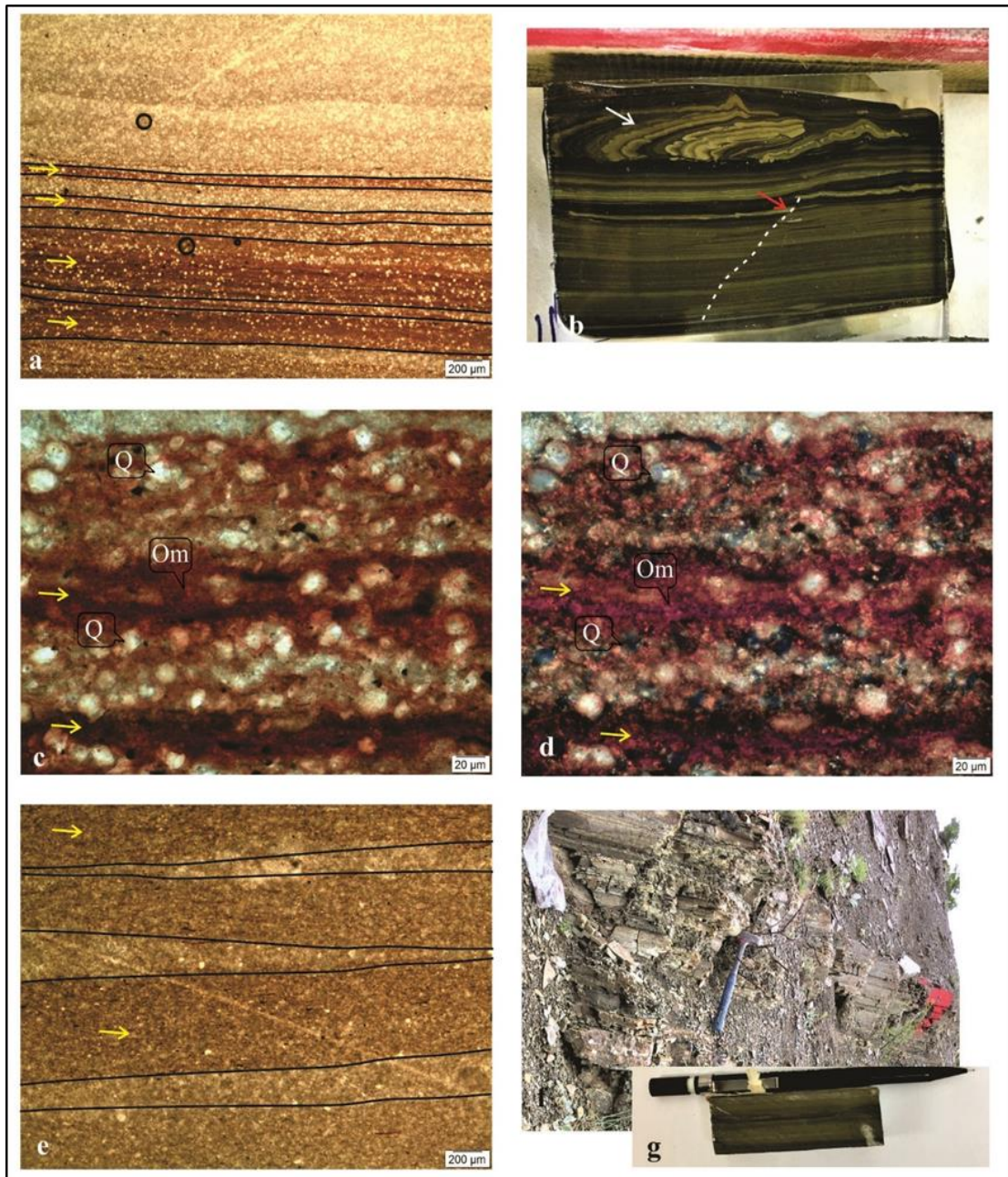


Figure 3.13. Photomicrographs of oil-shale presenting quartz (Q) and organic matter (Om). (Sample no. a) Laminated oil-shale, D40, PPI x4; b) field photography, D40, indicates convolute laminae (white arrow) and micro-fault (red arrow); c) D40, PPI, x100; d) D40, XPI, x100; e) Lenticular lamination, D69, PPI, x100; f) field photography of sample D69; g) Cut sample for thin section and show alternating dark and light laminae. (yellow arrow indicates organic-rich laminae-dark laminae) (Scale; Hammer and Pencil).

minerals (Cole, 1985). The presence of soft-sediment deformation structures and convolute bedding in lithofacies indicate episodically or seismically triggered during the deposition process.

#### **3.2.4. Calcareous Sandstone Facies (DA5)**

The sandstone is a sedimentary rock with coarse-grained character as compared to siltstone and mudrock. The sandstone is classified by Folk's (1974) and Pettijohn et al., (1987) with three end member i.e. feldspar-plagioclase member, quartz member and rock fragment member. The Folk's sandstone classification is also based on the matrix proportion and grain supported character (Figure 3.3). In the field, the sandstone facies are defining grayish orange, dark greenish gray, medium dark gray to medium gray color, thin to medium bedded sandstone units with interbedded oil-shale and marl at different intervals (Figures 2.7; 2.13; 2.14; 2.15; 2.16; 3.14; 3.16). The sedimentary structure observed in the field are low angle wavy ripple, very thin hummocky cross-stratification in the bedding and parallel lamination in the bedded sandstone units (Figures 2.14b; 3.14; 3.16; 3.17b; 3.18d). This facies appeared occasionally in the middle portion of the measured section and then followed by a regular appearance with increasing in the number of beds towards the top in the studied section. The upper and lower contact of the sandstone beds is sharp with underlying and overlying facies (oil-shale and marl). The intercalating oil-shale and/or marls units with sandstone exhibit heterolithic facies character (Figures 2.13; 2.14a; 2.15; 2.16) (McCauley, 2013; Collins et al., 2015; Rimkus, 2016). Microscopically, the sandstone facies is identified as having three mineralogical variations: Feldspathic litharenite, Feldspathic greywackes and lithic arkose, based on the Folk's (1974) and Pettijohn et al., (1987) sandstone classification (Tables 3.3; 3.4). The sandstone lithofacies are composed of predominantly quartz and rock fragments (includes polycrystalline quartz, shale, limestone and bioclasts) with the association of feldspar and plagioclase (Figures 3.17; 3.18). The observed accessory minerals in the lithofacies are chlorite, tourmaline, biotite, muscovite and rutile. The observed grains in the sandstone units are very fine-size to coarse sand-size, angular to sub-rounded,

moderate to well sorted and close to loosely packed (Table 3.4). The subordinate organic matter, charcoal (Mingram, 1998), oil staining and pyrite are also observed in the matrix. The fossils include foraminifera, Nummulites and other unidentified fragment also occur in the sandstone facies in the upper portion of measured stratigraphic section (Figures 3.17 d,e; 3.18). There is presence of bioturbation in the sandstone lithofacies but very rare (Figure 3.16e). The sandstone facies are periodically occurred in the middle portion of studied section and predominately present in the upper portion of the studied section (Figure 2.7).



*Figure 3.14. a) The field photograph of alternating shale and sandstone and showing bedding sandstone geometry planar to hummocky cross-stratification to wave ripple symmetry (Note; Close view hummocky cross-stratification in figure 3.14b).*

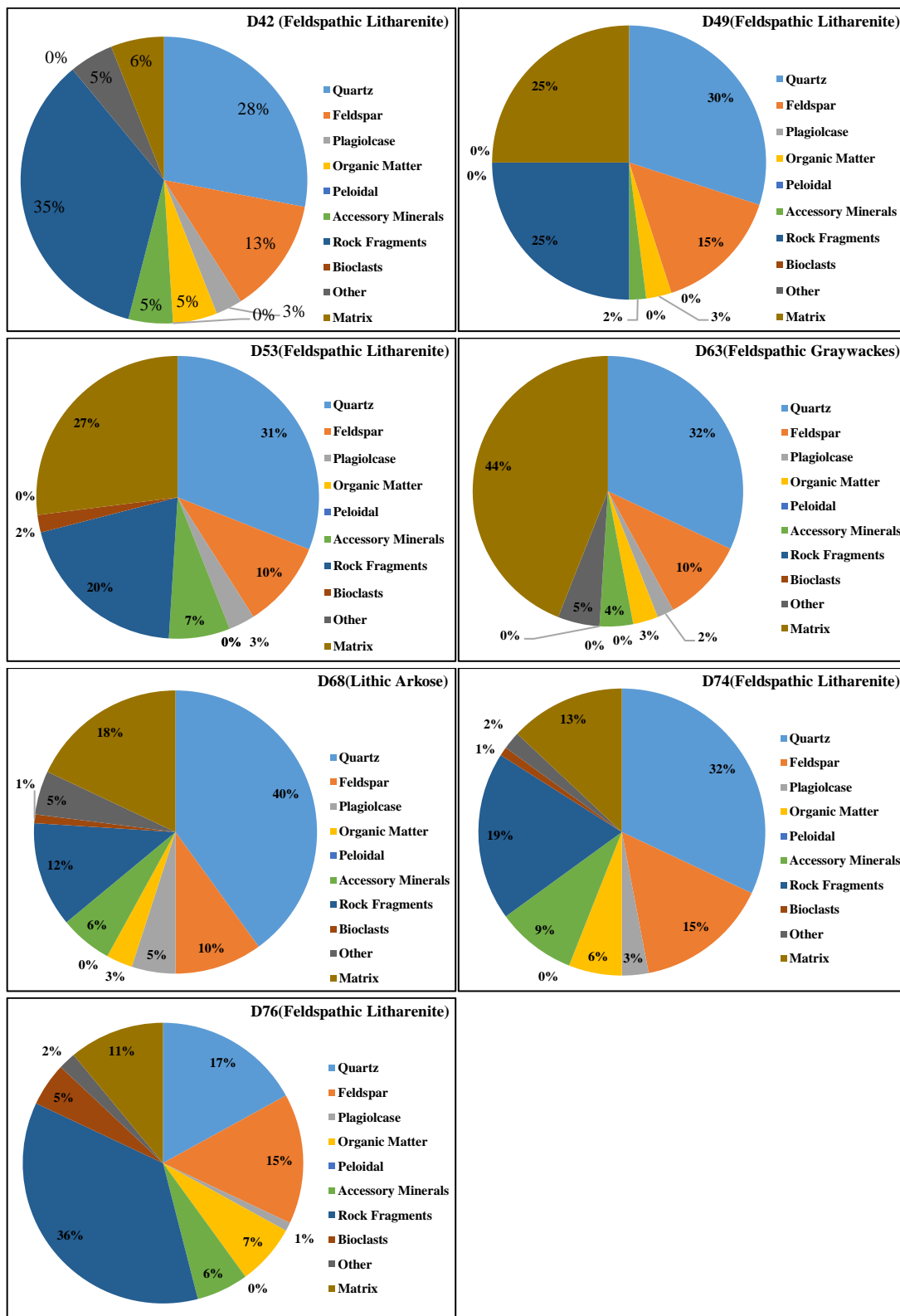


Figure 3.15. Pie graphs of the sandstone lithofacies in the Dağhacılar section.

### 3.2.4.1. Interpretation (DA5)

The fine-grained sandstone deposits with wave-rippled features and presence of burrow are deposited in a shallow lacustrine environment (Owen et al., 2015). The sandstone lithofacies in the studied section possesses horizontal lamination to wavy rippled features in the middle portion. This lithofacies with the absence of bioturbation is interpreted that it is deposited in a relative deeper lacustrine condition. The deeper environmental setting of fine sandstone is also supported by ripple crests rounded shape (Johansen, 2016).

The introduction of the marine environment (offshore transition facies) in the upper portion of the Dağhacılar measured section is recognized as intercalating sandstone-laminated oil-shale and occasionally marl. The evidence to identify marine sandstone in the studied section is an observation of marine fauna and rare bioturbation such as



Figure 3.16. The field photograph of interbedded marl and sandstone interbeds (arrow indicates planar sandstone bedding).

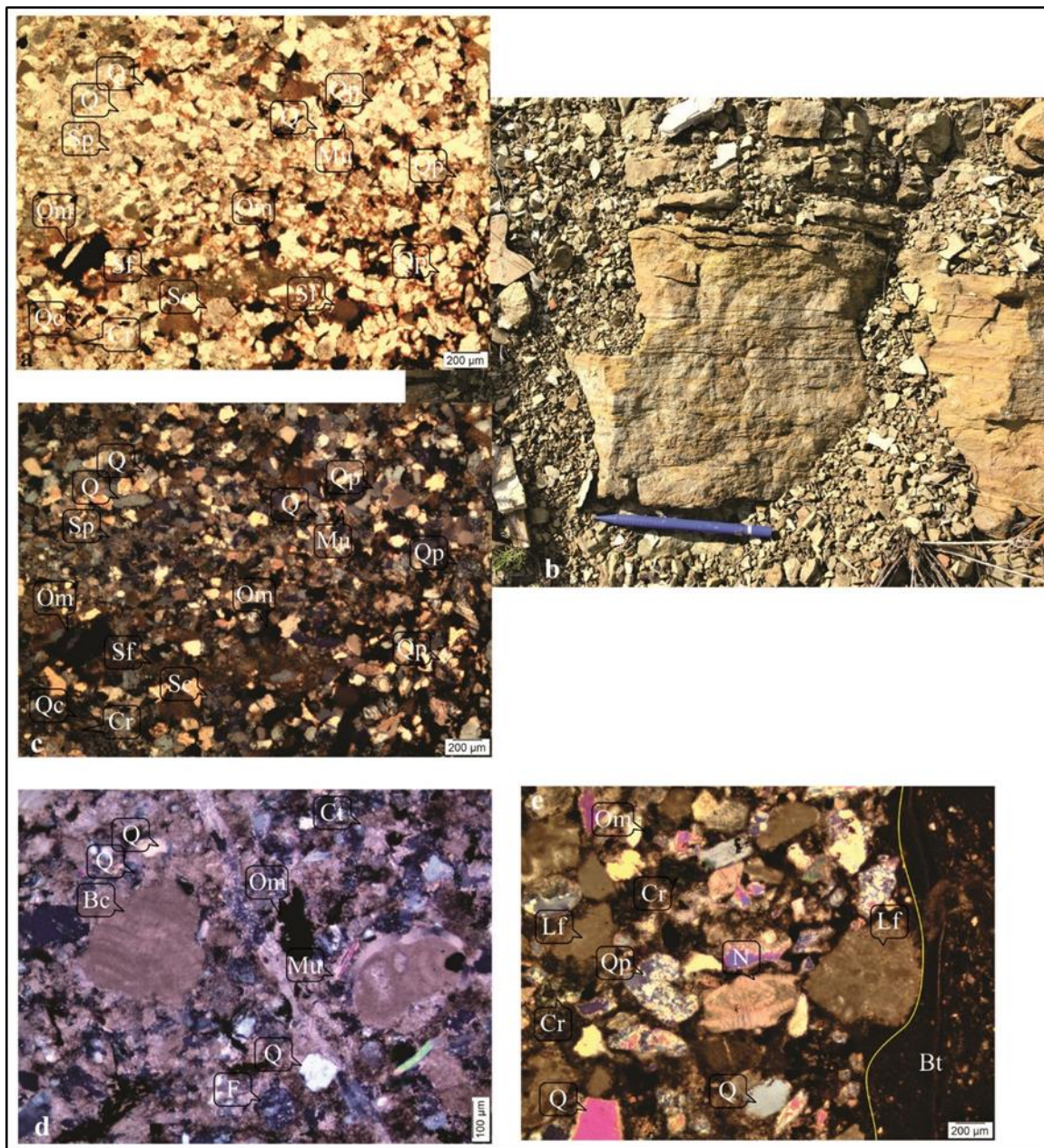


Figure 3.17. Photomicrographs of sandstone presenting quartz (Q), polyquartz (Qp), bioclasts (Bc, marine Bioclast), Nummulites (N), limestone fragment (Lf), shale fragment (Sf), microquartz (Qc), muscovite (Mu), sericitization (Sc), chlorite (Cr), sparite (Sp), feldspar (F), bioturbation (Bt, indicated by yellow line) and organic matter (Om). (Sample no. a) sandstone, D42, PPI x4; b) field photograph of low angle wavy laminated sandstone, D42, indicates deformed features (white arrow); c) a-XPI x4; d) Sandstone, D53, XPI, x10; e) sandstone with vertical bioturbation, D76, XPI, X4.

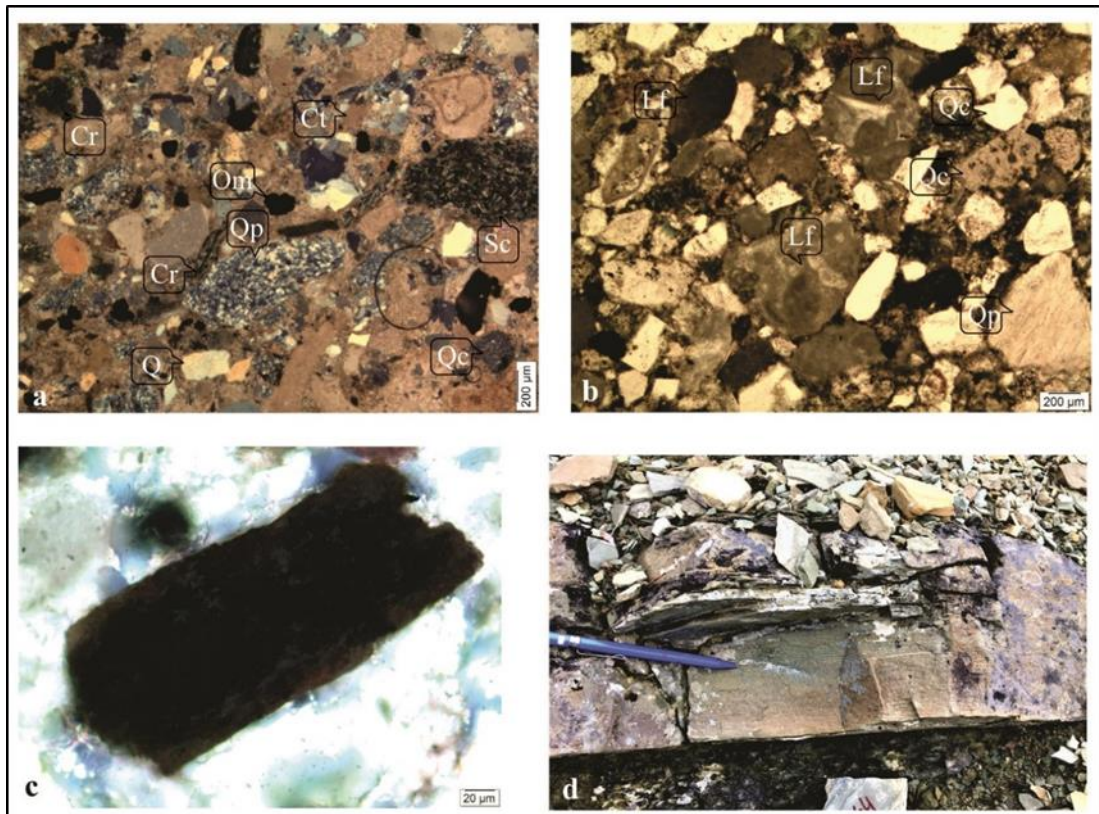


Figure 3.18. Photomicrographs of sandstone presenting quartz (Q), polycrystalline quartz (Qp), limestone fragment (Lf), shale fragment (Sf), cryptoquartz (Qc), muscovite (Mu), sericitization (Sc), chlorite (Cr), calcite fragment (Ct), and organic matter (Om). (Sample no. a) sandstone, D76, XPI, x4; b) sandstone, D76, PPI, x4; c) sandstone, charcoal, PPI, x100; d) Close view of hummocky cross-stratification, D64.

skolithic-cruziana ichnofacies (Johansen, 2016; Vakarelov et al., 2012). The presence of high content of carbonate matrix in the sandstone lithofacies indicates relatively deepening depositional condition (Figure 3.15). The heterolithic deposits character sandstone-oil-shale and/or marls reflects marine offshore fluctuating environmental condition. The sandstone lithofacies possesses hummocky cross-stratification, wave ripple and parallel lamination feature. The hummocky cross-stratification sandstone is characterized as deposited above storm weather wave base (SWWB) in the marine environmental condition (Walker and Plint, 1992). These identified feature in the sandstone lithofacies interpret storm event deposits (Abimbola, 2016). In the studied section, the observation of hummocky stratified sandstones, planar laminated

sandstone, ripple laminated sandstone, massively bedded with sharp and/or obscure contact with oil-shale and/marl, and sometimes with load-casts contact are identified as storm-induced wave oscillations deposits (Rees et al., 2014; Johansen, 2016). In general, these deposits are developed on the marine offshore-transitional environmental setting. The presence of marine fauna and calcareous cementation in the sandstone of Dağhacılar measured section also define marine influence deposited lithofacies (Huyghe et al., 2017) (Figure 3.15). In general, the calcareous sandstone lithofacies with the association of organic-rich shale and/or marl units interprets that the calcareous sandstone lithofacies are deposited in the marine offshore-transition environment between the fair-weather wave base and storm wave base and identified as the unit of turbiditic intervals. The associated organic-rich oil-shale and/or marl are settling from suspension under low energy depositional condition (Dahlgvist, 2018).

### 3.3. Microfacies of Hasanlar Section

In the Hasanlar measured section, three facies are categorized along the measure stratigraphic section based on the field and laboratory work studies (Figure 2.20; Tables 3.7; 3.8). The facies are described in detail as follow.

Table 3.7. Limestone, oil-shale and marl petrographic data and established/recognized facies in the Hasanlar studied section.

Sample No.	Q	F	Pg	Om	Pl	Pi	In	Bioclasts (Os/Ch/GUb/Al/Da/N/Br)	Other (P/He/Ph/Cr/Ce/Ct)	Matrix (Mi/Cl/Sp/Or D/Cr)	Field Nomenclature
H0a	5	-	-	-	-	-	3	11Os/1G=12	5P	53Mi+20D+Si	Bio-Limestone
H0b	5	-	-	-	-	-	-	-	-	75Mi+Or+20D	Oil-shale
H1	2	-	-	-	-	-	-	-	10P	88Mi+Or	Oil-shale
H3	5	-	-	2	-	-	-	-	10P	83Mi+Or	Oil-shale
H4	2	-	-	2	-	-	-	-	5P	91Mi	Limestone
H5	-	-	-	-	-	-	-	-	5P	75Mi+20D	Limestone
H9	1	-	-	-	-	-	-	-	1P	98Mi	Oil-shale
H10	15	-	-	5	10	10	-	-	-	60Mi	Bio-Limestone
H12	-	-	-	-	-	-	-	20Os/10Ub=12	2P	86Mi	Bio-Limestone
H13	15	-	-	2	-	-	-	20Os	6P	57Mi+Or	Oil-shale
H14	-	-	-	-	-	-	-	-	2P	98Mi+Or+Ct	Oil-shale
H15	20	-	-	5	-	-	-	-	5P	70Mi	Oil-shale
H19	-	-	-	5	-	-	-	5Os	5P	85Mi	Limestone
H20	5	-	-	5	-	-	-	5Os	12P	73Mi+Or	Oil-shale

Os-Ostracoda, Ch-Charopyta, G-Gastropod, Br-Brachiopod, Al-Algal, Da-Diatoms, N-Nummulites, Pl-Plant, Fr-Foraminifera, Py-Palynofacies, Ub-Unidentified Bioclasts, Q-Quartz, Qp-Polyquartz, Cr-Chlorite, Ct-Calcite, Mu-Muscovite, Mn-Manganese, P-Pyrite, Ce-Chert, F-Feldspar, Pg-Plagioclase, Sf-Shale fragment, Stf-Siltstone Fragment, Lf-Limestone fragment, Bo-Biotite, T-Tourmaline, Pi-Peloid, In-Intraclasts, R-Rutile, Z-Zircon, Sp-Sparite, Mi-Micrite, D-Dolomite, Cl-Clay, Or-Organic Rich, Om-Organic matter/Bitumen, He-Hematite, Ph-Phosphate, Se-Sphene

Table 3.8. Classifications of the limestone, oil-shale, marl and sandstone and established/recognized microfacies in the Hasanlar studied section.

Sample No.	Compositional Classification			Texture Classification*		Limestone Classification (Embry and Klovan's 1971)	Defined Facies in Studied Section
	Diaz's (2012) Mudstone (Unconventional)	Stow's (2005)	Allix's (2010) Shale	Folk's (1965)			
H0a						Bio-Wackestone	Wackestone
H0b	Carbonate-Dominated Lithotype	Calcareous	Calcareous Mudstone	Clay-Shale			Oil-shale
H1	Carbonate-Dominated Lithotype	Calcareous	Calcareous Mudstone	Clay-Shale			Oil-shale
H3	Carbonate-Dominated Lithotype	Calcareous	Calcareous Mudstone	Clay-Shale			Oil-shale
H4						Lime Mudstone	Lime Mudstone
H5						Lime Mudstone	Lime Mudstone
H8	Clay-rich Carbonate Mudstone	Marls	Calcareous Mudstone	Clay-Shale			Oil-shale
H9	Clay-rich Carbonate Mudstone	Marls	Argillaceous Mudstone	Clay-Shale			Oil-shale
H10						Bio-Wackestone	Wackestone
H12						Bio-Wackestone	Wackestone
H13	Mixed Carbonate Mudstone	Smarl	Argillaceous Mudstone	Mud-Shale			Oil-shale
H14	Clay-rich Carbonate Mudstone	Calcareous	Calcareous Mudstone	Clay-Shale			Oil-shale
H15	Mixed Argillaceous Mudstone	Smarl	Argillaceous Marlstone	Clay-Shale			Oil-shale
H18	Clay-rich Carbonate Mudstone	Marls	Argillaceous Mudstone	Clay-Shale			Oil-shale
H19						Lime Mudstone	Lime Mudstone
H20	Carbonate-Dominated Lithotype	Calcareous	Calcareous Mudstone	Clay-Shale			Oil-shale

\* Based on grains size of mud fraction, non-fissile/fissile and soft.

Table 3.8. Continues....

Sample No.	(Texture and/or Compositional)	Defined Facies in Studied Section
H0a	Oil stained, pyrite oxidized, highly stressed, Bio-Wackestone	Wackestone
H0b	Laminae, dolomitic grains, Oil-shale	Oil-shale
H1	Thin parallel laminated bedding, Oil-shale	Oil-shale
H3	Wavy Laminae, Oil-shale	Oil-shale
H4	Thin Bedded Marl	Lime Mudstone
H5	Thin-medium parallel bedded Dolomitic Mudstone, Patchy oil stained	Lime Mudstone
H8	Laminated horizontal bedded Oil-shale	Oil-shale
H9	Laminated horizontal bedded Oil-shale	Oil-shale
H10	Silt size quartz grains, plant fragments (phytoclasts/Cuticules)	Wackestone
H12	Thin Bedded, Bio-wackestone	Wackestone
H13	Laminated, having ostracods, Oil-shale	Oil-shale
H14	Lenticular wavy Laminae, Oil-shale	Oil-shale
H15	Oil-shale	Oil-shale
H18	Laminated to thin bedded, Oil-shale	Oil-shale
H19	Oil Lime Mudstone, Thin Bedded	Lime Mudstone
H20	Laminated, Oil-shale	Oil-shale

### 3.3.1. Limestone Facies

The limestone facies in the Hasanlar measured section is dominantly observed at regular interval with interbedded shale and occasionally marls (Figure 2.21). The detailed studies is carried out to define the microfacies character based on the field and petrographic features. The Embry and Klovan's (1971) classification is used to

classify the microfacies. A total of two sub-facies are classified in the limestone facies (Table 3.8).

#### **3.3.1.1. Lime Mudstone Microfacies (HA1)**

The lime mudstone microfacies is composed of very pale green to pale green, medium light grey, medium grey to light grey, thin-bedded strata (Figures 2.18; 2.19; 2.20; 2.21; 2.22C). Microscopic studies indicate that this microfacies consist of less than 10 percent allochem which is embedded in the micrite matrix (Table 3.8; Figure 3.19 a,b, d). Therefore, this facies is categorized as lime mudstone microfacies, based on the Embry and Klovan`s classification (1971). The allochem in this microfacies are composed of ostracods, organic matter and rare quartz grains (Figures 3.19a, b, d). Pyrite is observed in the form of framboidal type (Figure 3.19c) and also the presence of dolomitic patches in the single interval (Figure 3.19d). In the studied section, the lime mudstone microfacies present at regular interval with interbedded oil-shale and marl at different intervals (Figure 2.21).

#### **3.3.1.2. Interpretation (HA1)**

In the Hasanlar section, the deposition of lime mudstone intervals occurred in low energy lacustrine condition. The predominance of micrite matrix, high organic content, the absence of bioturbation and few grains of terrigenous clasts show distal depositional condition (Gingras et al., 2011; Amezcua, 2012). The occasional ostracods observation in the lime mudstone suggested relatively deeper lacustrine environments with anoxic conditions (Anan, 2014). The observation of framboidal form pyrite in the studied section corresponds to the relatively saline influence on the lacustrine environment (Brown and Cohen, 1995).

#### **3.3.1.3. Wackestone Microfacies (HA2)**

In the field, the wackestone microfacies recognized as moderate yellowish brown to very pale orange, thin-bedded units with occasionally intercalated fragile shale (Figure 2.21). On the basis of microscopic analysis, the facies are recognized as wackestone

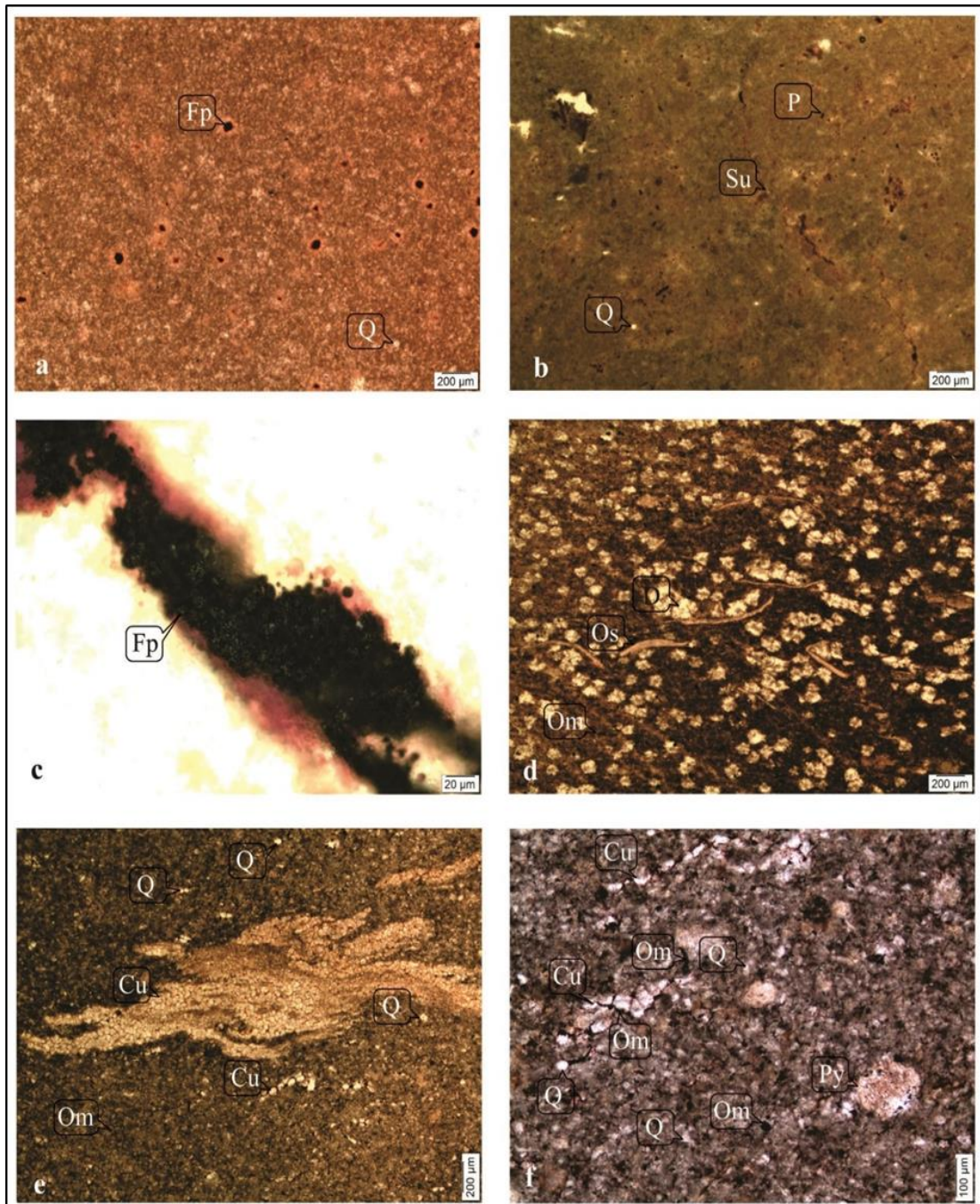


Figure 3.19. Photomicrographs of Lime Mudstone microfacies (a, b, c, d) and wackestone (e, f) presenting ostracod (Os), quartz (Q), pyrite (P), framboidal pyrite (Fp), organic matter (Om), rare dolomitic patches(D), phytoclast (Py), cuticles (Cu) and stylolite (Su). (Sample no. a) H4, PPl x4; b) H5, PPl x4; c) H5, PPl x100; d) H19, PPl x10; e) H10, PPl x4; f) H10, PPl x10.

microfacies under Embry and Klovan's classification (1971). The microfacies is composed of bioclasts and quartz grains which are embedded in micrite matrix (Table 3.8). The identified bioclastic fragments are ostracods, phytoclasts and cuticles (Fuhrmann, 2002; Gonçalves, 2014) (Figures 3.19 e, f; 3.20 a, b). There is the presence of subordinate pyrite and organic matter (Figure 3.19e, f). This facies is restricted to the lower portion of the measured stratigraphic section and occasionally in the middle part (Figure 2.20).

#### **3.3.1.4. Interpretation (HA3)**

The wackestone facies are commonly composed of phytoclasts, ostracods and rare intraclasts. The presence of ostracods with the association of phytoclasts/palynofacies and quartz grains in this limestone microfacies suggest moderate to relatively high energy environment condition in fluctuated lacustrine condition. This microfacies interpret relatively shallow alkaline lacustrine facies and characterized as the sublittoral environmental setting (Freytet and Plaziat, 1982; Sanjuan & Martín-Closas, 2012). The intraclast observation and palynofacies component in the microfacies may point to episodic turbulence and deposition from suspension and/or also eolian influence to the sublittoral depositional setting.

#### **3.3.2. Marl Facies (HA3)**

The Marl facies is defined by flaggy soft/loose character fine carbonate rock with high calcareous content (Pettijohn, 1975; Potter et al., 2005 and Stow, 2005). In the Hasanlar section, this facies occur in the form of yellowish gray, thin intercalated intervals with lime mudstone (Figures 2.20; 2.21A). This facies is restricted to the lower portion of the Hasanlar studied stratigraphic column (Figure 2.20).

##### **3.3.2.1. Interpretation (HA3)**

In the Hasanlar studied section, marl intervals are the deposition of unconsolidated lime mud from the suspension in the alkaline lacustrine setting. The marls facies are devoid of fossils and interbedded with lime mudstone and organic-rich shale units.

This facies in the studied section interpret deposition in dysoxic condition and relatively deeper lacustrine environment (Gierlowski-Kordesch, 2010; Sanjuan & Martín-Closas, 2012). The thin intervals of marl and interbedded with limestone microfacies and oil-shale imply deposition from suspension in a calm environmental condition (Pavelić et al., 1998).

### **3.3.3. Oil-shale Facies (HA4)**

In the Hasanlar section, the oil-shale facies is defined on the basis of composition, sedimentary structure and organic matter content (Tables 3.1; 3.5; 3.6; 3.7; 3.8; Figures 3.1; 3.2). In the field, the oil-shale facies is characterized as light brown, light gray, dusky yellow, black to brownish, laminated thin bedded to fragile laminated units (Figures 2.18; 2.19; 2.20; 2.21 and 2.22). Based on microscopic analysis, the facies is organized as alternating of organic-rich laminae and organic-poor laminae (Figures 3.20 c, d, e, f; 3.21). The laminae are arranged in the form of wavy to continuous to lenticular/discontinuous lamination in the studied shale facies (O'Brien, 1990, 1996; Wilkins, 2003) (Figures 3.20 c, d, e, f; 3.21). There is also occurrence of ostracods and euhedral pyrite in the facies with randomly silt-size quartz grains at different intervals (Figures 3.20 c, e; 3.21). At different horizons, the microdolomitization is observed in the oil-shale laminae (Figures 3.20 d, f). This facies is observed throughout the Hasanlar measured section with alternating lime mudstone (Figure 2.20).

#### **3.3.3.1. Interpretation (HA4)**

The occurrence of thick horizontal to wavy to lenticular laminae with the association of the ostracods in the oil-shale indicate relatively deeper lacustrine deposits and characterized as upper profundal depositional zone facies (Dyini & Hawkins, 1981; Gierlowski-Kordesch & Rust, 1994; Keighley, 2008; Tānavsuu-Milkeviciene & Frederick Sarg, 2012). The absence of bioturbation and high organic content in shale

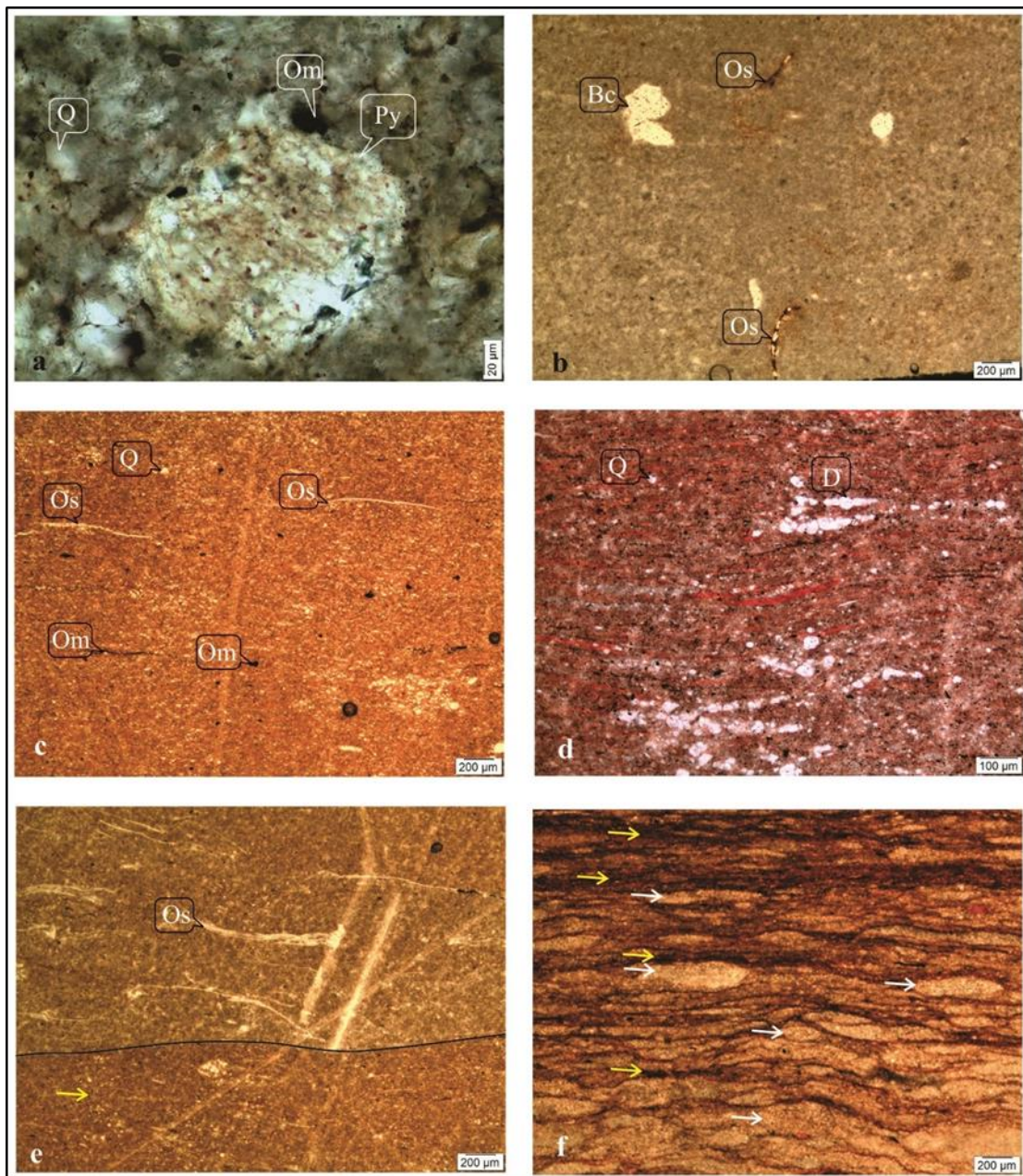


Figure 3.20. Photomicrographs of wackestone and oil-shale presenting quartz (Q), phytoclast (Py), Bioclast (Bc, dissolved fragment), ostracod (Os), micro dolomitic (D) and organic matter (Om). (Sample no. a) Wackestone, H10, PPI x100; b) Wackestone, H12, PPI, x4; c) organic-rich laminae oil-shale, H13, PPI, x4; d) close view, OIL stain lenses in organic-rich laminae, H13, PPI, x10; e) laminated organic-rich oil-shale (Yellow arrow indicates organic-rich laminae), H13, PPI, x4; f) lenticular/convoluted laminated oil-shale, PPI, x4 (yellow arrow indicates organic-rich laminae-dark laminae and white represent organic-poor lenses).

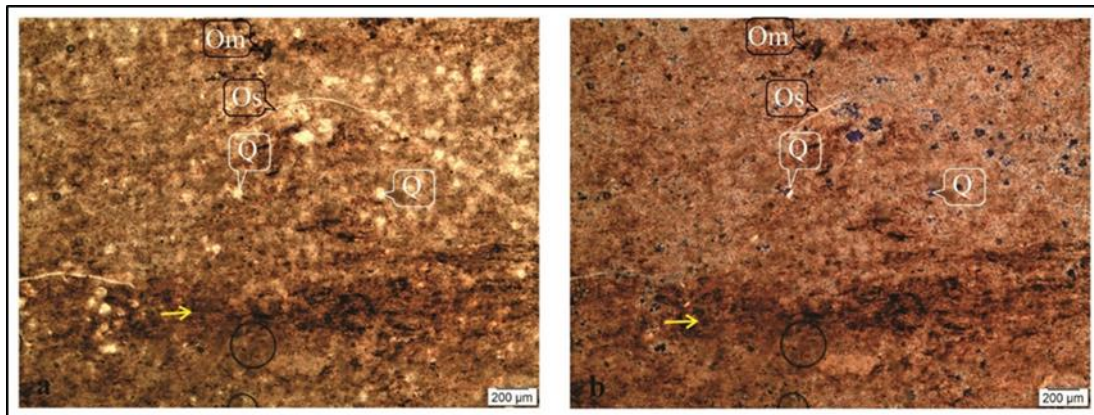


Figure 3.21. Photomicrographs of oil-shale presenting quartz (Q), ostracod (Os) and organic matter (Om). (Sample no. a) H2O, PPl x4; b) H2O, XPl, x4 (yellow arrow indicates organic-rich laminae-dark laminae).

lithofacies direct to relatively low energy environment and anoxic environmental condition (Zeller et al., 2015).

The recorded ostracods in the lithofacies in this succession reflect freshwater lacustrine water depositional setting. In the oil-shale, there is also occasionally framboidal pyrite which may be point to the relatively low saline influence on the lacustrine environment (Brown and Cohen, 1995). The intercalating organic-rich and organic-poor laminae in the shale reflect deposition from suspension under low energy condition. The rhythmic feature of the organic-rich shale represents linked to climatic seasonal changes (Caillaud et al., 2017). The disturbed lamina in the oil-shale may be short-term gravitational deposits in the profundal areas (Feng, 2011). The observation of thick lamina and wavy laminae to lenticular laminae in the oil-shale are characterized as relatively deeper anoxic depositional environment setting (O'Brien, 1990). Towards the top in the studied section, the oil-shale lithofacies is characterized by continuous to discontinuous thin parallel laminae features. These intervals are interpreted to be deposited in the relatively deeper depositional environment compared to lower portion thick laminated oil-shale.

### **3.4. Microfacies of Kösüre Section**

Along the Kösüre measured stratigraphic column, A total of 4 facies are recognized and categorized based on the field observation and petrographic classification (Tables 3.5, 3.6, 3.9, 3.10, 3.11; Figures 3.1; 3.2; 3.3).

#### **3.4.1. Limestone Facies**

In the measured stratigraphic column of the Kösüre section, it is observed that limestone facies define the upper lower portion to lower upper portion in the studied section (Figure 2.25). The documented thin to thick massive limestone facies intervals occur with alternating marl (Figures 2.25; 2.26; 2.28). The detailed observation in the field and microscopic studies help to identified and classified limestone facies. On the basis of the Embry and Klovan`s classification (1971), the limestone facies is classified into two sub-facies (Table 3.11).

##### **3.4.1.1. Wackestone Microfacies (KA1a)**

The wackestone microfacies in the studied section is characterized as very light gray, light olive gray, pinkish gray, light greenish gray, light brownish gray to brownish gray, thin to thick massive bedded intervals (Figures 2.25; 2.7B; 2.28; 3.22; 3.23a). In the field, there is also observation of clay patches in the wackestone facies at the single horizon. These clays are secondary percolation deposits in the bioturbated wackestone (Figures 3.24 d, e) (van der Meer & Menzies, 2011). Echinoderm fragments and abundant euhedral pyrite are also noticed in the wackestone facies in the upper part of the measured stratigraphic section (Figures 3.24f; 3.25a). In the microscopic analysis, this facies is composed of allochems between 10-50% which are embedded in micrite matrix (Tables 3.9; 3.11). The allochems are comprised of predominantly bioclasts, peloids and intraclasts with subordinate pyrite, quartz and rare phosphatic grain (Figures 3.24a, c). The identified bioclasts are ostracods, charophyte, bivalve fragments, gastropod fragments and other unidentified fossils fragments (Figures 2.27A; 3.24 a, b, d). In the measured stratigraphic column, this microfacies is observed

in the upper lower portion to lower upper portion with interbedded marls (Figures 2.25; 3.22; 3.23a).

#### **3.4.1.2. Packstone Microfacies (KA1b)**

Other identified limestone sub-facies in the measured Köşüre section is the Packstone microfacies, based on the Embry and Klovan`s (1971) classification. This facies is comprised of more than 50 percent particles and less than 50 percent micrite matrix (Tables 3.9; 3.11). The facies intervals in the field are thick bedded to massive bedded and very light gray to white color (Figure 3.23b). Microscopically, it composed of intraclasts, peloids, bioclasts which are surrounded by micrite matrix (Tables 3.9, 3.11; Figure 3.25b). The intraclasts are internally homogeneous and dominantly composed of micrites with having a bioclastic fragments internal display. The presence of peloids, intraclasts and micrite matrix indicate deposition in low energy environmental conditions (Figure 3.25b) (Tucker and Wright,1990). The recorded fossils in the facies are ostracod, bivalve fragments and another unidentified fragment. Pyrite is observed in the facies but rare and randomly distributed. This microfacies is restricted to the middle section of the Köşüre studied section (Figure 2.25).

#### **3.4.1.3. Interpretation (KA1a; KA1b)**

In the Köşüre stratigraphic section, wackestone-packstone microfacies correspond to moderate to high energy environment condition and categorized as oxic to dysoxic, relatively littoral-sublittoral depositional setting. The moderate to high energy environmental condition is also supported by the presence of intraclasts, peloidal observation and bivalve fragments in the wackestone-packstone microfacies in the studied section (Freytet and Plaziat, 1982; Sanjuan & Martín-Closas, 2012).

The thin to thick bedded wackestone-packstone microfacies in the lower portion of the studied section, are identified as shallow lacustrine with slightly brackish water character based on the presence of bivalve, bivalve fragments, fish tooth and absence of charophytes (Sanjuan & Martín-Closas, 2012; Anan, 2014). The appearance of charophytes in wackestone-packstone microfacies indicate the relatively freshwater



Figure 3.22. The field photograph of wackestone and marl microfacies of Kösiire measured stratigraphic section; a) Sample wackestone K6, K7, K8 with intercalated marl; b) Wackestone K25, K27 with intercalated marl (Sample K26).



Figure 3.23. The field photograph of a) intercalating wackestone and marl microfacies; b) Packstone microfacies of Köşüre measured stratigraphic section; a) Sample K31, K32, K33; b) packstone K11, K12.

Table 3.9. Limestone, oil-shale and marl petrographic data and established/recognized facies in the Köşüre studied section.

Sample No.	Q	F	Pg	Om	Pl	Pi	In	Bioclasts (Os/Ch/GUb/Al/Da/N/Br)	Other (P/He/Ph/Cr/Ce/Ct)	Matrix (Mi/Cl/Sp/ Or D/Cr)	Field Nomenclature
K2	10	-	-	3	-	-	-	1Ub	3P	83Mi	Marl
K3											Very Fine Sandstone
K6	3	-	-	-	-	35	-	5Bi/10Ub=15	1Ph	46Mi	Pel-Limestone
K9	3	-	-	-	-	5	15	13Bi/1G/2Ub=16	-	61Mi	Pel-Limestone
K11	-	-	-	-	-	40	25	5Os/5Bi/5Ub=15	3P	17Mi	Pel-Limestone
K13	20	-	-	-	-	-	-	2Bi	1P	77Cl	Oil-shale
K16	3	1	1	-	-	-	3	5Os/2Bi/3Ub=10	-	82Mi+Dolo	Bio-Limestone
K18											Sandstone
K19	12	-	1	-	-	-	-	-	1P	86Cl	Oil-shale
K21	-	-	-	-	-	-	-	5Os/15Bi/3Ub=23	2P	75Mi	Bio-Limestone
K24	2	-	-	-	-	5	-	-	2	91Cl	Oil-shale
K25	2	-	-	2	-	-	-	7Os/2Ch/2Ub/1Bn=12	-	84Mi	Bio-Limestone
K39											Sandstone
K40	7	-	-	-	-	3	-	-	2P	88Cl+Or	Oil-shale
K43											Fine Sandstone
K45	2	-	-	-	-	-	-	-	-	98Cl	Oil-shale
K47											Very Fine Sandstone
K49											Sandstone

Os-Ostracoda, Ch-Charopyta, G-Gastropod, Al-Algal, Da-Diatoms, N-Nummulites, Pl-Plant, Fr-Foraminifera, Py-Palynofacies, Ub-Unidentified Bioclasts, Q-Quartz, Qp-Polyquartz, Cr-Chlorite, Ct-Calcite, Mu-Muscovite, Mn-Manganese, P-Pyrite, Ce-Chert, F-Feldspar, Pg-Plagioclase, Sf-Shale fragment, Sst-Siltstone Fragment, Lf-Limestone fragment, Bo-Biotite, T-Tourmaline, Pi-Peloid, In-Intraclasts, R-Rutile, Z-Zircon, Sp-Sparite, Mi-Micrite, D-Dolomite, Cl-Clay, Or-Organic Rich, Om-Organic matter/Bitumen, He-Hematite, Ph-Phosphate, Se-Sphene, Si-silica

Table 3.10. Sandstone petrographic data and established/recognized facies in the Köşüre studied section.

Sample No.	Q	F	Pg	Om	Pl	Accessory Minerals	Rock Fragment	Bioclasts (Os/Ch/G/Ub/Al/Da/N/Br)	Other (P/He/Ph/Cr/Ce/Ct)	Matrix (Mi/Cl/Sp/Or D/Cr)	Field Nomenclature
K3	44	3	5	3	-	7Cr/1T=8	2Pq/2L/5Ct=9	-	-	28Sp	Fine Sandstone
K18	20	10	15	3	-	9Cr/1Bo/2Mu/ 0.5Z/0.5R=13	3Pq/6L/5Sf/6Ce= 20	-	-	19Sp	Medium Sandstone
K39	15	10	10	5	-	5Cr	15Pq/5L/7Sf/5Ce= 32	-	2P	21Sp	Medium Sandstone
K43	33	5	5	3	-	4.5Cr/1Bo/0.5 T/0.5R/0.5Z=7	10Pq/10Ce=20	-	2P	25Sp	Fine Sandstone
K47	27	5	5	3	-	5Cr/1Mu=6	5Pq/5Ce/5Lf=15	-	2P	37Sp	Fine Sandstone
K49	28	5	10	3	-	4.5Cr/0.5Z=5	15Pq/10Ce/10Lf= 35	-	2P	12Sp	Very Fine Sandstone

Os-Ostracoda, Ch-Charopyta, G-Gastropod, Br-Brachiopod, Al-Algal, Da-Diatoms, N-Nummulites, Pl-Plant, Fr-Foraminifera, Py-Palynofacies, Ub-Unidentified Bioclasts, Q-Quartz, Qp-Polyquartz, Cr-Chlorite, Ct-Calcite, Mu-Muscovite, Mn-Manganese, P-Pyrite, Ce-Chert, F-Feldspar, Pg-Plagioclase, Sf-Shale fragment, Sst-Siltstone Fragment, Lf-Limestone fragment, Bo-Biotite, T-Tourmaline, Pi-Peloid, In-Intraclasts, R-Rutile, Z-Zircon, Sp-Sparite, Mi-Micrite, D-Dolomite, Cl-Clay, Or-Organic Rich, Om-Organic matter/Bitumen, He-Hematite, Ph-Phosphate, Se-Sphene

Table 3.11. Sandstone petrographic data and established/recognized facies in the Köşüre studied section.

Sample No.	Compositional Classification of shale and marl			Texture Classification*	Limestone Classification (Embry and Klovan's 1971)	Sandstone Classification (Folk's 1974)	Defined Facies in Studied Section
	Diaz's (2012) Mudstone (Unconventional)	Stow's (2005)	Allix's (2010) Shale	Fine Grained Rock Folk's (1965)			
K2	Mixed Carbonate Mudstone	Marl	Argillaceous Marlstone	Clay-Shale			Marl
K3						Feldspathic Litharenite	Fine Sandstone
K6					Pel-Wackestone		Wackestone
K9					Intra-Wackestone		Wackestone
K11					Intra-Packstone		Packstone
K13	Mixed Mudstone	Smarl	Argillaceous Mudstone	Clay-Shale			Oil-shale
K16					Bio-Wackestone		Wackestone
K18						Lithic Arkose	Medium Sandstone
K19	Argillaceous/Carbonate Mudstone (Marl)	Smarl	Argillaceous Marlstone	Clay-Shale			Oil-shale
K21					Bio-Wackestone		Wackestone
K24	Carbonate-rich Argillaceous Mudstone	Marl	Argillaceous Mudstone	Clay-Shale			Oil-shale
K25					Bio-Wackestone		Wackestone
K39						Feldspathic Litharenite	Medium Sandstone
K40	Argillaceous/Carbonate Mudstone (Marl)	Marl	Argillaceous Marlstone	Clay-Shale			Oil-shale
K43						Feldspathic Litharenite	Fine Sandstone
K45	Carbonate-rich Argillaceous Mudstone	Marl	Argillaceous Mudstone	Clay-Shale			Oil-shale
K47						Feldspathic Litharenite	Fine Sandstone
K49						Feldspathic Litharenite	Fine Sandstone

\* Based on grains size of mud fraction, non-fissile/fissile and soft.

Table 3.11. Continues...

Sample No.	(Texture and/or Compositional)	Defined Facies in Studied Section
K2	Patchy Dolomite but rare	Marl
K3	Fine grains size, Well Sorted, Closely Packed	Fine Sandstone
K6	Pel-Wackestone, Bedded	Wackestone
K9	Intra-Wackestone, Bedded, Pyrite in bio-Chamber	Wackestone
K11	Intra-Packstone, Bedded	Packstone
K13	Oil-shale, Flaggy, Brachiopods	Oil-shale
K16	Bio-Wackestone, Bedded, Dolomitic patches in the matrix	Wackestone
K18	Medium-grained size, Moderated Sorted, loosely Packed, Charcoal	Medium Sandstone
K19	Oil-shale	Oil-shale
K21	Bio-Wackestone, Bedded	Wackestone
K24	Thin laminae, Oil-shale	Oil-shale
K25	Bio-Wackestone, Bedded, secondary clay percolation	Wackestone
K39	Medium-grained size, Poorly Sorted, Loosely Packed	Medium Sandstone
K40	Thin Laminae	Oil-shale
K43	Fine-grained size, Well Sorted, Loosely Packed	Fine Sandstone
K45	Laminae, Oil Stained	Oil-shale
K47	Fine-grained size, Moderately Sorted, Loosely Packed	Fine Sandstone
K49	Fine-grained size, Moderately Sorted, Closely Packed	Fine Sandstone

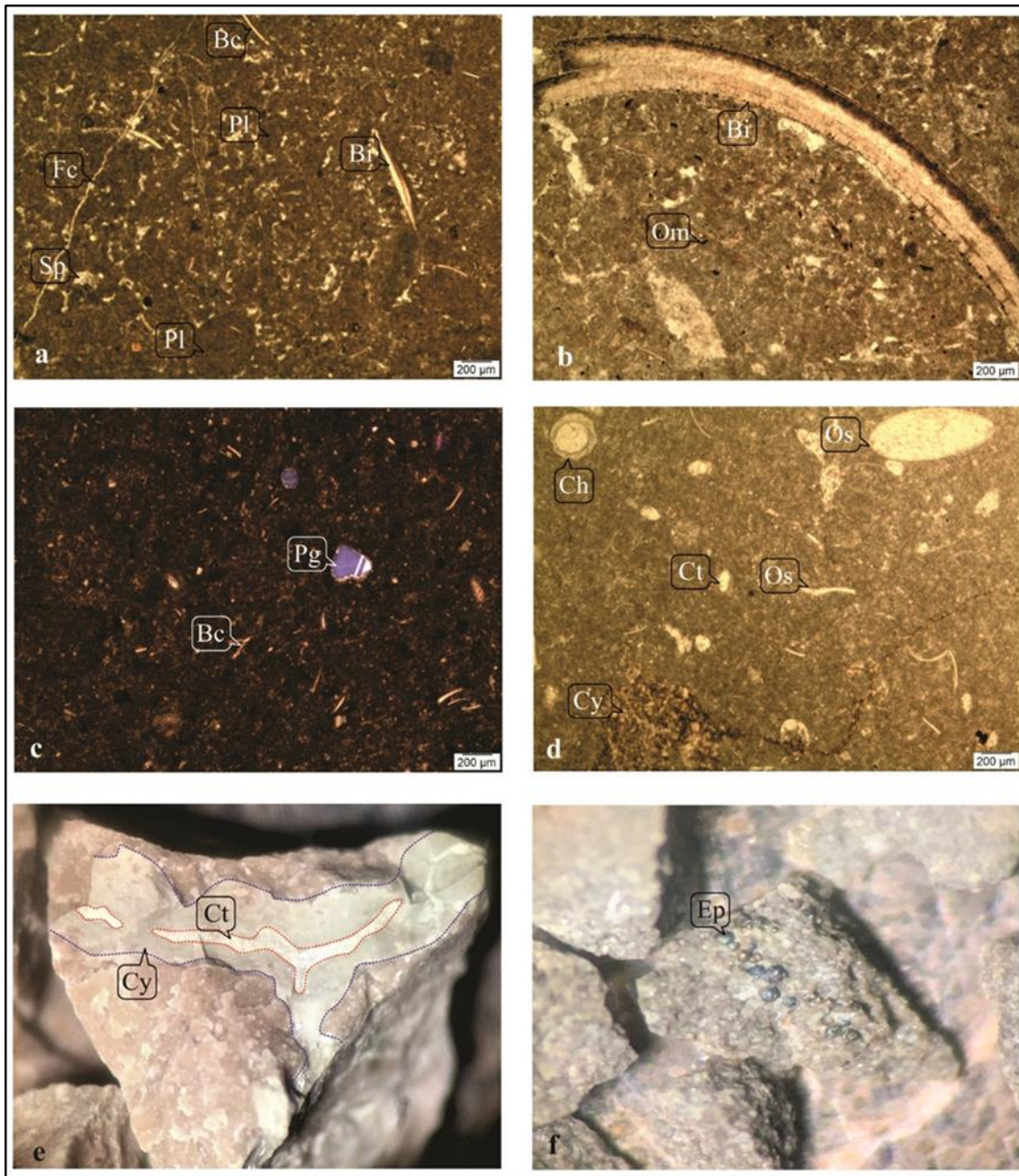


Figure 3.24. Photomicrographs of wackestone microfacies presenting charophyta (Ch), ostracod (Os), quartz (Q), plagioclase (Pg), bioclasts (Bc), calcite (Ct), peloid (Pl), clay (Cy), sparite (Sp), euhedral pyrite (Ep), Bivalve (Bi), organic matter (Om), sparite (Sp) and fracture (Fc). (Sample no. a) K6, PPI x4; b) K9, PPI x4; c) K16, XPI x4; d) K25, PPI x4; e) K25, x4; f) K34, x4.

depositional condition. The association with freshwater water ostracod in these intervals also suggests freshwater lacustrine environmental setting (Grosjean & Pittet, 2013).

The association of foraminifera, echinoderm fragment, fish teeth and diversified ostracods in the limestone argued marine condition (Huyghe et al., 2017). In the upper portion of the studied section, the wackestone-packstone microfacies contain echinoderm biota and appearance of abundant pyrite. The echinoderm association, absence of charophytes and abundant pyrite in the wackestone-packstone facies in the studied section interpret marine environmental facies (Baumiller & Gazdzicki, 1996). The pyrite formation in the studied section corresponds to the saline influence into the depositional basin (Brown and Cohen, 1995; Wang et al., 2013).

#### **3.4.2. Marl facies (KA2)**

Marl facies is the dominantly observed facies after wackestone facies in the Kösüre section (Figure 2.25). Marl is a fine-grained carbonate rock kind, which is characterized as a high proportion of calcareous character with relatively soft/loose sediment and non-fissile character (Pettijohn, 1975; Potter et al., 2005 and Stow, 2005; Figure 3.2). In the outcrop, the marl facies is observed as red thick interval at the base and then followed by dark greenish gray to greenish gray, thick to thin intervals with alternating limestone and occasionally sandstone lithofacies (Figures 2.24; 2.25; 2.26A, B; 2.28; 2.31; 2.32; 3.22b; 3.23a). Microscopic studies, the marl facies is composed of mainly lime mud matrix with the rare occurrence of silt-size quartz and bioclastic fragments (Tables 3.9, 3.11; Figures 3.25c, d, e). The extracted bioclasts include ostracods, fish-teeth and charophytes from the marl facies at different intervals (Figures 3.25d, e).

##### **3.4.2.1. Interpretation (KA2)**

Generally, marls facies are characterized as depositional facies in low energy and the relatively deeper environment in both lacustrine settings and in marine condition (Gierlowski-Kordesch, 2010; Sanjuan & Martín-Closas, 2012). In the Kösüre section,

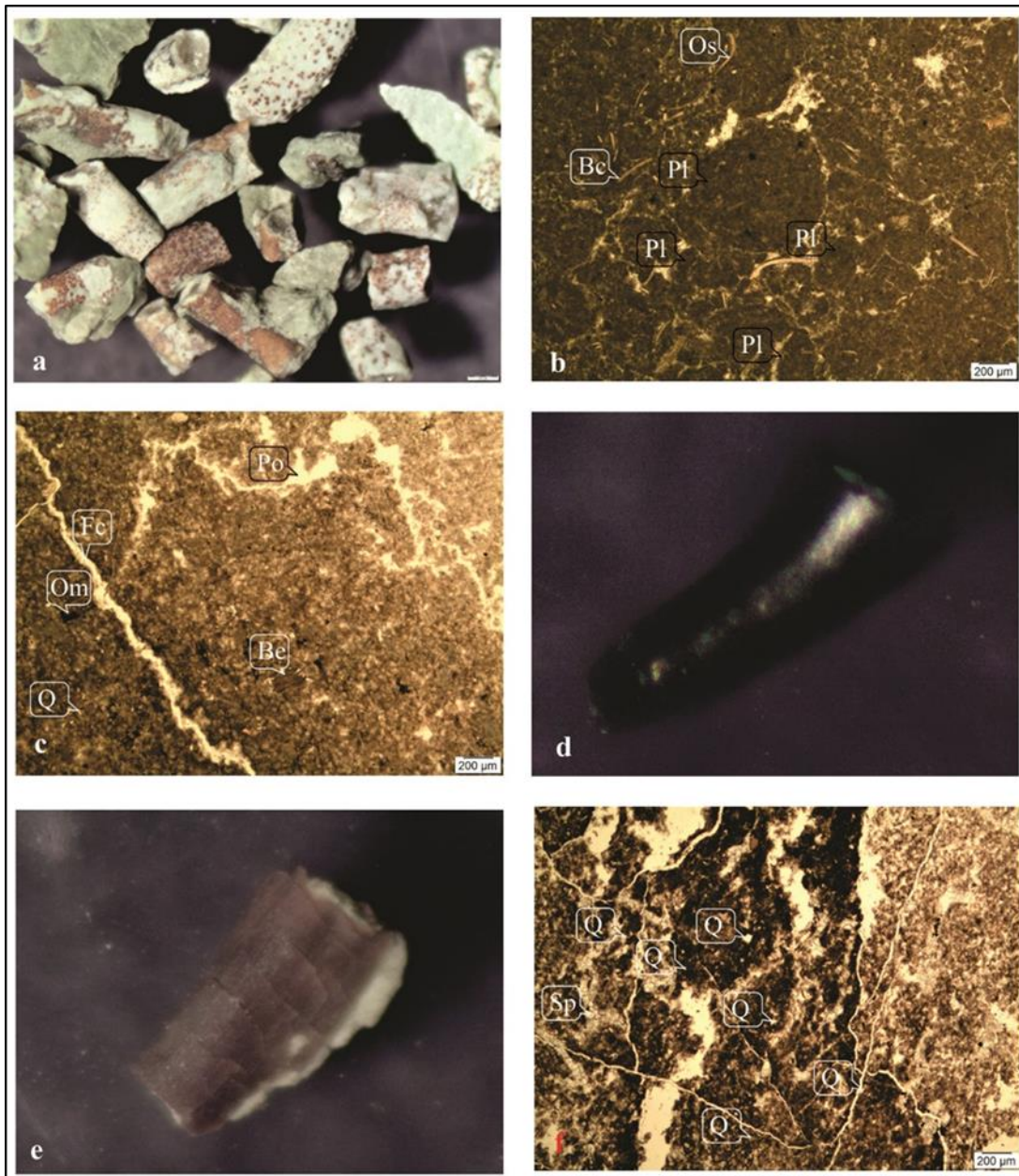


Figure 3.25. Photomicrographs of a) wackestone microfacies; b) packstone microfacies; c, d, e) marl facies and f) oil-shale facies presenting ostracod (Os), quartz (Q), bioclasts (Bc), peloid (Pl), biotite (Be), organic matter (Om), sparite (Sp) and porosity (Po). (Sample no. a) K38, Echinoderm, x4; b) K11, PPl x4; c) K2, PPl x4; d) K20, fish-tooth, x4; e) K28, fish-tooth, x4; f) K13, PPl, x4.

the thin to thick massive marl intervals interprets that it is deposited from the suspension in a relatively deeper (sublittoral zone) lacustrine. In the upper portion of the studied section, the documentation of ostracod and rare brackish-charophytes in the marls facies suggest slightly brackish water with dysoxic environmental condition (Pavelić et al., 1998). The recognition of rare fish tooth from the marls facies also indicate slightly brackish environmental condition setting.

### **3.4.3. Oil-shale Facies (KA3)**

The fine-grained sedimentary rocks can be described by a number of terms, includes shale or mudstone or claystone or mudrock. Number of researchers classified fine-grained sedimentary rocks on the basis of one or a combination of two or more features; includes composition, sedimentary structure and organic matter content, as shown in table 3.5; 3.6; 3.9; 3.11; Figures; 3.1A, B; 3.2 (Deng and Qian, 1990; Stow, 2005; Allix et al., 2010; Diaz et al., 2012; Wang, 2012; Jiang et al., 2013; Zou et al., 2010). Based on the above classification, this lithofacies is named as oil-shale facies in the Kösüre measured section (Tables 3.5; 3.6; 3.9; 3.11; Figures; 3.1A, B; 3.2).

The established oil-shale lithofacies is mainly reported at the middle and upper section of the measured stratigraphic column (Figure 2.25). In general, this lithofacies is appeared in the field as grayish green to grayish black, dark gray to black, laminated to thin planar bedded with discontinuous lamination to relatively homogeneous structureless intervals with fragile character (Figures 2.27B; 2.28; 2.29B; 2.31; 2.32B; 3.25e). At a single interval, the oil-shale facies characterize a thin parallel algal laminated feature (Figure 2.29B). By observing microscopically, in the field and chemical analysis data, it is interpreted that this lithofacies comprised of more clay matrix with comparatively organic-rich character. In this facies, the average matrix is observed more than 88 percent (Table 3.9). It contains a minor amount of silt-sized to very fine sand-size quartz grain and very rare pyrite and bioclasts (Figures 3.25f; 3.26a, b, c, d). There is also the observation of bioturbation in the facies but rare.

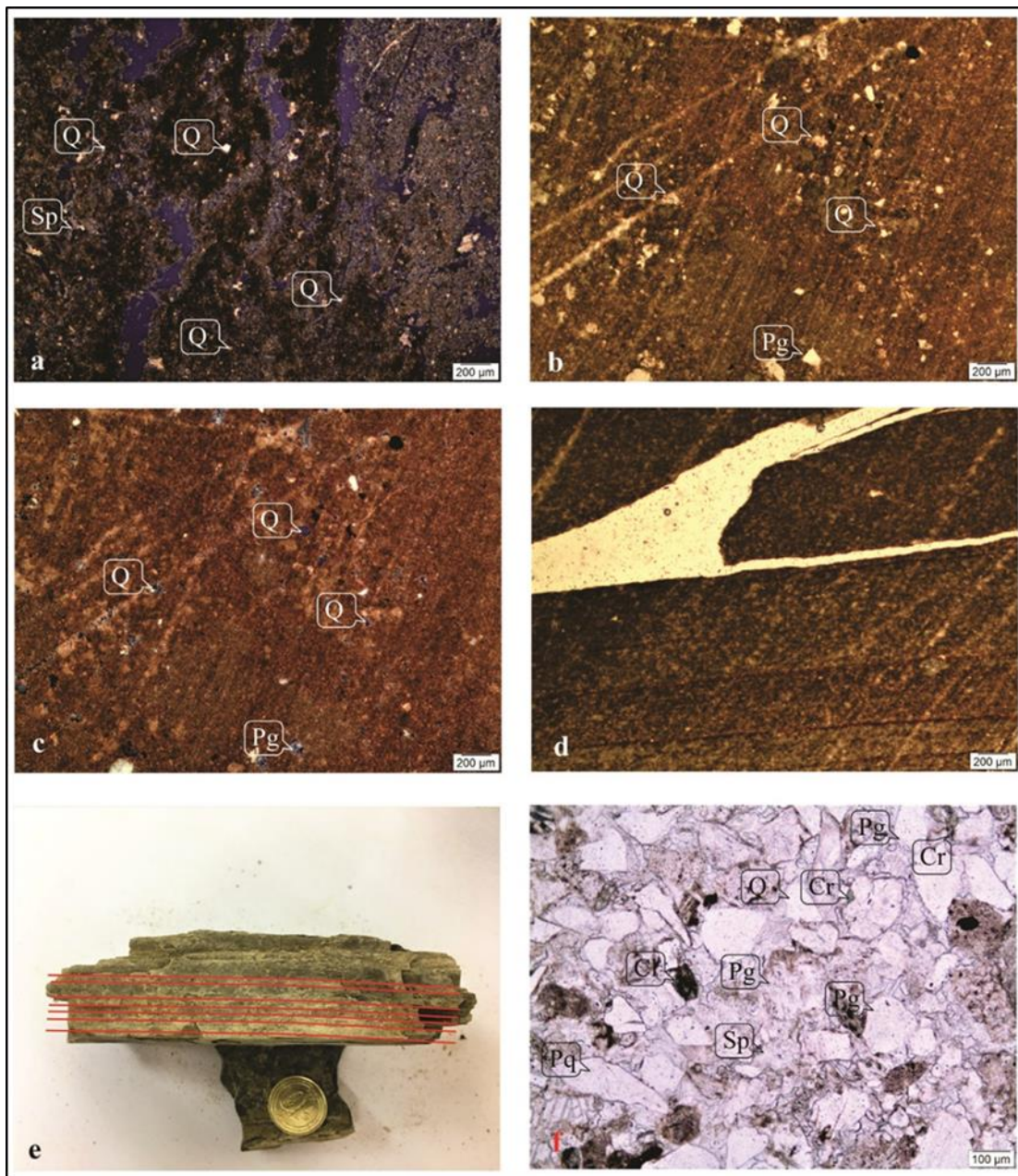


Figure 3.26. Photomicrographs of a, b, c, d, e) oil-shale facies; and f) sandstone facies presenting quartz (Q), plagioclase (Pg), calcite (Ct), polycrystalline quartz (Pq), chlorite (Cr), biotite (Be), organic matter (Om), and sparite (Sp) (Sample no. a) K13, Xpl, x4; b) K19, PPl, x4; c) K19, XPl, x4; d) K40, laminated oil-shale, PPl, x4; e) K40, hand specimen ; f) K18, PPl, x10.

#### **3.4.3.1. Interpretation (KA3)**

The organic-rich shale in the lacustrine environment is controlled by basin setting, sediment supply, climatic changes, salinity and redox condition of the depositional setting (Xu et al., 2015; Liang et al., 2018). In the Kösüre section, organic-rich shale first appears in the middle portion. These intervals are identified as massive, laminated, high organic content and lack of bioturbation. These features in the organic-rich shale indicate low energy, an anoxic condition in lacustrine environmental setting (Ma et al., 2016). General, these oil-shale horizons interpret deposition occur under low energy, calm water and upper profundal lacustrine environment (Gingras et al., 2011; Amezcua, 2012; Abouelresh et al., 2017). In the upper portion, the intercalating oil-shale with fine sandstone are interpreted as deposition from suspension in low energy marine offshore-transitional zone with anoxic depositional condition (Dyini & Hawkins, 1981; Gierlowski-Kordesch and Rust, 1994; Keighley, 2008; Tänavsuu-Milkeviciene & Frederick Sarg, 2012; Abouelresh et al., 2017).

#### **3.4.4. Calcareous Sandstone Facies (KA4)**

The sandstone lithofacies is defined on basis of three end member triangular classification, which are feldspar-plagioclase member, quartz member and rock fragment member (Folk, 1974 and Pettijohn et al., 1987; Figure 3.3). The recognized sandstone lithofacies in the studied section is greenish gray to grayish green, dusky yellow green to grayish yellow green very thin to thick massive bedded interval with occasionally marl intercalated horizons (Figures 2.25; 2.26A; 2.28; 2.29A). Occasionally, the sandstone lithofacies is characterized by nodularity and low angle wavy rippled to thin parallel bedding structures (Figure 2.29A; 2.33B; 3.27d; 3.28a, c). Generally, sandstone facies have sharp lower and upper contact with underlying and overlying facies (Figures 2.26A; 2.29A; 2.30; 2.31; 2.32; 2.33B; 3.27c). There is also the presence of preserved fish-tooth fossil in the sandstone lithofacies in the upper portion of the studied section (Figure 2.33A). In the measured stratigraphic column,

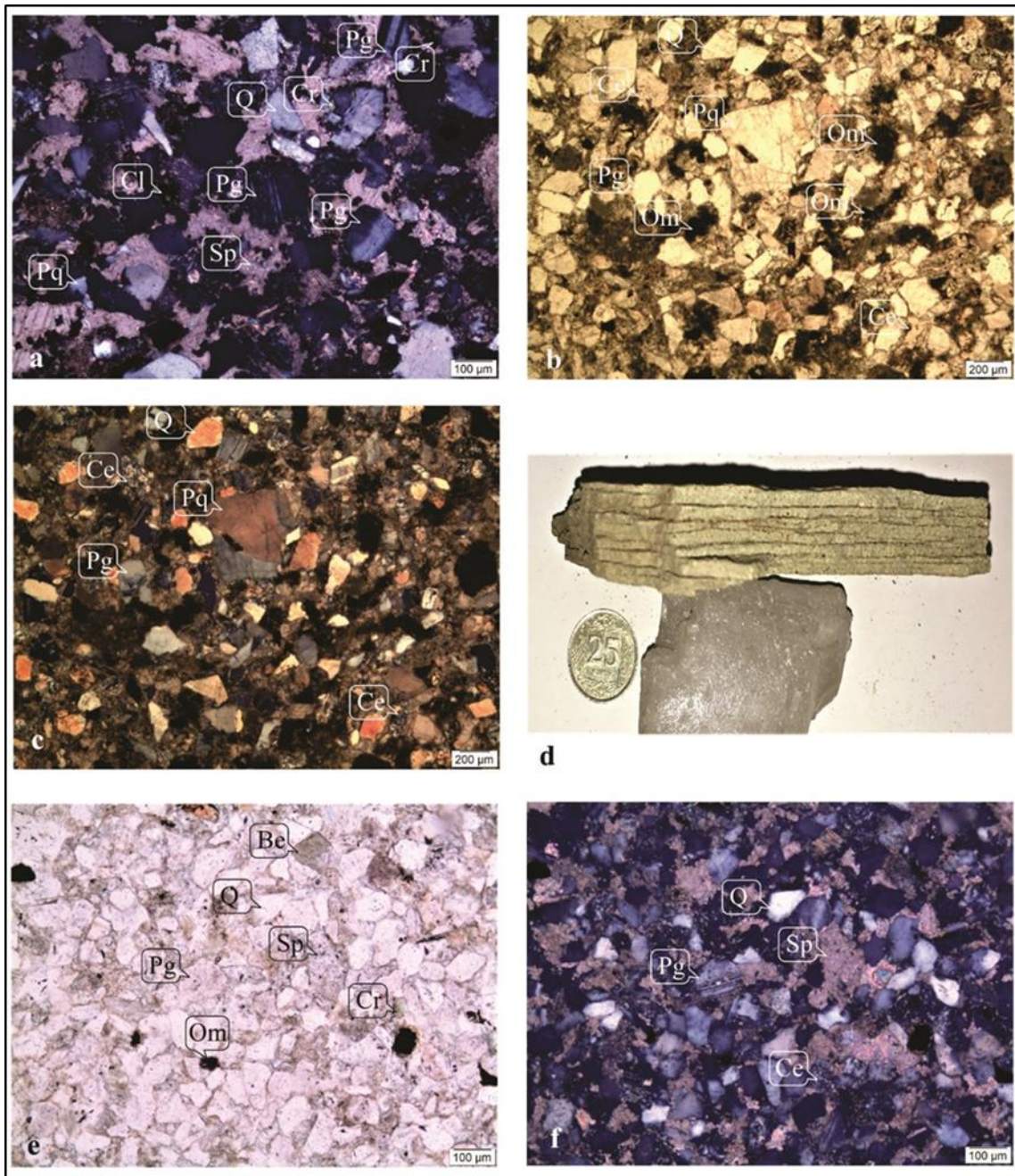


Figure 3.27. Photomicrographs of sandstone facies presenting quartz (Q), plagioclase (Pg), chert (Ce), polycrystalline quartz (Pq), chlorite (Cr), organic matter (Om), and sparite (Sp) (Sample no. a) K18, Xpl, x10; b) K39, PPl, x4; c) K39, XPl, x4; d) K43, long angle wavy very thin planar bedding, hand specimen; e) K43, PPl, x10; f) K43, XPl, x10.

this lithofacies is occasionally observed near the base, in the middle portion and dominantly upper portion (Figure 2.25). The petrographic data shows that this lithofacies is composed of two kinds of sandstone sub-lithofacies on the basis of the Folk's (1974) and Pettijohn et al., (1987) sandstone classification (Tables 3.3; 3.4; Figure 3.3). The classified sub facies are identified as feldspathic litharenite and lithic arkose sandstone (Tables 3.10; 3.11; Figure 3.3). The sandstone lithofacies are comprised of sand-size quartz grains, feldspar, plagioclase, rock fragments with a minor amount of accessory minerals and rare pyrite, bioclasts and organic matter (Figures 3.26f; 3.27; 3.29b). The identified rock fragments include polycrystalline quartz, limestone clast, chert and shale clasts. The sandstone lithofacies are cemented together by sparite. The identified accessory minerals are chlorite, tourmaline, biotite, muscovite, zircon and rutile. The particles in the facies are very fine sand-size to coarser sand size, angular to sub-rounded, poorly to moderate to well sorted with mostly loosely packed and rare close-packed (Figures 3.26f; 3.27; 3.29b).

#### **3.4.4.1. Interpretation (KA4)**

The sandstone intervals with intercalating shale and/or marl units are defined as heterolithic successions. These deposits are observed in both lacustrine and marine environmental setting and mostly characterized as offshore-transitional deposits. In the lower and middle portion of the studied section, the massive to nodular calcareous sandstone with alternating marl units are interpreted to be deposited in the offshore-transition zone in lacustrine environmental condition. These are recognized as the episodic influx of terrigenous clasts to the relatively deep lacustrine depositional setting (Rees et al., 2014; Meling, 2016).

The upper portion of the Kösüre section is characterized by increasing in the sandstone intervals and intercalating with organic-rich shale. These heterolithic deposits are identified as marine depositional units. These units show small-scale hummocky stratification, planar laminated, small ripple laminated sandstone, massively bedded features sandstone and represent sharp and/or obscure contact with oil-shale facies.

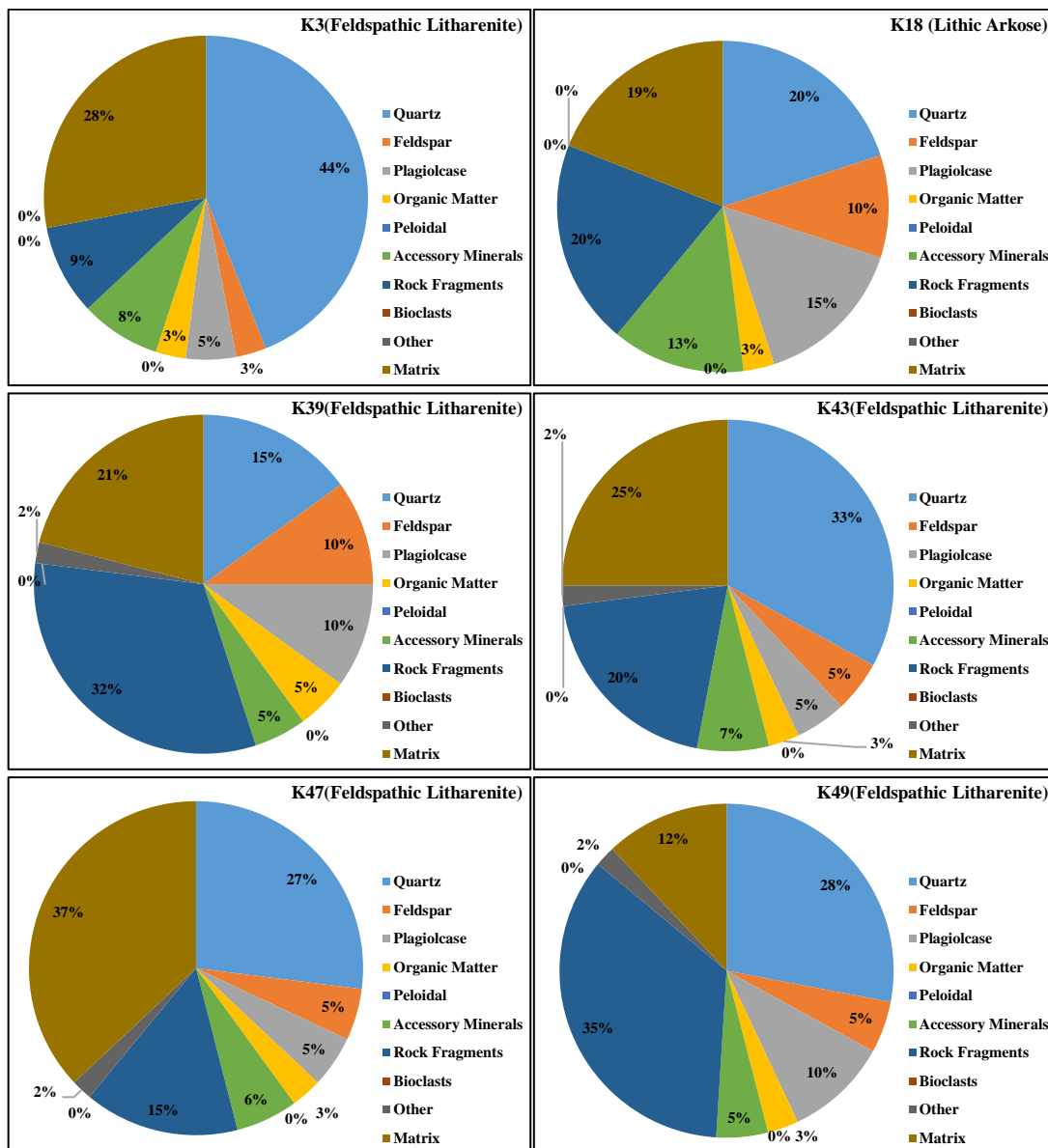


Figure 3.28. Pie graphs of the sandstone lithofacies in the Kösüre section.

On the basis of these features, these are recognized as storm-induced deposits on offshore-transition marine environment setting (Collinson et al., 2006; Rees et al., 2014; Johansen, 2016). The marine origin in the upper sandstone is also identified on the basis of observation of rare fish tooth fossil and overlying the marine limestone units (Huyghe et al., 2017). Overall, the calcareous sandstone lithofacies is deposited near the storm wave base on the marine offshore-transition setting and categorized as

turbiditic-tempestitic intervals (Figure 3.28). The high percent of calcareous matrix in the sandstone indicate deposition under relatively deeper water column (Figure 3.28). The organic-rich shale lithofacies are precipitated from suspension under anoxic, low energy depositional conditions (Dahlqvist, 2018).

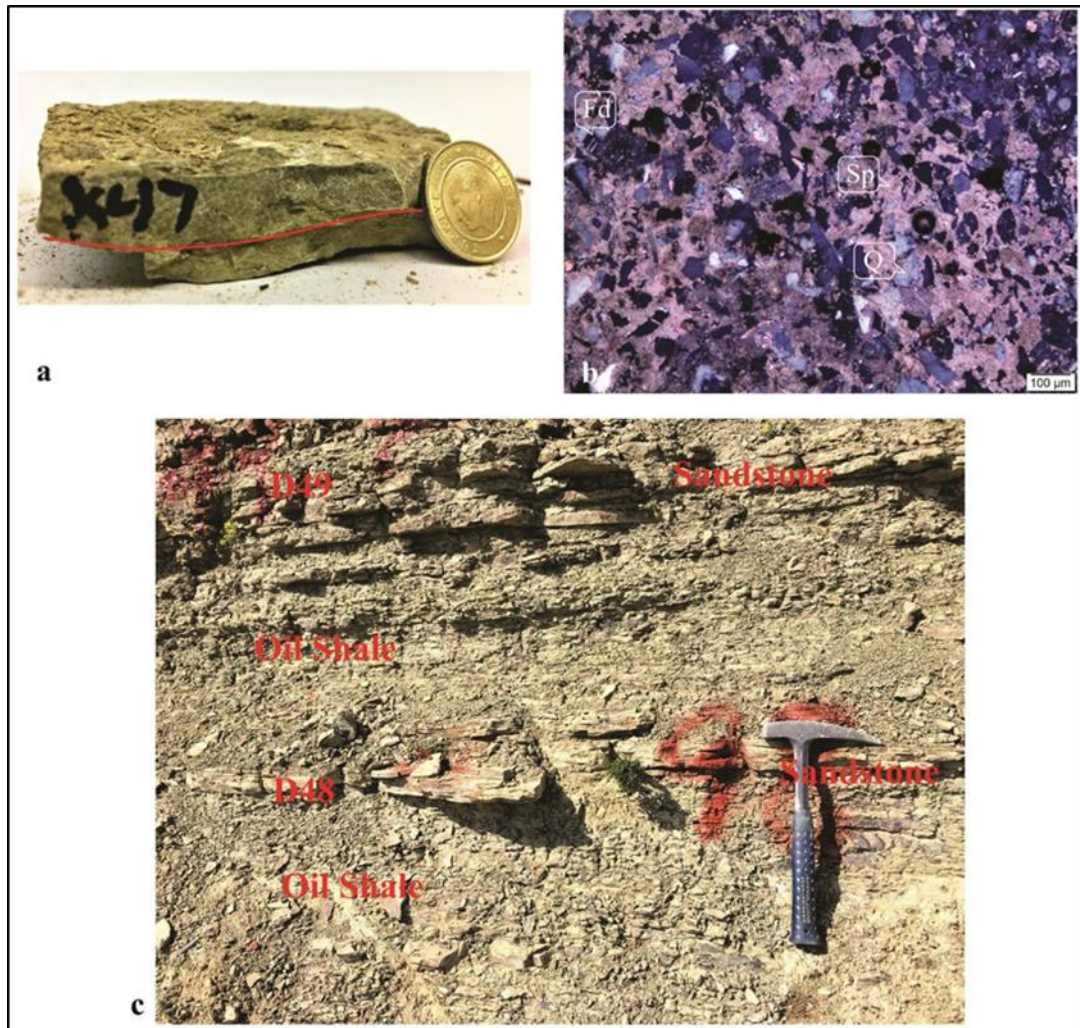


Figure 3.29. Photomicrographs of sandstone facies presenting quartz (Q), feldspar (Fd) and sparrite (Sp). (Sample no. a) K47, hand specimen, showing wavy rippled bedding (indicated by red line); b) K47, XPl x10; c) field photograph of interbedded sandstone and shale (K48, K49).

### 3.5. Microfacies of Karahisar Section

The Lutetian-Bartonian measured stratigraphic section near the Karahisar village, a total of three facies are categorized in the studied section, which are described in details as below (Tables 3.12, 3.13, 3.14);

#### 3.5.1. Limestone Facies

Based on the Embry and Klovan's classification (1971), the limestone facies is characterized as lime mudstone microfacies in the Karahisar stratigraphic section. The limestone facies is observed throughout the vertical measured section with alternating oil-shale (Figure 2.36).

##### 3.5.1.1. Lime Mudstone Microfacies (TA1)

The classified lime mudstone microfacies is documented as medium gray, medium dark gray to dark gray, very thin bedded to medium planar bedded units and having spherical to ellipsoidal ferrous-manganese nodules in the upper portion intervals of the studied section. The size of manganese nodules in the lime mudstone facies is ranging from microscopic (200 um) to approximately 1.5 cm (Figures 2.35; 2.38; 2.39A; 3.31b, c, f; 3.32a). There is also observation of small plant fragments (Figures

Table 3.12. Limestone, oil-shale and marl petrographic data and established/recognized facies in the Karahisar section.

Sample No.	Q	F	Pg	Om	Pl/Py	Pi	In	Bioclasts (Os/Ch/GUb/Al/Da/N/ Br)	Other (P/He/Ph/Cr/Ce/Ct)	Matrix (Mi/Cl/Sp/Or D/Cr)	Field Nomenclature
T1	15	-	-	5	-	-	-	-	-	80Mi+Or+D	Oil-shale
T4	17	-	-	-	-	-	-	-	-	83Mi+Or	Oil-shale
T5	5	-	-	5	-	-	-	-	10P	80Mi+Or	Oil-shale
T7	8	-	-	5	-	-	-	-	7P	80Mi	Lime Mudstone
T8	5	-	-	10	10	-	-	-	5P	70Mi	Lime Mudstone
T9	30	-	-	-	-	-	-	1Ub	-	69Mi	Oil-shale
T12	10	-	-	10	10	-	-	2Os	10Fe-Mn	58Mi	Lime Mudstone
T13	5	-	-	12	8	-	-	-	10Cl/10Fe-Mn=20	55Mi	Lime Mudstone
T16	5	-	-	15	-	-	-	-	11Fe-Mn	69Mi+D	Lime Mudstone
T17	15	-	-	3	1	-	-	-	3P	78Mi	Oil-shale
T22	15	-	-	15	-	-	-	-	5P	65Mi+Or	Oil-shale
T23	5	-	-	15	-	-	-	3Ub	5Cr/5Cl/10Fe-Mn=20	60Mi	Lime Mudstone
T27											Fine Sandstone

Os-Ostracoda, Ch-Charopyta, G-Gastropod, Al-Algal, Da-Diatoms, N-Nummulites, Pl-Plant, Fr-Foraminifera, Py-Palynofacies, Ub-Unidentified Bioclasts, Q-Quartz, Qp-Polyquartz, Cr-Chlorite, Ct-Calcite, Mu-Muscovite, Fe-Mn-Ferrous-manganese, P-Pyrite, Ce-Chert, F-Feldspar, Pg-Plagioclase, Sf-Shale fragment, Stf-Siltstone Fragment, Lf-Limestone fragment, Bo-Biotite, T-Tourmaline, Pi-Peloid, In-Intraclasts, R-Rutile, Z-Zircon, Sp-Sparite, Mi-Micrite, D-Dolomite, Cl-Clay, Or-Organic Rich, Om-Organic matter/Bitumen, He-Hematite, Ph-Phosphate, Se-Sphene, Si-silica

Table 3.13. Sandstone petrographic data and established/recognized facies in the Karahisar section.

Sample No.	Q	F	Pg	Om	P/Py	Accessory Minerals	Rock Fragment	Other (P/He/Ph/Cr/Ce/Ct)	Matrix (Mi/Cl/Sp/Or/D/Cr)	Field Nomenclature
T27	30	5	-	3	-	5Cr/0.5R/2Mu/1Bo/0.5T=9	5Pq/2Ce/5Sf=12	2Ph/10P=12	25Sp+4Ce	Fine Sandstone

Os-Ostracoda, Ch-Charopyta, G-Gastropod, Br-Brachiopod, Al-Algal, Da-Diatoms, N-Nummulites, Pl-Plant, Fr-Foraminifera, Py-Palynofacies, Ub-Unidentified Bioclasts, Q-Quartz, Qp-Polyquartz, Cr-Chlorite, Ct-Calcite, Mu-Muscovite, Mn-Manganese, P-Pyrite, Ce-Chert, F-Feldspar, Pg-Plagioclase, Sf-Shale fragment, Srf-Siltstone Fragment, Lf-Limestone fragment, Bo-Biotite, T-Tourmaline, Pi-Peloid, In-Intraclasts, R-Rutile, Z-Zircon, Sp-Sparite, Mi-Micrite, D-Dolomite, Cl-Clay, Or-Organic Rich, Om-Organic matter/Bitumen, He-Hematite, Ph-Phosphate, Se-Sphene

Table 3.14. Classifications of the limestone, sandstone, oil-shale, marl and sandstone and established/recognized microfacies in the Karahisar section.

Sample No.	Compositional Classification of shale and marl			Texture Classification*	Limestone Classification (Embry and Klovan's 1971)	Sandstone Classification (Folk's 1974)	Defined Facies in Studied Section
	Diaz's (2012) Mudstone (Unconventional)	Stow's (2005)	Allix's (2010) Shale	Fine-Grained Rock Folk's (1965)			
T1	Silica-rich dominated Carbonate Mudstone	Calcareous-Siliceous	Calcareous or Dolomitic Mudstone	Clay-Shale			Oil-shale
T4	Mixed Carbonate Mudstone	Calcareous-Siliceous	Siliceous Marlstone	Clay-Shale			Oil-shale
T5	Clay-rich Carbonate Mudstone	Calcareous-Siliceous	Siliceous Marlstone	Clay-Shale			Oil-shale
T7					Lime Mudstone		Lime Mudstone
T8					Lime Mudstone		Lime Mudstone
T9	Silica-rich dominated Carbonate Mudstone	Calcareous-Siliceous	Siliceous Marlstone	Mud-Shale			Oil-shale
T12					Lime Mudstone		Lime Mudstone
T13					Lime Mudstone		Lime Mudstone
T16					Lime Mudstone		Lime Mudstone
T17	Mixed Carbonate Mudstone	Calcareous-Siliceous	Argillaceous Marlstone	Clay-Shale			Oil-shale
T22	Mixed Carbonate Mudstone	Calcareous-Siliceous	Argillaceous Marlstone	Clay-Shale			Oil-shale
T23					Lime Mudstone		Lime Mudstone
T27						Feldspathic litharenite	Fine Sandstone

\* Based on grains size of mud fraction, non-fissile/fissile and soft.

Table 3.14. Continues...

Sample No.	(Texture and/or Compositional)	Defined Facies in Studied Section
T1	Thin to thick Laminae, organic-rich and organic-poor laminae, Oil-shale	Oil-shale
T4	Thick and Wavy Laminae, sub-round very fine sand- size quartz, Oil-shale	Oil-shale
T5	Thick Laminae, randomly distributed pyrite and quartz grains Oil-shale	Oil-shale
T7	Thick Laminae, silt-size quartz grains, Mudstone	Lime Mudstone
T8	Medium Bedded, Calcite Concertion, pyrite, phytoclasts	Lime Mudstone
T9	angular to sub-rounded, Silt to sand size quartz, Organic Poor Shale	Oil-shale
T12	Silty Lime Mudstone, Pollen and Spore, Bacterial Mucus, Oil Marl, Mn Nodules	Lime Mudstone
T13	Silty Lime Mudstone, Mn Nodules	Lime Mudstone
T16	Silty Lime Mudstone, Lenses, Mn Nodules	Lime Mudstone
T17	Thin Laminae, Oil-shale	Oil-shale
T22	Thin Laminae	Oil-shale
T23	Silty Lime Mudstone, Mn Nodules	Lime Mudstone
T27	Angular-sub-rounded, Well Sorted, loosely Packed, Charcoal, Oil Stained patches in matrix Patchy sparite	Fine Sandstone

3.30c, d, f; 3.31a, d) (Gonçalves, 2014). At a horizon, the facies bedding is characterized by calcareous concretion on the bedding surface with irregular shape (Figures 2.27B; 3.30b). Petrographic analysis, this facies is comprised of predominantly micrite matrix with subordinate quartz and rare ostracods and development of dolomitic patches with anhedral to euhedral form within the matrix (Tables 3.12; 3.14). The opaque particles such as organic matter, ferrous-manganese nodules, pyrite and phytoclasts fragments, cuticles fragments are randomly distributed in the facies (Figures 3.30; 3.31) (Fuhrmann, 2002; Shivanna & Singh, 2016).

### **3.5.1.2. Interpretation (TA1)**

In the Karahisar section, the lower portion non-ferromanganese bearing lime mudstone and the upper portion ferromanganese bearing lime mudstone microfacies are deposited in low energy, anoxic sublittoral-profundal lacustrine and shallow marine depositional environment, respectively. The lack of clastic particles in the lime mudstone microfacies suggest limited access of the terrigenous clasts to the depositional setting. Due to the anoxic bottom water condition, there is an absence of bioturbation and contains high organic content in the lime mudstone and suggest sublittoral-profundal deposits (Gingras et al., 2011; Amezcua, 2012). The small plant remains in the limestone are driven by either strongly influence episodic event deposits or eolian transport to the depositional setting (Tosal et al., 2018). The palynofacies and abundant amorphous organic matter also reflect that the lime mudstone is deposited in low energy and oxygen depleted environmental setting (Staplin, 1969; Tyson, 1995; Pittet & Gorin, 1997). The documentation of Fe-Mn nodules in the lime mudstone strata with association of black shales intervals indicate marine incursion to the restricted sublittoral-profundal lacustrine setting (Bolton & Frakes, 1985; Delian et al., 1992; Roy, 1992; Fuhrmann, 2002). The Fe-Mn nodules formed at the oxidizing-reducing interface and preserved in the lime mudstone in the anoxic bottom water condition (Tribovillard et al., 2006).

In the upper portion of the Karahisar studied section, the appearance of Fe-Mn small spherical nodules is indicated to be hydrogenetic origin in shallow marine environmental condition and associated with organic-rich shale (Wang et al., 2014). In the north-western regime of Turkey, there is the observation of Mn oxides in the Oligocene shallow marine deposits, which is linked with a rapid marine transgressive-regressive cycle. Generally, Fe-Mn oxides are formed at the interface of oxic-anoxic water and can be deposited in anoxic bottom water condition (Gültekin and Balci, 2018). In the Karahisar measured section, the Fe-Mn nodules in lime mudstone suggested forming in brackish water with low salinity in the depositional basin. The occurrence of brackish water condition and change in salinity condition in the lacustrine environment interpret marine incursion to the system. The absence of bioturbation in lithofacies infer stressed and anaerobic depositional settings (Egbobawaye, 2016). The absence of laminae in the lime mudstone also indicate very low sedimentation rate and/or deposition of homogeneous mud in a low-energy regime with the association of oxygen-poor environmental condition (Ekdale and Bromley, 1984; Meling, 2016).

### **3.5.2. Oil-shale Facies (TA2)**

The distinguished “oil-shale” facies is classified on the basis of composition, sedimentary feature and organic matter content (Tables 3.5; 3.6; 3.12; 3.14; Figures 3.1; 3.2; 3.3). The term “oil-shale” classification in the studied section is adapted from Stow`s (2005), Wang`s (2012) and Zou et al., (2010) shale classifications. Generally, the fine-grained sedimentary facies are defined by number of researcher and used different terminology to define fine-grained facies such as shale or mudstone or mudrock or claystone (Deng and Qian, 1990; Stow, 2005; Allix et al., 2010; Diaz et al., 2012; Wang, 2012; Jiang et al., 2013; Zou et al., 2010).

The documented oil-shale lithofacies in the Karahisar section is characterized as two-types of sub lithofacies based on sedimentary features, which are a) parallel to wavy laminated bedded shale, b) non-laminated bedding shale (Figure 2.35). In general, the

facies is comprised of olive gray, medium gray to medium dark gray, dark greenish gray intervals. The bedding and laminae feature are general observed as interlaminated very thin bedded to thin bedded units, and occasionally wavy laminae in the lower portion of the studied section (Figures 2.34; 2.35; 2.36). It is dominated facies with thick intervals in the measured stratigraphic section (Figure 2.35). The microscopic examination shows that it is consisting of non-laminated, alternating organic-rich laminae and organic poor laminae (Figures 3.32a, b, c, d; 3.33a, b, c). There is also the observation of lenticular laminae in the microscopic analysis. The observed particles in the facies are angular to rounded, silt to very fine sand-size quartz grains, opaque organic matters and occasionally anhedral to euhedral dolomitic appearance and pyrite in the matrix.

#### **3.5.2.1. Interpretation (TA2)**

The oil-shale deposition in the depositional settling depends on the number of factors such as basin setting, sedimentation rate, salinity changes and redox condition (Xu et al., 2015; Liang et al., 2018). Generally, the laminated calcareous shale with high organic-content and absence of bioturbation indicate low energy, reducing condition and relatively deeper environmental setting (Zeller et al., 2015). The algal laminated oil-shale is associated with the microbial organism (cyanobacteria). The heterogeneous grains within the laminated oil-shale are driven to the depositional environment through aeolian and/or from water suspension (de los Rios et al., 2004). Mostly, massive and thin laminated oil-shale are characterized as deep lacustrine setting or deep marine condition (Carroll and Bohacs, 2001). In the Karahisar section, lacustrine and marine oil-shale type are identified along the measured stratigraphic section based on laminae, stratigraphic position in the basin and associated facies feature. The lower portion of the Karahisar section is characterized by sublittoral to upper profundal lacustrine zone deposits. These are recognized as algal laminated to parallel laminated oil-shale and occasional lime mudstone intervals. This lithofacies also characterized by silt-size quartz grain which is transported by wind and/or high influx of terrigenous clasts and deposited from the suspension load.

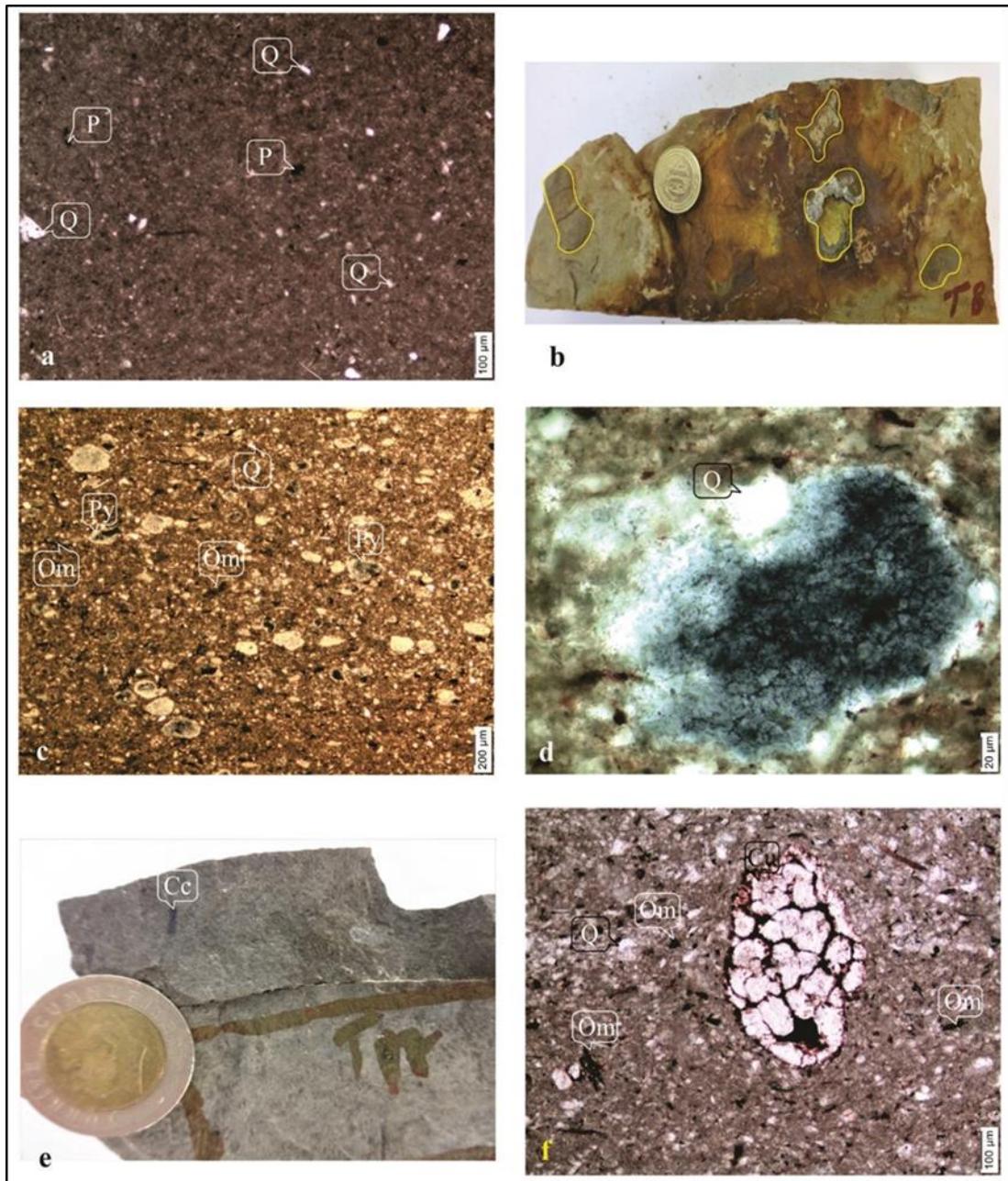


Figure 3.30. Photomicrographs of lime mudstone microfacies presenting quartz (Q), pyrite (P), phytoclast (Py), organic matter (Om), charcoal fragment (Cc) and cuticle (Cu). (Sample no. a) T7, PPL, x10; b) T8, hand specimen, yellow outline indicates calcareous concretion on the bedding plane; c) T8, PPL x4; d) T8, representing close view of phytoclast, PPL, x100; e) T11, hand specimen showing coaly wood fragment; f) T12, PPL, x10.

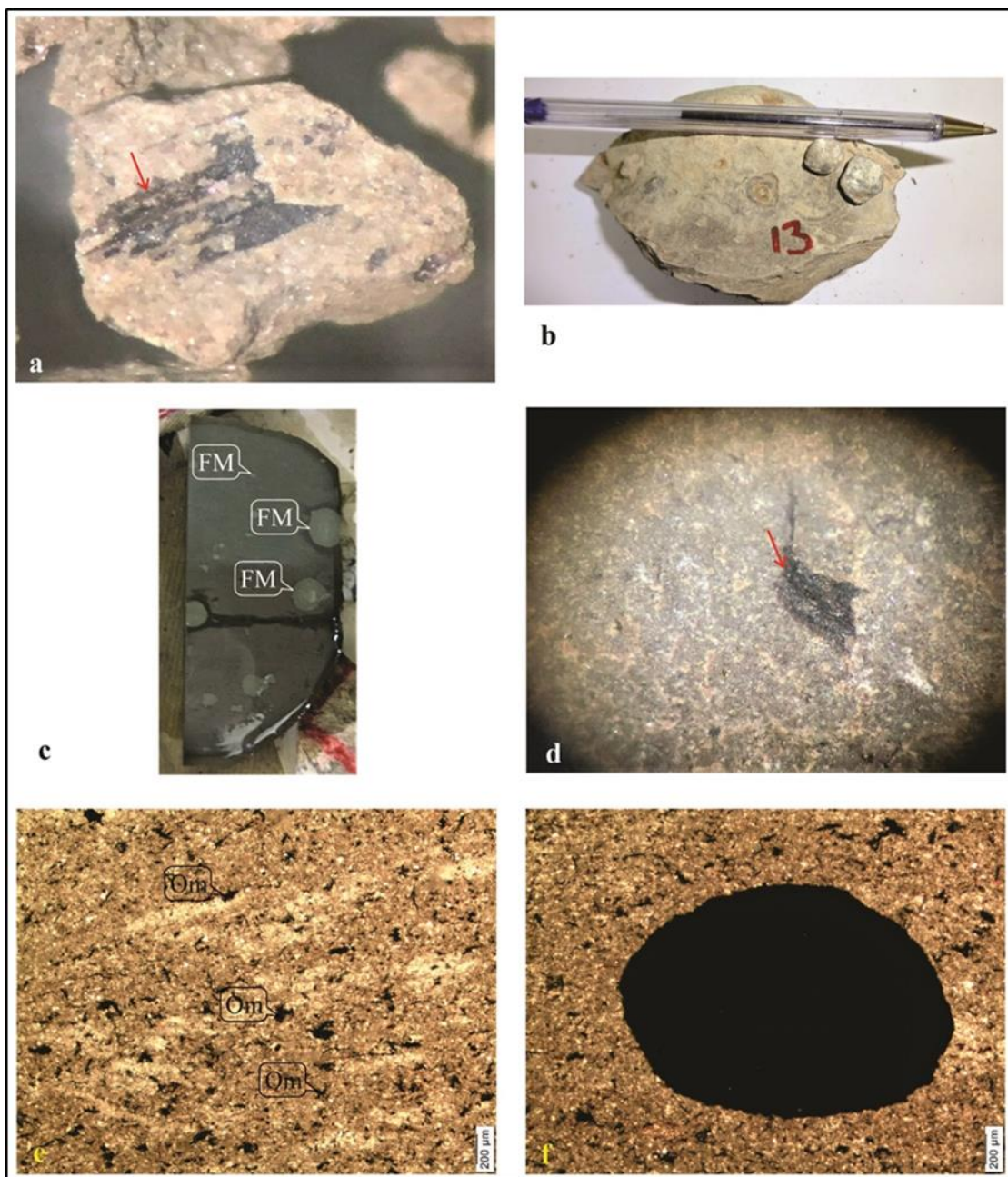


Figure 3.31. Photomicrographs of lime mudstone microfacies presenting ferrous-manganese (FM), oxidation of Fe-Mn modules (Ox) and organic matter (Om). (Sample no. a) T12, organic matter (charcoal fragment), x2.5; b) T13, hand specimen showing Fe-Mn nodules; c) T13, cross cut hand specimen showing Fe-Mn nodules; d) T16, organic matter (plant fragment), x2.5; e) T13, PPL x4; f) T13, Fe-Mn nodule, PPL, x4.

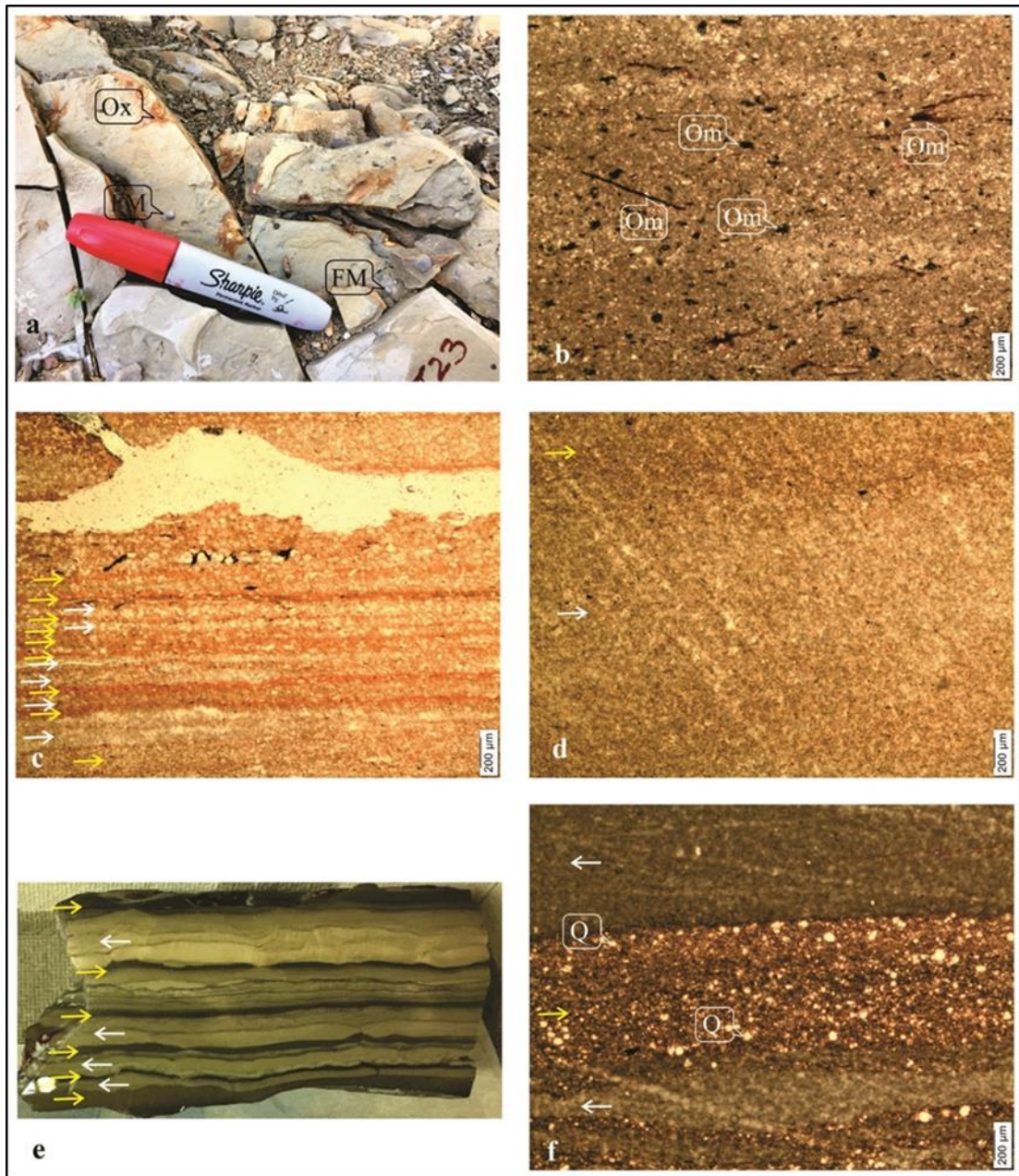


Figure 3.32. Photomicrographs of lime mudstone (a, b) and oil-shale (c, d, e, f) facies presenting organic-rich dark laminae (yellow arrow) and organic poor light laminae (white arrow), quartz (Q), and pyrite (P). (Sample no. a) T23, field photograph showing Fe-Mn nodules with outline oxidation; b) T12, PPl, x10; c) T1, parallel laminated, PPl, x4; d) T1, graded to thick laminae, PPl, x4; e) T4, hand specimen showing alternating organic-rich dark laminae (yellow) and organic-poor laminae (white arrow); f) T4, PPl, x4.

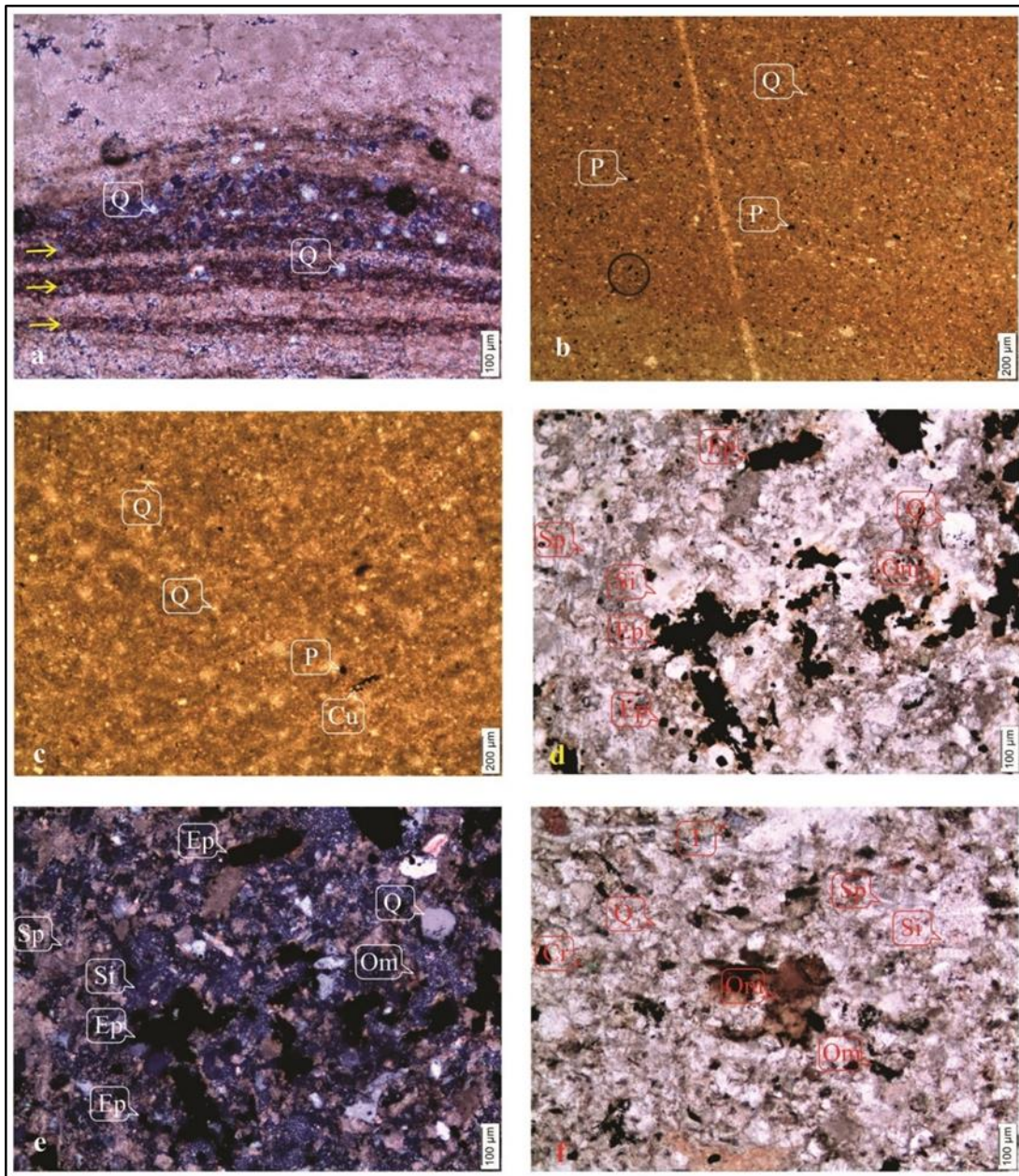


Figure 3.33. Photomicrographs of oil-shale (a, b, c) and sandstone (d, e, f) facies presenting quartz (Q), cuticle (Cu), euhedral pyrite (Ep), silica (Si), organic matter (Om), chlorite (Cr), blue tourmaline (T) and sparite cement (Sp). (Sample no. a) T4, XPl, x10; b) T5, PPl, x4; c) T17, non-laminated, PPl, x4; d) T27, PPl, x10; e) T27, XPl, x10; f) T27, PPl, x10.

In the upper portion of the Karahisar measured section, the massive to thick laminated calcareous oil-shale overlying Fe-Mn bearing lime mudstone are recognized as marine depositional intervals. The massive intervals and thick parallel horizontal laminated

bedded intervals are evidenced of deposition from suspension which is linked with storm deposits (O'Brien, 1990; Esteban, 2003). The marine oil-shale is interpreted as deposited in the low energy and anoxic marine environmental setting below storm wave base.

### **3.5.3. Calcareous Sandstone Facies (TA3)**

The periodically observed lithofacies in the Karahisar measured section is the sandstone lithofacies. The sandstone lithofacies is plotted as feldspathic litharenite in the Folk's (1974) ternary classification diagram of sandstone (Figure 3.4). The sandstone facies interval is appeared as medium dark gray color, thinly bedded with observing rippled sedimentary structure in the field. It is restricted to the upper portion of the studied section and having a sharp boundary with underlying and overlying lime mudstone units (Figure 2.35). The microscopic data identified that the lithofacies is comprised of mainly quartz grains with the association of feldspar, plagioclase, lithic fragment and accessory minerals (Table 3.13). The other randomly distributed subordinate grains are euhedral pyrite and rare organic matter (Figures 3.33b, c, d, e). the identified accessory minerals are chlorite, rutile, muscovite, biotite and tourmaline. The particles are surrounded by calcite cement with rare silica patches and oil stained patches (Figures 3.33d, e, f). Generally, the grains are very fine sand-size, angular-sub-rounded, well sorted and loosely packed character.

#### **3.5.3.1. Interpretation (TA3)**

In the upper portion of the Karahisar measured section, the single interval of rippled bedded sandstone is observed. This lithofacies is recognized as marine offshore transitional facies. The wavy ripple crests rounded feature, the absence of bioturbation, calcareous cementation and fine-grained sand-size sandstone suggest that it is deposited in relatively deeper environmental condition (Collinson et al., 2006; Johansen, 2016) (Figure 3.34). The sharp boundary of rippled calcareous sandstone with lime mudstone suggest storm event deposits on the marine offshore near storm wave base (Rees et al., 2014; Abimbola, 2016; Johansen, 2016).

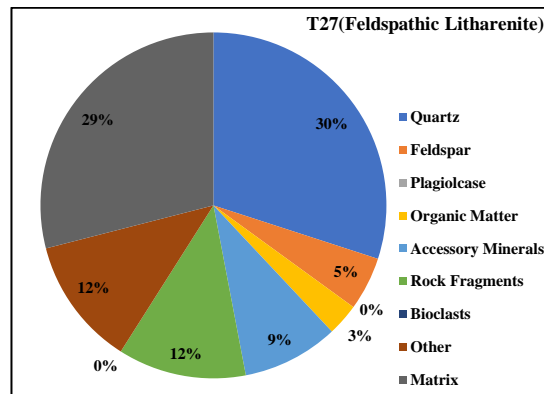


Figure 3.34. Pie graphs of sandstone lithofacies in the Karahisar section.

### 3.6. Microfacies of Sünnet Section

In the Sünnet section, during the field studies and microscopic examination, 4 numbers of facies are recognized along the measured studied section (Tables 3.15; 3.16 and 3.17).

#### 3.6.1. Limestone Facies

The recognized limestone facies in the Sünnet section is periodically observed along the measured stratigraphic section from bottom to top (Figures 2.41 and 2.42). This limestone facies are categorized into sub-facies, based on the Embry and Klovan's (1971) classification. The sub-facies of the limestone are identified on the basis of field character and microscopic analysis data (Tables 3.15 and 3.17).

##### 3.6.1.1. Lime Mudstone Microfacies (SA1)

In the field description, the lime mudstone specifies a very pale green color, medium bedded unit and highly fracture features. This microfacies is observed at a single locality and interbedded with shaly unit in the measured column (Figure 2.42). The distinguished sub-facies are composed of dominantly micrite matrix with identified subordinate fine-grained, angular quartz and association of rare feldspar, plagioclase and accessory mineral grains (Figure 3.35a, b). In the facies, there is also observation of rare micro-plant fragment, bivalve and pyrite.

### 3.6.1.2. Interpretation (SA1)

The lime mudstone texture defines the predominance of lime mud as matrix and less than 10% allochem and reflect low energy depositional setting. The lime mudstone in the Sünnet section indicates low energy and shallow marine depositional environment with rare siliciclastic influx. The observation of rare gastropod assemblage and small plant fragment also imitates a low-energy and relatively deeper environment (Carlucci et al., 2014).

Table 3.15. Limestone, oil-shale and marl petrographic data and established/recognized microfacies in the Sünnet studied section.

Sample No.	Q	F	Pg	Om	Pl	In	Accessory Minerals	Extra-clasts (Volcanogenic* /Rock Fragment^)	Bioclasts (Os/Ch/GU/Al/Da/N/Br)	Other (P/He/Ph/Cr/Ce/Ct)	Matrix (Mi/Cl/Sp/Or/D/Cr)	Field Nomenclature
S1												Coarse Sandstone
S5												Fine Sandstone
S6	12	5	2	3	-	-	3Cr/0.5T/0.5Z/1Bo/1Mu=6	5Pq/5Ce=10	-	-	62Cl	Oil-shale
S7	35	5	1	-	-	-	1T	3Pq	-	13P	42Mi	Oil-shale
S11	33	5	1	2	-	-	0.5T/1Mu/1.5Z=3	3Pq/1Ce=4	-	1p	51Cl	Oil-shale
S12	15	3	1	-	1	-	0.5Z/1R/0.5T=2	1Pq	-	1P/1Cr=2	75Mi	Limestone
S13	30	-	1	-	-	-	0.5T/0.5Z=1	1Pq	5G/2Bi/1Fr/7Ub=15	2P	50Cl+Or	Oil-shale
S15	35	-	-	5	-	-	-	-	-	-	60Cl+Or	Oil-shale
S16	2	-	-	10	5	-	-	-	10Os/5Bi/3Ch/12Ub=30	-	53Mi	Bio-Limestone
S17	10	-	-	8	4	-	-	-	15Os/27Ch/10Bi/5G/5Ub=61	-	17Mi	Bio-Limestone
S18												Very Coarse Sandstone
S20	50	-	-	10	-	-	2.5Mu/0.5T=3	-	-	2Cr	35Mi	Oil-shale
S21												Sandstone
S22	15	2	2	5	-	-	0.5BO/0.5T/1Mu=2	1Pq/3Ce=4	-	10Cr	60Mi	Oil-shale
S26	3	-	-	3	5	-	-	3Pq	25Al/2G/10Os/1Ch/2Ub=40	-	46Mi	Bio-Limestone
S27												Coarse Sandstone
S28	12	5	-	5	1	14	-	18Pq	15Bi/1Fr/4Ub=20	-	25Sp	Bio-Limestone
S29												Sandstone
S31												Sandstone
S33	15	5	-	5	-	5	1T/1S=2	5Pq	21Bi/15G/1N/9Ub=46	3Cr	14Sp	Bio-Limestone
S34												Sandstone
S35												Sandstone

Os-Ostracoda, Ch-Charopyta, G-Gastropod, Br-Brachiopod, Al-Algal, Da-Diatoms, N-Nummulites, Pl-Plant, Fr-Foraminifera, Py-Palynofacies, Ub-Unidentified Bioclasts, Q-Quartz, Qp-Polyquartz, Cr-Chlorite, Ct-Calcite, Mu-Muscovite, Mn-Manganese, P-Pyrite, Ce-Chert, F-Feldspar, Pg-Plagioclase, Sf-Shale fragment, Srf-Siltstone Fragment, Lf-Limestone fragment, Bo-Biotite, T-Tourmaline, Pi-Peloid, In-Intraclasts, R-Rutile, Z-Zircon, Sp-Sparite, Mi-Micrite, D-Dolomite, Cl-Clay, Or-Organic Rich, Om-Organic matter//Bitumen, He-Hematite, Ph-Phosphate, Se-Sphene

Table 3.16. Limestone, oil-shale and marl petrographic data and established/recognized microfacies in the Sunnet studied section.

Sample No.	Q	F	Pg	Om	Pl	Accessory Minerals	Rock Fragment	Bioclasts (Os/Ch/G/Ub/Al/Da/N/Br)	Other (P/He/Ph/Cr/Ce/Ct)	Matrix (Mi/Cl/Sp/Or/D/Cr)	Field Nomenclature
S1	11	15	7	10	-	4.9Cr/1Mu/0.5Z/0.5R/1T/0.1Gt=8	35Pq/5Ce/5Sf=45	-	-	4Sp	Fine Sandstone
S5	31	10	3	5	-	5Cr/0.5Z/0.5T/2Bo=8	15Pq	-	-	28Mi	Very Fine Sandstone
S18	20	10	1	5	-	5Cr	15Pq/10Ce/8L/5Sf=38	1Ch/2Bi/1Be=4	-	17Sp	Medium Sandstone
S21	32	-	1	9	-	4.5Cr/1Sp/0.5T=6	2Pq/5Ce=10	-	-	42Mi	Fine Sandstone
S27	20	5	20	8	-	1Cr/0.5Mu/0.5Sp=2	20Pq/15Ce/2Lf=37	-	-	8sp	Fine Sandstone
S29	47	5	5	10	-	0.5T/1.5Sp=2	7Pq/20Ce=27	-	-	4Sp	Very Fine Sandstone
S31	31	10	5	10	-	5Cr/0.5Sp/2Mu/0.5T=8	10Pq/17Ce=27	-	-	9Sp	Coarse Sandstone
S34	32	5	2	5	-	8Cr/1Sp/1Mu/1T=11	5Pq	-	-	40Sp	Sandstone
S35	29	3	1	5	-	5Cr/2Mu/0.5T/0.5Sp=8	6Pq	-	-	48Sp	Sandstone

Ch-Charopyta, Pl-Plant, Q-Quartz, Qp-Polyquartz, Cr-Chlorite, Ct-Calcite, Mu-Muscovite, Mn-Manganese, P-Pyrite, Ce-Chert, F-Feldspar, Pg-Plagioclase, Sf-Shale fragment, Srf-Siltstone Fragment, Lf-Limestone fragment, Bo-Biotite, T-Tourmaline, Pi-Peloid, In-Intraclasts, R-Rutile, Z-Zircon, Sp-Sparite, Mi-Micrite, D-Dolomite, Cl-Clay, Or-Organic Rich, Om-Organic matter/Bitumen, He-Hematite, Ph-Phosphate, Se-Sphene

Table 3.17. Classifications of the limestone, oil-shale, marl and sandstone and established/recognized microfacies in the Sunnet studied section.

Sample No.	Compositional Classification of shale and marl			Texture Classification*	Limestone Classification (Embry and Klovan's 1971)	Sandstone Classification (Folk's 1974)	Defined Facies in Studied Section
	Diaz's (2012) Mudstone (Unconventional)	Stow's (2005)	Allix's (2010) Shale	Fine-Grained Rock Folk's (1965)			
S1						Feldspathic litharenite	Sandstone
S5						Lith Graywackes	Sandstone
S6	Carbonate-rich Siliceous Mudstone	Siliceous Calcareous	Siliceous Mudstone	Mud-Shale			Oil-shale
S7	Mixed Siliceous Mudstone	Siliceous Calcareous	Siliceous Mudstone	Mud-Shale			Oil-shale
S11	Clay-rich Siliceous Mudstone	Sarl	Siliceous Mudstone	Mud-Shale			Oil-shale
S12					Lime Mudstone		Lime Mudstone
S13	Argillaceous/Siliceous Mudstone	Marl	Siliceous Mudstone	Mud-Shale			Oil-shale
S15	Argillaceous/Siliceous Mudstone	Marl	Siliceous Mudstone	Mud-Shale			Oil-shale
S16					Bio-Wackestone		Wackestone
S17					Bio-Packstone		Packstone
S18						Lith-arenite	Sandstone
S20	Mixed Siliceous Mudstone	Siliceous Calcareous	Siliceous Mudstone	Mud-Shale			Oil-shale
S21						Lith-arenite	Sandstone
S22	Mixed Mudstone	Marl	Argillaceous Mudstone	Clay-Shale			Oil-shale
S26					Bio-Wackestone		Wackestone
S27						Feldspathic litharenite	Sandstone
S28					Bio-Rudstone		Rudstone
S29						Feldspathic litharenite	Sandstone
S31						Feldspathic litharenite	Sandstone
S33					Bio-Rudstone		Rudstone
S34						Lithic Arkose	Sandstone
S35						Feldspathic litharenite	Sandstone

\* Based on grains size of mud fraction, non-fissile/fissile and soft.

Table 3.17. Continues...

Sample No.	(Texture and/or Compositional)	Defined Facies in Studied Section
S1	Coarse-size, sub-angular to sub-rounded, moderate to well sorted, closely packed	Sandstone
S5	Fragile, Clayey, fine-grained, loosely packed, angular to sub-rounded	Sandstone
S6	Oil-shale, Fragile, Clayey	Oil-shale
S7	Fragile, Clayey, Chalcopyrite and replaced by Malachite,	Oil-shale
S11	Oil-shale, Fragile, Clayey	Oil-shale
S12	Medium Bedded, fine-grained quartz	Lime Mudstone
S13	Oil-shale, very-fine grained quartz, sub-angular to sub-rounded, bivalve, foraminifera	Oil-shale
S15	Oil-shale	Oil-shale
S16	Bio-Wackestone, Charcoal, Plant, bivalve, ostracods	Wackestone
S17	Bio-Packstone, Thin Bedded, Plant fossil, Charcoal, fossiliferous	Packstone
S18	Thin bedded, coarse-grained, fish-bone, closely packed, poorly sorted, angular to sub-rounded	Sandstone
S20	Oil-shale	Oil-shale
S21	Massive bedded, fine-grained, angular to sub-rounded, loosely packed, plant fragments	Sandstone
S22	Oil-shale, Having Choritization in Matrix	Oil-shale
S26	Bio Wackestone, Algae filamentous, fossiliferous	Wackestone
S27	Very coarse-grained, poorly sorted, angular to sub-rounded	Sandstone
S28	Bio-Conglomerate	Rudstone
S29	Load cast, coarse-grained, sub-angular to sub-rounded, charcoal fragment, closely packed, moderately sorted	Sandstone
S31	Coarse-grained, sub-angular to sub-rounded, loosely to closely packed, moderately sorted	Sandstone
S33	Bio-Conglomerate	Rudstone
S34	Fine-grained, angular to sub-rounded, loosely packed, moderately to well sorted	Sandstone
S35	Concretion, fine-grained, angular to sub-rounded, loosely packed, moderately sorted	Sandstone

### 3.6.1.3. Wackestone Microfacies (SA2a)

The wackestone is another established microfacies from studied section based on the Embry and Klovan's classification (1971). It is comprised of light olive gray to medium dark gray, thin-bedded units in the field documentation (Figures 2.42; 2.51B). In the field studies, the recorded fauna and flora in the microfacies are plant fragment, gastropod, bivalve and rare tooth of pycnodont fishes (Figure 2.51B). This facies is present in the middle portion of the studied section (Figure 2.42). Under microscopic examination, it comprised of bioclasts with the subordinate association of quartz, opaque organic fragment and phytoclasts and rare pyrite, which are surrounded by micrite matrix (Tables 3.15; 3.17; Figures 3.35c, d, e) (Fuhrmann, 2002). The recognized microfossil in the microfacies are ostracods, bivalve, charophytes, gastropods, fish scale and algal fragment (Figures 3.35c, d, e).

#### **3.6.1.4. Packstone Microfacies (SA2b)**

In the Sünnet stratigraphic section, the Packstone microfacies define two intervals at a different level (Figures 2.42; 2.46 and 2.50B). In the field description, the Packstone microfacies are dark yellowish orange and thin-bedded limestone intervals (Figures 2.46 and 2.50B). The units are characterized by granular appears of abundant charophytes along with the association of plant materials (Figures 2.46; 2.50B and 3.36c). In the thin section microscopic studies, it consists of abundant bioclasts with the association of plant fragment and minor quartz grains and are embedded in micrite (Tables 3.15; 3.17 and Figures 3.35a; 3.36a, b). The bioclasts include predominantly charophytes, ostracods, gastropods, bivalve fragments and unidentified fossils. This microfacies is present in the middle portion of the studied section at two different localities and having sharp contact with lower and upper lithofacies.

#### **3.6.1.5. Interpretation (SA2a; SA2b)**

In the studied section, the wackestone facies include algal fragment, ostracods with the association of rare gastropods, charophytes and fish scale represent deposition in the comparative deeper condition with the relative agitative condition and also freshwater fluvial incursion to the marine environment (Martín-closas, 2009; Huyghe et al., 2017). The charophytes, plant materials, ostracods with associated of rare gastropod and bivalve in the packstone facies assemblages clearly indicate marshes environment with transgressive marine influence on the depositional setting (Martín-closas, 2009). The charophytes with the association of brackish ostracod, marine fauna such as ostracods and foraminifera in this microfacies suggest that charophytes were grown in brackish water condition nearby and transported to shallow marine condition (Sanjuan & Martín-Closas, 2014). Generally, the wackestone and packstone facies are deposited in moderate energy deposition condition (Flügel, 2004). The occurrence of plant fragment with the association of charophytes, ostracods and rare gastropod with minor algal fragments bearing black limestone indicate the development of short-term variable influence of fluvial-lacustrine on marine environment setting (Suarez-

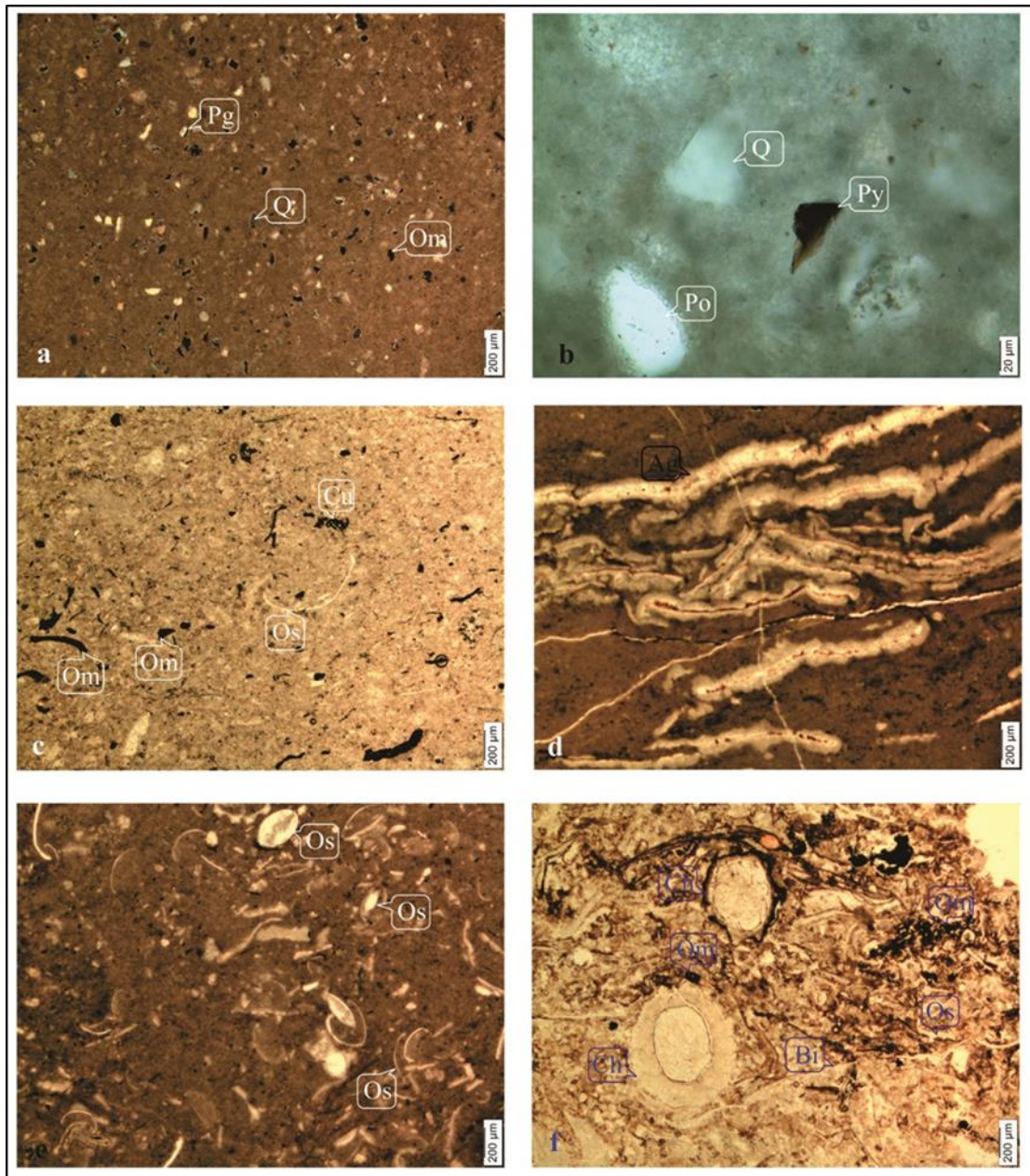


Figure 3.35. Photomicrographs of Lime Mudstone microfacies (a, b), wackestone (c, d, e) and packstone (f) presenting charophyta (Ch), ostracod (Os), plagioclase (Pg), quartz (Q), bivalve (Bi), phyoclast (Py), cuticle (Cu), algal filament (Ag) and organic matter (Om), pore (Po). (Sample no. a) S12, PPL, x4; b) S12, PPL, x100; c) S16, PPL, x4; d) S26, PPL, x4; e) S26, PPL, x4; f) S17, PPL, x4.

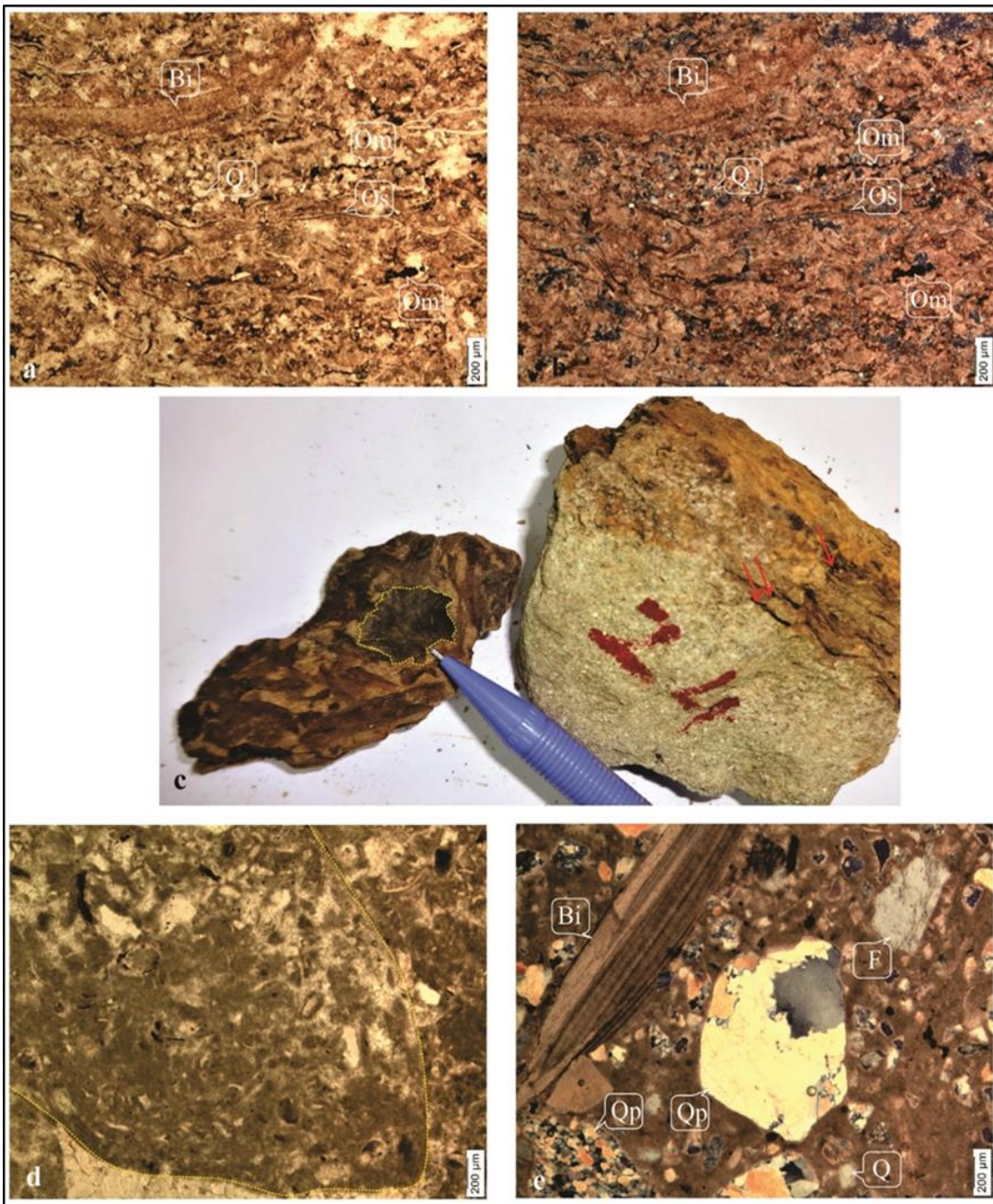


Figure 3.36. Photomicrographs of Packstone (a, b, c) and rudstone (d, e) presenting bivalve (Bi), quartz (Q), ostracod (Os), polycrystalline quartz (Qp), feldspar (F) and organic matter (Om). (Sample no. a) S17, PPI, x4; b) S17, XPI, x4; c) S17, Hand specimen, yellow dotted line showing leaf outline and red arrow pointing the plant fragments; d) S28, yellow outline indicates the intraclast, PPI, x4; e) S28, PPI, x4.

gonzalez et al., 2015). These intervals reflect charophytes rich beds with brackish ostracod laterally related to paralic marshes (Sanjuan & Martín-Closas, 2012). This environmental zone is shifted to open marine environment which is indicated by appearance of bivalve-rich bearing limestone units (bio-calicrudite) (Argakoesoemah, 2017).

#### **3.6.1.6. Rudstone microfacies (Bio-calicrudite) (SA3)**

According to Embry and Klovan (1971), the facies composed of more than 60 percent allochem and embedded in sparite cement, are classified as grainstone microfacies. In case of allochem more than 60 percent and size of allochem greater than 2mm, then this grainstone is characterized as Rudstone. In the measured studied section, this facies is classified as rudstone facies/bio-calicrudite, which is composed of abundant allochems with a size more than 2mm. In the Sünnet outcrop section, the rudstone is observed as greenish gray, fossiliferous thick bedded limestone unit (Figures 2.42; 2.47 and 3.37c). The identified macrofossils in the field are abundant bivalve with the association of subordinate gastropods shells (Figures 2.47 and 3.37). The observed siliciclastic grains are pebble to fine sand size quartz grains with sub-rounded to rounded shape geometry. In microscopic view, it is composed of bioclasts, monocrystalline and polycrystalline quartz, plagioclase, intra-clasts and rare foraminifera and nummulitic Foraminifera (Tables 3.15; 3.17 and Figures 3.36e, f; 3.37). The matrix is consisting of sparry calcite cement. The allochems are arranged in the form of poorly sorted and loosely packed in the sparry calcite cement. The rudstone microfacies is reported in the upper portion of the studied section (Figure 2.42).

#### **3.6.1.7. Interpretation (SA3)**

Rudstone lithofacies of the Sünnet section composed of grain-supported with sparry calcite cementation and their texture characteristic indicate high-energy marine shelf deposits with high terrigenous influx (Flügel 2004). Abundant bivalve with the association of benthic foraminifera, gastropod, gravel size quartz grains, intraclasts and rare miliolidae reflect high turbulent condition occurred in the relatively shallow

marine environment (Cunningham et al., 2006; Grosjean et al., Grosjean et al., 2012; Hadi et al., 2016). In the rudstone (calcirudite), there is no evidence of wave action, which shows that these are deposited below fair-weather wave base in the marine depositional setting.

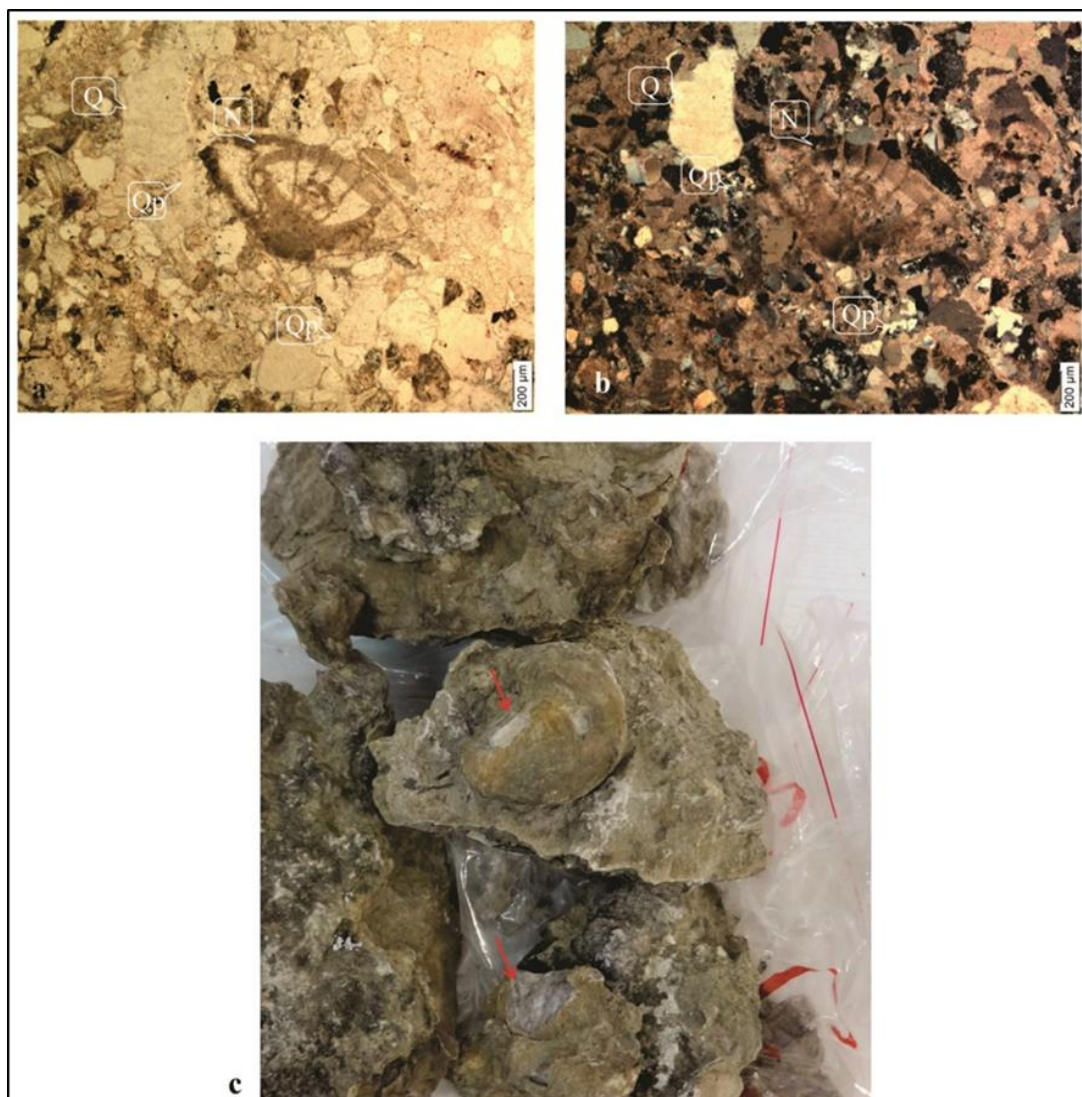


Figure 3.37. Photomicrographs of rudstone (a, b, c) presenting quartz (Q), polycrystalline quartz (Qp) and Nummulites (N). (Sample no. a) S33, PPL, x4; b) S33, XPL, x4; c) S33, hand specimen, red arrow pointing the bivalve.

### **3.6.2. Oil-shale Facies (SA4)**

Though, the shale or mudstone or claystone or mudrock are widely used terminology to describe fine-grained sedimentary rocks by researchers such as Deng and Qian, 1990; Stow, 2005; Allix et al., 2010; Diaz et al., 2012; Wang, 2012; Jiang et al., 2013; Zou et al., 2010 (Figures 3.1; 3.2 and Table 3.1). In this research, the shale term is used in the stratigraphic units to describe fine-grained sediments (Tables 3.15 and 3.17).

In the Sünnet section field studies, this facies is recognized as grayish red, medium dark gray, dark gray, olive gray, silty to gritty appearance, thin to thick intervals and having fragile character and rare observation of rhizoliths like features (Figures 2.42; 2.44B; 2.45). Rhizoliths are identified as the occurrence of gray patches in the reddish shale facies (Hembree & Bowen, 2017). This facies has shown transitional and sharp contact with occasional load cast boundary with overlying sandstone units at different localities in the measured section. At different intervals, samples are encountered with bivalve and gastropod fossils in the field (Figures 2.50A and 2.51A). Microscopically, this facies is characterized by the highest silt to very fine sand size quartz content with minor feldspar, plagioclase and accessory minerals and occasionally fossils content (Tables 3.15 and 3.17). The identified fossils in the facies include gastropod fragments, bivalve fragment, Foraminifera and unidentified bioclasts (Figures 3.38b, c). Pyrite is also observed in the matrix as disseminated grains at certain level. The chalcopyrite occurs at one of the shale facie which partially alter to green malachite. This facies is noticed at a regular interval from base to the middle portion and intercalated with sandstone lithofacies in the measured section (Figure 2.42). The oil-shale-sandstone interfaces are mostly defined as load structure and occasional sharp contact (Figures 2.44; 2.45; 2.48A).

#### **3.6.2.1. Interpretation (SA4)**

In the studied section, the red silty shale with gray mottling suggest pedogenic floodplain deposits (Figures 2.42; 2.43; 2.44) (Sanjuan & Martín-Closas, 2012). The

occurrence of red and gray mudstone with a lack of structure and bioturbation indicate deposited under the calm environmental setting (Collinson & Lewin, 1983).

Toward the top, the organic-rich shale is defining shallow marine with the terrigenous influx and anoxic condition. This facies have rare bivalve gastropod and milliodal foraminifera and support shallow marine conditional setting. The benthic fossils preserved in the lithofacies are either remnant of a stressed benthic community or they were transported to anoxic environment from oxic environmental condition (Berry and Wilde, 1978; Arthur and Sageman, 1994; Bingham-koslowski, 2015). The lack of bioturbation and high organic content in shale lithofacies indicate low energy, anoxic setting and interpreted as slope environmental condition (Zeller et al., 2015; Lettéron et al., 2018). The sharp contact of organic-rich shale with interbedded fine sandstone and also the observation of load coats reflects storm deposits below storm wave base (Collinson & Lewin, 1983).

### **3.6.3. Calcareous Sandstone Facies (SA5)**

This lithofacies of the Sünnet section are fine-grained to coarser-grained, gritty, grayish yellow, pale brown, light olive gray, greenish gray, thin to thick to massive bedded homogenous sandstone in the field studies (Figures 2.42; 2.44; 2.45; 2.48 and 2.49). This lithofacies possesses low angle wavy rippled lamination, parallel lamination, conglomerate lenses, sandstone concretion nodules, normal grading and occasionally fragile character at different intervals (Figures 2.42; 2.44; 2.45; 2.48 and 2.49). There is also the observation of load cast at sandstone-shale interfaces, and load casts and flute marks at coarser sandstone-fine sandstone interface (Figures 2.45; 2.48B). Generally, this facies appears throughout in the measured studied section (Figure 2.42). Petrographically, based on the monocrystalline quartz, feldspar/plagioclase and lithics fragments ternary classification diagram of Folk's (1974) and Pettijohn et al. (1987), this lithofacies encounters the lithic arkose, feldspathic litharenite, lith-arenite and lith graywackes quadrants (Tables 3.16; 3.17 and Figure 3.3). Microscopic studies indicate that it is comprised of predominantly

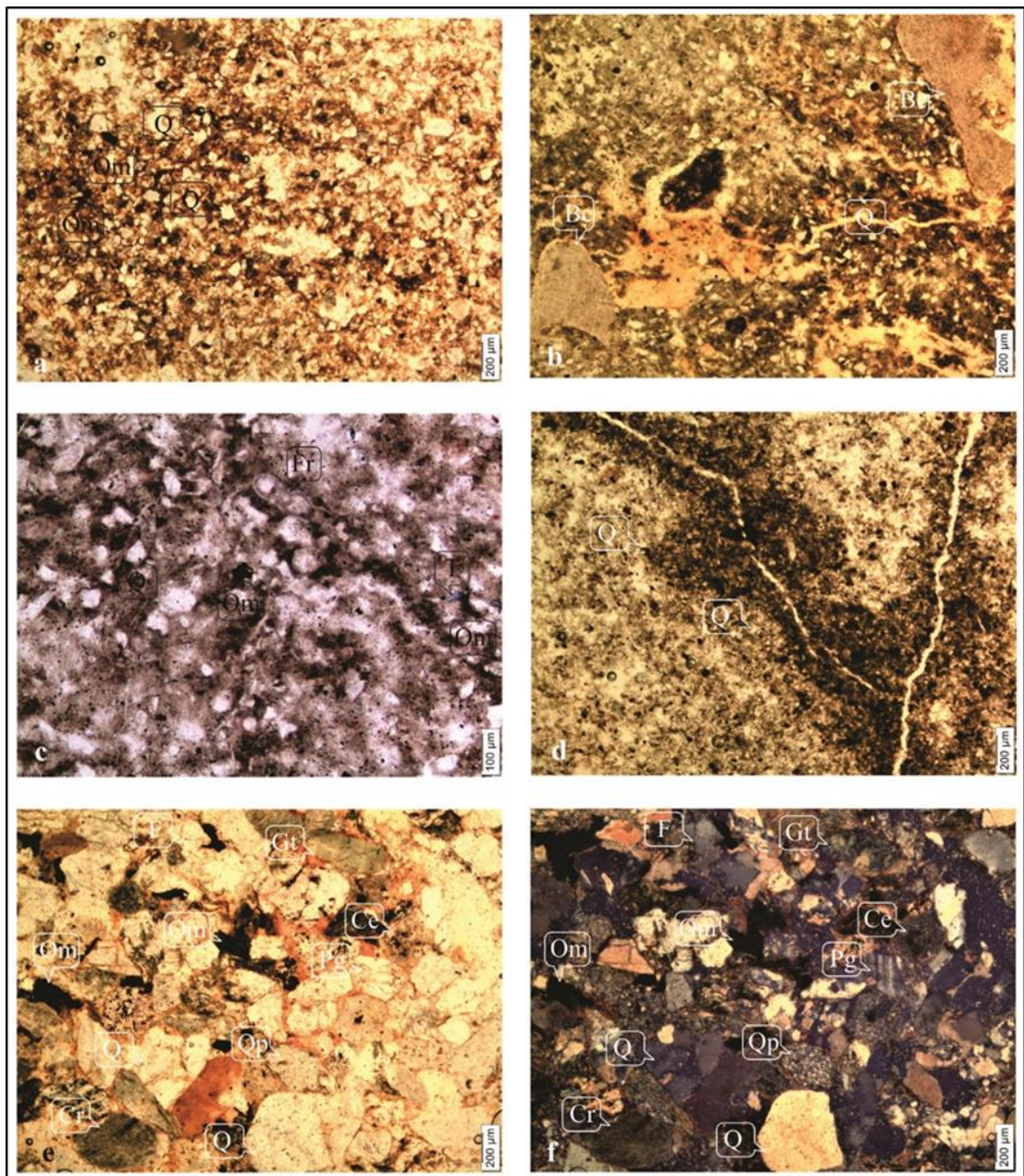


Figure 3.38. Photomicrographs of oil-shale (a, b, c, d) and sandstone (e, f) presenting quartz (Q), bioclast (Bc), foraminifera (Fr), tourmaline (T), feldspar (F), chert (Ce), polycrystalline quartz (Qp), chlorite (Cr), glauconite (Gt) and organic matter (Om). (Sample no. a) S11, PPl, x4; b) S13, PPl, x4; c) S13, PPl, x10; d) S20, PPl, x4; e) S1, PPl, x4; f) S1, XPl, x4.

quartz grains with the minor association of feldspar, plagioclase, accessory mineral and rock fragments (Table 3.16; Figures 3.38e, f; 3.41a, b, c, d). The subordinate associated accessory minerals in the studied section are chlorite, muscovite, rutile, tourmaline, sphene and biotite. At the certain horizon, there is a presence of charcoal, plant fragment and rare bivalve and bone fragment in this lithofacies (Mingram, 1998). The sandstone lithofacies are fine to very coarse-grained, poorly to well sorted and loosely to closely packed (Figures 3.38e, f; 3.41a, b, c, d).

### **3.6.3.1. Interpretation (SA5)**

In the studied section, three type of sandstone is observed based on fossil content, color change, and structural features. The absence of fossil, parallel lamination to cross stratified sandstone with having lenses conglomerate and fragile character is identified as floodplain deposits (Kangal et al., 2016). The presence of low matrix and high siliclastic content also reflect deposition under relatively high energy condition (Figure 3.39).

In the middle portion of the studied section, there is an observation of fossiliferous calcareous sandstone. It is interpreted as storm deposits on the outer shelfal marine environment (upper shoreface) based on the fossil fragment, lithic fragment and subangular grain character (Meling, 2016). The above calcareous sandstone intervals are characterized as sandstone dominated heterolithic facies intervals. The sharp contact and load cast feature indicate storm deposits in relatively shallow marine condition near/or below storm wave base (Snedden and Bergman, 1999; Suter and Clifton, 1999; Pattison, 2005; Dahlqvist, 2018). In the middle and upper studied section, this lithofacies is characterized by high carbonate content which suggest transgression in the depositional setting (Figure 3.40).

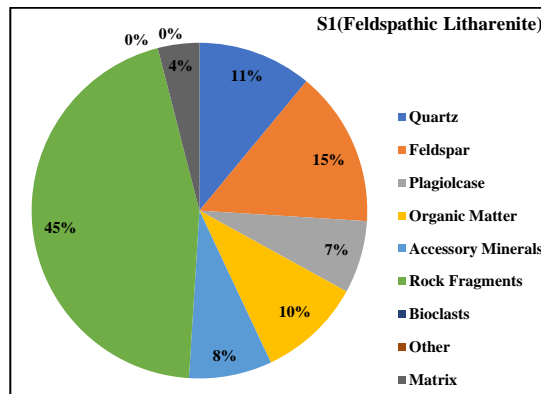


Figure 3.39. Pie graphs of the sandstone lithofacies of floodplain depositional environment in the Sünnet section.

### 3.6.4. Pebble-Conglomerate (SA6)

In the field, the pebble conglomerate facies observed as yellowish gray, poorly to moderately rounded, granule to pebbles, poorly sorted, massive bedded and characterized as a polymictic conglomerate (Figures 2.42; 2.44A; 3.41e, f). The defining facies are classified on basis of Miall's description of terrestrial facies (1977, 1978, 2006). This facies is recognized as clastic supported conglomeratic facies. The pebble-conglomerate lithofacies is also observed as lenticular and/or planar cross stratified within the sandstone lithofacies. In the studied stratigraphic section, this facies occurs periodically at different horizons along the measured column. The facies in the lower portion and middle portion in the studied section have sharp contact with underlying and overlying sandstone lithofacies (Figures 2.42; 2.44A). In the upper portion of the measured section, this facies represents erosional basal contact with facies and sharp upper contact with sandstone facies (Figures 2.42; 2.49).

#### 3.6.4.1. Interpretation (SA6)

In the nearshore environment, the conglomerate facies represent no indication of being reworked by marine processes. Generally, the conglomerate with lack of structural feature suggests fluvial channels deposition entering to the shallow marine environment (Collinson & Lewin, 1983).

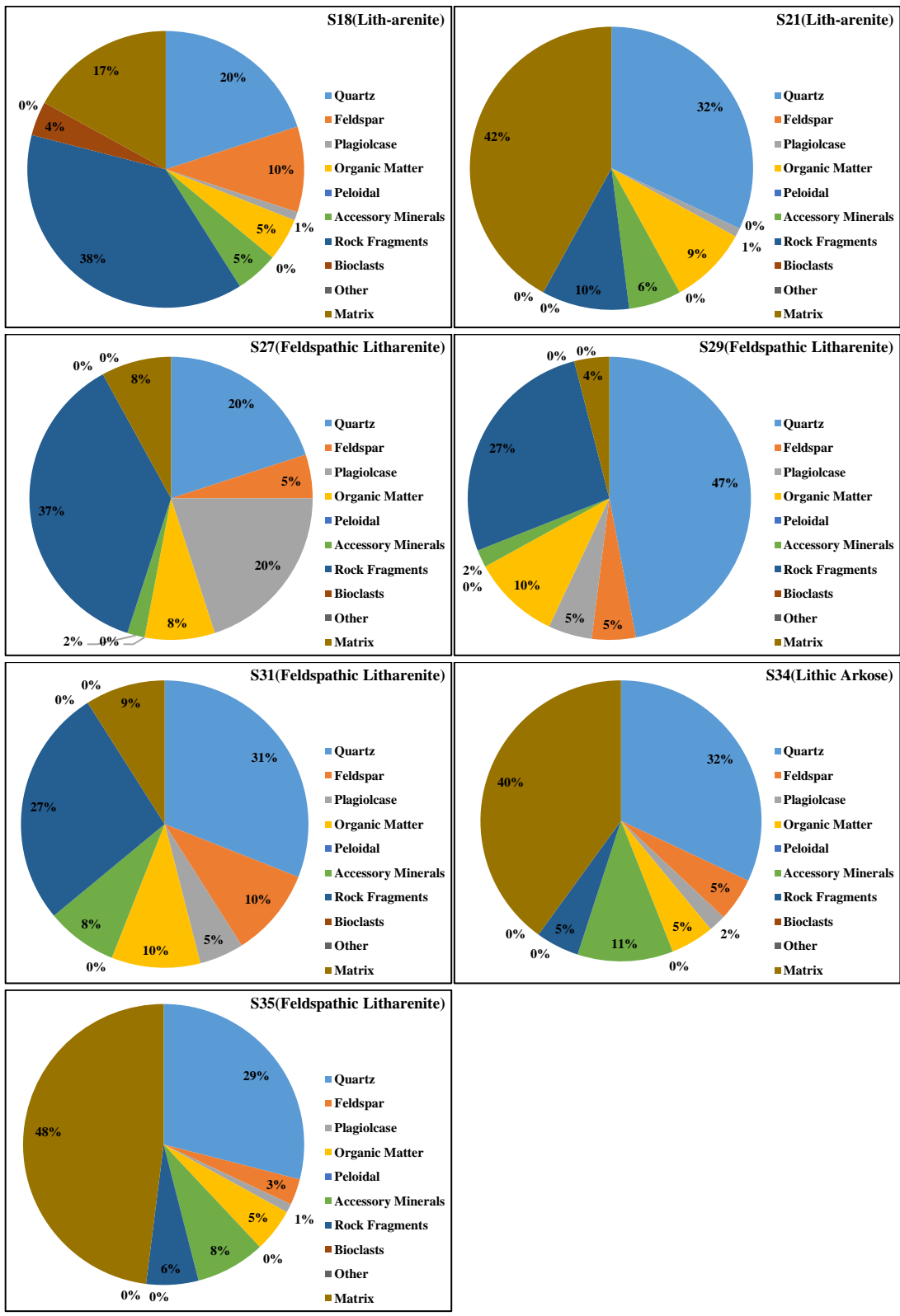


Figure 3.40. Pie graphs of the marine deposited sandstone lithofacies in the Sünnet section.

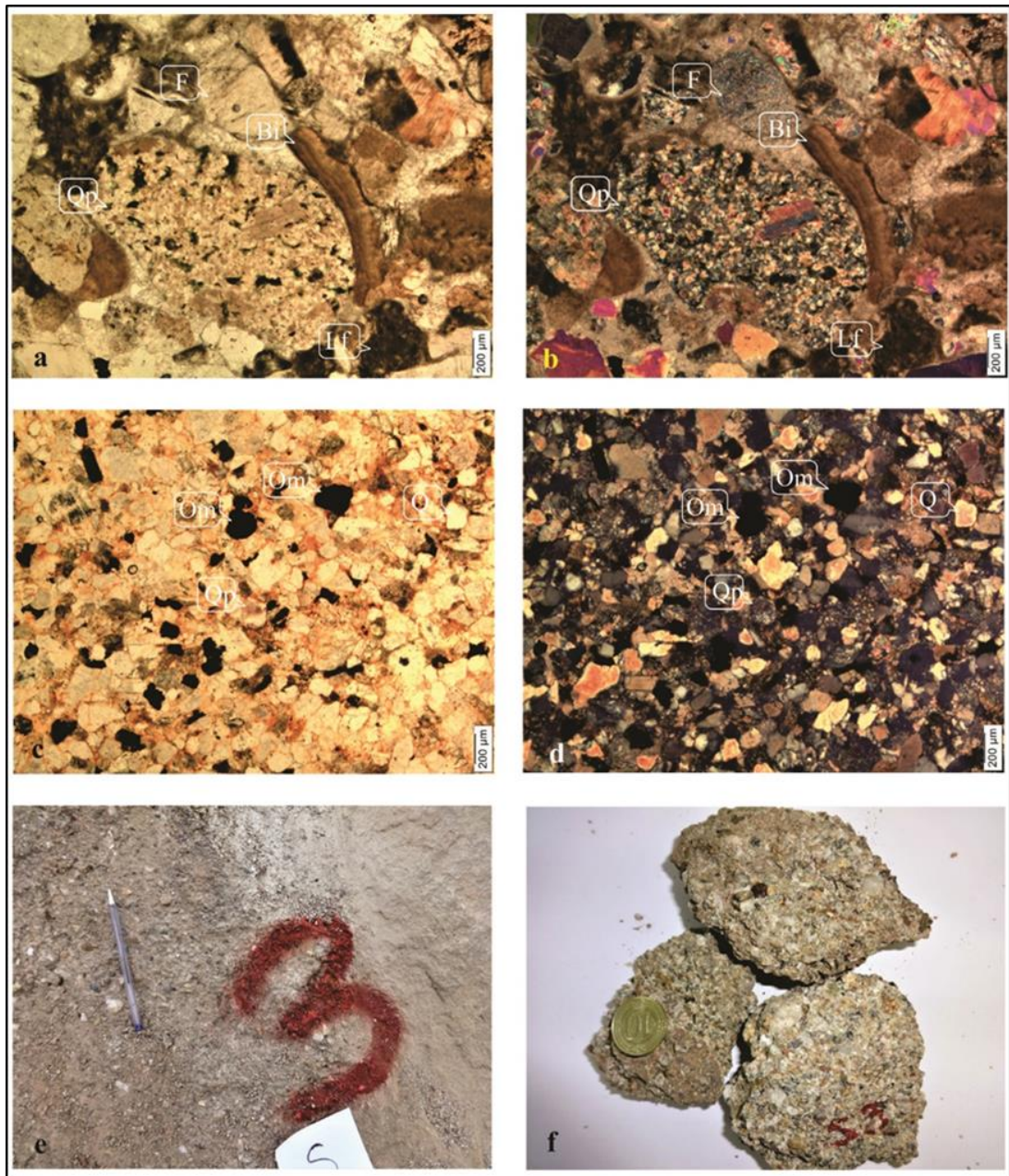


Figure 3.41. Photomicrographs of sandstone (a, b, c, d) and pebble-conglomerate (e, f) presenting quartz (Q), polycrystalline quartz (Qp), bioclasts (Bc), limestone fragment (Lf), feldspar (F) and organic matter (Om). (Sample no. a) S18, PPI x4; b) S18, XPI, x4; c) S29, PPI x4; d) S29, XPI, x4; e) field photography of S3 sample of pebble conglomerate; f) S3, Hand specimen.

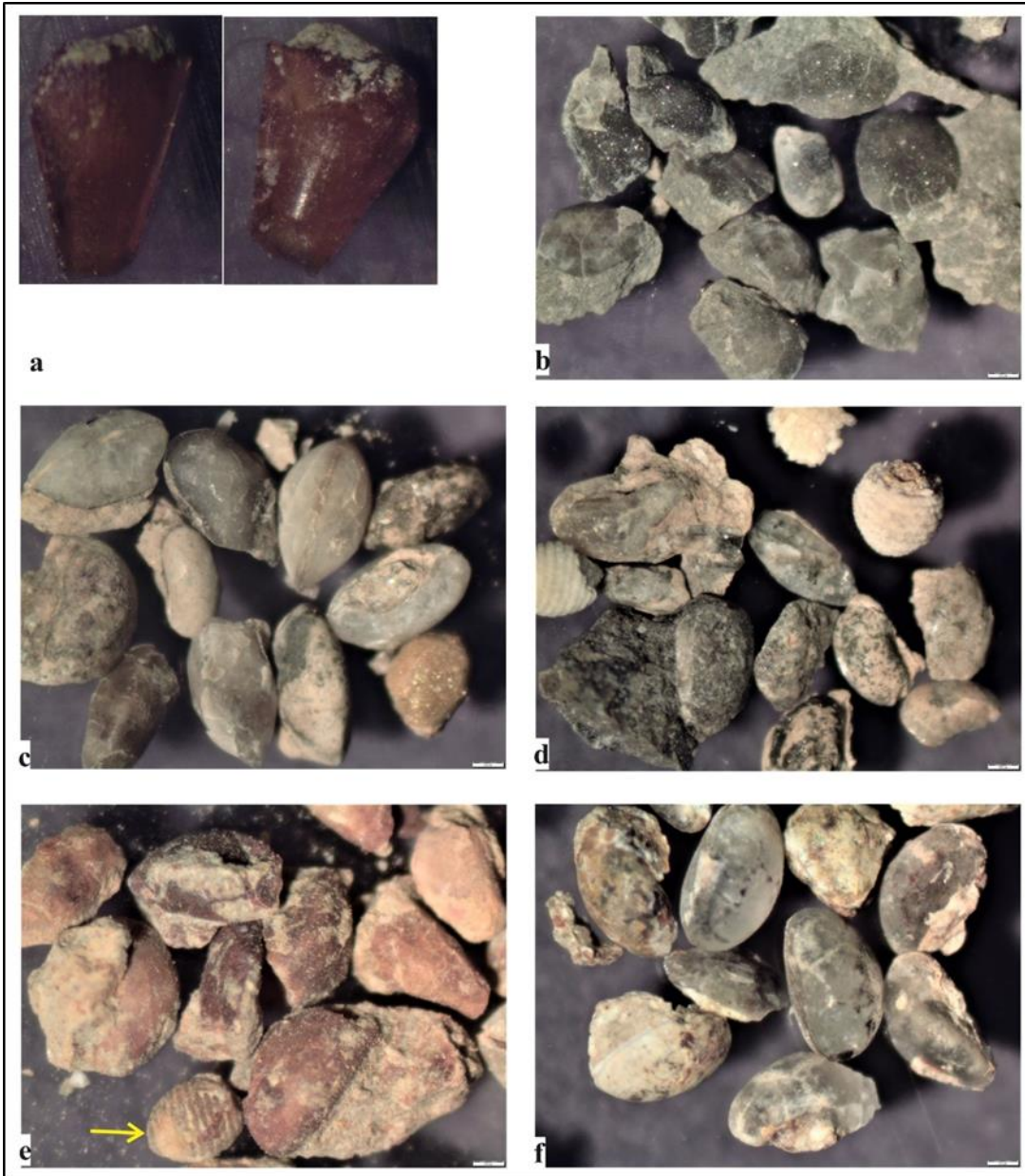


Figure 3.42. Photomicrographs of extracted fossils from Dağhacilar section presenting wackestone, packstone and marl facies. (Sample no. a) D6 wackestone, micro-tooth, x2.5; b) D6 wackestone, ostracods, x2.5; c) D14 wackestone, ostracods, x2; d) D17 wackestone, ostracods, x2; e) D11 packstone, ostracods, charophyta (yellow arrow), x2; f) D20 marl, ostracods, x2.5.

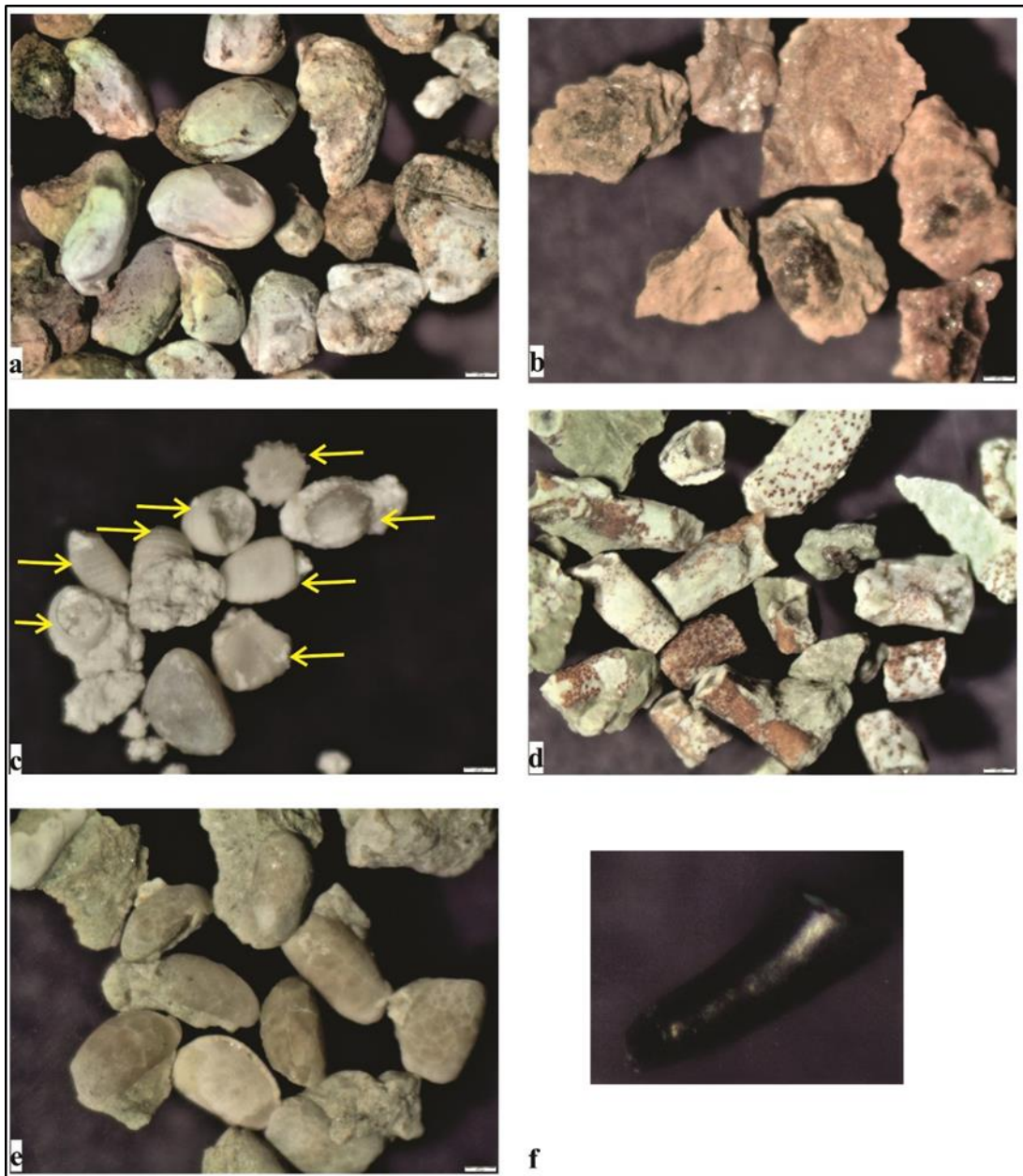


Figure 3.43. Photomicrographs of extracted fossils from Dağhacılar section (a), Hasanlar (b) and Köşüre sections (c, d, e, f) presenting wackestone, oil-shale and marl facies. (Sample no. a) D10 oil-shale, ostracods, x2.5; b) H13 oil-shale, ostracods, x2.5; c) K33 wackestone, ostracods and charophyte gyrogonites (yellow arrow), x3; d) K38 wackestone, crinoid, x1.5; e) K20 marl, ostracods, x2.5; f) K20 marl, micro-tooth, x2.5.

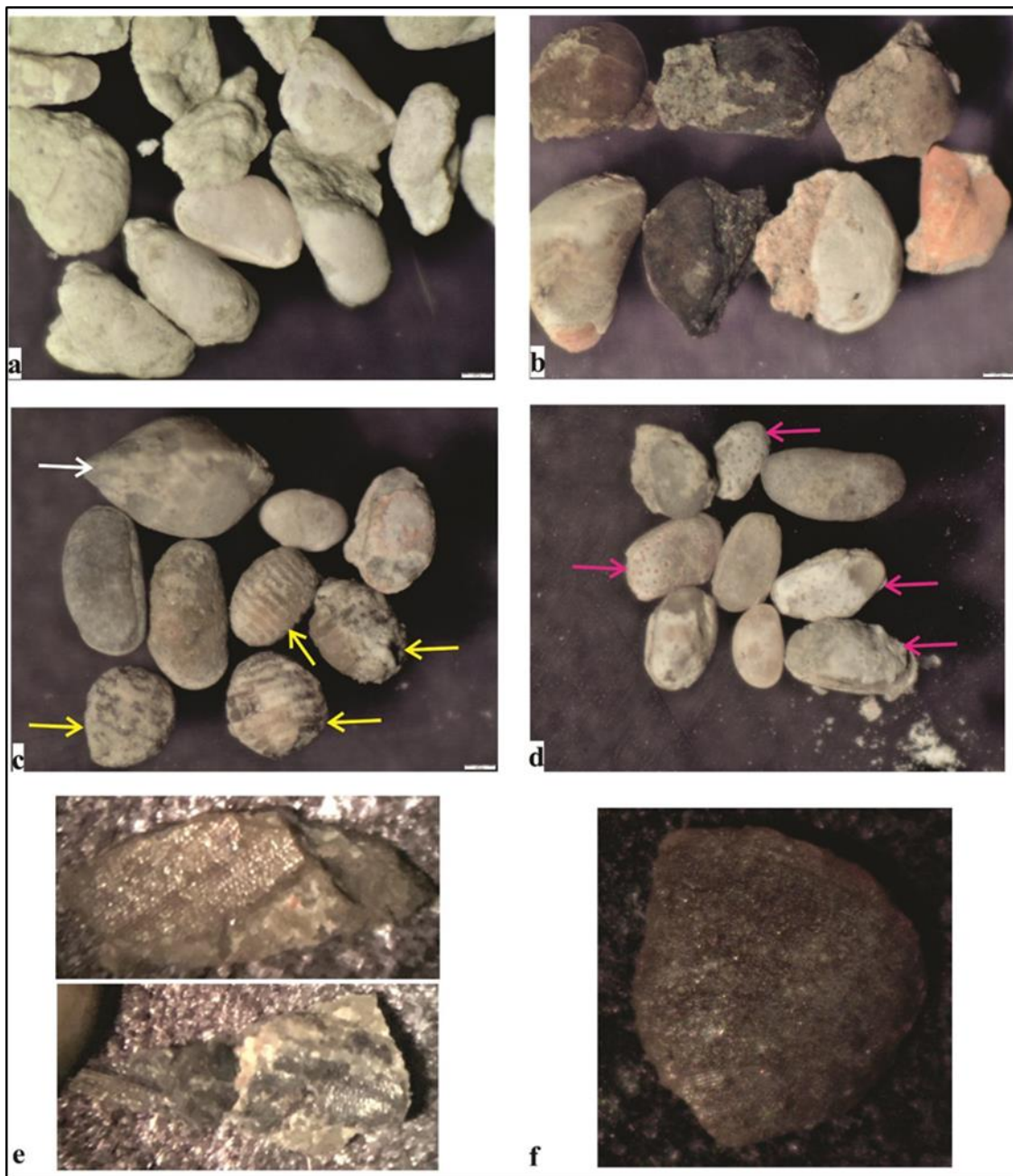


Figure 3.44. Photomicrographs of extracted fossils from Kösüre (a) and Sünnet sections (b, c, d, e, f) presenting wackestone, oil-shale and marl facies. (Sample no. a) K28 marl, ostracods, x2.5; b) S16 wackestone, ostracods, x2.5; c) S26 wackestone, ostracods, bivalve (white arrow) and charophyte gyrogonites (yellow arrow), x2.5; d) S26 wackestone, ostracods, perforated ostracods (pink arrow), x2.5; e) S26 wackestone, fish scales, x3; f) S13 oil-shale, bivalve fragment, x2.5.

In the studied section, the pebbly conglomerate characterizes littoral zone marine deposits. The littoral deposits conglomerate is consisting of moderately sorted and sub-rounded, and have a sharp to the slightly erosional base and a sharp to gradational upper contact. It is also supported by overlain palaeosols and underlain by well-bedded and sorted arenites. In contrast, the upper conglomerate in the upper portion of the studied sections are characterized as debris flow deposits. These are comprising of massive and poorly sorted, lack preferred orientation and vertical grain size trend. This interval facies indicate non-erosive contact and representing normal grading. These features are linked with debris flow deposits (Collinson & Lewin, 1983; Yang et al., 2010). The pebbly conglomerate bedding in the Sünnet section shows scarce erosional surface in the middle portion intervals. The laterally continuous intervals and sub-angular to sub-rounded grains indicates high wave energy marine shallow environmental deposits (Rees et al., 2014).

The topple conglomerate intervals are suggested as turbiditic deposits, which having erosional basal surface and then overlain by massive sandstone units (Yang et al., 2010).

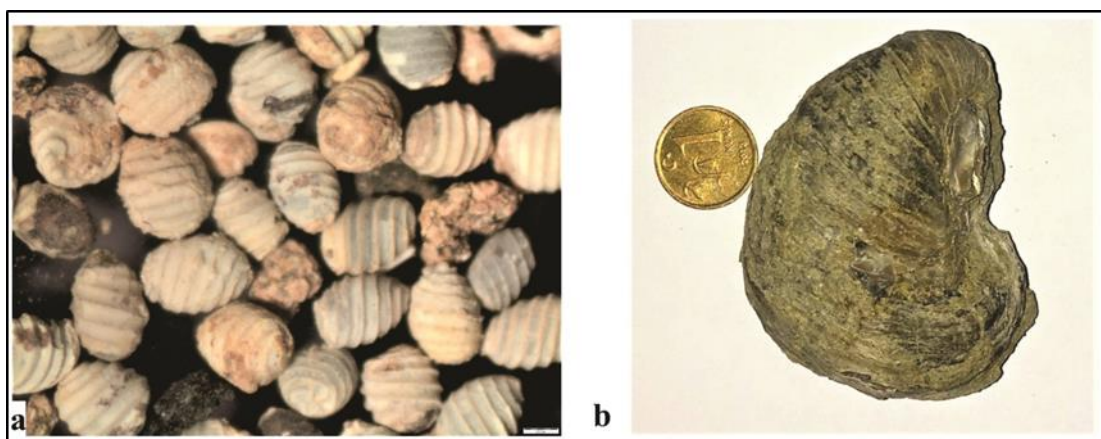


Figure 3.45. Photomicrographs of extracted fossils from Sünnet sections. (Sample no. a) S17 packstone, charophyte gyrogonites, x2.5; b) S32 rudstone, bivalve.



## CHAPTER 4

### OSTRACODS AND CHAROPHYTE GYROGONITES

#### 4.1. Introduction

The paleontological evidence provided characteristic features to identify and categorize the depositional setting and stratigraphic position of the studied successions in the basin. The studied region is comprised of sedimentary depositional successions which are related to the opening and closing of the northern branch of the Neo-Tethys ocean during the Late Cretaceous to Middle Eocene. As a result, deposited successions are of continental and marine depositional origin in the basin (Saner 1980b; Ocakoğlu et al. 2007; Şafak et al., 2015). Saner (1977, 1980b), Ocakoğlu et al. (2007; 2012) and Şafak et al. (2015) carried out a research in the Northwestern Turkey and documented a transitional lagoonal/lacustrine to deep marine depositional setting during the Middle Eocene period by analyzing sedimentological studies and Ostracoda assemblages. In this study, sedimentological analysis and fauna assemblages also indicate that the studied sections are initially deposited in Oligo-Mesohaline to brackish lacustrine and then evolved to the marine depositional environment in the later stage, barring the Sünnet section. The Sünnet section is evolved from the fluvio-lacustrine floodplain to the marine depositional environment.

In this study, the study of ostracods and charophyte gyrogonites in the studied successions is examined to identify and characterize the Middle Eocene marine-influence lacustrine condition. To achieve inclusive paleontological analyses on the studied measured sections, the desired microfossils are extracted from selected limestone, oil-shales and marls lithofacies (Appendices B1, B2, B3, B4, B 5). A total of 41, 14, 26, 21 and 15 samples are treated for ostracods and charophyte gyrogonites fossil extraction from the Dağhacılar section, Hasanlar section, Köşüre section,

Karahisar section and Sünnet section, respectively (Appendices B1, B2, B3, B4, B 5). Out of 117 samples, 23 samples give the desired fossils result and the remaining are devoid of ostracods and charophyte gyrogonites biofacies. The main objective of the extracted microfossils is to study ostracods and charophyte in relation to paleoenvironmental conditions and stratigraphic position of the studied sections. Thanks to Prof. Dr. Cemal Tunoğlu for the identification of ostracods in the samples.

#### **4.2. Charophyte Gyrogonites**

In the studied sections, the charophytes are recorded within the Dağhacılar, Köşüre and Sünnet sections with association of ostracods (Figure 4.2). In the studied sections, a total of 117 samples were examined in which 9 samples have well preserved Charophyte gyrogonites (sample D03, D11, D17, K25, K31, K33, S17, S24, S26).

In biostratigraphy studies, charophyte fossils record are known from the Silurian to present, based on their calcified fructifications (gyrogonites and utricles) (Figure 4.1) (Grambast, 1974; Feist et al., 2005). Generally, Cenozoic charophytes are considered as useful for biostratigraphic studies, without considering biogeographic text implications (Riveline, 1986; Soulié-Märsche et al., 2002; Bhatia, 2006; Sanjuan and Martín-closas, 2015). The charophyte gyrogonites studies are useful to predict the depositional environment and relative age of the stratigraphic successions. Charophytes are photic zone alkaline oligotrophic lacustrine macrophyte (Gierlowski-Kordesch, 2010; Amezcua, 2012). They are macrophytic green algae and are living in the fresh to brackish water condition. Therefore, it is considered as useful palaeoecologically indicators in the Eocene freshwater environment and in the brackish depositional environment. Charophytes are not only restricted to freshwater, it can be occasionally found in brackish and saline environment, in water depth of less than 10m, or down to a maximum 15m-20m (Platt, 1989; Sim et al., 2006; Soulié-Märsche, 2008). The co-occurrence of charophytes with ostracods and rare gastropods indicate freshwater to slightly brackish depositional environment with the alkaline condition (Freytet and Plaziat, 1982; Sanjuan & Martín-Closas, 2012; Grosjean &

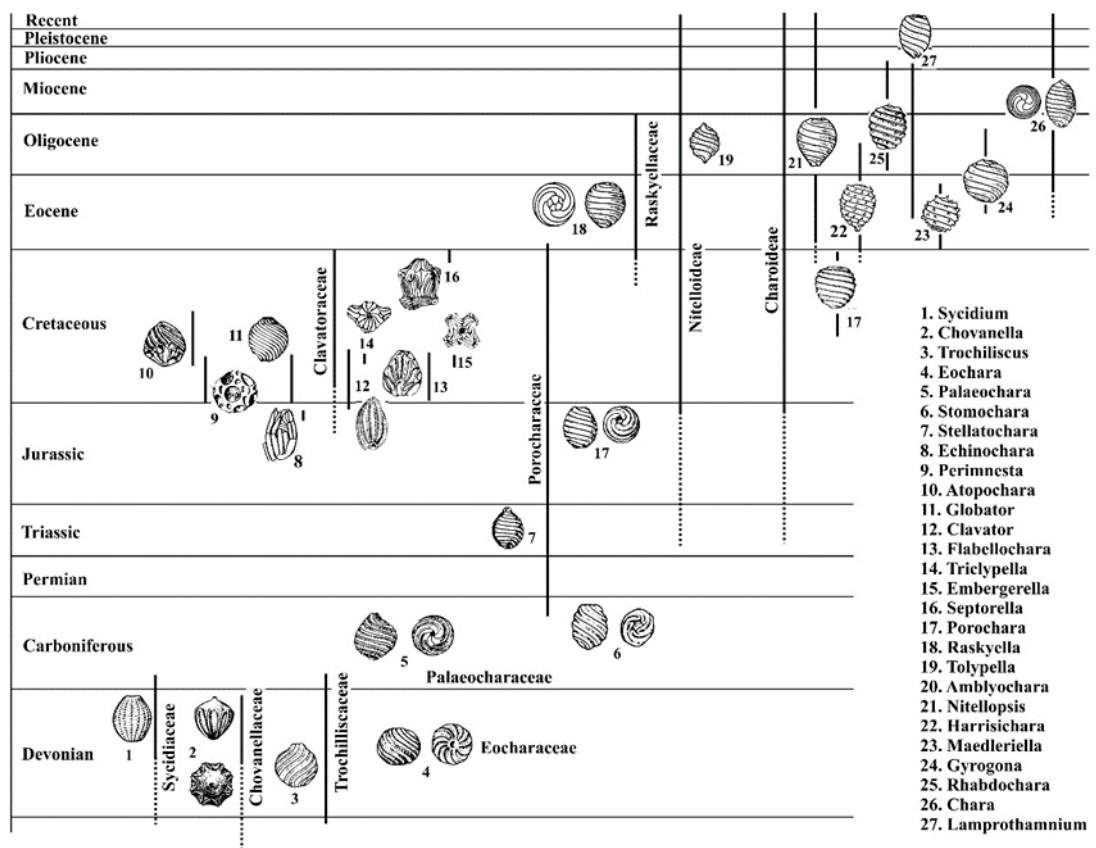


Figure 4.1. General evolutionary trend in Charophyte fructifications (Grambast, 1974).

Pittet, 2013). In general, the deposition of charophytes are resisted to shallow lacustrine depth and shoreline/marginal marine environment (Sanjuan & Martín-Closas, 2012).

Grambast (1962, 1964, 1974) is the first to establish the charophytes biostratigraphy for Tertiary period. In 1972, Grambast proposed the first charophytes biozonation for the European Paleogene. In this study, the charophyte gyrogonites genera are recognized. The charophyte gyrogonites genera are identified by studying number of articles on the charophyte gyrogonites such as Grambast (1962; 1964; 1972; 1974), Bhatia and Bagi (1991), Feist et al. (1994), Martín-Closas et al. (1999), Soulié-Märsche (1998), Soulié-Märsche et al. (2002), Sanjuan & Martín-Closas (2012; 2014; 2015).

In the Dağhacılar section, the observed Middle Eocene charophyte gyrogonites are identified as Family Characeae and Family Raskyellaceae (Figure 4.2) (Bhatia and Bagi, 1991; Riveline et al., 1996; Martín-Closas et al., 1999; Sanjuan and Martín-Closas, 2012, 2014, 2015; Huyghe et al., 2017). The identified Middle Eocene charophyte gyrogonites indicate close affinities with certain the Eocene charophyte gyrogonites from European and Sahara (Castel, 1968; Grambast, 1972; Feist, 1977; Riveline, 1983, 1986; Feist et al. 1994) and from the North West Sahara (Grambast and Lavocat, 1959; Bhatia & Bagi, 1991). The charophyte gyrogonites in the Dağhacılar section suggest relatively change in saline condition, which indicates occasional marine-influence on the lacustrine depositional environment (Soulié-Märsche, 1998; Sanjuan and Martín-Closas, 2012, 2014, 2015; Huyghe et al., 2017). The charophyte gyrogonites are restricted to the lower portion of the studied section. The other associated fauna with the charophyte gyrogonites are ostracod and gastropod (Figure 4.2). The charophyte gyrogonites with association of Middle Eocene ostracod in the studied section suggest Middle Eocene (Lutetian-Bartonian) age (Bhatia and Bagi, 1991; Riveline et al., 1996; Martín-Closas et al., 1999; Yi-yong et al., 2003; Sanjuan and Martín-Closas, 2012, 2014, 2015; Huyghe et al., 2017).

In the Köşüre section, the charophyte gyrogonites is documented from the middle portion of the studied stratigraphic section. The identified charophyte gyrogonites are from Family Characeae charophyte gyrogonites (Figure 4.2) (Bhatia and Bagi, 1991, Riveline et al., 1996; Martín-Closas et al., 1999; Martín-Closas and Ramos-Guerrero, 2005; Sanjuan and Martín-Closas, 2012, 2014, 2015; Huyghe et al., 2017). The recorded charophyte gyrogonites suggest lacustrine environment with slightly brackish condition (Soulié-Märsche, 1998; Martín-Closas and Ramos-Guerrero, 2005; Sanjuan and Martín-Closas, 2012, 2014, 2015). The charophyte gyrogonites and occurrence of ostracods in the intervals of the Köşüre studied succession suggest Middle Eocene (Lutetian-Bartonian) age and lacustrine depositional environment (Bhatia and Bagi, 1991; Riveline et al., 1996; Martín-Closas et al., 1999; Yi-yong et al., 2003; Sanjuan and Martín-Closas, 2012, 2014, 2015; Huyghe et al., 2017).

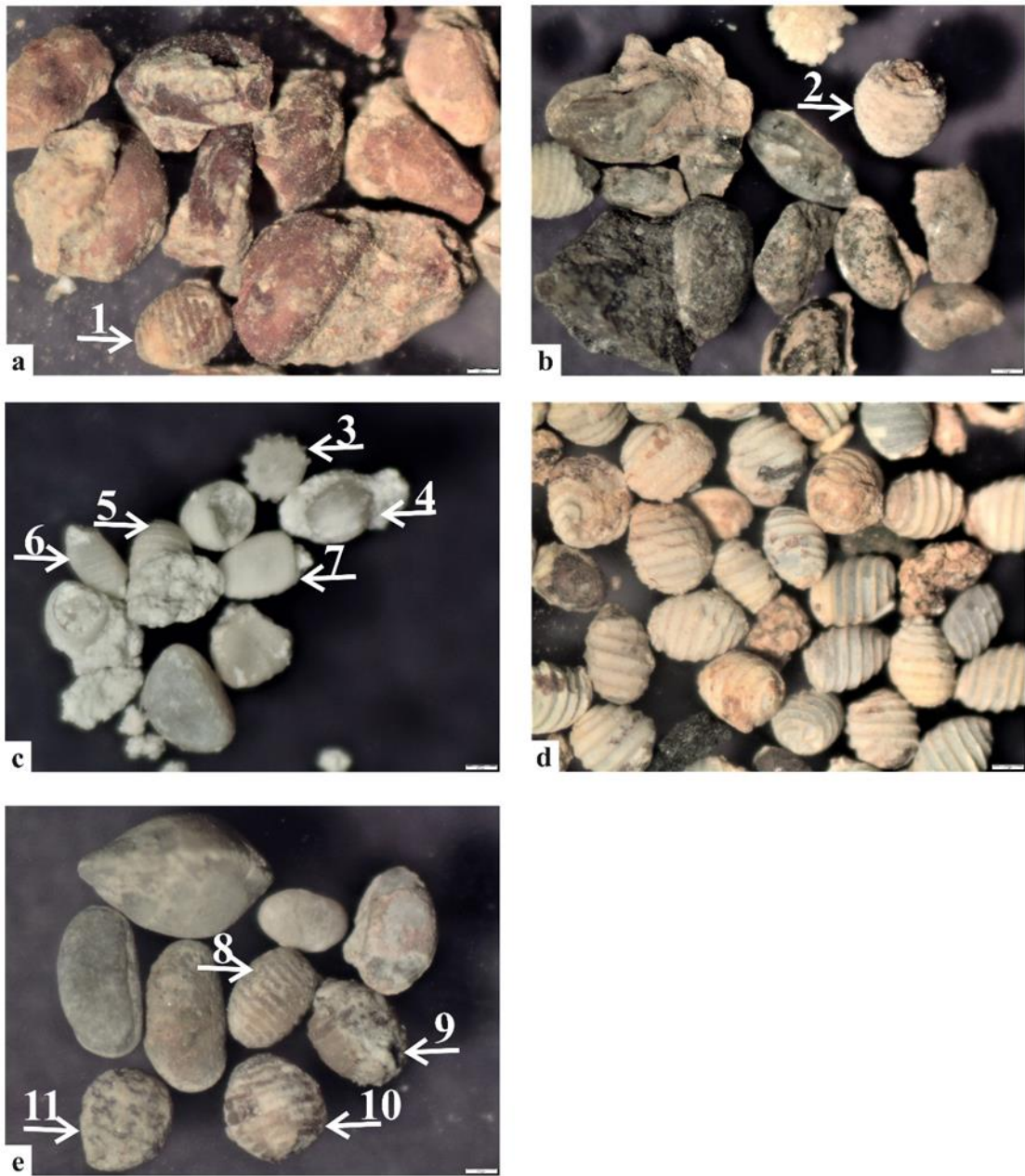


Figure 4.2. Photomicrographs of extracted fossils Charophyte gyrogonites from Dağhacılar section (a, b), Köşüre sections (c) and Sünnet section (d, e). (Sample no. a) D11 packstone, ostracods, charophyta (white arrow), x2; b) D17 wackestone, ostracods, x2; c) K33 wackestone, ostracods and charophyta (white arrow), x3; d) S17 packstone, charophytes, x2.5. e) S26 wackestone, ostracods, bivalve and charophyta (white arrow), x2.5; Charophyte Gyrogonites (1, 2, 3, 4, 5, 6, 7, 8, 9, 10, 11, Figure d)

In the Sünnet section, the recorded charophyte gyrogonites genera are of Family Characeae (Bhatia and Bagi, 1991; Feist et al., 1994; Sanjuan & Martín-Closas, 2012, 2014, 2015; Huyghe et al., 2017). The charophyta-bearing beds with plant fragments, ostracods and gastropods at different horizons indicate laterally related to paralic marshes and reflect Middle Eocene (Lutetian-Bartonian) age (Sanjuan & Martín-Closas, 2012, 2014, 2015; Huyghe et al., 2017).

### 4.3. Ostracods

Ostracods are important crustacean which occur in freshwater, brackish and aquatic marine environment. Their presence in different environmental condition provide important determination to predict ecology, hydrology, and aquatic chemistry of depositional environments which may not be possible through the study of other aquatic organisms (Smith et al., 2015). Previously, number of studied carried out on the Eocene ostracod fauna from different basins, in Turkey (Sönmez-Gökçen, 1973; Tunoğlu, 2001; Şafak et al., 2009, 2015; Şafak and Güldürek, 2016; Tunoğlu et al., 2013; Ocakoğlu et al., 2007, 2012; Şafak, 2018). In this study, the recorded ostracod in the Dağhacılar section, Hasanlar section, Kösüre section and Sünnet section are associated with freshwater to slightly brackish-lacustrine depositional environment and marine environment. The 11 ostracod genera are obtained from 23 samples out of 117 at different horizons in the Dağhacılar section, Hasanlar section, Kösüre section and Sünnet section. Previously, Ocakoğlu et al. (2007; 2012) and Şafak et al. (2015) identified number of ostracod assemblages and interpret their depositional environment from Middle to late Eocene successions in the central Sakarya region. The identified ostracod in their equivalent stratigraphic section studies are *Cyprinotus* and *Heterocypris* (oligomesohaline), *Cladarocythere*, *Neocyprideis*, and *Loxoconcha* (lagoonal), *Leptocythere*, *Cytheromorpha*, and *Cyamocytheridea* (lagoonal-littoral), *Hermanites*, *Quadracythere*, and *Uroleberis* (epineritic), *Monsmirabilia*, *Schuleridea*, and *Caudites* (epineritic-infraneritic), *Paracypris* (infraneritic), *Cytherella*, *Bairdia*, and *Cytheropteron* (epineritic-bathyal), and *Krithe* and *Macrocypris* (infraneritic-bathyal environmental conditions). These ostracod assemblages are comprised of a

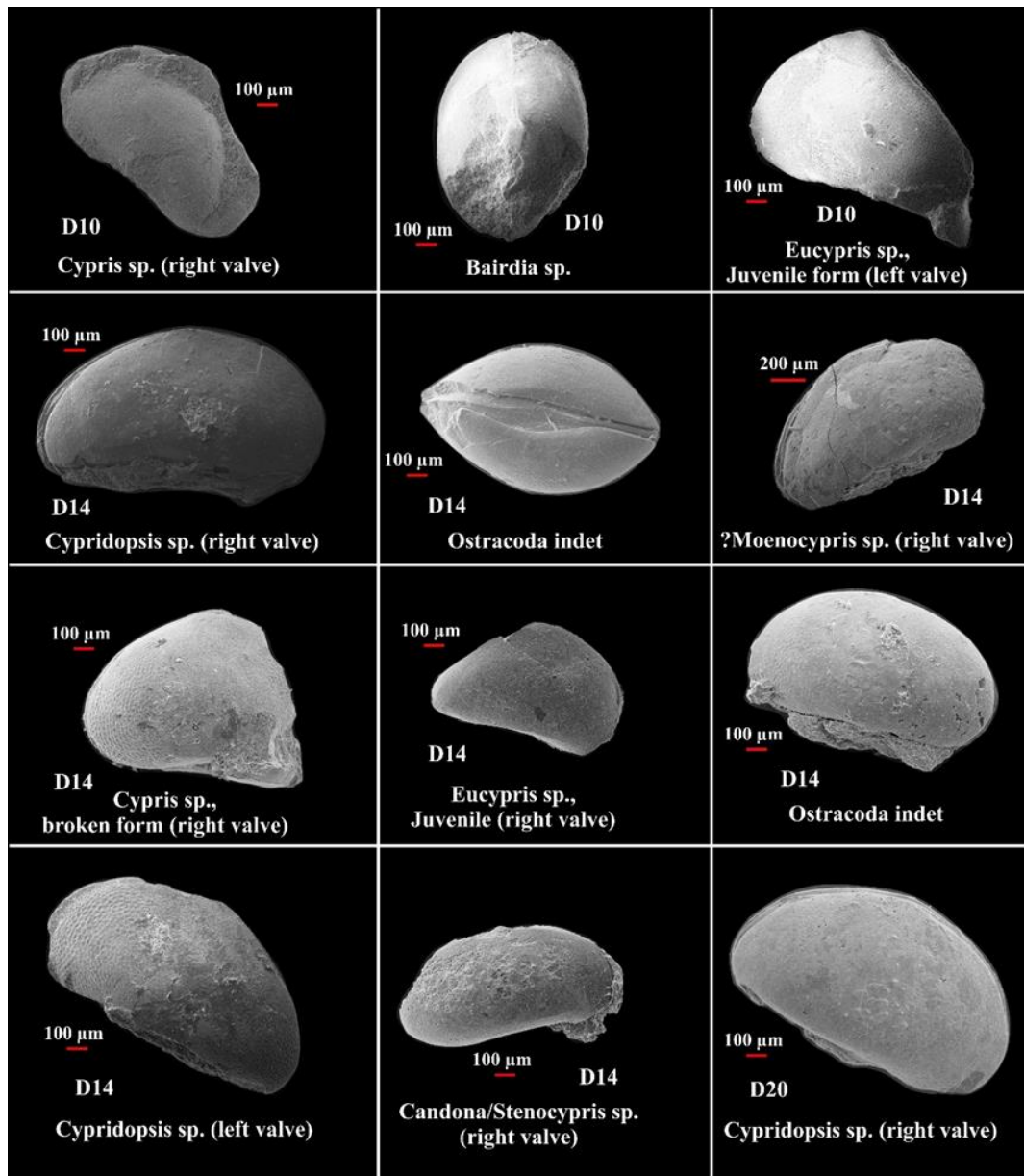


Figure 4.3. Scanning electron photomicrographs of the Dağhacılar ostracods genera. (D= Dağhacılar sample)

mixture of freshwater and euryhaline genera (Ocakoğlu et al., 2007, 2012; Şafak et al., 2015; Şafak, 2018). For the identification of ostracod genera in these Middle Eocene (Lutetian-Bartonian) studied sections, number of published data are overviewed such as Moore (1961), Van Morkhoven (1963), Yi-young et al. (2003), Atay & Tunoglu (2004), Nazik et al. (2008), Ocakoğlu et al. (2007, 2012), Khosla et al. (2011), Witt (2011), Tunoğlu et al. (2013), Şafak et al. (2015), Lettéron et al.

(2017), Şafak (2016; 2018) and also by Prof. Dr. Cemal Tunoğlu (personal communication).

During the Dağhacılar ostracod studies, the recorded ostracod genera in the lithofacies are *Cypris* sp., *Eucypris* sp., *Ostracoda indet*, *Candona/Stenocypris* sp., *?Moenocypris* sp., *Candona?* sp., *Cypridopsis* sp., *Eucythere/Eucypris* sp. and *Bairdia* sp. (Figures 4.3, 4.4). The identified ostracods illustrate freshwater to oligo-mesohaline genera, swim actively in the open water and reflects lacustrine depositional environment with slightly brackish character (Khosla et al., 2011; Witt, 2011; Mazzini et al., 2013; Şafak et al., 2015; Lettéron et al., 2017; Hammouda et al., 2018; Şafak, 2016; 2018). The recorded *Bairdia* sp. is related with marine environmental condition in the studied section. The *Candona* sp. and *Cypridopsis* sp. suggest oligo-mesohaline depositional condition (Khosla et al., 2011; Witt, 2011; Lettéron et al., 2017). Therefore, the ostracod bearing intervals in the lower portion of the Dağhacılar section interpret freshwater to oligo-mesohaline lacustrine depositional setting. The identified ostracods assemblage determines Middle Eocene (Lutetian-Bartonian) age to the studied section.

In the Köşüre section, the ostracods genera are mostly recorded in the middle portion of the measured section. The identified extracted ostracod genera from lithofacies are *Candona* sp.?, *Potamocypris* sp., *Cyprois* sp. and *Cyprinotus* sp. (Figure 4.4). The recorded ostracod in the studied samples describe a linked with freshwater to oligo-mesohaline lacustrine depositional environment (Khosla et al., 2011; Witt, 2011; Mazzini et al., 2013; Şafak et al., 2015; Lettéron et al., 2017; Hammouda et al., 2018; Şafak, 2016; 2018). The recorded ostracod genera evident of Middle Eocene (Lutetian-Bartonian) age in the Köşüre studied succession.

In the Sünnet section, the identified ostracod genera are comprised of *Neocyprideis aposteloscui* (Keij), *Cyprinotus* sp., *Candona?* sp., *Cypridopsis* sp., *Cyclocypris* sp., *Ostracoda indet* and reworked sp. (Figure 4.5). The *Cyprinotus* sp., *Candona?* sp., *Cypridopsis* sp., *Cyclocypris* sp., and *Ostracoda indet* are related with freshwater to

oligo-mesohaline environmental setting and can be found in the saline condition environment (Khosla et al., 2011; Witt, 2011; Mazzini et al., 2013; Şafak et al., 2015; Lettéron et al., 2017; Hammouda et al., 2018; Şafak, 2016; 2018). The *Neocyprideis aposteloscu* (Keij) are reported from mesohaline-hyperhaline environmental

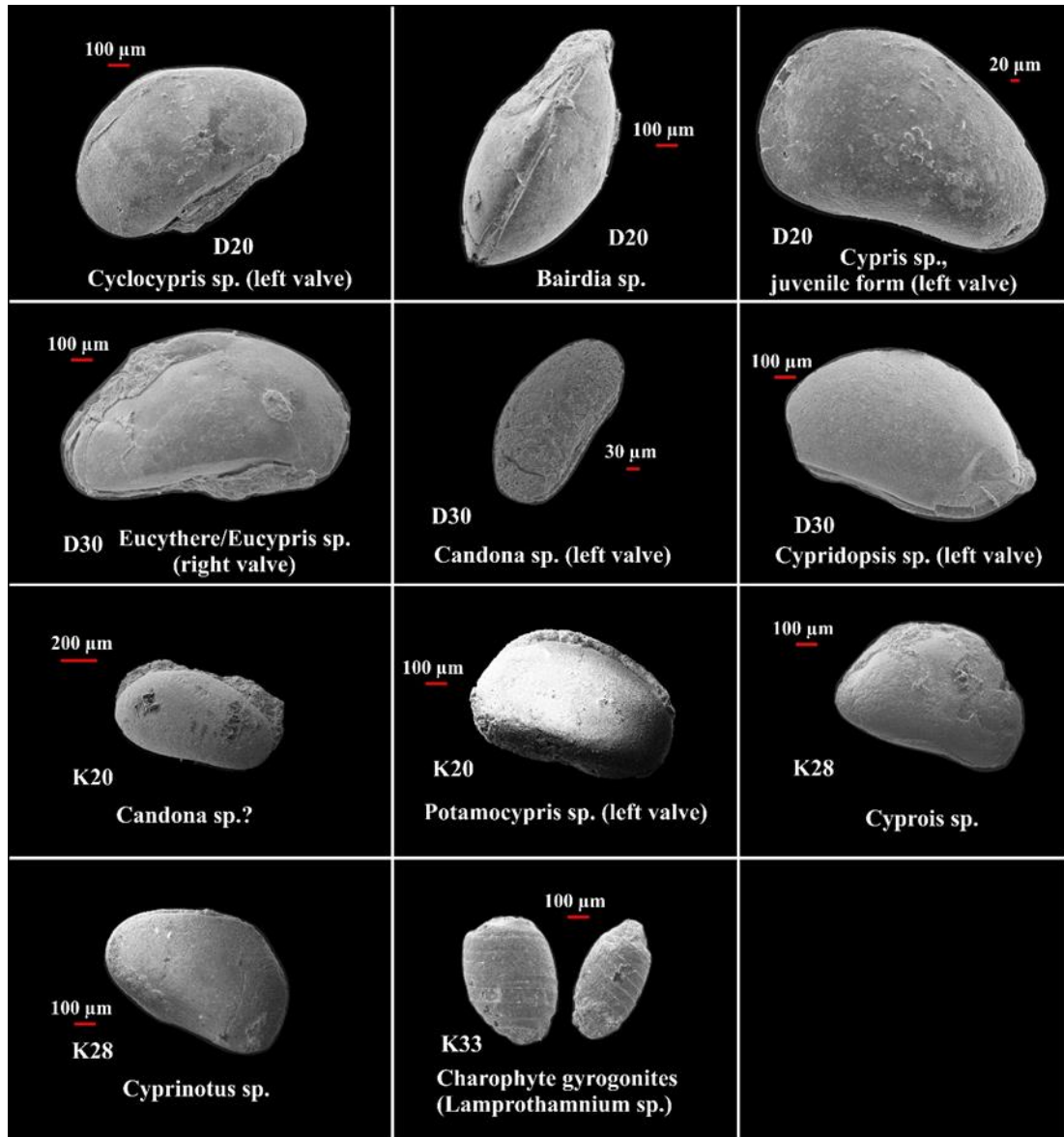


Figure 4.4. Scanning electron photomicrographs of the Dağhacılar and Köşüre ostracods genera. Note: Charophyte gyrogonites genera from Köşüre section. (D= Dağhacılar sample; K= Köşüre sample)

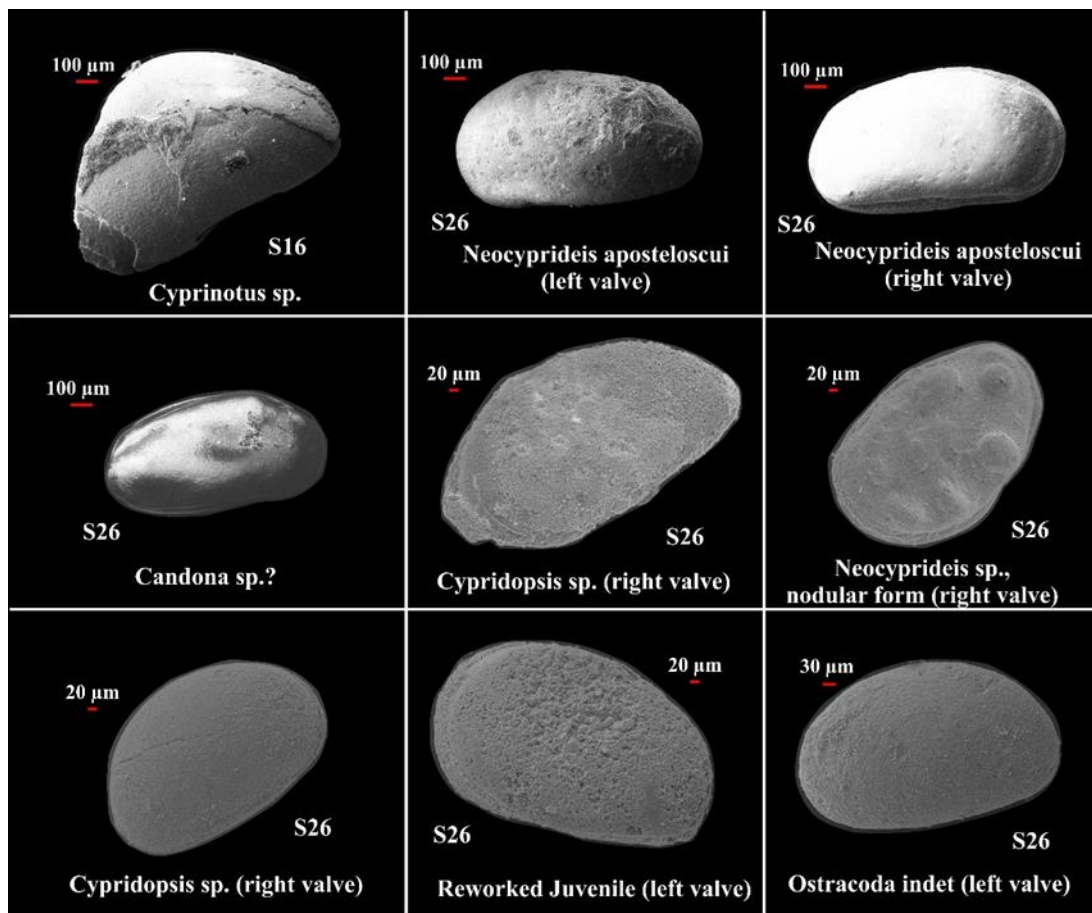


Figure 4.5. Scanning electron photomicrographs of the Sünnet ostracods genera. (S= Sünnet sample)

condition (Sandberg, 1964; Apostolescu and Guernet, 1992; Khosla et al., 2011; Witt, 2011; Mazzini et al., 2013; Şafak et al., 2015; Lettéron et al., 2017; Hammouda et al., 2018; Şafak, 2016; 2018). The recorded ostracods in the Sünnet section indicate a mixture of freshwater and euryhaline genera and suggested significant salinity fluctuation in the depositional regime. The Middle Eocene (Lutetian-Bartonian) age has been assigned to the studied section, based on the recorded Ostracoda assemblages in the studied section.

#### 4.4. Interpretation: Paleocology and Age Constraint for the Studied Sections

During this study, the Middle Eocene measured stratigraphic successions are identified as slightly brackish-lacustrine to transitional marine offshore depositional

environment in the central to southwest section (Dağhacılar section, Hasanlar section and Köşüre section), mesohaline-polyhaline brackish-lacustrine to transitional marine offshore depositional environment in the southeast section (Karahisar section) and fluvio-lacustrine to shallow marine depositional setting in the north (Sünnet section). The identified ostracods genera in the Dağhacılar, Köşüre and Sünnet studied successions are *Cypris* sp., *Eucypris* sp., *Candona/Stenocypris* sp., *?Moenocypris* sp., *Candona?* sp.; *Cypridopsis* sp., *Eucythere/Eucypris* sp., *Potamocypris* sp., *Cyprois* sp., *Cyprinotus* sp., *Neocyprideis aposteloscui* (Keij), *Cyclocypris* sp. and *Bairdia* sp. (Figures 4.3, 4.4, 4.5, 4.6). The identified ostracods genera are known as moderate to very active swimmers (Khosla et al., 2011). Along with ostracod, there is also recorded charophyte gyrogonites in the Dağhacılar, Köşüre and Sünnet studied sections (Figures 4.2, 4.6). Based on ostracod assemblages and association of charophyte gyrogonites and lateral and vertical correlation, it is interpreted that the successions were deposited during the Middle Eocene (Lutetian-Bartonian) period. The observed ostracods and charophyte gyrogonites in the Dağhacılar, Köşüre studied stratigraphic intervals and overlying occasional observed marine benthic fauna in the upper studied stratigraphic intervals, interpret that the studied successions were deposited in a slightly brackish lacustrine environmental, which was transitional evolved into marine transgressive environmental condition during the Middle Eocene period.

At some intervals in the lower portion of the Dağhacılar Section, the lithofacies have gastropod, ostracods and rare nummulites (Figures 3.9, 3.12, 3.42). The presence of gastropod with ostracods and rare nummulites at these intervals reflect the episodic incursion of marine condition into the lacustrine depositional environment and responsible for salinity changes in the depositional setting (Dolin et al., 1980; Şafak et al., 2015; Huyghe et al., 2017). This fossil mixing is evidence of significant fluctuation in the water salinity and depositional condition (Mazzini et al., 2013; Huyghe et al., 2017). The presence of ostracods and charophytes genera in the intervals also characterize slightly brackish-lacustrine depositional condition with no lagoonal character (gypsum) (Huyghe et al., 2017). Therefore, the lower portion of the

Dağhacılar section reflect Oligo-Mesohaline lacustrine environmental condition with depth of around + 70m. The upper calcareous sandstone with oil-shale and marl intervals in the studied section are characterized by subordinate benthic fossils, hummocky cross stratification and wavy rippled strata and interpret marine depositional environment deposits (Huyghe et al., 2017).

The presence of ostracods at different intervals in the Hasanlar measured section characterize lacustrine depositional setting.

Similarly, in the Kösüre section, the occasional presence of ostracods and mix freshwater-brackish charophytes at the intervals in the middle portion of the studied section suggest slightly brackish-lacustrine depositional condition (Figures 3.43, 3.44, 4.6). The hummocky cross stratification and wavy rippled calcareous sandstone with oil-shale intercalation, echinoderm bearing limestone in the upper portion of the Kösüre section suggest the marine depositional successions and are lying over the slightly brackish-lacustrine depositional successions (Guernet et al., 2012; Huyghe et al., 2017).

In the Karahisar section, there is rare observation of the ostracod which is identified under the microscopic analysis. The lower portion of the Karahisar section is interpreted as Meso-Polyhaline-lacustrine depositional environment which is overlain by marine environment deposits. It is also supported by the previous studies of Ocakoğlu et al. (2007; 2012) and Şafak et al. (2015) in the studied regime. In their studies, they recorded *Cyprinotus* and *Heterocypris*, *Neocyprideis* and *Cladarocythere*, *Leptocythere* and *Cytheromorpha*, *Cytherella*, and *Schuleridea*, *Monsmirabilia*, and *Paleomonsmirabilia* and interpreted a transition from hypohaline brackish-lacustrine to marine depositional environment.

In the Sünnet section, the association of fossils such as gastropod, bivalvia, fish-tooth and Oligo-Mesohaline to euhaline ostracods are indicating the marine environmental conditions (Figures 3.35, 3.36, 3.37) (Yi-yong et al., 2003; Schneider et al., 2005; Guernet et al., 2012; Huyghe et al., 2017). In the Middle Eocene Sünnet stratigraphic

section, the co-occurrence of fauna includes Bivalvia-occasional benthic foraminifera in the fossiliferous shale, ostracod-charophyta-gastropod in the limestone and gastropod-bivalvia-Nummulites shells in the calcirudite interpret marine shelf condition and lying over the fluvio-lacustrine floodplain deposits (Sanjuan & Martín-Closas, 2012; Huyghe et al., 2017).

Overall, in the studied sections, the ostracods and charophyte gyrogonites with occasional association of gastropod and rare Nummulites indicate oligomesohaline lacustrine inhabit and around + 70m lacustrine depth in the Dağhacılar, Hasanlar and Köşüre sections (Moore, 1961, Van Morkhoven, 1963). In the southeast, the Karahisar section reflect Meso-Polyhaline lacustrine based on lack of fauna and adjacent area previous studies (Ocakoglu et al., 2007; 2012 and Şafak et al., 2015). The northern studied section, near the Sünnet village, indicate mixing of brackish and polyhaline fauna and illustrate brackish lacustrine floodplain to marine depositional environment. In general view, from north to south in the studied region, the overlying successions on the brackish-lacustrine deposits are identified as marine-offshore transitional deposits. with occasional marine benthic fauna and demises of lacustrine fauna before the transition zone.

The stratigraphic position, ostracods and charophytes genera indicate Paleogene-Neogene period. The recorded *Cyclocypris* sp., *Candona* sp., *Potamocypris* sp., *Heterocypris* sp., *Stenocypris* sp., *Neocyprideis* sp. of ostracods genera and associated charophyte gyrogonites refer Middle-Late Eocene (Lutetian-Bartonian) age to the studied sections.

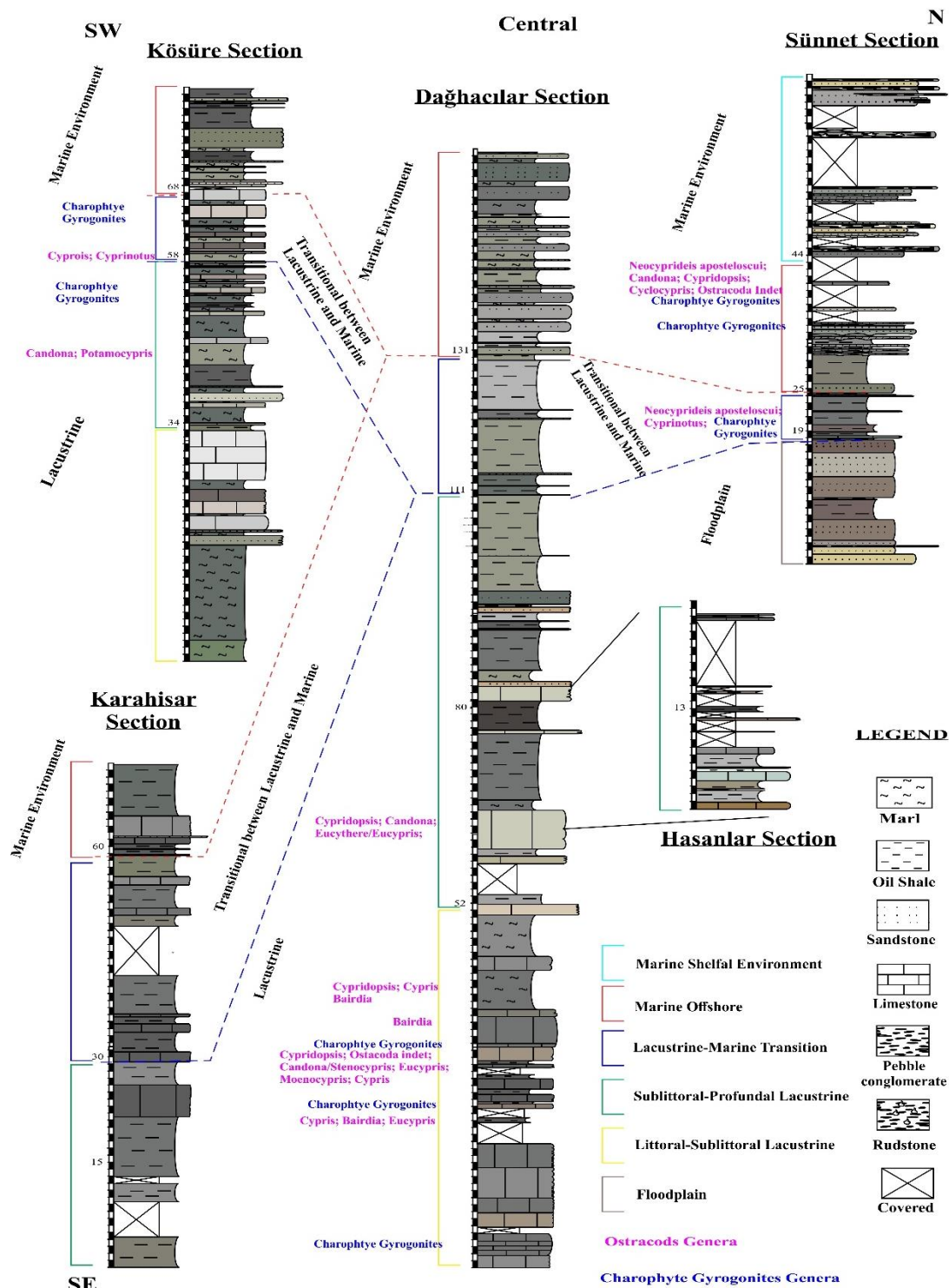


Figure 4.6. The identified ostracods and charophyte gyrogonites genera along the measured Dağaçlar section, Hasanlar section, Köşüre sections, Karahisar section and Sünnet section.

## CHAPTER 5

### FACIES ASSOCIATION, LACUSTRINE ENVIRONMENT AND TRANSITION TO MARINE ENVIRONMENT SETTING

#### 5.1. Introduction

In this study, sedimentological and petrographic analysis accompanied with fauna and flora are important tools to characterize the depositional environment in the measured stratigraphic sections (Martin, 1999). In the studied sections, the sediments generally reflect deposition in freshwater to slightly brackish lacustrine setting and marine influence overlain depositional environment. In the studied sections, the dominated limestone intervals interpret coarsening upward in the measured stratigraphic sections and deposited during fluctuation of lake level (Cyr et al., 2014). The intercalated marls facies with limestone units interpret that the marl facies are deposited in more distal and relatively deeper environment with the dysoxic condition. The overlying limestone on the marls facies illustrates lacustrine margins with increasing lime-producing organism activity (Gierlowski-Kordesch, 2010; Sanjuan & Martín-Closas, 2012).

The wackestone-packstone microfacies in the studied sections are commonly comprised of ostracods, gastropods, charophytes, rare echinoderm, benthic Foraminifera, bivalve, and phytoclast materials. These fossils bearing limestone intervals correspond to carbonate of the biogenic producer in oxygenated and shallow water condition. Generally, the wackestone and packstone facies represent moderate energy depositional setting. Frequent presence of intraclasts in the limestone suggest moderate to high energy environmental condition. The ostracods, gastropods with the association of charophytes in the wackestone-packstone facies interpret deposition in freshwater to brackish with the alkaline environmental condition (Freytet and Plaziat,

1982; Tunoğlu, 2001; Sanjuan & Martín-Closas, 2012). Generally, the predominance of lime mudstone-marl intercalating intervals suggests low energy depositional setting (Platt, 1989).

Lacustrine carbonate microfacies are generally categorized on the basis of charophytes remains and related fauna including freshwater-slightly brackish water ostracod, molluscs and other fauna. The carbonate intervals rich in charophytes represent the marginal to relatively deep lacustrine environment. In the case, the occurrence of abundant bioclasts with association of bioturbation in the micritic lithofacies would suggest oxygenated bottom waters condition. In the studied sections, the presence of relative content of bioclasts with lacking bioturbation reflect shallow lacustrine deposits with dysoxic condition in the lower portion of the measured stratigraphic sections (Figure 5.6). In the lacustrine deposits, the presence of freshwater to slightly brackish macrofossils, the absence of oolitic grains and evaporite minerals or remnant feature suggest that lacustrine water contain comparatively low water salinities (Kelts and Hsu 1978; Cyr et al., 2014). The presence of marine fauna and flora in the carbonate lithofacies indicate that the deposition of carbonate occur in marine environmental setting (Martín-closas, 2009). The recorded marine fauna in the lithofacies of the studied sections including bivalve, gastropod, ostracods, rare fish teeth and scale and echinoderm fragments indicate deposition occur in the marine environment with relatively saline condition.

Generally, charophyte gyrogonites do not show any evidence of fragmentation or erosion, indicating that they were buried in situ deposit. The absence of marine, together with the sedimentological and taphonomic analysis, suggest that charophyte assemblages grew in shallow brackish lakes. Similarly, the well-preserved documentation of molluscus and ostracod in the lithofacies also indicate that the biofacies assemblage were autochthonous in the depositional regime (Sanjuan & Martín-Closas, 2012). The presence of gastropods and charophytes in the lithofacies reflect brackish shallow lacustrine environment with a water depth of lesser than 10 m, or down to a maximum 15-20m (Platt, 1989; Sim et al., 2006; Wanas et al., 2015).

Abundant gastropod assemblages with the association of subordinate or rare ostracod in the studied section indicate low energy environment and slight deeper depositional setting. The dominance of gastropod in the lithofacies interpret relatively moderate salinity in the lacustrine depositional environment i.e shoreline lake deposits (Grosjean & Pittet, 2013). Oligohaline to brackish-lacustrine deposits are identified at certain intervals in the measured studied sections, i.e lower to the middle portion of the Dağhacılar section, Hasanlar section, lower to the middle portion of the Köşüre section and the lower portion of the Karahisar section (Figure 5.9). In the Sünnet section, the very thin brackish-lacustrine intervals are identified by observation of abundant charophytes deposit in the middle portion of the studied section at certain levels. The marine deposits are observed in the upper portion of the Dağhacılar section, Köşüre section, Karahisar section and Sünnet measured stratigraphic section, and are characterized as marine offshore-transitional deposits (Figure 5.9). The marine offshore-transitional deposits are mostly dominated by high percent of siliciclastic content with association of calcareous cementation and suggest deposition occurred under the influence of rising of water level (Young et al., 2008). The transgression of sea-water is also supported by demise of freshwater fauna and algal structure (algal varve) and occasional appearance of marine fauna in the upper measured stratigraphic successions (Figure 5.6). The marine shoreface-offshore transition sediments are composed of calcareous sandstone, calcareous oil-shale and rarely bioclasts of marine component except the Karahisar measured section (Figures 5.2; 5.3; 5.4; 5.5; 5.6; 5.7 and 5.8). In the Karahisar stratigraphic studied section, the marine depositional setting is identified on the basis of Fe-Mn nodules appearance in the lime mudstone facies which occurred as a result of change in physiochemical condition in the depositional environment (Figures 3.31b, c, f; 3.32a).

The recorded nummulites benthic foraminifera in the Dağhacılar studied section reveals the episodic influence of the marine environment to the lacustrine depositional setting (Argakoesoemah, 2017). The small plant remains in the studied section are the

climatically driven by strongly influence episodic small order sedimentary cycles (Tosal et al., 2018).

Generally, the organic-rich shale is deposited from suspension under anoxic or poorly-oxidized conditions (Chakraborty and Sarkar, 2005; Foix et al., 2013; Scherer et al., 2015). According to Ma et al. (2016), in the lacustrine environment, the massive calcareous mudstone represents shallow, relatively saline deposits with dysoxic-anoxic, cool and arid climatic conditions. In contrast, the laminated calcareous mudstone characterized a large and relatively deep stratified water with anoxic conditions bottom water and oxic surface water. The laminated calcareous mudstone also indicates more humid and warm character depositional condition. Such interpretations are observed in the organic-rich shale lithofacies of the studied sections. Laminae feature in the shale lithofacies are also useful tool to determine the depositional condition of oil-shale. The thick lamina indicate the evidence of bottom flowing current influence (most possibly persuaded by storms), the wavy laminae is characterized by benthic microbial mats (generally cyanobacteria), and the thin laminae in the organic-rich shale lithofacies reflect deposition from suspension in calm and relatively deeper environmental condition (Figure 5.1) (O'Brien, 1990). In the laminated organic-rich shale, the continuous planar laminae character reflects low energy depositional setting. The presence of pyrite and absence of trace fossils and bioturbation indicate deeper lake environment with anoxic condition (Cabrera et al., 2001; Tānavsuu-Milkeviciene & Frederick Sarg, 2012; Abouelresh et al., 2017). The laminae characterized by continuous, wavy laminated and ripple cross-laminated suggest wave activity in the depositional setting (Lazar et al., 2015). In the laminated oil-shale, the orientated ostracod shells and ripple cross-laminated indicate traction currents character deposits (O'Brian, 1996; Schieber et al., 2007; Macquaker and Bohacs, 2007; Macquaker et al., 2010). The alternation of organic-rich laminae and organic-poor laminae typically indicate sedimentological responses such as seasonal forced changes on water salinity, climatic changes, organic productivity, and runoff in lake catchment (Anderson and Dean, 1988; Lindqvist and Lee, 2009). The presence

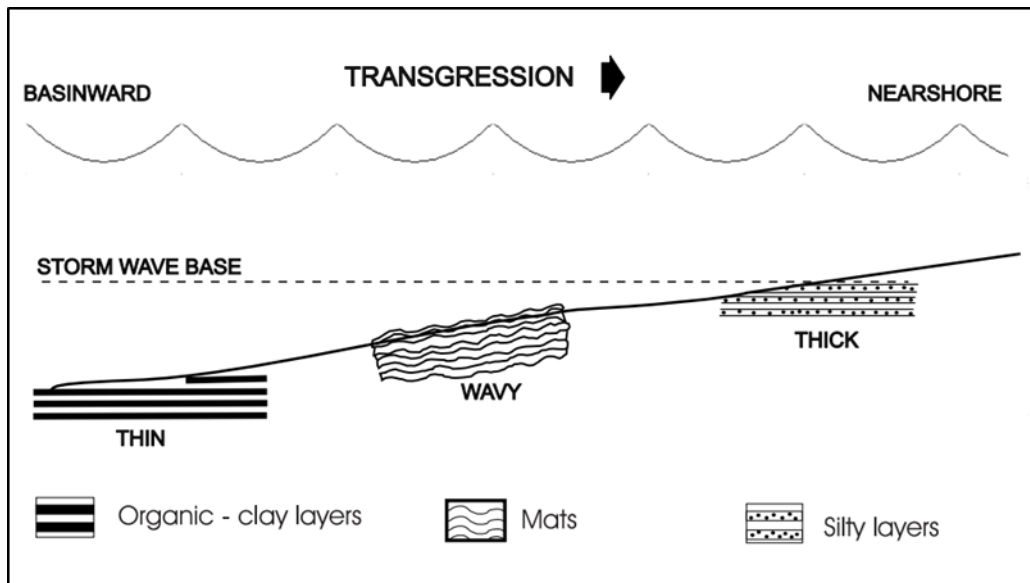


Figure 5.1. Generalized model for laminated mudrocks/shale type and their depositional setting (O'Brien, 1990).

of lenticular lamination in the organic-rich shale reflects sudden dilution and low-energy hyperpycnal flows (Caillaud et al., 2017).

The silt size or very fine sand size quartz grains in the shale intervals are interpreted to be transported into the basin through rivers or eolian processes (Sageman et al., 2003; Lazar, 2007). In the studied sections, the silt size or very fine sand size quartz grains in the oil-shales are defined as eolian transported and/or terrigenous influx to the basin through the hydrodynamic mechanism. In the upper portion of measured section, the documented calcareous sandstone with organic-rich shale revealed increasing percent of siliciclastic grains influx (Figures 5.2; 5.3; 5.4; 5.5; 5.6; 5.7 and 5.8). The increasing percent of siliciclastic grains influx support the hydrodynamic incursion of marine environment to lacustrine basin.

In the mixing zone between slightly brackish-lacustrine and marine water, is defined by low sedimentation rate and comparatively high organic content. It is due to change

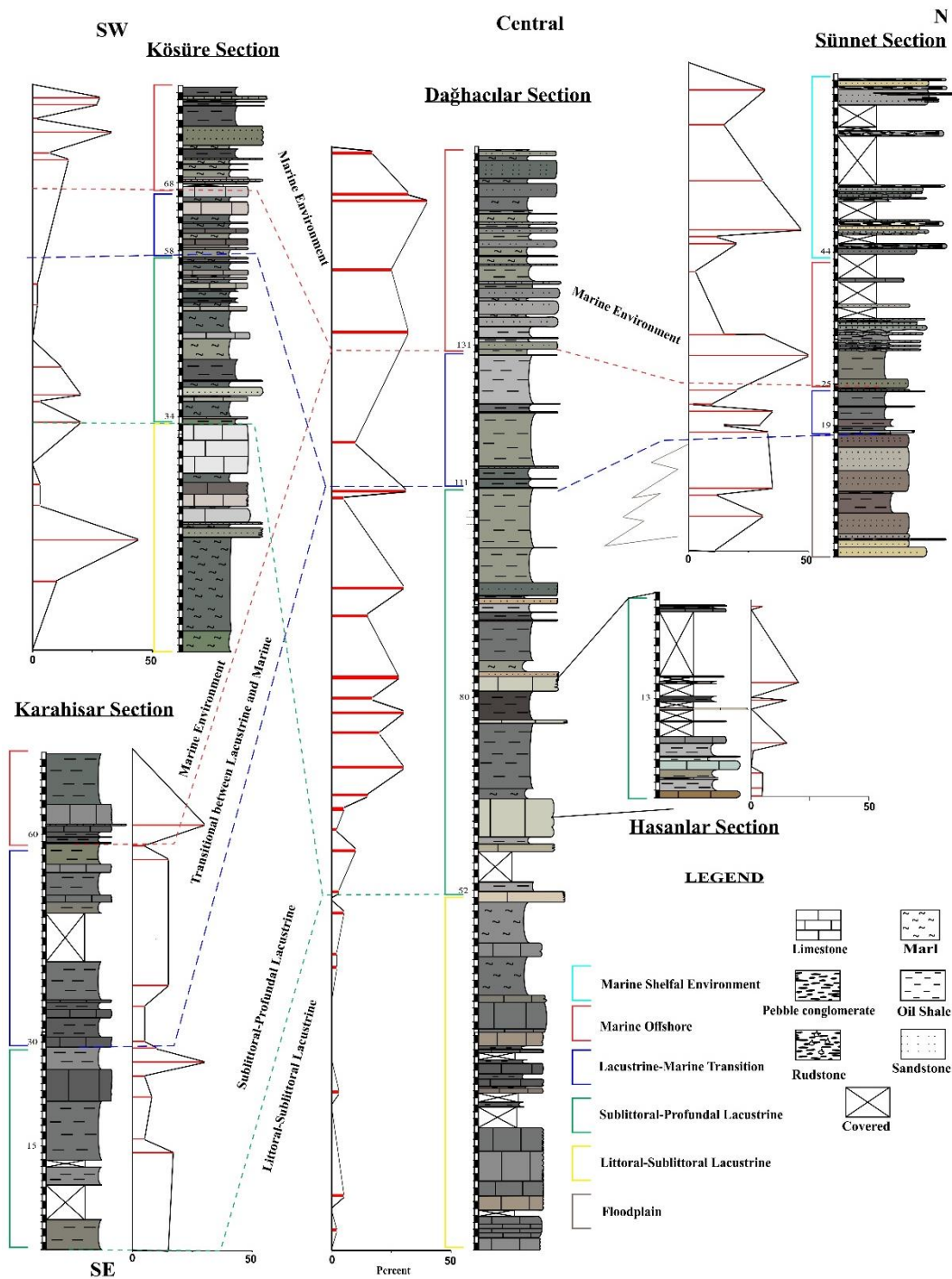


Figure 5.2. Graphic presentation of petrographic percent data of quartz along measured stratigraphic sections; Dağhacılar, Köşüre, Karahisar and Sünnet sections and their correlation.

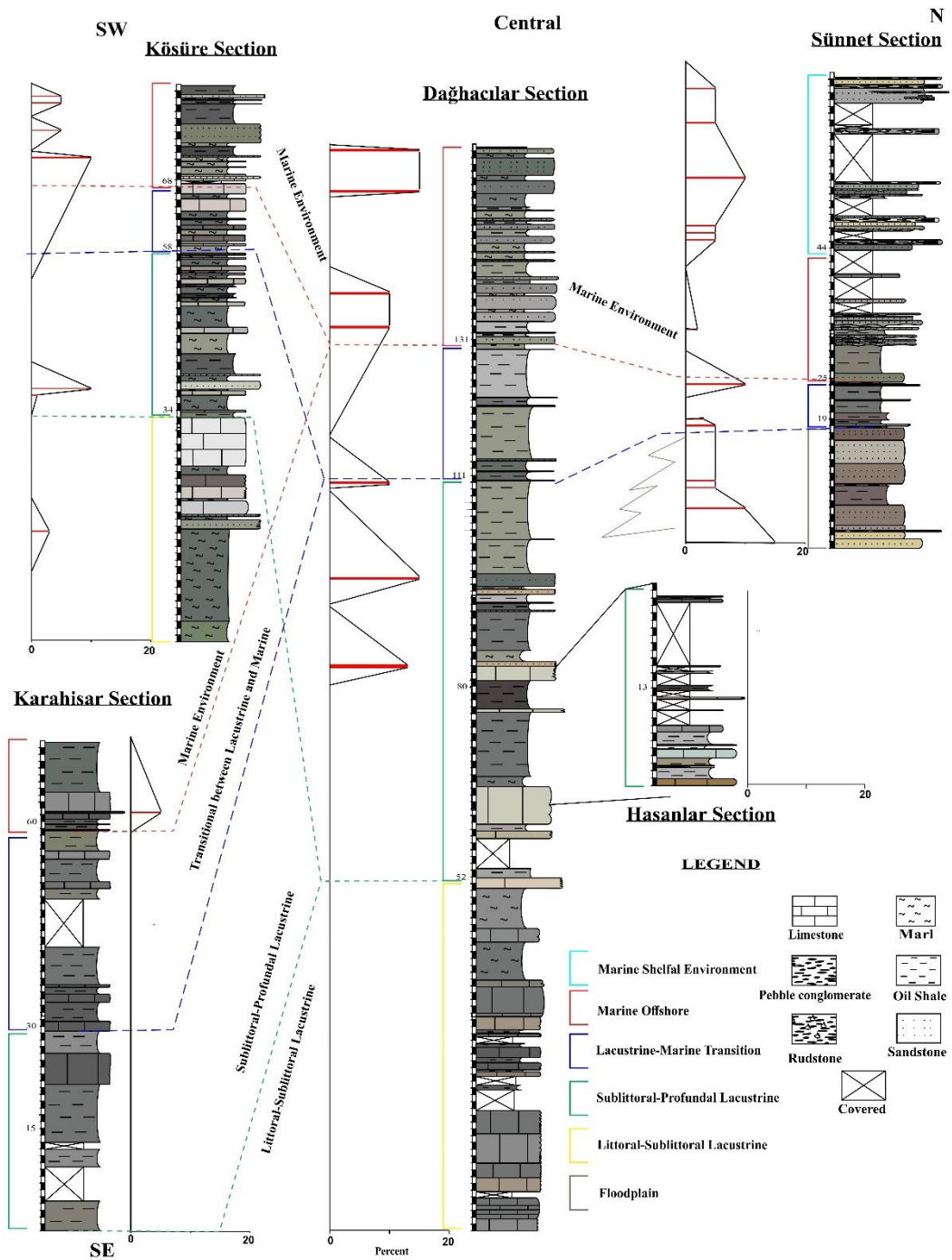


Figure 5.3. Graphic presentation of petrographic percent data of feldspar along measured stratigraphic sections; Dağhacılar, Köşüre, Karahisar and Sünnet sections and their correlation.

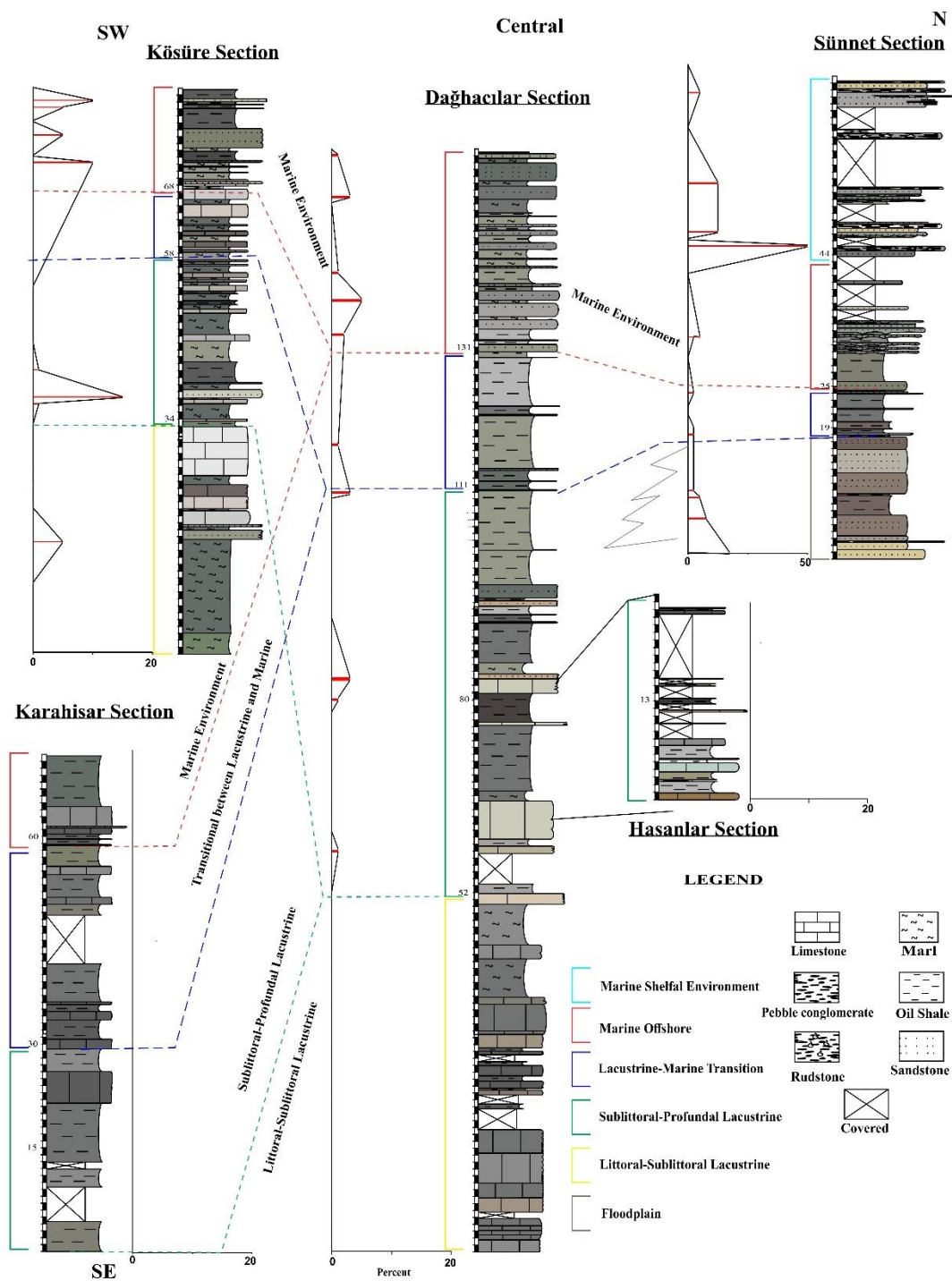


Figure 5.4. Graphic presentation of petrographic percent data of plagioclase along measured stratigraphic sections; Dağhacılar, Köşüre, Karahisar and Sünnet sections and their correlation.

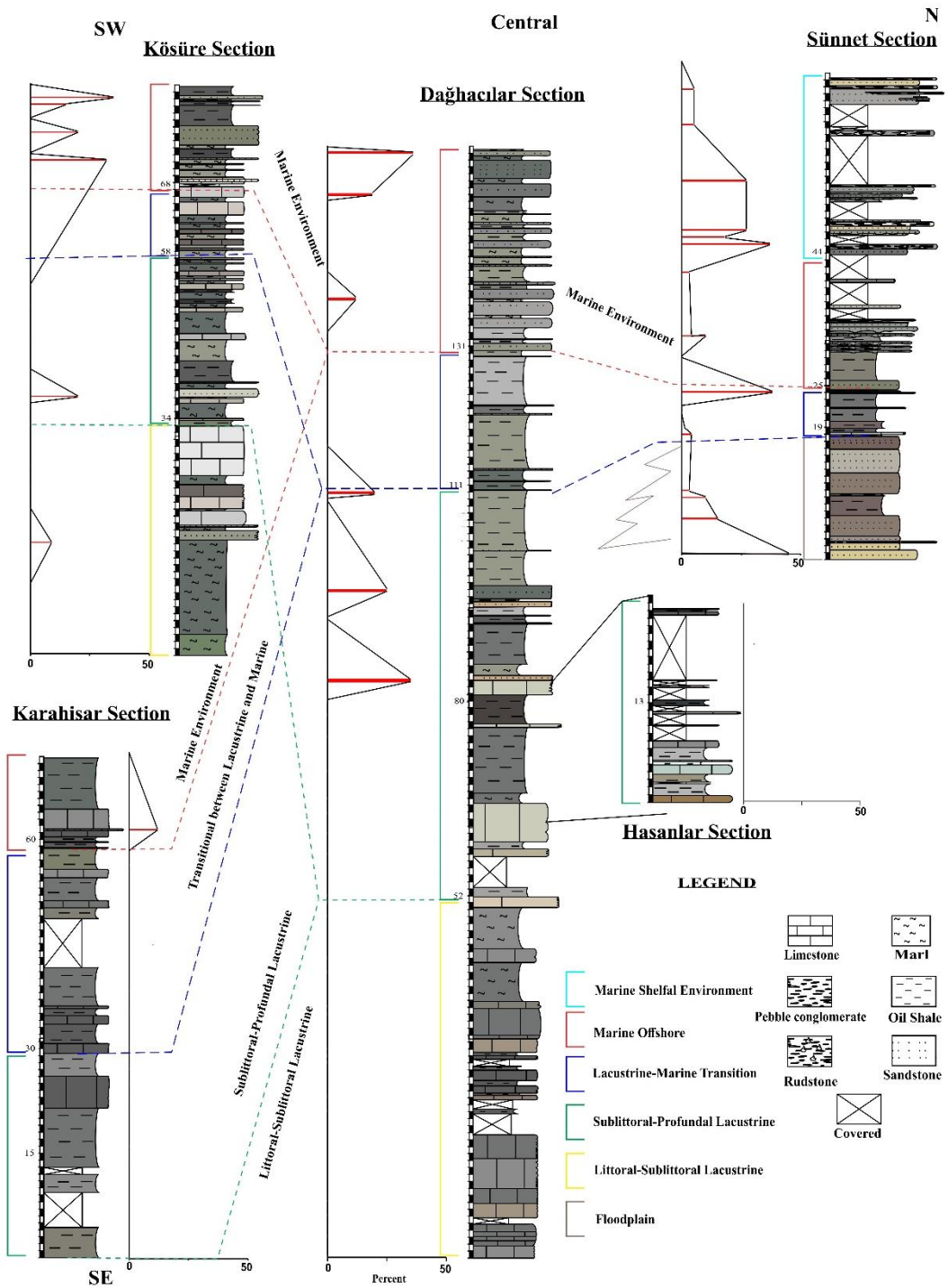


Figure 5.5. Graphic presentation of petrographic percent data of rock fragments along measured stratigraphic sections; Dağhacılar, Köşüre, Karahisar and Sünnet sections and their correlation.

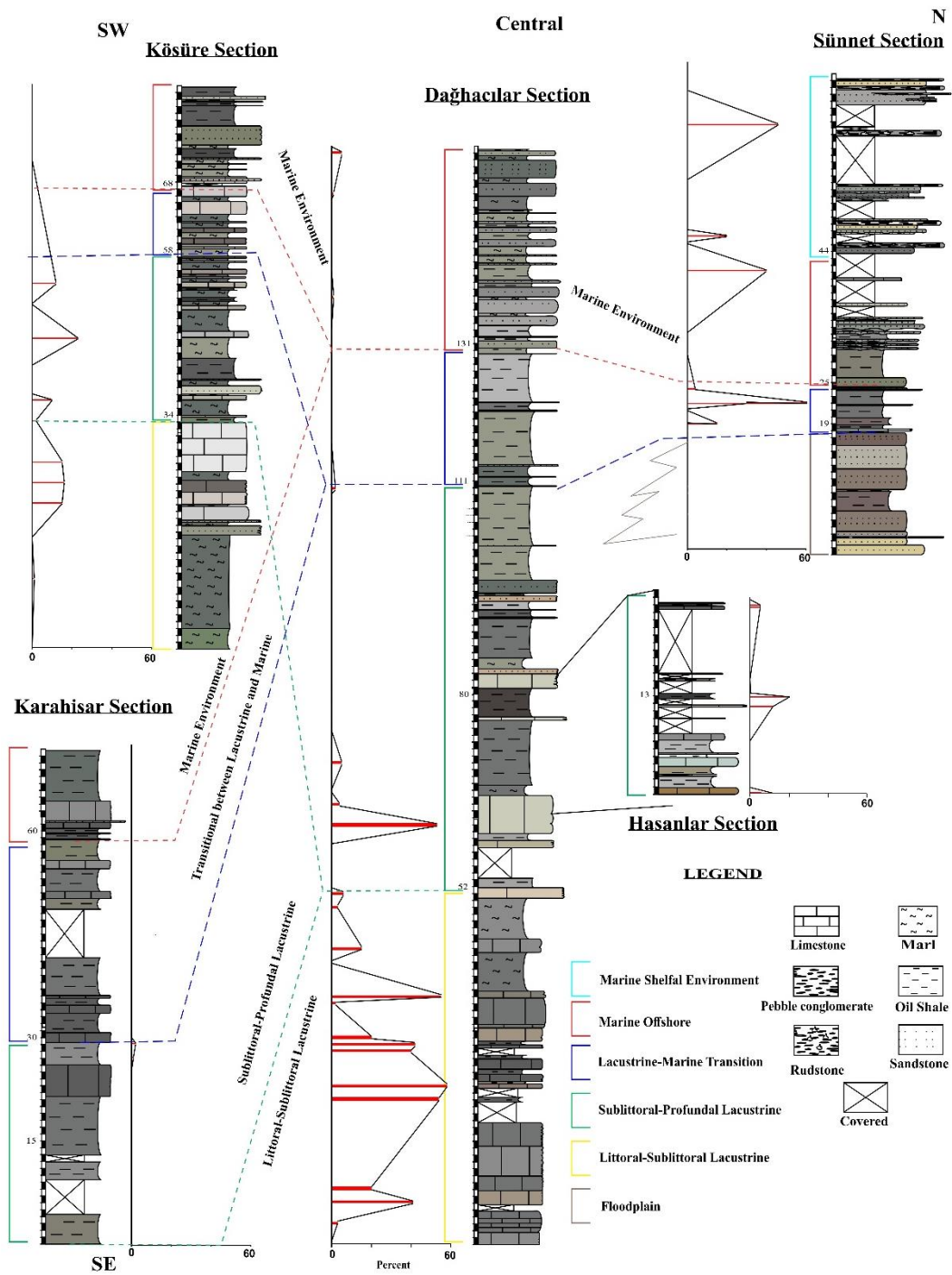


Figure 5.6. Graphic presentation of petrographic percent data of bioclasts along measured stratigraphic sections; Dağhaçlar, Köşüre, Karahisar and Sünnet sections and their correlation.

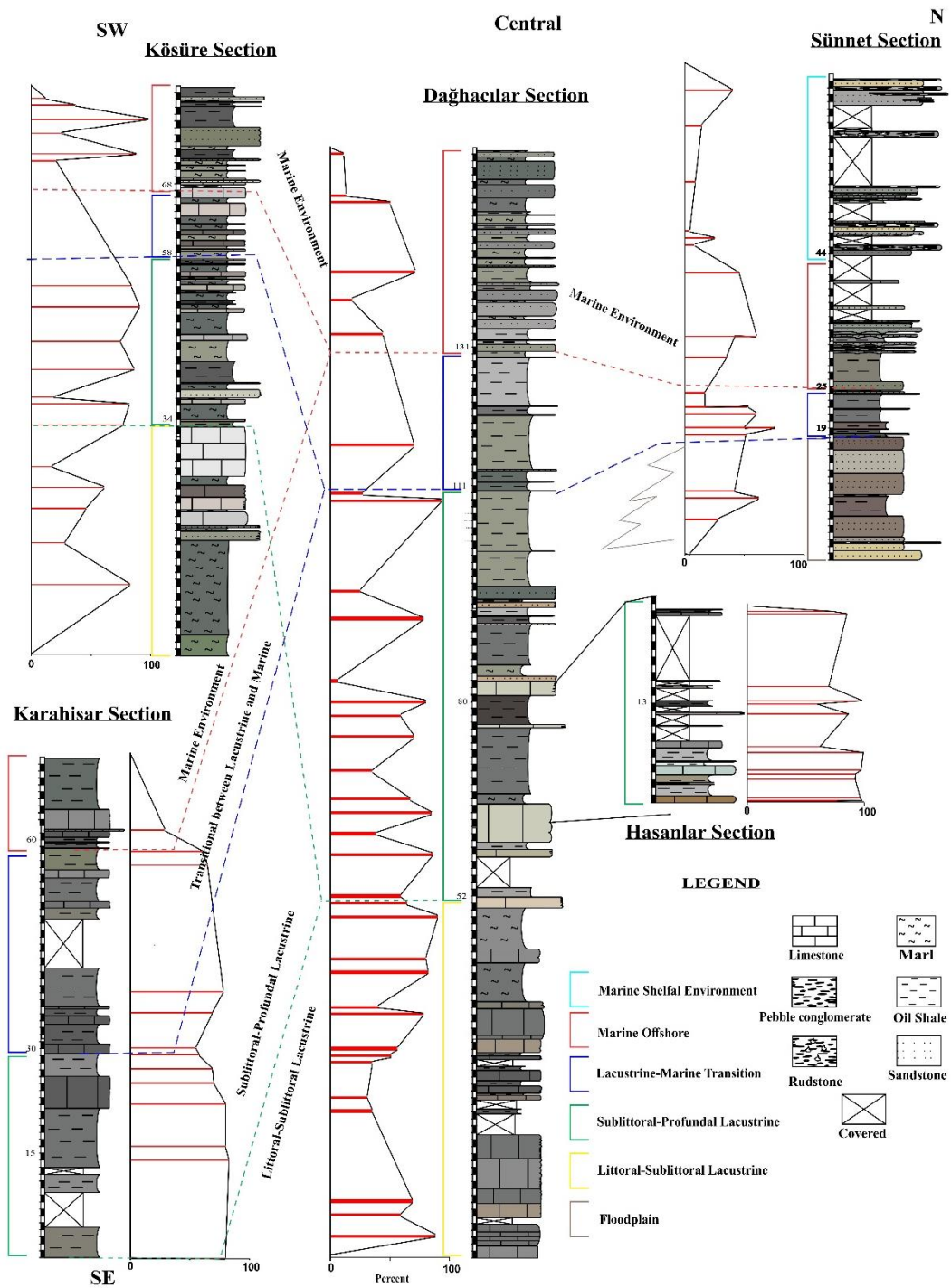


Figure 5.7. Graphic presentation of petrographic percent data of matrix along measured stratigraphic sections; Dağhacılar, Köşüre, Karahisar and Sunnet sections and their correlation.

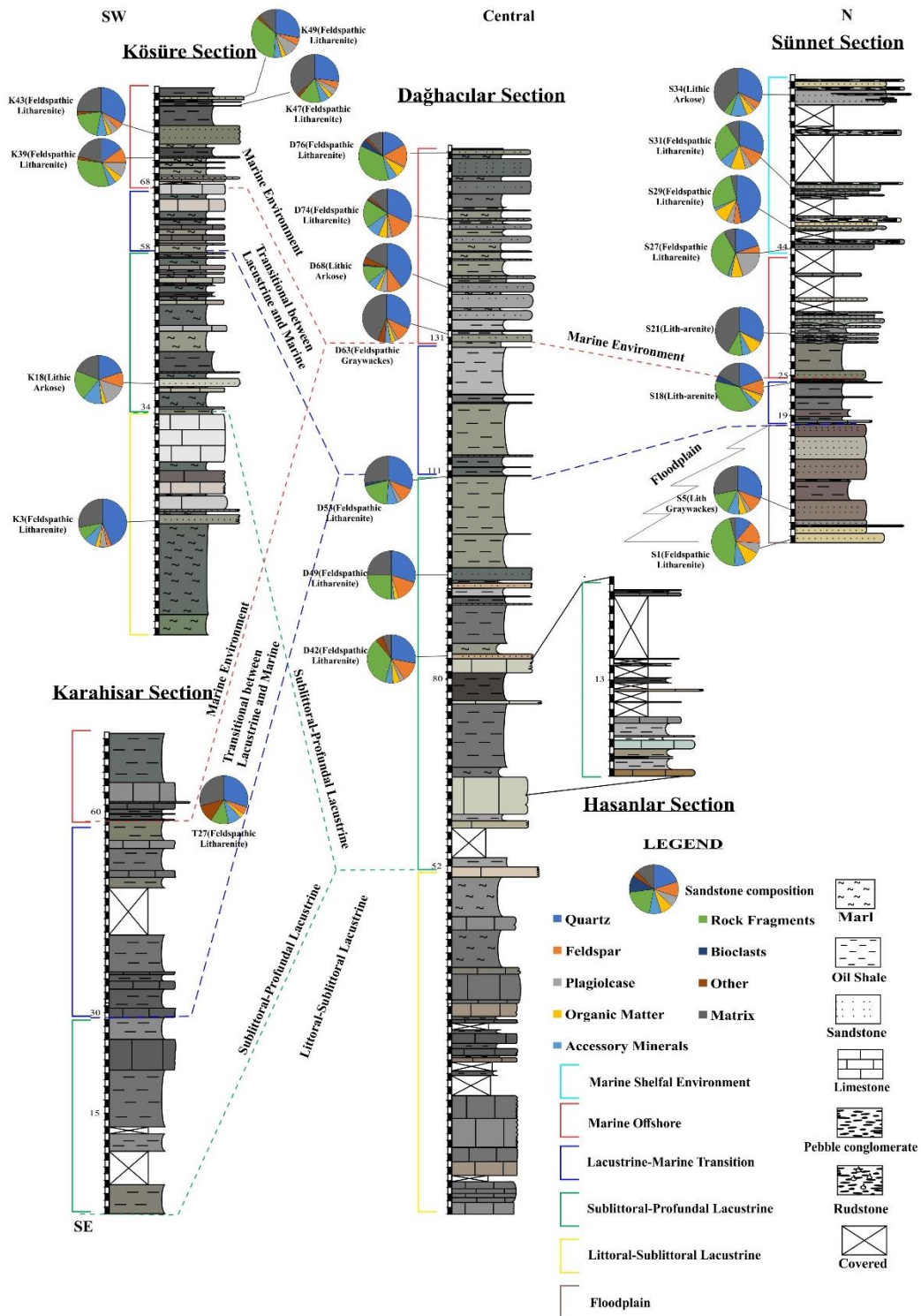


Figure 5.8. Graphic presentation of sandstone pie diagram (Chapter 3) along measured stratigraphic sections; Dağaçlar, Kösüre, Karahisar and Sünnet sections and their correlation.

in the physiochemical condition along the measured stratigraphic sections as a change from lacustrine to marine environment in a calm condition (Mingram, 1998). In the profile view, the quartz, feldspar and rock fragments components illustrate relatively low percent content in the transitional zone as compared to overlain marine successions (Figures 5.2; 5.3; 5.4 and 5.5). Thereafter, the marine successions in the studied sections are composed of turbiditic sedimentation with moderately high organic content shale lithofacies. In the studied sections, the increase in organic-rich shale-fine sandstone intercalation indicate relative high energy condition in the offshore-transition zone depositional setting and recognized as turbiditic deposits and occasionally tempestite deposits at different horizons (Abouelresh et al., 2017). These intervals in the studied sections are related to marine depositional environment. In the Karahisar section, the Fe-Mn nodules appearance suggest the physiochemical changes in the regime. This physiochemical change occurred due to the transgression of marine to lacustrine condition (Figures 3.31b, c; 3.32a).

The morphological study of pyrite is also useful in the prediction of the paleo-redox environmental condition and early diagenetic process (Table 5.1). The framboidal type of pyrite can be used to determine redox conditions in bottom waters by studying their characteristic, i.e densely packing, spherical aggregates of submicron-size pyrite crystals, and their size distribution (Wilkin et al., 1997; Wignall and Newton, 1998; Wignall et al., 2005; Zhou and Jiang, 2009; Wang et al., 2013). The occurrence of framboidal pyrite with size less than  $5\mu\text{m}$  is characterized as euxinic or anoxic environmental condition (Wignall and Newton, 1998). In the modern marine environmental studies, the direct formation of framboids pyrite was observed in the euxinic water condition. The size of this framboidal pyrite is mostly less than  $5\mu\text{m}$ . The framboidal pyrite grow within the sediments have no limitation in the size (can be greater than  $5\mu\text{m}$ ) and describe dysoxic or oxic water condition (Wilkin et al., 1997). The framboidal pyrite of the New Albany shale with average size more than  $5\mu\text{m}$  were interpreted to occur in the relatively shallow depositional environment with dysoxic condition (Lazar, 2007). The Kimmeridge clay framboid pyrite with a size of

Table 5.1. Formation and degree of pyrite related to redox depositional conditions (Lazar, 2007).

Environment Proxy	Euxinic	Anoxic	Dysoxic	Oxic	Reference
Pyrite framboids	<5µm Abundant framboids, less variable in size		>5µm Less abundant framboids, More variable in size	Little or no pyrite	1, 2, 3
DOP	0.75		0.42		4, 5, 6

1. (Wilkin et al., 1996); 2. (Wilkin & Barnes, 1997); 3. Wignall and Newton (1998); 4. Berner (1970); 5. (R. Raiswell et al., 1988); 6. (Jones & Manning, 1994).

3µm were interpreted as an anoxic water depositional setting (Wignall and Newton, 1998). The formation of euhedral pyrite is related to early and late diagenesis. During early diagenesis, framboidal form pyrite transformed to euhedral type pyrite (Raiswell, 1982). In the studied sections, rich framboidal pyrite in the oil-shales lithofacies are interpreted to be form under anoxic conditions (can be change from dysoxic-anoxic) and are comparatively deeper water conditions. The presence of framboidal form pyrite in the measured stratigraphic sections also correspond to the saline influence on the lacustrine environment (Brown and Cohen, 1995). In general, the formation of pyrite is linked to sulfate reduction in saline condition by anaerobic bacteria (Brown & Cohen, 1995).

The calcareous sandstone-oil-shale and/or marls intercalating are recognized as heterolithic deposit, which reflects the marine offshore-transition environment with turbiditic origin. Generally, the heterolithic sediments are associated with turbiditic depositional setting (Abimbola, 2016). Similarly, Ranson (2012) and Siddiqui et al. (2014) documented mudstone intercalation with very fine- to fine-grained, wave ripple, parallel lamination, hummocky cross-stratified sandstones in the Cretaceous Utah formation and Miocene Meragang Beach of China, respectively. These mudstone-sandstone intercalating intervals in the Cretaceous Utah and Miocene Meragang Beach of China were interpreted as marine offshore transitional facies in their study. The presence of hummocky cross-stratified sandstone intervals in the studied sections suggest episodic storm depositional event deposits in the marine-offshore transition environment (Ranson, 2012). The occurrence of rare ichnofacies

in the studied measured sections also predict that the sediments are deposited in marine offshore transition depositional environment (Boggs, 2011; Johansen, 2016).

## 5.2. Facies Association and Depositional Setting of the Studied Sections

In this section of the study, the identified facies have been grouped to facies association (Table 5.2). The facies association have been distinguished based on the stratigraphical grouping of sedimentary facies, identified sedimentary features, observation of flora and fauna, and facies interpretation. The facies associations describe genetically related facies to one another and represent a particular depositional environment (Reading and Levell, 1996). The established facies associations will help to construct the depositional model for the studied lacustrine successions and marine incursion to the lacustrine setting (Figures 5.2; 5.11 and 5.13).

Table 5.2. Facies Associations from established lithofacies of the studied sections and interpreted their depositional setting.

Facies association	Studied facies of the Measured Sections	Depositional setting
FA1	DA1; DA2; HA2; KA1; KA2; TA2	Littoral-sublittoral lacustrine (Shallow lacustrine)
FA2	DA1; DA3; DA4; DA5; HA2; HA3; HA4; KA2; KA3; TA1; TA2	Sublittoral-profundal lacustrine (Deep lacustrine)
FA3	DA3; DA4; DA5; KA1; KA3; KA4; TA1; TA2; TA3; SA4; SA5	Marine offshore transition
FA4	SA1; SA2; SA3; SA4; SA5; SA6	Marine Shelf environment
FA5	SA4; SA5; SA6	Floodplain paleosols

DA: Dağhacılar section; HA: Hasanlar Section; KA: Köşüre Section; TA: Karahisar Section; SA: Sünnet Section

### 5.2.1. Dağhacılar Section: Facies Association and Depositional Setting

The Dağhacılar measured section begin with lime mudstone-marl intercalation and shift to the wackestone-packstone intervals with fossiliferous organic-rich shale and marl interbeds. Then, it is followed by dominant laminated organic-rich shale-marl interbeds with occasional sandstone horizons. The laminated organic-rich shale-marl interbeds are topped by dominant alternating sandstone-laminated oil-shale and

occasionally marl intervals towards the top (Figure 5.9). The Dağhacılar depositional system give the idea that the sediments in the studied section are settled in different environmental condition stages. The lower stage is characterized by lime mudstone, marls to wackestone to packstone facies with rich in charophytes, ostracods and gastropods. It indicates shallow to the relatively deeper lacustrine environment with episodic marine influence. The episodic marine influence is responsible for the development of change salinity and relatively poor oxygenated bottom water conditions. Further upward, the middle portion of the Dağhacılar section is characterized by oil-shale-marl facies with occasional ostracod. This interval represents relative deepening in the lacustrine environment with low sedimentation rate and anoxic depositional condition. In the later stages, the Dağhacılar depositional system show transition from lacustrine to marine offshore transitional environment. The sandstone lithofacies in the studied section are characterized as turbiditic and storm deposits, and oil-shale/marl facies are defining the low energy deposits, settling from suspension. In general, these deposits are associated with marine offshore-transitional environment setting or between fair-weather and storm wave base marine environment deposits in the studied basin (Abimbola, 2016). In other words, these are characterized as event deposits, which occur in water depths near/or above storm-weather wave base and below fair-weather wave base in the marine depositional environment. The occurrence of *cruziana* and *skolithos* ichnofacies in the sandstone and marly facies also support that the deposition of successions occur below fair-weather wave base in the marine environment (Boggs, 2011; Pemberton et al., 1992 and Ranson, 2012). The depositional characterization of the Dağhacılar measured section is based on the facies association which are as following;

#### **5.2.1.1. Littoral-sublittoral Lacustrine (Relatively Shallow Lacustrine): Facies Association 1**

According to Ramos et al. (2001) and Cabrera et al., (2001), the couplet of lime mudstone-marl facies indicate deposition in the inner lacustrine (sublittoral lacustrine condition). In the Dağhacılar measured section, the observation of lime mudstone-

marl facies with the association of charophytes, ostracods and gastropods show sublittoral condition with relatively shallow lacustrine condition (Pierce, 1993). In the middle portion, the gastropod-ostracod bearing wackestone-packstone facies with interbedded organic-rich fine-grained sediments define the littoral-sublittoral lacustrine environmental setting carbonate deposits with relative low salinity and characterized as brackish intervals. These successions of FA1 (between 14m to 37m) in the studied section evolves to the brackish environmental condition by the episodic incursion of the marine environment to the lacustrine origin basin. These changes are observed by identification of oligo-mesohaline ostracod, gastropod and rare Nummulites fauna. Therefore, it is suggested that this depositional interval took place in a slightly brackish-lacustrine environment and indicate temporary linkage with the marine water (Abimbola, 2016). The presence of abundant gastropod with the association of ostracod also interpret low salinity condition and identify brackish depositional setting (Willmann, 1985; Pierce, 1993). In the studied section, the associated gastropod-ostracod assemblage intervals also prevailed the brackish water setting (Sanjuan & Martín-Closas, 2012). The oligo-mesohaline ostracod and molluscs bearing fossiliferous limestone display fairly oxygenated and destratified, shallow-water lake condition (Keighley et al., 2003).

#### **5.2.1.2. Sub-littoral-profundal lacustrine (Deep lacustrine): Facies Association 2**

The presence of brackish-freshwater fauna and the predominance of lime mudstone to wackestone feature indicate relatively deeper, low energy lacustrine environment (Alçiçek et al., 2007). In the studied section, the above facies column with the lime mudstone-wackestone facies and marl interbeds (Sample D20 to D36) in FA2 indicate sublittoral to the profundal lacustrine basin with the anoxic bottom condition. In the FA2, the observed oil-shale intervals with occasional ostracod also indicate deeper, low energy depositional setting. The observed ostracod in the lithofacies in this succession reflects lacustrine depositional environment. The presence of framboidal form of pyrite in the FA2 correspond to the saline influence into the lacustrine environment (Brown and Cohen, 1995). The Kimmeridge clay framboid pyrite with a

size of 3 $\mu$ m was interpreted to be formed in anoxic water condition (Wignall and Newton, 1998). Similarly, it is interpreted that rich framboidal pyrite oil-shales in these intervals are formed under anoxic conditions (Lazar, 2007).

The next lithofacies succession in the measured stratigraphic section is characterized by predominance laminated oil-shale-marls couplets with occasionally interbedded sandstone lithofacies. The laminated organic-rich shale lithofacies is represented by laminae structure, fine-grained, relatively high clay content, high organic matter content and absence of bioturbation. These mentioned features indicate deposition of sediments from suspension in a relatively low energy, calm water with anoxic condition (Abouelresh et al., 2017). The rhythmic features of the organic-rich shale deposits are probably linked to climatic seasonal change (Caillaud et al., 2017). The occasionally low angle wavy rippled sandstone to structureless thin to medium bedded sandstone lithofacies indicate relative high energy condition deposits in the basin and linked with event deposits. Overall, the portion of predominated laminated oil-shale with marl and occasionally sandstone of FA2 suggest low energy, calm water and profundal lacustrine environment.

### **5.2.1.3. Marine offshore transition: Facies Association 3**

Toward the top, the laminated oil-shale lithofacies are dominantly observed in the Dağhacılar section with a gradual increase of fine sandstone units and are characterized as FA3 (Figure 5.8). The alternating organic-rich and organic-poor laminated shale exhibit deposition from suspension and correspond to low energy environmental condition. The absence or decreasing of ostracod, brackish gastropod in the lithofacies suggest salinity increase in the depositional environment (Cole, 1985) (Figure 5.6). The oil-shale facies characterized by decreasing molluscus and algal structures, reflect relatively increase in salinity and deep, but not enough of salinity to precipitate saline minerals. This portion of the studied section also indicates a transitional change of lacustrine to marine condition with a gradual increase in the interbedded sandstone intervals toward the top. The occurrence of high organic

content in the shale shows anoxic bottom environmental condition with transgressive phase (Cole, 1985).

The intercalating organic-rich shale-fine sandstone indicate relative high energy condition in the marine offshore transition zone (Abouelresh et al., 2017). In the upper portion of the Dağhacılar section, the intercalating oil-shale-fine sandstone are observed and are interpreted as relatively high energy deposits on the offshore transition zone in the basin and associated with gravity flow under the influence of gravity and hydrodynamic forces (Homewood, 2001; Li et al., 1991). In this study, intercalation of thin-bedded sandstone with the association of parallel to wavy rippled feature and laminated oil-shale with a distinct sharp contact in the upper portion of the Dağhacılar measured section suggest turbiditic origin deposits (Mingram, 1998). These turbiditic intervals in deep environmental condition are identified as density flow current with some erosional effect at the microscopic level and interpreted as sedimentation in a relatively deeper, quiet, and poorly oxygenated environmental condition (Mingram, 1998; Wang et al., 2014).

The toward the top in the Dağhacılar section, FA3 represents dominated sandstone-laminated oil-shale intervals with occasional association of marly interval. The laminated oil-shale and marl of FA3 in the Dağhacılar section are characterized as anoxic to dysoxic condition, respectively. The marl lithofacies are characterized by rare bioturbation and occasionally pyrite distribution.

The fine sandstone-oil-shale/marl heterolithic bedding in the studied section reflect marine offshore-transitional environment, changes from the lacustrine condition. At a certain level in the measured stratigraphic section, the sandstone intervals illustrate hummocky cross-stratification, parallel interlaminated bedding and wavy rippled features. The presence of hummocky cross-stratification, occasional wavy ripples feature reflects storm-induced wave oscillations (Rees et al., 2014; Johansen, 2016). Occasionally, in the sandstone lithofacies, there is an observation of marine fauna and rare bioturbation. The sandstone lithofacies in the FA3 are characterized as turbiditic

and occasionally stormy character deposits in the offshore-transition depositional environment, and oil-shale/marl facies are defining the low energy offshore-transition deposits settling from suspension. In general, the heterolithic facies of FA3 in the Dağhacılar measured section, the observation of occasionally marine fauna, rare bioturbation and sharp contact in the interbedded sandstone-organic rich shale (heterolithic feature) interpreted as open marine facies character with the turbiditic depositional setting and on occasion affected by event deposits. The observation of sedimentary structures in these interbedded successions include sharp and/or obscure erosional sharp base, sometimes with load-casts, a massively thin to medium bedded and/or laminated lower portion, and wave-ripples portion also reflects the storm deposits. Commonly, this facies association in the Dağhacılar section exhibit offshore-transitional marine environment with occasionally storm depositional character (Johansen, 2016; Dahlgvist, 2018).

### **5.2.2. Hasanlar Section: Facies Association and Depositional Setting**

The Middle Eocene succession of the Hasanlar Section is comprised of wackestone, non-laminated to horizontal to lenticular laminated oil-shale with intercalation of lime mudstone and marl, and rare observation of ostracod. It interprets that sediments are deposited in sublittoral-profunda lacustrine and described as facies association 2 (Figure 5.9). The Hasanlar studied section depositional setting is categorized on facies association as below (Table 5.2);

#### **5.2.2.1. Upper sublittoral-profunda lacustrine (Deep lacustrine): Facies Association 2**

In the studied section, the limestone with wackestone texture are characterized by ostracod, micro-peloids, intraclasts and palynofacies, and suggest that these are deposited in a relatively sublittoral depositional lacustrine environment (Singh et al., 2017). The occurrence of organic-rich shale and marl interbeds in the studied section reflect that the carbonates are deposited in the deeper lacustrine zone with dysoxic-anoxic condition (Cabrera et al., 2001; Ramos et al., 2001). The phytoclasts in the

limestone intervals are present in the form of small size, sub-rounded to irregular shape. The transportation of the phytoclasts to the depositional setting may be introduced by turbiditic influence and/or eolian system (Biscara et al., 2011; McArthur et al., 2016). The phytoclast components in this FA2 interpret distal and low energy environment setting in the regime (Hopkins, 1950; Davids, 2000; Martin-Closas et al., 2005; Barron & Rengifo, 2007; Oskay, 2009). The occurrence of rare ostracod and the association of high organic content and absence of bioturbation in the Hasanlar section represent relatively deeper, anoxic, low energy lacustrine environment (Alçiçek et al., 2007). The upper portion of the Hasanlar section is composed of alternating laminated oil-shale and limestone with lime mudstone texture units, and also observation of few ostracod. The parallel to lenticular laminated oil-shale with the presence of ostracod, the absence of bioturbation and high organic content display low energy, anoxic lacustrine basinal condition (Zeller et al., 2015; Abouelresh et al., 2017). The occurrence of ostracod suggests relatively shallow water depth lacustrine conditional deposits (Lettéron et al., 2018). Overall, this facies association of the Hasanlar section indicate sublittoral-profundal zone deposits, based on laminated oil-shale and alternating of the oil-shale-limestone intervals in the studied section.

### **5.2.3. Köşüre Section: Facies Association and Depositional Setting**

The lower portion of the Köşüre section is composed of red to green marl with subordinate sandstone intervals and thin to thick limestone with thin marl facies. Then, it is followed by intercalating limestone-marl with occasional organic-rich shale and subordinate sandstone units. The upper portion of the Köşüre section is characterized by subordinate limestone and predominate intercalating sandstone-organic rich shale. Overall, the depositional setting of the Köşüre section from bottom to top is categorized as littoral-sublittoral to sublittoral-upper profundal to marine condition setting (Figures 5.9; 5.11 and 5.13). The facies association is used to describe and interpret the depositional setting of the Köşüre section are as following;

### **5.2.3.1. Upper littoral-sublittoral lacustrine (Relatively shallow lacustrine): Facies Association 1**

The Köüre section basal intervals illustrate red to green marl with subordinate sandstone intervals in the lower portion and may be identical to a relatively shallow oxygenate depositional environment. Then, the basal deposits are evolved to the relatively shallow lacustrine depositional environment, which is identified by the presence of ostracod and charophyta bearing limestone with interbedded marl facies and occasional oil-shale and rare sandstone units. In between, FA1 of the studied section, there is the occurrence of limestone microfacies with the occasional bivalve fragments, which indicate a brackish environmental condition, and suggest temporary link with the marine water (Abimbola, 2016). The presence of fish-teeth fossil also supports temporary linkage of this interval with the marine water. This facies association in the studied section defines upper littoral-sublittoral lacustrine environment.

### **5.2.3.2. Upper sublittoral-profundal lacustrine (Relatively deeper Lacustrine): Facies Association 2**

The FA2 of the studied section is characterized by the charophyta-ostracod limestone, bivalve fragmented limestone, and massive thick limestone intervals. It shows that carbonate rich of FA2 lacustrine facies are deposited in the relatively deeper condition (Murphy and Wilkinson 1980; Gierlowski-Kordesch 2010). The sporadic occurrence of clastic components in the FA2 of the studied section suggest episodic terrigenous influx to low-energy lake environment (Platt and Wright 1991; Calvo et al. 2000; Gierlowski-Kordesch 2010). The couplet of lime mudstone-marl facies in the FA2 of the Köüre section indicate deposition in the sublittoral lacustrine condition with dysoxic bottom water setting (Cabrera et al., 2001; Ramos et al., 2001). The limestone overlying the marls facies display lacustrine margins with increasing lime-producing organism activity (Gierlowski-Kordesch, 2010; Sanjuan and Martín-Closas, 2012). The predominance association of lime mudstone with marl in the FA2 of the Köüre

section implies low energy depositional setting (Platt, 1989). Limestone-marl intercalation formed in the deeper margin and also along the slope and basinal environment (Einsele and Ricken, 1991). These intercalating units reflect climatically induced changes in environmental condition (Fischer, 1991; Pittet, 2018).

The presence of laminated and massive organic-rich shale lithofacies in the FA2 of the Köşüre section suggest a shift to a relatively deeper profundal environmental condition (Abouelresh et al., 2017). The thick intervals of limestone facies with thick intervals of marl and occasionally organic-rich shale in the studied section indicate gradual fluctuation in a lacustrine environment (Sanjuan & Martín-Closas, 2012). The oil-shale intervals are deposited in anoxic bottom water from suspension sediment and microbial (cyano-bacteria) activity organism deposits (Chakraborty and Sarkar, 2005; Foix et al., 2013; Scherer et al., 2015). The brackish charophyte gyrogonites with oligo-mesohaline ostracod assemblages identify as in situ deposits and suggest that these are grown in shallow and slightly brackish-lacustrine condition (Sanjuan & Martín-Closas, 2012). The lack of biota, algal structure and certain low organic content intervals in the FA2 indicate slightly rise in salinity in the open lacustrine environment (Cole, 1985). The FA2 sediments suggest limited marine influence, which is indicated by appearance of fish tooth fossils, oligo-mesohaline ostracods and charophyte gyrogonites in the studied section. The upper portion of Köşüre section is characterized by single bioturbation, charophyta-ostracod (less than 15%) bearing wackestone microfacies. This microfacies display relatively shallow environment and dysoxic water condition (Asl & Aleali, 2016). This microfacies also construe episodic marine influence into lacustrine environmental condition. The above limestone microfacies with the association of charophytes, ostracods and rare fish tooth fossil identify brackish environmental FA2 deposits in the sublittoral lacustrine zone.

#### **5.2.3.3. Marine offshore transition: Facies Association 3**

In the FA3 in the Köşüre section, the occurrence of abundant octahedral pyrite limestone and echinoderm bearing limestone microfacies indicate marine depositional

environment, which transgresses the underlying the lacustrine depositional environment. The observation of echinoderm in the limestone facies indicate setup of marine depositional setting in the Kösüre studied section toward the top (Brown and Cohen, 1995; Baumiller & Gazdzicki, 1996; Elattaar, 2018). The association of echinoderm and fish teeth evident of marine condition (Huyghe et al., 2017). The echinoderm bearing limestone are covered by small scale hummocky cross-stratified, parallel lamination and wave rippled calcareous sandstone with interbedded organic rich shale and having a fish-tooth fossil. These intercalating calcareous sandstone and oil-shale facies represent marine offshore-transitional environment and indicate turbiditic and tempestitic character deposits (Büyüktoku et al., 2005; Ranson, 2012; Siddiqui et al., 2014; Johansen, 2016). The sandstone-organic-rich shale in FA3 display heterolithic feature depositional setting. The fine sandstone with intercalating organic-rich shale reflect comparative high energy condition on the marine offshore-transitional environment. The absence of bioturbation, high organic content and massive to laminated featured oil-shale reflect relatively low energy, anoxic depositional setting and deposited from suspension in the marine offshore-transitional environment (Abouelresh et al., 2017). The sharp and/or obscure erosional sharp base, thin horizontal and wave ripples indicate occasional storm deposit. In general, the sandstone-organic-rich shale intercalation with above identified feature interpret deposition in offshore-transitional marine environment with induced storm depositional character (Dahlqvist, 2018).

#### **5.2.4. Karahisar Section: Facies Association and Depositional Setting**

The Karahisar measured section begin with predominate oil-shale with occasional interbeds of lime mudstone and then is followed by lime mudstone-oil-shale intercalation with occasionally wavy rippled sandstone units near the top. The scarcity of fauna in the Karahisar studied section may be due to nearby fluvial development influx, which may lead to unfavorable condition for the development of biota in the moderate saline water (Ye et al., 2017). The facies association indicate two types of the sub-environment condition in the Karahisar section i.e Upper sublittoral-profundal

lacustrine (FA2) and marine deeper condition setting (FA3) (Table 5.2; Figures 5.9; 5.11 and 5.13). The depositional setting of Karahisar measured section is described by facies association which are as following;

**5.2.4.1. Upper sublittoral-profundal lacustrine (Relatively deeper lacustrine):  
Facies Association 2**

The FA2 of Karahisar measured section begin with predominate oil-shale with occasional interbeds of lime mudstone. The FA2 of the studied section is characterized lacustrine depositional environment, based on the observation of varve feature in the oil-shale. The alternating laminae in the oil-shale reflect precipitation from suspension under clam and anoxic environmental condition (Chakraborty and Sarkar, 2005; Foix et al., 2013; Scherer et al., 2015). In the studied section, the rhythmic feature in oil-shale of the Karahisar section indicate a linkage to climatic seasonal changes (Caillaud et al., 2017). The absence of bioturbation, fauna and fossils fragment suggest stressed and anaerobic conditions in the lacustrine setting as a result of circulation lacking in the water column (Hakala 2004; Grosjean & Pittet, 2013; Egbobawaye, 2016). At certain intervals, the small plant fragment remains are documented in the FA2, which may be driven by strongly influence episodic small depositional cycles and/or eolian transport (Tosal et al., 2018). The palynofacies and abundant amorphous organic matter in the studied section suggest low energy, oxygen-depleted conditions and related to sublittoral-profundal environmental zone (Staplin, 1969; Tyson, 1995; Pittet & Gorin, 1997). The lithological character and observation of small plant fragments suggest relatively shallow lacustrine setting during deposition of FA2 intervals (Carroll et al., 1992; Wang et al., 2011).

At certain level in the measured stratigraphic section, there is slightly increase in the silt size quartz grains in the lithofacies represent higher clastic influx to the system, which also effect the laminae feature and indicate that there is a change in the lacustrine stratification and/or climatic condition (Mingram, 1998) (Figure 5.2). In the lime mudstone of the studied section, the occurrence of irregular flattened calcareous

concretion nodules interprets very slow sedimentation stage, interface in the depositional setting (Alshahrani, 2013).

#### **5.2.4.2. Marine offshore transition: Facies Association 3**

The brackish/freshwater and marine water interface zone characterize low sedimentation rate and relatively high organic content, due to a change in the physiochemical condition (Mingram, 1998) (Figure 5.2). In the Karahisar studied section, the episodic mixing zone between freshwater and marine water is characterized by the appearance of Fe-Mn nodules in the lime mudstone and suggest that Fe-Mn nodules develop due to change in the physiochemical condition in the water column. The physiochemical change in the depositional condition occurred due to the transgression of a marine into lacustrine condition. Manganese-rich carbonate deposits are mostly associated with black shales and restricted to relatively deeper basinal environmental condition (Bolton & Frakes, 1985; Delian et al., 1992; Roy, 1992; Fuhrmann, 2002). Similarly, in the Black Sea, high Mn concentration solution is formed in the stratified anoxic environmental setting in the basin. Later, the Mn precipitation took place from Mn concentrated solution in the basin at redox interface. These Mn oxides are embedded in carbonate. Mn-carbonate are associated with black shale. It is suggested that Mn deposits occur during the transgressive phase (Roy, 1992). In the Baltic Sea, the manganese-rich sediment deposition restricted to deepest part of the basin and linked to intense microbial activity at the sediment-water interface. The Baltic Sea composed of brackish water and characterized low salinity water (Huckriede & Meischner, 1996; Fuhrmann, 2002). Formation of manganese oxide occurred at the oxidizing-reducing condition and deposited in the anoxic condition (Tribovillard et al., 2006). In the marine condition, there is the identification of three types of Mn-oxyhydroxides deposited (Glasby, 2006), such as Mn-nodules in the deep ocean, Mn crust on submarine seamounts, and ferromanganese nodules in shallow-marine condition. The Mn nodules are characterized as hydrogenous in origin and form directly from the oxidizing condition in the marine environment. The Mn crusts and concretion can be form either from hydrogenously or hydrothermally (Yu

et al., 2016). In the deep-ocean, accumulation of Mn-nodules also depends on the slow sedimentation rate (Glasby, 2006; Yu et al., 2016). The presence of Fe and Mn oxides imitate change in redox condition associated with depositional condition and also associated with variable sporadic water table (McCarthy et al., 1998; Tanner and Locus, 2006; Wanas et al., 2015). In the Karahisar studied section, the appearance of Fe-Mn small spherical nodules indicates hydrogenetic origin and deposited in shallow marine environment. The described origin and setting of the Fe-Mn nodules in the Karahisar section is also supported by organic-rich shale associated facies (Wang et al., 2014; Yu et al., 2016). In the north-western regime of Turkey, there is the documentation of Mn oxides in the Oligocene shallow marine deposits, which are linked with a rapid marine transgressive-regressive cycle. Generally, Fe-Mn oxides are formed at the interface of oxic-anoxic water and can be deposited in relatively oxygen-depleted bottom water condition (Alçiçek et al., 2007).

In the upper portion of the Karahisar measured section, there is documentation of the thick parallel laminated to massive oil-shale, lime mudstone and wavy ripple calcareous sandstone interval. This portion of studied section suggest offshore-transition marine environmental setting with occasionally turbidite influence deposits. The organic-rich shale lithofacies represent high clay content and absence of bioturbation. These organic-rich lithofacies are deposited from suspension in a relatively low energy, calm water and anoxic bottom water on the offshore-transition marine environment (Abouelresh et al., 2017). Overall, the organic-rich shale with association of sandstone and Fe-Mn bearing lime mudstone intervals are characterized as FA3 and interpret marine-offshore transitional influence environment deposits.

#### **5.2.5. Sünnet Section: Facies Association and Depositional Setting**

The Sünnet section is comprised of terrestrial deposits at the base. The terrestrial deposits are overlain by the marine shelf environment with occasional charophytes rich-plant fragments deposits of fluvio-lacustrine invasion. The studied section is composed of predominantly sandstone, fossiliferous and non-fossiliferous organic-

rich oil-shale, fossiliferous limestone and occasional conglomerate facies. The facies association revealed the detailed depositional setting of the measured Sünnet section in the studied regime (Table 5.2; Figure 5.9).

#### **5.2.5.1. Marine Shelf Environment: Facies Association 4**

In the Sünnet section, the FA4 of the measured stratigraphic section are characterized by fossiliferous organic-rich oil-shale, interbedded fossil bearing sandstone, coarser siliciclastic sediments (conglomeratic interval) and fossiliferous limestone facies. Generally, it is interpreted that organic-rich shale and/or marls with the association of pyrite are deposited in calm condition from suspension under oxygen deficient environment. In contrast to organic-rich shale, organic-rich silty shales are interpreted relative similar depositional setting as sandstone depositional setting. The organic-rich silty shales are deposited in relatively high energy and high terrigenous influx environmental setting as compared to organic-rich shale (Figures 5.2 and 5.8) (Ghadeer & Macquaker, 2011). Siliciclastic deposits on the marine shelf environment are controlled by number of complex interplays, which includes wave energy effect, terrestrial input, gravity and biological activity (Ghadeer & Macquaker, 2011). The floodplain coarser sandstone with occasional conglomerate and red silty shale are overlain by fossil bearing silty shale, occasional limestone having bivalve, ostracods, charophytes, gastropods, plant fragments, rare Foraminifera and fossil bearing coarser sandstone. The fossil bearing silty shale, bivalve-charophyta-gastropod-plant fragments-rare foraminifera bearing limestone units and fossil bearing coarser sandstone specify shallow shelf marine environmental condition and indicate marine transgressive phase (Figure 5.9) (Li et al., 2009). The abundant charophytes and associated plant fragments indicate episodic fluvio-lacustrine incursion to the marine depositional setting (intermixing zone between brackish and marine environment). The charophytes rich horizons refer laterally related to paralic marshes (Sanjuan & Martín-Closas, 2012; Argakoesoemah, 2017). Later, this environmental zone is vertically shifted to bivalve bearing lithofacies intervals of the marine environment (Argakoesoemah, 2017). The absence of bioturbation expression frequent reworking

and a high sedimentation rate (Aigner & Reineck, 1982). Above this facies interval, the studied section is characterized by organic-rich shale with few bivalve-gastropod and then is followed by interbedded sandstone-organic-rich shale intervals of the lower shoreface deposits. More episodic storm and gravity flows are responsible for the deposition of the interbedded sandstones and organic-rich shales in the studied section (Meling, 2016). Between the sandstone horizons, there is another phase of brackish-lacustrine influence on the shallow marine setting, which is identified by thin bedded charophytes-plant fragments bearing limestone facies and then is followed by shallow marine fossiliferous limestone units. The marine fossiliferous limestone units are composed of rare glossifungite bioturbation, plant fragments, algal fragments, ostracod and gastropod. The marine fossiliferous limestone is covered by fossiliferous coarser sandstone and bivalve siliciclastic limestone/molluscus-calcirudite intervals in the studied section. The association of sandstone, fossiliferous limestone and molluscus bearing calcirudite (rudstone) and organic-rich shale illustrate lower shoreface facies with storm depositional character (Hadi et al., 2016; Meling, 2016). The siliciclastic sediments with the association of fossiliferous limestone units and organic-rich shale also support storm-induced deposits (Carvalho et al., 2000). In the Mengen region, stratigraphic equivalent Tokmaklar Formation is composed of coarser carbonate units, sandstone, conglomeratic facies, organic-rich shale and documentation of foraminifera, gastropods and other macrofossils in the formation. The Tokmaklar Formation in the Mengen region interpret shallow marine environmental setting (Koralay, 2009). The FA4 of studied section encounter similar character and can be interpreted as deposition occur in the shallow marine condition. Toward the top, the siliciclastic sediment include conglomerate, sandstone and occasionally organic-rich shale with non-erosional lower and upper contact are characterized as upper shoreface deposits (Yang et al., 2010). In the middle portion, the conglomerate intervals in the studied section without cross-stratification suggest that conglomerate intervals are deposited from shallow depth gravity flow deposits (Collinson & Lewin, 1983). The matrix-support conglomerate in the FA4 having non-erosive contact, normal grading is linked with debris flow deposits (Collinson &

Lewin, 1983). The various load marks in the studied section indicate rapid deposition of sediments (Rees et al., 2014). In the next stage, there is a change from lower shoreface to a relatively high-energy environment (a transition zone between upper shoreface and lower foreshore). It is identified by observation of conglomerate intervals deposited over the massive to wavy laminated sandstone units (Hiroki & Terasaka, 2005).

The upper portion of the studied section is characterized by molluscus-nummulitic bearing calcirudite (rudstone), fine sandstone and conglomerate-sandstone beds. It is interpreted that deposition of molluscus-nummulitic bearing calcirudite (rudstone) and fine sandstone deposits are associated with the shallow benthic zone environment deposits and are overlain by sandstone of shoreface. This succession is topped by subaqueous channelized influence conglomerate deposits with the erosional basal surface (Xiafei & Zhonghua, 2000). These are covered by coarser sandstone and the matrix-support conglomerate having non-erosive contact and normal graded bedding. It is interpreted that coarser sandstone and the matrix-support conglomerate are deposited from debris flow in the shallow marine condition (Collinson & Lewin, 1983). Generally, the presence of flute casts and load casts in the upper portion of coarser sandstone indicate sandstone of turbiditic origin in the studied section (Güray, 2014).

#### **5.2.5.2. Floodplain Paleosols: Facies Association 5**

The basal portion of the Sünnet measured section is observed in the field as parallel laminated to cross-stratified sandstone to graded conglomerate horizon and then followed by red sandstone and occasionally silty shale with gray mottling. The lithofacies are devoid of fossils and are characterized as facies association 5. The parallel laminated to cross-stratified sandstone, conglomerate-red sandstone and red to grayish shale intervals are characterized as pedogenic floodplain deposits. The red silty shale is formed by suspended fine-grained sediments after turbulence condition (Sanjuan & Martín-Closas, 2012). The red shale intervals may reflect palaeosols with

lack of bioturbation and sedimentary structure (Ranson, 2012). This interpretation is supported by interbedded grayish organic-rich silty shale between the floodplain and shallow marine carbonate deposits (wackestone-packstone). Red color intervals are generally of paleosols development on the floodplain (Dini et al., 1998).

### **5.3. Lacustrine Environment and Transition to Marine Environment in the Studied Basin**

During the Eocene times, there is occurrence of closing in the Neo-Tethys ocean in the North Anatolia (Figure 5.10). As a result, the Anatolian block begin to experience internal deformation (Okay and Tüysüz, 1999; Görür and Tüysüz, 2001). This south-north shortening in the region are accompanied by shoaling upward sequence in marine deposits. Later on, the marine deposits in the region were covered by shallow marine and lagoonal or lacustrine deposits of the pre-existing comparatively deeper fore-arc basin (Görür et al., 1998). These Eocene lacustrine/lagoonal to marine environmental deposits are documented in the Mudurnu-Göynük basin and adjacent region (Saner 1977, 1980b; Ocakoğlu et al., 2007 and 2012). Therefore, the studied Middle Eocene (Lutetian-Bartonian) successions in the five different localities in the Mudurnu-Göynük basin provide the opportunity to study the paleoenvironmental fluctuations and transition from lacustrine to marine environmental condition. Based on the facies analyses, biotic observation and facies association, the middle Eocene successions exhibit an evolution of the basin from oligomesohaline/brackish-lacustrine to the marine transgressive environment (Figures 5.9, 5.11, 5.12 and 5.13).

Carrol and Bohacs (1999) and Bohacs et al. (2000) classified three type of the lacustrine basin, based on the physical, chemical and biological factor. The classified lacustrine basins are overfilled lake basin, balanced-fill lake basin and underfilled lake basin (Table 5.3). The overfilled lake types characterize fluvial-lacustrine facies deposits. The lacustrine deposited with fluvial-lacustrine facies character contains marlstone, coquina, bioclastic grainstone, the association of carbonaceous mudstone, sandstone, coals and presence of freshwater- oligomesohaline biota. The I to III type

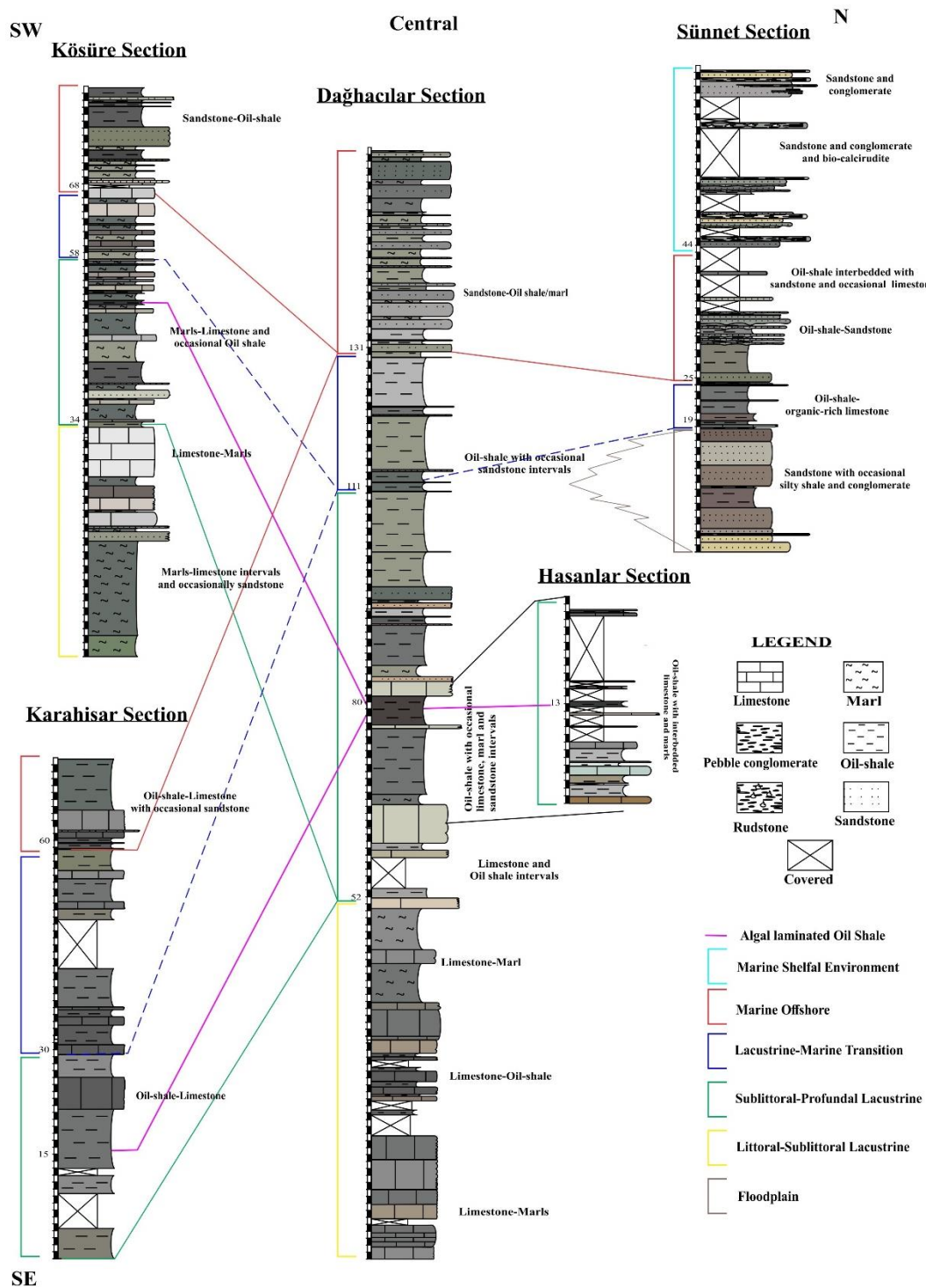


Figure 5.9. Depositional setting and correlation of the studied sections.

Table 5.3. Representative Attributes of Three Major Lacustrine Facies Associations (Carrol and Bohacs, 1999; Bohacs et al., 2000).

<b>Lake basin type</b>	<b>Overfilled Lake basin type</b>	<b>Balanced fill Lake basin type</b>	<b>Underfilled Lake basin type</b>
<b>Features</b>			
<b>Lacustrine Facies Association</b>	Fluvial-Lacustrine	Fluctuating Profundal	Evaporitive
<b>Lake Hydrology</b>	Open	Open during TST-HST Closed during LST	Closed
<b>Water Table</b>	High	Fluctuating	Low
<b>Stratal Stacking Patterns</b>	Dominantly progradation Indistinctly expressed parasequences	Mixed progradation and aggradation, distinctly expressed parasequences	Dominantly aggradation Distinctly to indistinctly parasequences
<b>Sedimentary Structures</b>	Physical Transport: ripples, dunes, flat bed, root casts, burrows (Infaunal & epifaunal)	Physics and biogenic; flat bed, current, wave, and wind, ripples; stromatolites, pisolites, oncolites, mudcracks, burrows (epifaunal)	Physical, Biogenic, & Chemical: climbing currently ripples, flat bed, stromatolites, displacive fabrics, cumulate textures
<b>Lithofacies</b>	Mudstone, sandstone, marl, coquina, coaly shale, coal	Marl, mudstone, siltstone, sandstone, carbonate grainstone, wackestone, micrite, kerogenite	Mudstone, kerogenite Evaporite, Siltstone, sandstone, Grainstone, boundstone, flat-pebble conglomerate
<b>Organic matter</b>	Freshwater biota, Land-plant, charophytes and aquatic algal organic matter, low to moderate TOC, terrigenous and Algal biomarkers	Salinity tolerant fauna, aquatic algal Organic matter, Minimal land plants, moderate to high TOC, Algal biomarkers	Low-diversity, halophytic biota, Algal-bacterial organic matter, Low to high TOC, expressed Hypersaline biomarkers

of kerogen are linked with overfilled lake basin type. The balanced-fill lake basin type consists of fluctuating profundal facies, fresh to saline water fauna and represents type I kerogen of algal-bacterial origin. The balanced-fill lake basin type can be open or closed basin. The associated facies with balanced-fill lake basin type are consisting of interbedded heterogenous lithofacies such as carbonate, siliciclastic, argillaceous and organic-rich mudstone. In the underfilled lacustrine basin, the facies are characterized by evaporative facies association, occurred in a closed basin, composed of a wide variety of lithofacies (i.e evaporites, grainstone, clastic sandstone and kerogenite) and low diversity, high salinity and salinity tolerant fauna and represent type I kerogen type.

In this study, the lacustrine facies association of the Dağhacılar, Hasanlar, Köşüre, and Karahisar measured sections indicate overfilled-lake to balanced-fill lake basin type. The Karahisar lacustrine facies association suggest that it is deposited in balanced-fill lacustrine basin type with relatively restricted condition. The lacustrine facies association in the studied sections are characterized by predominantly fluctuating profundal facies association, representing lower littoral-sublittoral to profundal zones with high organic carbon shale (oil-shale), relatively deeper carbonate, marl and occasionally calcareous fine sandstone.

In the Later stages, the studied lacustrine facies successions are overlain by marine offshore transitional facies successions and are characterized by organic-rich shale-sandstone with occasional marl and presence of rare benthic fossils in some measured stratigraphic successions at different intervals. The organic-rich shale-sandstone intercalation and occasional marl are mostly associated with gravity flow deposits (Turbiditic). The marine transgression into the lacustrine setting regime occur in the open lacustrine phase. It is recognized by observing the unchanged lithofacies across the transition and indicate continuous sedimentation between lacustrine and marine environments across the transitional interval. In the case of intercalating sandstone and organic-rich shale, it is difficult to distinguish between the lake deposits and low energy marine deposits. In this case, the documentation of fossils and algal structure are reliable indicators to predict the change in the depositional environment (Willmann, 1985; Nichols, 2009; Lorente et al., 2014). The morphology of the studied lacustrine basin successions changed to marine basin during relative rising of the sea level. A change of environment from lacustrine to marine also affects the freshwater-brackish fauna, flora and algal structure in the previously lacustrine basin. The calcareous oil-shale and fine sandstone in the studied sections represent alternatively hydrologically open and closed basin and changing from oligomesohaline/brackish to saline condition (Carroll and Bohacs, 1999; Bohacs et al., 2000). It is purposed that geographic setting, climate and tectonics are factors involving in the marine incursion to lacustrine in the measured stratigraphic successions.

The presence of benthic fauna in the studied section at different intervals also indicate marine influence. In the Dağhacılar studied section, it is noticed repeatedly marine incursions in the lacustrine environment and can be traced by means of fauna recorded in the lower portion at different intervals. The freshwater fauna is not complete devoid in this portion and survive the episodic marine water invasions. The survival fauna may evolve to brackish water fauna. Later, the Dağhacılar and other studied sections are evolved to marine environment during the transgressive phase in the region during Late Eocene period. This change leads to the disappearance of the lacustrine and brackish fauna during the evolving marine transgressive phase. Generally, the deposited facies of the studied sections indicate the alkaline condition with low salinity. It is interpreted on the observation of high carbonate content, low occurrence of ostracods and charophytes in the deposited studied succession in the region (Cole, 1985). In 1978a, Saner also observed marine transgressive deposits overlying the lake deposits in the Eocene period in the studied region. According to him, the lake formation occurred due to marine regression, which was once again overtaken by marine transgression in the late Eocene (Figure 5.10). The Sünnet section is interpreted as barrier deposits between lacustrine and marine environmental setting. The basal portion of the Sünnet section is identified as floodplain paleosol deposits. In the Sünnet section, it is indicated that the above portion of the middle Eocene studied section is characterized by marine shelf deposits with occasionally thin intervals of charophytes rich Fluvio-lacustrine beds intervals. The Abundant bivalves and gastropod assemblages with siliciclastic material indicate that marine sediments are deposited below the storm wave base.

Overall, the deposited carbonate, organic-rich shale, marl and occasional siliciclastic cycles of lacustrine succession are transgressively overlain by marine deposits in the Dağhacılar, Köşüre and Karahisar measured section. The underlying lacustrine deposits are characterized as littoral-sublittoral to fluctuating profundal environmental deposits facies (Figures 5.9; 5.11, 5.12 and 5.13).

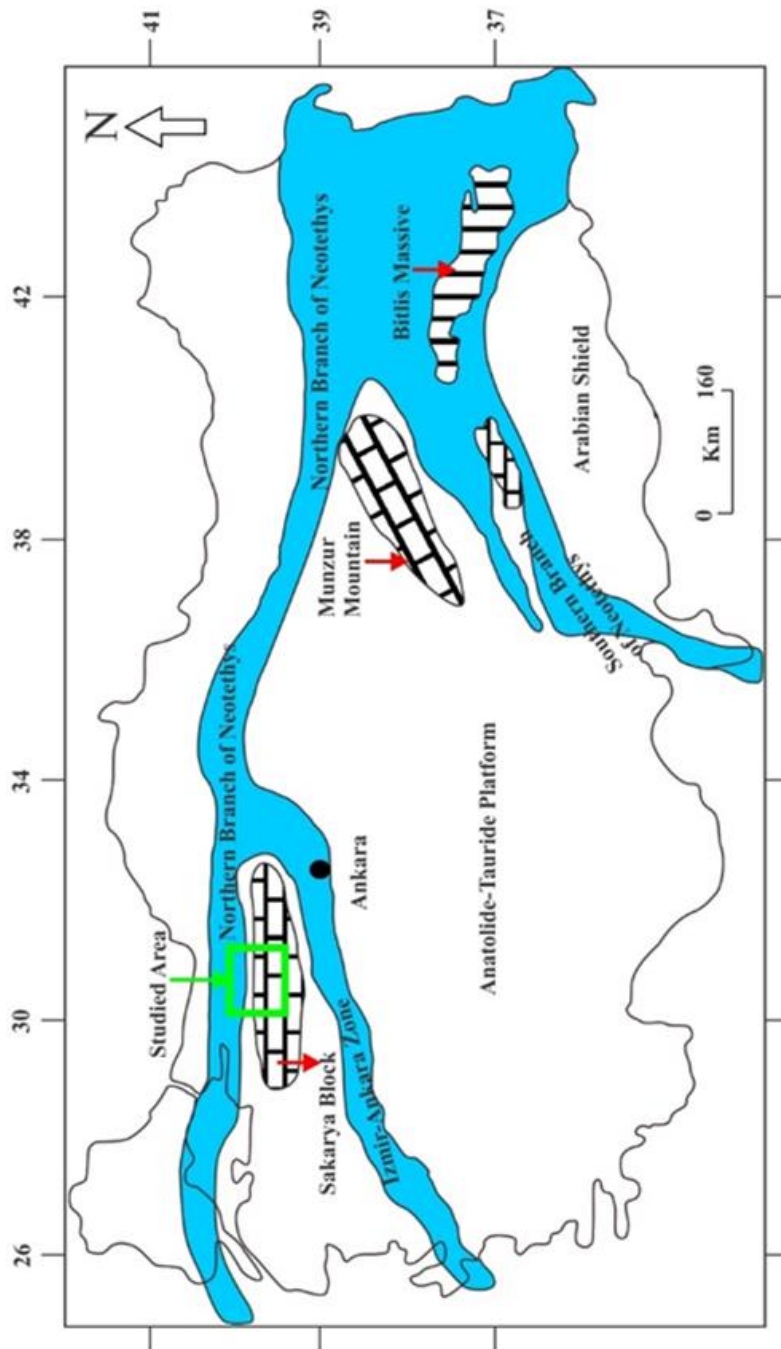


Figure 5.10. The paleogeographic position of studied area related with the Neo-Tethys (Studied regime is represented by green rectangle) (Şengör and Yılmaz, 1983).

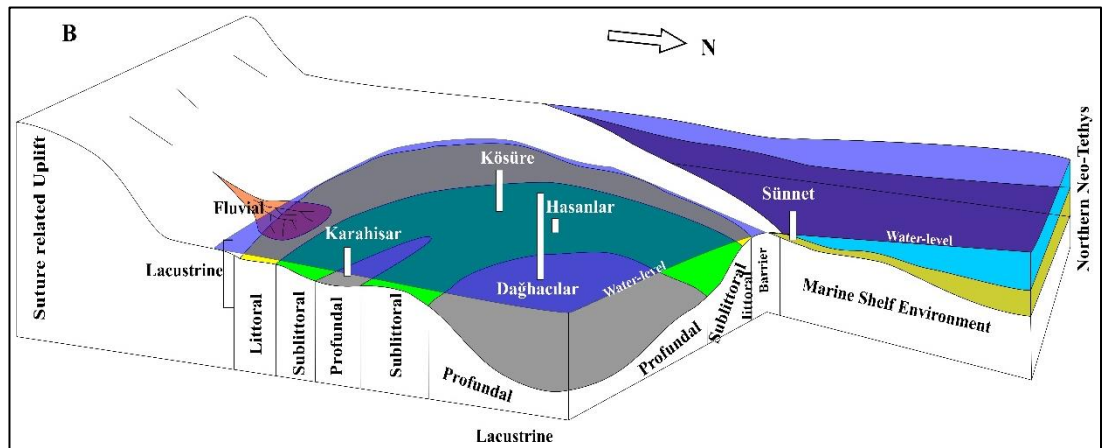
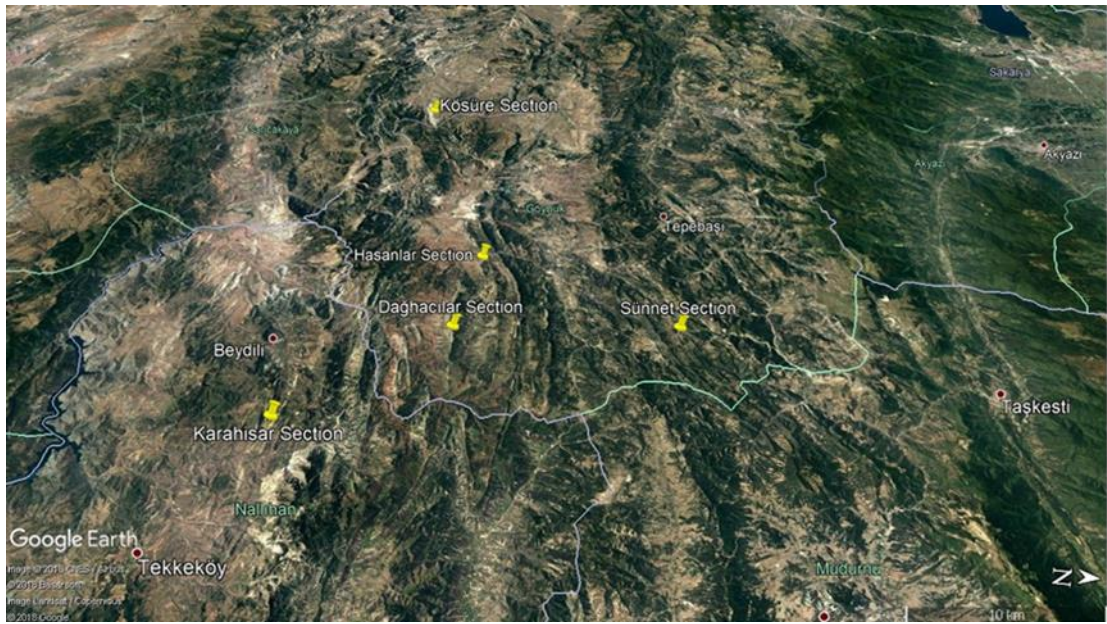


Figure 5.11. A) Satellite image of studied sections; B) Depositional setting stage of the studied sections during Middle Eocene. The first stage of lacustrine setting development in the studied regime after the marine regression. According to Saner (1978), development of lacustrine due to marine regression in the studied regime. (White block represents studied sections and transparent blue represent water level; arrow shows north direction).

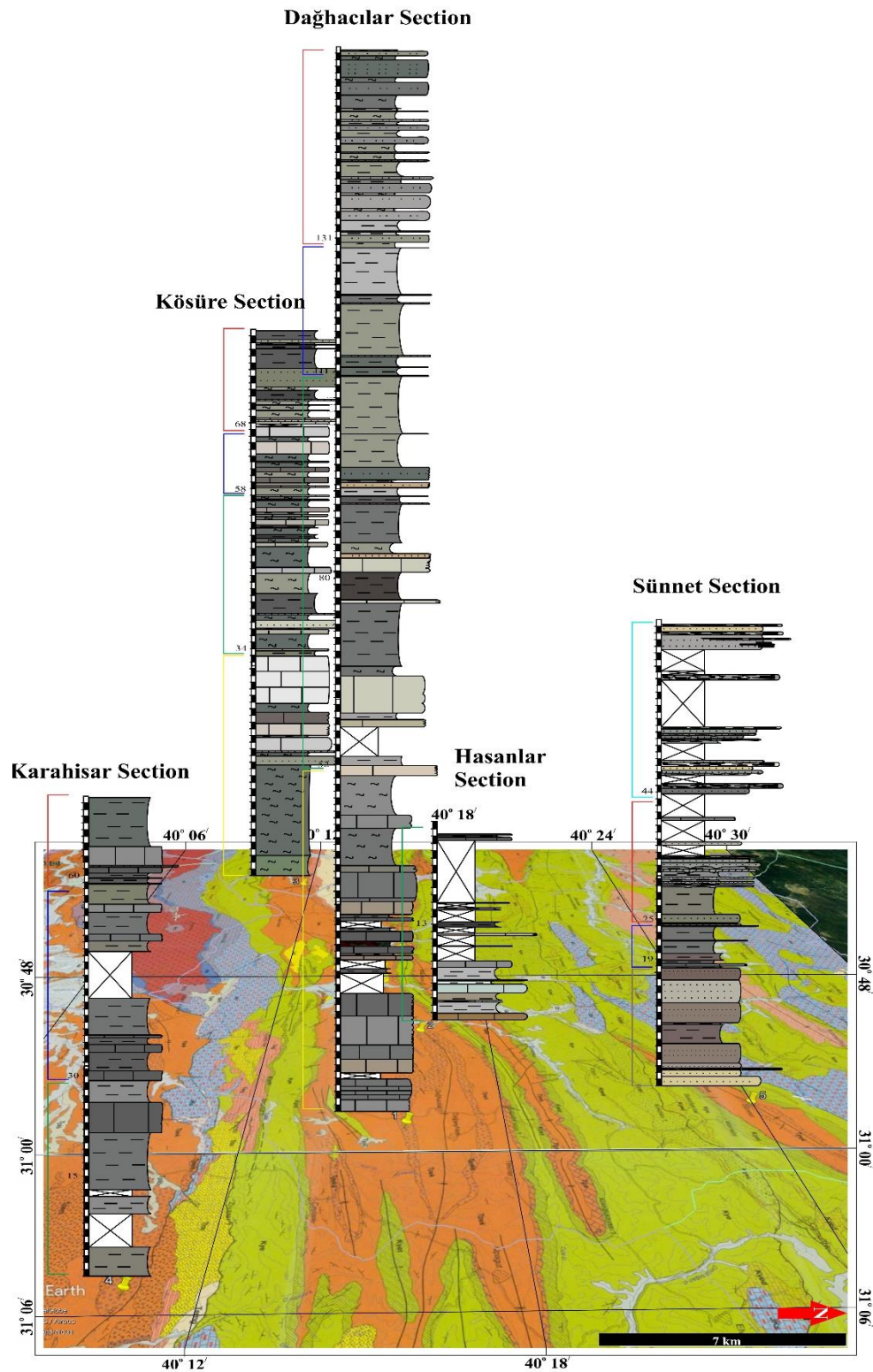


Figure 5.12. 1/100000 Geological map of the Northwestern Anatolia, Turkey (Adapazarı-H25 and Adapazarı-H26) (Timur and Aksay, 2002; Gedik and Aksay, 2002) and studied stratigraphic sections in the area. (red arrow-North direction).





## CHAPTER 6

### CYCLOSTRATIGRAPHY

#### 6.1. Introduction

The Early Paleogene period has been characterized as a period of the last thermal maximum and apparently ice-free greenhouse period in the of the Earth`s history. In relation to it, different studies have been carried out to study the fluctuation of eustatic sea level and changes in climatic condition in the Early Paleogene period that indicate probably linkage with the orbital forcing as a background external controlled forces (Miller et al., 1987; Sloan and Morrill, 1998; Zachos et al., 2001, 2008). The documentation of cyclic or quasi-cyclic depositional stacking pattern in the Green River Formation of Wyoming, Colorado and Utah (West USA) are related to the climatic changes. It has been interpreted that the climatic changes in the Green River Formation of Wyoming and Utah are controlled by Earth`s orbitally forces (Fischer and Roberts, 1991; Pietras et al., 2003; Machlus et al., 2008). Similarly, it has been recorded that high frequency cyclic generation in the foreland successions are also linked with orbitally forcing climatic changes (Vail et al., 1977; Pujalte et al., 1993; Devlin et al., 1993; Matthews and Perlmutter, 1994; Juhasz et al., 2007; Ocakoğlu et al., 2012). In the Northwest Anatolian foreland regime, it has been suggested that the high frequency depositional cyclic stacking pattern are enforced by orbitally forced climatic changes and tectonic activities (Ocakoğlu et al., 2012). In this study, the Lutetian-Bartonian studied successions have been studied to construct and examine the nature of cycles and analyze relative sea-level/water-level fluctuation in the studied regime and interpret their linkage with orbitally forced climatic changes.

The cyclostratigraphy terminology was introduced by Fischer et al. (1988). He represented sedimentary successions with cycles, which are so-called Milankovitch

band (Strasser et al., 2006; Hinnov, 2013). In the cyclostratigraphy, the high-frequency cycles are classified by distinct lithofacies successions. The distinct lithofacies successions are bounded by surfaces along which there is indication of relative change in the sea-level/lacustrine depth-level (Kerans and Tinker, 1997). The defining cyclostratigraphy in the studied sections are used to describe the depositional environment setting and develop the transgressive-regressive cycle and sequence stratigraphic framework in the studied regime. The Middle Eocene lacustrine studied successions with marine incursion represent transgressive-regressive cycles, which are identified on basis of limestone, organic rich oil-shale, marl and interbedded sandstone facies depositional cyclic pattern. The littoral-sublittoral, sublittoral-profundal and profundal to marine facies associations occur in high-frequency depositional cycles and display periods of lacustrine and marine relative water-level fluctuation and accommodation space (Figures 6.12; 6.15; 6.21; 6.22) (Smoot, 1983; Yang et al., 2018). In each cycle, the development of different facies associations is characterized by facies partitioning (Homewood, 1996; Yang et al., 2018). The fluctuation in sea level, sediment supply and preservation potential affect the depositional cycles partitioning. The recognition of sharp bedding surfaces and/or obscure erosion surfaces bounding the beds/or cycles are used as criteria for the identifying the high-frequency cycles in the studied successions. These sharp bedding surfaces are classified as sharp changes in sedimentation or non-depositional surfaces due to fluctuation of relative water-level (Schwarzacher, 2000; Strasser et al., 1999, 2005; Bádenas et al., 2005; Val et al., 2017).

The field observation and petrographic analysis of the studied successions lead to distinguish depositional cyclic stacking patterns in the studied sections. The studied sections intervals display different cyclic hierarchies and expresses various frequencies of the relative water-level fluctuation and Milankovitch bands (Figure 6.12; 6.15; 6.21; 6.22). The studied sections are identified as the Middle Eocene (Lutetian-Bartonian) age, based on recorded ostracods and charophytes fauna in the studied sections, stratigraphic succession position, and previous studies in the region

i.e Şener and Şengüler, 1998; Gedik and Aksay, 2002; Ocakoğlu et al., 2007 and 2012; Koralay, 2009 and Şafak et al., 2015. Hence, it is assumed that studied sections may roughly correspond to approximately 6.0 Ma (45.0 to 39.0  $\pm$ 1.0Ma) Dağhacılar section,  $\approx$ 1.0 Ma (42.5 to 41.5  $\pm$ 1.0Ma) Hasanlar section,  $\approx$ 2.5 Ma (42.0 to 39.5  $\pm$ 1.0Ma) Kösüre section,  $\approx$ 2.0 Ma (41.5 to 39.5  $\pm$ 1.0Ma) Karahisar section and  $\approx$ 2.0 Ma (42.0 to 40.0  $\pm$ 1.0Ma) Sünnet section.

Within the Middle Eocene studied successions, the established hierarchical cyclic order is comprised of centimeter to meter-scale order cycles. The cyclicity in the studied sections are established by using the sedimentological character and microscopic data of the lithofacies and lateral and vertical changes in the lithofacies. Generally, the centimeter-meter-scale cyclicity in the marine influence lacustrine environment in the studied sections are comprised of limestone-marl, limestone-oil-shale, marl-oil-shale, sandstone-marl and represent relative transgressive cycle. The identified centimeter to meter scale cycles in the marine environment in the studied sections are couplets of oil-shale-sandstone, marl-sandstone, limestone-sandstone, coarser sandstone-fine sandstone, pebble conglomerate-sandstone and generally indicate regressive cycle.

The vertical facies variation and minimum-maximum accommodation mark the bounding surfaces between the successive cycles. The bounding surfaces in the studied sections are described as flooding surface which separates younger unit from older one and across which change in the paleowater depth (Van Wagoner et al., 1988; Van Wagoner et al., 1990). The hierarchical cyclic order in the studied sections are mostly characterized by symmetrical to asymmetrical rhythmic cycles. The cyclic alternation of facies in the studied sections are limestone-marl, limestone-oil-shale, limestone (packstone-wackestone), oil-shale-marl, sandstone-oil-shale and sandstone-marl (Figures 6.3; 6.5; 6.7; 6.9; 6.11). The symmetrical rhythmic cycles of lithofacies suggest repetitive change in the depth of lacustrine-marine and/or fluctuating sediments influx (Cabrera et al., 2001). (Goldhammer et al., 1990; D'Argenio et al., 1997). The 12, 3, 8, 3, 12 cycle types are recorded along the Dağhacılar, Hasanlar,

Kösüre, Karahisar and Sünnet sections, respectively (Figures 6.2; 6.4; 6.6; 6.8; 6.10). The cyclic type in the studied sections are comprised of mostly two lithofacies. In the Dağhacılar, Kösüre and Karahisar studied sections, generally the first segment of cyclic pattern corresponds to relative shallow cycles (alternating of limestone and oil-shale/marl), while the second depositional cyclic pattern indicates progressively transgressive cycles (dominated by oil-shale and marl). The third cyclic pattern corresponds to siliciclastic cycles (sandstone- oil-shale/marl cycles) and indicate progressively regressive condition cycles. In the Sünnet section, the first segment of cyclic pattern corresponds to floodplain cycles (alternating of coarser and fine siliciclastic and oil-shale/limestone), while the second depositional cyclic pattern indicates progressively transgressive cycles (dominated by siliciclastic and limestone cycles). The third cyclic pattern corresponds to siliciclastic cycles (sandstone, pebble conglomerate cycles) and interpreted as regressive cycles.

Table 6.1. Number of Beds and Cycles and their thickness in the Middle Eocene (Lutetian-Bartonian) studied sections.

Studied Sections	Total Thickness (m)	Beds		cm-m scale Order Cycles	
		No.	Average Thickness/(m)	No.	Average cycles Thickness/(m)
Dağhacılar	159.50	392	0.41	108	1.48
Hasanlar	25.20	51	0.49	23	1.10
Kösüre	81.80	139	0.59	42	1.95
Karahisar	71.80	149	0.48	21	3.42
Sünnet	69.30	69	1.00	24	2.88

Table 6.2. Number of Beds and Cycles and their thickness in the Middle Eocene (Lutetian-Bartonian) studied sections.

Studied Sections	Age (Kyr) (Appr.) <sup>1</sup>	Precession	Obliquity
		Kyr/6 <sup>th</sup> Cycle or Bed	Kyr/cm-m scale order Cycle
Dağhacılar	6000	15.31	55.55
Hasanlar	1000	19.60	43.47
Kösüre	2500	17.98	59.52
Karahisar	2000	13.42	95.24
Sünnet	2000	28.98*	83.33*

<sup>1</sup> Based on ostracods-charophyte fauna in the studied sections; Ocakoğlu et al., 2007, 2012 and Şafak et al., 2015. (\* high value due to number of covered intervals in the measured section)

The cyclic evolution of the studied successions (lacustrine-marine successions) are in good settlement with relative sea-level fluctuation and tectonic evolutionary

component of the global cyclostratigraphy model curve. In the studied lacustrine and marine successions of cyclically stacked transgressive/ regressive facies, Milankovitch periodicities can be useful indicator to predict the climatic changes linked with earth`s orbitally forces (Schwarzacher, 1993; Fredriksen et al., 1998; Martínek et al., 2006). The centimeter to meter scale cycles in the studied sections are around 43.47 ka to 95.24 ka (Table 6.1; 6.2). The time of duration per cycle are obtained by dividing the time duration of studied intervals by the number of cycles counted in each studied section.

## **6.2. Cyclic Hierarchy in the Studied sections**

The field observation and petrographic studies of the studied sections led to recognition of cyclic stacking pattern in the lacustrine and marine facies.

The facies variation along the successions reflect cyclic changes in depositional environment. To determine cyclic changes in depositional environment in the studied sections, it requires a facies model architecture. A facies model architecture is determined by interpretation of facies in depositional environment setting (Figure 6.1). The vertical variation and lithological character leads to recognize the centimeter to meter scale order cycles in the successions (Colombié and Strasser, 2003; Colombié et al., 2012).

## **6.3. Dağhacılar Section Depositional Cyclicity**

In the Dağhacılar section, a total of 392 beds with 0.41 average bed per meter are documented along the 159.50-meter stratigraphic column (Table 6.1; Figure 6.3). The Dağhacılar section is comprised of limestone microfacies, marl, organic-rich oil-shale, and sandstone lithofacies. The facies change along the measured section indicate change in relative water-level and interpret a transgression from lacustrine to marine depositional cycles (Figures 6.3; 6.12; 6.21; 6.22). The lower succession in the studied section is comprised of medium to thick limestone in packstone, wackestone to lime mudstone microfacies with gastropods, ostracods and charophytes and alternating with marl and/or oil-shale facies. The middle portion intervals in the studied section

are defined by centimeter to meter thick intervals of oil-shale with thin marl and occasionally sandstone interbedded. These are overlain by dominated calcareous sandstone with intercalated oil-shale and/or marl lithofacies. The depositional cyclic pattern from limestone in the lower portion to dominated oil-shale in the middle portion in the studied section indicate transgression/relatively deepening upward trend cycles.

In this studied section, a total of 108 centimeter to meter scale order cycles are recognized with 1.48 average cycles thickness in meter (Tables 6.1; 6.2). The cycles begin with marl facies at the bottom and are overlain by limestone microfacies with charophytes, ostracods and gastropods and indicate relative fall in the water-level for short period. The overlying dominated oil-shale and marl facies on the limestone-dominated intervals indicate transgression in the water depth (Fischer and Arthur, 1977; Oçakoğlu et al., 2012; Foix et al., 2013; Scherer et al., 2015). The cycles with oil-shale, marl with sandstone facies indicate shallowing upward trend in the depositional cyclic stacking pattern toward the top in the studied section and associated with marine offshore-transitional environment.

In the Dağhacılar section, 12 types of centimeter to meter scale cycles are recorded along the measured section (Figures 6.2; 6.3). The cycles A1 type in the studied section are composed of marl at the base and limestone in lime mudstone microfacies at the top which is generally possessing few gastropods, charophytes and ostracods. The limestone facies in the cycles identified as decrease in the relative water-level. This type of cycles is observed predominately in the lower portion of the studied section with repeated rhythmic pattern. Another relatively thick A1 type cycle is observed in the middle portion of the studied section. The cycles A2 type in the studied section begin with wackestone facies and are overlain by packstone microfacies. It is observed in the lower portion of the studied section. The cycles A3 type are formed by thick bedded wackestone microfacies at base and oil-shale facies at the top. It is recorded at three different portions in the studied section. The A4 type cycles are rare

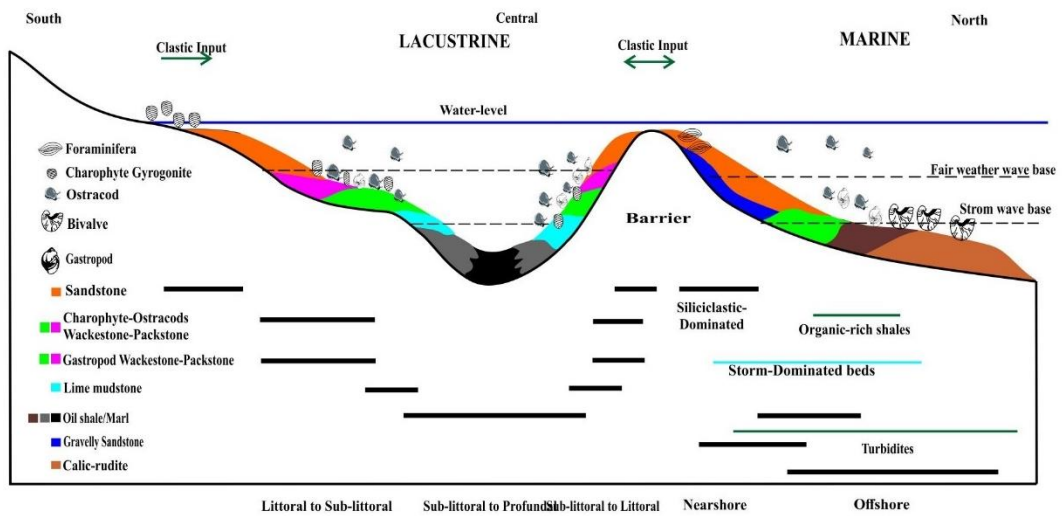


Figure 6.1. Facies distribution depositional diagram as interpreted from sedimentological analysis and stacking pattern. (Not to the scale) (Abouelresh et al., 2017; Platt & Wright 1991)

### LEGEND

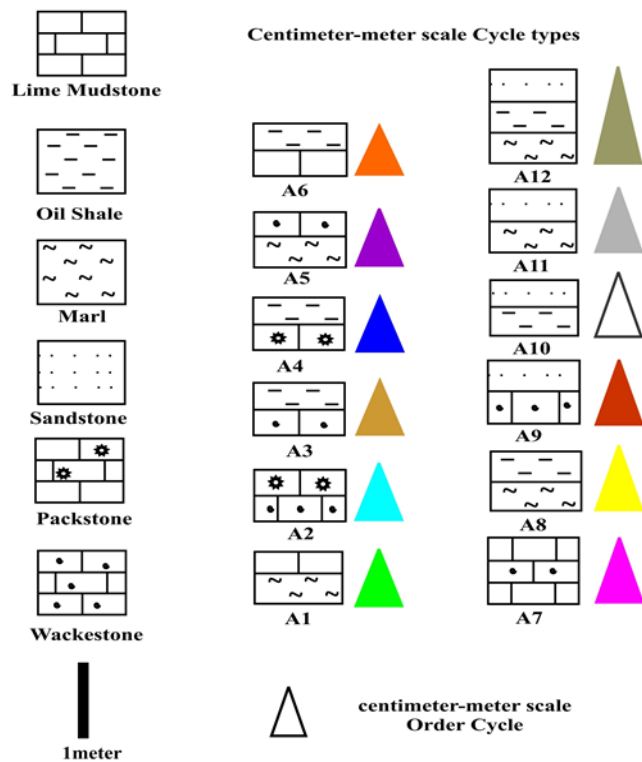


Figure 6.2. Types of cycle determined in the Dağhaclar Section.

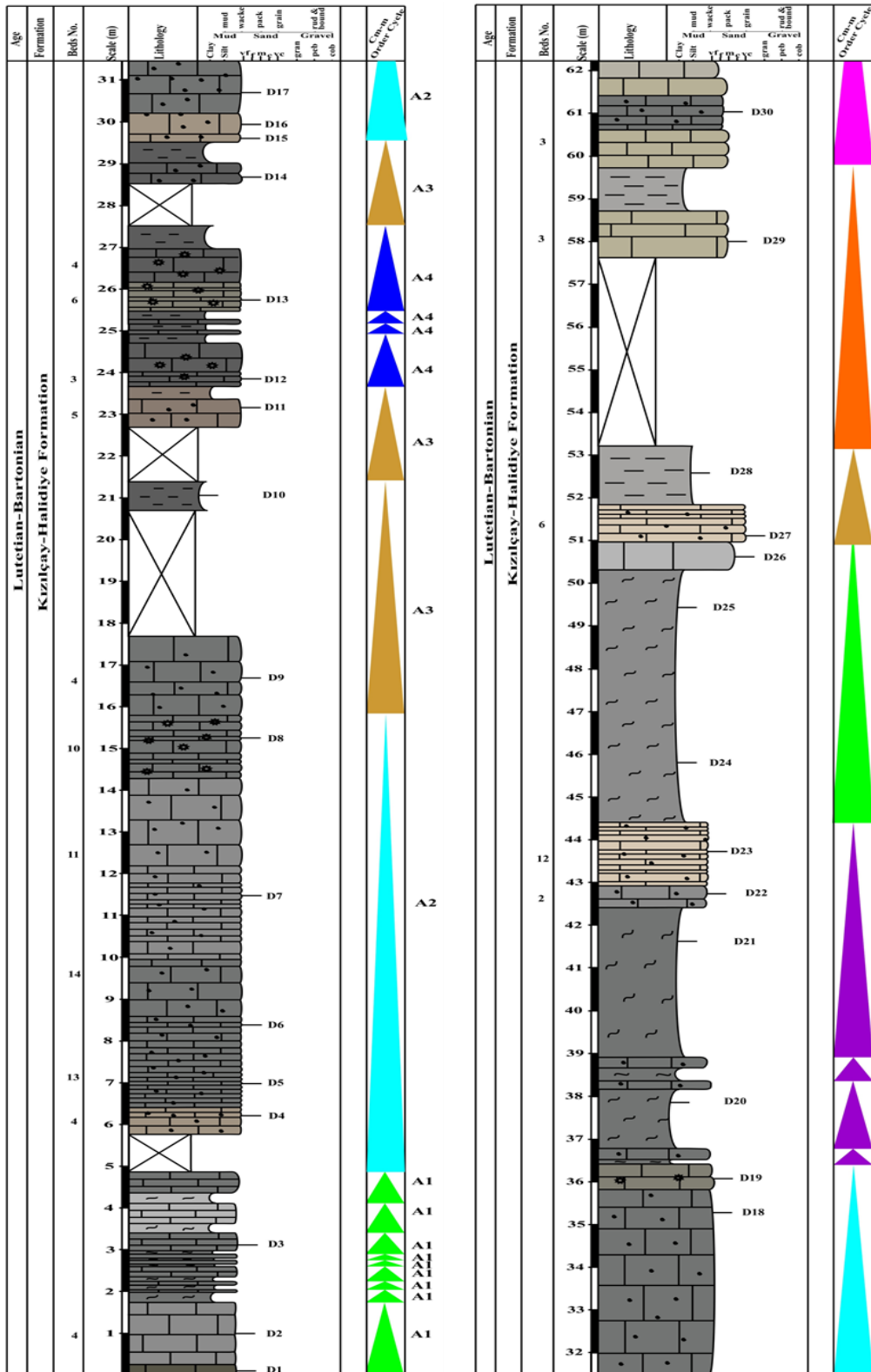


Figure 6.3. Types of cycle along the Dağhacılar Section. Triangles indicate centimeter to meter scale cycles. (for legend; Figure 6.2).



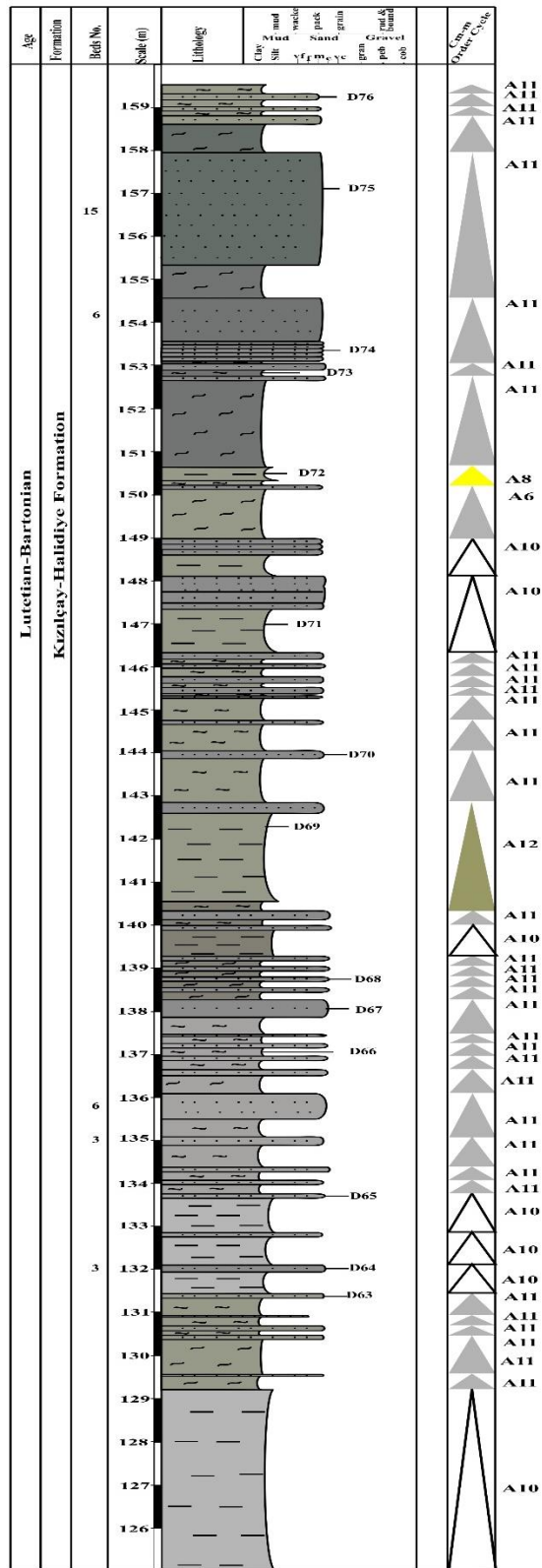


Figure 6.3. Continues... (125.10m-159.50m)

observed in the measured section and are defined by packstone microfacies with abundant gastropod and ostracod at the bottom and oil-shale facies present at the top of the depositional centimeter-meter scale cycle. The cycle A5 types are the cycles that occurred between marl and limestone facies and indicate shallowing upward trend. The A6 cycle types are composed of oil-shale facies which is underlain by medium bedded limestone. It is rare documented in the studied section. The A7 type cycles include lime mudstone at the bottom and then followed by wackestone and capped by lime mudstone. The cycles A8 type are composed of rhythmic intercalation of marl and oil-shale facies. The cycles A8 type are identified in the middle portion of the Dağhacılar section. The A9 type of cycles are composed of wackestone at the bottom and thin to medium bedded wavy rippled sandstone with devoid of fossil at the top. The type A10 cycles are consisting of thick interval of oil-shale facies at the base and thin bedded sandstone lithofacies at the top. This cycle type is predominately present in the upper portion of the studied section. The cycle A11 types are characterized by marl facies which is capped by sandstone lithofacies. The A12 type cycles are composed of marl facies at the base and then followed by oil-shale and sandstone lithofacies at top. It is occasionally observed in the studied section (Figure 6.1). In the studied section, it is interpreted that limestone interval topped by marl and/or oil-shale facies indicate relative rise in the water-level and identified as transgressive cycles (Ocakoğlu et al., 2012). The deeper cycles with dominated oil-shale with alternating thin sandstone (cycle type A10) corresponds to maximum rise in the water level (defined as maximum flooding zone) and indicates a transition period from lacustrine to marine transition environment. Then, it is followed by cycle types of oil-shale/ marl at the bottom and is topped by dominated relatively thicker siliciclastic facies. These cycles correspond to aggradational-progradational stacking pattern of marine transition environment and interpreted as regressive cycles. Overall, the centimeter to meter scale cycle in the studied section correspond to 55.55ka time of duration per cycles (Table 6.2).

#### 6.4. Hasanlar Section Depositional Cyclicality

A total of 51 number of beds with 0.49 average thickness in meter are recorded along the 25.20m thick measured Hasanlar section (Table 6.1; Figure 6.5). The cyclic pattern in the Hasanlar section are composed of lime mudstone, wackestone, marl and oil-shale. The cyclic pattern of facies in the studied section display transgressive depositional cyclic trend. Three types of cycle are documented along the Hasanlar measured section (Figures 6.4; 6.5). The total observed centimeter to meter scale order cycles along the measured section are 23 number of cycles with 1.10-meter average cycle thicknesses (Table 6.1; Figure 6.5). The A1 type cycles are composed of wackestone microfacies with overlying oil-shale facies. A2 type cycles are comprised of lime mudstone at bottom and marl facies at top in the cycle. The cycles A3 type are defined by lime mudstone facies at the bottom and oil-shale facies at the top (Figure 6.5). These centimeter-meter scale cycles are identical to transgressive portion of the studied section with rhythmic character. The time duration per cycles in the studied section is around 43.47ka (Table 6.2).

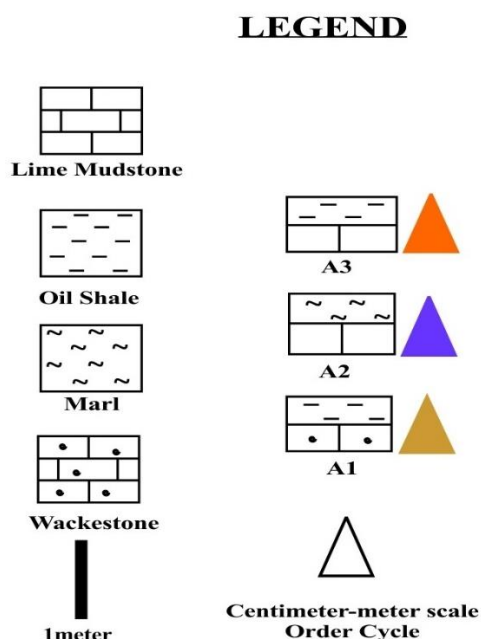


Figure 6.4. Types of cycle determined in the Hasanlar Section.



## 6.5. Kösüre Section Depositional Cyclicality

A total thickness of the Kösüre section is 81.80 m along which 139 number of beds are recorded with 0.59 average value thicknesses in meter (Table 6.1; Figure 6.7). The Kösüre section is consist of limestone, marl, oil-shale and sandstone lithofacies. The vertical and lateral changes in the lithofacies along the stratigraphic section are related with fluctuation of relative water-level in the lacustrine depositional setting and with overlying marine transitional deposits (Figure 6.7). In comparison to Dağhacılar section, the Kösüre section display relatively marginal depositional character with dominate limestone and marl intercalation cycles and occasional oil-shale and marl-sandstone cycles in the lower and middle portion. It is followed by dominate siliciclastic lithofacies with oil-shale cycles in the upper portion of the studied section.

In the Kösüre section, 42 number of centimeters to meter scale order cycles with 1.95 average cycle thickness in meter are determined along the measured section. A total of 8 different centimeter to meter scale cycle types are recorded along the measured section (Table 6.1; Figures 6.6; 6.7). The cycle in the Kösüre section start with marl at the bottom and sandstone at the top. Toward the top, the studied section composed of thick limestone and marl centimeter to meter scale cycles and occasional oil-shale and marl cycles, which represent as a relative rise in the water-level and indicate transgressive cyclic pattern. At the top, the boundary between the thick limestone-marl cycle and overlain sandstone-marl/oil-shale cycles suggest maximum flooding zone and fluctuation from lacustrine to marine transitional environment. The sandstone and oil-shale/marl centimeter to mater scale cycles indicate relative gradual fall in the water-level which is associated with marine transitional condition and represent regressive cyclic pattern.

8 types of cycles are determined in the Kösüre section with transgressive and regressive centimeter to meter scale order cycle trend. The type A1 cycles and type-A2 cycles are characterized by wackestone microfacies and sandstone lithofacies at the bottom which are topped by marl facies, respectively. The cycles A3 type are

consist of oil-shale at the base, marl interbedded and end with charophyta and ostracod bearing wackestone at the top. This cycle type may indicate relative fall of water-level in the lacustrine environment for a short-term. The cycle A4 type are composed of packstone microfacies at the bottom and oil-shale at the top. This meter scale cycle corresponds to sudden relative rise in the water-level in the region. The cycles type-A5 are comprised of thin to thick marl interval at the base and medium to thick bedded wackestone microfacies at the top. This cycle is predominately noticed in the studied section and represent rhythmic cyclic pattern and indicate aggradational stacking pattern. It also represents maximum rise in the relative water-level and reaches to transgressive transitional phase which indicate a change from lacustrine to marine transitional environment at the end. The cycle A6 type is composed of sandstone lithofacies and thick oil-shale facies interval. It started from sandstone lithofacies and capped by oil-shale facies. The A7 type of cycles are characterized by oil-shale at the bottom and sandstone lithofacies at the top. It is observed in the upper portion of the studied section and represent regressive cycles in the studied section.

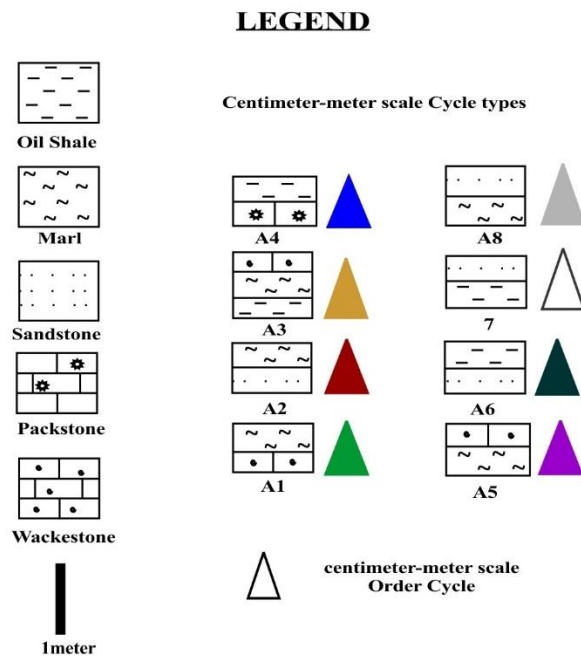


Figure 6.6. Types of cycle determined in the Kösüre Section.

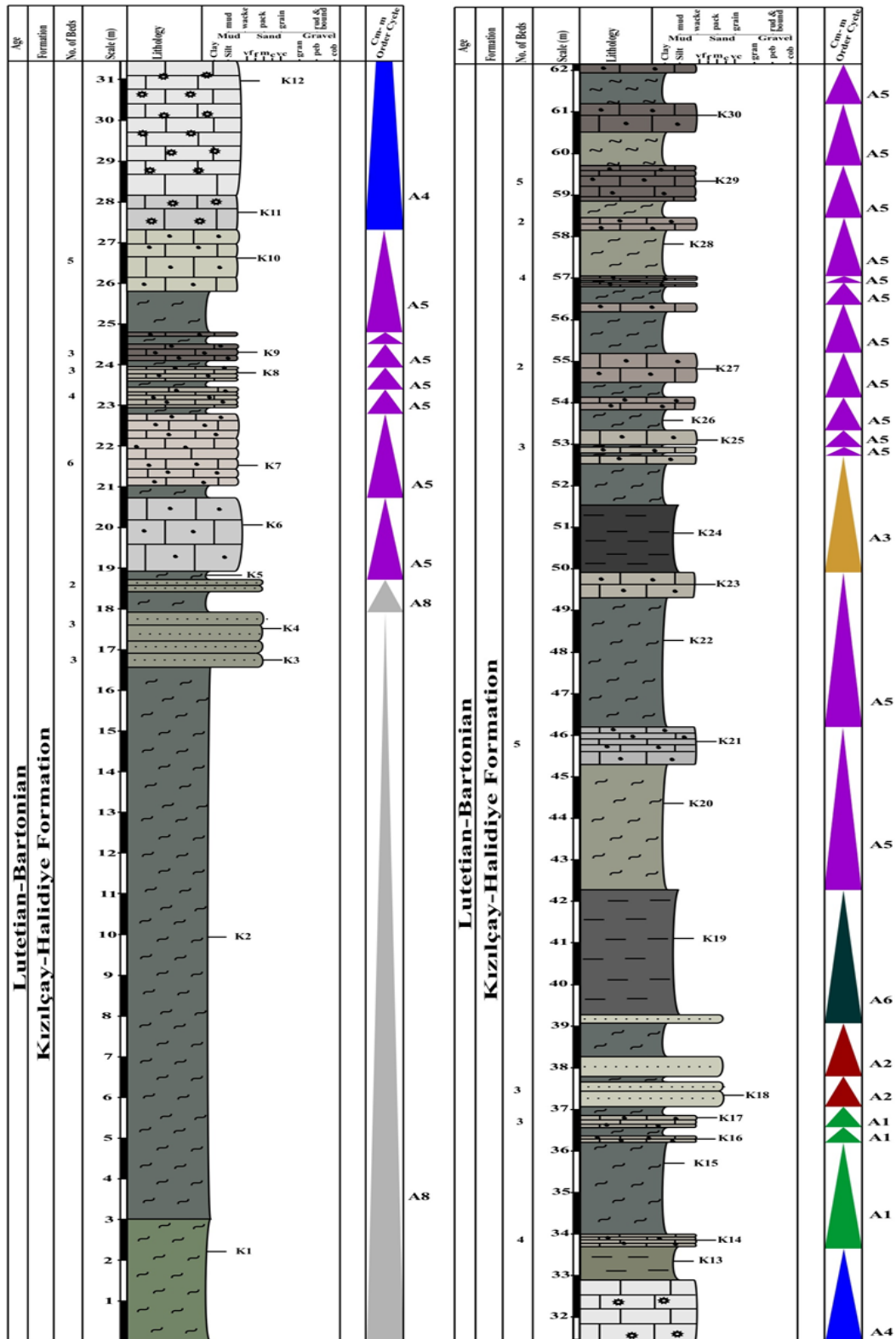


Figure 6.7. Types of cycle along the Kösiire Section. Triangles indicate centimeter to meter scale cycles. (For legend: Figure 6.6)

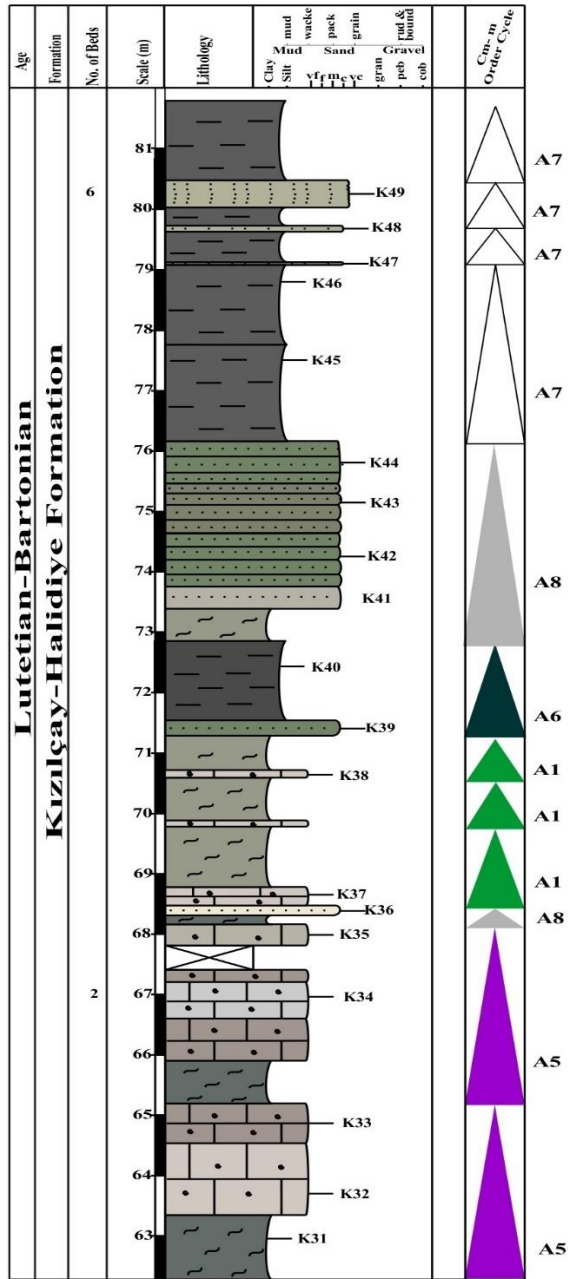


Figure 6.3. Continues... (62.5m-81.80m)

A8 type cycle are based on the marl facies at bottom, which is covered by sandstone lithofacies at the top. It is restricted in the lower portion and upper portion of the measured section (Figure 6.7). The recorded centimeter to meter scale cycles in the Kösüre section represent about 59.52ka time duration per cycle (Table 6.2).

## 6.6. Karahisar Section Depositional Cyclicity

In the Karahisar region, a total of 71.80m stratigraphic section is measured. 149 number of beds and 0.48 bed per meter are counted along the 71.80m measured section (Figure 6.9). The Karahisar succession is composed of predominately alternation of lime mudstone and oil-shale with occasional presence of sandstone lithofacies. Generally, this studied section mostly indicate transgressive to dominate aggradation cyclic stacking pattern. A total of three types of cycles are recorded along the studied section (Figures 6.8; 6.9). The identified centimeter to meter scale order cycles in the studied section are 21 number of cycles with 3.42 average cycle thickness in meter (Table 6.1 and Figure 6.9). The A1 type cycles are comprised of medium to thick interval of oil-shale at the bottom which is overlain by lime mudstone microfacies at the top. The studied section is predominately characterized by A1 type cycles and defined most of the studied stratigraphic section (Figure 6.9). In the middle portion of the studied section, A1-type cycles correspond to maximum rise of the water-level and related with transitional boundary between lacustrine and marine environmental condition. There is also decrease in the thickness of A1-type cycles toward the top

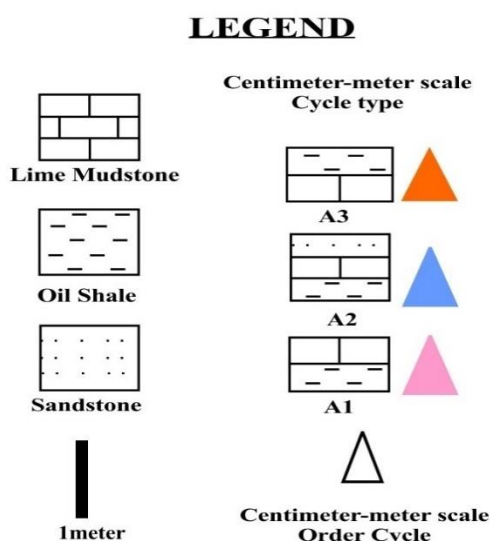


Figure 6.8. Types of cycle determined in the Karahisar Section.

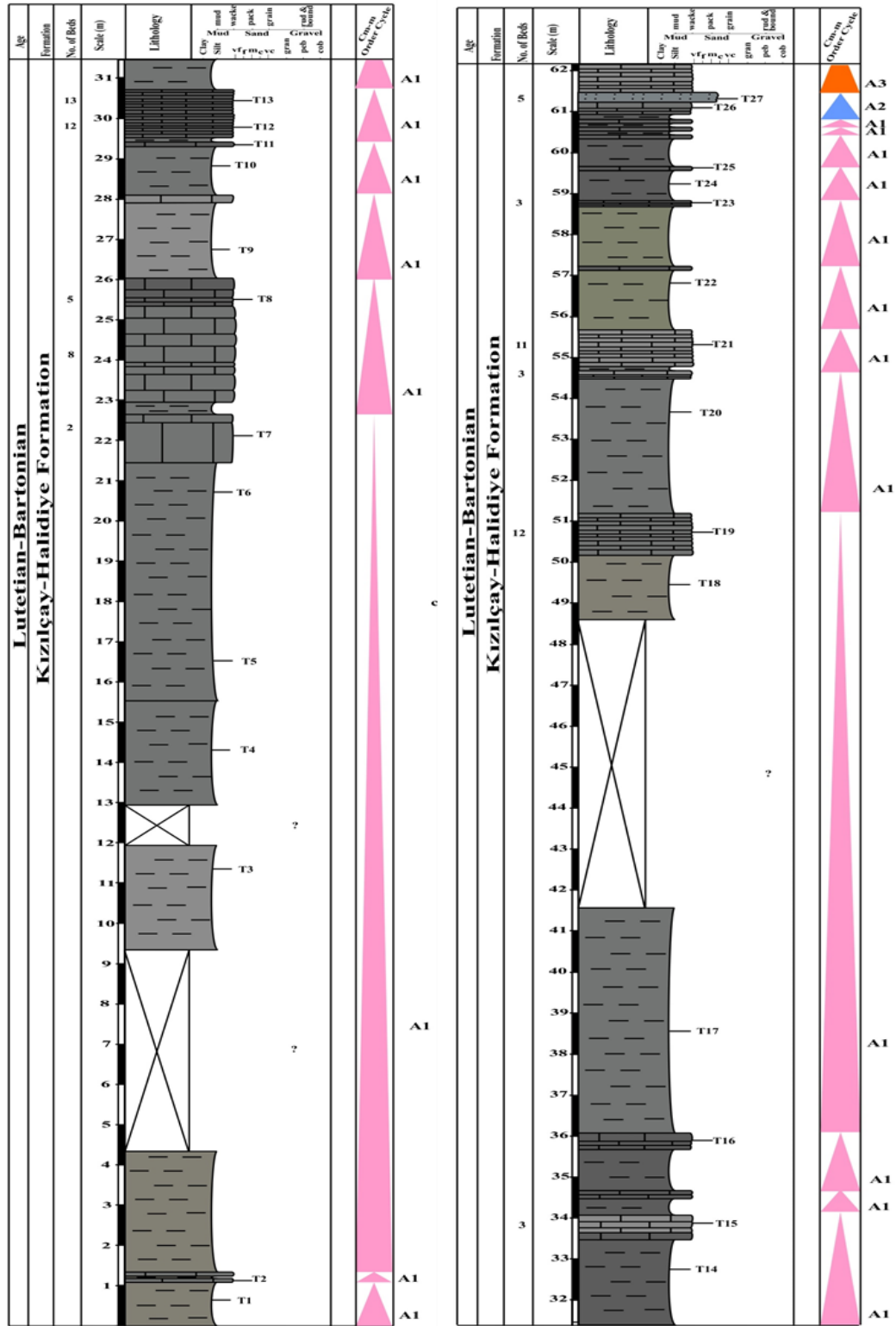


Figure 6.9. Types of cycle along the Karahisar Section. Triangles indicate centimeter to meter scale cycles. (For legend; Figure 6.8)

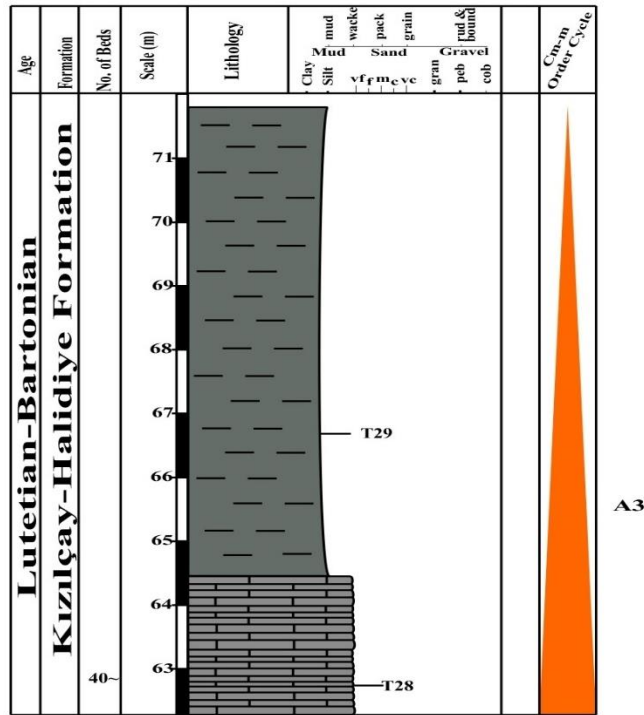


Figure 6.3. Continues... (31.50m-81.80m)

which also reflect change in the depositional condition. A2 type cycles are composed of oil-shale at the bottom, passed to lime mudstone and capped by sandstone lithofacies at the top. A3 type cycles started from lime mudstone at the bottom and end upward with oil-shale facies. The upper portion of the studied section with oil-shale-lime mudstone cycles and oil-shale-limestone-sandstone indicate aggradation cyclic stacking pattern (Figure 6.9). In the Karahisar section, the recorded centimeter to meter scale cycles correspond to about 95.24ka time duration per cycle (Table 6.2).

### 6.7. Sünnet Section Depositional Cyclicity

Along 69.30 m measured Sünnet section, A total of 69 number of beds are recorded with average 1.00 per meter (Table 6.1; Figure 6.11). The recorded beds in the studied section are composed of fine and coarse-grained sandstone, oil-shale, conglomerate and limestone microfacies includes rudstone, packstone, wackestone and lime mudstone. The variation in the facies along the measured section illustrate transgressive-regressive depositional cycles and defining the relative sea-level

fluctuation in the regime. The depositional facies in the measured section is composed of floodplain deposits and are overlain by shelfal marine deposits. Based on the identified facies, a total of 12 types of cycles are documented in the measured stratigraphic section (Figure 6.10). The observed centimeter to meter scale cycles are 24 cycles with 2.88 average thickness of cycle in meter (Table 6.1; Figure 6.11). In the Sünnet section, the cycles are started with predominate floodplain siliciclastic deposits. Further upward in the studied section, the cycles are composed of transitional deposits between fluvial-lacustrine and shallow marine environment. Toward the top, the cycles dominated with siliciclastic deposits with intercalated oil-shale and occasionally limestone units which illustrate transgressive cycles. The appearance of bioclastic-limestone (rudstone), placing over siliciclastic facie interpret maximum flooding zone in the studied sections. Then, it is followed by the regressive cycles which are composed of coarser siliciclastic dominated cycles.

12 types of cycles are recorded in the Sünnet section (Figure 6.10). The cycles type with coarse-grained sandstone at the bottom and fine-grained sandstone at the top are named as A1 type cycles. It is present at different horizons in the studied measured section. Cycles A2 type are comprised of ostracod bearing wackestone at the bottom and abundant charophyta bearing packstone microfacies at the top. The A3 type cycles begin at the bottom with conglomerate, pass to fine-grained sandstone and end at the top with oil-shale facies. Next type of cycle in the studied section is characterized as A4 type. It consists of packstone microfacies with abundant charophytes at the base and oil-shale facies at the top. The A5 type cycles are categorized by thick interval of oil-shale with bivalve at the bottom and thin bedded coarser-grained sandstone with bioclastic fragment at the top. The cycles A6 type are comprised of lime mudstone microfacies at the bottom and oil-shale facies with bivalve at the top. The cycle A7 types are fine sandstone at the base and coarser-grained sandstone at the top. The cycles A8 type begin with wackestone microfacies and passes to fine-grained sandstone and end with rudstone/calcirudite facies with *Bivalvia* mollusk. The cycles A9 type are identified as coarser sandstone at the base and oil-shale at the top. The

cycles A10 type in the studied section are started with fine sandstone lithofacies which is covered by conglomeratic intervals. The cycles A11 type are composed of fine-grained sandstone with overlying oil-shale facies having bivalve fauna. A12 type cycles are composed of conglomerate bed which is overlain by rudstone microfacies. The about 83.33ka time of duration per cycles is determined for recorded centimeter to meter scale cycles in this studied section (Table 6.2).

### LEGEND

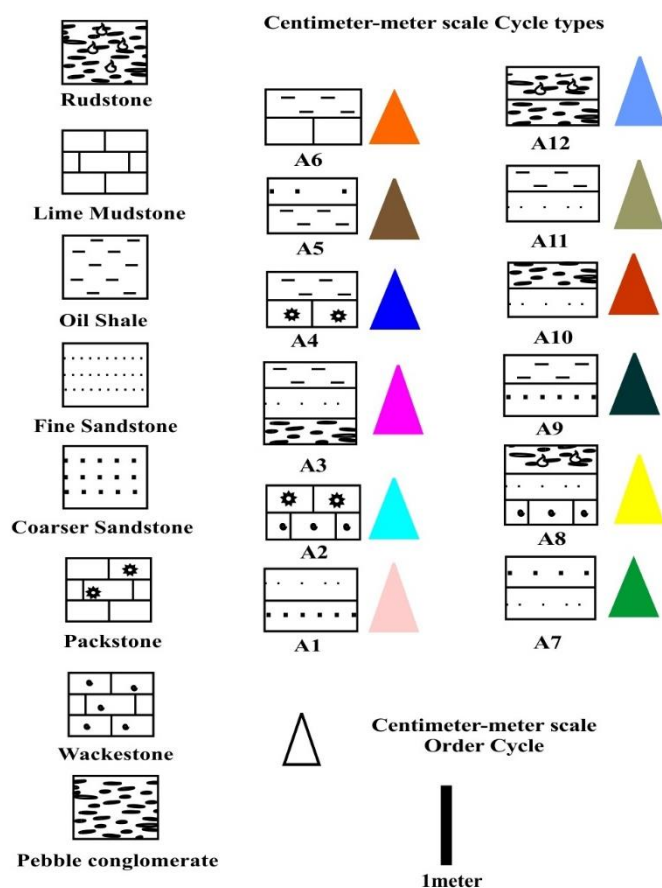


Figure 6.10. Types of cycle determined in the Sünnet Section.

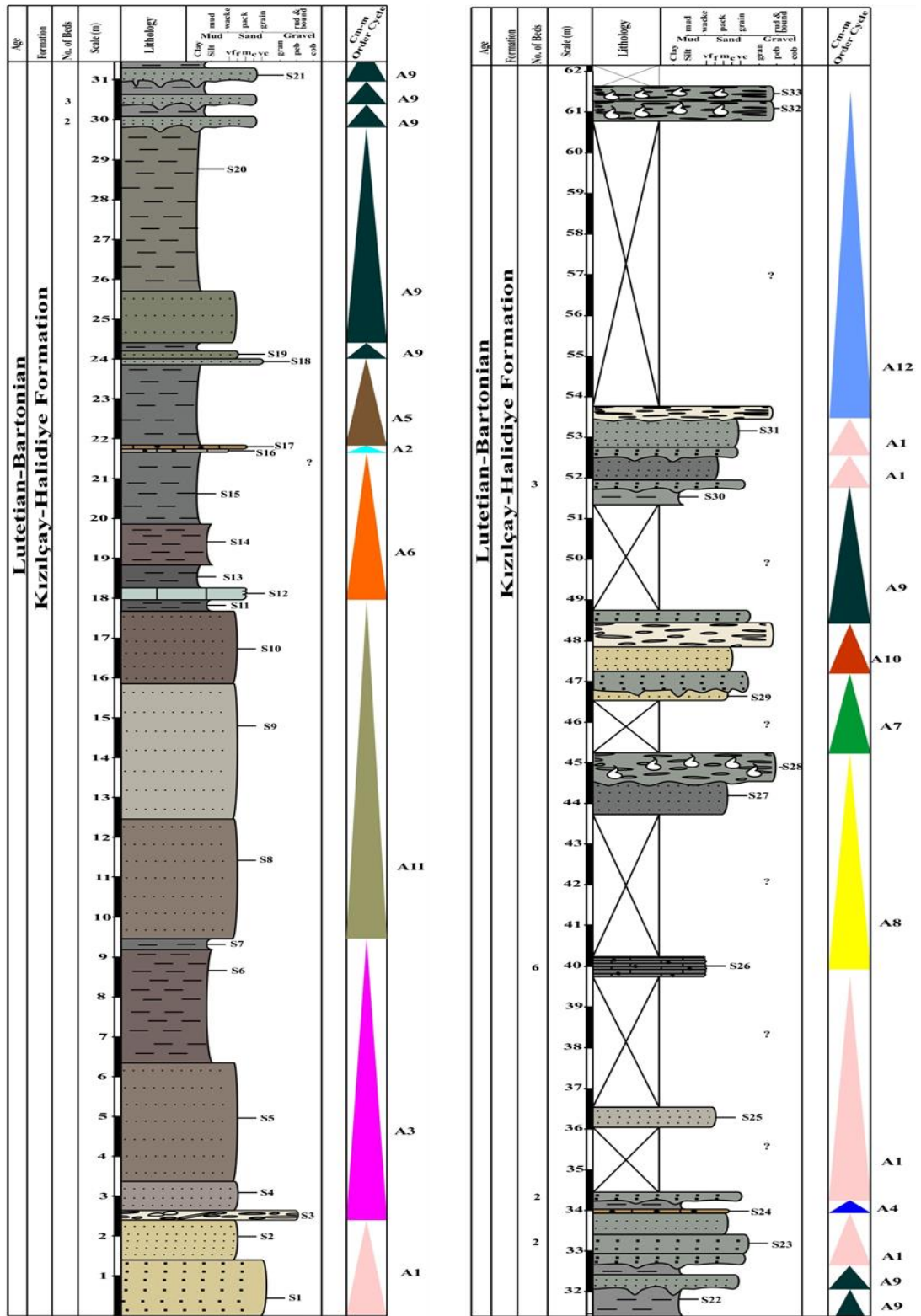


Figure 6.11. Types of cycle along the Sünnet Section. Triangles indicate centimeter to meter scale cycles. (For legend; Figure 6.10)

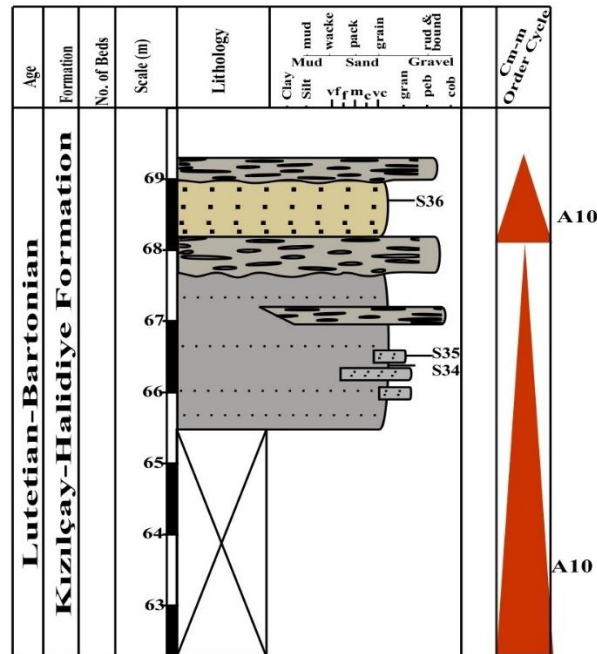


Figure 6.11. Continues... (62.10m-69.20m)

## 6.8. Interpretation

### 6.8.1. Milankovitch Periodicity Analysis

In the cyclostratigraphy, Milankovitch periodicity is an important concept that linked to depositional cycles. Milankovitch periodicity is defined by depositional cycles which occur due to systematic changes in the Earth's eccentricity, obliquity and precession (Fischer, 1980; Berger et al., 1992; Wu et al., 2013). The physical, chemical or paleontological proxies from sedimentary successions are used to predict paleoclimatic condition changes and to study the orbitally forced control cyclicity pattern (Mader et al., 2004).

The total number of beds, centimeter-meter scale order cycles in the studied sections are analyzed by ordinary statistical parameters (Tables 6.1; 6.2). The statistical studies indicate significant change in the average centimeter-meter scale order cycles in the studied sections, which are probably related with climatic control changes linked with orbitally forced parameters. The maximum average thick order cycles are observed in the Karahisar section (Table 6.1; Figures 6.12; 6.14). The minimum average order

cycles are recorded in Hasanlar section (Table 6.1; Figures 6.12; 6.14). In the studied sections, the average thickness of centimeter-meter scale order cycles are thicker in the Karahisar section> Sünnet section> Dağhacılar section> Köşüre section> Hasanlar section (Table 6.1; Figures 6.12; 6.14). Generally, the average thickness of cycles is comparatively closer to each other within studied sections (Table 6.1). The average bed per meter in the studied sections are relatively closer with each other except Sünnet section. In the Dağhacılar section, Hasanlar section, Köşüre section, Karahisar section are ranging between 0.41-0.59 average bed thickness per meter. In the Sünnet section, it is 1 average bed thickness per meter (Table 6.1). The beds in the studied sections are categorized as 6th order cycle. The precession of Milankovitch bands is recorded 13.42kya to 28.98kya/bed in the Dağhacılar section, Hasanlar section, Köşüre section, Karahisar section and Sünnet section (Table 6.2). In the Dağhacılar section, Hasanlar section, Köşüre section, Karahisar section and Sünnet section, each centimeter-meter scale order cycle is 55.55ka, 43.47ka, 59.52ka, 95.24ka and 83.33ka, respectively (Table 6.2). It is interpreted that centimeter-meter scale order cycles in the Dağhacılar section, Hasanlar section, Köşüre section, Karahisar section and Sünnet section correspond to the Milankovitch cycles of obliquity band range (Einsele et al., 1991) (Table 6.2). Therefore, it is interpreted that the change in the relative water depth in the lacustrine associated with marine setting are enforced by the climatic control linked with earth`s orbital forced.

### **6.8.2. Fischer Plot Workflow**

The Fischer plot is a graphical presentation of analyze centimeter to meter scale cyclic stacking patterns in the beds or laminae by plotting cumulative departure from mean cycle thickness as a function of time or cycle number and thickness (Husinec et al., 2008; Figures 6.12; 6.13; 6.14; 6.15). This Fischer plots diagram illustrate change in accommodation spaces in the region (Read and Goldhammer, 1988; Sadlaer et al., 1993). The Fischer plot is used to define the accommodation space changes in response of relative sea-level fluctuation and/or tectonic subsidence in the studied successions with time. The relative change in water-level/sea-level can be interpreted

from the Fischer plot graphical presentation of the cycles data. The Fischer plot analyses are applied on the centimeter to meter scale order cycles of the Dağhacılar, Hasanlar, Köşüre, Karahisar and Sünnet measured sections (Figures 6.12; 6.13; 6.14; 6.15). The cycle thickness change along each studied section has been analyzed independently from facies association. Their departure from mean cycle thickness is charted against cycle numbers for each section (Sadler et al., 1993). The vertical stacking patterns of the studied sections cycles are illustrated on the Fischer plot diagram (Figures 6.12; 6.13; 6.14; 6.15). Fischer plot graphic diagram show relatively similar pattern within studied sections (Figures 6.12; 6.13; 6.14; 6.15). In the Dağhacılar section, the Fischer plot indicate three peaks of increasing in accommodation space and four limbs of declining in accommodation spaces (Figures 6.12; 6.13; 6.14; 6.15). In the Hasanlar section, there is two phases of short-term increasing in accommodation spaces and two stages of low angle declining in accommodation space (Figures 6.12; 6.13; 6.14; 6.15). The Köşüre section shows relatively similar pattern of increasing and decreasing in the accommodation space in the Fischer plot as in the Dağhacılar section (Figures 6.12; 6.13; 6.14; 6.15). In the Karahisar section Fischer graphic representation, there is observation of two decreasing patterns and two increasing patterns in the accommodation space (Figures 6.12; 6.13; 6.14; 6.15). In the Sünnet section, the Fischer graphically diagram indicate an increase in the accommodation space and then followed by declining limb (Figures 6.12; 6.13; 6.14; 6.15). Overall, the last declining limb in the studied sections except Hasanlar section are associated with siliciclastic influxes with alternating oil-shale and marl. These siliciclastic influxes are linked with marine environmental setting which replaces the previous lacustrine depositional environment in the region (Figures 6.12; 6.13; 6.14; 6.15). Additionally, the Fischer plot diagram of the studied sections are correlated according to the stratigraphic depositional correlation and exhibit relatively similar pattern within studied sections (Figures 6.12; 6.13; 6.14; 6.15).

Generally, in the studied sections, it is interpreted that marl overlying the limestone or sandstone, and oil-shale overlying the limestone or sandstone intervals are related with

relative rise of sea level. The siliciclastic lithofacies correspond to relatively regressive setting. while, oil-shale and marl are associated with relatively transgressive condition (Hunt and Tucker, 1993; Strasser, 1994; Wright, 1984). The cyclic nature of the studied sections demonstrates that climatic control linked with earth`s orbital forcing is driving factor in the relative water-level/sea-level changes in the studied region. The studied successions are identified as marine-influence lacustrine deposit to marine deposits. The depositional cyclic stacking pattern in the studied successions suggest that relative sea-level change in the studied regimes correspond to minor change which may be not greater than 30m (Ocakoglu et al., 2012). The siliciclastic influxes dominated cycles in the upper portion of the studied section argue that change in relative sea-level is also linked with minor tectonic factors (Devlin et al., 1993; Matthews and Perlmutter, 1994; Ocakoglu et al., 2012). The siliciclastic influxes also interpret marine transgression to the lacustrine setting.

### **6.8.3. Carbonate and Organic Matter Content relationship with Cyclostratigraphy**

Along the measured stratigraphic section, the determined carbonate content and organic matter content are correlated with recorded centimeter to meter scale cycles within the measured sections (Figures 6.16; 6.17; 6.18; 6.19; 6.20; 6.21; 6.22). In the limestone units, the carbonate content is higher and organic matter content is lower compared to marl and oil-shale. In the graphic representation, the change in the carbonate content and organic matter content curves correspond to changes in the cyclic facies pattern (Figures 6.16; 6.17; 6.18; 6.19; 6.20; 6.21; 6.22). The carbonate content and organic matter content curve also interpret cyclicity imprint as recorded in the facies along the measured stratigraphic section (Figures 6.16; 6.17; 6.18; 6.19; 6.20; 6.21; 6.22).

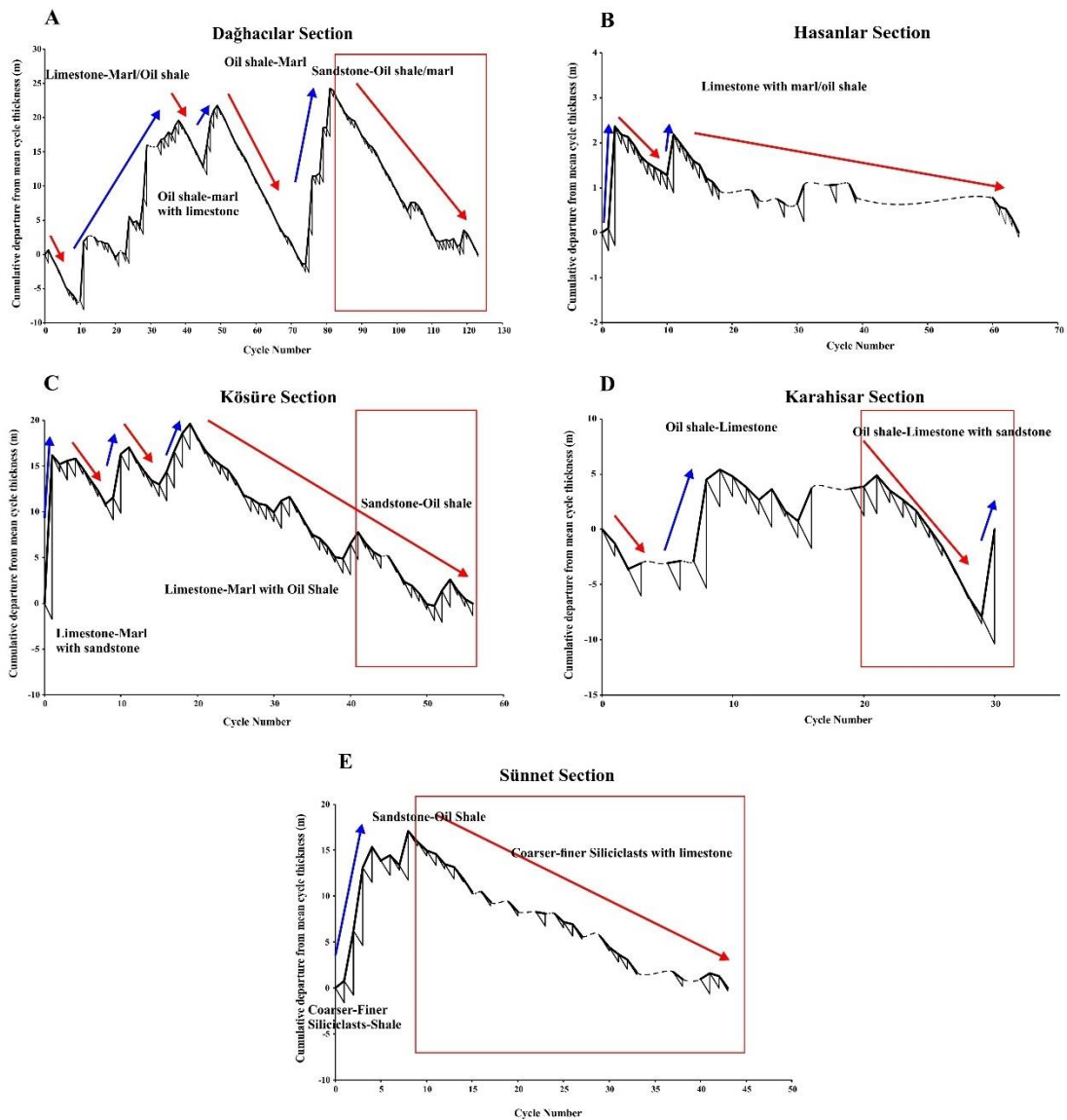


Figure 6.12. Fischer plot of the Middle Eocene (Lutetian-Bartonian) studied sections. Blue arrow indicates increase in accommodation space and red arrow indicates decrease in accommodation spaces. Red rectangle indicates marine successions in the upper portion of the studied sections.

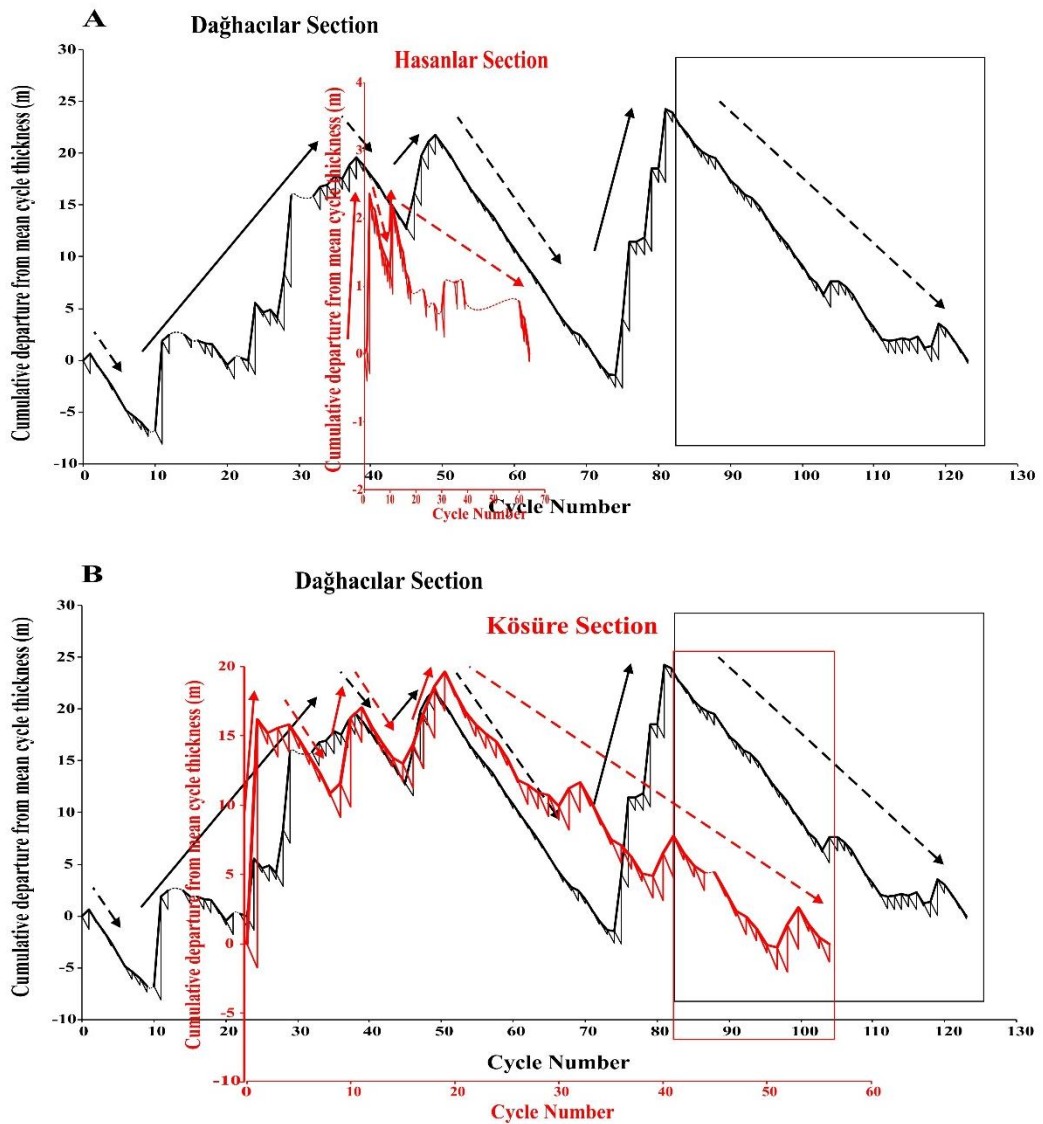


Figure 6.13. Correlation of Fischer plot of the Middle Eocene (Lutetian-Bartonian) studied sections, A) Hasanlar Section and B) Köşüre Section with the Dağhacılar Section. Rectangle indicates marine depositional cycles in the studied sections.

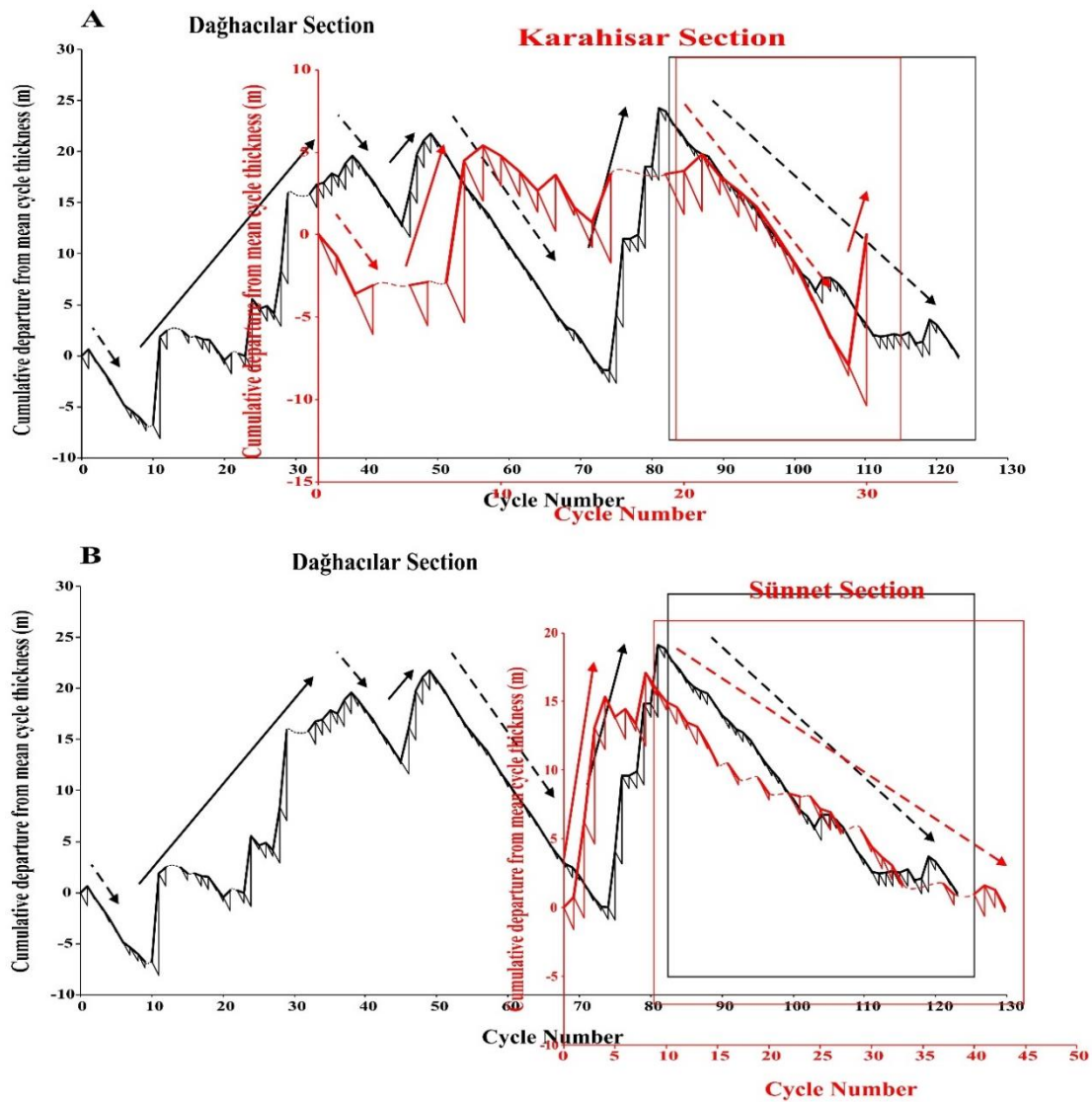


Figure 6.14. Correlation of Fischer plot of the Middle Eocene (Lutetian-Bartonian) studied sections, A) Karahisar Section and B) Sünnet Section with the Dağhacılar Section. Rectangle indicates marine depositional cycles in the studied sections

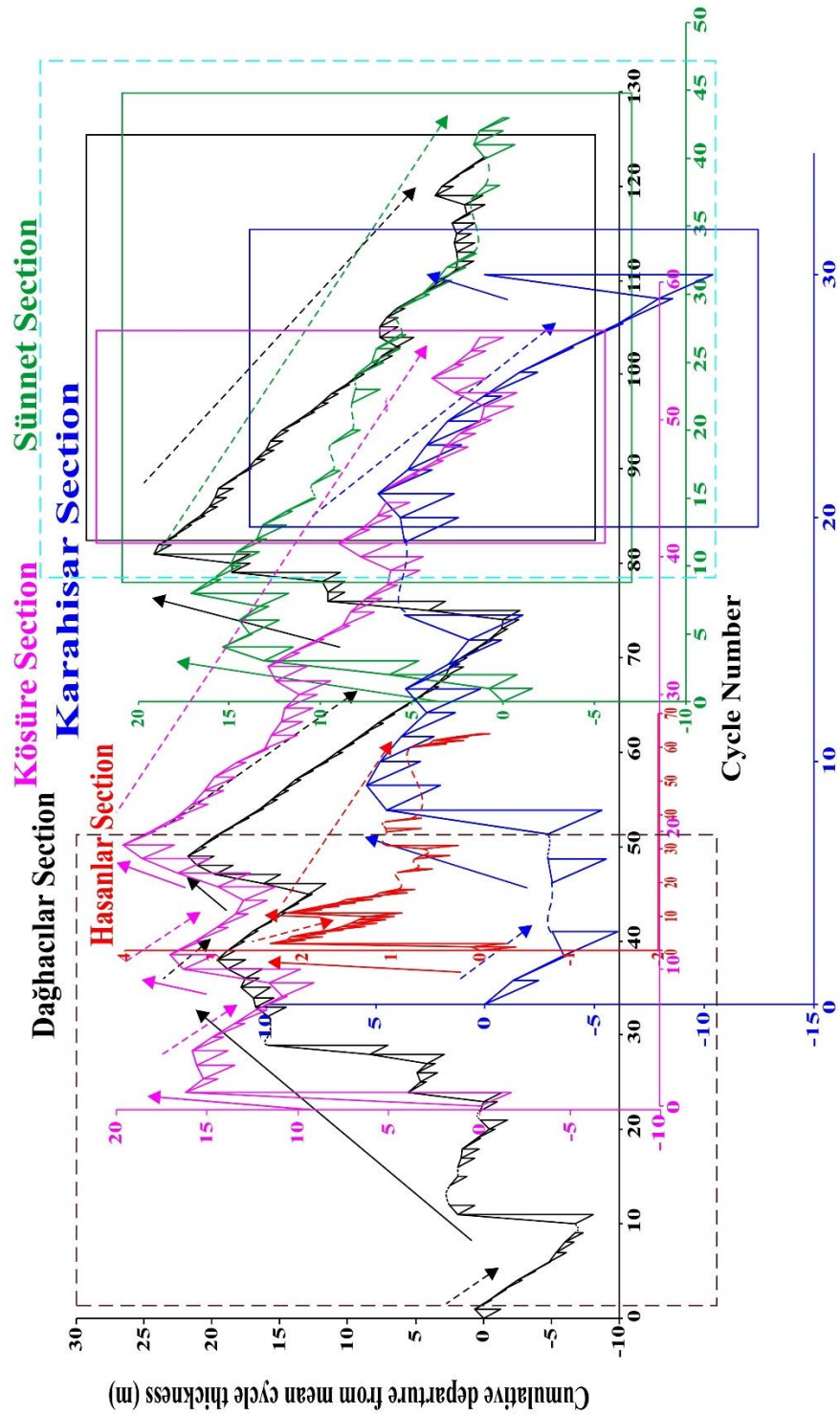


Figure 6.15. Correlation of Fischer plot of the Middle Eocene (Lutetian-Bartonian) studied sections. Solid arrows indicate increase in accommodation space and Dotted arrows indicate decrease in accommodation spaces. Solid line rectangle indicates marine depositional cycles in the upper portion of the studied sections. Dotted brown rectangle shows overall deepening trend and Dotted light blue shows overall shallowing trend.

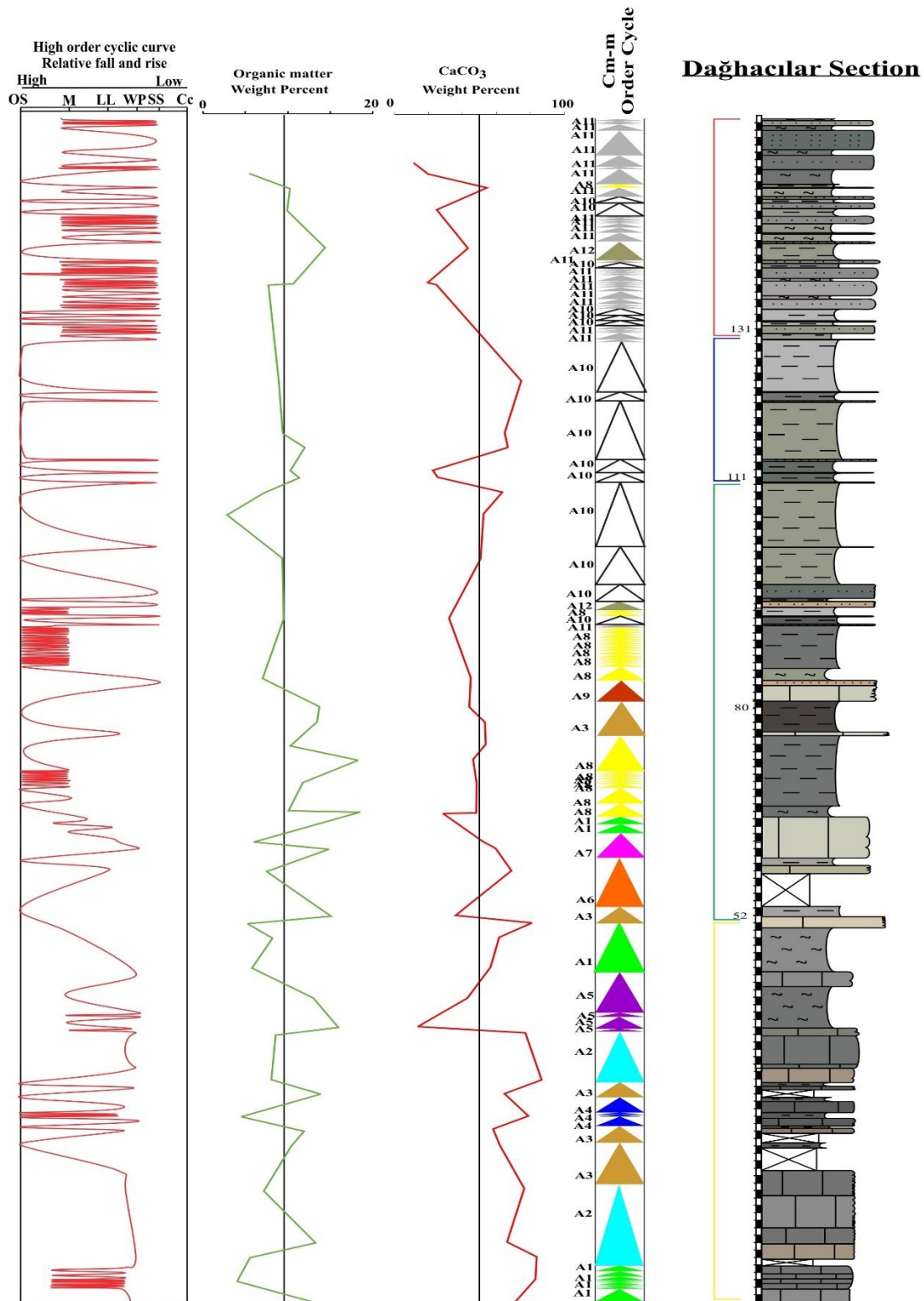


Figure 6.16. Relationship between organic matter content, carbonate content and centimeter to meter scale order cycles of the Dağhacılar section.

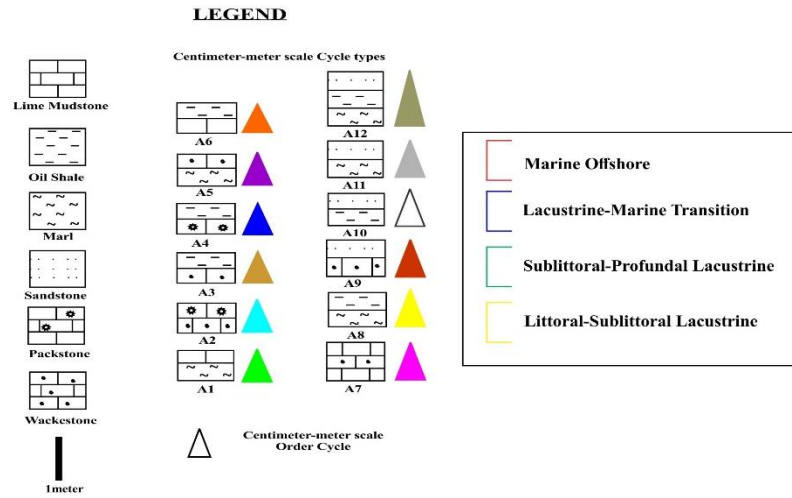


Figure 6.12. Continues...

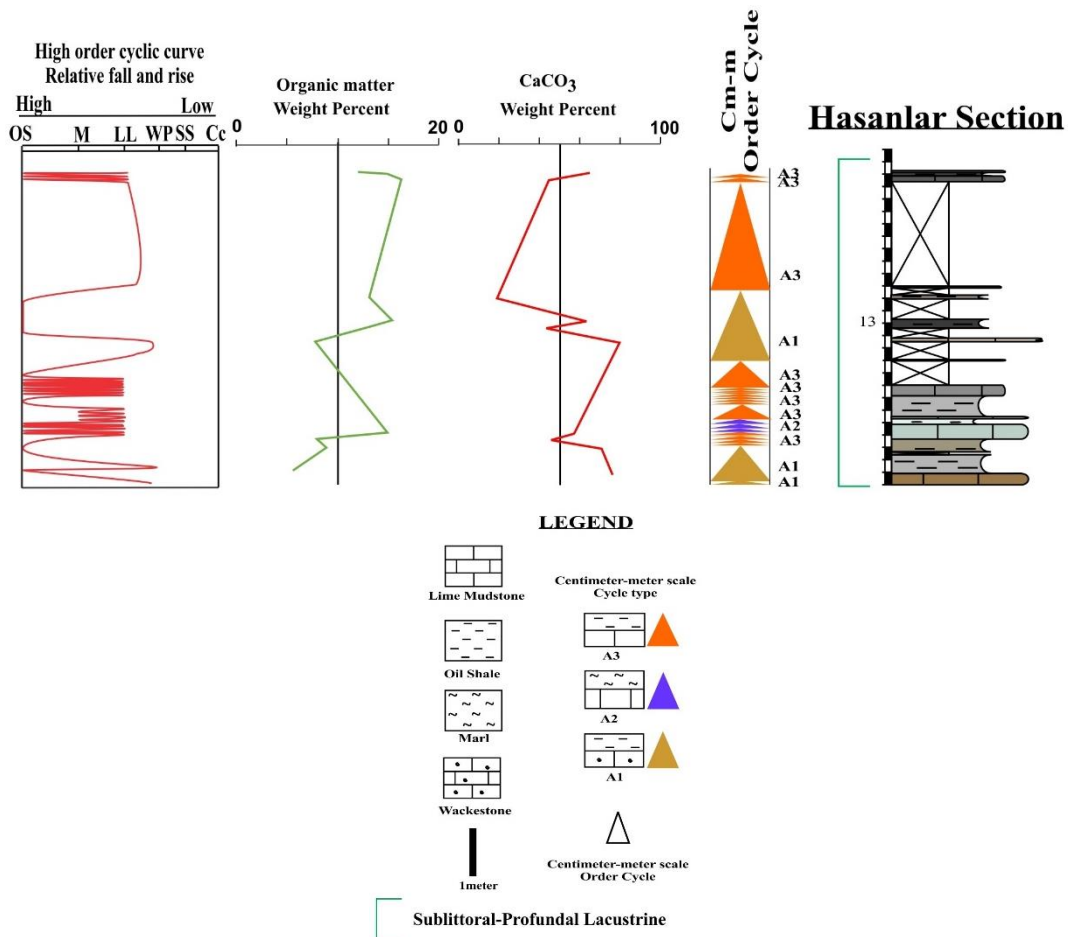
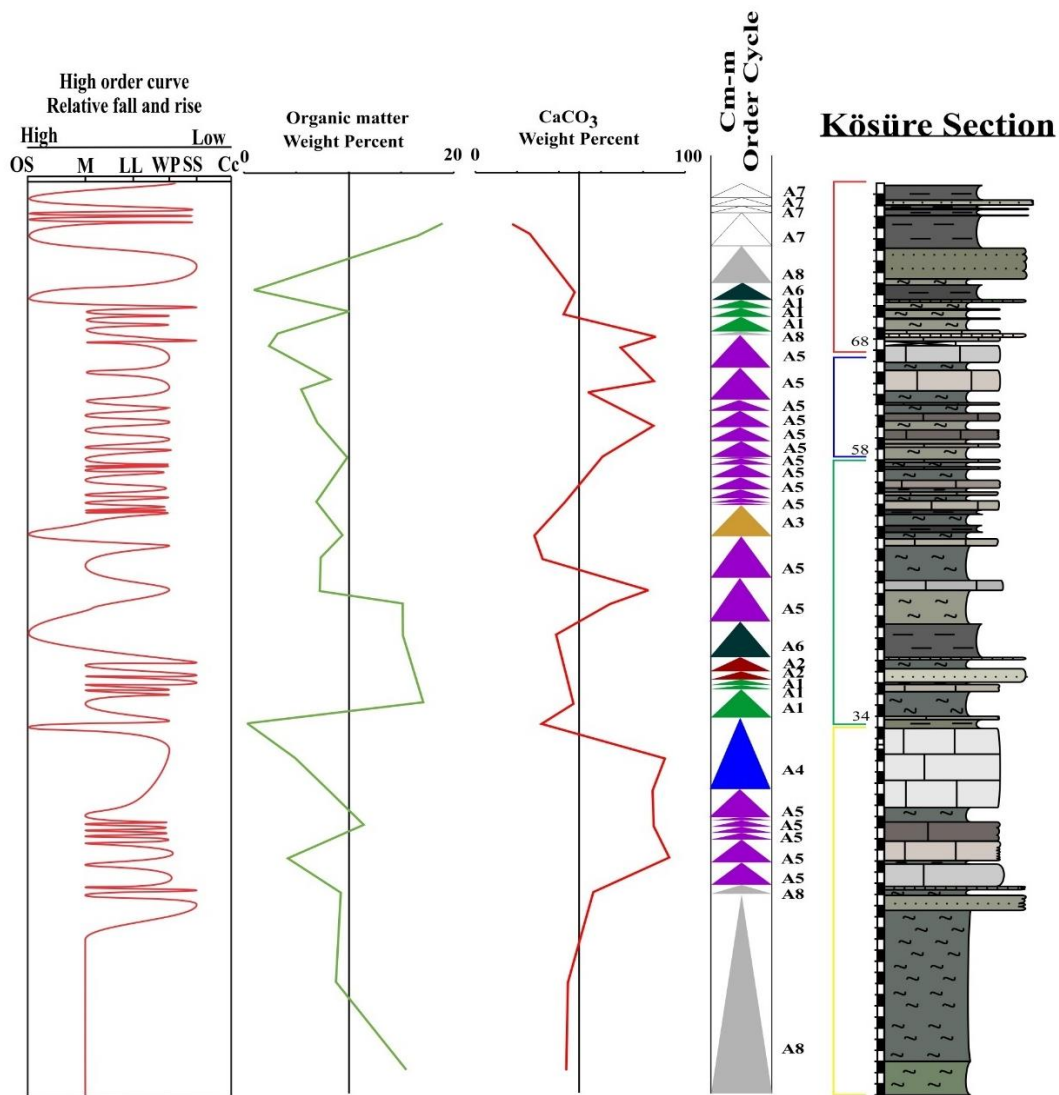


Figure 6.17. Relationship between organic matter content, carbonate content and centimeter to meter scale order cycles of the Hasanlar section.



**LEGEND**

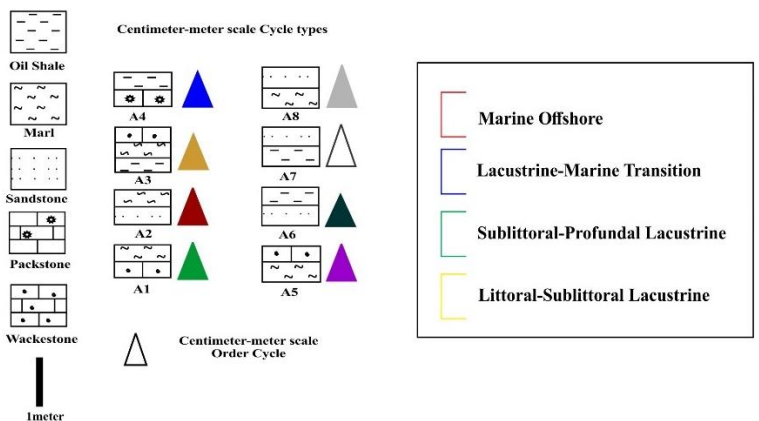


Figure 6.18. Relationship between organic matter content, carbonate content and centimeter to meter scale order cycles of the Kösiire section.



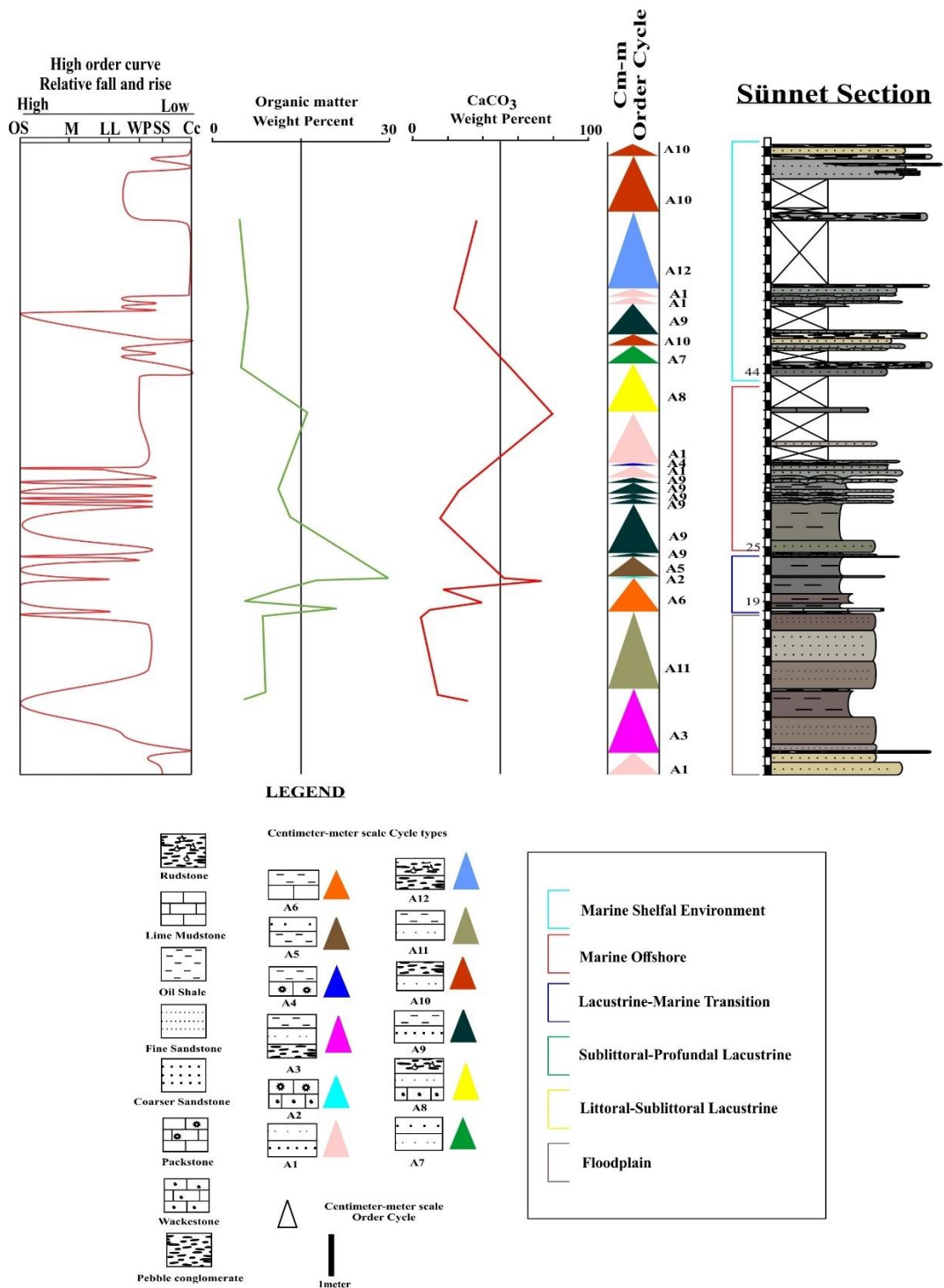
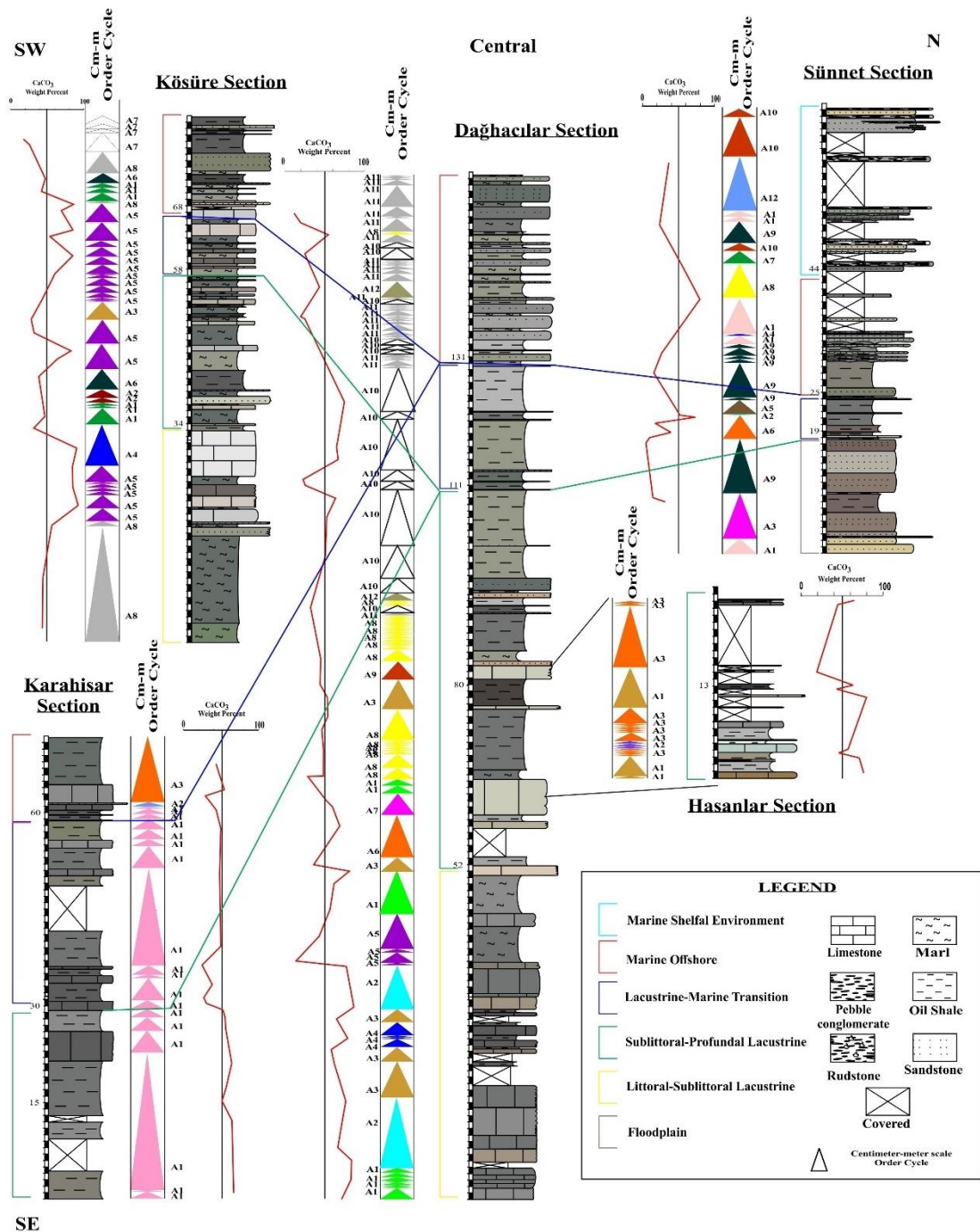
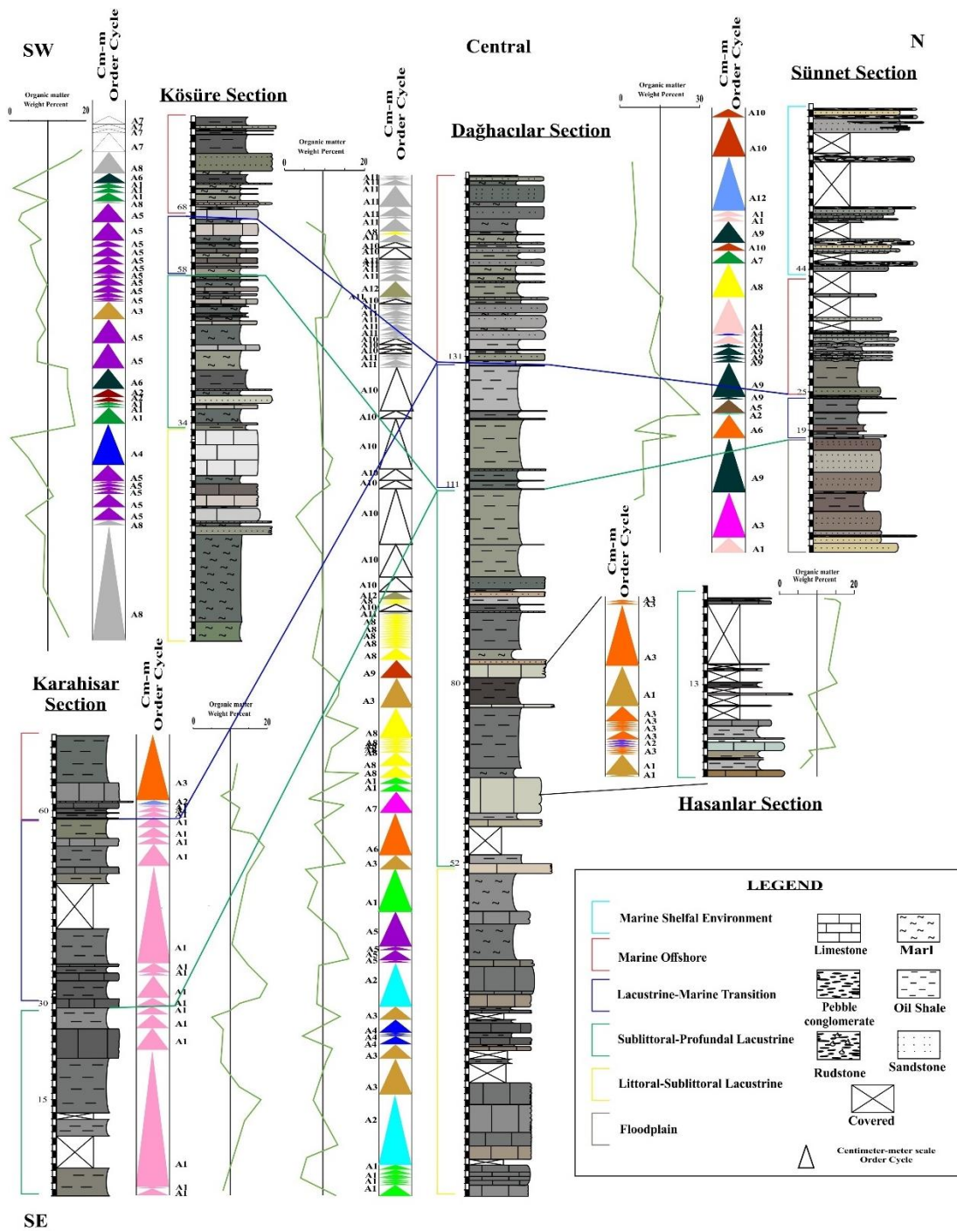


Figure 6.20. Relationship between organic matter content, carbonate content and centimeter to meter scale order cycles of the Sünnet section.



SE  
 Figure 6.21. Relationship between carbonate content and centimeter to meter scale order cycles within the studied sections.



SE  
 Figure 6.22. Relationship between organic matter content and centimeter to meter scale order cycles within the studied sections.

## CHAPTER 7

### SEQUENCE STRATIGRAPHY

#### 7.1. Introduction

The sequence stratigraphic analysis techniques were initially based on the seismic sections and well log profiles (Mitchum et al., 1977) and Vail et al., 1977). In recent decade, the sequence stratigraphic analysis is not only performed on the seismic profiles and well logs, but also perform on the basis of detailed field observation and sedimentological analysis (Beaubouef and Friedmann, 2000; Zeng et al., 2001, Zeng and Hentz, 2004; Wei et al., 2017). The eustatic sea-level changes are figured out as the driving factor for the sequence development (Vail et al., 1984). In 1987 and 1988, Haq et al. presented the global sea-level curve from Triassic to recent. Van Wagoner et al. (1988) defined and described the concepts of sequence stratigraphy in detail and also presented the concepts of parasequence in the sequence stratigraphy. Later on, the sequence stratigraphy is further evolved and not only restricted to siliciclastic successions but also applied to carbonate dominate-systems (Sarg, 1988; Weimer and Posamentier, 1993). In this study, the Van Wagoner et al. (1988), Sarg (1988) and Handford and Loucks (1993) sequence stratigraphic terminologies are applied to study the sequence stratigraphic framework of the studied sections. The studied successions comprised of distinct lowstand systems tract (LST), transgressive systems tract (TST) and highstand systems tract (HST). Study of systems tracts also helpful in the identification of flooding surfaces (FS) and maximum flooding zones (MFZ) (Catuneanu, 2006; Holland and Patzkowsky, 1998). Generally, the similar concepts of sequence stratigraphy of marine basin successions are applied to lacustrine basin successions. As, the depositional base level is controlled by the changes in the lake level such as sea level fluctuation in the marine basins. Though, in the lacustrine basins, especially in the active-tectonic lacustrine basins, the depositional systems

tracts, sequence architecture pattern and the sequence boundaries origins are far distinctive from models of sequence stratigraphy for marine basins. Therefore, the concept of sequence stratigraphy in the tectonically active lacustrine basins require modification to describe the lacustrine sequences intricacy and the depositional systems tracts distribution in the basins (Li et al., 1992; Changsong, Eriksson, & Sitian, 2001). In this study, sequence stratigraphy frameworks are established in Middle Eocene marine-influence lacustrine basin through combination of detailed field analysis, sedimentological studies and depositional cyclic stacking pattern. The depositional cyclic stacking pattern of the intervals are categorized as high resolution parasequence. The aim of this chapter is to evaluate the measured stratigraphic sections in terms of facies variation and high-resolution sequence stratigraphy framework.

In the Dağhacılar, Hasanlar, Köşüre and Karahisar studied sections, based on the sedimentology, petrography and fossils analyses, the depositional character in the Middle Eocene (Lutetian-Bartonian) studied sections are transgressively evolved from lacustrine to transitional marine depositional environment. The northern Sünnet section defines the transgressive phase and change from fluvial-lacustrine to shelf marine environment. The lacustrine transgression-phase in the Dağhacılar, Hasanlar, Köşüre and Karahisar studied sections is defined by the occurrence of interbedded limestone-marl facies and overlying oil-shale-marl intercalation, which are deposited under dysoxic to anoxic environments in relatively shallower to deeper lacustrine, respectively (Huang et al., 2017). These successions are overlain by transition phase of marine offshore character and are composed of interbedded calcareous sandstone-oil-shale and occasionally marl lithofacies (Figure 7.6). Similar conditions are also documented in the Beibuman Basin in Paleogene successions (Huang et al., 2017). Saner (1977, 1978a, 1980b) and Ocakoğlu et al. (2007, 2012) also observe marine transgression in the Mudurnu-Göynük basin during Middle Eocene period.

In Middle Eocene (Lutetian-Bartonian) stratigraphic sections, the observed changes in the marine-influence lacustrine level in the south and changes in the relative sea

level in the north exhibit relatively synchronous with global sea level curve in Middle Eocene (Lutetian-Bartonian) period (Figure 7.7) (Haq et al., 1987; Wang and Li, 2009). In the upper portion of the studied sections, a transitional change from lacustrine deposits to marine-transitional offshore deposits in the studied sections indicate major landward shift of the deposits and recognize as maximum relative sea-level rise/shift in the studied region (Figure 7.6).

Generally, the Late Lowstand systems tract is also observed in the Sünnet Section which is characterized by siliciclastic deposits of fluvio-lacustrine floodplain environment and overlain by transgressive systems tract (Figures 7.5; 7.6). The Early transgressive systems tract is characterized in the lower portion of littoral-sublittoral deposits in the Dağhacılar section which are composed of charophyta-gastropod-ostracod bearing limestone intervals with occasional interbedded marl units and rare fossiliferous oil-shale (Gale et al., 2006) (Figures 7.1; 7.6). The transgressive systems tract in the Dağhacılar, Hasanlar, Köşüre and Karahisar studied sections are characterized by limestone microfacies with interbedded marl, presence of abundant pyrite, organic-rich lithofacies and lack of clastic influx (Figures 7.1; 7.2; 7.3; 7.4; 7.6). The overlying marine influence successions on the transgressive systems tract in the studied sections are defined by calcareous siliciclastic intervals with interbedded organic rich shale and occasional marl and lime mudstone horizons. These depositional successions are identifying as highstand systems tract deposits in the studied sections and characterized as marine transgression to the depositional setting (Figures 7.1; 7.2; 7.3; 7.4; 7.6) (Ocakoğlu et al., 2007; Lash & Blood, 2011). It is also supported by presence of abundant quartz and lacking clay content in the siliciclastic deposits of highstand systems tract in the studied sections (Lash, 2011) (Figures 4.8; 5.26). In general, in the sequence stratigraphic framework, the Dağhacılar, Hasanlar, Köşüre and Karahisar sections are composed of carbonate and oil-shales deposits of transgressive systems tract which are overlain by dominated siliciclastic, oil-shale and occasional marl intervals of the highstand systems tract deposits (Figures 7.1; 7.2; 7.3; 7.4; 7.5; 7.6). Herein, the transitional changes in the lithofacies from lacustrine to

marine environment reflect High-accommodation systems tract (Wanas et al., 2015). The profundal lacustrine-transitional marine oil-shale and carbonate overlain by sandstone in the Dağhacılar, Köşüre and Karahisar sections exhibit maximum flooding zones in the studied stratigraphic columns (Keighley et al., 2003). In the Sünnet measured section, the intervening parasequences or depositional cycles of marine shelf fossiliferous oil-shale and carbonate, overlying the fluvio-lacustrine deposits exhibit relative sea-level rise and identified as flooding surface (Amorosi and Marchi, 1999; Miller and West, 2012) (Figures 7.5; 7.6). The appearance of biocalcirudite with abundant bivalve, gastropod and benthic foraminifera in the Sünnet section are identified as maximum flooding zones. Such types of lithofacies intervals are defined as upper boundary of the transgressive systems tract (Amorosi and Marchi, 1999; Miller and West, 2012). In the Sünnet section, the organic rich shale and calcareous sandstone with occasional carbonate deposit of the transgressive systems tract are overlain by period of highstand relative sea-level and are characterized by mixed siliciclastic and carbonate deposits of the Highstand systems tract (Figures 7.5; 7.6). Generally, in the studied sections, there is absence of condensed section intervals. Therefore, the oil-shale depositional cycles/parasequences stacking pattern deposits and/or carbonate assemblages in the studied sections are used to recognize the maximum flooding zones (Montañez and Osleger, 1993; Miller & West, 2012). The Transgressive systems tract in the studied sections are thicker than average intervals and are composed of relatively homogenous sediments and deposited in the deeper environmental condition (Figures 7.1; 7.2; 7.3; 7.4; 7.5; 7.6). The observed highstand systems tract (HST) successions in the Dağhacılar, Köşüre and Karahisar sections represent thinner than average intervals and are dominantly comprised of fine-grained turbiditic deposits and having high vertical heterogeneity (Figures 7.1; 7.2; 7.3; 7.4; 7.6) (Bohacs, Carroll, Neal, & Mankiewicz, 2000). In the studied basin, the tectonic uplift (İzmir-Ankara suture) in the south, lake level fluctuation, relative sea level rise, marine-incurion and sediment influx are responsible for the formation of such types of depositional systems tract in the marine-influence lacustrine environment and transgressive marine depositional environment.

## **7.2. Sequence stratigraphy framework in the Dağhacılar section**

The studied section begins with retrogradational parasequence pattern which is composed of limestone microfacies with interbedded marl and occasional fossiliferous oil-shale and identified as Early transgressive systems tract deposits. It is then pass to occasional limestone, dominate intervals of oil-shale with intercalated marl, and indicates transgressive systems tract successions within the system (Figure 7.1) (Gale et al., 2006; Huang et al., 2013). It is also supported by lack of coarser grains in this portion and implies low energy depositional condition (Jin et al., 2014).

The transition from dominated limestone units to oil-shale units with intercalated marl and rare calcareous sandstone units interpret transgressive systems tract deposits. The transgressive systems tract in the studied section is also evident by determination of high organic matter content in the black laminated to massive shale (Lazar, 2007). The deposits over the transgressive systems tract successions in the studied section are identified as the highstand systems tract deposits. The highstand systems tract deposits consist of predominantly aggradational-progradational parasequences pattern and composed of intercalated oil-shale-calcareous sandstone intervals with occasional marl facies (Figure 7.1). The intervals of calcareous sandstone units increase in number and thickness toward the top which indicates aggradational to progradational shift in the studied section deposits. According to Lazar (2007), the intervals composed of gray shales with intercalated sandstone beds can be interpreted as Highstand systems tract in the fine-grained sequence stratigraphy. The intercalated sandstone-oil-shale successions in the studied section explain the highstand systems tract with marine character which are linked to relative sea-level rise in the region (Ocakoglu et al., 2007, 2012; Sanjuan and Martín-Closas, 2012; Wei et al., 2017). The maximum flooding surfaces in the studied section is defined as maximum flooding zones. The maximum flooding zones in the studied section is characterized by upper

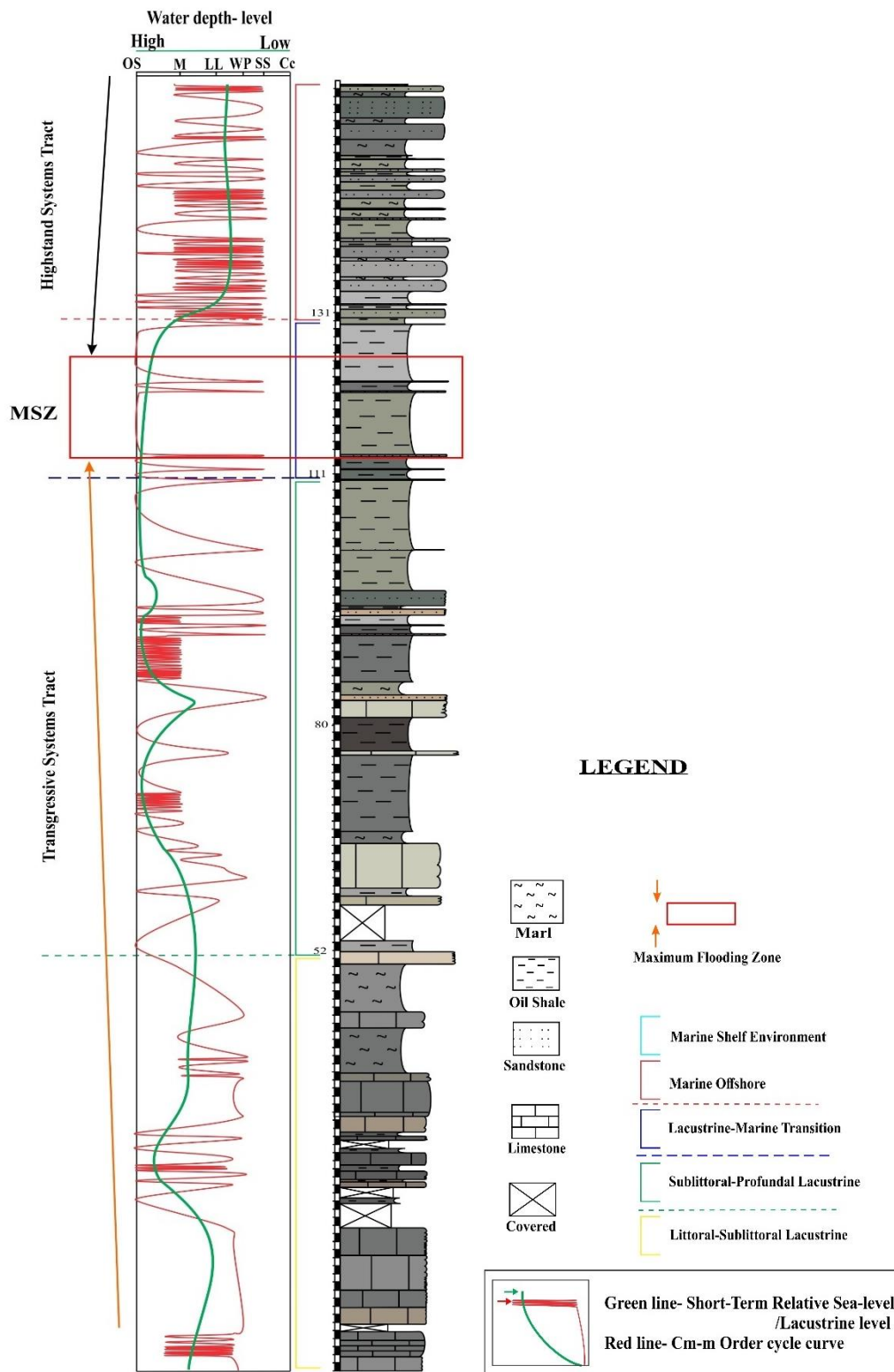


Figure 7.1. Sequence stratigraphic interpretation of the Dağhacılar section. (OS-oil-shale; M-marl; LL-Lime mudstone; Wp-wackestone-packstone; SS-sandstone; Cc-conglomeratic)

portion of sublittoral-profunda to transitional lacustrine-marine oil-shale intervals, which occur between the transgressive systems tract and highstand systems tract (Figure 7.1) (Wei et al., 2017). A maximum flooding zone is marked around 110m to 125m where observation of dominate oil-shales and from that point upward, progressively increasing calcareous sandstone intervals toward top (Figure 7.1). In addition, the above successions are also indicating absence of biofacies which support the parasequences of highstand systems tract (Wei et al., 2017).

### 7.3. Sequence stratigraphy framework in the Hasanlar section

The Hasanlar succession displays the retrogradational parasequence pattern. It is composed of limestone-marl and limestone-oil-shale cyclic deposits (Figure 7.2). The lime mudstone with interbedded oil-shale/marl lithofacies reflect transgressive system tract within the depositional succession (Huang et al., 2013).

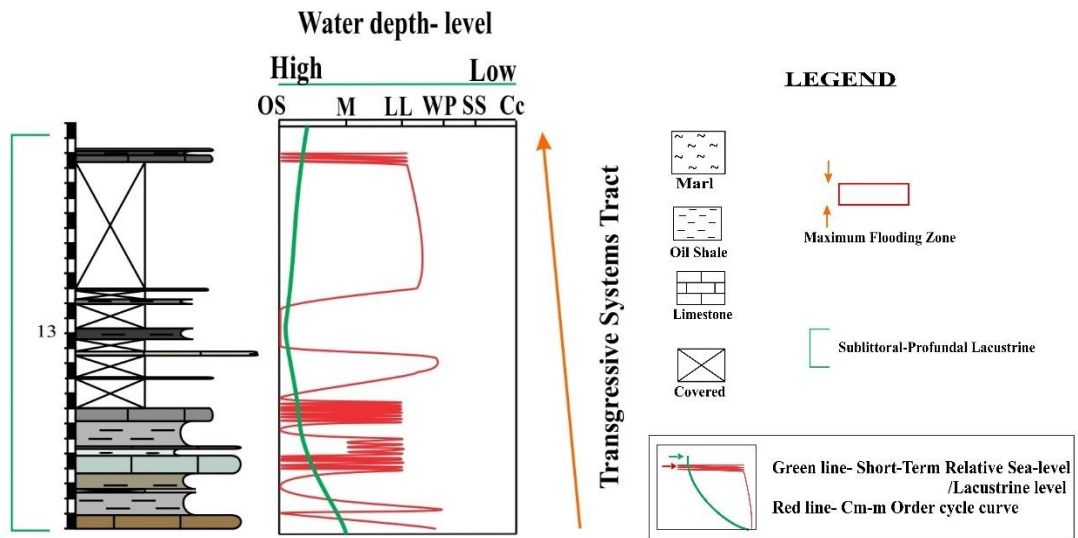


Figure 7.2. Sequence stratigraphic interpretation of the Hasanlar section. (OS-oil-shale; M-marl; LL-Lime mudstone; Wp-wackestone-packstone; SS-sandstone; Cc-conglomeratic)

#### **7.4. Sequence stratigraphy framework in the Kösüre section**

In the Kösüre stratigraphic column, the medium to thick limestone facies intervals with intercalated thin marly lithofacies and occasional calcareous sandstone lithofacies in the lower portion, pass vertically into the thick limestone-marl dominated successions with occasional presence of oil-shale intervals and calcareous sandstone lithofacies at different horizon indicate relative deepening in the lacustrine succession. As, the studied section display a shift from littoral-sublittoral lacustrine sub-environment to sublittoral-profundal lacustrine sub-environment. This change in depositional sub-environment in the Kösüre section reflect retrogradational-aggradational depositional stacking pattern and indicate transgressive systems tract deposits (Figure 7.3). The Transgressive systems tract in this portion of the studied succession is also supported by the presence of limestone of wackestone and packstone microfacies with interbedded marl and occasional shale facies deposits (Carlucci et al., 2014). The maximum flooding zones is placed within the lacustrine-marine transitional carbonate deposits which are overlain by the siliciclastic parasequences (Figure 7.3; 7.6). The successions within the lacustrine-marine transitional deposits in the studied section display aggradational depositional pattern. The above portion with marine depositional character indicates a shift from aggradation to progradational dominated siliciclastic intervals with oil-shale and occasionally limestone facies. This overlying portion describe the highstand systems tract in the studied section (Figure 7.3) (Carlucci et al., 2014; Wei et al., 2017). In the fine-grained sequence stratigraphy, the successions composed gray shales with intercalated sandstone beds can be defined as highstand systems tract (Lazar, 2007; Wei et al., 2017).

#### **7.5. Sequence stratigraphy framework in the Karahisar section**

The basal portion of the Karahisar section is identified by dominate oil-shale intervals with lime mudstone microfacies and acknowledged as transgressive systems tract (Figure 7.4). The oil-shale in the middle portion of the Karahisar sections are identified

as maximum flooding zones. This oil-shale with association of Fe-Mn carbonate deposits in the middle portion indicate marine transgression and define the lacustrine-marine transitional zone in the studied section. The overlying depositional cyclic

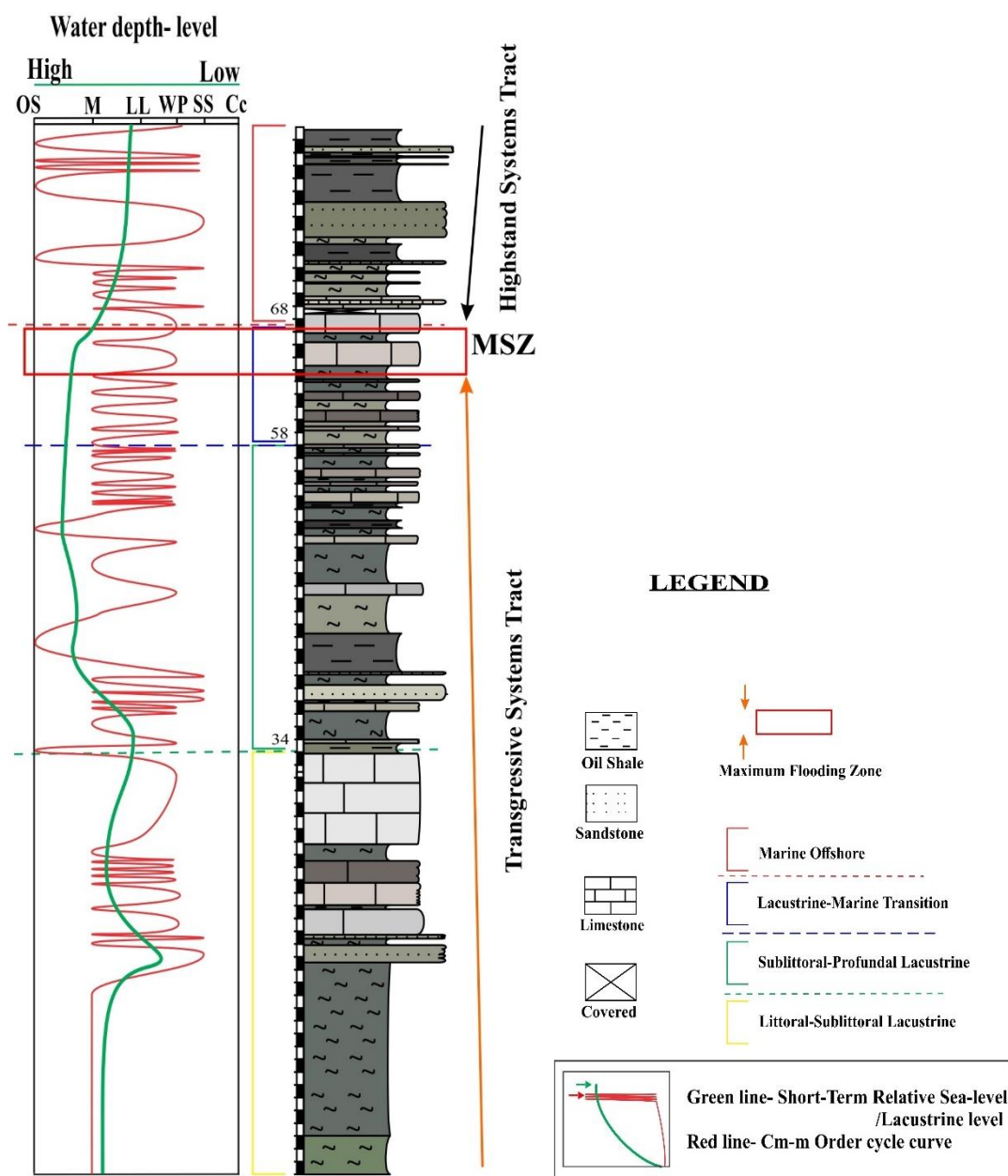


Figure 7.3. Sequence stratigraphic interpretation of the Kösiüre section. (OS-oil-shale; M-marl; LL-Lime mudstone; Wp-wackestone-packstone; SS-sandstone; Cc-conglomeratic)

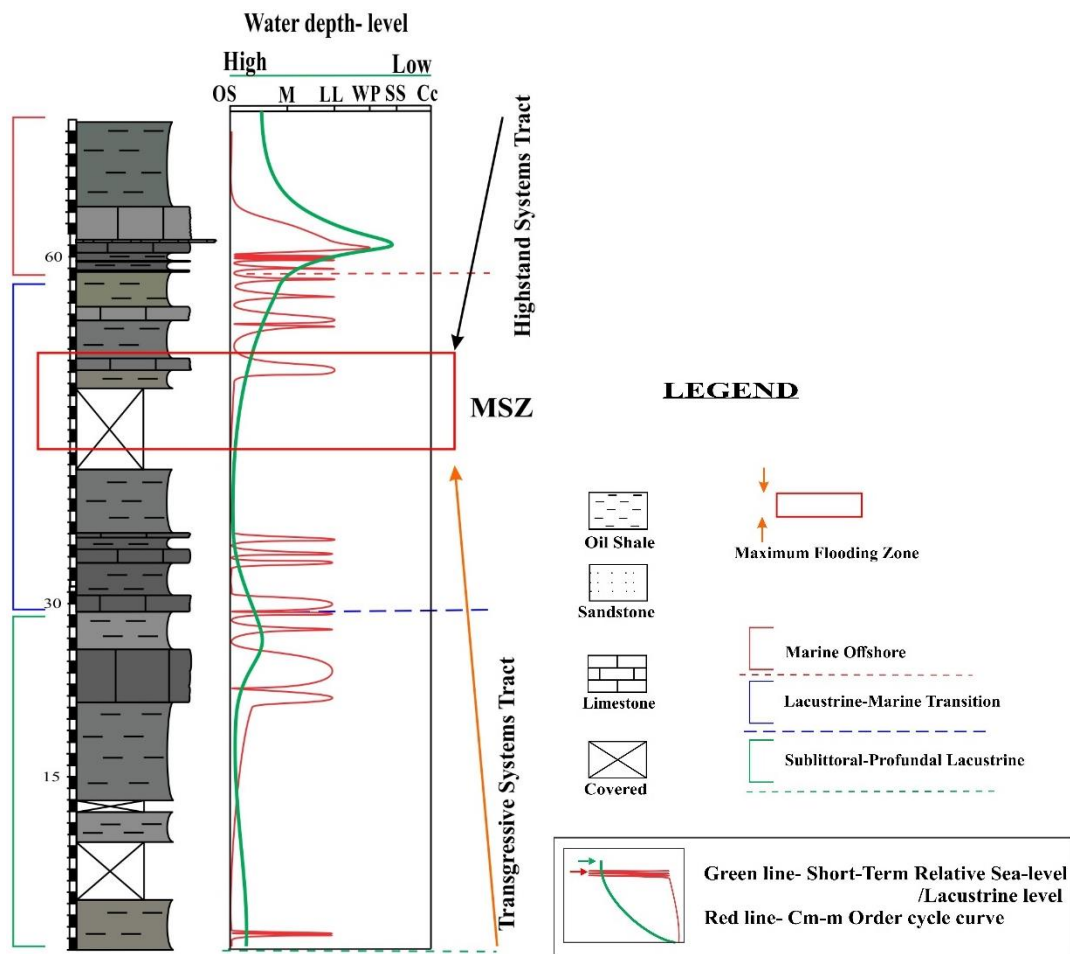


Figure 7.4. Sequence stratigraphic interpretation of the Karahisar section. (OS-oil-shale; M-marl; LL-Lime mudstone; Wp-wackestone-packstone; SS-sandstone; Cc-conglomeratic)

stacking pattern of the Karahisar section illustrate aggradational parasequence geometry by the oil-shale-lime mudstone intervals with rare calcareous sandstone lithofacies (Figure 7.4). Therefore, the overlying sequence above the maximum flooding zones oil-shale in middle portion of the studied stratigraphic column is characterized as highstand systems tract successions (Lazar, 2007).

## 7.6. Sequence stratigraphy framework in the Sünnet section

In the Sünnet sections, the basal portion is composed of coarser calcareous sandstone with occasional conglomerate, red calcareous fine sandstone and red and gray shale. This basal portion define fluvio-lacustrine floodplain deposits (Figure 7.5). These

deposits are interpreted as Lowstand systems tract deposits. It is overlain by calcareous sandstone with silty oil-shale, fossiliferous oil-shale and rare limestone having benthic bivalve, gastropods, rare Foraminifera which specifies coastal to shallow shelf/neritic environmental condition (Figure 7.5). Such retrogradational depositional pattern in the studied succession indicate marine transgression and interprets transgressive systems tract depositional sequence (Li et al., 2009).

In the upper middle portion of the studied section, the limestone successions are characterized by ostracod and gastropod. It has sharp contact with above bio-calcirudite (bio-rudstone) and overlying transgressive systems tract depositional sequence. The appearance of bio-calcirudite carbonate intervals in the measured succession indicate boundary between transgressive systems tract and highstand systems tract and identified as upper limit of the transgressive systems tract deposits. The appearance of bio-calcirudite carbonate intervals in the measured studied section interpret maximum flooding zones. The deposits overlain the maximum flooding zones are interpreted as Highstand systems tract deposits with progradational depositional stacking pattern (Figure 7.5). The Highstand systems tract deposits are comprised of calcareous sandstone units, bio-calcirudite (bio-rudstone) and pebbly conglomeratic beds. The calcareous sandstone intervals are overlain by eroded basal surface pebbly conglomeratic horizons. The introduction of later rudstone with association of abundant bivalvia, gastropod and benthic Foraminifera are associated with the highstand event in the studied section (Dix and Parras, 2014). Similarly, in the Black Sea, during Pliocene, the introduction of bivalvia to the basin, it was characterized as highstand event in the basin (Baak et al., 2015). The floodplain deposits are overlain by transgressive organic rich shale with occasional intercalating calcareous sandstone and limestone, changing upwards into shelf marine siliciclastic-bio-calcirudite deposits. This depositional sequence exhibits a rapid landward shift of marine depositional system during the Middle Eocene (Lutetian-Bartonian) and indicate relative sea-level rise in the measured Sünnet stratigraphic section for short period.

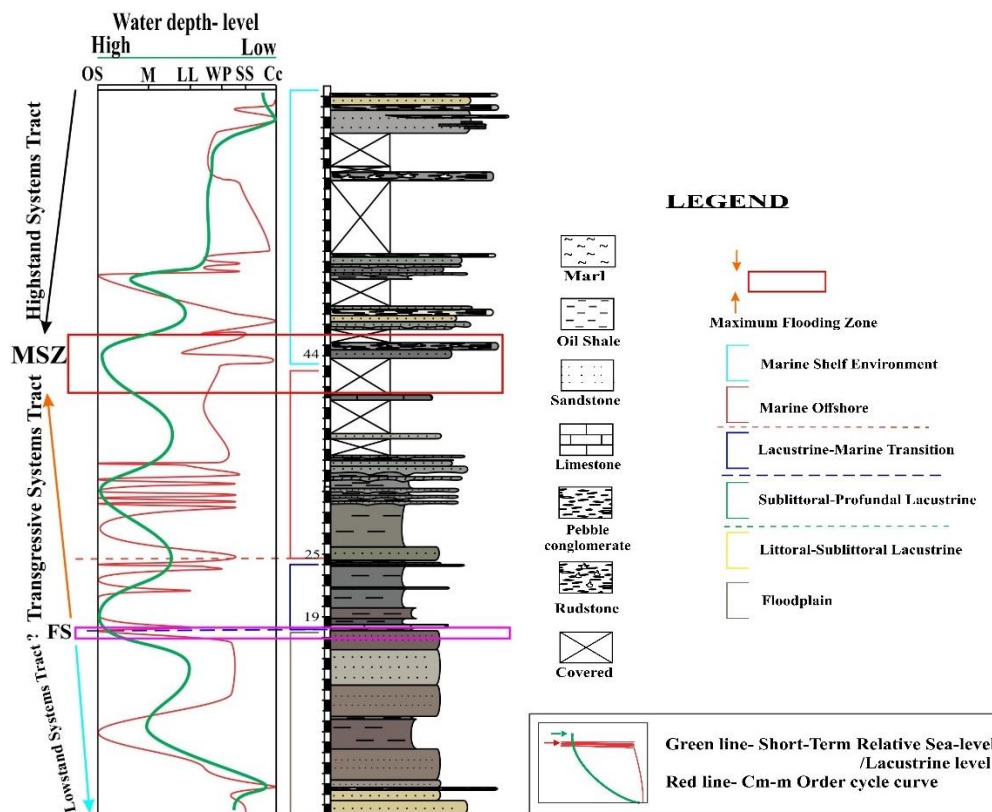


Figure 7.5. Sequence stratigraphic interpretation of the Sünnet section. (OS-oil-shale; M-marl; LL-Lime mudstone; Wp-wackestone-packstone; SS-sandstone; Cc-conglomeratic)

## 7.7. Sequence stratigraphic framework and correlation of the studied sections in the Basin

The sequence stratigraphic framework basically concerned with the depositional sequence record. In the depositional sequence, the formation of systems tract is related with available accommodation space for the sediment deposits and are determined with relative sea-level changes.

Sequence stratigraphic framework in the studied basin is figured out on the basis of sedimentology, depositional cyclic pattern and parasequence geometry in the sediments within the Middle Eocene (Lutetian-Bartonian) measured stratigraphic successions. Generally, the successions in the studied sections are recognized as

transgressive systems tract and highstand systems tract deposits (Figure 7.6). The lowstand systems tract is identified only in the Sünnet Section (Figure 7.6). The documented relative sea-level curve in the studied successions are comparatively fit within Middle Eocene (Lutetian-Bartonian) global sea level curve of Haq et al. (1987) (Figure 7.7).

The spatial depositional system packages and systems tracts geometry varies significantly within depositional sequences. The depositional system packages and systems tracts formed in the different phases of the basin evolution. The identified systems tract geometry stacking pattern and major surfaces in the studied sections are as below;

#### **7.7.1. Lowstand Systems Tract (LST)**

The LST are defined by the depositional stacking patterns that occur after the onset of the relative sea level rise (Posamentier and Allen, 1999). The Lowstand systems tract in the Sünnet section is characterized by siliciclastic deposits of fluvio-lacustrine deposits (Figures 7.5; 7.6) (Sun et al., 2014a; Ma et al., 2015).

#### **7.7.2. Flooding Surfaces (FS)**

The Flooding surfaces define first significant flooding interval in the successions, which occurs between the lowstand systems tract and transgressive systems tract (Bohacs and Schwalbach, 1992). In the Sünnet studied section, the flooding surface is placed between the fluvio-lacustrine siliciclastic deposits and overlying organic rich shale and calcareous sandstone transgressive systems tract deposits (Figures 7.5; 7.6) (Amorosi and Marchi, 1999).

#### **7.7.3. Transgressive Systems Tract (TST)**

The transgressive systems tract is comprised of depositional successions which are deposited in the period of rapid relative sea level rise and display retrogradational or deeper depositional stacking pattern (Bohacs and Schwalbach, 1992; Posamentier and Allen, 1999; Catuneanu, 2002, 2006). In the Dağhacılar, Hasanlar, Kösüre and

Karahisar successions, the transgressive systems tract is characterized by limestone units, limestone units with the interbedded marl and oil-shales-marls depositional stacking pattern (Figures 7.1; 7.2; 7.3; 7.4; 7.6). They are deposited in the littoral-sublittoral to sublittoral-profundal lacustrine to marine transitional depositional environment, respectively (Figures 7.1; 7.2; 7.3; 7.4; 7.6). In the Sünnet section, the transgressive systems tract is identified by a transgression from fluvio-lacustrine siliciclastic deposits to fossiliferous oil-shale with occasional interbedded limestone unit and calcareous sandstone of the marine shelf deposits (Figures 7.5; 7.6). In the transgressive systems tract, the depositional stacking pattern are generally thick interval and illustrate retrogradational stacking pattern in the studied depositional successions (Figure 7.6).

The overlying oil-shales with increasing intercalated sandstone interval and occasional marl lithofacies in the Dağhacılar section and Kösüre section are construed as the transition to highstand condition. In the Karahisar section, the transition to highstand condition is marked by changing to calcareous oil-shale with frequent thin interbedded limestone units (Figures 7.1; 7.2; 7.3; 7.4; 7.6) (Schwarz and Howell, 2005). The transition to highstand condition in the Sünnet section is characterized by appearance of bio-calcirudite (*Bivalvia rudstone*) and overlying sandstone intervals within measured section (Figures 7.5; 7.6).

#### **7.7.4. Maximum Flooding Zones (MFZ)**

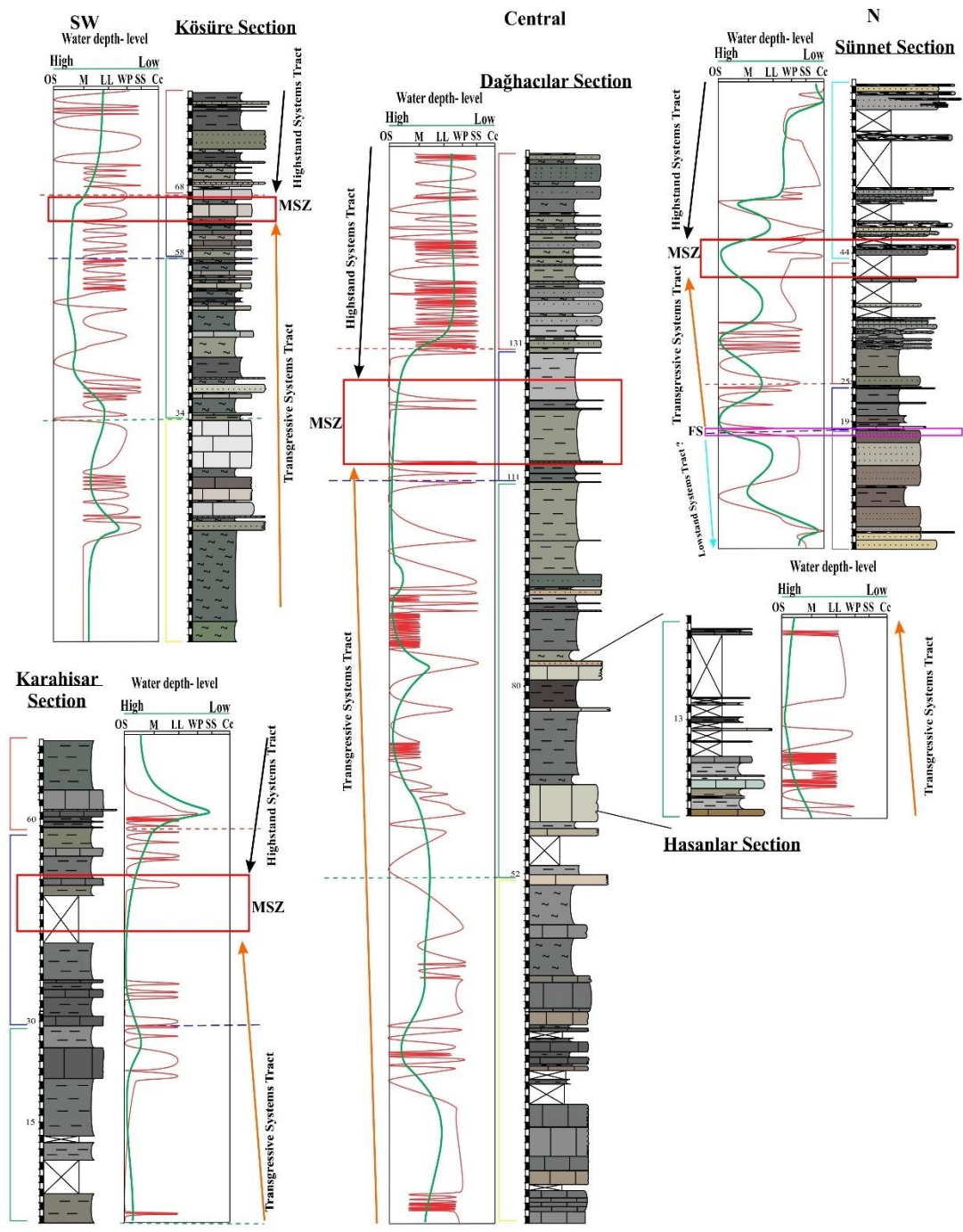
The maximum flooding zones indicate maximum landward progression of the marine/lacustrine water within a depositional succession (Posamentier et al., 1988; Van Wagonar et al., 1988; Bohacs and Schwalbach, 1992). The below and above this surface, the depositional stacking pattern shift from retrogradational to aggradational-progradational pattern, respectively (Bohacs and Schwalbach, 1992; Bohacs, 1998; Catuneanu, 2002, 2006). In the study, maximum flooding zone terminology is used instead of maximum flooding surface. As, maximum flooding zone in the studied successions does not show any of the features related with condensed section such as

diagenetic mineral enrichment, burrowed surfaces or fossil concentration (Holland and Patzkowsky, 1998). The fossil concentration is observed only in Kösüre section and Sünnet section, which are defining maximum flooding zones with association of fossil concentration. In the studied sections, the maximum flooding zones are recognized within transitional lacustrine-marine organic rich shale deposits and/or carbonate which are overlain by siliciclastic deposits of marine depositional environment (Figures 7.1; 7.2; 7.3; 7.4; 7.5; 7.6) (Montañez and Osleger 1993; Pasquier and Strasser 1997; Holland and Patzkowsky, 1998; Keighley et al., 2003; Martínek et al., 2006). In case of lacking or absences of oil-shale, the maximum flooding zones is also interpreted in the zones where immediately placing of siliciclastic parasequence over the carbonate parasequence. The above siliciclastic parasequences in the studied sections define the portion of highstand systems tract (Keighley et al., 2003). In the Dağhacılar section, Kösüre section and Karahisar section, the maximum flooding zones is associated with lacustrine-marine transitional depositional zone which is onset of marine environment transgression and indicate a change in the depositional environment from lacustrine to marine depositional environment (Figures 7.1; 7.3; 7.4; 7.6). The maximum flooding zones deposits within lacustrine-marine transitional deposits indicate maximum relative sea-level landward shift in the region. Thereafter, the lacustrine environmental condition is replaced by marine environmental condition in the studied region from north to south. In the Sünnet section, the maximum flooding zones is defined by the appearance of abundant bivalve, gastropod and benthic foraminifera bearing rudstone and interpreted as extensive fossil lag deposits and indicate a change from the proximal siliciclastic to distal shelly-rich horizons (Figures 7.5; 7.6) (El-Azabi, 2006; Oçakoğlu et al., 2007; Dix and Parras, 2014).

#### **7.7.5. Highstand Systems Tract (HST)**

The highstand systems tract is defined as set of aggradational-progradational depositional stacking pattern which occur after the maximum flooding zones and related with end of the relative sea level rise or gradual beginning part of the relative

sea level fall (Hunt and Tucker 1995; Neal and Abreu, 2009; Abreu et al., 2010). In the highstand systems tract, the parasequence stacking pattern display aggradation to progradational pattern (Bohacs and Schwalbach, 1992; van Wagoner et al. 1988; Bohacs, 2006; Catuneanu, 2006). The presence of organic rich shale- calcareous sandstone and occasional calcareous sandstone-marl intercalation with association of sharp contact, occasional hummocky cross stratification and wavy rippled, indicate the influence of highstand systems tract in the studied successions of the Dağhacılar, Köşüre and Karahisar measured sections (Peters et al., 2009; Rivandi et al., 2013). In general, in these studied sequences, the highstand systems tract are characterized by the presence of dominate intervals of calcareous sandstone lithofacies with intercalating oil-shale and occasionally marlly intervals (Figures 7.1; 7.2; 7.3; 7.4; 7.5; 7.6) The calcareous sandstone with intercalating oil-shale and occasionally marlly intervals in the upper portion of the studied sections are generally recognized as marine influence environmental deposits. These sandstone-dominated intervals exhibit aggradational to progradational stacking pattern in the Dağhacılar, Köşüre and Karahisar studied successions (Figure 7.6). The highstand systems tract deposits are composed of relatively thin to medium intervals of turbiditic sandstones of lacustrine to marine offshore transitional deposits in the Dağhacılar, Köşüre and Karahisar studied successions (Figure 7.6) (Lin et al., 2001; Dix and Parras, 2014). In the Sünnet section, the highstand systems tract depositional sequence is comprised of coarser sandstone intervals with occasional pebbly conglomeratic horizons and calcirudite and are representing progradational stacking pattern (Figures 7.5; 7.6). Generally, the rudstone (calcirudite) with abundant bivalve, gastropod and benthic foraminifera in the Sünnet section are interpreted as rapid relative sea-level rise and are overlain by calcareous siliciclastic deposits (Figures 2.47; 3.37; 7.6). It is interpreted as the depositional sequence of the highstand systems tract with progradational stacking pattern (El-Azabi, 2006; Dix and Parras, 2014; Paredes et al., 2015).



SE

Figure 7.6. Correlation of the sequence stratigraphic interpretation of the studied sections and relative change of the sea-level/lacustrine level in the studied sections. (FS-flooding surface; MFZ-maximum flooding zones; OS-oil-shale; M-marl; LL-Lime mudstone; Wp-wackestone-packstone; SS-sandstone; Cc-conglomeratic)

## LEGEND

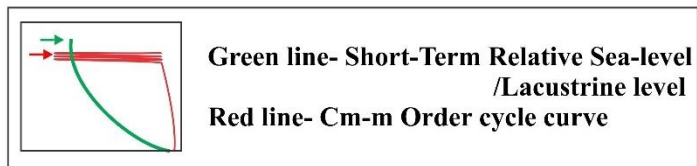
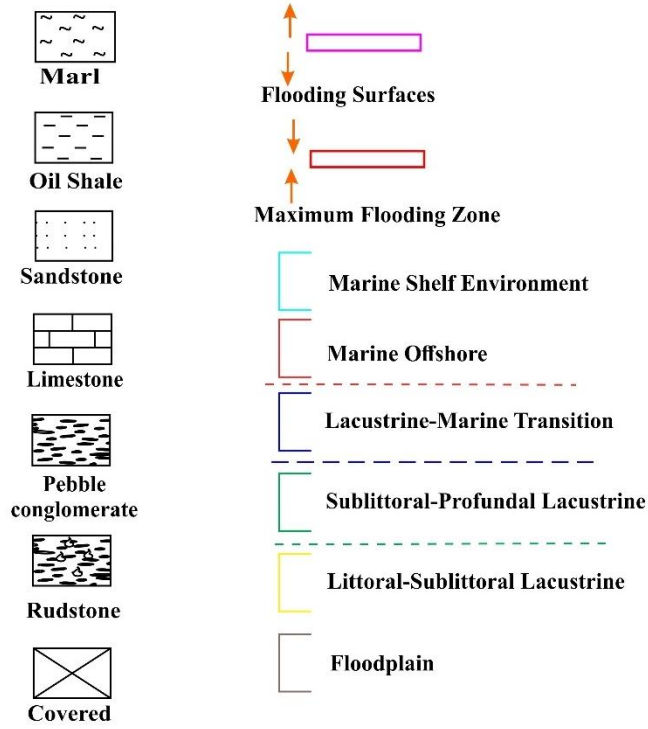


Figure 7.6. Continued.

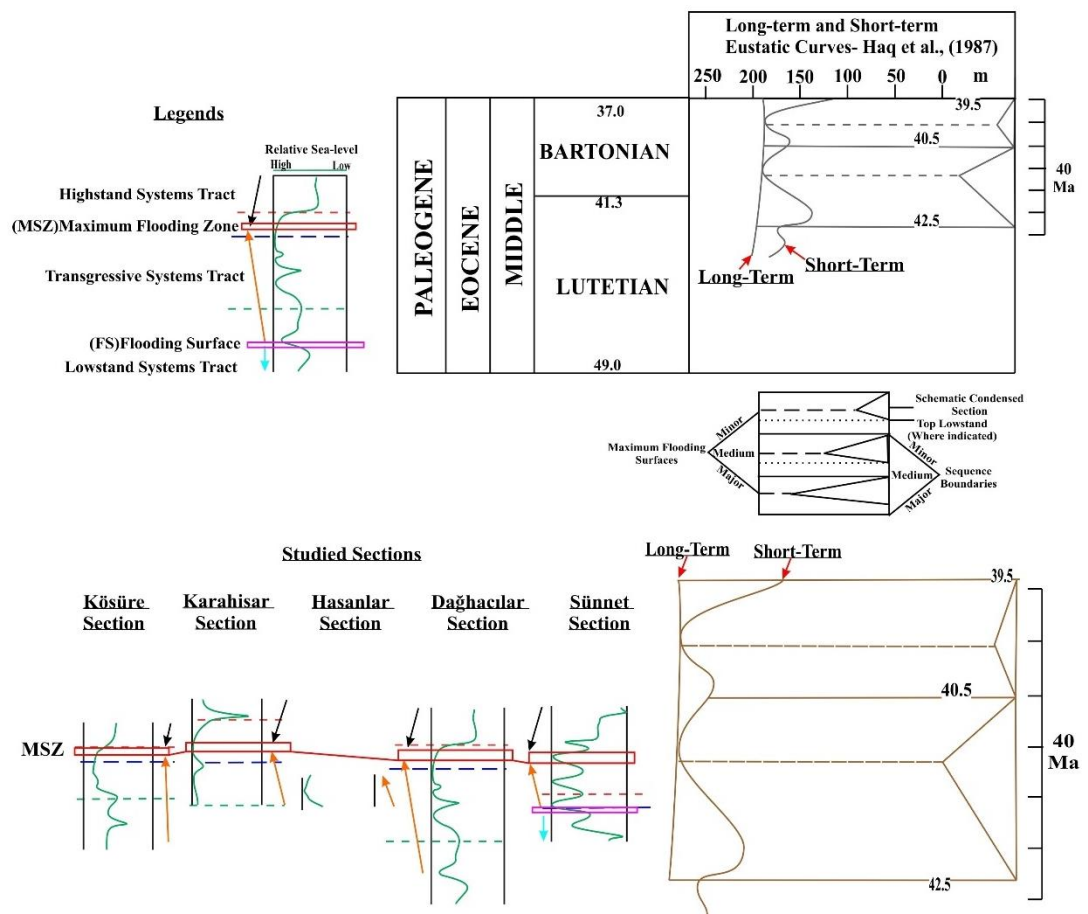


Figure 7.7. Correlation of Sequences and maximum flooding zones between the studied sections and with Eustatic Sea-level Curve chart (Haq et al., 1987).



## CHAPTER 8

### GEOCHEMICAL ANALYSES AND HYDROCARBON DEPOSITS

#### 8.1. Introduction

The organic-rich deposits are generally deposited in the different environmental conditions, either lacustrine or brackish or marine depositional environment. Generally, the most favorable condition for the deposition of organic-rich facies is anoxic lacustrine environment (Wartes et al., 2000; Martínek et al., 2006; Lyons et al., 2011; Tänavsuu-Milkeviciene et al., 2017). It has been documented that the well preserved organic-rich facies mostly occur in the deep, fresh to the alkaline lacustrine environment. Such conditions are formed during the humid and warm climate intervals and are associated with transgressive phases depositional condition (Martínek et al., 2006; Lyons et al., 2011; Tänavsuu-Milkeviciene et al., 2017). In terms of oil-shale, some of the largest and richest oil-shales have been reported from the large lacustrine basins such as Green River Formation of Eocene age in the western United States, the Albert Shale of Early Carboniferous (Mississippian) age in New Brunswick, Canada, and Cenozoic deposits in Europe and Asia. Organic-rich facies of lacustrine and marine deposited are correspondingly important source rock and unconventional reservoir rock (Bruhn, 1999; Carroll and Bohacs, 2001; Bohacs et al., 2003; Wang et al., 2011; Ma et al., 2015; Ma et al., 2016). In the studied sections, organic-rich facies were deposited in two sets during the Middle Eocene time, including the lacustrine and marine member. Firstly, the transgressive phase in the lacustrine environment deposited the organic-rich deposits, and then followed by another transgressive phase having organic-rich deposits are related to marine incursion to the lacustrine depositional condition in the studied sections. Therefore, the organic-rich facies are not only observed in a lacustrine environment in the studied sections but also associated with the marine conditions in the upper portion of the

studied sections (Figures 8.3; 8.7; 8.11; 8.15 and 8.19). The presence of high organic content in the marine successions is related to a change in the physiochemical condition, which is occurred during the transgression of the marine environment to a lacustrine environmental condition (Mingram, 1998). Generally, the organic-rich deposits with the alkaline character in the lacustrine and in the marine environment are likely to be richer in organic matter content (Yen and Chilingarian, 1976). According to Bohacs et al. (2000), more than 20 percent of the world's hydrocarbon production is probably related to lacustrine deposits.

The aim of this chapter is to study the organic content in the Middle Eocene facies, their relationship with other minerals (inorganic matter) and their source rock characteristics. In the studied sections, the organic-rich character is possessed by marl, carbonate and predominantly oil-shale, and defined as hydrocarbon deposits or oil-shale. The term "Oil-shale" in this chapter is not only restricted to the shale lithofacies. It also includes the sedimentary rock such as carbonate and marl which have immature high organic content and can yield the oil through destructive distillations or pyrolysis (Tissot and Welte, 1984; Suárez-Ruiz et al., 2012; Sun et al., 2013; Alali et al., 2015).

## **8.2. Minerals and Organic Matter**

The dominant constituents throughout the Middle Eocene studied sections are carbonate, organic matter, clay materials, and quartz/feldspar, based on the microscopic studies and geochemical analysis (Tables 3.2; 3.7; 3.9; 3.12; 3.15; Appendices A1; A2; A3; A4; A5; A6; A7; A8; A9; A10). The organic matter and minerals component (inorganic matter) are varying in their chemical and physical properties, which depends on the physical, chemical and biological processes that occur during the depositional setting. As a result, a series of organic matters and minerals association are formed. Therefore, the study of organic matter and their association with minerals are important to analyze their different interaction in the oil deposits facies (Zeng et al., 2018). In this study, the organic matter and minerals component (inorganic matter component) are studied to recognize individual character,

their relationship and source rock character in the limestone facies, marl facies and oil-shale facies (Figures 8.3; 8.5; 8.8; 8.9; 8.11; 8.12; 8.13; 8.15; 8.16; 8.17; 8.19; 8.20; 8.21; 8.22; 8.23; 8.24; 8.25; 8.26; 8.27; 8.28; 8.29; 8.30; 8.31; 8.33). The studied sections display distinct mineral and organic matter composition (Tables 8.1; 8.2; 8.3; 8.4; 8.5; Appendices A2; A4; A6; A8; A10; Figures 8.28; 8.29; 8.30; 8.31). The average carbonate content is highest in the Dağhacılar section and lowest in the Sünnet section. The average clay content is highest in the Karahisar section and lowest in the Sünnet measured section; The average weight percent of quartz/feldspar content are highest in the Sünnet section and lowest in the Kösüre studied sections (Figures 8.21; 8.28; 8.30; 8.31). The average organic matter content decreases from high to low in the Karahisar section> Hasanlar section> Sünnet section> Dağhacılar section> Kösüre section, respectively (Tables 8.1; 8.2; 8.3; 8.4; 8.5; Figures 8.2; 8.5; 8.8; 8.11; 8.14; 8.21; 8.29).

### **8.2.1. Carbonate Content in the Studied Sections**

Generally, high calcareous and siliceous minerals content lithofacies possesses brittle character and susceptible to fracturing (Jiang et al., 2015; Tingwei et al., 2017). The calcareous and/or siliceous content in the lithofacies should be more than 40% to achieve the brittleness character. It is interpreted that the carbonate-rich lithofacies (oil-shale, marl and limestone) are of particular interest, as they include some of the high-grade oil deposits accumulation (Yen and Chilingarian, 1976). In this study, the observed carbonate content in the lithofacies of measured sections are mostly higher than 40% (Figures 8.2; 8.5; 8.8; 8.11; 8.14; 8.21). The carbonate content in the Dağhacılar measured section is ranging from 21 wt.% to 89.03 wt.% with an average of 56.42 wt.% (Appendices A2). In terms of lithofacies, the packstone microfacies show high carbonate content around 78.43wt.% average value, then followed by wackestone (76.13wt.% average value)> lime mudstone (71.06wt.% average value)> oil-shale (51.71 wt.% average value)> marls (38.28 wt.% average value) (Table 8.1; Figure 8.2). The littoral-sublittoral successions in the Dağhacılar section represent

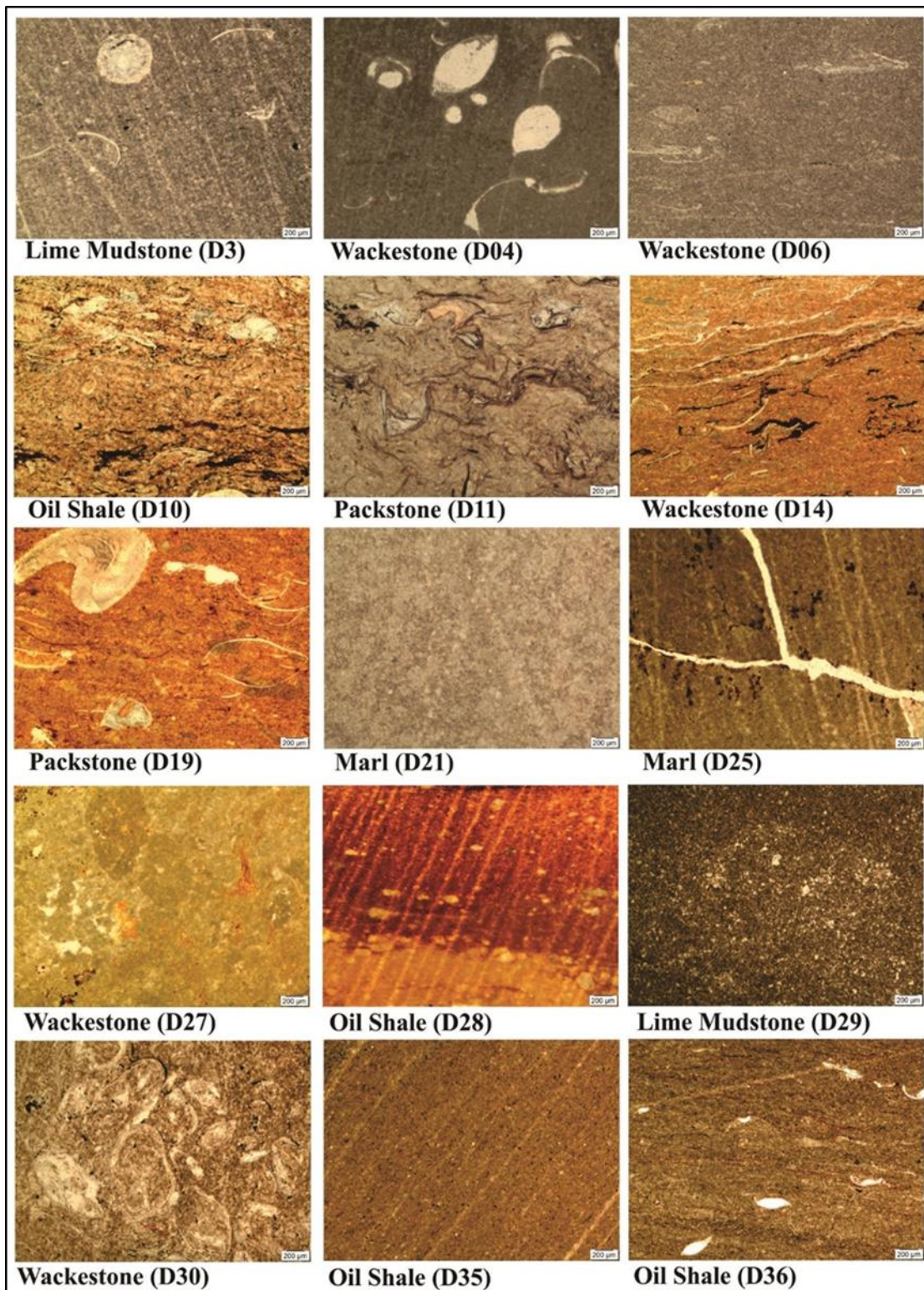


Figure 8.1. Photomicrographs of the Dağhacılar lithofacies, examined for chemical analysis (PPI, x4).

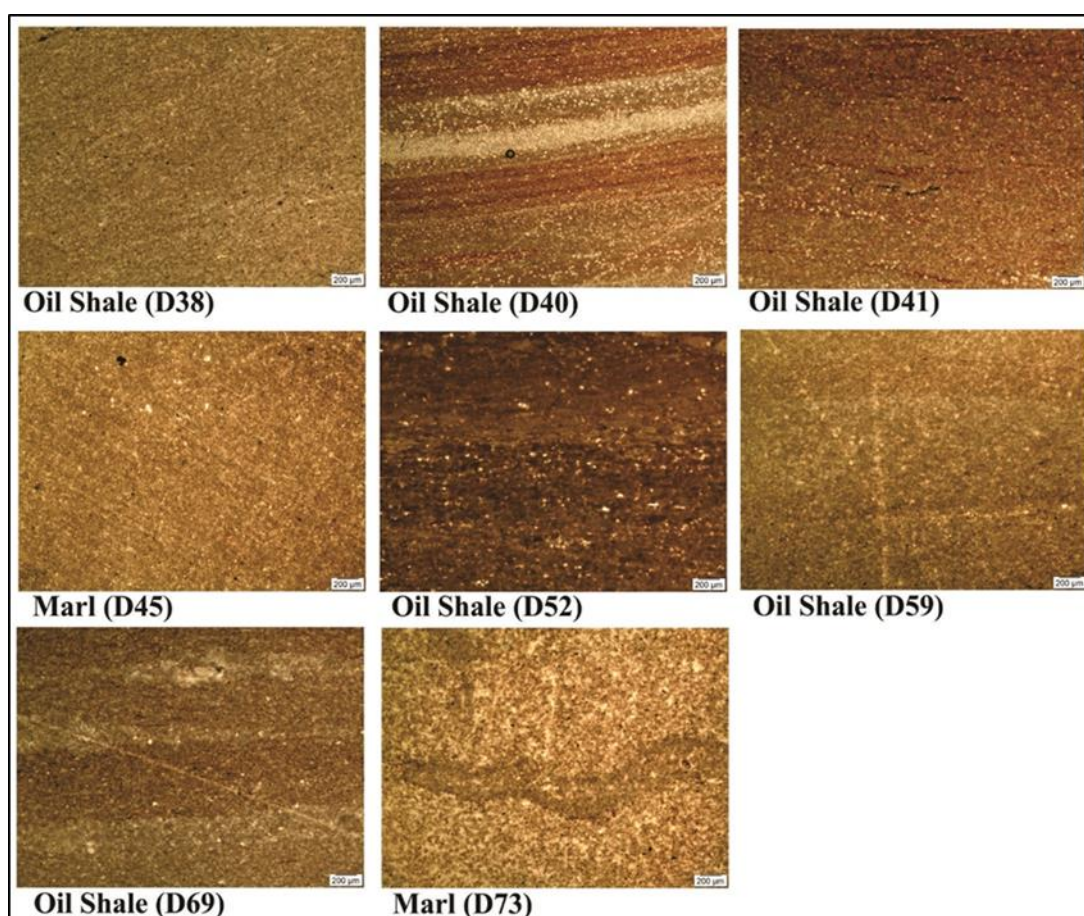


Figure 8. 1: Continues...

Table 8.1. The minimum, maximum and average weight percent values of lithofacies from the Dağhacılar measured section.

Lithofacies	% Weight carbonate			% Weight Organic Matter			% Weight Clay			% Weight Quartz/Feldspar		
	Min	Max	Average	Min	Max	Average	Min	Max	Average	Min	Max	Average
Lime Mudstone	54.37	88.33	71.06	4.49	13.47	8.09	9.18	39.16	19.73	0.00	3.50	1.13
Wackestone	61.80	89.03	76.13	8.71	18.28	10.58	2.48	22.92	12.95	0.00	2.00	0.33
Packstone	61.55	81.08	78.43	8.27	12.35	8.56	10.63	28.11	18.76	0.00	1.00	0.25
Marl	16.00	63.95	38.28	8.91	16.42	9.65	10.60	68.45	37.27	0.00	60.10	16.42
Oil-shale	24.78	77.86	51.71	3.30	18.99	11.90	0.00	67.23	23.92	0.00	53.57	14.96
Overall Section	16.00	89.03	58.42	3.30	18.99	10.55	0.00	68.45	24.04	0.00	60.10	10.47

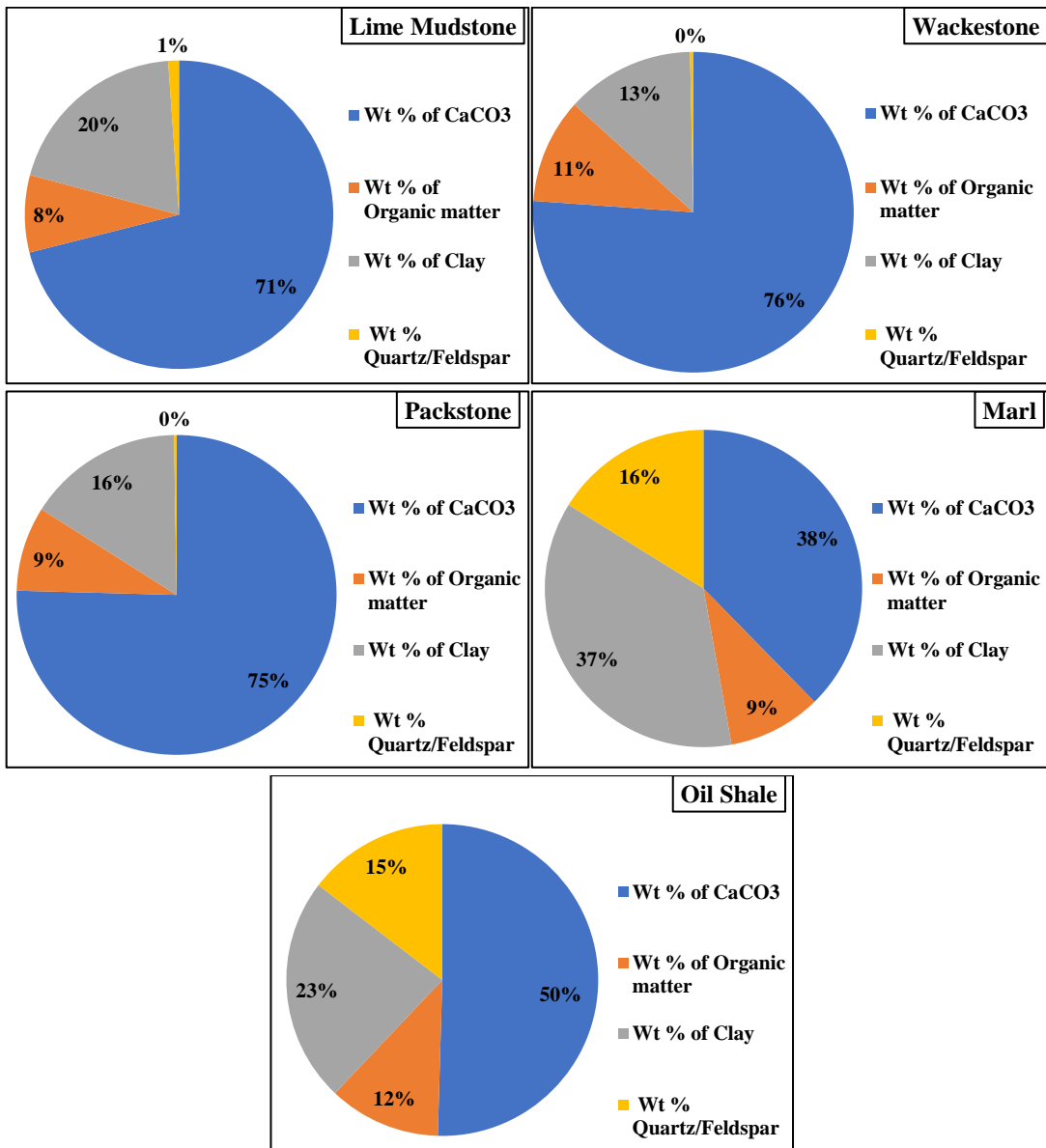


Figure 8.2. The pie chart of average weight percent values of lithofacies from the Dağhacılar measured section.

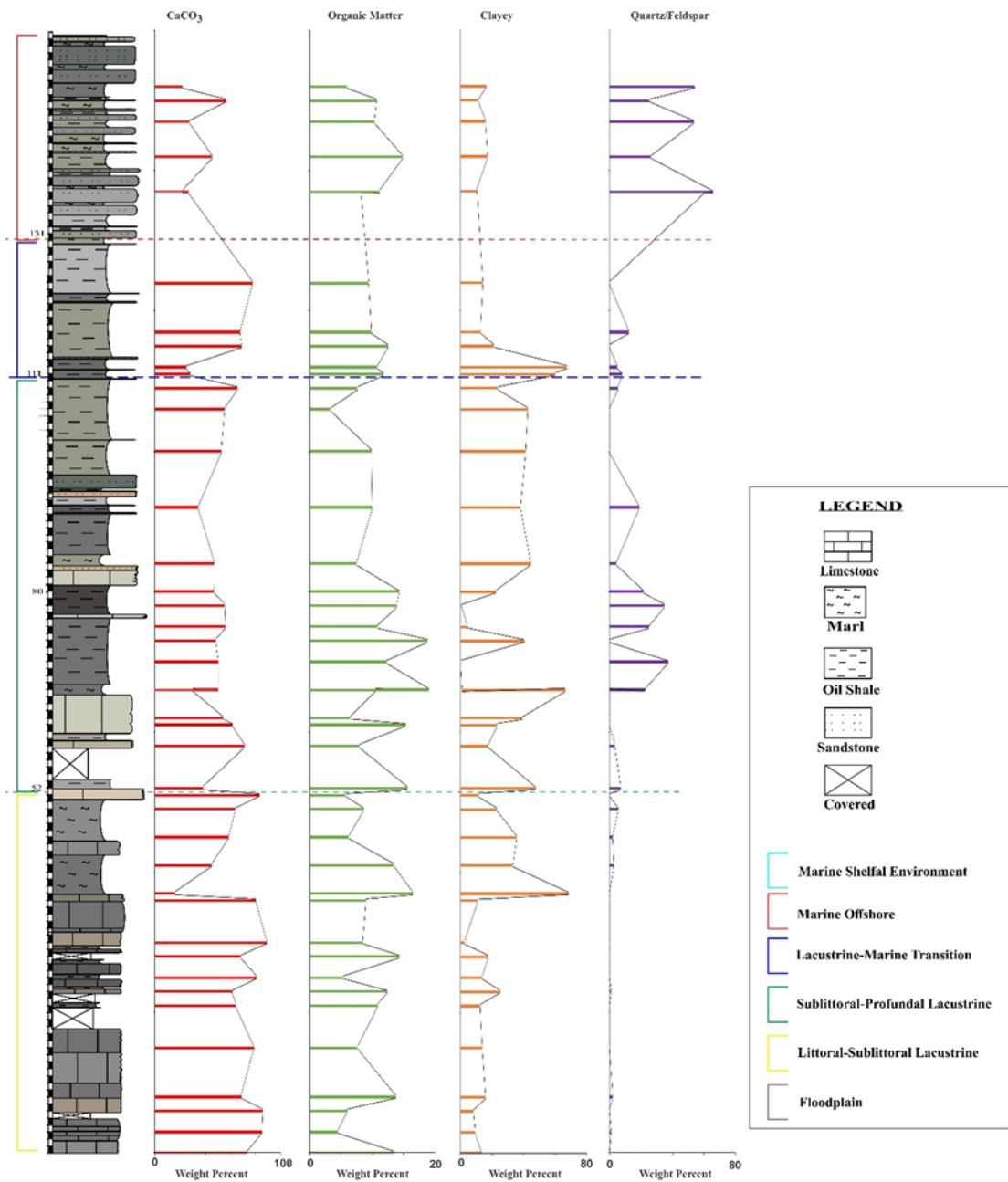


Figure 8.3. Representing the Dağhacalar measured stratigraphic log and graphical representation of geochemical analysis data of weight percent CaCO<sub>3</sub>, organic matter, clay and quartz/feldspar and their comparison along the measured stratigraphic log.

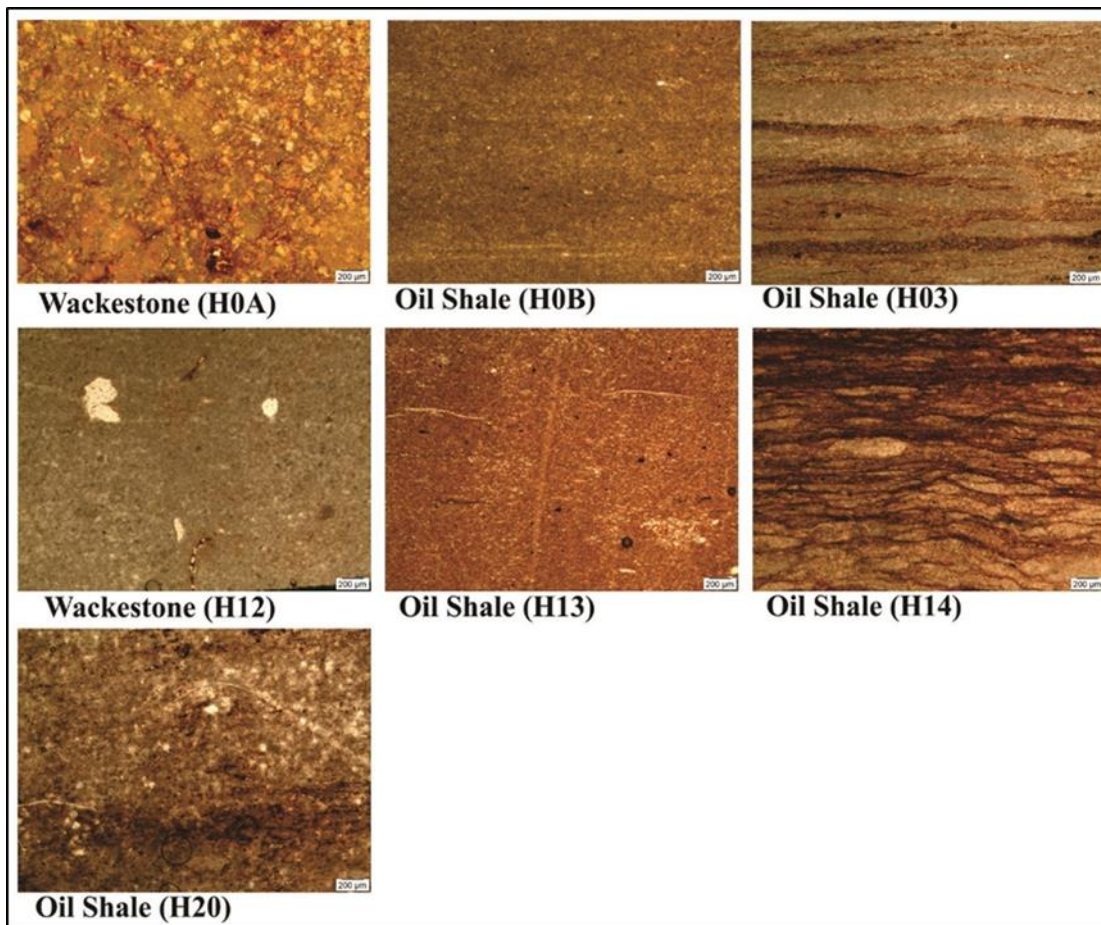


Figure 8.4. Photomicrographs of the Hasanlar lithofacies, examined for chemical analysis (PPI, x4).

Table 8.2. The minimum, maximum and average weight percent value of lithofacies from the Hasanlar section.

Lithofacies	% Weight carbonate			% Weight Organic Matter			% Weight Clay			% Weight Quartz/Feldspar		
	Min	Max	Average	Min	Max	Average	Min	Max	Average	Min	Max	Average
Lime Mudstone	44.27	64.70	54.49	7.74	11.66	9.70	21.64	47.99	34.82	0.00	2.00	1.00
Wackestone	7.31	79.32	43.31	7.85	14.26	11.06	12.83	78.43	44.13	0.00	3.00	1.50
Oil-shale	18.43	76.45	53.35	8.31	16.39	12.87	4.95	51.87	26.96	0.00	28.57	8.08
Overall	7.31	79.32	51.86	8.31	16.39	12.04	12.83	78.43	31.13	0.00	28.57	28.57

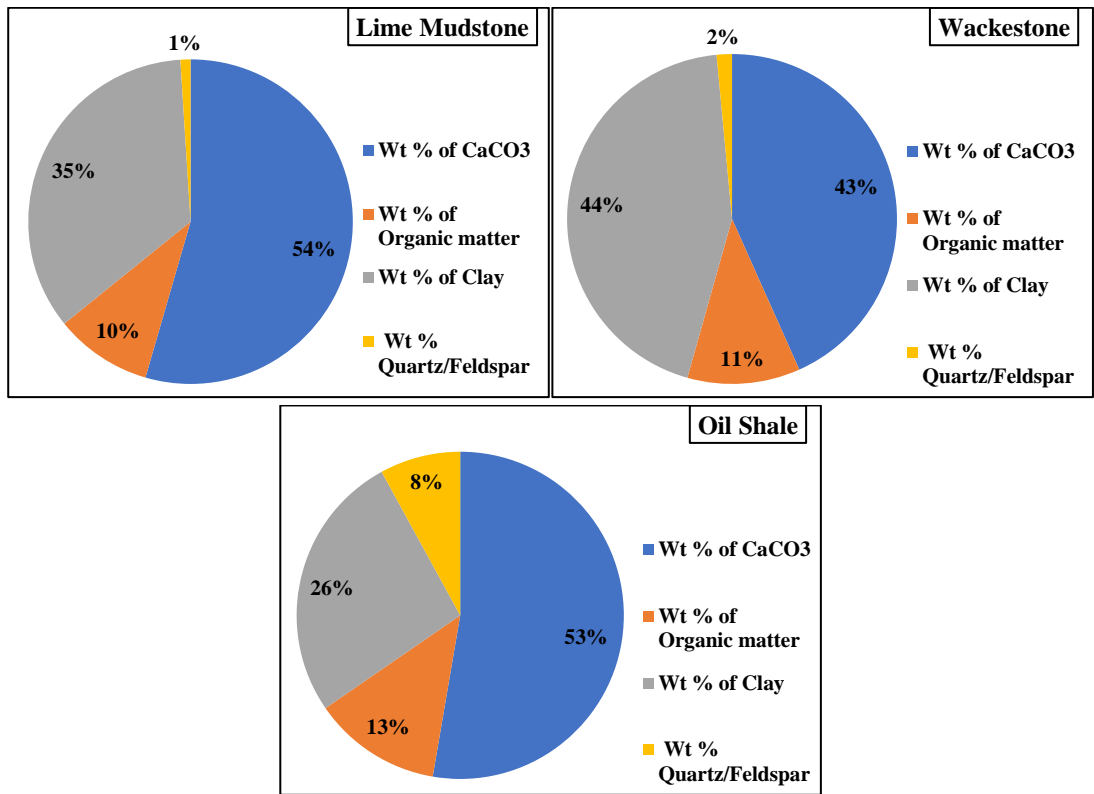


Figure 8.5. The pie chart of average weight percent values of lithofacies from the Hasanlar measured section.

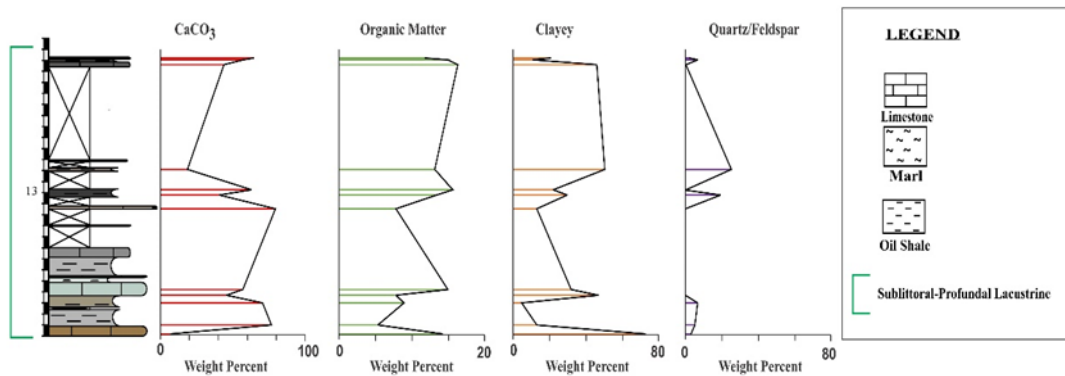


Figure 8.6. Representing the Hasanlar measured stratigraphic log and graphical representation of geochemical analysis data of weight percent CaCO<sub>3</sub>, Organic Matter, Clay and Quartz/feldspar and their comparison along the measured stratigraphic log.

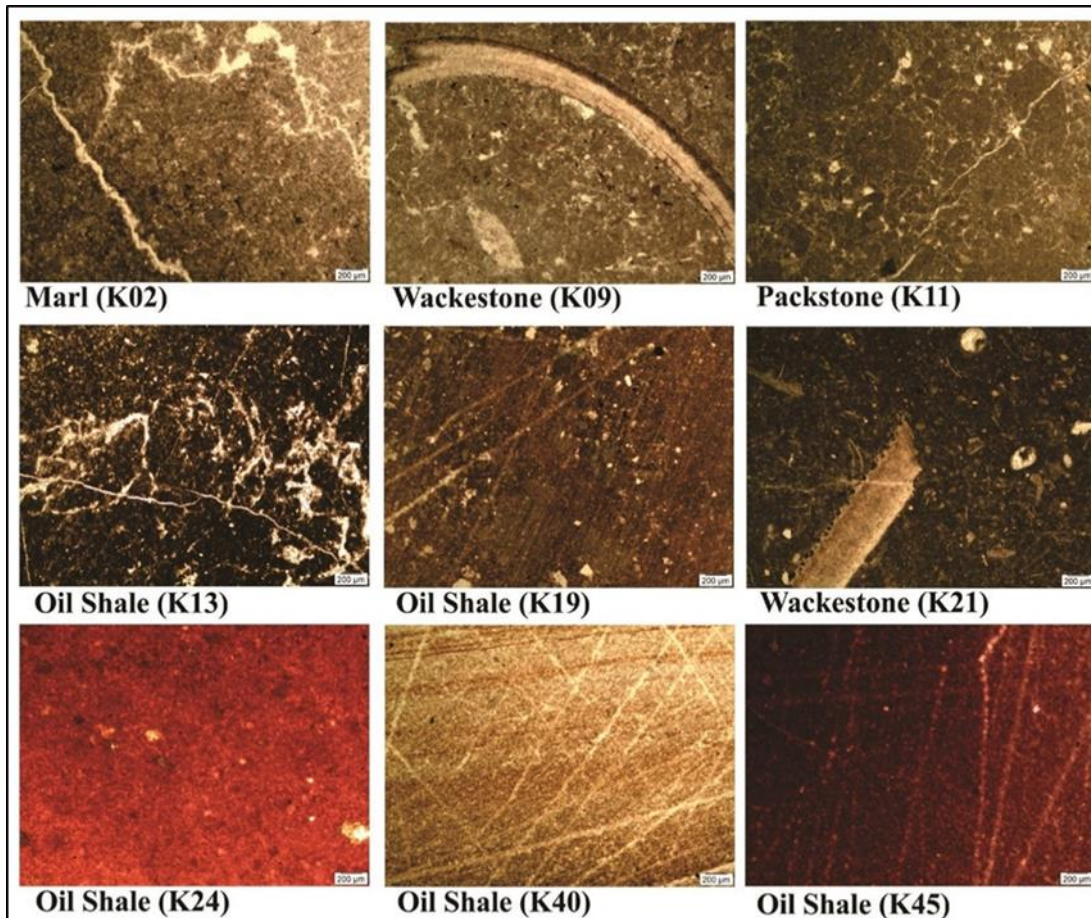


Figure 8.7. Photomicrographs of the Kösiire lithofacies, examined for chemical analysis (PPL, x4).

Table 8.3. The minimum, maximum and average weight percent data of lithofacies from the Kösiire measured section.

Lithofacies	% Weight Carbonate			% Weight Organic Matter			% Weight Clay			% Weight Quartz/Feldspar		
	Min	Max	Average	Min	Max	Average	Min	Max	Average	Min	Max	Average
Wackestone	42.18	92.66	78.74	2.43	11.46	6.77	3.10	47.65	14.49	0.00	0.00	0.00
Packstone	84.57	90.44	87.50	4.94	8.42	6.68	4.63	7.01	8.82	0.00	0.00	0.00
Marl	33.11	64.48	49.57	8.49	17.10	10.62	21.88	63.86	39.03	0.00	18.69	4.74
Oil-shale	17.72	47.55	31.79	0.35	18.99	10.26	39.10	78.66	58.73	1.37	20.92	8.28
Overall	17.72	92.66	53.93	0.35	18.99	8.29	3.10	78.66	39.72	0.00	20.92	1.18

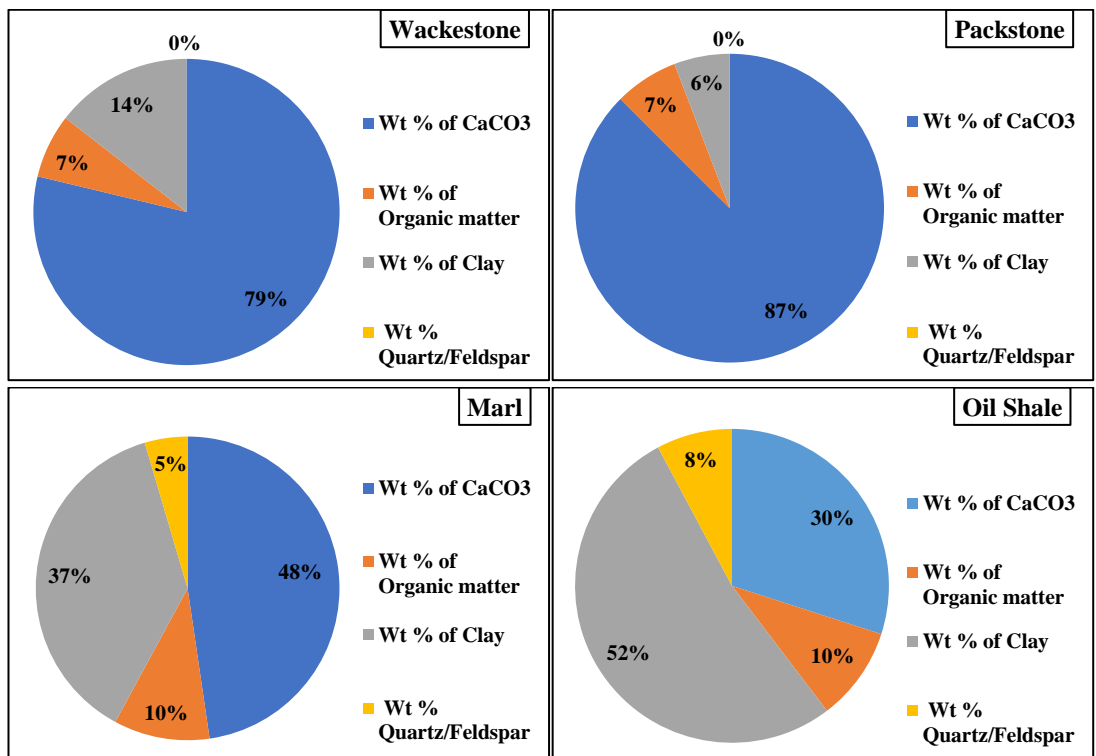


Figure 8.8. The pie chart of average weight percent data of lithofacies from the Kösüre measured section.

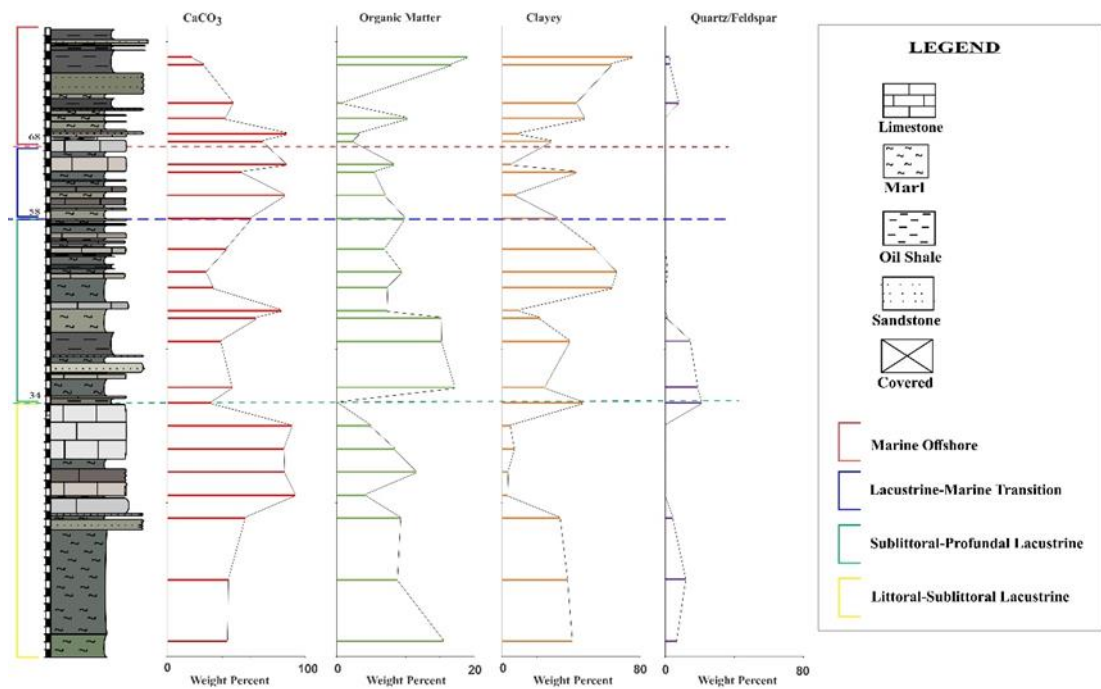


Figure 8.9. Representing the Kösüre measured stratigraphic log and graphical representation of geochemical analysis data of weight percent CaCO<sub>3</sub>, Organic Matter, Clay and quartz/feldspar and their comparison along the measured stratigraphic log.

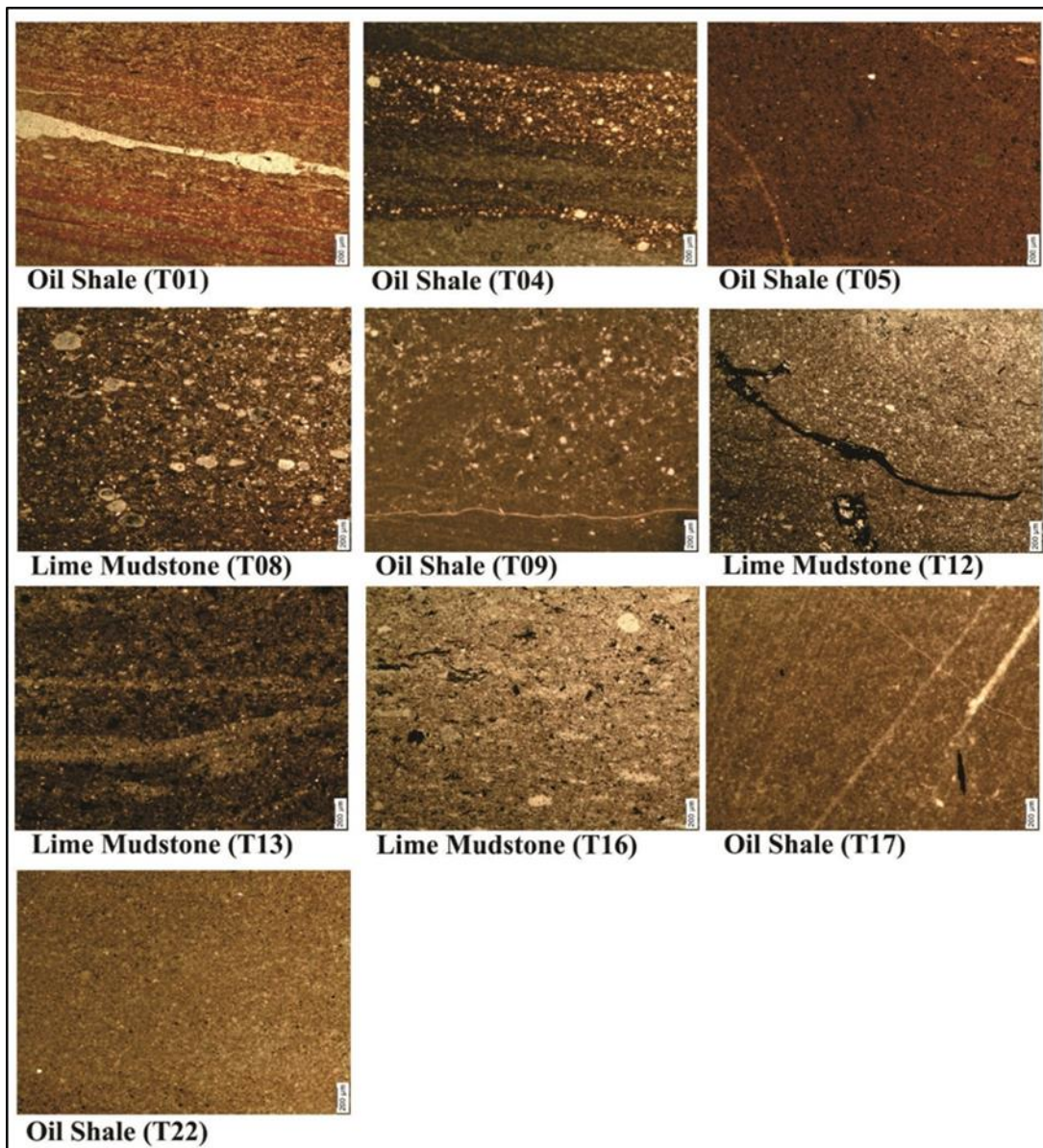


Figure 8.10. Photomicrographs of the Karahisar lithofacies, examined for chemical analysis (PPL, x4).

Table 8.4. The minimum, maximum and average weight percent values of lithofacies from the Karahisar measured section.

Lithofacies	% Weight carbonate			% Weight Organic Matter			% Weight Clay			% Weight Quartz/Feldspar		
	Min	Max	Average	Min	Max	Average	Min	Max	Average	Min	Max	Average
Lime Mudstone	24.71	56.22	38.69	7.56	17.94	12.52	34.74	63.46	48.79	0.00	0.00	0.00
Oil-shale	38.31	66.84	52.44	8.03	19.93	12.42	3.80	44.72	27.22	0.00	38.11	8.65
Overall	24.71	66.84	47.86	8.03	19.93	12.45	3.80	63.46	34.41	0.00	38.11	8.77

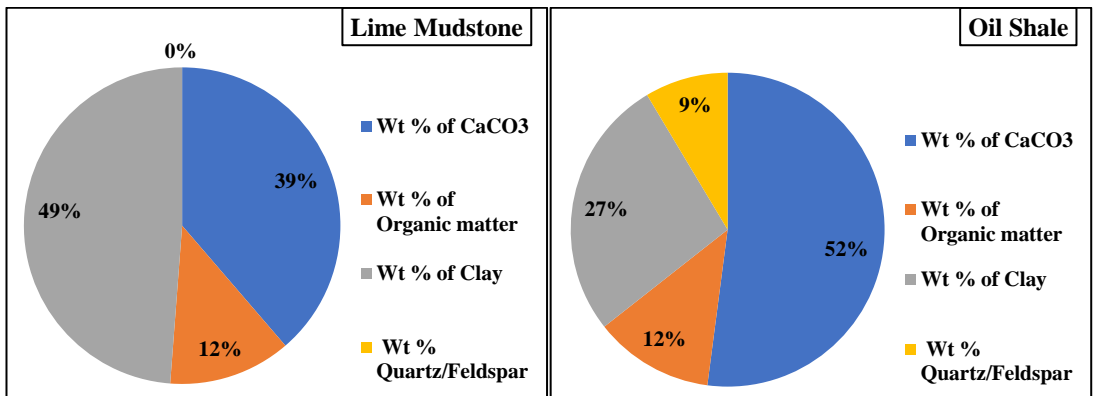


Figure 8.11. The pie chart of average weight percent values of lithofacies from the Karahisar section.

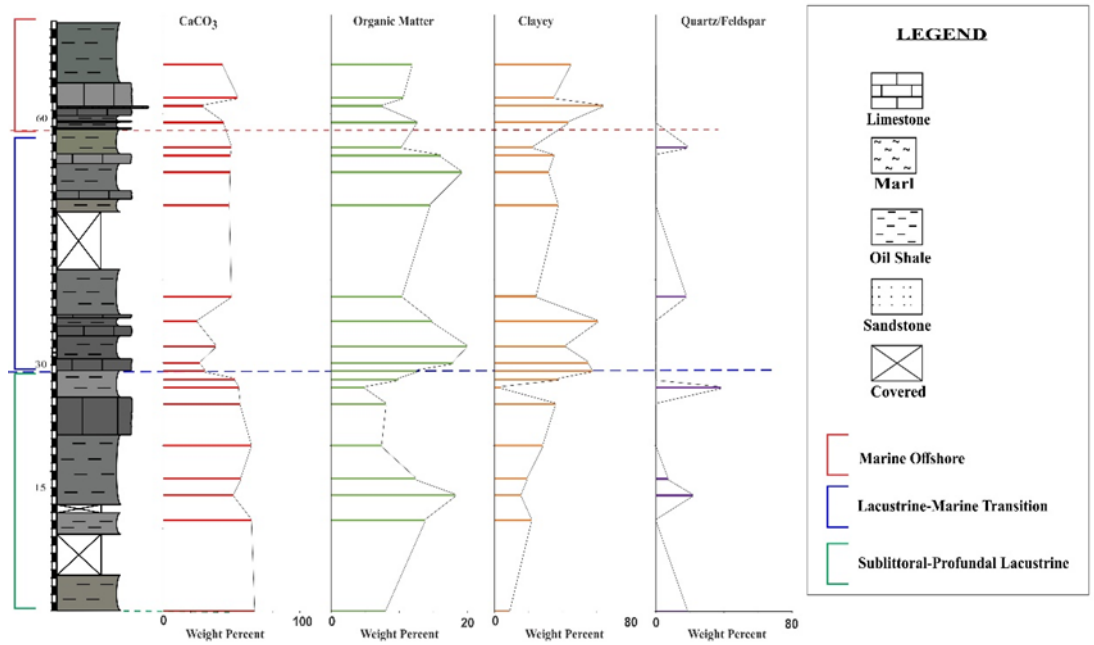


Figure 8.12. Representing the Karahisar measured stratigraphic log and graphical representation of geochemical analysis data of weight percent CaCO<sub>3</sub>, Organic Matter, Clay and Quartz/feldspar and their comparison along the measured stratigraphic log.

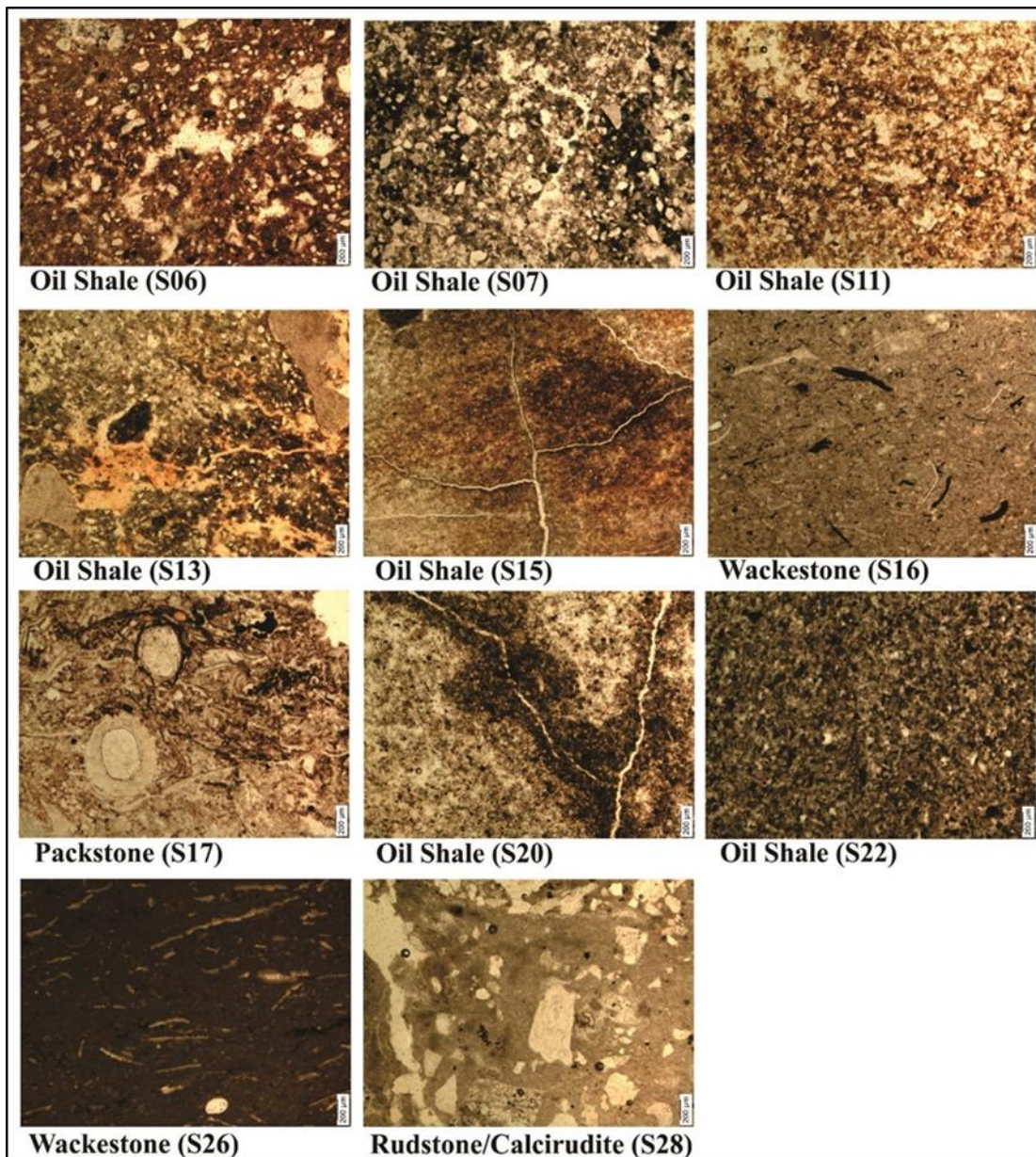


Figure 8.13. Photomicrographs of the Sünnet lithofacies, examined for chemical analysis (PPI, x4).

Table 8.5. The minimum, maximum and average weight percent values of lithofacies from the Sünnet measured section.

Lithofacies	% Weight carbonate			% Weight Organic Matter			% Weight Clay			% Weight Quartz/Feldspar		
	Min	Max	Average	Min	Max	Average	Min	Max	Average	Min	Max	Average
Wackestone	73.20	79.50	76.35	16.01	18.35	17.18	0.00	38.35	17.68	8.45	31.64	20.05
Packstone	54.35	54.35	54.35	29.91	29.91	29.91	0.00	0.00	0.00	18.74	18.74	18.74
Rudstone	36.34	58.56	48.95	4.36	4.64	4.50	0.00	0.00	0.00	39.80	59.31	49.55
Oil-shale	4.33	39.16	20.12	8.09	21.05	10.09	0.00	41.81	18.40	41.67	70.69	58.20
Overall	4.33	79.50	34.28	4.36	29.91	11.72	0.00	41.81	14.35	8.45	70.69	48.48

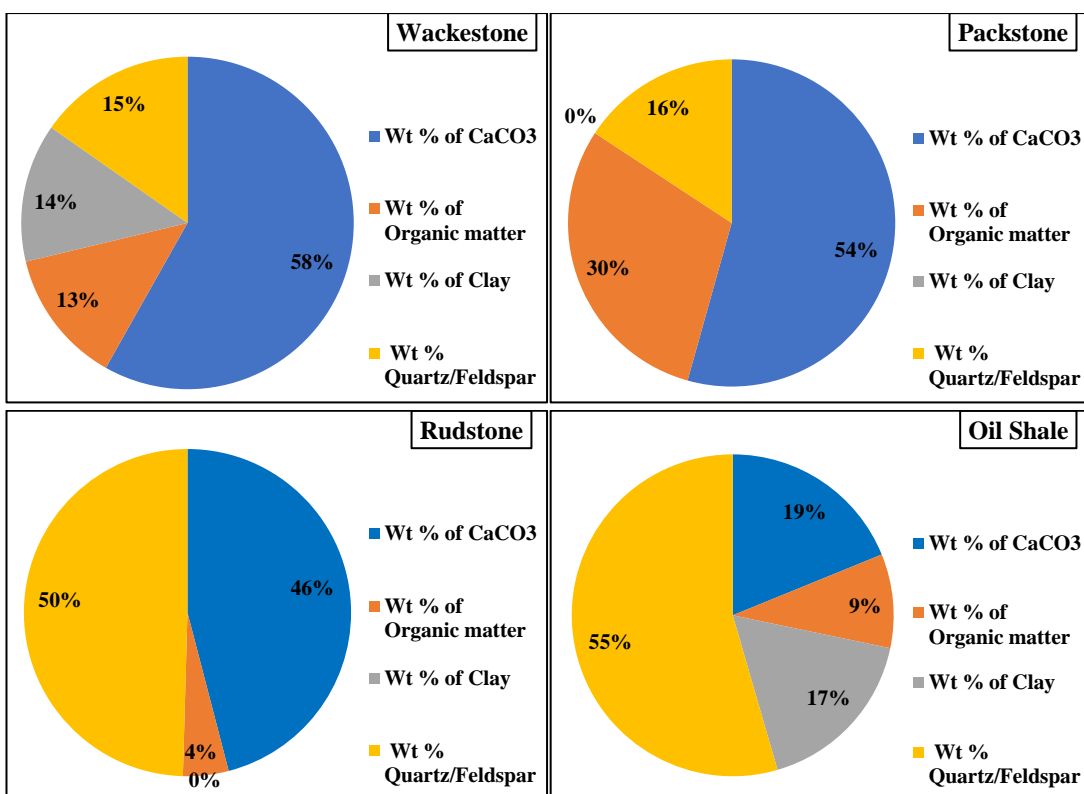


Figure 8.14. The pie chart of average weight percent values of lithofacies from the Sünnet measured section.

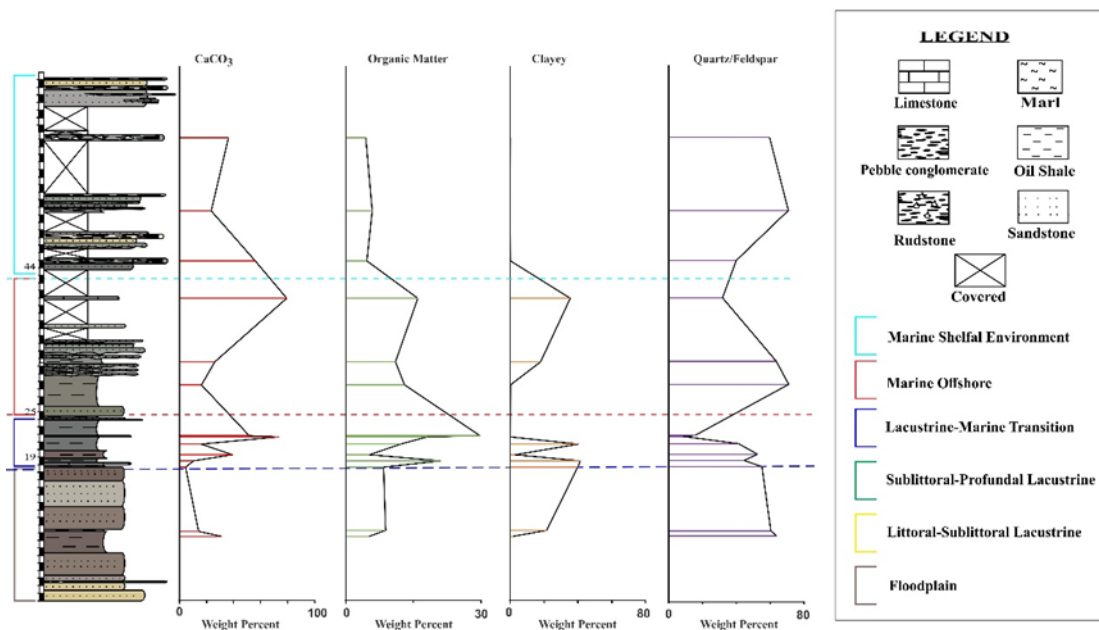


Figure 8.15. Representing the Sünnet measured stratigraphic log and graphical representation of geochemical analysis data of weight percent  $\text{CaCO}_3$ , organic matter, Clay and quartz/feldspar and their comparison along the measured stratigraphic log.

maximum carbonate content curve as compared to a sublittoral-profundal zone, which mostly show relatively low carbonate content. In the transitional zone, there is a sudden decrease in the carbonate content, then followed by an increasing trend toward the top. The sandstone-shale intervals in the marine zone, there is a gradual decreasing in the carbonate content curve line (Figure 8.3). In the Hasanlar section, the minimum and maximum carbonate weight percent are 7.31 wt.% and 79.32 wt.%, respectively. The average value of carbonate content in the Hasanlar is around 51.86 wt.% (Appendices A4). 54.49 wt.%, 53.35 wt.% and 43.31 wt.% average values are obtained from lime mudstone>oil-shale> wackestone, respectively (Table 8.2; Figure 8.5). The carbonate curve line in the Hasanlar section is mostly on the maximum value side with few left trend curves. At the middle portion in the measured section, there is sudden shift of the carbonate content line to left and show decrease in the carbonate content and then followed by right shift in the curve line and represent increasing trend in the carbonate content (Figure 8.6). The Kösüre section lithofacies are composed of 17.72 wt.% to 92.66 wt.% of carbonate content (Table 8.3). 53.93

wt.% is average wt.% carbonate content in the studied section (Appendices A6). The average minimum values of carbonate content in the Kösüre section lithofacies are represented by oil-shale <marl <wackestone <packstone (Table 8.3; Figure 8.8). The general trend in the carbonate content curve in the studied section is relatively low and then followed by the relatively increasing trend. This trend sharply decreases in the begin of the sublittoral-profunda zone. After that, there is gradually increasing and then decreasing trend in the carbonate curve line in the Kösüre section. There is a steady increasing in the carbonate content toward the transitional zone. The transitional zone carbonate content is at maximum with few minimum carbonates trend curve line. In the marine zone, there is decreasing in the carbonate content toward the top in the studied section (Figure 8.9). The obtained weight percent of carbonate content in the Karahisar section is ranging from 24.71 wt.% to 66.84 wt.% and the average value is 47.86 wt.% (Appendices A8). The average value of the carbonate content in the Karahisar lithofacies is 38.69 % in the lime mudstone and 52.44 wt.% in the oil-shale (Table 8.4; Figure 8.11). The carbonate curve line in the Karahisar section is generally a stable curve line with few left peaks along the measured stratigraphic column. At the beginning of the transitional lacustrine-marine zone, there is observation of left shift in the carbonate content curve line and then followed by right shift in the curve line and the relatively constant trend toward the upper portion of the studied section (Figure 8.12). The Sünnet section indicates 4.33 wt.% minimum, 79.50 wt.% maximum and 34.28 wt.% average value carbonate content (Appendices A10). In the lithofacies of the Sünnet section, the carbonate content is decreasing from wackestone> packstone> rudstone> oil-shale (Table 8.5; Figure 8.14). The carbonate content in the lower portion of the studied section is appeared low. Toward the top, there is an increase in the carbonate content and curve line shifted toward the right. In the marine condition zone, the carbonate trend line define a decreasing trend and followed by increasing and again decreasing trend (Figure 8.15). Generally, the observed decreasing curve peaks in the carbonate content along the studied sections are characterized as a transitional change from arid climatic stage to warm-humid climatic condition (He et al., 2017).

### 8.2.2. Clay Content in the Studied Sections

Generally, the lithofacies with a clay content more than 40% represent strong plasticity character. Such lithofacies are least favorable to fracturing (Jiang et al., 2015; Tingwei et al., 2017). The clay constituent in the lithofacies are present in the form of clay-rich laminae or homogeneous mud matrix or association with organic-rich laminae. The clay-rich feature and matrix are formed as result of flocculation of clay minerals or other minerals particles during dominant terrigenous influx (Liu and Wang, 2013; Zeng et al., 2018). In the studied sections, the clay content is second dominated inorganic constituents after the carbonate content except for the Sünnet section. The average weight percent values observed in the studied sections are 24.04 wt.% in the Dağhacılar section, 31.23 wt.% in the Hasanlar section, 39.72 wt.% in the Kösüre section, 34.41 wt.% in the Karahisar section and 14.35 wt.% in the Sünnet section (Appendices A2; A4; A6; A8; A10; Figure 8.21). In the studied section, the clay content curve lines indicate mostly opposite relation to the carbonate content except for the Sünnet Section (Figures 8.3; 8.6; 8.9; 8.12; 8.15). Generally, it is observed along the measured stratigraphic sections, i.e if there is an increase in the clay content, in response, there will be a decrease in carbonate content in the lithofacies and vice versa (Figures 8.3; 8.6; 8.9; 8.12). In the Dağhacılar section, the average clay content weight percent is higher in the marl lithofacies (37.27 wt.%) compared to other lithofacies in the measured section, i.e (37.27 wt.%) marl > (23.92 wt.%) oil-shale > (19.73 wt.%) lime mudstone > (18.76 wt.%) packstone > (12.95 wt.%) wackestone (Table 8.1; Figure 8.2). The minimum, maximum and overall average clay content in the studied section are 0.00 wt.%, 68.45 wt.%, and 24.04 wt.%, respectively (Appendices A2; Table 8.1; Figure 8.2). The graphic curve line of the clay content in the Dağhacılar section is on the left side in the lower portion. Then, there is a shift in the curve line to higher values with occasional lower values diverted peaks in the middle portion of the studied section. In the upper portion, there is high value peak in the clay curve line in the transitional zone, and then toward the top, the clay curve line is shifted to the left side of graphs with comparatively constant character in the upper

portion of the studied section (Figure 8.3). In the Hasanlar section, the clay content in the studied samples are ranging from 4.95 wt.% to 78.43 wt.% and the average clay content in the studied section is 31.13 wt.% (Appendices A4; Figure 8.21). The average clay content in the Hasanlar section lithofacies are (4.13 wt.% in the wackestone> 34.82 wt.% in the lime mudstone> 26.96 wt.% in the oil-shale (Table 8.2; Figure 8.5). In the graphic diagram of the Hasanlar section, the clay content curve line in the lower portion indicate lower value peaks with few high peaks and then followed by higher value curve line in the upper portion and topped by lower peak values curve line (Figure 8.6). In the Kösüre section, the documented clay content values are between 3.10 wt.% to 78.66 wt.% and 39.72 wt.% average clay content value (Appendices A6; Figure 8.21). The high clay content is observed in the oil-shale lithofacies with 58.73 average wt.%. In the other lithofacies, the average clay content is 39.03 wt.% in marl, 14.49 wt.% in wackestone and 8.82 wt.% in the packstone (Table 8.3; Figure 8.8). The clay content curve along the measured section indicate high peaks in the marl and oil-shale. The curve line of clay content is minimum in the wackestone and packstone intervals in the Kösüre section (Figure 8.9). The low, high and average weight percent of clay content in the Karahisar section is 3.80 wt.%, 63.46 wt.% and 34.41 wt.%, respectively (Appendices A8). The average clay content values in the lime mudstone and oil-shale lithofacies are 48.79 wt.% and 27.22 wt.%, respectively (Table 8.4; Figure 8.11). In the Karahisar section, the oil-shale intervals in the stratigraphic section indicate generally high trend curve line except for few intervals. The sublittoral-profundal zone of the studied section shows low clay content trend line. In the transitional zone, the clay curve line moves toward the right side and then followed by relative constant curve line pattern toward the top. In the marine zone, the curve line of clay content illustrates high-value peaks and then relatively low-value curve line toward the top (Figure 8.12). The observed clay content in the Sünnet section is comparable lower than the other studied sections (Figure 8.21). The observed weight percent of clay content is ranging from 0.00 wt.% to 41.81 wt.% with 14.35 wt.% average values in the Sünnet section (Appendices A10; Table 8.5; Figure 8.21). Along the stratigraphic section, the clay curve line appears as low peaks in the

floodplain, which is increased near transitional condition environment. In the transitional zone, there is an episodically shift from high to low values in the clay content curve line. In the marine condition, there is occasional appearance of relatively low to high clay content (Figure 8.15).

### **8.2.3. Quartz/Feldspar Content in the Studied Sections**

The quartz/feldspar contents are characterized as the detrital grains. The appearance of quartz/feldspar content in the rock suggest that quartz/feldspar constituents are deposited in the basin via gravity flow under influence of gravity and hydrodynamics, and aeolian processes (Reynolds et al., 1991; Yang et al., 2015). On average, the quartz/feldspar content in the Dağhacılar section is 11.75 wt.%. The quartz/feldspar content in the Dağhacılar section are ranging from 0.00 wt.% to 65.52 wt.% (Appendices A2). The quartz/feldspar average weight percent in the lithofacies of the Dağhacılar section are 16.42 wt.% in marl> 14.96 wt.% in oil-shale> 1.13 wt.% in lime mudstone> 0.33 wt.% in wackestone> 0.25 wt.% in packstone (Table 8.1; Figure 8.2). The profile curve of quartz/feldspar content in the lower portion of the Dağhacılar section indicate low weight percent quartz/feldspar curve line, near to 0.00 wt.%. In the sublittoral-profunda, the quartz/feldspar profile curve show moderate peaks and then followed by low peaks near and after the transitional environment. In the upper portion, the quartz/feldspar curve illustrate shift to the higher values. Generally, there is an increase in quartz/feldspar content toward the upper portion of the studied section (Figure 8.3). The Hasanlar studied section is characterized by low quartz/feldspar content. The observed low and high values in the studied section are 0.00 wt.% and 25.57 wt.%, respectively (Appendices A4). The average obtained value of the quartz/feldspar content in the Hasanlar section is 5.80 wt.%. The oil-shale (8.08 wt.%)> wackestone (1.50 wt.%)> lime mudstone (1.00 wt.%) are the average values of quartz/feldspar content in the studied section lithofacies (Table 8.2; Figure 8.5). Low-value peaks of quartz/feldspar profile curve line are present in the lower portion and high-value peaks curve line of quartz/feldspar are observed in the upper portion (Figure 8.6). In the Köşüre section, the limestone microfacies show zero

quartz/feldspar content (Appendices A6). The oil-shale and marl facies represent 0.00 wt.% to 18.69 wt.% and 1.37 wt.% to 20.92 wt.% quartz/feldspar content in the Kösüre section, respectively (Appendices A6; Table 8.3; Figure 8.8). The overall average value of the quartz/feldspar content in the Kösüre section is 1.18 wt.% (Figure 8.21). The graphic line of quartz/feldspar content along the Kösüre section show few peaks in the lower, middle and upper portion of the studied section (Figure 8.9). In the Karahisar section, a lower quartz/feldspar content is observed in the lithofacies which is ranging from 0.00 wt.% to 38.11 wt.% (Appendices A8). The average weight percent of quartz/feldspar content in the studied section is 5.77 wt.% (Figure 8.21). The lime mudstone facies show zero quartz/feldspar content, while oil-shale lithofacies display 8.65 wt.% average value (Table 8.4; Figure 8.11). In the Karahisar profile, the quartz/feldspar peaks are occasionally observed along the stratigraphic column (Figure 8.12). In the Sünnet section, the quartz/feldspar content observed to be 70.69 wt.% at maximum and 8.45 wt.% at a minimum (Appendices A10). The obtained average of quartz/feldspar content in the Sünnet section is 48.48 wt.%. On average, quartz/feldspar content in the lithofacies are 58.20 wt.% in oil-shale > 49.55 wt.% in rudstone/calcirudite > 20.05 wt.% in wackestone > 15.74 wt.% in packstone (Table 8.5; Figure 8.14). Generally, quartz/feldspar content profile line of the Sünnet section indicate high-value peaks along the stratigraphic column from bottom to top portion with occasional few low peaks interval in the transitional zone and near top portion in the marine offshore zone (Figure 8.15).

#### **8.2.4. Organic Matter Content in the Studied Sections**

The organic matter accumulation of oil-rich lithofacies in a depositional environment is the result of numerous factors, including the organic matter source, deposition and preservation. These factors are commonly linked to high organic matter influx, anoxic depositional condition and the combination of both factors (Xu et al., 2015; He et al., 2017). The organic matter is preserved in the sedimentary rock in the form of organic-rich laminae or organic-rich mud matrix or high plant fragments (Zeng et al., 2018). The obtained geochemical analysis data shows that organic matter content in the

studied sections are ranging from 0.35 wt.% to 29.91 wt.% (Figure 8.21; 8.26). In the Dağhacılar section, minimum, maximum and average organic matter content in the each of lithofacies are 4.49 wt.%, 13.47 wt.% and 8.09 wt.% in lime mudstone; 5.71 wt.%, 15.28 wt.% and 10.58 wt.% in wackestone; 5.27 wt.%, 12.35 wt.% and 8.56 wt.% in packstone; 5.91 wt.%, 16.42 wt.% and 9.65 wt.% in marl; 3.30 wt.%, 18.99 wt.% and 11.90 wt.% in oil-shale, respectively (Appendices A2; Table 8.1: Figure 8.2). In the profile view, the organic matter content mostly displays increasing character with declining carbonate content and linear relation with clay content (Figure 8.3). The sublittoral-profundal zone exhibit high organic matter content curve line trend as compared to other sub-depositional zones (Figure 8.3). The organic matter content in the Hasanlar section is ranging from 5.31 wt.% to 16.39 wt.% with an average of 12.04 wt.% (Appendices A4; Figure 8.21). In each lithofacies of the Hasanlar section, the average organic matter content decrease from high to low in oil-shale (12.87 wt.%), wackestone (11.06 wt.%) and lime mudstone (9.70 wt.%) (Table 8.2; Figure 8.5). In the graphic presentation, the organic matter content mostly displays similar pattern as clay content curve line along the Hasanlar section. The lower portion of the studied section show negative encroachment organic matter curve line, whereas display a positive trend in the upper portion of the studied section (Figure 8.6). The obtained organic matter data from the Köşüre section samples are 0.35 wt.% to 18.99 wt.% (Appendices A6). The organic matter content in each of lithofacies is different from each other; marl lithofacies has highest average organic matter content of 10.62 wt.%, followed by oil-shale (10.26 wt.%), wackestone (6.77 wt.%) and packstone (6.68 wt.%) (Table 8.3: Figure 8.8). In the profile assessment, the organic matter content line is present at higher value side, which is followed by a gradually decline pattern in the organic matter curve line. At the sublittoral-profundal zone, there is a sudden increase in the organic matter trend line and then followed by relative fall in the organic matter curve line. At the start of the marine condition, organic matter content curve line display rapid fall and then followed by rapid stepwise rise in the organic matter curve line toward the upper portion of the studied section (Figure 8.9). The minimum and maximum organic matter content in the Karahisar section is 5.03

wt.% and 19.93 wt.%, respectively, with a mean value of 12.45 wt.% (Appendices A8). The average organic matter content in the lime mudstone and oil-shale lithofacies are 12.45 wt.% and 12.42 wt.%, respectively (Table 8.4; Figure 8.11). The Karahisar section begin with a low weight percent of organic matter content curve line and then sudden high peaks and followed by a gradual fall in the organic matter curve line. This gradual fall in the organic matter curve line is followed by another sudden rise in the organic matter curve line and then steady fall and rise in the curve line of organic matter toward the upper portion of the studied section (Figure 8.12). The average of organic matter values in the Sünnet section lithofacies are 29.91 wt.% in packstone, 17.18 wt.% in wackestone, 10.09 wt.% in oil-shale and 4.50 wt.% in the rudstone/calcirudite (Appendices A10; Table 8.5: Figure 8.14). The profile view of the Sünnet section displays an increase in the organic matter with few low-value peaks. After reaching to a maximum value, there is a gradual decline in the organic matter curve line along the measured section toward the top (Figure 8.15).

### **8.3. Organic Matter and mineral associations**

Numerous types of minerals and organic matter types would show in the various organic matter and minerals associations, as a result of the difference in their properties. The organic matter and minerals vary in their physical and chemical properties. These physical and chemical properties are influenced by the chemical, physical and biological processes that occur during sedimentation. During chemical, physical and biological processes, a series of organic matter and mineral association types are formed (Bennet et al., 1991). The facies and minerals deposition in different lithofacies are dominated by different processes. The study of the relationship between minerals and organic matter is based on the chemical and petrographic data parameters. In this study, the relationship between organic matter with CaCO<sub>3</sub>, Clay content and detrital content (quartz/feldspar) is observed and discuss the reflected result as below;

### **8.3.1. The relationship between CaCO<sub>3</sub> vs Organic matter**

The total carbonate content in the Dağhacılar, Hasanlar, Köşüre, Karahisar and Sünnet section is ranging from 16 wt.% to 89.23 wt.%, 7.31 wt.% to 79.32 wt.%, 17.72 wt.% to 92.66 wt.%, 24.71 wt.% to 66.84 wt.% and 4.33 wt.% to 79.50 wt.%, respectively (Appendices A2; A4; A6; A8; A10; Figure 8.28). The CaCO<sub>3</sub> vs organic matter cross-plots represent scatter points with negative correlation coefficient (r) except for the Sünnet section (Figures 8.16; 8.17; 8.18; 8.19; 8.20). This negative relationship is interpreted as declining in the organic matter with increasing of CaCO<sub>3</sub> content (Figures 8.3; 8.6; 8.9; 8.12; 8.15). The changes in the carbonate influx may be as a result of differences in the primary productivity, cementation or dissolution which concentrated or diluted the organic matter of the deposits. The Hasanlar section (number of samples (n) = 12; correlation coefficient (r) = -0.47) <Köşüre section (n = 25; r = -0.39) <Karahisar Section (n= 21; r = -0.37) <Dağhacılar Section (n= 42; r = -0.33) shows high negative correlation coefficient with organic matter (Figures 8.16; 8.17; 8.18; 8.19). According to Liu (2013) and Zeng et al. (2018), the negative correlation coefficient of the carbonate content vs organic matters is related with precipitation of carbonate minerals by microbes or nanoplankton activity and deposited through biochemical process. The CaCO<sub>3</sub> and organic matter in the Sünnet section reflects positive correlation coefficient (n = 14; r = 0.27) (Figure 8.20). The positive correlation coefficient suggests that a relative decrease in productivity in the basin, which result in diluting the carbonate component and causing a decrease in the organic matter and a synchronized increase in the clastic content in the studied section.

### **8.3.2. The relationship between clay content vs organic matter**

The obtained Clay content data in the studied section are ranging from 0.00 wt.% to 68.45 wt.% in the Dağhacılar section, 4.95 wt.% to 75.43 wt.% in the Hasanlar, 3.10 wt.% to 75.66 wt.% in the Köşüre section, 3.80 wt.% to 63.46 wt.% in the Karahisar section and 0.00 wt.% to 41.81 wt.% in the Sünnet section (Appendices A2; A4; A6; A8; A10; Figure 8.30). In the studied sections, the cross-plot of Clay content vs

organic matter of the studied samples indicate positive correlation coefficient. The observed positive correlation coefficient in the studied sections are ( $n = 12$ ,  $r = 0.36$ ) in the Hasanlar section, ( $n = 25$ ,  $r = 0.28$ ) in the Kösüre section, ( $n = 21$ ,  $r = 0.26$ ) in the Karahisar section, ( $n = 14$ ,  $r = 0.18$ ) in the Sünnet section and ( $n = 42$ ,  $r = 0.10$ ) in the Dağhacılar section (Figures 8.16; 8.17; 8.18; 8.19; 8.20). The observed very weak positive correlation coefficient in the studied sections exhibit that with increase of clay content, there is a relative increase in the organic matter content or show no obvious effect on the deposition environment during the accumulation of organic matter. The positive correlation coefficient of clay content with organic matter suggests that deposition of clay content with organic matter is physiochemical and biochemical process accumulation (Zeng et al., 2018).

### **8.3.3. The relationship between Quartz/Feldspar vs organic matter**

In the depositional sediment, the variations in the detrital input can also affect the organic matter content (Ding et al., 2015). Enhanced detrital input may lead to providing the sites for organic matter adsorption in and on the aluminosilicates or either serving as a variable that controls the dilution of the organic matter (Rimmer et al., 2004). It may influence indirectly by rapid burial rate of the organic matter which controls the bacterial decomposition of the organic matter (Canfield, 1994; He et al., 2017). The Quartz/feldspar content in the Dağhacılar section, Hasanlar section, Kösüre section, Karahisar section and Sünnet section are ranging from 0.00 wt.% to 60.10 wt.%; 0.00 wt.% to 25.57 wt.%; 0.00 wt.% to 20.92 wt.%; 0.00 wt.% to 38.11 wt.% and 8.45 wt.% to 70.69 wt.%, respectively (Appendices A2; A4; A6; A8; A10; Figure 8.31). The correlation coefficient analysis of the quartz/feldspar content and organic matter reflect very weakly positive correlation or no correlation. The obtained quartz/feldspar content vs organic matter correlation coefficient in the studied section are ( $n = 42$ ,  $r = 0.06$ ) in the Dağhacılar section, ( $n = 12$ ,  $r = 0.07$ ) in the Hasanlar section and ( $n = 25$ ,  $r = 0.13$ ) in the Kösüre section (Figures 8.16, 8.17, 8.18). It indicates that the positive relationship of the quartz/feldspar content with organic matter favored to the organic matter deposition and preservation. Whereas,

quartz/feldspar vs organic matter cross-plot exhibit negative correlation coefficient in the Karahisar (n = 21, r = -0.37) and Sünnet sections (n = 14, r = -0.68) (Figures 8.19, 8.20). This relation indicates decreasing in the organic matter content with increasing the quartz/ feldspar content (Figures 8.3; 8.6; 8.8; 8.12; 8.15). The negative correlation also indicates a rapid influx of quartz/feldspar content to the depositional environment, which help in the rapid burial of the organic matter and controls the bacterial decomposition (Li and Bennett, 1991; Homewood, 2001; Zeng et al., 2018).

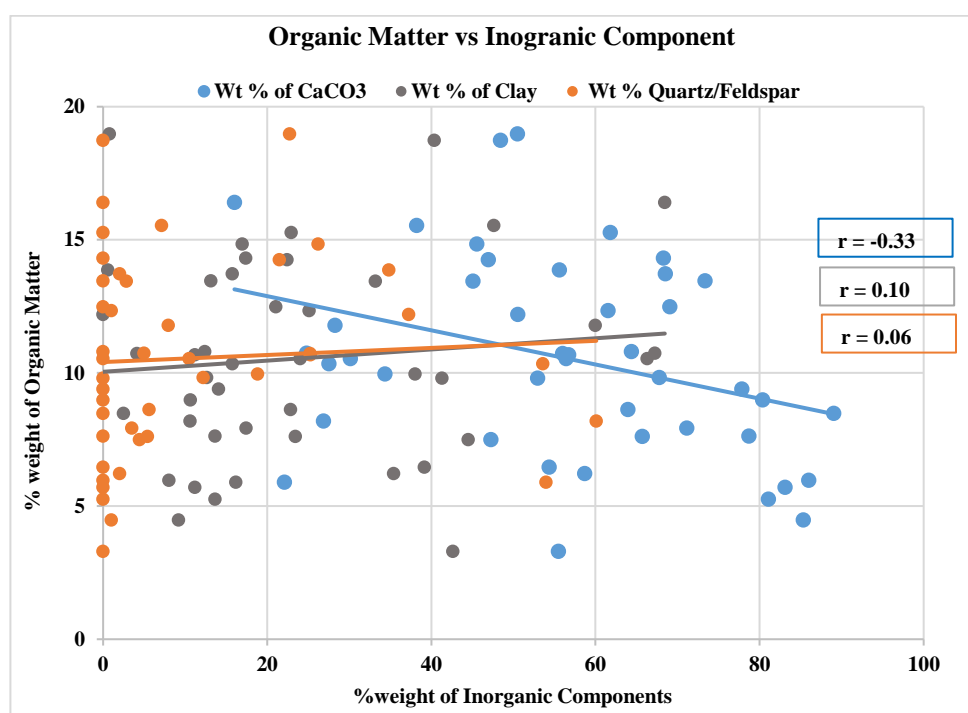


Figure 8.16. Cross-Plot of wt.% Organic matter vs wt.% CaCO<sub>3</sub>, wt.% organic matter vs wt.% clay content and wt.% organic matter vs wt.% quartz/feldspar content of the Dağhacılar geochemical studied samples data. CaCO<sub>3</sub> represent a negative linear trend to organic matter, Clay and quartz /feldspar show a positive linear trend to organic matter (Solid line shows a linear trend of the minerals component).

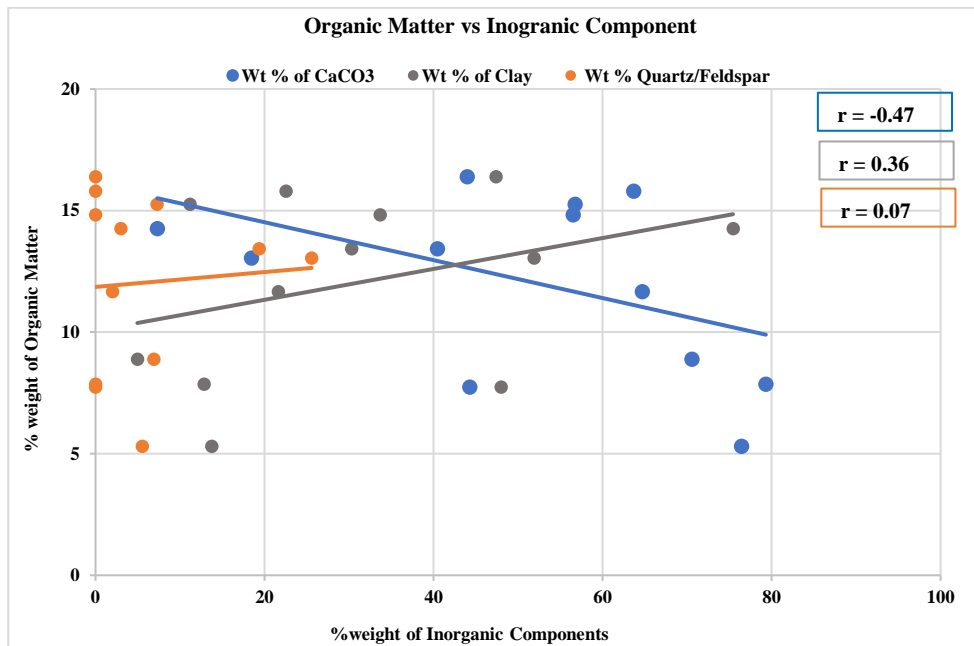


Figure 8.17. Cross-Plot of wt.% Organic matter vs wt.% CaCO<sub>3</sub>, wt.% organic matter vs wt.% clay content and wt.% organic matter vs wt.% quartz/feldspar content of the Hasanlar geochemical studied samples data. CaCO<sub>3</sub> represent a negative linear trend to organic matter, Clay and quartz /feldspar show a positive linear trend to organic matter (Solid line shows a linear trend of the mineral component).

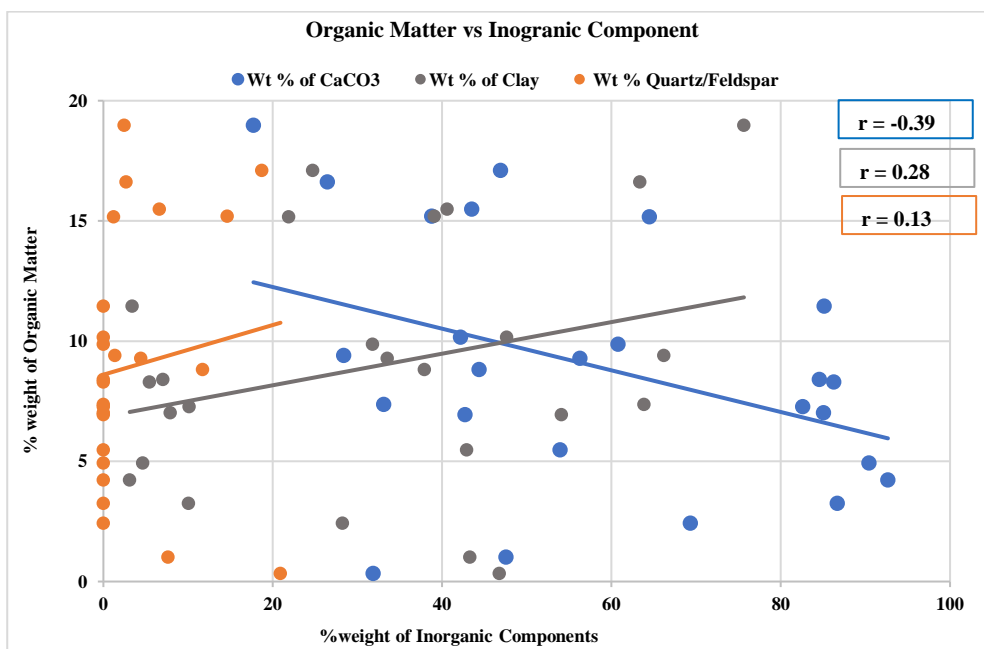


Figure 8.18. Cross-Plot of wt.% Organic matter vs wt.% CaCO<sub>3</sub>, wt.% organic matter vs wt.% clay content and wt.% organic matter vs wt.% quartz/feldspar content of the Kösüre geochemical studied samples data. CaCO<sub>3</sub> represent a negative linear trend to organic matter, Clay and quartz /feldspar show a positive linear trend to organic matter (Solid line shows a linear trend of the mineral component).

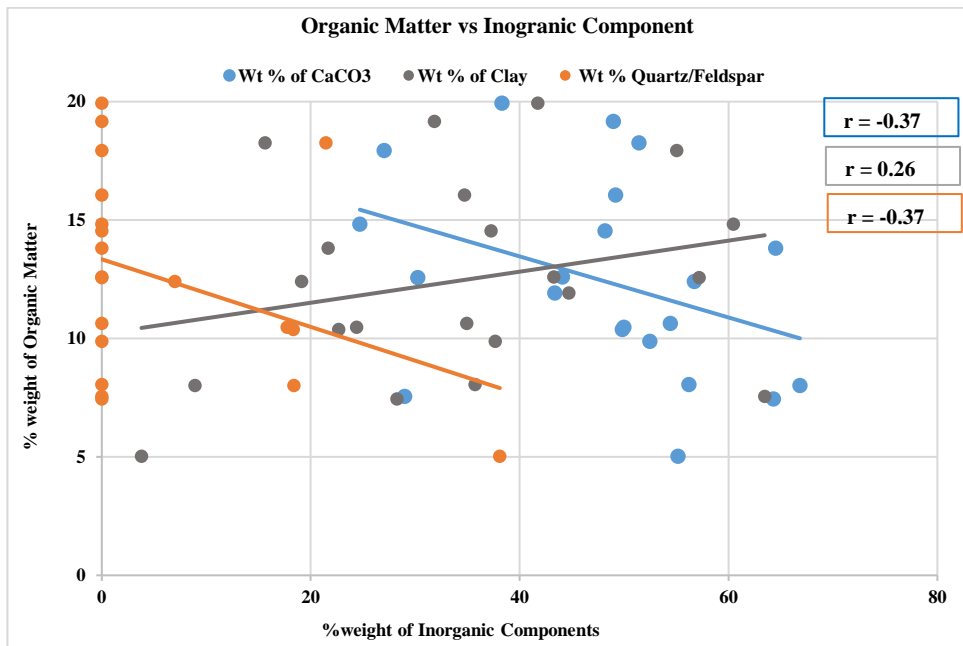


Figure 8.19. Cross-Plot of wt.% Organic matter vs wt.% CaCO<sub>3</sub>, wt.% organic matter vs wt.% clay content and wt.% organic matter vs wt.% quartz/feldspar content of the Karahisar geochemical studied samples data. CaCO<sub>3</sub> represent a negative linear trend to organic matter, Clay and quartz /feldspar show a positive linear trend to organic matter (Solid line shows a linear trend of the mineral component).

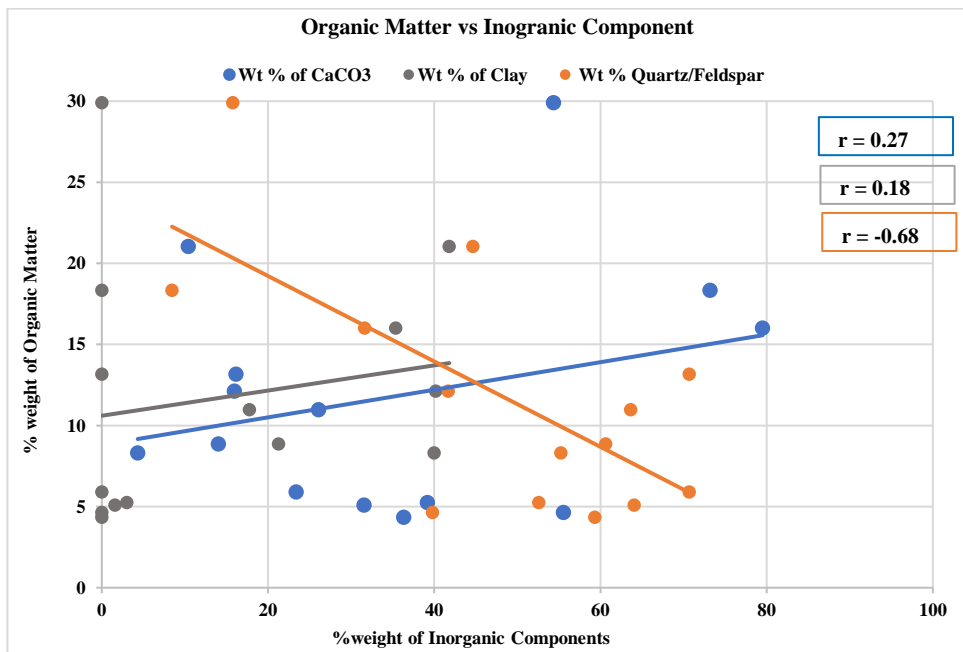


Figure 8.20. Cross-Plot of wt.% Organic matter vs wt.% CaCO<sub>3</sub>, wt.% organic matter vs wt.% clay content and wt.% organic matter vs wt.% quartz/feldspar content of the Sünnet geochemical studied samples data. CaCO<sub>3</sub> represent a negative linear trend to organic matter, Clay and quartz /feldspar show a positive linear trend to organic matter (Solid line shows a linear trend of the minerals component).

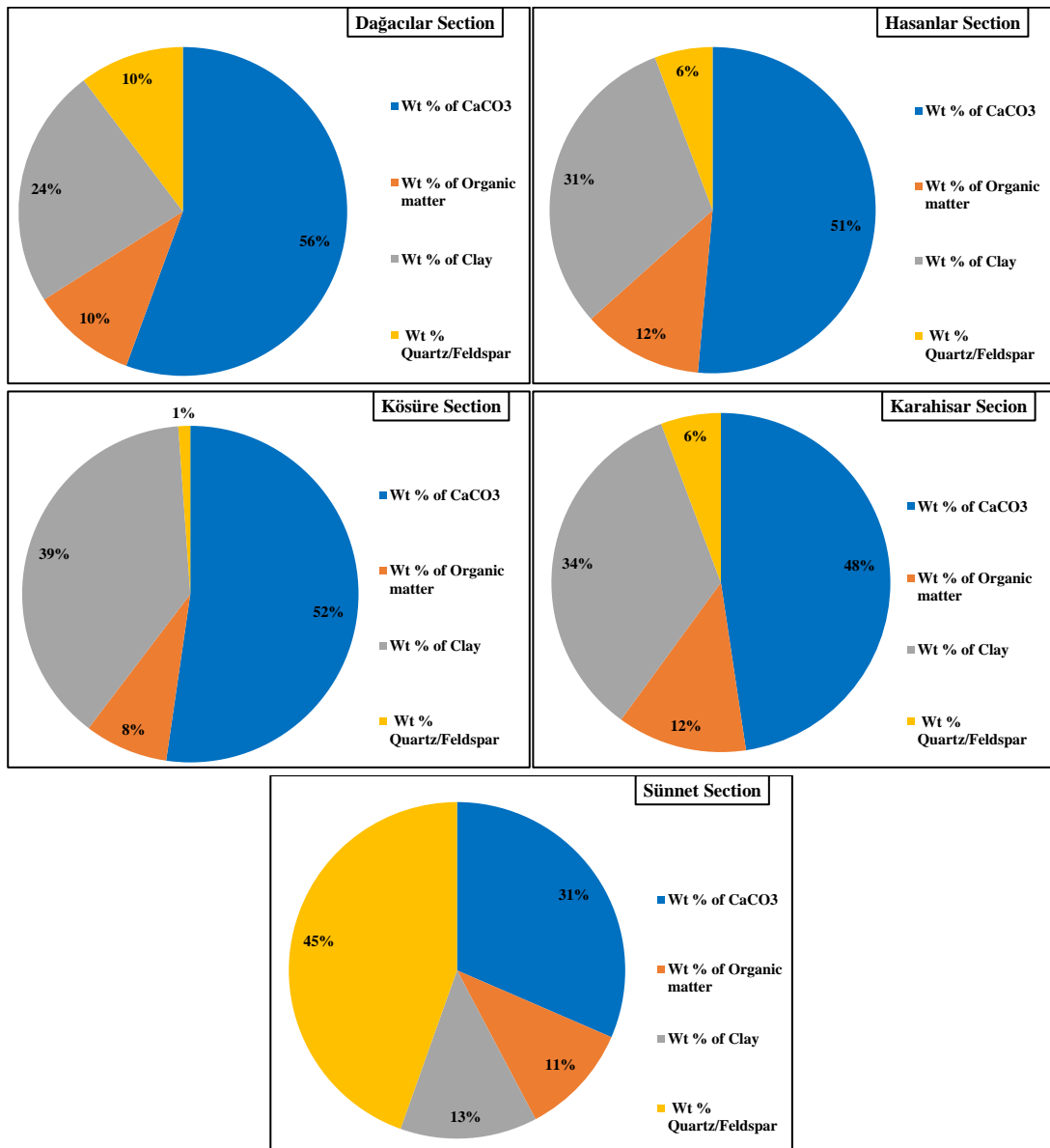


Figure 8.21. The pie chart of average weight percent values of the CaCO<sub>3</sub>, organic matter, clay content and quartz/feldspar in the Dağacılar, Hasanlar, Köşüre, Karahisar and Sünnet measured sections.

### 8.3.4. Characterization and interpretation of the CaCO<sub>3</sub>, Clay, Quartz/ Feldspar contents vs Organic matter

The organic matter preservation is enhanced by biological blooms. It can produce a large amount of organic matter, which causes depletion in oxygen due to oxygen

consumption by the biological activity. Therefore, it creates favorable condition for the preservation of organic matter (Curtis, 2002). A humid climatic condition and low salinity are the favorable conditions for the nourishment of biological activity. In addition, the terrestrial influx supplies the nutrient for the development of biological activity (Deng and Qian, 1990). The development of the anoxic condition in the water column protects the organic matter from oxidation (Zhang et al., 2013). In the case of carbonate content, clear and enclosed water without detrital influx provides a favorable depositional environment for carbonate deposition (Scholle et al., 1983; Zhu et al., 2005). Therefore, the carbonate content exhibits a negative correlation with clay and quartz/feldspar contents in the studied sections. Generally, the appropriate environment for the deposition of carbonate content is related to high salinity. Such conditions are unfavorable for the development of biological activity but favorable for the development of anaerobic bacteria i.e cyanobacteria and sulfate bacteria (Yang et al., 2012; Tingwei et al., 2017). Hence, the negative correlation observed between carbonate content and organic matter in the studied sections except for the Sünnet section (Figures 8.16; 8.17; 8.18; 8.19; 8.20). It is interpreted that relatively high deposition of carbonate content in the lacustrine environment indicate hydrological open environmental condition with temporary linkage of marine environment (Figure 8.28) (Fuhrmann, 2002; Cyr et al., 2014). The high occurrence of carbonate content in the studied sections also indicate transgressive depositional environment in the region (Figures 8.21, 8.28) (Lash & Blood, 2011). A negative correlation interprets as exhibiting dilution of organic matter and terrigenous clay content by carbonate influx (Ricken, 1993). Generally, four major sources of calcium carbonate precipitation are suggested, which are responsible for their deposition. These carbonate sources are detrital carbonate from fluvial, biogenic carbonate from various organism skeletal, inorganically-precipitation and diagenetic carbonate (Jones & Bowser, 1978; Fuhrmann, 2002).

The weakly positive correlation of the clay content with organic matter in the measured studied sections indicate dual depositional character which can either amass

with organic matter or co-deposits with detrital sediments (Zeng et al., 2018). In the Karahisar and Sünnet sections, the positive relation of organic matter with clay content and negative relation with quartz/feldspar content exhibit rapid incursion of terrestrial influx to the depositional system (Figures 8.19; 8.20) (Tingwei et al., 2017). A substantial amount of organic-rich sediments can be preserved to deposit organic-rich lithofacies by increase the accommodation and relatively rapid influx of clastic sediments and organic productivity (Huang et al., 2013). Therefore, this correlation suggests that relatively high rate of clastic sedimentation occur in the depositional setting and lead to the development of the oxygen-deficient condition in the depositional setting.

#### **8.4. Porosity Types and Visual Estimated Porosity**

The petrographic analyses and imageJ software processed petrographic images of selected samples from the five Middle Eocene studied sections are evaluated for the porosity types and their potential percentage calculation. In last decade, a number of researches have been carried out to describe and recognize different types of pore in lithofacies (Loucks et al., 2012; Schieber, 2013). The petrographic image studies used to obtain total visible porosity estimate by the help of ImageJ software (Tables 8.6; 8.7; 8.8; 8.9; 8.10; Figures 8.22; 8.23; 8.24; 8.25; 8.26; 8.27). The total porosity values are estimated in the oil-shale, marl and limestone lithofacies from the Dağhacılar, Hasanlar, Köüre, Karahisar and Sünnet sections, which mostly have high organic matter content (Figure 8.21). The obtained total porosity in the Dağhacılar, Hasanlar, Köüre, Karahisar and Sünnet sections are ranging from 0.00% to 22.76%, 0.04% to 3.36%, 0.00% to 11.49%, 0.00% to 5.50% and 0.00% to 23.15%, respectively (Tables 8.6; 8.7; 8.8; 8.9; 8.10). The average total porosity in the studied sections are 5.35% in the Sünnet Section >4.72% in the Dağhacılar section >1.84% in the Köüre section >1.47% in the Hasanlar section and >0.73% in the Karahisar section (Tables 8.6; 8.7; 8.8; 8.9; 8.10). By using microscopic analysis and ImageJ software, different types of pore and micro-fracture porosity are identified and classified in the studied sections (Figures 8.23, 8.24). The observed pore types and micro-fracture related

Table 8.6. Total porosity % and types of porosity in the Dağhacılar section.

Sample No.	Lithofacies	Visible Porosity %	Types of Porosity
D03	Lime Mudstone	0.00	Nil
D04	Wackestone	18.04	Intraparticle pores
D06	Wackestone	0.00	Nil
D10	Oil-shale	9.53	Interparticle pores and Intraparticle pores
D11	Packstone	6.68	Intraparticle pores
D14	Wackestone	4.16	Intraparticle pores and Fracture type
D15	Wackestone	2.83	Intraparticle pores
D17	Wackestone	0.00	Nil
D18	Lime Mudstone	0.00	Nil
D19	Packstone	22.76	Intraparticle pores
D21	Marl	0.66	Interparticle pores
D23	Wackestone	1.88	Intraparticle pores and Interparticle pores
D25	Marl	5.91	Intraparticle pores and Fracture type
D27	Wackestone	14.32	Interparticle pores
D28	Oil-shale	7.15	Fracture type
D29	Lime Mudstone	18.04	Interparticle pores
D30	Wackestone	2.28	Intraparticle pores
D33	Lime Mudstone	1.71	Interparticle pores
D35	Oil-shale	0.00	Nil
D36	Oil-shale	0.66	Intraparticle pores
D38	Oil-shale	0.57	Interparticle pores
D40	Oil-shale	1.61	Intraparticle pores
D41	Oil-shale	0.12	Intraparticle pores
D45	Marl	1.35	Interparticle pores
D52	Oil-shale	0.03	Intraparticle pores and Interparticle pores
D59	Oil-shale	0.04	Intraparticle pores
D69	Oil-shale	7.62	Interparticle pores and Fracture type
D73	Marl	4.15	Interparticle pores and Fracture type
	Average	4.72	
	Min	0.00	
	Max	22.76	

Table 8.7. Total porosity % and types of porosity in the Hasanlar section.

Sample No.	Lithofacies	Visible Porosity %	Types of Porosity
H0A	Wackestone	2.27	Intraparticle pores and Interparticle pores
H0B	Oil-shale	0.11	Intraparticle pores
H01	Oil-shale	0.04	Intraparticle pores
H03	Oil-shale	2.79	Interparticle pores and Fracture type
H04	Lime Mudstone	0.05	Intraparticle pores
H05	Lime Mudstone	0.43	Intraparticle pores
H08	Oil-shale	0.00	Nil
H09	Oil-shale	0.19	Interparticle pores
H10	Wackestone	2.59	Interparticle pores
H12	Wackestone	1.38	Intraparticle pores
H13	Oil-shale	0.62	Interparticle pores
H14	Oil-shale	3.36	Interparticle pores and Fracture type
H15	Oil-shale	2.55	Interparticle pores
H19	Lime Mudstone	2.21	Intraparticle pores
H20	Oil-shale	2.02	Interparticle pores
	Average	1.47	
	Min	0.04	
	Max	3.36	

Table 8.8. Total porosity % and types of porosity in the Kösüre section.

Sample No.	Lithofacies	Visible Porosity %	Types of Porosity
K02	Marl	8.74	Interparticle pores and Fracture type
K06	Wackestone	1.12	Interparticle pores
K09	Wackestone	0.49	Interparticle pores
K11	Packstone	0.15	Interparticle pores and Fracture type
K13	Oil-shale	11.49	Interparticle pores and Fracture type
K16	Wackestone	0.01	Intraparticle pores
K19	Oil-shale	0.14	Interparticle pores
K21	Wackestone	0.00	Nil
K24	Oil-shale	0.09	Interparticle pores
K25	Wackestone	3.45	Interparticle pores and Fracture type
K40	Oil-shale	0.01	Interparticle pores
K45	Oil-shale	0.03	Intraparticle pores
	Average	1.84	
	Min	0.00	
	Max	11.49	

Table 8.9. Total porosity % and types of porosity in the Karahisar section.

Sample No.	Porosity %	Visible Porosity %	Types of Porosity
T01	Oil-shale	5.50	Interparticle pores and Fracture type
T04	Oil-shale	1.10	Interparticle pores and Fracture type
T05	Oil-shale	0.53	Interparticle pores
T07	Lime Mudstone	0.36	Interparticle pores and Fracture type
T08	Lime Mudstone	0.10	Intraparticle pores
T09	Oil-shale	0.09	Intraparticle pores
T12	Lime Mudstone	0.00	Nil
T13	Lime Mudstone	0.01	Intraparticle pores
T16	Lime Mudstone	0.00	Nil
T17	Oil-shale	0.69	Interparticle pores and Fracture type
T22	Oil-shale	0.40	Interparticle pores
T23	Lime Mudstone	0.00	Nil
	Average	0.73	
	Min	0.00	
	Max	5.50	

Table 8.10. Total porosity % and types of porosity in the Sünnet section.

Sample No.	Lithofacies	Visible Porosity %	Types of Porosity
S6	Oil-shale	3.30	Interparticle pores
S7	Oil-shale	2.30	Interparticle pores
S11	Oil-shale	9.11	Interparticle pores
S12	Lime Mudstone	0.00	Nil
S13	Oil-shale	23.15	Interparticle pores
S15	Oil-shale	1.93	Interparticle pores and Fracture type
S16	Wackestone	0.01	Nil
S17	Packstone	12.77	Interparticle pores
S20	Oil-shale	6.12	Interparticle pores and Fracture type
S22	Oil-shale	0.00	Nil
S26	Wackestone	0.21	Intraparticle pores
S28	Rudstone	0.00	Nil
	Average	5.35	
	Min	0.00	
	Max	23.15	

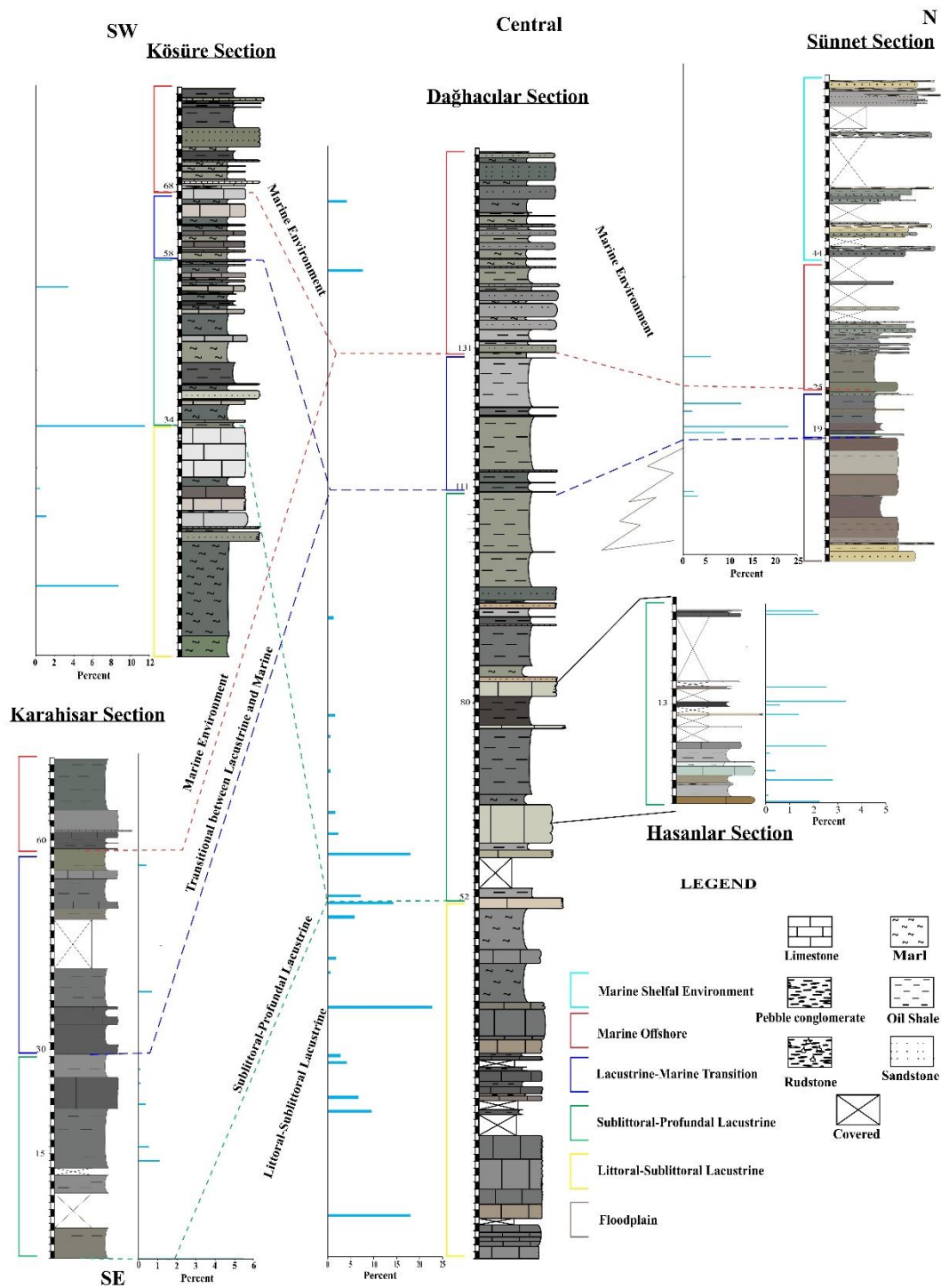


Figure 8.22. Graphic presentation of total porosity% along measured stratigraphic section of the Dağhacılar, Köşüre, Karahisar and Sünnet sections and their correlation.

porosity are classified by using Loucks et al. (2012) pore type classification (Tables 8.6; 8.7; 8.8; 8.9; 8.10). Based on Loucks et al. (2012) pore types classification, the identified pore types in the studied sections sample are intraparticle pores, interparticle pores and microfracture-related porosity (Tables 8.6; 8.7; 8.8; 8.9; 8.10; Figures 8.23; 8.24; 8.25; 8.26; 8.27).

#### **8.4.1. Intraparticle Pores Type**

In general, the intraparticle pores are related to the pore spaces, occurring within the particles (Loucks et al., 2012). It is identified in the form of moldic, intracrystalline and dissolution rim. In the studied sections, intraparticle pore spaces are mostly diagenetic, but some might be primary in the origin. The observed intraparticle pores in the studied sections are in the form of moldic which is developed after the fractional or comprehensive dissolution of a fossil shell fragment, intrafossil pores, intracrystalline, intragranular pores and dissolution rim (Figures 8.23; 8.24; 8.25; 8.26; 8.27).

#### **8.4.2. Interparticle Pores Type**

The interparticle pores are identified as pore spaces that are formed among mineral grains within the matrix (Loucks et al., 2012). It is also characterized as framework pores. It is generally occurred as primary porosity but also occur as secondary porosity. The secondary interparticle porosity is form due to the partial or complete dissolution or removal of matrix from the lithofacies during diagenetic alternations. The interparticle pore types are identified within the samples of the Dağhacılar, Hasanlar, Köşüre, Karahisar and Sünnet studied sections (Tables 8.6; 8.7; 8.8; 8.9; 8.10; Figures 8.23; 8.24; 8.25; 8.26; 8.27). It is randomly observed in the studied sections and poorly to moderately connected.

#### **8.4.3. Micro-Fracture Type Porosity**

In the microscopic studies, micro-fracture and laminae-fractures containing porosity are noticed within the selected studied sections samples (Figures 8.23; 8.24; 8.25;

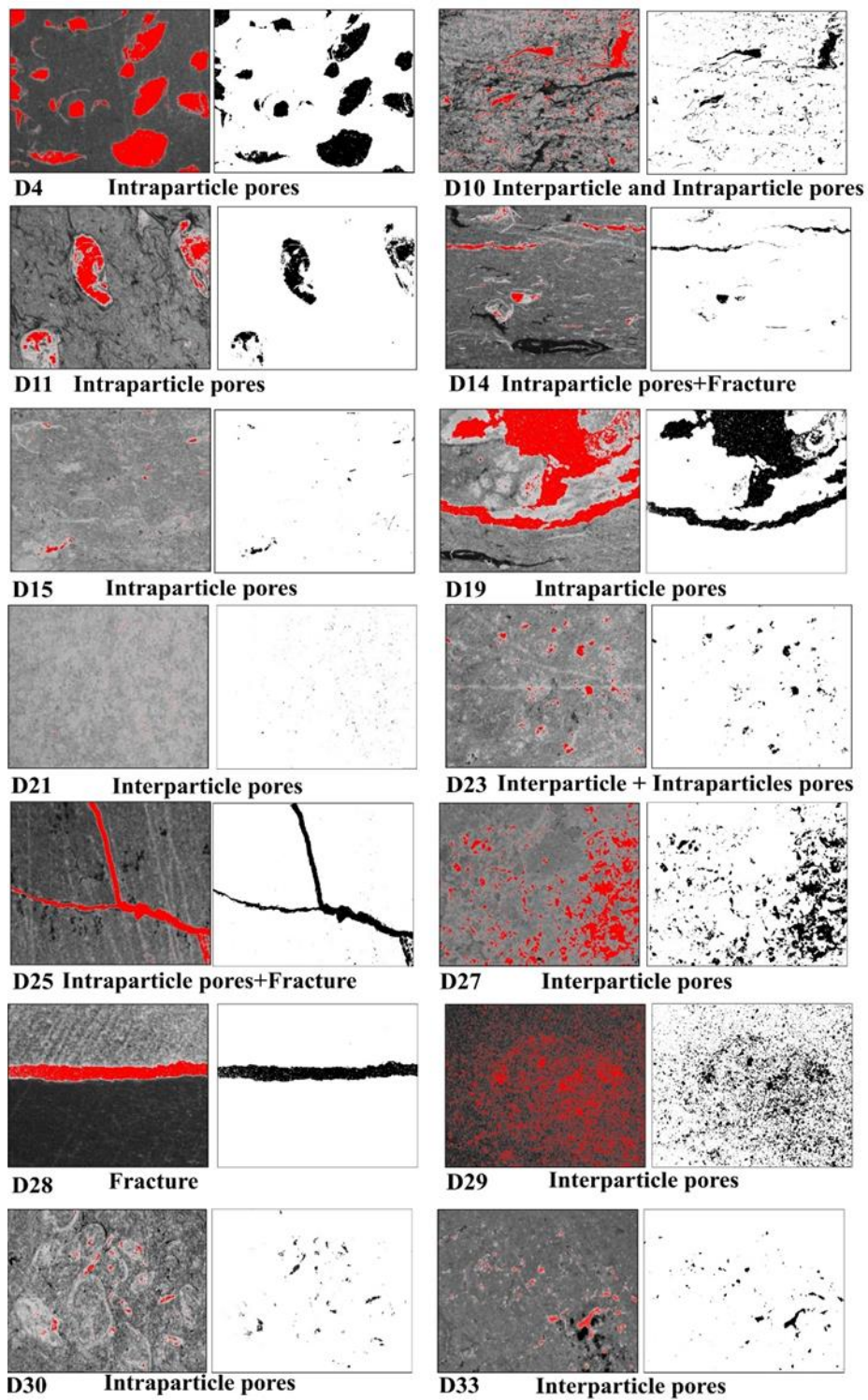


Figure 8.23. Photomicrographs and porosity sketch of the Dağhacılar section (D) samples. The red color indicates pore spaces in the photomicrographs. Black patches within the white square background indicates pore spaces sketch in the photomicrographic image. (PPI, x04).

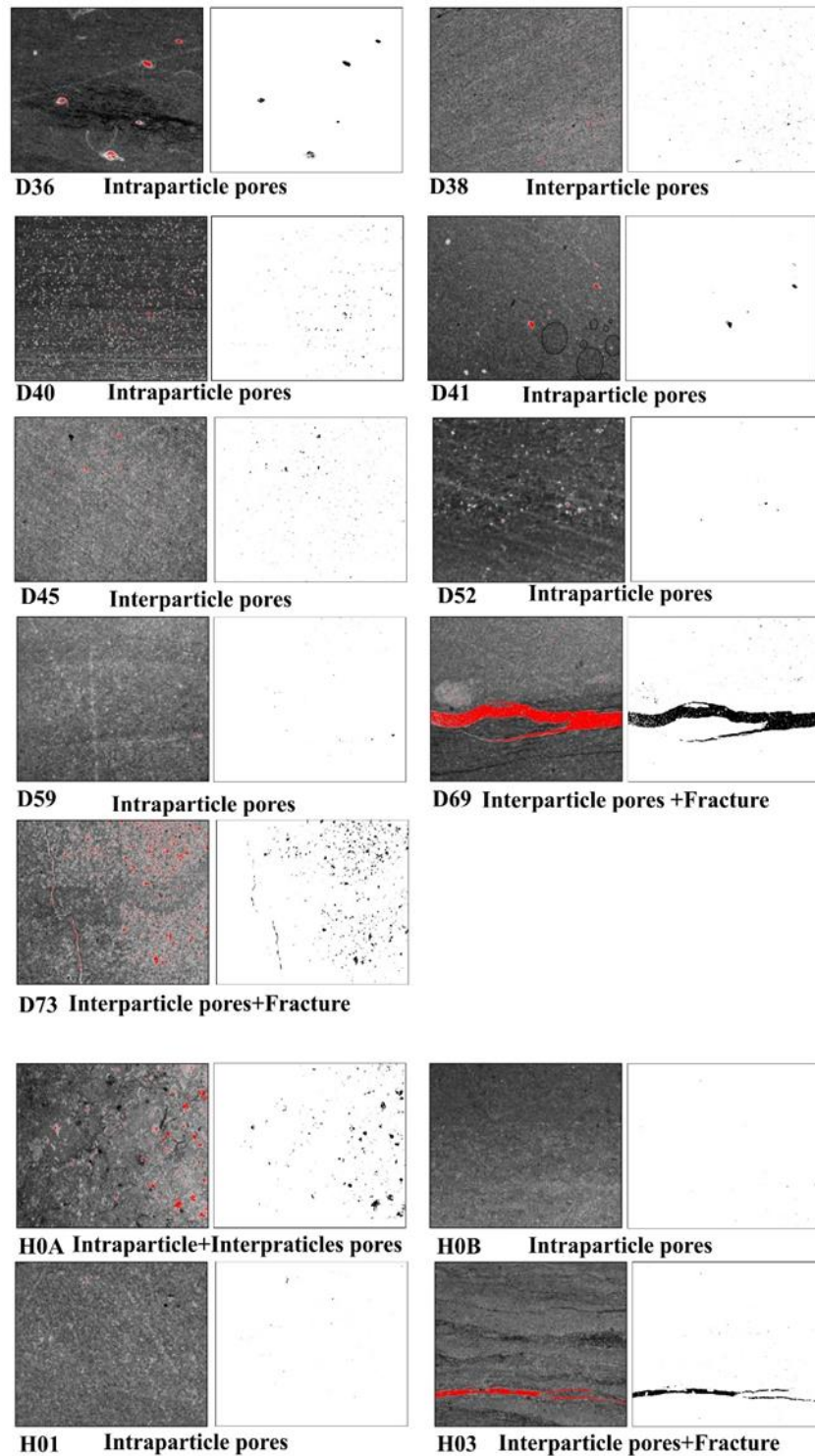


Figure 8.24. Photomicrographs and porosity sketch of the Dağhacılar section (D) and Hasanlar section (H) samples. The red color indicates pore spaces in the photomicrographs. Black patches within the white square background indicates pore spaces sketch in the photomicrographic image. (PPI, x04).

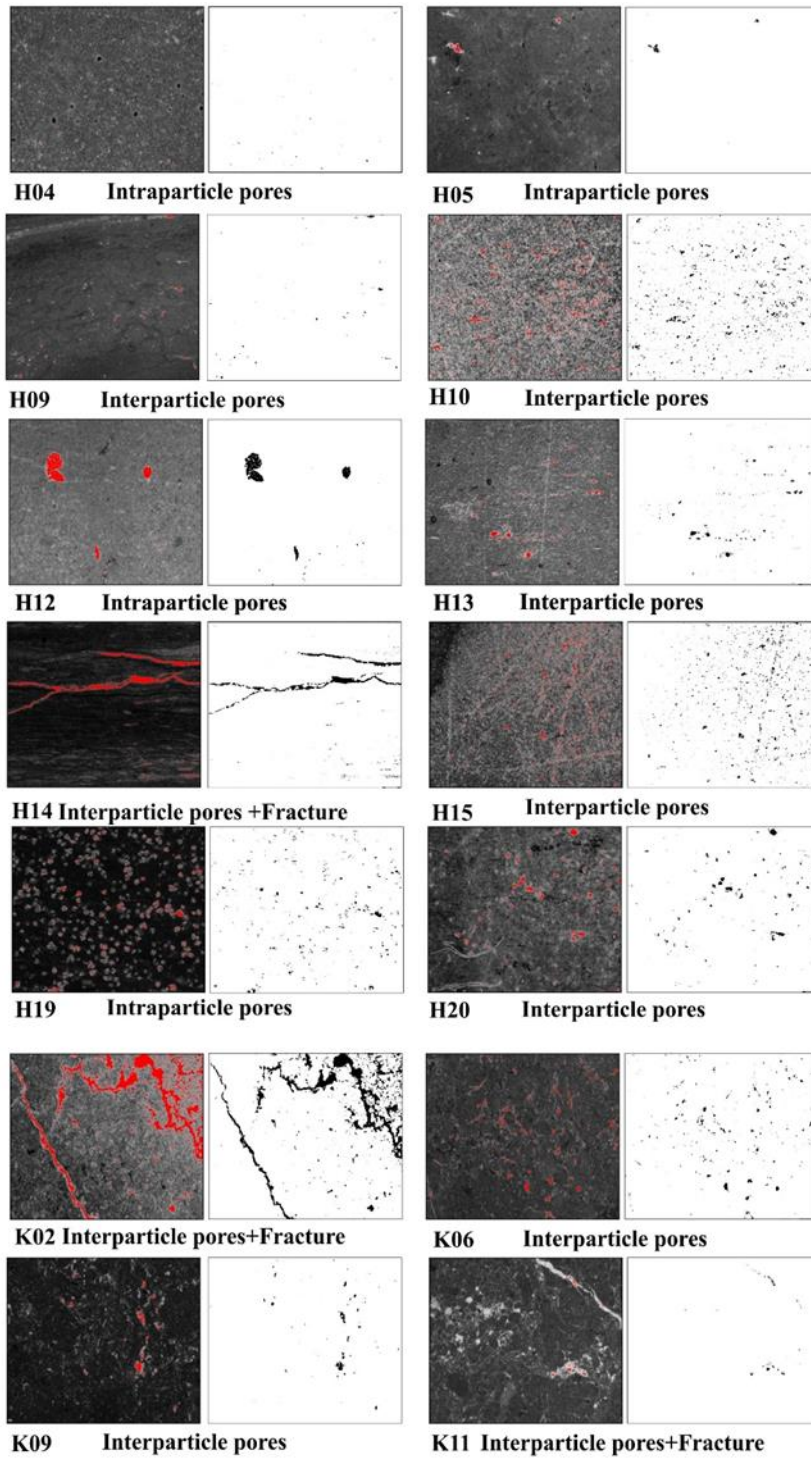


Figure 8.25. Photomicrographs and porosity sketch of the Hasanlar section (H) and Köşüre section (K) samples. The red color indicates pore spaces in the photomicrographs. Black patches within the white square background indicates pore spaces sketch in the photomicrographic image. (PPI, x04).

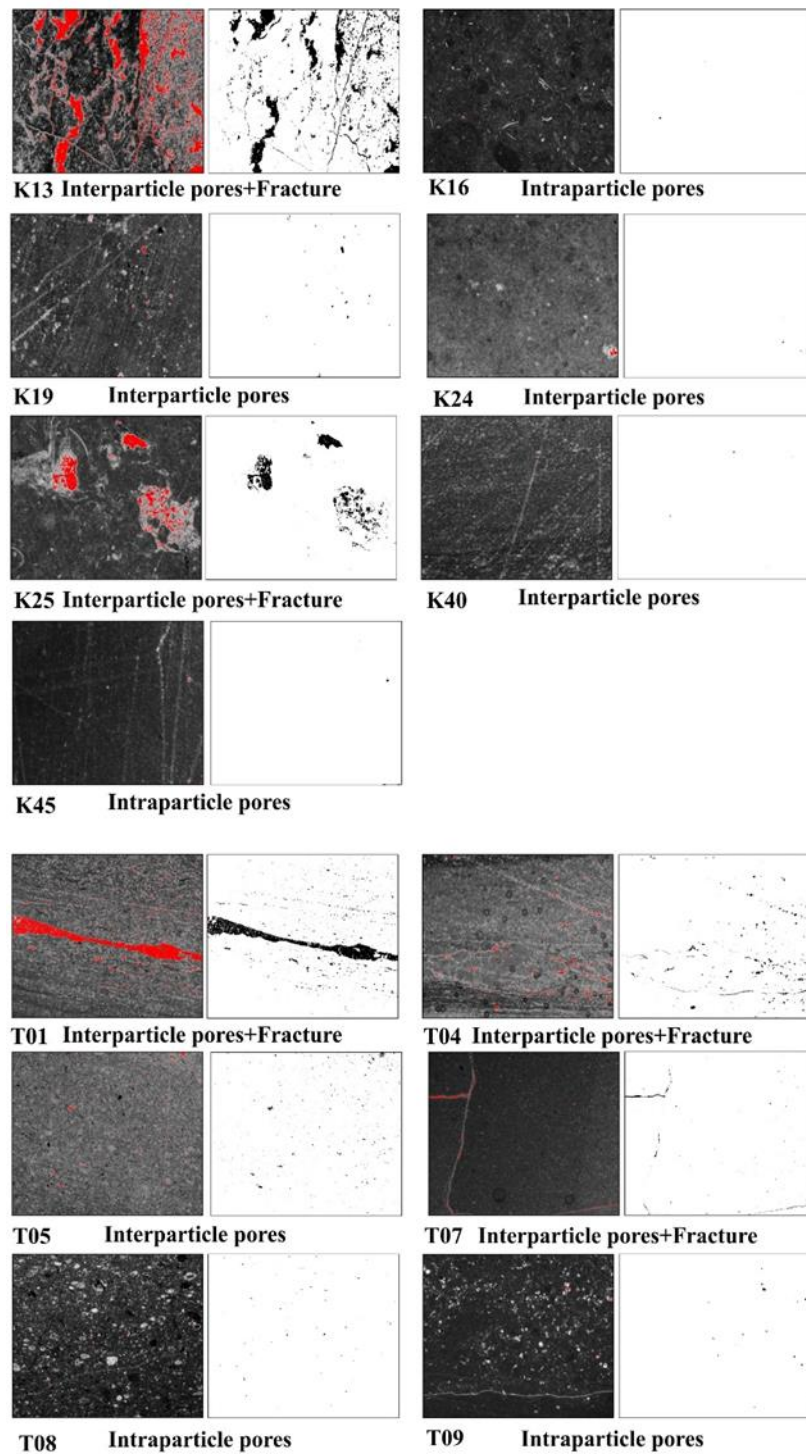


Figure 8.26. Photomicrographs and porosity sketch of the Köşüre section (K) and Karahisar section (T) samples. The red color indicates pore spaces in the photomicrographs. Black patches within the white square background indicates pore spaces sketch in the photomicrographic image. (PPI, x04)

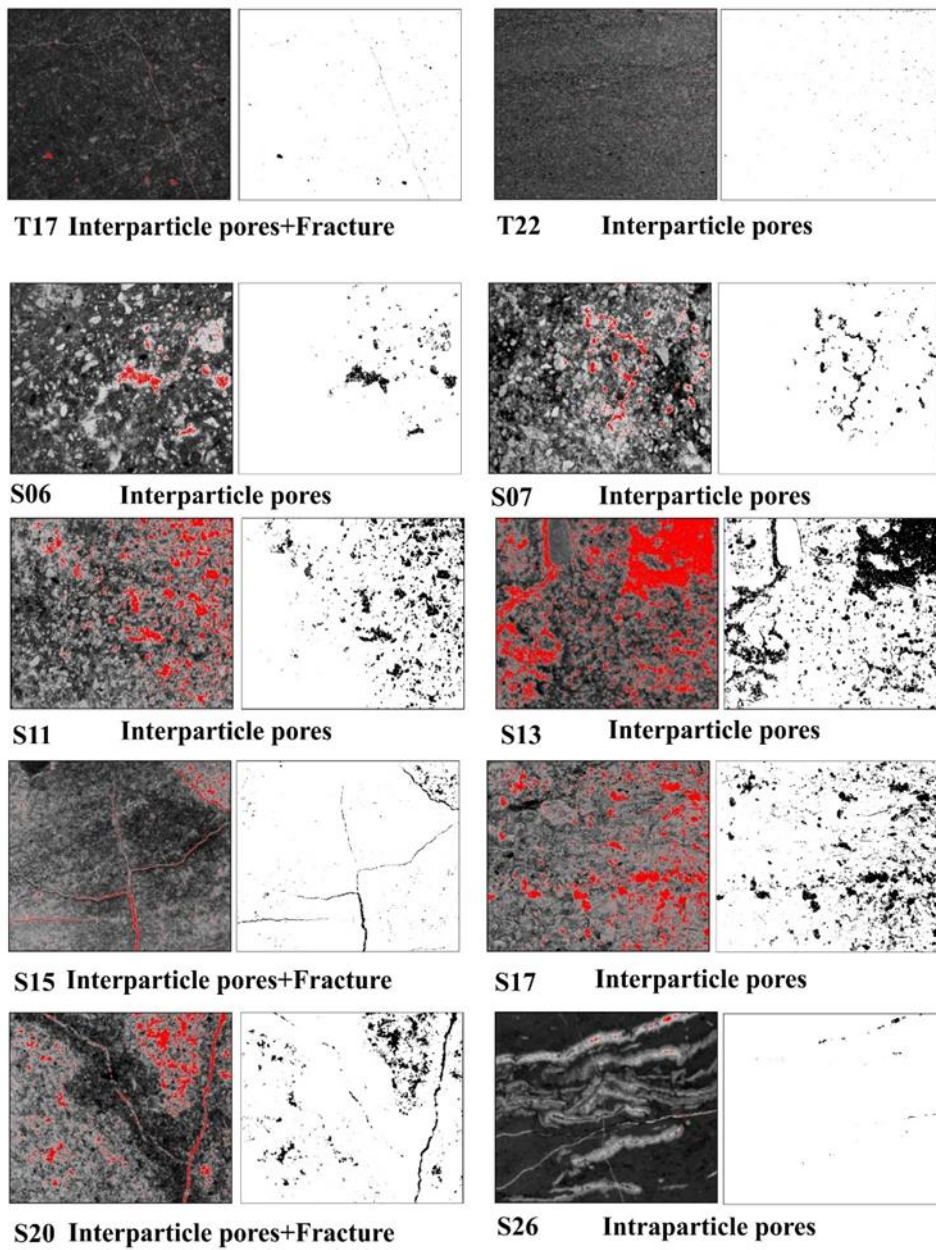


Figure 8.27. Photomicrographs and porosity sketch of the Karahisar section (T) and Sünnet section (S) samples. The red color indicates pore spaces in the photomicrographs. Black patches within the white square background indicates pore spaces sketch in the photomicrographic image. (PPI, x04).

8.26; 8.27). The micro-fracture porosity is formed as a result of tectonic stress on the high brittle mineral content bearing lithofacies. The laminae-fracture porosity types are defined as the dissolution of calcite laminae along the laminae edge and/or fracture opening along the laminae features.

### **8.5. Source Rock Potential on the Petrographic and Geochemical Approaches in the Studied Sections**

Source rocks are defined as organic-rich sediments that can be deposited in a various sedimentary environment with oxygen-depleted conditions such as deep marine, lacustrine and deltaic environmental settings (Hunt, 1991; Magoon and Dow, 1994). Generally, the term source rock is used to a rock that contains enough organic matter and suitable chemical composition to generate and extract hydrocarbons through biogenic or thermal methods (Miles, 1994). The source rock term is applied regardless of whether its organic matter is mature or immature (Tissot and Welte, 1984; Belaid et al., 2010). The organic matter content in the source rock may be less than 1% (Taylor et al., 1998). Generally, the 1-2 wt.% organic carbon content (TOC) in the shale and carbonate-type are good source rock and higher than 2 wt.% are characterized as very good source rock (Cornford, 1998; Feng, 2011; Cornford et al., 2014). Higher organic matter content precedes to higher production of hydrocarbon. The Oil-shale is defined as sedimentary rock types (carbonate, shale and marl) that contain immature high organic matter content. The immature organic matter contents in the oil-shale are insoluble in organic solvent but extract liquid oil-like hydrocarbon through destructive distillations, i.e 500-600 °C temperature with a minimum oil yield of approximately 5% (Alali et al., 2015). The estimated organic matter content in the organic-rich lithofacies in the studied sections are generally high, which are between 0.35wt.% to 29.91wt.% (Appendices A2; A4; A6; A8; A10; Figure 8.29). The obtained values of organic matter from Middle Eocene measured stratigraphic sections are approximately identical to the Himmetoğlu oil-shale and Hatıldığ oil-shale field in Göynük (Şener and Gündoğdu, 1996; Şener and Şengüler, 1998), Beypazarı oil-

shales (Şener et al., 2013), Seyitömer oil-shale (Kök et al., 2001), Paleocene-Eocene oil-shales in the Nallıhan Region (Sari & Aliyev, 2006; Altun et al., 2006).

In the recent era, around the world, the organic-rich deposits are mainly focused for the oil and gas exploration and as well as unconventional exploration (Liang et al., 2017). For this purpose, the source rock potential in the studied sections are evaluated through the analysis of geochemical obtained data and petrographic studies. The geochemical data and microscopic image analyses help in the identifying the intervals of high organic matter content, carbonate content, clay content and detrital grains content and visual porosity character in the studied sections (Figures 8.28; 8.29; 8.30; 8.31; 8.33). Generally, organic-rich deposits refer to fine-grained sedimentary rocks, such as shale and mudstone associated with marine, marine-terrestrial transitional and lacustrine (Zou et al., 2010). In the study, the oil-shale term is not only associated with organic-rich shale or marl lithofacies but also includes organic-rich limestone facies, which indicate source rock character and possesses high organic matter content (Figure 8.33). In the exploration geology and geochemical studies, the term oil-shale is used for the rocks that are immature regarding hydrocarbon generation. In general, any sedimentary rock which generates oil through pyrolysis, are characterized as oil-shale (Tissot and Welte, 1984). Therefore, oil systems are used to describe the organic-rich deposits, which yielding the oil upon the pyrolysis (Tissot and Welte, 1984; Suárez-Ruiz et al., 2012).

The organic-rich shale lithofacies in the studied sections generally have highest brittle character mineral content, relatively low clay content and having microscale porosity (Figures 8.22; 8.23; 8.24; 8.25; 8.26; 8.27; 8.28; 8.29; 8.30; 8.31; 8.33). Similarly, the limestone units in the studied sections have a brittle character with microscale porosity and having high organic matter content. Generally, the amount of organic matter in the sedimentary rock are also described as total organic carbon (Hunt, 1995). It is purposed that the good unconventional oil-shale reservoir composed of TOC more than 2% and more than 40% brittle character (Table 8.11) (Zou et al., 2010; Wang et al., 2014; Ma and Holditch, 2015; Jiang et al., 2016). Along the organic matter content

and brittle character, low-permeability and nano to microscale pores are also important factor for the productivity of unconventional reservoir (Curtis et al., 2010; Afsharpoor and Javadpour, 2016). The evaluation of the organic geochemical data and microscopic analysis indicate that organic-rich oil-shale, organic-rich marl and organic-rich limestone facies in the studied sections possess relatively excellent potential as source rock and may have good reservoir character (Figure 8.21; 8.33). The observed pore types in the organic-rich lithofacies of the studied sections are interparticle pores, intraparticle pore and micro-fracture (Figures 8.23; 8.24; 8.25; 8.26; 8.27). The presence of high brittle mineral content and low clay content in the lithofacies of studied sections promote natural and artificial fractures, which are important characteristics, more specifically in terms of unconventional reservoir exploration (Figures 8.21; 8.33).

The organic-rich lithofacies of the studied sections possess high organic content (0.35 wt.% to 29.91 wt.%), high carbonate content (7.31 wt. % to 92.66 wt.%) and relatively moderate porosity (Appendices A2; A4; A6; A8; A10; Figures 8.22; 8.28; 8.29). The organic-rich lithofacies in the Dağhacılar section, Hasanlar section and Sünnet section are characterized as excellent source rock potential and can have good reservoir properties except certain level along the measured stratigraphic column, where the organic matter content is less than 3.5 wt. %, relatively high clay content and relatively zero or near to zero porosity (Figure 8.33) (Hongjun et al., 2016). The Köşüre and Karahisar sections are identified as good-excellent source rock potential with mostly ductile rock character, based on the relatively high clay content at certain levels and very low porosity character. Generally, sublittoral-profunda depositional intervals in the studied sections indicate high organic matter content with brittle mineral content and specify the excellent source rock character. The marine condition in the studied sections are mostly dominated by sandstone lithofacies with interbedded organic-rich shale and occasional marl. The organic-rich shale in the marine intervals possesses good source rock potential (Figure 8.33). The sandstone in the intervals are well cemented character and illustrate poor reservoir feature.

Based on the geochemical data and petrographic analysis, the most prospective oil intervals in the region are in the Sünnet section and Dağhacılar measured section and then followed by the Hasanlar, Karahisar and Köşüre sections (Figure 8.33).

#### **8.5.1. Source rock potential on the petrographic and geochemical approaches in the Dağhacılar section**

The Dağhacılar section lithofacies indicate high average organic matter content (around 10 average wt.%) and 4.72 average wt.% visible porosity (Appendices A2; Table 8.6; Figure 8.21). The lithofacies of the studied section represent high carbonate content (58.42 average wt.%), low clay content (24.04 average wt.%) and detrital grains (10.47 average wt.%) (Figure 8.21). The identified porosity types in the lithofacies are intraparticle pores, interparticle pores and fracture porosity (Figures 8.23; 8.24). In the measured stratigraphic section, the porosity is higher in the lower and middle portion as compared to the upper portion of the studied section (Figure 8.22). Based on the geochemical data and petrographic analyses, it is interpreted that the Dağhacılar section describes excellent source rock potential (Tables 8.1, 8.11; Figure 8.33). In the Dağhacılar section, there is also observation of oil staining in the oil-shale at certain level (Figure 8.32)

#### **8.5.2. Source rock potential on the petrographic and geochemical approaches in the Hasanlar section**

In the Hasanlar section, the 12.04 average wt.% organic matter content is observed with 1.47 % average visible porosity calculated in the organic-rich lithofacies (Appendices A4; Table 8.7; Figure 8.21). Generally, the Hasanlar section is characterized by high carbonate content, relatively low clay content and low detrital grains (Table 8.7). The recognized pores type in the lithofacies are intraparticle pores type, interparticle pores type and occasionally micro-fracture porosity (Figures 8.24, 8.25). The Hasanlar section is defining relatively excellent source rock potential (Tables 8.2, 8.11). It possesses high organic matter content and low visible porosity in the lithofacies (Figure 8.33).

### 8.5.3. Source rock potential on the petrographic and geochemical approaches in the Kösüre section

The samples of the Kösüre section are characterized by variable organic matter content, clay content and detrital content at different intervals (Appendices A6; Figure 8.9). The average organic matter content, average carbonate content, average clay content and average detrital content are 8.29 wt.%, 53.93 wt.%, 39.72 wt.% and 1.18 wt.% (Appendices A6; Figures 8.21). This studied section shows low visible porosity percent compared to Dağhacılar studied section (Figures 8.22; 8.25; 8.26). The average visible porosity in the studied section is 1.84% (Table 8.8). The studied section indicates good to very good source rock. At certain level in the studied section, source rocks indicate ductile character source having high clay content (more than 40%) and/or very low percent of visible porosity (Figures 8.9; 8.22; 8.25; 8.26). Generally, the Kösüre section characterize as very good to excellent source rock (Tables 8.3, 8.11; Figure 8.33).

Table 8.11. Geochemical parameters used to determine the oil potential (Quantity) of an immature source rock. (Tissot and Welte, 1984; Jarvie, 1991; Peters and Cass, 1994)

Peters and Cass (1994)		Tissot and Welte (1984)		Jarvie (1991)	
Corganic (wt. %)	Oil potential	Corganic (wt. %)	Oil potential	Corganic (wt. %)	Oil potential
0 - 0.5	Poor	0.1 – 0.5	Weak	0 – 0.5	Insufficient
0.5 - 1	Fair	0.5 – 1	Moderate	0.5 – 1	Moderate
1 - 2	Good	1 – 2	Good	> 1	Enough
2 – 4	Very Good	2 - 10	Rich		
> 4	Excellent				

### 8.5.4. Source rock potential on the petrographic and geochemical approaches in the Karahisar section

The lithofacies of the Karahisar section contains around 12.45 average weight percent organic matter content, 47.86 average wt.% carbonate content, 34.41 average wt.% clay content and 8.77 average wt.% detrital grains (Appendices A8; Figures 8.12;

8.21). The porosity types in the studied section are commonly interparticle pores, intraparticle pores and micro-fracture porosity (Figures 8.26; 8.27). The observed porosity in the lithofacies is very low. The obtained average visible porosity from the studied samples is 0.73% which is lowest compared to other studied sections (Table 8.3; Figure 8.22). The Karahisar section is identified as excellent source rock potential (Tables 8.4, 8.11; Appendices A8).

#### **8.5.5. Source rock potential on the petrographic and geochemical approaches in the Sünnet section**

The Sünnet section lithofacies have the highest detrital contents (8.45 wt.%-70.69 wt.%), and moderate carbonate enrichment (about 34.28 wt.%) (Appendices A10). The content of organic matter in the studied section is high, with 4.36 wt.% minimum, 29.91 wt.% maximum and 11.72 average wt.% value (Appendices A10). The dominant porosity types in the samples are interparticle pores with a good connectivity and occasionally presence of fracture porosity and intraparticle porosity (Figure 8.27). The fields studies, petrographic analysis and geochemical data interpret that the Sünnet section is composed of organic-rich deposits with brittle mineral content and abundant detrital grains (Figure 8.15). The Middle portion of the studied section is categorized as excellent source rock potential (Tables 8.5, 8.11; Figure 8.33). At certain horizon in the studied section, there is observation of oil staining in the sandstone lithofacies (Figure 8.32).

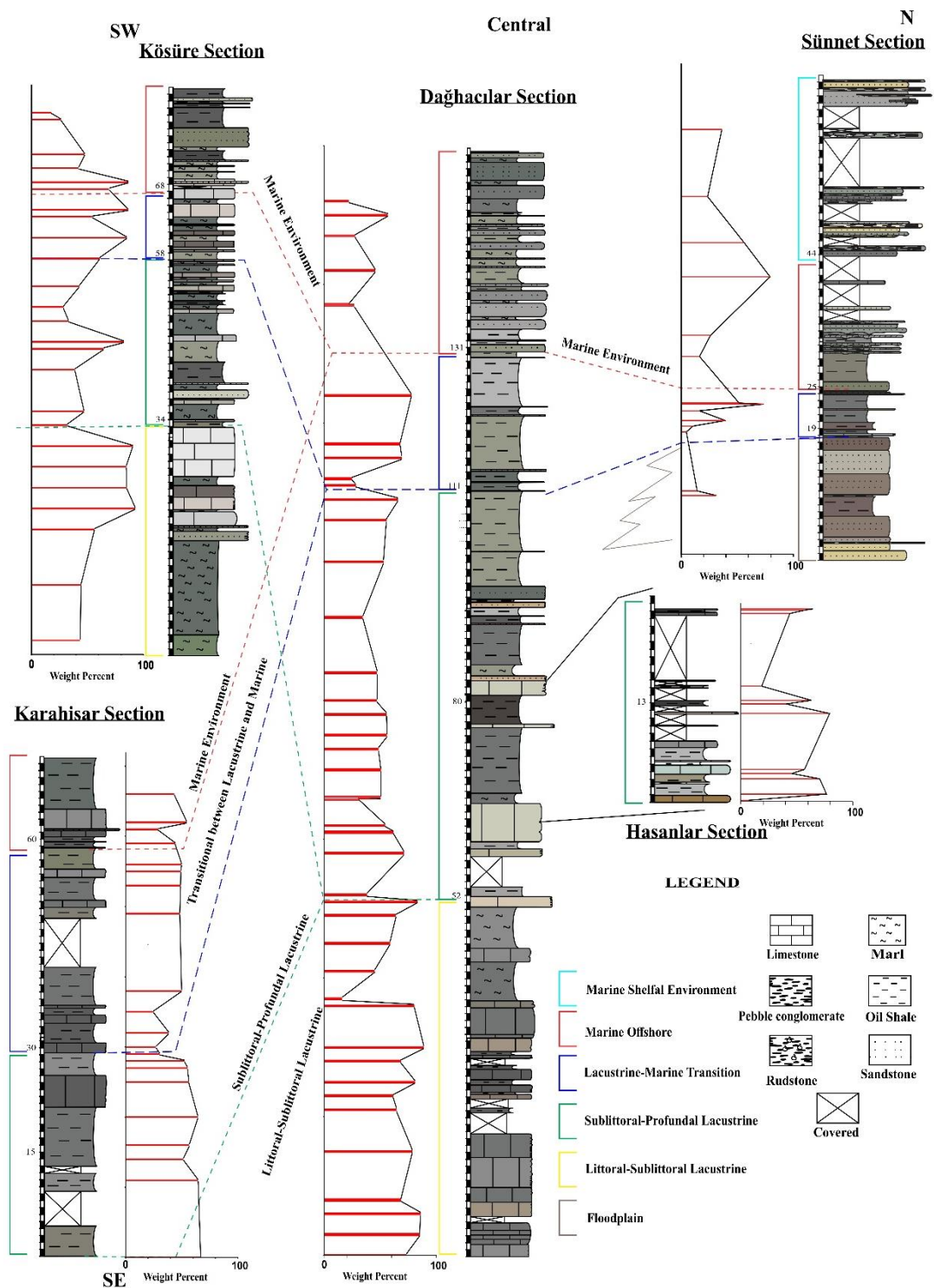


Figure 8.28. Graphic presentation of the  $\text{CaCO}_3$  wt.% along measured stratigraphic sections of the Dağhacılar, Köşüre, Karahisar and Sünnet sections and their correlation.

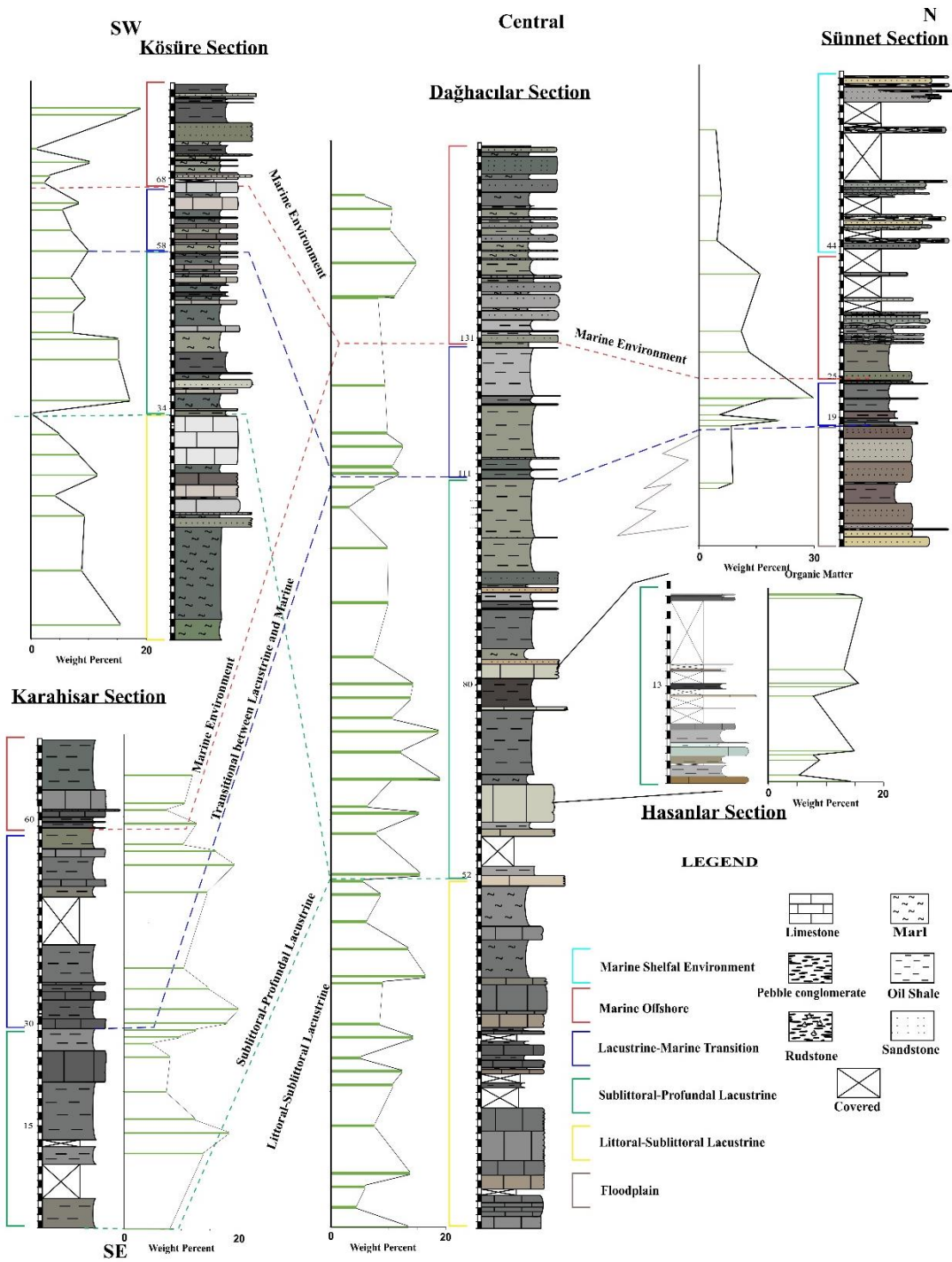


Figure 8.29. Graphic presentation of the organic matter content wt.% along measured stratigraphic sections of the Dağhacılar, Köşüre, Karahisar and Sünnet sections and their correlation.

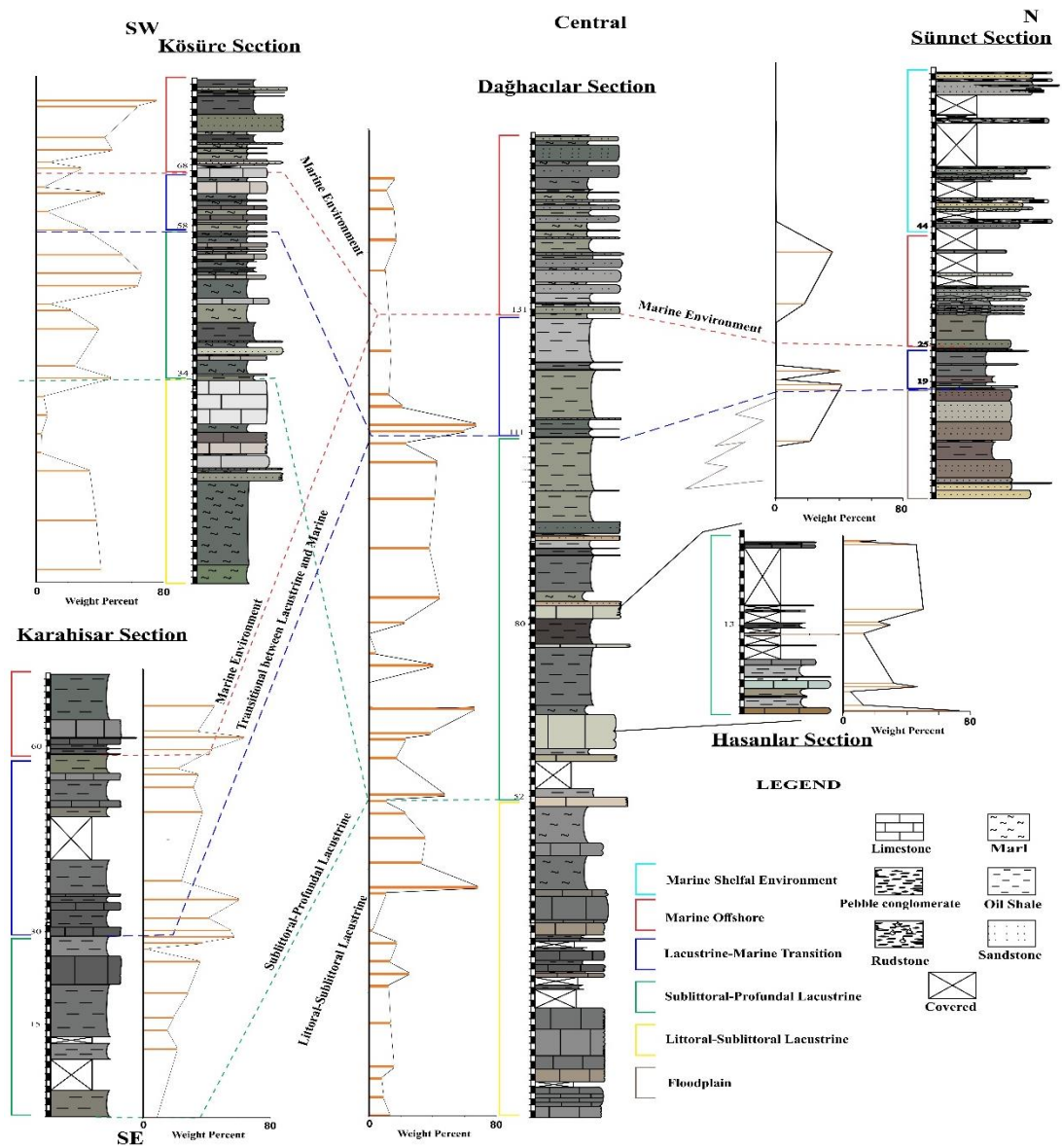


Figure 8.30. Graphic presentation of the clay content wt.% along measured stratigraphic sections of the Dağhacılar, Köşüre, Karahisar and Sünnet sections and their correlation.

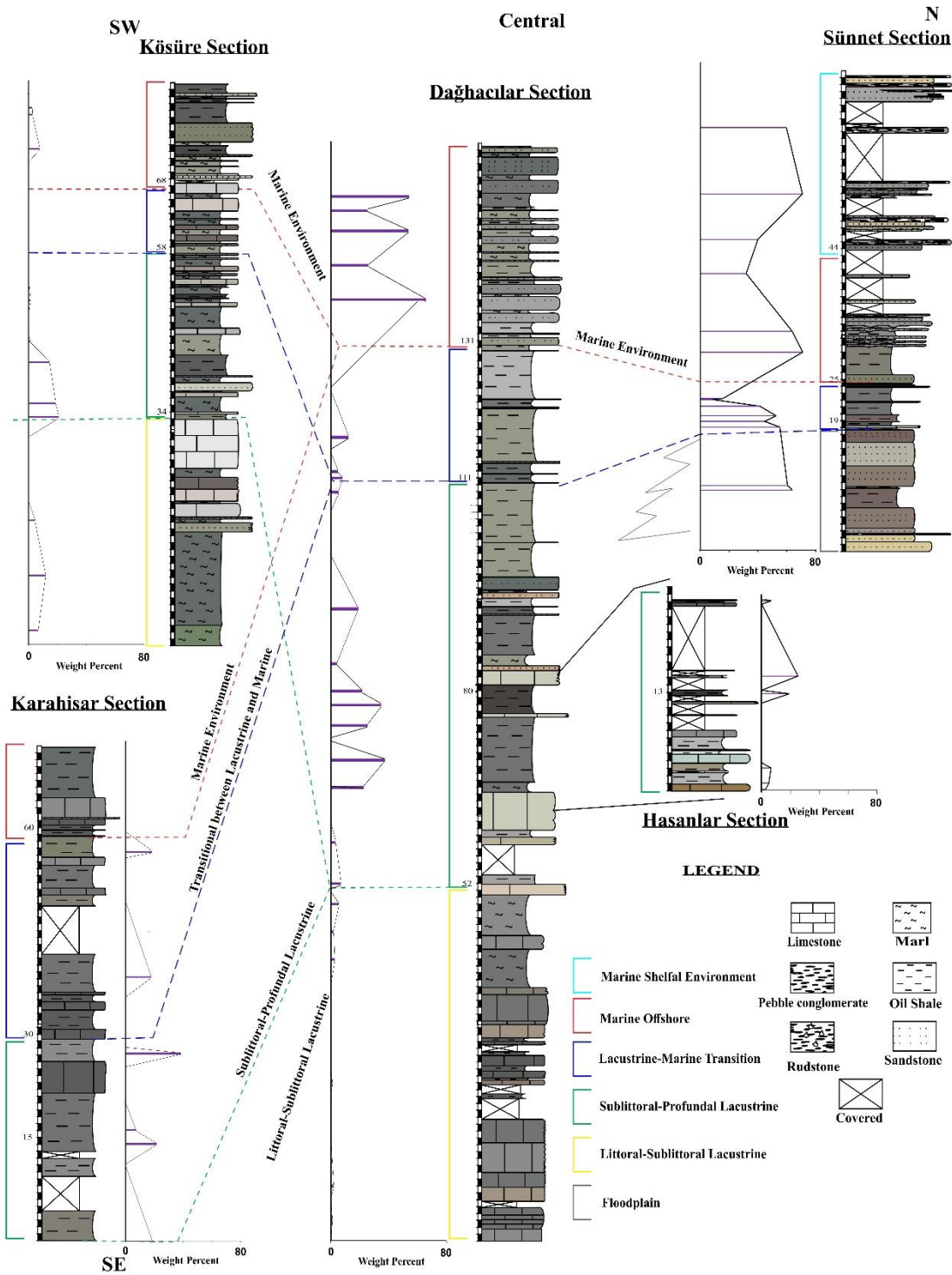


Figure 8.31. Graphic presentation of the quartz/feldspar content wt.% along measured stratigraphic sections of the Dağhaclar, Köşüre, Karahisar and Sünnet sections and their correlation.

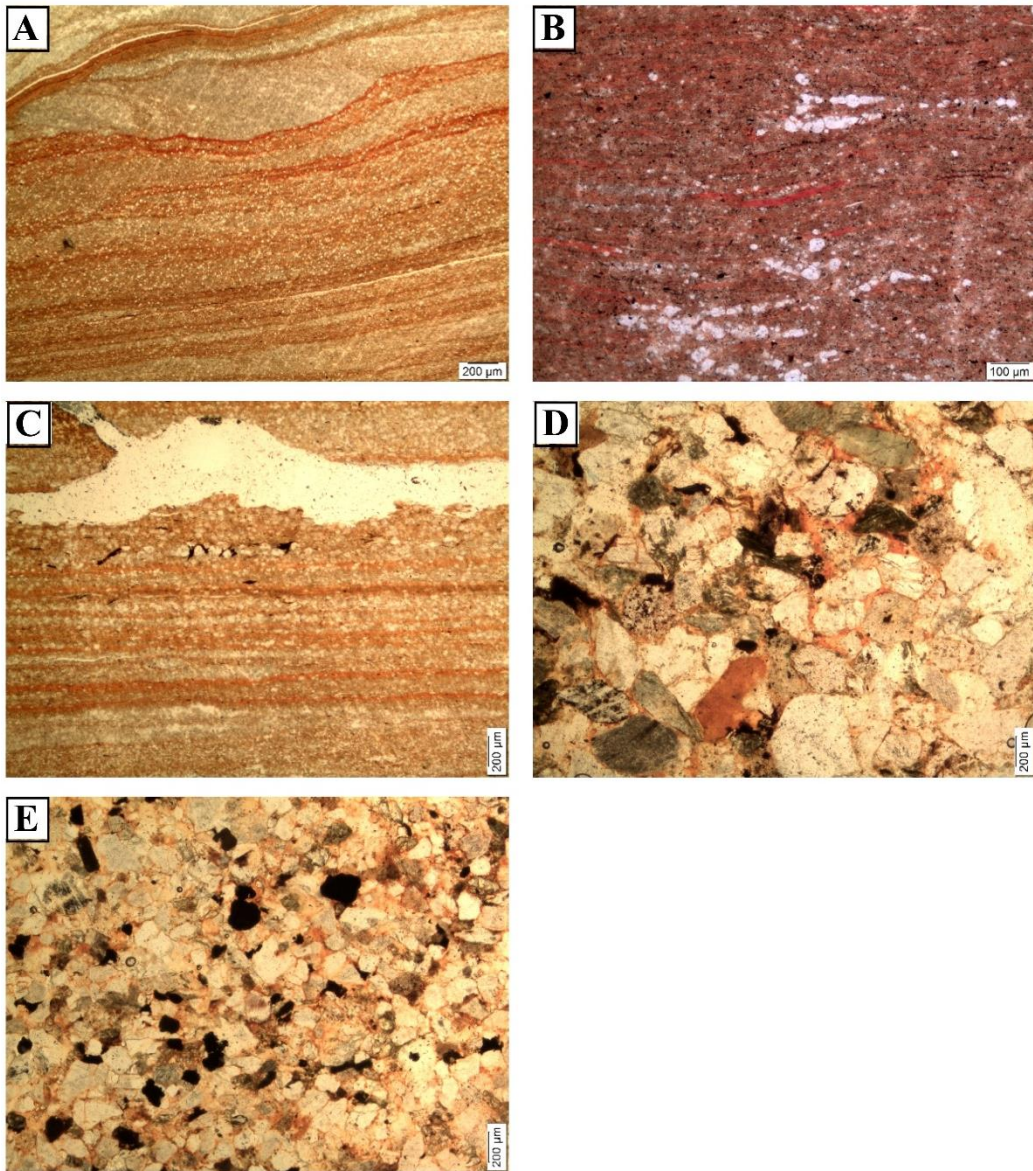


Figure 8.32. Representing photomicrographs of oil stained shale and sandstone from the A) Dağhacılar (sample D40, x4, PPI), B) Hasanlar (sample H13, x10, PPI), C) Karahisar (sample T1, x4, PPI) and D-E) Sünnet sections (S1 and S29, x4, PPI).

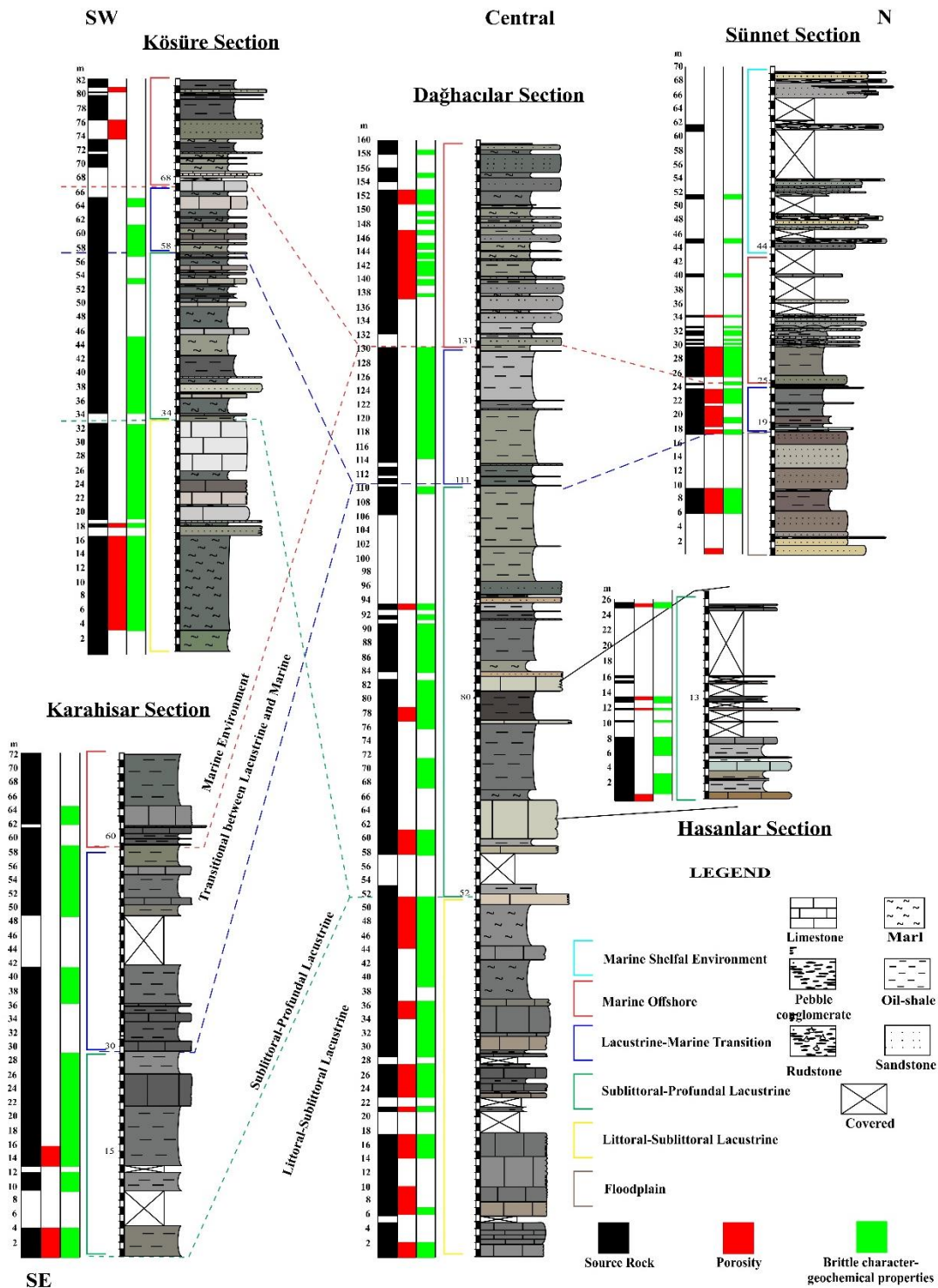


Figure 8.33. Graphic presentation of the source rock, porosity and brittle character composition along measured stratigraphic section of the Dağaçlar, Köüre, Karahisar and Sünnet sections.

## CHAPTER 9

### DISCUSSION

The Middle Eocene (Lutetian-Bartonian) successions are measured from five different localities in the Mudurnu-Göynük basin, Northwestern Turkey. Generally, it has been interpreted that the several lacustrine basins are developed in the central and western Anatolia, during the Paleocene to Upper Miocene. Such tectonic settings in the region are resulted in the response of basin-scale uplift at the end of the Late Cretaceous and ends at the end of the Eocene period. This tectonic event is related to the opening and closing of the Neo-Tethys ocean. The resulting depositional facies in the region are characterized by continental- shallow marine deposits in the southern part of the basin and deep marine deposits in the northern part of the basin (Saner, 1977, 1980b; Şengör and Yılmaz, 1981; Şener, et al., 1995; Şener and Göncüoğlu, 1996; Ocakoğlu et al., 2007). During the Paleogene, the development of lagoonal/lacustrine systems in the Mudurnu-Göynük basin and the adjacent regions are associated to this Neo-Tethys tectonic event. It has been reported that some of them are important for the oil-shale and coal exploration. The lagoonal/lacustrine deposits in the studied basin are overlain by marine deposits (Saner, 1980b; Şener, et al., 1995; Şener and Gündoğdu, 1996; Sarı and Aliyev, 2005; Ocakoğlu et al., 2007, 2012) (Figure 1.4). In this study, the measured Middle Eocene (Lutetian-Bartonian) successions in the Mudurnu-Göynük basin are carried out for the oil-shale facies, sedimentology analysis, depositional environment, depositional cyclic stacking pattern and sequence stratigraphic interpretation, source rock; their visual porosity and geochemical character. Tectonically and geologically, the studied successions describe lacustrine deposits with episodic marine-influence and overlain by marine deposits from north to south. It has been interpreted that the lacustrine deposits in the Mudurnu-Göynük basin are separated from marine environment in the north by barrier deposits (Figures 5.11, 5.12

and 5.13) (Saner, 1977, 1980b; Şengör and Yılmaz, 1981; Şener, et al., 1995; Şener and Göncüoğlu, 1996; Ocakoğlu et al., 2007, 2012).

### **9.1. Facies Distribution in the Middle Eocene (Lutetian-Bartonian) studied sections**

The Middle Eocene (Lutetian-Bartonian) studied sections are recognized in this study as Upper Kızılçay Formation and Halidiye Formation, based on stratigraphic position and previous stratigraphic studies of the studied region (Ocakoğlu et al., 2007, 2012; Şafak et al., 2015). Based on the recorded fossil assemblages in the Kızılçay Formation and Halidiye Formation, it has been identified that the formations belong to Lutetian-Priabonian periods (Ocakoğlu et al., 2007, 2012; Şafak et al., 2015). In this study, the measured successions in the Dağhacılar, Hasanlar, Köşüre and Karahisar regions are brackish-lacustrine depositional succession, which are overlain by marine-transitional deposits in the basin toward the top. Near the Sünnet village, the formation indicates floodplain deposits at the base, which is topped by marine offshore transitional deposits. Simply, the transgression in the basin result in the eventual linkage of lacustrine environment in the south to the marine depositional environment in the north. In the study, it is estimated that the lacustrine environment is approximately >35km wide between the Köşüre marginal southwest section and the Sünnet floodplain-marine environment (Barrier) succession in the north; and approximately >25km wide between the Karahisar relative deeper marginal southeast section and the Sünnet floodplain-marine environment (Barrier) succession in the north. Based on this framework, the Dağhacılar section and Hasanlar section are characterized as the central portion of the lacustrine environment in the studied region. The studied sections generally comprise of limestone, oil-shale, intercalating marl intervals and fine to coarser-grained sandstone lithofacies. In the northern studied section, near the Sünnet village, presences of occasional conglomeratic beds and calcirudite beds are observed. The recorded fauna in the measured sections are ostracods, brackish charophytes, gastropods, bivalvia, benthic Foraminifera (including nummulites and other Foraminifera), fish-teeth and scales, echinoderms,

algal filamentous and plant fragments. In the proximity of the Dağhacılar village, the measured section consists of very thick to very thin bedded, ostracod-gastropod bearing limestone, lime mudstone, marl, laminated and non-laminated oil-shale and very fine to coarser sandstone. The measured section in the basin represents central portion of the lacustrine depositional environment and is overlain by the siliciclastic, oil-shale and marl facies of marine deposits towards the top. To the southwest and southeast of the Dağhacılar section, the measured section includes Köşüre section and Karahisar section, which depicts the marginal to relative deeper lacustrine deposits, composed of limestone with interbedded marl, lime mudstone, occasional oil-shale, sandstone lithofacies; and intercalating oil-shale-lime mudstone units, respectively. Furthermore, the upper portion of the Köşüre section indicate siliciclastic-oil-shale and occasional limestone units of marine origin. The Karahisar section suggested restricted lacustrine environment deposits, which is overlain by the marine lime mudstone-oil-shale with occasional Fe-Mn spherical nodule and sandstone deposits. The Hasanlar section, in the west of the Dağhacılar measured section is composed of lime mudstone and oil-shale with occasional marl and define central portion of the lacustrine environment. In the north of the Dağhacılar measured section, the barrier deposits in the Sünnet section are composed of siliciclastic floodplain deposits, which is overlain by marine shelf deposits. The marine shelf deposits are composed of predominate fine and coarser siliciclastic deposits with association of fossiliferous limestone and organic rich shale. Generally, the shale lithofacies in the studied sections are predominately of calcareous character. Similarly, the sandstone lithofacies also possess calcareous character. The interpreted depositional setting in the studied region indicate lacustrine-marine offshore-transitional deposits in the south and barrier -marine deposits in the north (Figures 5.11; 5.12 and 5.13).

## **9.2. Paleoenvironment and Age; based on fossil assemblages**

The paleontological evidences from the studied sections are also important in terms of depositional condition, paleoenvironmental setting and interpretation of stratigraphic position of the successions in the studied region. In the studied sections, the Dağhacılar

section and Sünnet section contain high abundance of fauna as compared to the Köüre section> Hasanlar section> Karahisar section (Figure 5.6). The recorded fauna in the studied sections are freshwater-brackish ostracods, brackish-charophyte gyrogonites, gastropod, bivalve, nummulites, echinoderms, algal filamentous, fish-teeth, fish scales and plant fragments (Figures 3.9; 3.12; 3.25; 3.36; 3.37; 3.42; 3.43; 3.44; 3.45; 4.3; 4.4; 4.5; 4.6). The extracted ostracods and charophytes fauna species from the studied sections indicate Oligo-Mesohaline lacustrine depositional setting which is transgressively overlain by marine environment toward the top. In the wackestone-packstone microfacies, the presence of ostracods, gastropods and charophytes indicate deposition in the alkaline environment setting with slightly brackish character (Freytet and Plaziat, 1982; Tunoğlu, 2001; Sanjuan & Martín-Closas, 2012). The demise of the freshwater, brackish lacustrine fauna and appearance of marine fauna at different locates such as nummulites, echinoderms, bivalve, gastropod and ostracod also support the marine transgression into lacustrine environment in the studied successions. The recorded marine fauna and flora in the successions refer to the marine depositional condition (Martín-closas, 2009).

The Middle Eocene (Lutetian-Bartonian) age has been assigned to the measured sections by recording ostracod assemblages that includes *Cyclocypris* sp., *Candona* sp., *Potamocypris* sp., *Heterocypris* sp., *Stenocypris* sp., *Neocyprideis* sp. genera and associated charophyte gyrogonites. The ostracods and charophyte assemblages age are also supported by stratigraphic position and equivalent to different stratigraphic successions in the region (Şener and Şengüler, 1997, 1998; Gedik and Aksay, 2002; Ocağolu et al., 2007, 2012; Şafak et al., 2015). Based on these evidences, it is also predicted that the Dağhacılar section, Hasanlar section, Köüre section, Karahisar section and Sünnet section may approximately correspond to 6.0 Ma (45.0 to 39.0 ±1.0Ma), ≈1.0 Ma (42.5 to 41.5 ±1.0Ma) ≈2.5 Ma (42.0 to 39.5 ±1.0Ma), ≈2.0 Ma (41.5 to 39.5 ±1.0Ma) and ≈2.0 Ma (42.0 to 40.0 ±1.0Ma), respectively.

The lithological character and recorded fauna assemblages in the studied sections also support the Oligo-Mesohaline to brackish-lacustrine depositional environment. Such

Oligo-Mesohaline to brackish-lacustrine depositional condition in the studied sections occur due to episodic marine incursion to lacustrine environment. Relatively high percent of carbonate content deposition in the lacustrine environment in the studied sections support hydrological open environment, which have temporary linked with marine environment (Figure 8.28) (Fuhrmann, 2002; Cyr et al., 2014). The weakly positive correlation in the clay content and organic matter also indicate marine influence on the lacustrine environmental condition (Zeng et al., 2018). The overlain siliciclastic successions with occasional association of marine fauna indicate a switch from the lacustrine depositional condition to the transgressive marine environment, close to the Lutetian-Bartonian boundary. The fluctuation of mix fauna, lateral and vertical lithofacies variation in the studied region significant reflect the variation in the salinities and paleoenvironmental condition.

### **9.3. Variation in the relative lacustrine level and relative sea-level (Oligo-Mesohaline/Brackish-lacustrine and marine offshore transitional)**

Based on the facies association study, the Middle Eocene studied sections in the Mudurnu-Göynük Basin are divided into littoral-sublittoral to sublittoral-profundal lacustrine facies, marine offshore transitional depositional facies and floodplain paleosols facies to marine shelf environment facies. In the studied sections, the sediments generally reflect the deposition in the lacustrine environment, which later switches to marine environment.

In the Dağhacılar and Köşüre sections, the intercalating limestone-marl facies are related to the deposition in the littoral-sublittoral lacustrine condition (Pierce, 1993; Ramos et al., 2001 and Cabrera et al., 2001). The intercalating limestone-marl facies is characterized as inner lacustrine facies. The observation of lime mudstone-marl intercalation with occasional charophytes, ostracods and gastropods represent sublittoral condition with relative shallow lacustrine environment in the Dağhacılar section. The abundant gastropod-ostracod bearing wackestone-packstone facies with interbedded organic-rich shale and marl indicate littoral-sublittoral brackish-lacustrine

deposits in the Dağhacılar section. The brackish character gastropods, ostracods, charophytes and the presence of occasional nummulites in the studied section signify episodic marine incursion to the lacustrine basin (Willmann, 1985; Pierce, 1993; Sanjuan & Martín-Closas, 2012; Abimbola, 2016). In the southwest, the Kösüre section facies association indicate relative shallow oxygenate, calm condition, slightly brackish-lacustrine environment as compared to the Dağhacılar section. In the north, the Sünnet section facies association are characterized by floodplain deposits. The floodplain deposits are composed of coarser sandstone to fine-grained sandstone with conglomeratic, silty shale with gray mottling (Dini et al., 1998; Ranson, 2012). The floodplain deposits are topped by marine fossils bearing carbonate, fossiliferous coarser sandstone and bivalvia bearing organic rich shale and indicate paralic-marine shelf environmental deposits (Li et al., 2009).

In the next phase, the lacustrine successions in the Dağhacılar section, the southeast Karahisar section and southwest Kösüre section indicate relative rise in the lacustrine water depth. The relative shallow lacustrine facies are replaced by the dysoxic to anoxic condition, deeper facies such as predominate oil-shale with occasional interbedded marl and fine-grained sandstone in the central region, oil-shale with intercalating lime mudstone in the southeast studied section (Karahisar) and marl with interbedded limestone and oil-shale in the southwest region (Kösüre). This phase of the lacustrine deposition is categorized by dysoxic to anoxic condition, sublittoral-profunda lacustrine environment. Rhythmic symmetry within the succession indicate probable linkage to climatic fluctuation (Caillaud et al., 2017). The episodic siliciclastic beds in this studied intervals are related with periodic influx of terrigenous to the lacustrine in the low energy depositional condition (Platt and Wright 1991; Mingram, 1998; Calvo et al. 2000; Gierlowski-Kordesch 2010).

The transitional zone in the studied sections is the zone where a gradual change of open lacustrine environment transgressed into the marine depositional environment. In the Dağhacılar section and Karahisar section, the transitional zone is described by low sedimentation rate and comparatively high organic matter content, which occur

in response to change in the physiochemical condition (Mingram, 1998). In the Kösüre section, the transitional zone is defined by limestone-marl intercalation. The limestone unit is occasional characterized by abundant octahedral pyrite and appearance of echinoderms (Brown and Cohen, 1995; Baumiller & Gazdzicki, 1996; Elattaar, 2018). In the Sünnet section, the transitional zone is defined by abundant charophytes, brackish ostracods and plant fragment carbonate deposits (Sanjuan & Martín-Closas, 2012; Argakoesoemah, 2017). In the contrast, the Karahisar section represents restricted depositional condition. The transitional zone is described by the appearance of Fe-Mn spherical nodules bearing limestone with intercalating oil-shale lithofacies. The development of Fe-Mn spherical nodules in the limestone intervals are linked with physiochemical changes, and occur because of marine transgression into lacustrine condition, which possesses Fe-Mn concentration (Bolton & Frakes, 1985; Delian et al., 1992; Roy, 1992; Fuhrmann, 2002; Alçiçek et al., 2007; Wang et al., 2014; Yu et al., 2016).

The later phase in the basin, the lacustrine depositional environment in the studied sections are prevailed by marine environment from north to south. The facies associations define marine offshore transitional environment. In the Dağhacılar and Kösüre sections, the marine offshore transitional deposits are characterized by the predominate calcareous sandstone-oil-shale intercalation lithofacies with occasional marl and fossiliferous limestone and are deposited between fair-weather and storm wave base (Abimbola, 2016). These heterolithic character lithofacies are associated with turbiditic origin. There is also presence of occasional intervals of episodic storm deposits of Tempestite character in the Dağhacılar and Kösüre sections (Büyüktoku et al., 2005; Ranson, 2012; Siddiqui et al., 2014; Abimbola, 2016; Johansen, 2016)). In the north, the Sünnet section also indicates a change in the relative sea-level rise and deposited marine shelf lithofacies and marine fauna over the floodplain deposits. The rapid transition to marine shelf environment is specified by the bivalvia bearing organic rich shale and calcareous sandstone-organic rich shale interbeds deposits. The upper Sünnet section is characterized by abundant Nummulites-gastropod bivalve

limestone (bio-calcurudite) with conglomerate interval, coarser sandstone and occasional organic rich shale and indicate marine transgression phase (Carvalho et al., 2000; Li et al., 2009). The southeast Karahisar section represents relatively restricted depositional condition. The marine transgression into the lacustrine deposits in the Karahisar section is evident by the Fe-Mn small spherical nodules occurrence in the limestone deposits. The Fe-Mn small spherical nodules are of hydrogenetic origin and linked with physiochemical changes in the relatively restricted depositional condition. It occurs due to the concentration of Fe-Mn dissolution in the restricted lacustrine environment. It interacts with marine environmental condition and causes the formation of the Fe-Mn small spherical nodules at the interface and deposited at the depositional base (Bolton & Frakes, 1985; Delian et al., 1992; Roy, 1992; Fuhrmann, 2002; Alçiçek et al., 2007). The marine-offshore transitional environment in the Karahisar section is also argued by the wavy ripple calcareous sandstone beds with interbedded oil-shale and lime mudstone units.

Based on the facies analyses, biotic observation and facies association, the studied Middle Eocene (Lutetian-Bartonian) sections in the Mudurnu-Göynük basin indicate Oligo-Mesohaline lacustrine deposits in the south and barrier-marine deposits in the north. During the Middle Eocene (Lutetian-Bartonian), the lacustrine and marine environment shows progressive transgression in the region, which results in the linkage of lacustrine with marine environment in the north. Later on, formerly lacustrine deposits switch to marine-offshore transitional deposits (Figures 5.11; 5.12 and 5.13).

#### **9.4. Type of Lacustrine Basin and Marine transgression**

Based on the Carrol and Bohacs`s (1999) and Bohacs et al.`s (2000) lacustrine basin classification, it is interpreted that lacustrine deposits in the Dağhacılar, Hasanlar and Köşüre studied sections comprise of balanced-fill lake basin type and occasionally evolved to overfilled-lake basin type character between successions. The Karahisar section is interpreted as balanced-fill lake basin type with close lake hydrology. The

first stage of lacustrine basin indicates fresh to brackish water, retrogradational depositional patterns and moderate to high organic matter content (Figures 7.6; 8.29). In the next stage, lacustrine basin is characterized by facies association of predominately fluctuating sublittoral-profundal environment and having retrogradational to aggradational depositional trend (Figures 7.6; 8.30). This zone in the studied sections indicates relatively high organic matter content and comprises of marl-oil-shale with occasional sandstone in the Dağhacılar section, oil-shale, marl-lime mudstone in the Kösüre section and Oil-shale with occasional interbedded lime mudstone in the Karahisar section. The evaporate facies are absent in the studied sections, which also figures out that the lacustrine basin in the studied region is of balance-fill lake type basin with open lake hydrology. In the later stages, the depositional pattern of the facies consists of aggradational to progradational depositional pattern in the studied sections, which are characterized by calcareous sandstone from north to southwest and southeast in the studied sections and can be interpreted as an overfilled lake type (Figures 5.8; 7.6). This stage is related with the evolution of lacustrine to the marine depositional environment. It is interpreted that the lacustrine basin evolved to marine-offshore transitional environment from north to south (Figures 5.11; 5.12 and 5.13). The lacustrine evolution to marine transgression in the studied regime occurs in the open lacustrine phase. The transgression of marine environment is interpreted as a gradual change from the lacustrine successions. Therefore, continuous sedimentation is recorded across the transition from lacustrine to marine environment and deposition of the unchanged lithofacies across the evolution of lake into marine transgression environment. The continuous sediment successions are characterized by calcareous fine-grained sandstone and organic-rich shale in the central and southern studied sections. In such cases, it is difficult to recognize the transitional boundary between deeper lacustrine deposits and marine-offshore transitional deposits. Therefore, the absence or presence of fauna and algal structures are important evidence to predict the environmental changes in the studied sections (Willmann, 1985; Nichols, 2009; Lorente et al., 2014). The change of fauna, algal structure, presence of calcareous oil-shale and calcareous

sandstone in the studied sections illustrate alternatively opening and closing of lacustrine basin and changing the environmental condition from lacustrine to saline condition (Carroll and Bohacs, 1999; Bohacs et al., 2000). It is proposed that geographic setting, tectonics and predominately climatic changes are factors involved in the marine incursion to lacustrine in the measured stratigraphic successions. The Sünnet section in the north describe barrier deposits, and occur as a result of marine regression and basin-scale tectonic uplift in the Paleogene period (Saner, 1978a, 1980b; Ocakoğlu et al., 2007; Şafak et al., 2015). The recorded fauna and depositional succession in the Sünnet section is divided into floodplain deposits, which are transgressively overlain by open shelf marine environment (Figure 5.9). The transitional zone between floodplain and marine depositional environment reflect fluvio-lacustrine facies deposits, which illustrate the linkage of lacustrine basin with marine environment in the north. Later on, the rise in the relative Sea-level invaded the lacustrine environment from north and result in the deposition of marine-offshore deposits from north to south and replaced the previously lacustrine environment in the studied basin.

### **9.5. Cyclostratigraphic Framework**

In the Mudurnu-Göynük basin, the cyclostratigraphic framework of the Middle Eocene (Lutetian-Bartonian) lacustrine to marine-offshore studied successions suggest orbital control forced climatic changes and minor tectonic influence. Similarly, the orbital forced climatic changes are also interpreted by Ocakoğlu et al. (2012) in the Mudurnu-Göynük basin. The depositional cyclic stacking patterns in the studied sections are identified on the basis of limestone-marl, limestone-oil-shale, limestone (packstone-wackestone), oil-shale-marl, sandstone-oil-shale and sandstone-marl intercalation. In the studied sections, different cyclic hierarchies of various frequencies are observed within the measured section (Figure 6.6; 6.7). It occurs due to the repetitive change in the depth of lacustrine-marine environment and/or fluctuating sediments influx in the basin. It also results in the development of the symmetrical rhythmic cycles to asymmetrical cycles in the studied sections (Cabrera

et al., 2001). In the studied sections, the identified cycles are corresponding to the centimeter to meter scale order cycles (Figures 6.1; 6.2; 6.3; 6.4; 6.5; 6.7). Generally, in the studied sections, centimeter to meter scale order cycles exhibit relatively deepening stacking pattern to shallowing stacking pattern towards the top. It indicates that there is an increase in the accommodation space, followed by a decrease in accommodation space in the regime. The Fischer plot diagrams of the studied sections also indicate similar interpretation the studied successions (Figures 6.6; 6.7; 6.8; 6.9). The indicated changes in the relative accommodation space in relation with water-level fluctuations with time are marked by the Fischer plot and yielded comparatively similar pattern for the studied sections (Figures 6.8; 6.9; 6.10). These centimeter-meter scale order cycles in the Middle Eocene (Lutetian-Bartonian) studied sections are linked with obliquity Milankovitch orbital element. With global cyclostratigraphy model, the transgressive-regressive cycles evolution of the Middle Eocene (Lutetian-Bartonian) studied successions have approximately linear relation with sea-level fluctuation. The complex interaction of centimeter-meter scale order cycles in the studied sections are established in the time scale of around cycle is 55.55ka, 43.47ka, 59.52ka, 95.24ka and 83.33ka (Tables 6.1; 6.2). These higher frequency cycles in the studied sections suggest orbitally forced event. Similarly, the high frequency cycles are determined with 20 ka – 500 ka in the Green River formation and are related with orbital driven forces (Matthews and Perlmutter, 1994) (Tables 6.1; 6.2). Therefore, it is interpreted that the depositional cyclic stacking patterns in the studied sections correspond to changes in earth`s orbitally forced and belong to obliquity band (Einsele et a., 1991). These depositional centimeter to meter scale cycles in the studied section are suggested to be linked with climatic changes, which are induced by earth`s orbitally forces as a background external control forces in the studied regime and also accompanied by tectonic factors in the later stages. The change in relative water-level linked with minor tectonic subsidence factors are asserted by siliciclastic influxes in the upper depositional cycles pattern (Devlin et al., 1993; Matthews and Perlmutter, 1994; Ocakoğlu et al., 2012).

## 9.6. Sequence Stratigraphic Framework

In the sequence stratigraphic framework, it is indicated that Middle Eocene (Lutetian-Bartonian) sections show transgression in the lacustrine successions in the south, central and in the marine environment in the north (Figures 5.11; 5.13). Later on, this transgression in the Middle Eocene (Lutetian-Bartonian) sections in the region overcome the barrier deposits and lead to lacustrine environment to evolve into marine-offshore transitional environment from north to south, during Middle Eocene (Lutetian-Bartonian). Based on the chemical analysis, the determination of alkaline environmental conditions in the studied sections also support the transgression in the depositional environment. These alkaline environmental conditions are related with humid and warm climate and transgressive condition (Martínek et al., 2006; Lyons et al., 2011; Tānavsū-Milkevičienė et al., 2017). The geochemical determination of high carbonate content in the lithofacies of the studied sections reflect transgressive depositional condition in the regime (Figures 8.21; 8.28) (Lash & Blood, 2011). The interpreted relative water-level curve in the Middle Eocene (Lutetian-Bartonian) exhibits relative synchronous with global sea level curve of Middle Eocene (Lutetian-Bartonian) period (Figure 7.7) (Haq et al., 1987; Wang and Li, 2009).

In the studied sections, the sequence stratigraphic framework is demonstrated by the changes in the marine level and lake level from north to south (Figures 7.1; 7.6). The sequence stratigraphic framework in the studied sections are determined by on the basis of field studies, sedimentological analysis and depositional cyclic stacking pattern. In the lacustrine successions of the Dağhacılar, Hasanlar, Kösüre and Karahisar sections, the limestone-marl facies are overlain by oil-shale-marl facies, which indicates retrogradational depositional stacking pattern. It reveals the relative rise in the water-level in the studied sections and is associated with transgressive systems tract (Figure 7.6). In the north, floodplain-dominated siliciclastic deposits of lowstand systems tract are transgressively replaced by the marine shelf deposits, which are calcareous sandstone with oil silty shale, fossiliferous oil-shale and rare limestone having marine fauna, this displays retrogradational stacking pattern. The

flooding surface in the north is marked by first appearance of the organic rich shale and calcareous sandstone of the marine environment, which overlies the floodplain-siliciclastic deposits. It reflects relative rise in the Neo-Tethys sea-level in the north and displays a change in transgressive systems tract deposits.

From north to south, the upper portion studied sections are graded into marine deposits with aggradational-progradational depositional stacking patterns. The marine deposits are composed of siliciclastic-oil-shale intercalation and limestone in the south and center, and coarser siliciclastic-oil-shale horizons, mollusc-rich siliciclastic-carbonate and pebbly conglomerate in the north (Figures 5.9; 7.6). These marine successions are associated with highstand systems tract deposits and reflect maximum shift of the Neo-Tethys from north to south in the studied region during the Middle Eocene (Lutetian-Bartonian) period (Figures 5.11; 5.12; 5.13; 7.6). In the south, the maximum flooding zones is defined within lacustrine-marine transitional successions, which is composed of organic rich shale deposits and/or carbonate. Thereafter, the depositional successions are graded into siliciclastic-dominant lithofacies (calcareous sandstone intercalating with oil-shale/marls) of marine environment. It is suggested from the marine deposit thicknesses that the relative sea-level rises upto >30m approximately in the studied basin (estimated after replaced lacustrine succession). In the north, the maximum flooding zones is characterized by the first appearance of mollusc-rich siliciclastic-carbonate (Figures 7.5; 7.6) (El-Azabi, 2006; Ocakoğlu et al., 2007; Dix and Parras, 2014). Inclusive, the maximum flooding zones in the studied sections is marked around Lutetian-Bartonian boundary (approximately  $40.60 \pm 0.5$  Ma) and can be correlatable with Haq et al.'s (1987) and Ocakoğlu et al.'s (2007, 2012) Lutetian-Bartonian maximum flooding surfaces. In the studied sections, the lateral and vertical changes in the depositional environment indicate tectonically active regime which was anticipated by rise and fall of Northern Neo-Tethys oceans during the Eocene period.

## **9.7. Source rock potential on the petrographic and geochemical approaches**

Generally, the oil-shale lithofacies are deposited in the dysoxic or anoxic condition in different depositional environment, which could be brackish, lacustrine or marine environmental setting (Wartes et al., 2000; Martínek et al., 2006; Lyons et al., 2011; Tānavsū-Milkeviciene et al., 2017). Therefore, both lacustrine and marine oil-shale deposits are similar substantial source rock and unconventional reservoir potential (Bruhn, 1999; Carroll and Bohacs, 2001; Bohacs et al., 2003; Wang et al., 2011; Ma et al., 2015; Ma et al., 2016). In the studied sections, the oil-shale deposits comprise of marl, carbonate and predominantly oil-shale, which has high percent of immature organic matter content and can yield oil through destructive distillation or pyrolysis. In the Middle Eocene (Lutetian-Bartonian) studied sections, oil-shale rocks are determined in the lacustrine intervals and also in the transgressively overlying marine deposits (Figures 8.3; 8.8; 8.11; 8.15 and 8.19). It is evaluated that the oil-shale in the studied sections are settled in the alkaline environmental condition, which result in the deposition and well preservation of organic-rich facies in the studied regime. It also indicates that the oil-shale lithofacies attains high percent organic matter content in the studied Middle Eocene (Lutetian-Bartonian) successions (Martínek et al., 2006; Lyons et al., 2011; Tānavsū-Milkeviciene et al., 2017). The geochemical analysis indicates the high percent carbonate content in the oil-shale lithofacies. It shows that the oil-shale is deposited in the hydrological open lacustrine environmental setting and transgressive phase and have temporary linkage with marine environment (Figure 5.11; 5.13; 8.21; 8.28) (Fuhrmann, 2002; Cyr et al., 2014). Later on, this transgressive phase in the studied region result in the marine environment shift into the lacustrine environment from north to south (Figures 5.11; 5.13). The negative correlation coefficient between clay and quartz/feldspar content in the studied sections define episodic marine-influence into the lacustrine depositional setting. The positive correlation of organic matter with clay content and negative correlation with quartz/feldspar contents suggest relatively high rate of sedimentation influx and lead

to the development of the dysoxic-anoxic condition in the depositional environment (Figures 8.20; 8.21) (Huang et al., 2013).

The geochemical analysis and petrographic studies of oil-shale are useful tools to evaluate organic matter content and their source rock properties in the studied regime. Based on the obtained statistical data of the lithofacies, it is observed that the average organic matter content in the studied sections is higher than 8 wt. % (Table 9.1). The higher organic matter content in the studied sections might provide to be higher oil yield through pyrolysis. The average higher organic matter content in the lithofacies indicate excellent source rock potential in the Middle Eocene (Lutetian-Bartonian) studied successions (Figures 8.21; 8.33). The geochemical character and geochemical properties of the oil-shale of the studied sections are evaluated through the study of the organic matter content, carbonate content, clay content, detrital grains content and visual microscopic porosity determination (Table 9.1; Figures 8.21; 8.22; 8.23; 8.24; 8.25; 8.26; 8.27; 8.28; 8.29; 8.30; 8.31; 8.33). The formation of different types of pore structures and late impact on the reservoir is controlled by different mineral compositions in the rocks. In the studied sections, the organic-rich lithofacies generally possess high content of brittle minerals (> 40%) and relatively low clay content (<40%) (Table 9.1; Figure 8.21). The high brittle mineral content in the studied lithofacies facilitates nature and artificial fracturing and may interconnect the pores during the oil-shale exploitation. The average visual porosity percent is 4.72 % in the Dağhacılar section, 1.47 % in the Hasanlar, 1.84 % in the Köşüre section, 0.73 % in the Karahisar section and 5.35 % in the Sünnet section (Tables 8.6; 8.7; 8.8; 8.9; 8.10; 9.2; Figures 8.22; 8.23; 8.24; 8.25; 8.26; 8.27; 8.28; 8.29; 8.30; 8.31; 8.33). For the excellent unconventional reservoir, it is proposed that the organic matter content in the oil-shale should be more than 4%, while the brittle mineral content should be greater than 40% (Table 8.11; Figure 8.21) (Zou et al., 2010; Wang et al., 2014; Ma and Holditch, 2015; Jiang et al., 2016). The statistical data of the organic matter content, brittle mineral content, clay content and visual porosity percent in the Middle Eocene (Lutetian-Bartonian) studied sections determine excellent source rock

potential and brittle geochemical character of the oil-shale deposits in the studied regime and are graded as higher percent brittle mineral content in the north and central regime and low brittle mineral content in the southwest and southeast in the studied regime (Table 9.1; Figures 8.21; 8.22; 8.33). Based on the geochemical analyses and petrographic studies, it is interpreted that the Dağhacılar and Sünnet sections are considered as excellent source rock potential, possessing high brittle geochemical mineral character oil-shale deposits (Figure 8.33).

Table 9.1. The obtained minimum, maximum and average weight percent of CaCO<sub>3</sub>, organic matter, clay content, quartz/feldspar content and visual porosity from the Middle Eocene (Lutetian-Bartonian) measured succession.

Studied Sections		Dağhacılar section	Hasanlar section	Kösüre section	Karahisar section	Sünnet section	
Weight percent	Carbonate	Min	16.00	7.31	17.72	24.71	24.71
		Max	89.03	79.32	92.66	66.84	79.5
		Average	58.42	51.86	53.93	47.86	34.28
	Organic Matter	Min	3.30	8.31	0.35	8.03	4.36
		Max	18.99	16.39	18.99	19.93	29.91
		Average	10.55	12.04	8.29	12.45	11.72
	Clay	Min	0.00	12.83	3.10	3.80	0.00
		Max	68.45	78.43	78.66	63.46	41.81
		Average	24.04	31.13	39.72	34.41	14.35
	Quartz/ Feldspar	Min	0.00	0.00	0.00	0.00	8.45
		Max	60.1	28.57	20.92	38.11	70.69
		Average	10.47	28.57	1.18	8.77	48.48
Visual Porosity %	Min	0.00	0.04	0.00	0.00	0.00	
	Max	22.76	3.36	11.49	5.5	23.15	
	Average	4.72	1.47	1.84	0.73	5.35	

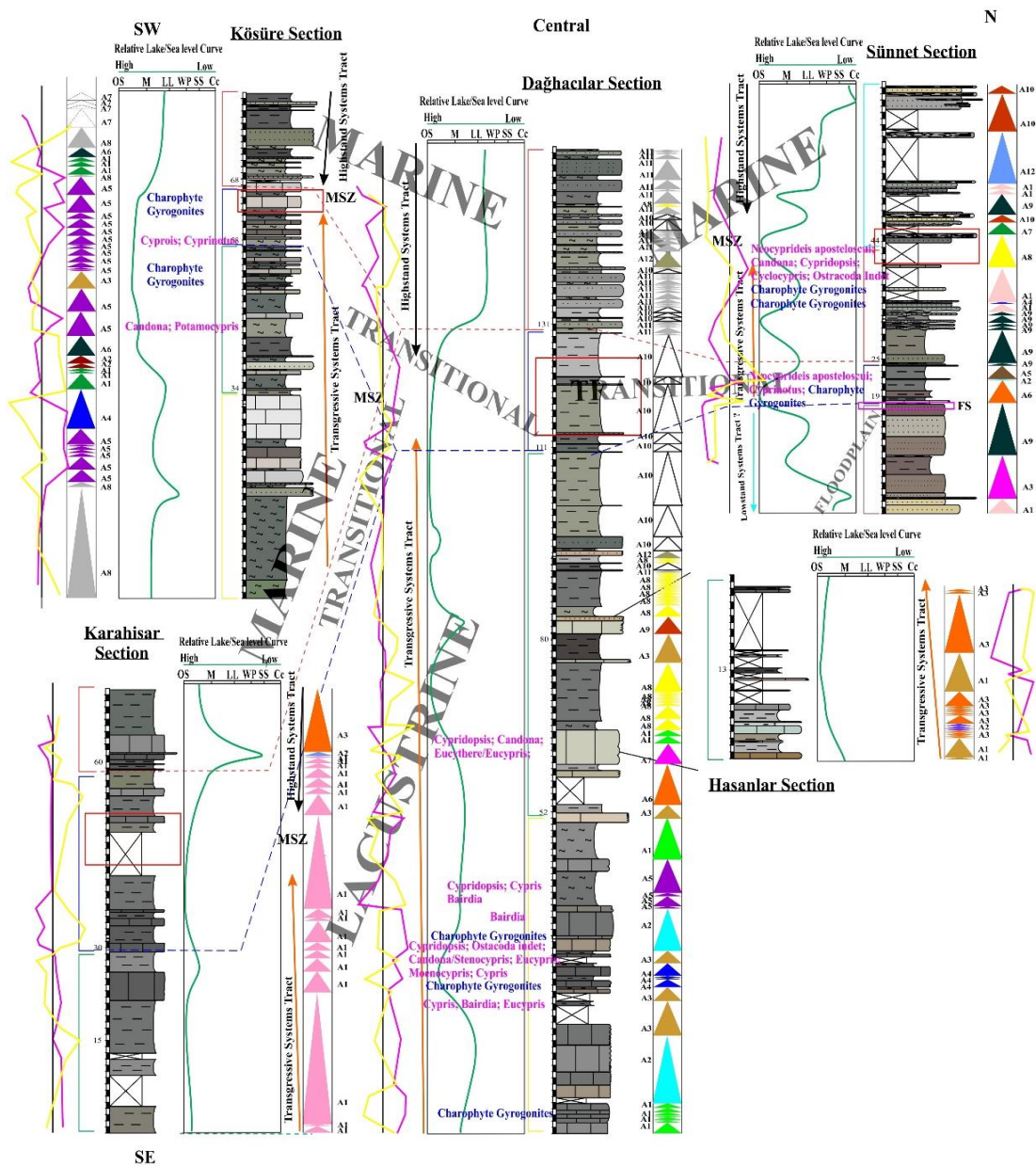
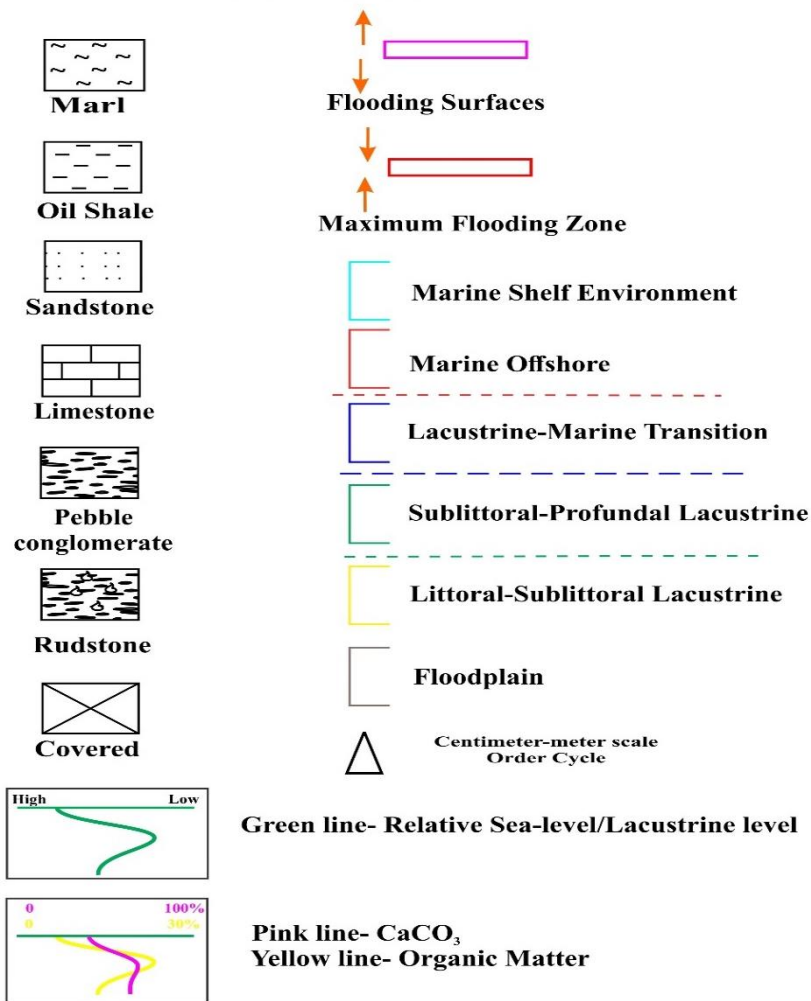


Figure 9.1. Correlation of the sequence stratigraphic interpretation, centimeter-meter scale cycles, relative lake level/sea-level, organic matter content,  $\text{CaCO}_3$ , and charophytes and ostracods within the studied sections from south to central to north. (FS-flooding surface; MFZ-maximum flooding zones; OS-oil-shale; M-marl; LL-Lime mudstone; Wp-wackestone-packstone; SS-sandstone; Cc-conglomeratic)

# LEGEND



**Blue Name: Charophyte Gyrogonites**

**Pink Name: Ostracods**

*Figure 9.1. Continues...*

## CHAPTER 10

### CONCLUSION

- The studied area is located in the Bolu province, NW Anatolia, Turkey. The five stratigraphic sections are measured in the vicinity of Dağhacılar village, Hasanlar village, Köşüre village, Karahisar village and Sünnet village. These sections were measured through the Middle Eocene (Lutetian-Bartonian) Upper Kızılcay Formation and the Halidiye Formation in the Mudurnu-Göynük Basin, NW Turkey (Ocakoglu et al., 2007, 2012 and Şafak et al., 2015).
- The recognized lithofacies are generally composed of limestone, marl, calcareous oil-shale, fine to coarser sandstone and occasional conglomeratic beds and calcirudite. A total of 4, 3, 4, 4, 4 microfacies with sub-microfacies are identified in the Dağhacılar, Hasanlar, Köşüre, Karahisar and Sünnet section, respectively. The recorded fauna along the stratigraphic sections at different intervals are ostracods, charophyte gyrogonites, gastropods, bivalve and occasionally benthic foraminifera, rare fish-teeth and scale, echinoderms, algal filamentous and plant fragments.
- Based on the recorded ostracod assemblages (*Cyclocypris* sp., *Candona* sp., *Potamocypris* sp., *Heterocypris* sp., *Stenocypris* sp., *Neocyprideis* sp.) and associated charophyte gyrogonites, the Middle Eocene (Lutetian-Bartonian) age is assigned to the studied intervals.
- The lithofacies and recorded fossil assemblages indicate Oligo-Mesohaline to brackish-lacustrine depositional environment in the lower portion of the

studied sections. Relatively high carbonate content, weak but positive correlation of clay content with organic matter suggest episodic marine incursion into the lacustrine environmental condition of the studied sections.

- The predominated siliciclastic successions with oil-shale and marl intercalation and presence of occasional marine benthic fauna indicate a shift from the lacustrine depositional environment to the transgressive marine environment, around the Lutetian-Bartonian boundary. Overall, the studied sedimentary sequence initially reflect deposition in the lacustrine environment and then is transformed to marine depositional environment. Based on the unchanged lithofacies across the transition and continuous sedimentation across the transitional interval suggest that the marine transgression into the lacustrine setting occurred in an open lacustrine phase.
- In the north, the Sünnet studied section, the successions with dominate-siliciclastic deposits with oil-shale, fossiliferous limestone, coarser to pebble conglomerate and calcirudite indicate barrier deposits with transgressively overlying marine environment.
- Based on the detailed studies of facies associations, five depositional patterns as sub-environment are recognized in the studied sections. In the central and south sections, facies associations are composed of littoral-sublittoral lacustrine, sublittoral-profundal lacustrine and marine offshore-transitional deposits. In the north, facies associations comprise of floodplain deposits and marine shelf deposits.
- Two major types of depositional environments are identified in the Middle Eocene (Lutetian to Bartonian) studied sections from bottom to top, in the Mudurnu-Göynük Basin, based on the detailed studies of lithofacies and facies

associations. In the central and southern sections, the lacustrine deposits are transitional overlain by the marine-offshore deposits. In the north, there is absence of lacustrine deposits. In this region, the siliciclastic dominated floodplain deposits of fluvio-lacustrine environment are overlain by paralic-marine shelf deposits.

- The lacustrine lithofacies and facies associations in the Dağhacılar, Hasanlar, Köşüre and Karahisar section show balanced-fill lake basin type deposits and marine offshore transitional deposits towards the top. The Dağhacılar and Hasanlar sections depict the central portion of the lake. The Köşüre and Karahisar sections characterize marginal to relatively deeper lake marginal deposits, respectively. In the north, the Sünnet section exhibit barrier deposits (between lacustrine and marine environmental setting) and marine shelf deposits towards the top.
- During Middle Eocene (Lutetian-Bartonian), the lacustrine environment gradually transgressed to marine environment due to the relative rise in the sea-level, in the Mudurnu-Göynük Basin.
- Within the Middle Eocene (Lutetian-Bartonian) studied successions, the established hierarchical order cyclicity are identified as centimeter to meter scale order cycles. The hierarchical high order depositional cycles in the studied sections are recorded by limestone-marl, limestone-oil-shale, limestone (packstone-wackestone), oil-shale-marl, sandstone-oil-shale and sandstone-marl. The symmetrical rhythmic cycles in the studied sections reflect repetitive changes in the relative water-depth and/or fluctuating sediments influx. The centimeter to meter scale order cycles are cycle is 55.55ka, 43.47ka, 59.52ka, 95.24ka and 83.33ka duration, which correspond to the Milankovitch cycles of obliquity band range. These changes in the

Middle Eocene (Lutetian-Bartonian) period indicate a linkage with the changes in earth's orbital forces. The Fischer plot diagram display comparatively similar accommodation spaces graphic pattern within studied sections. It indicates the relatively similar changes in relative depositional space in relation to fluctuation of the relative water-level with time in the studied sections.

- In the sequence stratigraphic framework, the Middle Eocene (Lutetian-Bartonian) sediments are recognized as transgressive systems tract and highstand systems tract deposits. In the central to southeast and southwest, the lacustrine deposits in the studied regime belong to transgressive systems tract, then are overlain by marine offshore-transitional deposits, which are interpreted as highstand systems tract. In the north section (Sünnet section), the floodplain deposits associated lowstand systems tract are overlain by marine deposits, which are interpreted as transgressive systems tract and highstand systems tract deposits.
- The obtained relative water-level curve in the studied successions exhibit comparatively synchronous trend with global sea level curve in Middle Eocene (Lutetian-Bartonian) period of Haq et al. (1987). The identified maximum flooding zones in the studied sections is determined around Lutetian-Bartonian boundary (approximately  $40.60 \pm 0.5$  Ma), which relatively coincide with Haq et al.'s (1987) and Ocakoğlu et al.'s (2007, 2012) Lutetian-Bartonian maximum flooding surface at 40.40 Ma.
- Geochemical data and petrographic analysis indicate that both lacustrine and marine organic-rich lithofacies (oil-shale, marl and limestone) in the studied sections interpret excellent source rock potential. The organic matter content in the lithofacies are ranging from 0.35wt.% to 29.91wt.% with effectively

thick intervals. The identified pore types in the studied samples are intraparticle pores, interparticle pores and microfracture related porosity.

- The geochemical and petrographic studies interpret that the organic rich lithofacies in the central (Dağhacılar section, Hasanlar section) and north sections (Sünnet section) are characterized as high brittle mineral content and relatively low clay content, which facilitates both natural and artificial fractures and inferring good unconventional reservoir properties. The southwest (Kösüre section) and southeast (Karahisar section) sections have relatively high clay content at certain levels and very low porosity. The southwest (Kösüre section) and southeast (Karahisar section) sections are categorized as low-quality unconventional reservoir character. Therefore, it is concluded that oil-shale in the Dağhacılar, Hasanlar and Sünnet sections are favorable potential target for exploration and production of hydrocarbon.



## REFERENCES

- Abdüsselamoglu, M.S., 1959. Geology of Almacikdağı, Mudurnu and Göynük Region," Istanbul University Science Faculty, No. 14, 95.
- Abimbola, D. A., 2016. A Re-evaluation of the Depositional Environments and Sedimentary Facies of Middle Miocene Paralic Deposits (Agbada Formation), Ewan and Oloye Marine Science: Research & Development, 6(3). <https://doi.org/10.4172/2155-9910.1000193>
- Abouelresh, M. O., Babalola, L., Bokhari, A. K., Boyde, D., Thomas, K. and Omer, M., 2017. Understanding reservoir properties of the organic-rich Qusaiba Shale, a potential shale gas reservoir, NW Saudi Arabia: an outcrop approach. Search and Discovery, 11004; 1-4.
- Abreu, V., Neal, J. E., Bohacs, K. M. and Kalbas, J. L., 2010. Sequence stratigraphy of siliciclastic systems e the ExxonMobil methodology. SEPM Concepts in Sedimentology and Paleontology 9, 226
- Afridi, B. Z., 2014. Stratigraphical, sedimentological, geochemical and cyclostratigraphical analyses of Upper Cretaceous (Upper Santonian-Campanian) pelagic successions of Haymana and Mudurnu-Göynük basins of the Sakarya continent, Turkey. Master Thesis, METU, Ankara.
- Afsharpoor, A. and Javadpour, F., 2016. Liquid slip flow in a network of shale noncircular nanopores. Fuel 180, 580-590.
- Aigner T. and Reineck H.-E., 1982. Proximality trends in modern storm sands from the Helegoland Bight (North Sea) and their implications for basin analysis. Senckenbergiana marit., 14, 183- 215.
- Akarsu, I., 1971. II Geological report of the AR/TPO/747 area. Türkiye Petrolleri Anonim Ortaklığı (unpublished).

- Akarsu, İ. 1974. Göynük, Gölpaazarı, Bolu, Nallıhan, Beypazarı yöresi ile geniş çevresinde bitümlü şeyllerin jeolojik etüd incelemesi. TPAO Araştırma Merkezi Rapor No: 898.
- Akkuş, İ., Sümer, A., Şengüler, İ., Taka, M., Pekatan, R. ve Işık, A. 1982. Beypazarı Çayırhan yöresinin jeoloji ve bitümlü şeyl olanakları. MTA Rapor No: 7837.
- Aksenova, O. V, Bolotov, I. N., Gofarov, M. Y., Kondakov, A. V, Vinarski, M. V, Bespalaya, Y. V, ... Palatov, D. M., 2018. Species Richness, Molecular Taxonomy and Biogeography of the Radicine Pond Snails (Gastropoda : Lymnaeidae) in the Old World, (July), 1-17. <https://doi.org/10.1038/s41598-018-29451-1>
- Alçiçek, H., Varol, B. and Özkul, M., 2007. Sedimentary facies, depositional environments and palaeogeographic evolution of the Neogene Denizli Basin, SW Anatolia, Turkey. *Sedimentary Geology - Sediment Geol.* 202. 596-637.
- Alali, J., Salah, A. A., Yasin, S. M. and Al Omari, W., 2015. Geology of Oil-shale in Jordan, Ministry of energy and mineral resources, mineral status and future opportunity. *Oil-shale, Memeoir.*
- Aliyev, S., Sarı, A., Koralay, D. B. and Koç, S., 2009. Investigation of organic carbon and trace metal enrichments of rocks at the Paleocene-Eocene boundary, NW Turkey. *Petroleum Science and Technology*, Vol. 27: 56-71.
- Allix, P., Burnham, A., Herron, M. and Kleinberg, R., 2010. Gas Shale, Oil-shale, and Oil-Bearing Shale: Similarities and Differences: American Association of Petroleum Geologists Search and Discovery, Abstract.
- Alnawafleh, H. and Fraige, F., 2015. Shale Oil Solvent Extraction of Central Jordan El-Lajjun Oil-shale. *Journal of Analytical Sciences, Methods and Instrumentation*, 5, 35-43. doi: 10.4236/jasmi.2015.53004.
- Alshahrani, S., 2013. Depositional environment, history, diagenesis, and petroleum geology of the Cleveland shale member, Northeastern Ohio.

- Altner, D., 1991. Microfossil biostratigraphy (mainly foraminifers) of the Jurassic-Lower Cretaceous carbonate successions in Northwestern Anatolia (Turkey). *Geologica Romana*, Vol. 27, pp. 167-215.
- Altner, D. and Özkan S., 1991. Calpionellid zonation in North-Western Anatolia (Turkey) and calibration of the stratigraphic range of some benthic Foraminifera at the Jurassic-Cretaceous boundary. *Geologica Romana*, Vol. 27 (1), pp. 215-236.
- Altner, D., Koçyiğit, A., Farinacci, A., Nicosia, U. and Conti, M. A., 1991. Jurassic-Lower Cretaceous stratigraphy and paleogeographic evolution of the southern part of North-Western Anatolia (Turkey). *Geologica Romana*, Vol. 27, pp. 13-81.
- Altınlı, İ. E., 1973a. Bilecik Jurassigi. Cumhuriyetin 50. Yılı Yerbilimleri Kongresi tebliğleri. Maden Tetkik Arama Yayını, 102-110. (In Turkish).
- Altınlı, İ. E., 1973b. Orta Sakarya' nın jeolojisi. 50. Yıl Yerbilimleri kongresi, Tebliğler kitabı, 159-187, Ankara.
- Altınlı, İ.E., 1975. Yenisehir Havzası'nın jeolojik ve hidrojeolojik incelenmesi., İstanbul Üniversitesi Fen Fakültesi Mecmuası B 30, 31-51. (In Turkish).
- Altınlı, İ.E., 1976. Geology of the northern portion of the Middle Sakarya River. İstanbul Üniversitesi Fen Fakültesi Mecm. Seri B 41 (1-4), s.35-s.36.
- Altınlı, İ. E, 1977. Geology at the eastern territory of Nallihan (Ankara, province). İstanbul Üniversitesi Fen Fakültesi, Mecmuası, B, Vol. 42, (1-2), pp. 29-44.
- Altun, N. E., Hıçılmaz, C., Hwang, J.-Y., Bağcı, A. S. and Kök, M. V., 2006. Oil Shales in the World and Turkey; Reserves, Current Situation and Future Prospects: a Review. Estonian Academy Publishers, 23(3), 211-227.

- Amezcuca, N., 2012. Stratigraphy and Facies of the Pliocene Mayrán Lacustrine Basin System, Northeast México. # Thesis.
- Amorosi, A. and Marchi, N., 1999. High-resolution sequence stratigraphy from piezocone tests: an example from the Late Quaternary deposits of the southeastern Po Plain, 128, 67–81.
- Anderson, R. Y. and Dean, W., 1988. Lacustrine varve formation through time. *Palaeogeography, Palaeoclimatology, Palaeoecology*. 62. 215-235.
- Apostolescu, V. and Guernet, C., 1992. Les ostracodes de la région Forcalquier-Manosque (Bassin continental d'Apt, Haute-Provence). *Revue de Micropaleontologie* 35, 91–115
- Arabu, N., 1934-1935. Contribution a l'étude géologique des environs de la mer de Marmara. C.R. geological institute of Roumanie, pp. 23.
- Argakoesoemah, I., 2017. Middle Eocene Palaeogeography of the Greater Makassar Strait Region, Indonesia: A Review of Eocene Source Rock Distribution. <https://doi.org/10.29118/IPA.50.17.247.G>
- Arikan, Y., 1975. Tuzgölü havzasının jeolojisi ve petrol imkanları. *Mineral Research and Exploration of Turkey*, No. 85, pp. 17-38.
- Arthur, M. A. and Sageman, B. B., 1994. Marine black shales: depositional mechanisms and environments of ancient deposits. *Annual Review of Earth and Planetary Sciences* 22, 499-551
- Asl, S. S. and Aleali, M., 2016. Microfacies Patterns and Depositional Environments of the Sarvak Formation in the Abadan Plain, Southwest of Zagros, Iran, 201-209.

- Atay, G. and Tunođlu, C., 2004. Kilitbahir (Eceabat/Çanakkale) Sondaj ÖrneKlerinin ostrakod faunasına bađlı Kronostratigrafisi ve Paleortamsal Yorumu, Türkiye Jeoloji Bülteni, 47, 2, 5-23.
- Aydın, M., Demir, O., Serdar, H.S., Ozaydın, S. and Harput, B., 1995. Tectono-sedimentary evolution and hydrocarbon potential of the SinopBoyabat Basin, North Turkey: in A. Erler, E. Tuncay, E. Bingol, and S. Orcan (eds.), Geology of the Black Sea Region, General Directorate of Mineral Research and Exploration (MTA), Ankara, p. 254–263.
- Aygen, T., 1956. Balya bölgesi jeolojisinin incelenmesi. Mineral Research and Exploration Institute (MTA) of Turkey publication Bulletin, No. 11, pp. 1-95.
- Aysal, N., Ustaömer, T., Öngen, S., Keskin, M., Köksal, S., Peytcheva, I. and Fanning, M., 2012. Origin of the Lower-Middle Devonian magmatism in the Sakarya zone, NW Turkey: Geochronology, geochemistry and isotope systematics. Journal of Asian Earth Sciences, 45, 201-222.
- Baak, C. G. C. Van., Mandic, O., Lazar, I., Stoica, M. and Krijgsman, W., 2015. The Slanicul de Buzau section, a unit stratotype for the Romanian stage of the Dacian Basin (Plio-Pleistocene, Eastern Paratethys). Palaeogeography, Palaeoclimatology, Palaeoecology, 440, 594–613.  
<https://doi.org/10.1016/j.palaeo.2015.09.022>
- Barron, E. and Comas-Rengifo, M. J., 2007. Differential accumulation of miospores in Upper Miocene sediments of the La Cerdana basin (eastern Pyrenees, Spain). Paleovol, 6, 157-168.
- Baumiller, T. K. and Gazdzicki, A., 1996. New crinoids from the Eocene La Meseta Formation of Seymour Island, Antarctic Peninsula.
- Bádenas, B., Aurell, M. and Gröcke, D. R., 2005. Facies analysis and correlation of high-order sequences in middle-outer ramp successions: variations in exported carbonate in basin-wide  $\delta^{13}\text{C}_{\text{carb}}$  (Kimmeridgian, NE Spain). Sedimentology 52, 1253-1276

- Beauboeuf, R. T. and Friedmann, S. J., 2000. High-resolution seismic/sequence stratigraphic framework for the evolution of pleistocene intra slope basins, western Gulf of Mexico: depositional models and reservoir analogs. In: Weimer, P., Slatt, R.M., Coleman, J., Rosen, N.C., Nelson, H., Bouma, A.H., Styzen, M.J., Lawrence, D.T. (Eds.), *Deep-water Reservoirs of the World*. Gulf Coast Society of the Society of Economic Paleontologists and Mineralogists Foundation, 20th Annual Research Conference, pp. 40–60.
- Belaid, A., Krooss, B. M. and Littke, R., 2010. Thermal history and source rock characterization of a Paleozoic section in the Awbari Trough Basin, SW Libya. *Marine and Petroleum Geology* 27: 612–632
- Benda, L., Meulenkamp, J. E., Schmidt, R. R., Steffens, P., and Zachariasse, J. W., 1977. Biostratigraphic correlations in the Eastern Mediterranean Neogene. 2. Correlation between sporomorph associations and marine microfossils from the Upper Oligocene-Lower Miocene of Turkey. *Newsl. Stratigr.*, 6: (1), 1-22.
- Bennett, R. H., O'Brien, N. R. and Hulbert, M. H., 1991. Determinants of Clay and Shale Microfabric Signatures: Processes and Mechanisms. In: Bennett R.H. et al. (eds) *Microstructure of Fine-Grained Sediments*. *Frontiers in Sedimentary Geology*. Springer, New York, NY
- Berger, A., Loutre, M. F. and Laskar, J., 1992. Stability of the astronomical frequencies over the Earth's history for paleoclimate studies: *Science*, v. 255, no. 5044, p. 560-566.
- Berner, R. A., 1984, Sedimentary pyrite formation: an update: *Geochimica et Cosmochimica Acta*, v. 48, p. 605-615
- Berry, W. B., and Wilde, P., 1978. Progressive ventilation of the oceans; an explanation for the distribution of the lower Paleozoic black shales. *American Journal of Science* 278, 257-275.
- Beseme, P., 1967. Kabalar senklinalinin (Göynük - Bolu) genel ve uygulamalı jeolojik etüdü: MTA Raporu (No: 4629).

- Bhatia, S. B., 2006. Ecological parameters and dispersal routes of *Lychnothamnus barbatus* (Characeae) in the Early-Middle Holocene from Ganga plain, India. *Cryptogam. Algal.* 27, 341–356
- Bhatia, S. B. and Bagi, H., 1991. Early Lutetian charophyta from the Shimla Hills, Lesser Himalayas. *Ulletin de La Société Botanique de France. Actualités Botaniques*, 138, 7–14. <https://doi.org/10.1080/01811789.1991.10827037>
- Bingham-koslowski, N. E., 2015. High resolution stratigraphy and paleoenvironmental reconstruction of the Upper Devonian Kettle Point Formation, southwestern Ontario, Canada.
- Biscara, L., Mulder, T., Martinez, P., Baudin, F., Etcheber, H., Jouanneau, J. and Garlan, T., 2011. Transport of terrestrial organic matter in the Ogooué deep sea turbidite system. *Marine and Petroleum Geology*, 28(5), 1061-1072. <https://doi.org/10.1016/j.marpetgeo.2010.12.002>
- Blumenthal, M., 1937. Bolu vilayeti dahilindeki Gökdağ mintikası bitümlü şist sahasının jeolojisi hakkında rapor. MTA Rapor No: 269, Ankara.
- Boggs, S. J., 1995. *Principles of Sedimentology and Stratigraphy*. Prentice Hall, Upper Saddle River, N.J., 774 pp.
- Boggs, S., 2011. *Principles of sedimentology and stratigraphy*, Fifth Edition. Pearson Prentice Hall.
- Bohacs, K. M., 1998, Contrasting expressions of depositional sequences in mudrocks from marine to non-marine environs, in J. Schieber, W. Zimmerle, and P. Sethi, eds., *Mudstones and Shales*, vol. 1, Characteristics at the basin scale: Stuttgart, Schweizerbart'sche Verlagsbuchhandlung, p. 32-77.
- Bohacs, K. M., 2006. Lithofacies, organic matter, depositional environments, lake-facies associations, and lake-basin types of the Rundle and Curlew formations (Middle-Late Eocene), Queensland, Australia in the ERD-110 core. In:

Abstracts with Geological Society of America, 2006 Annual Meeting, 38(7): 84

Bohacs, K. M. and Schwalbach, J. R., 1992, Sequence stratigraphy of fine-grained rocks with special reference to the Monterey Formation, in J.R. Schwalbach and K.M. Bohacs, eds, Sequence stratigraphy in fine-grained rocks: examples from the Monterey Formation: Pacific Section SEPM Guidebook 70, 80p.

Bohacs, K. M., Carroll, A. R., Neal, J. E. and Mankiewicz, P. J., 2000. Lake-basin type, source potential, and hydrocarbon character: an integrated-sequence-stratigraphic-geochemical framework. In: Lake basins through space and time (Ed. by E.H. Gierlowski-Kordesch and K. Kelts); AAPG Studies in Geology, Vol. 46, pp. 3-34. <http://dx.doi.org/10.1306/E4FD42AB-1732->

Bohacs, K. M., Carroll, A. R. and Neal, J. E., 2003, Lessons from large lake systems - thresholds, nonlinearity, and strange attractors, in M.A. Chan, and A.W. Archer, eds., Extreme depositional environments: Mega end members in geologic time: GSA Special Paper 370, p. 75-90.

Bolton, B. R. and Frakes, L. A., 1985. Geology and genesis of manganese colite, Chiatara, Georgia, U.S.S.R. GSA Bulletin, 96, 1398-1406

Brown, K. E. and Cohen, A. D., 1995. Stratigraphic and micropetrographic occurrences of pyrite in sediments at the confluence of carbonate and peat-forming depositional systems, southern Florida, U.S.A. Organic Geochemistry. [https://doi.org/10.1016/0146-6380\(95\)90011-X](https://doi.org/10.1016/0146-6380(95)90011-X)

Bruhn, C. H., 1999. Reservoir architecture of deep-lacustrine sandstones from the Early Cretaceous Reconcavo rift basin, Brazil. AAPG Bull. 83, 1502-1525

Büyüktutku, A. G., Sari, A., and Karaçam, A., 2005. The reservoir potential of the Eocene carbonates in the Bolu Basin, West of Turkey. Journal of Petroleum Science and Engineering, 49(1-2), 79-91. <https://doi.org/10.1016/j.petrol.2005.07.002>

- Cabrera, Â., Hagemann, H. W., Ramos, E., Pickel, W. and Zamarren, I., 2001. Palaeogene lacustrine record in Mallorca (NW Mediterranean, Spain): depositional, palaeogeographic and palaeoclimatic implications for the ancient southeastern Iberian margin, 172.
- Caillaud, A., Blanpied, C. and Delvaux, D., 2017. The Upper Jurassic Stanleyville Group of the eastern Congo Basin: An example of perennial lacustrine system. *Journal of African Earth Sciences*, 132,80-98.  
<https://doi.org/10.1016/j.jafrearsci.2017.05.002>
- Calvo, J. P., Gomez-gras, D., Alonso-zarza, A. M. and Jimenez, S., 2000. Architecture of a bench-type carbonate lake margin and its relation to fluvially dominated deltas, Las Minas Basin, Upper Miocene, Spain, 70(1), 240-254.
- Canfield, D. E., 1994. Factors influencing organic carbon preservation in marine sediments. *Chem. Geol.* 114, 315-329.
- Carlucci, J. R., Westrop, S. R., Brett, C. E. and Burkhalter, R., 2014. Facies architecture and sequence stratigraphy of the Ordovician Bromide Formation (Oklahoma): a new perspective on a mixed carbonate-siliciclastic ramp, 987–1012. <https://doi.org/10.1007/s10347-014-0412-6>
- Carroll, A. R. and Bohacs, K. M., 1999. Stratigraphic classification of ancient lakes: Balancing tectonic and climatic controls: *Geology*, v. 27, no. 2, p. 99-102.
- Carroll, A. R. and Bohacs, K. M., 2001. Lake-type controls on petroleum source rock potential in nonmarine basins *American Association of Petroleum Geologist*, v. 85, no. 6, p. 1033-1053.
- Carvalho, M. D. de, Praça, U. M., Jr., A. C. da S.-T., Jahnert, R. J. and Dias, J. L., 2000. Bioclastic Carbonate Lacustrine Facies Models in the Campos Basin (Lower Cretaceous), Brazil. *AAPG Studies in Geolog*, 46, 245-256.

- Castel, M., 1968. Zones de Charophytes pour l'Oligocène d'Europe Occidentale. *Comptes Rendus Sommaire des Séances de la Société Géologique de France*, 4: 121–123.
- Cater, J. M. L., Hanna, S. S., Ries, A. C. and Turner, P., 1991. Tertiary evolution of the Sivas Basin, Central Turkey. *Tectonophysics* 195, 29–46.
- Catuneanu, O., 2002. Sequence stratigraphy of clastic systems: concepts, merits, and pitfalls. *Journal of African Earth Sciences* 35, 1-43.
- Catuneanu, O., 2006. *Principles of Sequence Stratigraphy*. Elsevier, Amsterdam, pp. 386.
- Cestari, N., 2015. Reservoir and Source Potential of Eocene Microbialites, Green River Formation, USA. MS Thesis. University of Kansas, USA.
- Chakraborty, T. and Sarkar, S., 2005. Evidence of lacustrine sedimentation in the Upper Permian Bijori Formation, Satpura Gondwana basin: palaeogeographic and tectonic implications. *Journal of Earth System Science* 114, 303–323
- Changsong, L., Eriksson, K. and Sitian, L., 2001. Sequence Architecture, Depositional Systems, and Controls on Development of Lacustrine Basin Fills in Part of the Erlian Basin, Northeast China.
- Cole, R. D., 1985. Depositional environments of oil-shale in the Green River Formation, Douglas Creek arch, Colorado and Utah: in Picard, M.D., ed., *Geology and energy resources, Uinta Basin of Utah: Utah Geological Association Publication* 12, p. 211-224.
- Collinson, J. D. and Lewin, J., 1983. *Modern and Ancient Fluvial Systems*. Special Publication 6 of the International Association of Sedimentologists.

- Collins, J., Kenyon-roberts, S., Cullen, B., White, J., Floch, N. B., Downey, J., ... London, W., 2015. Arran Field: a complex heterolithic reservoir on the margins of the Forties Fan System, 185-217.
- Cornford, C., 1998. Source rocks and hydrocarbons of the North Sea. In: Glennie, K.W. (Ed.), *Petroleum Geology of the North Sea* (4th eds). Blackwell Science Ltd., London, pp. 376-462
- Cornford, C., Birdsong, B. and Groves, G., 2014. Offshore unconventional oil from the Kimmeridge Clay Formation of the North Sea: a technical and economic case. In: *Unconventional Resources Technology Conference Proceedings*, 25-27.
- Cunningham, K. J., Renken, R. a, Wacker, M. a, Zygnerski, M. R., Robinson, E., Shapiro, M. and Wingard, G. L., 2006. Application of carbonate cyclostratigraphy and borehole geophysics to delineate porosity and preferential flow in the karst limestone of the Biscayne aquifer, SE Florida. *Perspectives on Karst Geomorphology, Hydrology, and Geochemistry*, 404(303), 191–208. [https://doi.org/10.1130/2006.2404\(16\)](https://doi.org/10.1130/2006.2404(16))
- Curtis, J. B., 2002. Fractured shale-gas systems. *American Association of Petroleum Geologists Bulletin* 86 (11), 1921-1938
- Curtis, M. E., Ambrose, R. J. and Sondergeld, C. H., 2010. Structural Characterization of Gas Shales on the Micro-and Nano-scales, *Canadian Unconventional Resources and International Petroleum Conference*. Society of Petroleum Engineers.
- Cyr, A. J., Currie, B. S., Rowley, D. B., The, S., September, N., Cyr, A. J., ... Rowley, D. B., 2014. Geochemical Evaluation of Fenghuoshan Group Lacustrine Carbonates, North - Central Tibet: Implications for the Paleoaltimetry of the Eocene Tibetan Plateau *Geochemical Evaluation of Fenghuoshan Group Lacustrine Carbonates, North-Central Tibet: Implica*, 113(5), 517–533.
- Czaja, A., Estrada-Rodríguez, J. L. and Méndez, U. R., 2014. Freshwater mollusks of the Valley of Sobaco, Coahuila, Northeastern Mexico - a subfossil ecosystem

similar to Cuatrociénegas. *Boletín de La Sociedad Geológica Mexicana*, 66(3), 459-469. <https://doi.org/10.18268/BSGM2014v66n3a4>

Çimen, O., Koç, Ş. and Sarı, A., 2013. Rare Earth Element (REE) geochemistry and Genesis of oil-shales around Dağhacılar Village, Göynük-Bolu, Turkey. *Oil Shale*, Vol. 30, (3), pp. 419-440.

Çiner, A., Deynoux, M., Ricou, S. and Koşun, E., 1996a. Cyclicity in the middle Eocene Çayraz Carbonate Formation, Haymana Basin, Central Anatolia. *Palaeogeography, Palaeoclimatology, Palaeoecology*, Vol. 121, pp. 313-329.

Çiner, A., Deynoux, M. and Koşun, E., 1996b. Cyclicity in the Middle Eocene Yamak turbidite complex of the Haymana basin, Central Anatolia, Turkey. *Geologische Rundschau*, Vol. 85, pp. 669-682.

Çoğulu, E., 1967. Etude pétrographique de la région de Mihaliççik (Turquie). *Schweiz. Mineral. Petrogr. Mittl.*, 47, 683-824.

Davids, M. B., 2000. Palynology after Y2K-understanding the source of area of pollen in sediments. *Annual Review of Earth and Planetary Science*, 28, 1-18.

Dahlqvist, P., 2018. Late Ordovician (Hirnantian) depositional pattern and sea-level change in shallow marine to shoreface cycles in central Sweden, 141, 605-616. <https://doi.org/10.1017/S0016756804009446>

D'Argenio, B., Amodio, S., Ferreri, F. and Pelosi, N., 1997. hierarchy of high frequency orbital cycles in Cretaceous carbonates in northern Italy. *Am. J. Sci.* 287, 853 -892.

Delaloye, M. and Bingöl, E., 2000. Granitoids from Western and Northwestern Anatolia: Geochemistry and modeling of geodynamic evolution. *International Geology Review*. 42. 241-268.

- De los Rios, A., Ascaso, C., Wierzchos, J., Ferna, E. and Quesada, A., 2004. Microstructural Characterization of Cyanobacterial Mats from the McMurdo Ice Shelf, Antarctica. *Applied and Environmental Microbiology*, 70(1), 569-580. <https://doi.org/10.1128/AEM.70.1.569>
- Delian, F., Tiebing, L. and Le, Y., 1992. The process of formation of manganese carbonate deposits hosted in black shale series. *Economic Geology*, 87, 1419-1420.
- Demaison, G. J. and Moore, G. T., 1980. Anoxic environments and oil source bed genesis. *American Association of Petroleum Geologists Bulletin* 64, 1179-1209.
- Deng, H. and Qian, K., 1990. The genetic types and association evolution of deep lacustrine facies mudstones. *Acta Sedimentologica Sinica* 8 (3).
- Deveciler, E., et al., 1989. Çatalzeytin (Kastamonu) dolayının jeolojisi, MTA rapor no. 8617 (Yayınlanmamış).
- Devlin, W. J., Rudolph, K. W., Shaw, C. A. and Ehman, K. D., 1993. The effect of tectonic and eustatic cycles on accommodation and sequence-stratigraphic framework in the Upper Cretaceous foreland basin of southwestern Wyoming. In: Posamentier, H.W., Summerhayes, C.P., Haq, B.U., Allen, G.P. (Eds.), *Sequence Stratigraphy and Facies Associations*, vol. 18. Spec. Publ. Int. Ass. Sediment, pp. 501-520.
- Diaz, H. G-, Miller, C. and Lewis, R., 2012. sCore: A Classification Scheme for Organic Mudstones Based on Bulk Mineralogy. *American Association of Petroleum Geologists, Southwest section convention, Fort Worth, Texas.*
- Ding, X. J., Liu, G. D., Zha, M., Huang, Z. L., Gao, C. H., Lu, X. J., Sun, M. L., Chen, Z. L., Liu, X. X. and Zhuang, 2015. Relationship between total organic carbon content and sedimentation rate in ancient lacustrine sediments, a case study of Erlian basin, northern China. *J. Geochem. Explor.* 149, 22-29.

- Dini, M., Tunis, G. and Venturini, S., 1998. Continental, brackish and marine carbonates from the Lower Cretaceous of Kolone-Barbariga (Istria, Croatia): stratigraphy, sedimentology and geochemistry, 140, 245–269.
- Dix, G. R. and Parras, A., 2014. Integrated diagenetic and sequence stratigraphy of a late Oligocene-early Miocene, mixed-sediment platform (Austral Basin, southern Patagonia): Resolving base-level and paleoceanographic changes, and paleoaquifer characteristics. *Sedimentary Geology*, 307, 17–33. <https://doi.org/10.1016/j.sedgeo.2014.04.003>
- Dolin, C., Dolin, L. and Le Renard, J., 1980. Inventaire systématique des mollusques de l’Auversien à «faciès charrié» de Baron (Oise), et remarques paléontologiques. *Bull. inf. Géolog. bass. Paris*, 17 (2): 26-48.
- Durand, B., 1980. Sedimentary organic matter and kerogen. Definition and quantitative importance of kerogen. In: Durand, B. (Ed.), *Kerogen, Insoluble Organic Matter from Sedimentary Rocks*. Editions Technip, Paris.
- Dyni, J. R. and Hawkins, J. E., 1981. Lacustrine turbidites in the Green River Formation, northwestern Colorado. *Geology*, 9, 235-238.
- Dyni, J. R., 2003. Geology and resources of some world oil-shale deposits. *Oil-shale* 20 (3), 193–252.
- Einsele, G., Ricken, W. and Seilacher, A., 1991. *Cycles and Events in Stratigraphy*. Springer Verlag, Berlin Heidelberg, pp. 23–47.
- Embry, A. F. and Klovan, E. J., 1971. The Upper Devonian stratigraphy of northeastern Banlts Island has. *Bulletin of Canadian Petroleum Geology*, 19(4), 730-781.
- Egbobawaye, E. I., 2016. Sedimentology and Ichnology of Upper Montney Formation Tight Gas Reservoir, Northeastern British Columbia, Western Canada Sedimentary Basin. *International Journal of Geosciences*, 07(12), 1357-1411. <https://doi.org/10.4236/ijg.2016.712099>

- Elattaar, A. A., 2018. Middle Eocene echinoids from El Sheikh Fadl-Ras Gharib stretch, Eastern Desert, Egypt : systematics, stratigraphy, palaeobiogeography.
- El-Azabi, M., 2006. Sedimentological characteristics, palaeoenvironments and cyclostratigraphy of the Middle Eocene sequences in Gabal El-Ramliya, Maadi-Sukhna stretch, North Eastern Desert, Egypt. proceedings of the 8th int. conf. on the geology of the arab world (gaw 8), cairo university, egypt. vol. ii. 459-484.
- Erk, S., 1942. Etude geologique de la region entre Gemlik et Bursa. Mineral Research and Exploration Institute (MTA) of Turkey publication Bulletin, No. 9.
- Eroskay, S. O. 1965. Paşalar Boğazı-Gölpazarı sahasının jeolojisi. İ. Ü. F. F. Mecm. Seri B, 3-4, 135-170.
- Esmeray, S., 2008. Cretaceous/Paleogene boundary in the Haymana basin, Central Anatolia, Turkey: Micropaleontological, Mineralogical and Sequence Stratigraphic Approach. MS Thesis; Middle East Technical University, Ankara.
- Esteban, S. B., 2003. Biogenic and physical sedimentary structures in latest Cambrian-earliest Ordovician mudrock facies (Famatina Range, northwestern Argentina). *Geologica Acta*, 1(1), 85-94.
- Feist, M., 1977. Evolution of the charophyten floras in the Upper Eocene and Lower Oligocene of the Isle of Wight. *Palaeontology* 20: 143-157.
- Feist, M., Anadón, P., Sáez, M., Choi, S. J., Cabrera, L. and Colombo, F. 1994. Upper Eocene - Lowermost Miocene charophyte succession in the Ebro Basin (Spain). Contribution to the charophyte biozonation in Western Europe. *Newsletters on Stratigraphy*, 30(1), 1-32. <https://doi.org/10.1127/nos/30/1994/1>
- Feist, M., Grambast-Fessard, N., Guerlesquin, M., Karol, K., Lu, H., Mccourt, R. M., Wang, Q. and Shenzen, Z., 2005. Treatise on Invertebrate Paleontology. Part B., Protozoa 1. Charophyta, The Geological Society of America, Kansas, 170p.

- Feng, J., 2011. Source rock characterization of the Green River oil-shale, Piceance Creek Basin, Colorado. Thesis, 1-96.
- Fischer, A. G., 1980. Gilbert-bedding rhythms and geochronology. *Geol. Soc. Am., Spec.*, 183, 107-149.
- Fischer, A. G., 1991. Orbital cyclicity in Mesozoic strata, in Einsele, G., Ricken, W., and Seilacher, A., eds., *Cycles and events in stratigraphy*. Berlin, Springer-Verlag, p. 48-62
- Fischer, A. G. and Roberts, L. T., 1991. Cyclicity in the Green River formation (lacustrine Eocene) of Wyoming. *J. Sediment. Petrol.* 61, 1146-1154
- Fischer, A. G., De Boer, P. L. and Premoli Silva, I., 1988. Cyclostratigraphy. In: Beaudoin, B. & R. N. Ginsburg (eds.): *Global Sedimentary Geology Program: Cretaceous Resources, Events, and Rhythms*. -NATO ASI Series, Kluwer, 139-172, Dordrecht.
- Flügel, E., 2004. *Microfacies of Carbonate Rocks: Analysis, Interpretation and Application*. Springer (pp. 1–996). <https://doi.org/10.1007/978-3-642-03796-2>
- Foix, N., Paredes, J.M. and Giacosa, R.E., 2013. Fluvial architecture variations linked to changes in accommodation space: Río Chico Formation (Late Paleocene), Golfo san Jorge basin, Argentina. *Sedimentary Geology* 294, 342–355.
- Folk, R. L., 1965. *Petrology of Sedimentary Rocks*. 2nd Edition Hemphill, Bookstore, Austin.
- Folk, R. L., 1974. *Petrology of Sedimentary Rocks*. 3rd Edition Hemphill, Austin, Texas.
- Forsman, J. P. and Hunt, J. M., 1958. Insoluble organic matter (kerogen) in sedimentary rocks. *Geochimica et Cosmochimica Acta*, 15(3), 170–182. [https://doi.org/10.1016/0016-7037\(58\)90055-3](https://doi.org/10.1016/0016-7037(58)90055-3)

- Fourquin, C., 1975. L'anatolie du Nord-Ouest, marge méridionale du continent européen, histoire paléogéographique, tectonique et magmatique durant le Secondaire et Tertiaire. Bulletin Society of Géology of France, Vol. 7, pp. 1058-1070.
- Fredriksen, K. S., Clemmensen, L. B. and Lawætz, H. S., 1998. Sequential architecture and cyclicity in Permian desert deposits, Brodrick Beds, Arran, Scotland. J. Geol. Soc. (Lond.) 155, 677-683.
- Freytet, P. and Plaziat, J.-C., 1982. Continental carbonate sedimentation and Pedogenesis-Late Cretaceous and Early Tertiary of Southern France. Contributions to Sedimentology 12, 1-213.
- Fuhrmann, A., 2002. Geochemical Indicators of Paleoenvironmental and Paleoclimatic Change in Ancient and Recent Lake Deposits : Facies Models , Facies Distributions and Hydrocarbon Aspects. Thesis.
- Gedik, İ. ve Aksay, A., 2002. 1/100.000 ölçekli Türkiye Jeoloji Haritaları, No: 38. Adapazarı-H25 paftası. 34 s.
- Ghadeer, S. G. and Macquaker, J. H. S., 2011. Sediment transport processes in an ancient mud-dominated succession: a comparison of processes operating in marine offshore settings and anoxic basinal environments. Journal of the Geological Society, 168(5), 1121-1132. <https://doi.org/10.1144/0016-76492010-016>
- Gingras, M. K., MacEachern, J. A., and Dashtgard, S. E., 2011, Process ichnology and the elucidation of physico-chemical stress: Sedimentary Geology, v. 237, p. 115-134.
- Gierlowski-Kordesch, E.H. and Rust, B.R., 1994. The Jurassic East Berlin Formation, Hartford basin, Newark Supergroup (Connecticut and Massachusetts): a saline lake-playa-alluvial plain system. In: Sedimentology and Geochemistry of Modern and Ancient Saline Lakes (Eds R.W. Renaut and W.M. Last), SEPM Spec. Publ., 50, 249-265.

- Gierlowski-Kordesch, E. H., 2010. Chapter 1 Lacustrine Carbonates. Developments in Sedimentology (Vol. 61). Elsevier. [https://doi.org/10.1016/S0070-4571\(09\)06101-9](https://doi.org/10.1016/S0070-4571(09)06101-9)
- Glasby, G.P., 2006. Manganese: predominant role of nodules and crusts. In: Schulz HD, Zabel M (eds) Marine geochemistry. Springer, Heidelberg, pp 371-428
- Gonçaves, P. A., 2014. Characterization of organic facies and identification of potential source rocks in Jurassic sedimentary sequences of the Lusitanian Basin (Portugal).
- Goldhammer, R. K., Dunn, P. A. and Hardie, L. A., 1990. Depositional cycles, composite sea-level changes, cycle stacking pattern and the hierarchy of stratigraphic forcing. Examples from Alpine Triassic platform carbonates. Geol. Soc. Am. Bull. 102, 535-562.
- Göncüoğlu, M. C., 2010. Introduction to Geology of Turkey: Alpine and pre-Alpine geodynamic evolution of tectonic units. Mineral Research and Exploration of Ankara, Turkey, Monograph Series, No. 5, pp. 1-69.
- Göncüoğlu, M. C., Turhan, N., Şentürk, K., Uysal, Ş., Özcan, A. and Işık, A. 1996. Nallıhan-Sarıcakaya Arasında Orta Sakarya'daki Yapısal Birimlerin Jeolojik Özellikleri [Geological Characteristics of the Structural Units in Central Sakarya Between Nallıhan-Sarıcakaya]. MTA Report no. 10094 [in Turkish, unpublished].
- Göncüoğlu, M. C., Turhan, N., Şentürk, K., Özcan, A., Uysal, S. and Yalınız, M. K., 2000. A geotraverse across northwestern Turkey: tectonic units of the Central Sakarya region and their tectonic evolution. In: Bozkurt, E., Winchester, J.A. & Piper, J.D. (eds) Tectonics and Magmatism in Turkey and the Surrounding Area Geological Society, London, Special Publications 173, 139–162
- Görmüş, S., 1980. Yığılca (Bolu NW) yöresinin jeolojik incelenmesi. Doktora Tezi, Hacettepe Üniversitesi, 197 s., Ankara.

- Görür, N. and Tüysüz, O., 2001. Cretaceous to Miocene palaeogeographic evolution of Turkey: implications for hydrocarbon potential. *J. Petrol. Geol.* 24 (2), 119-146.
- Görür, N., Tüysüz, O. and Sengör, A. M.C ., 1998. Tectonic evolution of the Central Anatolian Basins. *Int. Geol. Rev.* 40, 831-850.
- Görür, N., Şengör, A. M. C., Akkök, R. and Yılmaz, Y., 1983. Pontidlerde Neotetis'in kuzey kolunun açılmasına ilişkin sedimantolojik veriler. *Türkiye Jeoloji Kurumu Bülteni* 26 (1), 11–20 (in Turkish with English abstract).
- Grambast, L., 1957. Ornementation de la gyrogonite et systématique chez les charophytes fossiles. *Rev. Gén. Bot.* 64, 1–24.
- Grambast, L., 1962. Classification de l'embranchement des Charophytes. *Naturalia Monspelienis (serie Botanique)*, 14, 63–86.
- Grambast, L., 1964. Précisions nouvelles sur la phylogénie des Charophytes. *Natur. Monspel. Bot.* 16: 71-77,
- Grambast, L., 1972. Principes de l'utilisation stratigraphique des charophytes. Applications au Paléogène d'Europe occidentale. *Mémoires du Bureau de Recherches Géologiques et Minières*, 77: 319–328.
- Grambast, L. 1974. Phylogeny of the Charophyta. *Taxon*, 23 (4), 463-481. <https://doi:10.2307/1218769>
- Grambast, L., and Lavocat, R., 1959. Sur la présence dans la région du Dra (Sahara nord-occidental) de couches éocènes datées par les charophytes. *Comptes rendus sommaires des Séances de la Société Géologique de France* (6): 153.
- Granit, S. ve Şener, M., 1987. Sarıcakaya (Eskişehir) ve Çamalan-Beydili (Ankara) bölgesinin jeolojisi ve bitümlü şeyl olanakları. MTA Rapor No: 8400.

- Grosjean, A. S., Pittet, B., Ferry, S., Mahéo, G. and Gardien, V., 2012. Reconstruction of Tertiary palaeovalleys in the South Alpine Foreland Basin of France (Eocene–Oligocene of the Castellane arc). *Sedimentary Geology*, 275–276, 1-21. <https://doi.org/10.1016/j.sedgeo.2012.05.022>
- Grosjean, A. S. and Pittet, B., 2013. Facies analysis and depositional environments of the Taulanne Limestone Formation in the South Alpine Foreland Basin (Oligocene, southeastern of France). *Facies*, 59(4), 717-736. <https://doi.org/10.1007/s10347-012-0350-0>
- Guernet, C., Huyghe, D., Lartaud, F., Merle, D., Emmanuel, L., Geély, J. P., Michel, F. and Pilet, O. 2012. Les Ostracodes de la falunieère de Grignon (Lutétien du Bassin de Paris): implications stratigraphiques. *Geodiversitas*, 34, 909-959.
- Guo, Q., Xie, H., Mi, S., et al., 2009a. Fractal model for petroleum resource distribution and its application. *Acta Petrolei Sinica* 30 (3), 379-385.
- Guo, W., Zhaojun, L., Yuqin, S., et al., 2009b. Genetic type and features of oil-shale in the Minhe Basin, QinghaieGansu provinces. *China Geological Bulletin of China* 28 (6), 780-786.
- Gülbay, R. K. and Korkmaz, S., 2008. Organic geochemistry, depositional environment and hydrocarbon potential of the tertiary oil-shale deposits In NW Anatolia, Turkey. *Oil-shale*, Vol. 25, (4), pp. 444-464.
- Gültekin, A. H. and Balci, N., 2018. Geochemical Characteristics of Sedimentary Manganese Deposit of Binkılıç, Trache Basin, Turkey. *Journal of Geology & Geophysics*. 07. <https://doi.org/10.4172/2381-8719.1000336>
- Güray, A., 2014. Planktonic foraminiferal biostratigraphy of the Paleocene-Eocene sequences in the western and central Black Sea region, Turkey. PhD Thesis, ODTU.
- Hadi, M., Mosaddegh, H. and Abbassi, N., 2016. Microfacies and biofabric of Nummulites accumulations (Bank) from the Eocene deposits of Western Alborz

(NW Iran) *Journal of African Earth Sciences*, 124, 216-233.  
<https://doi.org/10.1016/j.jafrearsci.2016.09.012>

Hakala, A., 2004. Meromixis as part of lake evolution-observations and a revised classification of true meromictic lakes in Finland. *Boreal Environ Res* 9:37–53

Hakyemez, Y., Barkut, M. Y., Bilginer, E., Pehlivan, Ş., Can, B., Dağer, Z. and Sözeri, B., 1986. Yapraklı-Ilgaz-Çankırı-Çandır dolayının jeolojisi. MTA Report No: 7966, unpublished.

Hammouda, S. A., Sames, B., Adaci, M. and Bensalah, M., 2018. First record of non-marine ostracods from the Paleogene “hamadian deposits” of Méridja area, west of Bechar (southwestern Algeria). *Annales de Paleontologie*, 104(1), 27–44.

Handford, C. R. and Loucks, R. G., 1994. Carbonate depositional sequences and systems tracts - responses of carbonate platforms to relative sea-level changes: in R.G. Loucks and I.F.R. Sarg, eds., *Carbonate Sequence Stratigraphy*, American Association of Petroleum Geologists Memoir 57, p. 3-42.

Haq, B. U., Hardenbol, J. and Vail, P. R., 1987. Chronology of fluctuating sealevels since the Triassic. *Science*, 235, 1156-1167.

Haq, B. U., Hardenbol, J. and Vail, P. R., 1988. Mesozoic and Cenozoic chronostratigraphy and cycles of sea-level change. In: Wilgus, C.K., Hastings, B.S., Kendall, C.G.St.C., Posamentier, H.W., Ross, C.A., van Wagoner, J.C. (Eds.), *Sea-Level Changes: An Integrated Approach*, SEPM (Society for Sedimentary Geology), Special Publications, 42, 71–108.

He, J., Ding, W., Jiang, Z., Jiu, K. and Li, A., 2017. Mineralogical and chemical distribution of the Es<sub>3</sub><sup>L</sup> oil-shale in the Jiyang Depression, Bohai Bay Basin ( E China ): Implications for paleoenvironmental reconstruction and organic matter accumulation. *Marine and Petroleum Geology*, 81, 196–219.  
<https://doi.org/10.1016/j.marpetgeo.2017.01.007>

Hembree, D. I. and Bowen, J. J., 2017. Paleosols and ichnofossils of the Upper

Pennsylvanian-Lower Permian Monongahela and Dunkard groups (Ohio , USA): A multi-proxy approach to unraveling complex variability in ancient terrestrial landscapes containing ichnofossils as well as vertebrate, 295-320.

Hinnov, L. A., 2013. Cyclostratigraphy and its revolutionizing applications in the earth and planetary sciences. *Bulletin of the Geological Society of America*, 125(11-12), 1703-1734. <https://doi.org/10.1130/B30934.1>

Hiroki, Y. and Terasaka, T., 2005. Wavy lamination in a mixed sand and gravel foreshore facies of the Pleistocene Hosoya Sandstone, Aichi, central Japan. *Sedimentology*, 52(1), 65-75. <https://doi.org/10.1111/j.1365-3091.2004.00682.x>

Homewood, P. W., 1996. The carbonate feedback system: Interaction between stratigraphic accommodation, ecological succession and the carbonate factory. *Bulletin de la Societe Geologique de France*. 167. 701-715.

Homewood, P., 2001. Fine-Grained Turbidite Systems. *Basin Res.* 13, 377

Hongjun, W., Feng, M. A., Xiaoguang, T., Zuodong, L. I. U., Xinshun, Z., Zhenzhen, W. U., ... Liuyan, Y., 2016. Assessment of global unconventional oil and gas resources, 43(6), 925–940. [https://doi.org/10.1016/S1876-3804\(16\)30111-2](https://doi.org/10.1016/S1876-3804(16)30111-2)

Hopkins, J.S., 1950. Differential flotation and deposition of coniferous and deciduous tree pollen. *Ecology*, 31, 633-641

Huang, B., Tian, H., Wilkins, R. W. T., Xiao, X. and Li, L., 2013. Geochemical characteristics, palaeoenvironment and formation model of Eocene organic-rich shales in the Beibuwan Basin, South China Sea. *Marine and Petroleum Geology*, 48, 77–89. <https://doi.org/10.1016/j.marpetgeo.2013.07.012>

Huang, B., Zhu, W., Tian, H., Jin, Q., Xiao, X. and Hu, C., 2017. Characterization of eocene lacustrine source rocks and their oils in the Beibuwan Basin, offshore South China Sea. *AAPG Bulletin*, 101(9), 1395–1423. <https://doi.org/10.1306/10171615161>

- Huckriede, H. and Meischner, D., 1996. Origin and environment of manganese-rich sediments within black-shale basins. *Geochimica et Cosmochimica Acta*, 60(8), 1399-1413.
- Hunt, J. M., 1991. Generation of gas and oil from coal and other terrestrial organic matter. *Org. Geochem.* 17, 673-680
- Hunt, D. and Tucker, M.E., 1995. Stranded parasequences and the forced regressive wedge systems tract: deposition during base-level fall - reply. *Sediment. Geol.* 95, 147-160.
- Husinec, A., Basch, D., Rose, B. and Read, J. F., 2008. FISCHERPLOTS: An Excel spreadsheet for computing Fischer plots of accommodation change in cyclic carbonate successions in both the time and depth domains. *Computers and Geosciences*, 34(3), 269–277. <https://doi.org/10.1016/j.cageo.2007.02.004>
- Hutton, A. C., 1982. Organic Petrology of Oil-shales. PhD thesis, University of Wollongong (unpubl.).
- Hutton, A. C., 1987. Petrographic classification of oil-shales. *Int. J. Coal Geol.* 8, 203–231.
- Hutton, A. C., 1991. Classification, organic petrography and geochemistry of oil-shale. In: *Proceedings of 1990 Eastern Oil-shale Symposium*. Institute for Mining and Minerals Research, University of Kentucky, Lexington, KY, pp. 163–172.
- Hutton, A. C., Kantsler, A. J., Cook, A. C. and McKirdy, D. M., 1980. Organic matter in oil-shales. *APEA J.*, 20: 44-67.
- Huyghe, D., Emmanuel, L., Renard, M., Lartaud, F., Génot, P., Riveline, J. and Merle, D., 2017. Significance of shallow-marine and non-marine algae stable isotope ( $\delta^{18}\text{O}$ ) compositions over long periods : Example from the Palaeogene of the Paris Basin. *Palaeogeography, Palaeoclimatology, Palaeoecology*, 485, 247-259. <https://doi.org/10.1016/j.palaeo.2017.06.017>

- Jarvie, D. M., 1991. Total organic carbon (TOC) analysis; In: Source migration processes and evaluation techniques. Merrill, R. K. (ed), AAPG, Treatise of petroleum geology handbook of petroleum geology, pp. 113-118, New York
- Jiang, Z., Chao, L., Wu, J., Jianguo, Z., Zhang, W., Wang, Y., Liu, H., and Chen, X., 2013. Several issues in sedimentological studies on hydrocarbon-bearing fine-grained sedimentary rocks. *Shiyou Xuebao/Acta Petrolei Sinica*. 34. 1031-1039.
- Jiang, Z., Tang, X., Cheng, L., Li, Z., Zhang, Y., Bai, Y., Yuan, Y. and Hao, J., 2015. Characterization and origin of the Silurian Wufeng-Longmaxi Formation shale multiscale heterogeneity in southeastern Sichuan Basin, China: Interpretation, 3, no. 2, SJ61–SJ74, <https://doi.org/10.1190/INT-2014-0151.1>
- Jiang, S., Xu, Z., Feng, Y., Zhang, J., Cai, D., Chen, L., Wu, Y., Zhou, D., Bao, S. and Long, S., 2016. Geologic characteristics of hydrocarbon-bearing marine, transitional and lacustrine shales in China. *J. Asian Earth Sci.* 115, 404-418.
- Jin, S., Wang, H., Cao, H., Chen, S., Lin, Z., Yu, J. and Pan, S., 2014. Sedimentation of the Paleogene Liushagang Formation and the response to regional tectonics in the Fushan, 1.
- Johansen, S. K., 2016. Sedimentology and facies distribution of the Upper Triassic De Geerdalen Formation in the Storfjorden area and Wilhelmøya, eastern Svalbard. MSc thesis, Norwegian University of Science and Technology, Trondheim.
- Jones, F. G. and Bowser, C. J., 1978. The mineralogy and related chemistry of lake sediments. In: *Lakes: Chemistry, Geology and Physics* (Ed. by A. Lerman), pp. 179-235. Springer-Verlag, Berlin.
- Jones, B. and Manning, D. A. C., 1994. Comparison of geochemical indices used for the interpretation of palaeoredox conditions in ancient mudstones. *Chemical Geology*. [https://doi.org/10.1016/0009-2541\(94\)90085-X](https://doi.org/10.1016/0009-2541(94)90085-X)
- Juhasz, Gy., Pogacsas, Gy., Magyar, I. and Vakarcs, G., 2007. Tectonic versus climatic control on the evolution of fluvio-deltaic systems in a lake basin, eastern

Pannonian Basin. *Sediment. Geol.* 202, 72-95.

Kadolsky, D., 2015. *Lutetiella*, a new genus of hydrobioids from the Middle Eocene (Lutetian) of the Upper Rhine Graben and Paris Basin (Mollusca: Gastropoda: Rissooidea s. lat.). *Journal of Central European Geology*, 61(1), 35–51

Kangal, Ö., Erdem, N. Ö. and Varol, B., 2016. Depositional stages of the Eğribucak inner basin (Terrestrial to marine evaporite and carbonate) from the Sivas Basin (Central Anatolia, Turkey). *Turkish Journal of earth sciences*, 25, pp. 1-20. <https://doi.org/10.3906/yer-1606-7>

Katz, B. J., 1990. Controls on distribution of lacustrine source rocks through space and time. In: Katz, B.J.(Ed): *Lacustrine Basin Exploration-Case Studies and Modern Analogues*. AAPG Memoir 50. American Association of Petroleum Geologists, pp 61-76.

Kaymakci, N., White, S. H., Vandijk, P. M., 2003. Kinematic and structural development of the Çankiri Basin (Central Anatolia, Turkey): a paleostress inversion study. *Tectonophysics* 364 (1-2), 85-113.

Kazancı, N. and Gökten, E., 1986. Sedimentary characteristics of terrestrial Paleocene deposits in northern Ankara region, Turkey. *Commun. Fac. Sci. Univ. Ank. Serie C* 4, 153–163.

Keighley, D., Flint, S., Howell, J. and Moscariello, A., 2003. Sequence Stratigraphy in Lacustrine Basins: A Model for Part of the Green River Formation (Eocene), Southwest Uinta Basin, Utah, U.S.A. *Journal of Sedimentary Research*, 73(6), 987-1006. <https://doi.org/10.1306/050103730987>

Keighley, D., 2008. A lacustrine shoreface succession in the Albert Formation, Moncton Basin, New Brunswick. *Bull. Can. Petrol Geol.*, 56, 235-258.

Kelts, K., and Hsu, K. J., 1978. Freshwater carbonate sedimentation. In Lerman, A., ed. *Lakes: chemistry, geology, physics*. New York, Springer, p. 295–323.

- Kerans, C. and Tinker, S.W., 1997. Sequence Stratigraphy and Characterization of Carbonate Reservoirs. In: Society of Economic Paleontologists and Mineralogists Short Course Notes, 40, p. 130.
- Ketin, İ., 1966. Tectonic units of Anatolia (Asia Minor). Mineral Research and Exploration Institute of Turkey Bulletin, No. 66, pp. 23-34.
- Khosla, S. C., Nagori, M. L., Jakhar, S. R. and Rathore, A. S., 2011. Early Danian lacustrine- brackish water Ostracoda from the Deccan Inter-trappean beds near Jhilmili, Chhindwara District, Madhya Pradesh, India, 57(3), 223–245.
- Kim, J. Y., Keighley, D. G., Pickerill, R. K., Hwang, W. and Kim, K-S. 2005. Trace fossils from marginal lacustrine deposits of the Cretaceous Jinju Formation, southern coast of Korea. *Palaeogeography, Palaeoclimatology, Palaeoecology*, v. 218, p. 105–124.
- Koçyiğit, A., 1991. An example of an accretionary fore-arc basin from Central Anatolia and its implications for the history of subduction of Neo-Tethys in Turkey. *Geological Society of American Bulletin*, Vol.103, (1), pp. 22-36.
- Koçyiğit, A., Özkan, S. and Rojay, B., 1988. Examples of the fore-arc basin remnants at the active margin of northern Neo-Tethys: development and emplacement ages of the Anatolian Nappe, Turkey. *Middle East Technical University Journal of Pure and Applied Sciences*, Vol. 3, pp. 183-210.
- Koçyiğit, A., Altıner, D., Farinacci, A., Nicosia, U. and Conti, M. A., 1991. Late Triassic-Aptian evolution of the Sakarya divergent margin: implications for the opening history of the Northern Neo-Tethys, in the North-Western Anatolia, Turkey. *Geologica Romana*, v. 27, p; 81-101.
- Koralay, D. B., 2009. Investigation of hydrocarbon potential and trace element distributions of Eocene bituminous shales in Bolu Basin, PhD thesis, Ankara University.
- Kök, M. V., Şengüler, İ., Hufnagel, H. and Sonel, N., 2001. Thermal and geochemical

investigation of Seyitomer oil-shale. *Thermochimica Acta*, 371(1–2), 111–119.  
[https://doi.org/10.1016/S0040-6031\(01\)00415-4](https://doi.org/10.1016/S0040-6031(01)00415-4)

Lash, G. G., 2011. Sequence Stratigraphy Manifested in Source and Reservoir Properties of Shale Successions – Examples from the Middle Devonian Marcellus Formation , Appalachian Basin, 1–8.

Lash, G. and Blood, R., 2011. Sequence Stratigraphy as Expressed by Shale Source Rock and Reservoir Characteristics-Examples from the Devonian Succession , Appalachian Basin, 80168, 103–107.

Lazar, O. R., 2007, Redefinition of the New Albany Shale of the Illinois Basin: An integrated, stratigraphic, sedimentologic, and geochemical study, Ph.D thesis, Indiana University,

Lazar, O. R., Bohacs, K. M., Macquaker, J. H. S., Schieber, J. and Demko, T. M., 2015. Capturing Key Attributes of Fine-Grained Sedimentary Rocks In Outcrops, Cores, and Thin Sections: Nomenclature and Description Guidelines. *Journal of Sedimentary Research*, 85(3), 230–246. <https://doi.org/10.2110/jsr.2015.11>

Lefebvre, C., Meijers, M. J. M., Kaymakci, N., Peynircioğlu, A., Langereis, C. G. and van Hinsbergen, D., J. J., 2013. Reconstructing the geometry of central Anatolia during the late Cretaceous: Large-scale Cenozoic rotations and deformation between the Pontides and Taurides. *Earth and Planetary Science Letters*, Vol. 366, pp. 83-98.

Lettéron, A., Fournier, F., Hamon, Y., Villier, L., Margerel, J. P., Bouche, A., ... Joseph, P. (2017). Multi-proxy paleoenvironmental reconstruction of saline lake carbonates: Paleoclimatic and paleogeographic implications (Priabonian-Rupelian, Issirac Basin, SE France). *Sedimentary Geology*, 358, 97–120.  
<https://doi.org/10.1016/j.sedgeo.2017.07.006>

Lettéron, A., Hamon, Y., Fournier, F., Séranne, M., Pellenard, P. and Joseph, P., 2018. Reconstruction of a saline, lacustrine carbonate system (Priabonian, St-Chaptes Basin, SE France): Depositional models , paleogeographic and paleoclimatic implications, 367, 20-47. <https://doi.org/10.1016/j.sedgeo.2017.12.023>

- Lewis, D. W. and McConchie, D. M., 1994. *Analytical Sedimentology*. Chapman & Hall, New York.
- Li, H. and Bennett, R. H., 1991. The significance of sediment-flow dynamics on clay microstructure development: Riverine and continental shelf environments. In *Microstructure of Fine-Grained Sediments*; Chiou, W., Faas, R., Kasprovicz, J., Li, H., Lomenick, T., O'Brien, N., Pamukcu, S., Smart, P., Weaver, C., Yamamoto, T., Eds.; Springer: New York, NY, USA, pp. 193-202.
- Li, Q., Zhong, G. and Tian, J., 2009. Stratigraphy and Sea Level Changes. In: Wang P., Li Q. (eds) *The South China Sea. Developments in Paleoenvironmental Research*, vol 13. Springer, Dordrecht, pp 75-170. <https://doi.org/10.1007/978-1-4020-9745-4>
- Li, S., Cheng, S., Yang, S., Huang, Q., Xie, X., Jiao, Y., et al., 1992. *Sequence Stratigraphy and Depositional System Analysis of the Northeastern Ordos Basin*. Beijing: Geological Publishing House.
- Liang, C., Cao, Y., Jiang, Z., Wu, J., Guoq Yen T. F. and Chilingarian, G. V., 1976. *Oil-shale*. Elsevier Scientific Publishing Company, 291 p., New York. i, S., & Wang, Y. (2017). Shale oil potential of lacustrine black shale in the Eocene Dongying depression: Implications for geochemistry and reservoir characteristics. *AAPG Bulletin*, 101(11), 1835–1858. <https://doi.org/10.1306/01251715249>
- Liang, C., Wu, J., Jiang, Z., Cao, Y. and Song, G., 2018. International Journal of Coal Geology Sedimentary environmental controls on petrology and organic matter accumulation in the upper fourth member of the Shahejie Formation (Paleogene, Dongying depression, Bohai Bay Basin, China). *International Journal of Coal Geology*, 186, 1-3. <https://doi.org/10.1016/j.coal.2017.11.016>
- Lindqvist, J. K. and Lee, D., 2009. High-frequency paleoclimate signals from Foulden Maar, Waipiata Volcanic Field, southern New Zealand: An Early Miocene varved lacustrine diatomite deposit. *Sedimentary Geology*. 222. 98-110.
- Linye, Z., Yitao, S. and Guangli, W., 2006. Organic compositions of lacustrine source

rocks in Jiyang super-depression and its implication to petroleum geology. *Chinese Science Bulletin*, 51(5), 573–584. <https://doi.org/10.1007/s11434-006-0573-y>

Lirer, F., 2000. A new technique for retrieving calcareous microfossils from lithified lime deposits. *Micropaleontology* 46, 365–369.

Liu, C., Wang, P. and Xu, J., 2001. Algal blooms: the primary mechanism in the formation of lacustrine petroleum source rocks. *Geol. Rev.* 2001, 47, 207-210.

Liu, Z., Hulin, Y., Qinshui, D., et al., 2009a. *Oil-shale in China*. Petroleum Industry Press, Beijing.

Liu, Z., Qingtao, Y., Rong, L., 2009b. Characteristics and genetic types of continental oil-shales in China. *Journal of Palaeogeography* 11 (1), 105-114.

Liu, C. and Wang, P., 2013. The role of algal blooms in the formation of lacustrine petroleum source rocks-Evidence from Jiyang depression, Bohai Gulf Rift Basin, eastern China. *Palaeogeogr. Palaeoclimatol. Palaeoecol.* 2013, 388, 15-22.

Lokman, K., 1929. Bituminous schist of Bolu (Mengen) // MTA report number: 268, Ankara, (unpublished) [in Turkish with English abstract].

Lorente, F. L., Pessenda, L. C. R., Oboh-Ikuenobe, F., Buso, A. A., Cohen, M. C. L., Meyer, K. E. B., ... Macario, K., 2014. Palynofacies and stable C and N isotopes of Holocene sediments from Lake Macuco (Linhares, Espírito Santo, southeastern Brazil): Depositional settings and palaeoenvironmental evolution. *Palaeogeography, Palaeoclimatology, Palaeoecology*, 415, 69–82. <https://doi.org/10.1016/j.palaeo.2013.12.004>

Loucks, R. G., Reed, R. M., Ruppel, S. C. and Hammes, U., 2012. Spectrum of pore types and networks in mudrocks and a descriptive classification for matrix-related mudrock pores. *Aapg Bull.* 96, 1071-1098.

- Luciani, V., 2002. High-resolution planktonic foraminiferal analysis from the Cretaceous-Tertiary boundary at Ain Settera (Tunisia): evidence of an extended mass extinction. *Palaeogeography, Palaeoclimatology, Palaeoecology*, 178, 299-319.
- Lucius, M., 1928. Çağa Çay (Bolu) bitümlü şist yatakları hakkında rapor. MTA Rapor No: 265, 7 s., Ankara.
- Lyons, R. P., Scholz, C. A., Buoniconti, M. R. and Martin, M. R., 2011. Late Quaternary stratigraphic analysis of the Lake Malawi Rift, East Africa: an integration of drillcore and seismic-reflection data: *Palaeogeography, Palaeoclimatology, Palaeoecology*, v. 303, p. 20-37
- Ma, Z. and Holditch, S., 2015. *Unconventional oil and Gas Resources Handbook: Evaluation and Development*, Gulf Professional Publishing, P.550
- Ma, P., Wang, L., Wang, C., Wu, X. and Wei, Y., 2015. Organic-matter accumulation of the lacustrine Lunpola oil-shale, central Tibetan Plateau: controlled by the paleoclimate, provenance, and drainage system. *Int. J. Coal Geol.* 147, 58–70.
- Ma, Y., Fan, M., Lu, Y., Liu, H., Hao, Y., Xie, Z., ... Hu, H., 2016. Climate-driven paleolimnological change controls lacustrine mudstone depositional process and organic matter accumulation: Constraints from lithofacies and geochemical studies in the Zhanhua Depression, eastern China. *International Journal of Coal Geology*, 167, 103-118. <https://doi.org/10.1016/j.coal.2016.09.014>
- Machlus, M. L., Olsen, P. E., Christie-Blick, N. and Hemming, S. R., 2008. Spectral analysis of the lower Eocene Wilkins Peak Member, Gren Formation, Wyoming: Support for Milankovitch cyclicity. *Earth Planet. Sci. Lett.* 268, 64-75.
- Macquaker, J. H. S. and Bohacs, K. M., 2007. Geology-On the accumulation of mud: *Science*, v. 318, p. 1734-1735
- Macquaker, J. H. S., Keller, M. A. and Davies, S. J., 2010. Algal Blooms and “Marine Snow”: Mechanisms That Enhance Preservation of Organic Carbon in Ancient

Fine-Grained Sediments. *Journal of Sedimentary Research*, 80(11), 934-942.  
<https://doi.org/10.2110/jsr.2010.085>

Mader, D., Cleaveland, L., Bice, D. M., Montanari, A. and Koeberl, C., 2004. High-resolution cyclostratigraphic analysis of multiple climate proxies from a short Langhian pelagic succession in the Cònero Riviera, Ancona (Italy). *Palaeogeography, Palaeoclimatology, Palaeoecology*, 211(3-4), 325-344.  
<https://doi.org/10.1016/j.palaeo.2004.06.001>

Magoon, L. B., and Dow, W. G., 1994, The petroleum system, in L.B. Magoon and W.G. Dow, eds., *The Petroleum System--From Source to Trap: AAPG Memoir 60*, p. 3-24.

Martin, D. M., 1999. Depositional setting and implications of Paleoproterozoic glaciomarine sedimentation in the Hamersley Province, Western Australia. *Geological Society of America Bulletin*, 111. 189-203.

Martín-closas, H. C. C., 2009. Charophyte-rich microfacies in the Barremian of the Eastern Iberian Chain (Spain), 387-400. <https://doi.org/10.1007/s10347-008-0173-1>

Martín-Closas, C., Serra-kiel, J., Busquets, P. and Ramos-Guerrero, E., 1999. New correlation between charophyte and larger foraminifera biozones (Middle Eocene, Southeastern Pyrenees). *Geobios*, 32(1), 5–18.  
[https://doi.org/https://doi.org/10.1016/S0016-6995\(99\)80080-1](https://doi.org/https://doi.org/10.1016/S0016-6995(99)80080-1).

Martín-Closas, C. and Ramos-Guerrero, E., 2005. Palaeogene Charophytes of the Balearic Islands (Spain). *Geologica acta: an international earth science journal*, ISSN 1695-6133, Vol. 3, No. 1, pp 39-58.

Martin-Closas, H. C. C., Permanyer, A. and Jesus-Villa, M., 2005. Palynofacies distribution in a lacustrine basin. *Geobios*, 38, 197-210.

Martínek, K., Blecha, M., Daněk, V., Franců, J., Hladíková, J., Johnová, R., & Uličný, D., 2006. Record of palaeoenvironmental changes in a Lower Permian organic-

rich lacustrine succession: Integrated sedimentological and geochemical study of the Rudník member, Krkonoše Piedmont Basin, Czech Republic. *Palaeogeography, Palaeoclimatology, Palaeoecology*, 230(1–2), 85–128.  
<https://doi.org/10.1016/j.palaeo.2005.07.009>

Matthews, M. D. and Perlmutter, M. A., 1994. Global cyclostratigraphy. In: Boer, P.L., Smith, D.G. (Eds.), *Orbital Forcing and Cyclic Sequences*, vol. 19. *Spec. Publ. Int. Ass. Sediment.*, pp. 459-481.

Mazzini, I., Hudáčková, N., Joniak, P., Kováčová, M. and Mikes, T., 2013. Palaeoenvironmental and chronological constraints on the Tuğlu Formation (Çankırı Basin, Central Anatolia, Turkey), 747-777.

Mcarthur, A. D., Kneller, B. C., Wake, M. I., Souza, P. A. and Kuchle, J., 2016. Palynofacies classification of the depositional elements of confined turbidite systems: Examples from the Gres d'Annot, SE France, 77.  
<https://doi.org/10.1016/j.marpetgeo.2016.08.020>

McCarthy, P. J., Martini, I. P. and Leckie, D. A., 1998. Use of micromorphology for paleoenvironmental interpretation of complex alluvial paleosols: an example from the Mill Creek Formation (Albian), southwestern Canada. *Palaeogeography, Palaeoclimatology, Palaeoecology* 143, 87-110.

McCauley, A. D., 2013. Sequence stratigraphy, depositional history, and hydrocarbon potential of the Mancos Shale, Uinta Basin, Utah. Thesis.

McGlue, M. M., Soreghan, M. J., Michel, E., Todd, J. A., Cohen, A. S., Mischler, J. and Nkotagu, H. H., 2010. Environmental controls on shell-rich facies in tropical lacustrine rifts: A view from Lake Tanganyika's littoral. *Palaios* 25 (7), 426-438.

Meling, S. V., 2016. Sedimentology and Sequence Stratigraphy of the Corinth Canal, Central Greece.

Meriç, E., ve Şengüler, İ., 1986. Göynük (Bolu, KB Anadolu) çevresinde Üst KretasePaleosen stratigrafisi üzerine yeni görüşler. *Jeoloji Müh.*, 29, 61-64.

- Miall, A. D. 1977. A review of the braided-rivers depositional environment. *Earth Science Review*, 13, 1-62.
- Miall, A. D. 1978. Lithofacies types and vertical profile models in braided-rivers deposits: a summary. In: Miall, A.D.(Ed.), *Fluvial Sedimentology*. Canadian Society of Petroleum Geologists Memoir, 5, 597–604. Calgary, Canadian Society of Petroleum Geologists.
- Miall, A. D. 2006. Reconstructing the architecture and sequence stratigraphy of the preserved fluvial record as a tool for reservoir development: A reality check. *The American Association of Petroleum Geologists Bulletin*, 90, 989-1002.
- Mingram, J., 1998. Laminated Eocene maar-lake sediments from Eckfeld (Eifel region, Germany) and their short-term periodicities. *Palaeogeography, Palaeoclimatology, Palaeoecology*, 140(1-4), 289-305.  
[https://doi.org/10.1016/S0031-0182\(98\)00021-2](https://doi.org/10.1016/S0031-0182(98)00021-2)
- Miles, J. A., 1994. *Illustrated glossary of petroleum geochemistry*. Oxford university press, Oxford.
- Miller, K. B. and West, R. R., 2012. Identification of Sequence Boundaries within Cyclic Strata of the Lower Permian of Kansas , USA : Problems and Alternatives Identification of Sequence Boundaries within Cyclic Strata of the Lower Permian of Kansas , USA : Problems and Alternatives 1. *Alternatives*, 106(2), 119–132.
- Miller, K. G., Fairbanks, R. G. and Mountain, G. S., 1987. Tertiary isotope synthesis, sea level history, and continental margin erosion. *Paleoceanography* 2 (1), 1-19.
- Mitchum, R. M., Vail, P. R. and Thomson, S., 1977. Seismic stratigraphy and global changes of sea-level, Part 2: The depositional sequences as a basic unit of for stratigraphic analysis. *Applications to Hydrocarbon Exploration*. AAPG Memoir, 26, 53-62.
- Montañez, I. P. and Osleger, D. A., 1993. Parasequence stacking patterns, third-order accommodation events, and sequence stratigraphy of Middle to Upper Cambrian

platform carbonates, Bonanza King Formation, southern Great Basin, in Loucks R.G., and Sarg, J.F., eds., Carbonate Sequence Stratigraphy: American Association of Petroleum Geologists, Memoir 57, p. 305–326.

Moore, C. R., 1961. Treatise on Invertebrate Paleontology, Arthropoda 3, Crustacea, Ostracoda, Geological Society of America, University of Kansas Press, 442p.

Murphy, D. H. and Wilkinson, B. H., 1980. Carbonate deposition and facies distribution in a central Michigan marl lake. *Sedimentology* 27, 123-135.

Nazik, A., Türkmen, İ., Koç, C., Aksoy, E., Avşar, N. and Yayık, H., 2008. Fresh and Brackish Water Ostracods of Upper Miocene Deposits , Arguvan / Malatya (Eastern Anatolia). *Turkish Journal of Earth Sciences*, 17, 481–495.

Neal, J. and Abreu, V., 2009. Sequence stratigraphy hierarchy and the accommodation succession method. *Geology*, 37(9), 779-782.  
<https://doi.org/10.1130/G25722A.1>

Nichols, G., 2009. *Sedimentology and stratigraphy* (2nd ed.). Chichester, UK; Hoboken, NJ: Wiley-Blackwell.

O'Brien, N. R., 1990. Significance of lamination in Toarcian (Lower Jurassic) shales from Yorkshire, Great Britain. *Sedimentary Geology*, 67(1-2), 25-34.  
[https://doi.org/10.1016/0037-0738\(90\)90025-O](https://doi.org/10.1016/0037-0738(90)90025-O)

O'Brien, N. R., 1996. Shale lamination and sedimentary processes. *Geological Society, London, Special Publications*, 116(1), 23-36.  
<https://doi.org/10.1144/gsl.sp.1996.116.01.04>

Ocakoğlu, F., 1997. Evolution of the Lutetian-aged depositional systems in Çankırı–Çorum Basin, Central Anatolia, Turkey. Hacettepe University, Institute of Natural Sciences. PhD Thesis, 158p.

Ocakoğlu, F., ve Çiner, A., 1995. Orhaniye-Güvenç (KB Ankara) karasal çökellerinin

Paleosen-E. Eosen Sedimanter evrimi, Türkiye Jeoloji Bülteni 38 (2), 53–66.

Ocakođlu, F., Yılmaz, Ö. İ., Demircan, H., Özkan-Altınır, S., Hakyemez, A., İslamođlu, Y., Önođlu, N., Tekin, U. K., Yıldız, A., Uchman, A., Szulc, A. and Açıkalın, S., 2007. Orta Sakarya bölgesi Geç Kretase-Paleojen çökellerinin sekans stratigrafisi. TUBITAK Proje No.: YDABÇAG 104Y153.

Ocakođlu, F., Açıkalın, S., Yılmaz, İ. Ö., Altınır, S. Ö., Hakyemez, A., Tekin, K., İslamođlu, Y., 2008. Overview of the Late Cretaceous to Late Eocene sequence stratigraphic framework of the Central Sakarya Region: Evidences for Distinct Imprints of Global Cycle. In: 26th IAS Regional Meeting/SEPM-CES SEDIMENT 2008, Abstract Book, p. 202.

Ocakođlu, F., Açıkalın, S., Yılmaz, İ. Ö., Şafak, Ü. ve Gökçeođlu, C., 2012. Evidence of orbital forcing in lake-level fluctuations in the Middle Eocene oil-shale-bearing lacustrine successions in the Mudurnu-Göynük Basin, NW Anatolia (Turkey). *Journal of Asian Earth Sciences*, 56, 54-71.  
<https://doi.org/10.1016/j.jseaes.2012.04.021>

Okay, A. İ., 2008. Geology of Turkey: A synopsis. *Anschnitt*, Vol. 21, pp. 19-42.

Okay, A.I. and Altınır, D., 2004, Uppermost Triassic limestone in the Karakaya Complex - stratigraphic and tectonic significance. *Turkish Journal of Earth Sciences*, 13, 187-199.

Okay, A. İ. and Tüysüz, O., 1999. Tethyan sutures of northern Turkey. In: Durand, B., Jolivet, L., Horváth, D., and Séranne, M. (eds) *The Mediterranean basins: Tertiary extension within the Alpine Orogen*: Geological Society of London, Special Publication, Vol. 156, pp. 475-515.

Okay, A. İ., Tüysüz, O. and Tansel, I., 2001. Obduction, subduction and collision as reflected in the Upper Cretaceous-Lower Eocene sedimentary record of western Turkey. *Geological Magazine UK*, Vol. 138, (2), pp. 117-142.

Okay, A. İ., Monod, O. and Monié, P., 2002. Triassic blueschists and eclogites from

- northwest Turkey: vestiges of the Paleo-Tethyan subduction. *Lithos*, Vol. 64, pp. 155-178.
- Okay, A. and Göncüoğlu, M. C., 2004. The Karakaya Complex: A Review of Data and Concepts. *Turkish Journal of Earth Sciences*. 13. 77-95.
- Okay, A. İ., Satir, M. and Siebel, W., 2006a. Pre-Alpide Palaeozoic and Mesozoic orogenic events in the Eastern Mediterranean region In: Gee, D. G. and Stephenson, R. A. (eds). *European Lithosphere Dynamics*. Geological Society of London, *Memoirs*, Vol. 32, pp. 389-405.
- Okay, A. İ., 2008. *Geology of Turkey: A synopsis*. *Anschnitt*, Vol. 21, pp. 19-42.
- Oskay, R. G., 2009. Palynofacies analyses of coal bearing sediments in the Çanakkale-Çan Basin (NW Turkey). Thesis, Dokuz Eylül University.
- Owen, A., Nichols, G. J., Hartley, A. J., Weissmann, G. S. and Scuderi, L. A., 2015. Quantification of a distributive fluvial system: the Salt Wash DFS of The Morrison, 544-561.
- Özkan, S., 1993a. Calcareous nannofossil and calpionellid biostratigraphy of the Upper Jurassic-Lower Cretaceous in Northwest Anatolia, Turkey. Ph.D. Thesis, University College London, pp. 336.
- Özkan, S., 1993b. Calcareous nannofossils from the Late Jurassic-Early Cretaceous of Northwest Anatolia, Turkey. *Geological Journal*, Vol. 28, pp. 295-307.
- Özkan-Altıner, S., 1996. Calcareous nannofossil biostratigraphy of Valanginian-Aptian in Northwest Anatolia, Turkey. *Revue de Paléobiologie*, Vol. 15, (2), pp. 479-498.
- Özkan-Altıner, S., 1999. Rock-forming Nannofossils in Uppermost Jurassic-Lower Cretaceous Rock Units of Northwest Anatolia: *Nannoconus* and Its Revised Taxonomy. *Turkish Journal of Earth Sciences*, Vol. 8, pp. 19-43.

- Özcan, Z., Okay, A.I., Özcan, E., Hakyemez, A. and Özkan-Altiner, S., 2012, Late Cretaceous - Eocene geological evolution of the Pontides in northwest Turkey between the Black Sea coast and Bursa. *Turkish Journal of Earth Sciences*, 21, 933-960.
- Özcan, E., Okay, A.I., Bürkan, K.A., Yücel, A.O., Özcan, Z., 2018, The Bartonian-Priabonian marine record of the Biga Peninsula, NW Anatolia (Turkey): larger benthic foraminifera, revised stratigraphy and implications for the regional geology. *Geologica Acta*, 16, 163-187.
- Pamukcu, S. and Tuncan, M., 1991. Influence of Some Physicochemical Activities on Mechanical Behavior of Clays. In *Microstructure of Fine-Grained Sediments*, 1st ed.; Chiou, W., Faas, R., Kasprovicz, J., Li, H., Lomenick, T. O'Brien, N., Pamukcu, S., Smart, P., Weaver, C., Yamamoto, T., Eds.; Springer: New York, NY, USA; pp. 241–253.
- Paredes, M., Irigoyen, M., Moscoso, P. and Giordano, S., 2015. A late Eocene-early Oligocene transgressive event in the Golfo San Jorge basin : Palynological results and stratigraphic implications *Journal of South American Earth Sciences* A late eocene-early Oligocene transgressive event in the Golfo San Jorge basin : *Journal of South American Earth Sciences*, 63(October), 293–309.  
<https://doi.org/10.1016/j.jsames.2015.08.009>
- Pasquier, J. B. and Strasser, A., 1997. Platform-to-basin correlation by high-resolution sequence stratigraphy and cyclostratigraphy (Berriasian, Switzerland and France). *Sedimentology* 44, 1071 – 1092.
- Paterson, D. M., 1997. Biological mediation of sediment erodibility: ecology and physical dynamics. In *Cohesive Sediments* (Burt, N., Parker, R. & Watts, J., eds), pp. 215–229. John Wiley and Sons, Chichester.
- Pattison, S. A. J., 2005. Isolated highstand shelf sandstone body of turbiditic origin, lower Kenilworth Member, Cretaceous Western Interior, Book Cliffs, Utah, USA. *Sedimentary Geology*, 177(1-2), 131–144.  
<https://doi.org/10.1016/j.sedgeo.2005.02.005>

- Pavelić, D., Miknić, M. and Sarkotić-Šlat, M., 1998. Early to Middle Miocene facies succession in lacustrine and marine environments on the southwestern margin of the Pannonian Basin System (Croatia). *Geologica Carpathica*. 49. 433-443.
- Pemberton, S. G., Frey, R. W., Ranger, M. J. and MacEachern, J. A., 1992: The conceptual framework of ichnology; in, *Applications of ichnology to petroleum exploration-A core workshop*, S. G. Pemberton, ed.: Society of Economic Paleontologists and Mineralogists, Core Workshop 17, p. 1-32.
- Peters, E. K. and Cassa, M. R., 1994. *Applied source rock geochemistry*. AAPG Memoir. 60, p. 93-120
- Peters, S. E., Antar, M. S. M., Zalmout, I. S., & Gingerich, P. D., 2009. Sequence Stratigraphic Control on Preservation of Late Eocene Whales and Other Vertebrates At Wadi Al-Hitan, Egypt. *Palaios*, 24(5), 290–302. <https://doi.org/10.2110/palo.2008.p08-080r>
- Petrizzo, M. R., 2000. Upper Turonian–lower Campanian planktonic foraminifera from southern mid–high latitudes (Exmouth Plateau, NW Australia): biostratigraphy and taxonomic notes. *Cretaceous Research*, 21, 479–505.
- Pettijohn, F. J., 1975. *Sedimentary Rocks*, 3rd Edition, Harper and Row, New York.
- Pettijohn, F. J., Potter, P. E. and Siever, R., 1987. *Sand and sandstone*. New York: Springer-Verlag.
- Pierce, H. G., 1993. The Nonmarine Mollusks of the Late Oligocene-Early Miocene Cabbage Patch Fauna of Western Montana III. *Aquatic Mollusks and Conclusions*, 67(6), 980-993.
- Pietras, J. T., Carroll, A. R., Singer, B. S. and Smith, M. E., 2003. 10 k.y. depositional cyclicity in the early Eocene: stratigraphic and  $^{40}\text{Ar}/^{39}\text{Ar}$  evidence from the lacustrine Green River Formation. *Geology* 31, 593-596.

- Pittet, B., and Gorin, G. E., 1997. Distribution of sedimentary organic matter in a carbonate-siliciclastic platform environment: Oxfordian of the Swiss Jura mountains: *Sedimentology* , v. 44, p. 915-937.
- Pittet, B., Strasser, A. and Mattioli, E., 2000. Depositional Sequences in Deep-Shelf Environments: A Response to Sea-Level Changes and Shallow-Platform Carbonate Productivity (Oxfordian, Germany and Spain). *Journal of Sedimentary Research*, 70(2), 392–407. Retrieved from
- Platt, N. H., 1989. Lacustrine carbonates and pedogenesis: sedimentology and origin of palustrine deposits from the Early Cretaceous Rupelo Formation, W Cameros Basin, N Spain. *Sedimentology*, 36(4), 665-684. <https://doi.org/10.1111/j.1365-3091.1989.tb02092.x>
- Platt, N. H. and Wright, V. P., 1991. Lacustrine carbonates: facies models, facies distributions and hydrocarbon aspects. In: Anado'n, P., Cabrera, Ll., Kelts, K. (Eds), *Lacustrine Facies Analysis*. International Association of Sedimentologists Special Publication 13, pp. 57-74.
- Posamentier, H. W. and Allen, G. P., 1999. Siliciclastic Sequence Stratigraphy- Concepts and Applications. In: *SEPM Concepts in Sedimentology and Paleontology*, vol. 7, p. 210.
- Posamentier, H. W., Jervey, M. T. and Vail, P. R., 1988. Eustatic controls on clastic deposition, I: conceptual framework. In: Wilgus, C.K., Hastings, B.S., Kendall, C.G.St.C., Posamentier, H.W., Ross, C.A., Van Wagoner, J.C. (Eds.), *Sea Level Changes: an Integrated Approach*. SEPM Special Publication, vol. 42, pp. 110-124
- Potter, P. E., Maynard, J. B. and Depetris, P. J., 2005. Mud and mudstones introduction and overview: New York, Springer Berlin Heidelberg, pp. 297.
- Pujalte, V., Robles, S., Robador, A., Baceta, J. I. and Orue-Etxebarria, X., 1993. Shelf to basin Paleocene paleogeography and depositional sequences, western Pyrenees, north, Spain. In: Posamentier, H.W., Summerhayes, C.P., Haq, B.U., Allen, G.P. (Eds.), *Sequence Stratigraphy and Facies Associations*, vol. 18. Spec.

Publs. Int. Ass. Sediment, pp. 369-395.

Raiswell, R., 1982. Pyrite texture, isotopic composition and the availability of iron. American Journal of Science. <https://doi.org/10.2475/ajs.282.8.1244>

Raiswell, R., Buckley, F. and Bern, R.A., 1988. Degree of pyritization of iron as a paleoenvironmental indicator of bottom-water oxygenation. SEPM Journal of Sedimentary Research. <https://doi.org/10.1306/212F8E72-2B24-11D7-8648000102C1865D>

Ramos, E., Cabrera, L., Hagemann, H. W., Pickel, W. and Zamarreño, I., 2001. Palaeogene lacustrine record in Mallorca (NW Mediterranean, Spain): depositional, palaeogeographic and palaeoclimatic implications for the ancient southeastern Iberian margin. Palaeogeography, Palaeoclimatology, Palaeoecology, 172(1-2), 1-37. [https://doi.org/10.1016/S0031-0182\(01\)00277-2](https://doi.org/10.1016/S0031-0182(01)00277-2)

Ranson, A. M., 2012. Transitional facies and sequence stratigraphic complexity of shallow-marine Star Point Formation to Coastal-Plain Blackhawk Formation along Depositional-Strike, Wasatch Plateau, Utah, 46.

Read, J. F. and Goldhammer, R. K., 1988. Use of Fischer plots to define third-order sea-level curves in Ordovician peritidal cyclic carbonates, Appalachians. Geology 16, 895-899.

Reading, H. G. and Levell, B. K., 1996. Controls on the sedimentary rock record. In: Sedimentary Environments: Processes, Facies and Stratigraphy (Ed. by H.G. Reading), Blackwell Science, Oxford, pp. 5-36.

Reckamp, J. U. and Özbey, S., 1960. Petroleum geology of Temelli and Kugtepe structures, Polatlı area: Pet. İis. Gen. Md., Ankara (Unpublished).

Rees, A. J., Thomas, A. T., Lewis, M., Hughes, H. E. and Turner, P., 2014. Chapter 2 Lithostratigraphy and palaeoenvironments of the Cambrian in SW Wales, (1871), 33-100.

- Reynolds, S. and Gorsline, D. S., 1991. Silt Microfabric of Detrital, Deep Sea Mud(stone)s (California Continental Borderland) as Shown by Backscattered Electron Microscopy. In *Microstructure of Fine-Grained Sediments: From Mud to Shale*, 1st ed.; Bennett, R.H., Bryant, W.R., Hulbert, M.H., Chiou, W.A., Faas, R.W., Kasprowicz, J., Li, H., Lomenick, T., O'Brien, N.R., Pamukcu, S., et al., Eds.; Springer: New York, NY, USA, pp. 203–211.
- Ricken, W., 1993. Variation of sedimentation rates in rhythmically bedded sediments—distinction between depositional types. In: Einsele, G., Ricken, W., Seilacher, A. (Eds.), *Cycles and Events in Stratigraphy*. Springer-Verlag, Berlin, pp. 167–187
- Rigo da Righi, M. and Cortesini, A., 1959. Regional studies central Anatolian basin, progress report 1. Turkish Gulf Oil Company: Pet. iş. Gen. Md., Ankara (Unpublished).
- Rimkus, A., 2016. A high-resolution depositional model of the tidally-influenced Middle Jurassic Curtis Formation, Humbug Flats, Utah, USA. Master Thesis, Department of Geosciences, University of Oslo, Norway.
- Rimmer, S. M., Thompson, J. A., Goodnight, S. A. and Robl, T. L., 2004. Multiple controls on the preservation of organic matter in Devonian-Mississippian marine black shales: geochemical and petrographic evidence. *Palaeogeogr. Palaeoclimatol. Palaeoecol.* 215, 125-154.
- Riveline, J., 1983. Proposition d'une échelle zonale de Charophytes pour le Tertiaire (Danien a Burdigalien) de l'Europe occidentale. *C. R. Ac. Sc.*, Paris, 296, 1077-1080.
- Riveline, J., 1986. Les Charophytes du Paléogène et du Miocène Inférieur d'Europe Occidentale, *Cahiers de Paléontologie*. Centre National de la Recherche Scientifique, Paris.
- Riveline, J., Berger, J. P., Bilan, W., Feist, M., Martín-Closas, C., Schudack, M.E. and Soulié-Märsche, I., 1996. European Mesozoic-Cenozoic Charophyte Biozonation. *Bulletin de la Société Géologique de France*, 167, 453-468.

- Roberts, J., Jepsen, R., Gotthard, D. and Lick, W., 1998. Effects of particle size and bulk density on erosion of quartz particles. *J. Hydraul. Eng.*, 124(12), 1261–1267
- Robertson, A. H. F., Clift, P. D., Degnan, P. J. and Jones, G., 1991. Palaeogeographic and palaeotectonic evolution of the Eastern Mediterranean Neotethys. *Palaeogeography, Palaeoclimatology, Palaeoecology*, 87, 289–343.
- Rojay, B. and Altiner, D., 1998. Middle Jurassic-Lower Cretaceous biostratigraphy in central Pontides (Turkey): remarks on the paleogeography and tectonic evolution. *Rivista Italiana di Paleontologia e Stratigrafia*, Vol. 104, (2), pp. 167-180.
- Roy, S., 1992. Environments and processes of manganese deposition. *Economic Geology*, 87(5), 1218-1236. <https://doi.org/10.2113/gsecongeo.87.5.1218>
- Sageman, B. B., Murphy, A. E., Werne, J. P., Ver Straeten, C. A., Hollander, D. J. and Lyons, T. W., 2003. A tale of shales: the relative roles of production, decomposition, and dilution in the accumulation of organic-rich strata, Middle Upper Devonian, Appalachian basin: *Chemical Geology*, v. 195, p. 229-273
- Sadler, P. M., Osleger, D. A., and Montañez, P., 1993. On the labeling, length, and objective basis of Fischer plots. *Journal of Sedimentary Research* 63, 360-368.
- Sandberg, P. A., 1964. The Ostracod Genus *Cyprideis* in the Americas. *Acta Universitatis Stockholmiensis: Stockholm Contributions in Geology* 12, 178 pp.
- Saner, S., 1977. Geyve-Osmaneli-Gölpazarı-Taraklı Alanının Jeolojisi; Eski Çökeltme Ortamları ve Çökeltmenin Evrimi. *MTA Enst. Derleme No: 6306*, 312s.
- Saner, S. 1978a. Geology and the environments of deposition of Geyve-Osmaneli-Gölpazarı-Taraklı area. *Istanbul Üniversitesi Fen Fakültesi Mecmuası, Seri B* 43, 63–91.

- Saner, S. 1978b. Depositional relations during the Upper Cretaceous–Palaeocene–Eocene in the central Sakarya and their importance for petroleum exploration. Proceedings, Fourth Petroleum Congress of Turkey, pp. 95–114. Ankara.
- Saner, S., 1980a. Batı Pontitler'in kom'ü havzaların oluşumlarının levha tektoniği kuramıyla açıklaması, Mineral Research and Exploration Institute (MTA) of Turkey Publications, No. 93/94, pp. 1-20.
- Saner, S., 1980b. The paleogeographical interpretation of the Mudurnu-Göynük basin based on the depositional features of the Jurassic and later ages: Türkiye Jeoloji Kurultayı Bülteni, Vol. 23, pp. 39-52.
- Sanjuan, J. and Martín-Closas, C., 2012. Charophyte palaeoecology in the Upper Eocene of the Eastern Ebro basin (Catalonia, Spain). Biostratigraphic implications. Palaeogeography, Palaeoclimatology, Palaeoecology, 365-366, 247-262. <https://doi.org/10.1016/j.palaeo.2012.09.031>
- Sanjuan, J. and Martín-Closas, C., 2014. Taxonomy and palaeobiogeography of charophytes from the Upper Eocene-Lower Oligocene of the Eastern Ebro Basin (Catalonia, NE Spain). Geodiversitas, 36(3), 385-420. <https://doi.org/10.5252/g2014n3a3>
- Sanjuan, J. and Martín-closas, C., 2015. Biogeographic history of two Eurasian Cenozoic charophyte lineages. Aquatic Botany, 120, 18–30. <https://doi.org/10.1016/j.aquabot.2014.05.018>
- Sarg, J. F., 1988. Carbonate sequence stratigraphy. In: Sea-level Changes: An integrated approach. Wilgus, C. K., Hastings, B. S. et al. (eds.), The Society of Economic Paleontologist and Mineralogist, Special Publication, 42, 155-181.
- Sarı, A., 1999. Himmetoğlu formasyonu (Göynük-Bolu) bitümlü şeyllerinin organik jeokimyasal incelenmesi. 1. Batı Anadolu Hammadde Kaynakları Sempozyumu, s. 143-149, İzmir
- Sarı, A., and Aliyev, S. A., 2005. Source rock evaluation of the Lacustrine Oil-shale

bearing deposits, Göynük/Bolu, Turkey. *Energy Sources* 27:271–279.

Sarı, A. and Aliyev, S. A., 2006. Organic geochemical characteristics of the Paleocene-Eocene oil-shales in the Nallıhan Region, Ankara, Turkey. *Journal of Petroleum Science and Engineering*, 53(1–2), 123–134.  
<https://doi.org/10.1016/j.petrol.2006.04.001>

Sarı, A. and Geze, Y., 2008. Organic geochemical valuations of bituminous rock and coals in Miocene Himmetoğlu Basin (Bolu, Turkey). *Petroleum Science and Technology*, Vol. 26, (6), pp. 649-664.

Sarı, A. and Sonel, N., 2000. Organic geochemical characteristics and economic usability of lacustrine bituminous shales. *Geosound* 37:55–73 (in Turkish).

Sarı, A., Üzmez, B., and Aliyev, S. A., 2004a. Hydrocarbon potential of the bituminous shales around Mengen (Bolu). *Eng. Faculty's Earth Sciences Review* 37:10–20 (in Turkish).

Sarı, A., Koca, D., and Aliyev, A. S., 2004b. Organic geochemical investigation of oil rocks from Çakirköy (Gökçesu-Bolu) area. *Journal of the Engineering and Architecture Faculty of Selcuk University* 19:69–79 (in Turkish).

Sarı, A., Aliyev, S. A. and Koralay, D. B., 2007. Source rock evaluation of the eocene shales in the gökçesu area (Bolu/Turkey). *Energy Sources, Part A: Recovery, Utilization and Environmental Effects*, 29(11), 1025–1039.  
<https://doi.org/10.1080/00908310500434002>

Sarı, A., Vosoughi Moradi, A. and Akkaya, P., 2015. Evaluation of source rock potential, matrix effect and applicability of gas oil ratio potential factor in Paleocene-Eocene bituminous shales of Çamalan Formation, Nallıhan e Turkey. *Mar. Pet. Geol.* 67, 180-186.

Saxby, J. D., 1970. Isolation of kerogen in sediments by chemical methods. *Chemical Geology*, 6(C), 173–184. [https://doi.org/10.1016/0009-2541\(70\)90017-3](https://doi.org/10.1016/0009-2541(70)90017-3)

- Scherer, C. M. S., Goldberg, K. and Bardola, T., 2015. Facies architecture and sequence stratigraphy of an early post-rift fluvial succession, Aptian Barbalha Formation, Araripe Basin, northeastern Brazil. *Sedimentary Geology*, 322, 43–62. <https://doi.org/10.1016/j.sedgeo.2015.03.010>
- Schieber, J., Southard, J. B. and Thaisen, K., 2007. Accretion of mudstone beds from migrating floccule ripples: *Science*, v. 318, p. 1760-1763
- Schieber, J., 2013. SEM Observations on Ion-milled Samples of Devonian Black Shales from Indiana and New York: the Petrographic Context of Multiple Pore Types.
- Schmidt, G., C., 1960. AR/MEM/365-266-367 sahalarının nihai terk raporu. Pet. İş. Gen. Md., Ankara.
- Scholle, P. A., Bebout, D. G. and Moore, C. H., 1983. Carbonate Depositional Environments. AAPG Memoir, 33.
- Schwarz, E. and Howell, J., 2005. Sedimentary evolution and depositional architecture of a lowstand sequence set: The Lower Cretaceous Mulichinco Formation, Neuquén. *Sedimentary evolution and depositional architecture of a lowstand sequence set: the Lower Cretaceous Mulichinco Formation, Neuquén*, (January). <https://doi.org/10.1144/GSL.SP.2005.252.01.06>
- Schwarzacher, W., 1993. Cyclostratigraphy and the Milankovitch theory: Elsevier London.
- Schwarzacher, W., 2000. Repetitions and cycles in stratigraphy. *Earth-Science Reviews* 50, 51-75.
- Scouten, C., 1990. Part IV: Oil-shale. Chapters 25–31. In: Speight, J.G. (Ed.), *Fuel Science and Technology Handbook*. Marcel Dekker Inc., New York.

- Shivanna, M. and Singh, H., 2016. Depositional environment and hydrocarbon potential of marginal marine sediments of Eocene from western India: A palynofacies perspective. *Marine and Petroleum Geology*, 73(March), 311-321. <https://doi.org/10.1016/j.marpetgeo.2016.03.021>
- Shrivastava, J. P. and Ahmad, M., 2004. Compositional studies on organic matter from iridium enriched Anjar intertrappean sediments: Deccan volcanism and palaeoenvironmental implications during the Cretaceous / Tertiary boundary, 31, 167–177.
- Siddiqui, U. A., El-Ghali, M. A., Bin Abd Rahman, A. H., Mijinyawa, A. and Ben-Awuah, J., 2013. Depositional Environment of Shallow-Marine Sandstones from Outcrop Gamma-Ray Logs, Belait Formation, Meragang Beach, Brunei Darussalam. *Research Journal of Environmental and Earth Sciences*. 5. 305-324.
- Sim, L. L., Chambers, J.M. and Davis, J.A., 2006. Ecological regime shifts in salinised wetland systems. I. Salinity thresholds for the loss of submerged macrophytes. *Hydrobiologia* 573, 89-107
- Sloan, L. C. and Morrill, C., 1998. Orbital forcing and Eocene continental temperatures. *Palaeogeogr., Palaeoclimatol., Palaeoecol.* 144, 21-35
- Smith, A. J., Horne, D. J. and Schön, I., 2015. Class Ostracoda. *Ecology and General Biology: Thorp and Covich's Freshwater Invertebrates (Fourth Edi)*. Elsevier. <https://doi.org/10.1016/B978-0-12-385026-3.00030-9>
- Singh, A., Shivanna, M., Mathews, R. P., Singh, B. D., Singh, H., Singh, V. P. and Dutta, S., 2017. Palaeoenvironment of Eocene lignite bearing succession from Bikaner-Nagaur Basin, western India: Organic petrography, palynology, palynofacies and geochemistry. *International Journal of Coal Geology*, 181, 87-102. <https://doi.org/10.1016/j.coal.2017.08.009>
- Smoot, J. P., 1983. Depositional sub-environments in an arid closed basin; Wilkins Peak Member of the Green River Formation (Eocene), Wyoming, U.S.A. *Sedimentology* 30, 801–827.

- Snedden, J. W. and Bergman, K. M., 1999. Isolated shallow marine sand bodies: deposits for all interpretations. In: Bergman KM, Snedden JW, editors. Isolated shallow marine sand bodies: sequence stratigraphic analysis and sedimentological interpretation. Soc. Sed. Geol. Spec. Publ., vol. 64, p.1-11.
- Sonel, N., Kayabalı, K., Sarı, A. ve Ethem Tozlu., 1987a. Ahmetbeyler-Göynük-Bolu civarının jeolojisi ve yapısal özellikleri. S. Ü. Müh-Mim Fak. Derg., 2, 37-50.
- Sonel, N., Sarı, A. and Tozlu, E., 1987b. Geological investigation of the lignitic formation at Himmetoglu Area/Göynük-Bolu. J. Fac. Eng. Arch. Selcuk Univ. 2:51-67 (in Turkish).
- Soulié-Märsche, I., 1998. Fossil *Lamprothamnium papulosum* (Charophyta), a biomarker for seasonal rainfall in northern Mauritania. *Palaeoecology of Africa and the surrounding Islands* 25, 65-76.
- Soulié-Märsche, I., 2008. Charophytes, indicators for low salinity phases in North African sebkhet. *Journal of African Earth Sciences*, 51(2), 69-76. <https://doi.org/10.1016/j.jafrearsci.2007.12.002>
- Soulié-Märsche, I., Benammi, M. and Gemayel, P., 2002. Biogeography of living and fossil *Nitellopsis* (Charophyta) in relationship to new finds from Morocco. *J. Biogeogr.* 29, 1703-1711.
- Sönmez-Gökçen, N., 1973. Etude paléontologique (ostracodes) et stratigraphique de niveaux du Paléogène du Sud-Est de la Thrace, Maden Tetkik Arama Enstitüsü Yayınlarından, no. 147, pp. 1-118, XII pl.
- Staplin, F. L., 1969. Sedimentary organic matter, organic metamorphism and oil and gas occurrence. *Bull. Can. Pet. Geol.* 17, 47-66
- Stepinsky, V., 1940. Geological investigation of the Beypazari-Nallihan-Bolu-Gerede regions. MTA Report No: 1363 (in Turkish).

- Stow, D. A. V., 2005. *Sedimentary rocks in the field: A colour guide*: Manson Publishing.
- Strasser, A., Hilgen, F.J., and Heckel, P.H., 2006. Cyclostratigraphy-Concepts, definitions and applications: *Newsletters in Stratigraphy*, v. 42, p. 75–114, <https://doi.org/10.1127/0078-0421/2006/0042-0075>
- Strasser, A., Pittet, B., Hillgärtner, H. and Pasquier, J. B., 1999. Depositional sequences in shallow carbonate-dominated sedimentary systems: concepts for a high-resolution analysis. *Sedimentary Geology* 128, 201-221.
- Strasser, A., Aurell, M., Bádenas, B., Meléndez, G. and Tomás, S., 2005. From platform to basin to swell: orbital control on sedimentary sequences in the Oxfordian, Spain. *Terra Nova* 12, 407-413.
- Suarez-gonzalez, P., Quijada, I. E. and Benito, M. I., 2015. Sedimentology of ancient Coastal Wetlands: Insights from A Cretaceous, 95–117.
- Suárez-Ruiz, I., Flores, D., Mendonça Filho, J. G., Hackley, P. C., Filho, J. G. M. and Hackley, P. C., 2012. Review and update of the applications of organic petrology: Part 1, geological applications. *International Journal of Coal Geology*, 99, 54–112. <https://doi.org/10.1016/j.coal.2012.03.005>
- Sun, P., Liu, Z., Gratzner, R., Xu, Y., Liu, R., Li, B., Meng, Q. and Xu, J., 2013. Oil yield and bulk geochemical parameters of oil-shales from the Songliao and Huadian Basins, China: A grade classification approach. *Oil-shale*. 30 (3). 402-418. <https://doi.org/10.3176/oil.2013.3.03>
- Sun, J. M., Xu, Q. H., Liu, W. M., Zhang, Z. Q., Xue, L. and Zhao, P., 2014a. Palynological evidence for the latest Oligocene-early Miocene paleoelevation estimate in the Lunpola Basin, central Tibet. *Palaeogeogr. Palaeoclimatol. Palaeoecol.* 399, 21–30.
- Sunardi, E., 2015. The Lithofacies Association of Brown Shales In Kiliran Jao Subbasin, West Sumatra Indonesia. *Indonesian Journal on Geoscience*, 2(2), 77-

90. <https://doi.org/10.17014/ijog.2.2.77-90>

Suter, J. R. and Clifton, H. E., 1999. The Shannon Sandstone and isolated linear sand bodies: interpretations and realizations. In: Bergman KM, Snedden JW, editors. Isolated shallow marine sand bodies: sequence stratigraphic analysis and sedimentological interpretation. Soc. Sed. Geol. Spec. Publ., vol. 6, p. 321-56.

Szary, W. A., 2014. Introduction to Global Plate Tectonics: Plate Tectonics Theory; Paleogeography; And, the Ocean Basins. Createspace Independent Pub.

Sümengen, M., Terlemez, İ., Bilgiç, T., Gürbüz, M., Ünay, E., Ozaner, S. ve Tüfekçi, K., 1987. Şarkışla-Gemerek dolaylı Tersiyer havzasının stratigrafisi, sedimantolojisi ve jeomorfolojisi. MTA Genel Müdürlüğü Derleme No: 8118, 232 s.

Şafak, Ü., 2018. Distribution of Eocene-Oligocene Ostracods in Turkey. *Stratigraphy and Geological Correlation*, 26(7), 798–823.  
<https://doi.org/10.1134/S0869593818070043>

Şeker, H. and Kesgin, Y., 1991. Geology and petroleum possibilities of around Nallıhan Mudurnu-Senen- Beypazarı regions. TPAO report no: 2907.

Şafak, Ü. and Güldürek, M., 2016. The ostracoda assemblage of the Eocene–Oligocene transition in northwestern Thrace, Kırklareli–Edirne area (northwestern Turkey), *J. Afr. Earth Sci.*, 2016, vol. 117, pp. 62–85.

Şafak, Ü., Kapucuoglu, U., and Heybeli-Donat, D., 2009. BesniKahta (Adıyaman) Civarında Yer Alan Tersiyer istifinin ostrakod faunası ve Ortamsal Yorumu, *Çukurova Üniversitesi Mühendislik Mimarlık Fakültesi Dergisi*, 24 (1-2), pp. 193-208.

Şafak, Ü., Ocakoğlu, F. and Açıkalın, S., 2015. Ostracoda assemblage and the environmental characteristics of the Eocene succession of the Central Sakarya Region. *Micropaleontology*, 61(1-2), pp. 49-68.

- Şafak, Ü. and Güldürek, M., 2016. The ostracoda assemblage of the Eocene-Oligocene transition in northwestern Thrace, Kırklareli-Edirne area (northwestern Turkey), *J. Afr. Earth Sci.*, 117, pp. 62-85.
- Şenalp, M. and Gökçen, L. S., 1978. Sedimentological Studies of the Oil-Saturated Sandstones of the Haymana Region. Geological Society of Turkey, Vol. 21, pp. 87-94 (in Turkish).
- Şener, M. and Gündoğdu, M. N., 1996. Geochemical and petrographical investigation of Himmetoğlu oil-shale field, Göynük, Turkey. *Fuel*, Vol.75, no. 11, pp. 1313-1322, Elsevier.
- Şener, M. ve Şengüler, İ., 1992. Hatıldağ (Bolu-Göynük) bitümlü şeyl sahasının jeolojisi ve teknolojik kullanım olanakları. MTA Rapor No: 9445, 56 s., Ankara.
- Şener, M. and Şengüler, İ., 1998. Geological, mineralogical and geochemical characteristics of oil-shale bearing deposits in the Hatıldağ oil-shale field, Göynük, Turkey. *Fuel*, 77(8), 871–880.
- Şener, M., Sengüler, I. and Kök, M. V., 1995. Geological considerations for the economic evaluation of oil-shale deposits in Turkey. *Fuel* 74:999–1003.
- Şener, M., Şengüler, I., Taka, M. and Şener, M. F., 2013. The Stratigraphic, Mineralogical, and Geochemical Characterization of the Beypazarı Oil-shales, Central Anatolia, Turkey. *Energy Sources, Part A: Recovery, Utilization, and Envir., Effects*, 35(18), 1741–1752.  
<https://doi.org/10.1080/15567036.2010.531502>
- Şengör, A. M. C., 1987. Tectonics of the Tethysides: orogenic collage development in a collisional setting. *Annual Reviews of Earth and Planetary Sciences* 15, 213-244.
- Şengör, A. M. C. and Yılmaz, Y., 1981. Tethyan evolution of Turkey: a plate tectonic approach. *Tectonophysics*, Vol. 75, pp. 181-241.

- Şengör, A. M. C. and Yılmaz, Y., 1983. Evolution of Neo-Tethyan in Turkey. Turkish Geol. Soc. Special Pub., 1: 75.
- Şengör, A. M. C., Yılmaz, Y. and Sungurlu, O., 1984. Tectonics of the Mediterranean Cimmerides: nature and evolution of the western termination of Paleo-Tethys. In: Dixon, J. E., and Robertson, A. H. F., (eds). The geological evolution of the Eastern Mediterranean. Geological Society of London, Special Publication, Vol.17, pp. 77-112.
- Şengüler, İ., 1999. Investigation of Economically Utilization Possibilities of the Seyitömer (Kütahya, Western Turkey) Area Oil-shales, Ph.D. thesis, Ankara University, Graduate School of Natural and Applied Sciences Department of Geology, Ankara, Turkey, (in Turkish).
- Şengüler, İ., 2001. Türkiye bitümlü şeyllerinin GAP bölgesinde toprak güçlendirici olarak kullanılma imkanlarının araştırılması ve geliştirilmesi. MTA Genel Müdürlüğü Enerji Hammadde Etüt ve Arama Daire Başkanlığı, 21 s., Ankara
- Taka, M. ve Şener, M., 1988. Himmetoğlu (Göynük-Bolu) sahasının bitümlü şeylleri ve sondajları. MTA Rap. No:8533, Ankara.
- Tanner, L. H. and Lacus, S. G., 2006. Calcareous paleosols of the Upper Triassic Chinle Group, Four Corners region, southwestern United States: Climatic implications. Geological Society of America, Special paper 416, pp. 53-74.
- Taylor, G. H., Teichmüller, M., Davis, A., Diessel, C. F. K., Littke, R. and Robert, P., 1998. Organic Petrology. Borntraeger, Berlin, Stuttgart.
- Tänavsuu-Milkeviciene, K. and Frederick Sarg, J., 2012. Evolution of an organic-rich lake basin - stratigraphy, climate and tectonics: Piceance creek basin, eocene green river formation. Sedimentology, 59(6), 1735-1768. <https://doi.org/10.1111/j.1365-3091.2012.01324.x>

- Tänavsuu-Milkeviciene, K., Sarg, J. F. and Bartov, Y., 2017. Depositional cycles and sequences in an organic-rich lake basin : Eocene Green Abstract : Early to middle Eocene Green River Formation lacustrine deposits in the eastern portion of Lake Uinta formed in two subbasins , the Piceance basin and the Uinta bas. *Journal of Sedimentary Research*, 87, 210–229.
- Tekeli, O., 1981. Subduction complex of pre-Jurassic age, northern Anatolia, Turkey. *Geology*, Vol. 9, pp. 68-72.
- Timur, E. ve Aksay, A., 2002. 1/100 000 Ölçekli Türkiye Jeoloji Haritaları No: 39, Adapazarı-H26 Paftası [1/100 000 Scale Geological Maps of Turkey No: 39, Adapazarı-H26 Sheet]. Mineral Research and Exploration Institute (MTA) of Turkey Publications.
- Tingwei, L., Jiang, Z., Chenlu, X. and Liu, G., 2017. Effect of sedimentary environment on shale lithofacies in the lower third member of the Shahejie formation , Zhanhua Sag , eastern China Technical papers t Effect of sedimentary environment on shale lithofacies in the lower third member of the Shahejie Fo, (October). <https://doi.org/10.1190/INT-2017-0016.1>
- Tissot, B. P. and Welte, D. H., 1984. Petroleum formation and occurrence. 2nd ed., 538 p., Heidelberg: Springer Verlag, New York.
- Toker, V., 1975. Haymana yöresinin (SW Ankara) planktonik foraminifera ve nannoplanktonlarla biyostratigrafik incelenmesi. PhD. Thesis, Ankara Üniversitesi Fen Fakültesi, pp. 1-57.
- Topuz, G., Altherr, R., Kalt, A., Satır, M., Werner, O. and Schwarz, W.H., 2004. Aluminous granulites from the Pulur complex, NE Turkey: a case of partial melting, efficient melt extraction and crystallization. *Lithos* 72:183-207
- Topuz, G., Okay, A., Altherr, R., Meyer, H.-P. and Nasdala, L., 2006. Partial high-pressure aragonitization of micritic limestones in an accretionary complex, Tavşanlı Zone, NW Turkey. *Journal of Metamorphic Geology*. 24. 603-613.
- Topuz, G., Altherr, R., Schwartz, W. H., Dokuz, A. and Meyer, H. P., 2007. Variscan

amphibolites-facies rocks from the Kurtođlu metamorphic complex (Gümüřhane area, Eastern Pontides, Turkey). *International Journal of Earth Sciences*, Vol. 96, pp. 861-873.

Tosal, A., Sanjuan, J., Cartanyà, J. and Martín-closas, C., 2018. Taphonomy and palaeoecology of the uppermost Eocene flora from Sarral (Eastern Ebro Basin): Palaeoclimatic implications. *Palaeogeography, Palaeoclimatology, Palaeoecology*, 497, 66-81. <https://doi.org/10.1016/j.palaeo.2018.02.006>

Tribovillard, N., Algeo, T.J., Lyons, T. and Riboulleau, A., 2006. Trace metals as paleoredox and paleoproductivity proxies: an update. *Chem. Geol.* 232, 12-32.

Tucker, M. E. and Wright, V.P., 1990. *Carbonate Sedimentology*. Blackwell Scientific Publications, Oxford, 482. <http://dx.doi.org/10.1002/9781444314175>

Tunođlu, C., 2001. Eocene (Lutetian–Bartonian) ostracoda of the Sinop Basin, Black Sea Coast of Turkey, Proc. 2nd Int. Symp. on Petrol. Geol. Hydrocarbon Potential of the Black Sea Area, September 22–24, 1996, řile–İstanbul–Turkey, Turkish Ass. Petrol. Geol. Spec. Publ., no. 4, pp. 149–163.

Tunođlu, C., Tuncer, A., Özgen, N., and Kangal, Ö., 2013. Oligocene ostracoda from the Sivas Basin (Central Anatolia, Turkey), Proc. 17th Int. Ostracoda Symp., *IL Naturalista Siciliano*, vol. XXXVII, no. 1, pp. 411–412

Türkünal, S., 1957. Çamdađ oolitic demir cevherlerinin dođu ve batı istikametinde devamı : MTA Rep. 2626, Ankara-Turkey.

Tüysüz, O. and Yiđitbař, E., 1994. The Karakaya Basin: a Palaeo-Tethyan marginal basin and its age of opening. *Acta Geologica Hungarica*, Vol. 37, (3-4), pp. 327-350.

Tyson, R. V., 1995. *Sedimentary Organic Matter; Organic Facies and Palynofacies*. Chapman & Hall, London, p. 615

- Ünalın, G., Yüksel, V., Tekeli, T., Göneaç, O., Seyirt, Z. and Hüseyin, S., 1976. Stratigraphy and paleogeographical evolution of Upper Cretaceous- lower Tertiary sediments in the Haymana-Polatlı region (SW Ankara): Geological Society of Turkey Bulletin, v. 19, p; 159-176.
- Ünalın, G. ve Yüksel, V., 1985. Haymana-Polatlı havzasının jeolojisi ve petrol olanakları. Mineral Research and Exploration Institute (MTA) of Turkey, Petrol ve Jeotermal Enerji Dairesi Raporu.
- Vaasma, T., 2008. Grain-size analysis of lacustrine sediments: A comparison of pre-treatment methods. *Estonian Journal of Ecology*, 57(4), 231–243. <https://doi.org/10.3176/eco.2008.4.01>
- Vail, P. R., Mitchum, R. M. and Thompson, S., 1977. Seismic stratigraphy and global changes of sea-level, Part 4: Global cycles of relative changes of the sea-level, in payton, C. E., eds., seismic stratigraphy. Application to Hydrocarbon Exploration. AAPG Memoir, 26, 83-97.
- Vail, P. R., Hardenbol, J. and Todd, R. G., 1984. Jurassic unconformities, chronostratigraphy and sea-level changes from seismic stratigraphy. In: Interregional Unconformities and Hydrocarbon Exploration (ed. By J. S Schlee). Memoir of the AAPG, Tulsa, 33, 129-144.
- Vail, P. R., Mitchum, R. M., Todd, R. G., et al., 1977. Seismic stratigraphy and global changes in sea level. In: Payton, C.E. (Ed.), *Seismic Stratigraphy - Applications to Hydrocarbon Exploration*, vol. 26. Mem. Am. Assoc. Petrol. Geol., pp. 49-212
- Vakarelov, B. K., Ainsworth, R. B. and MacEachern, J. A., 2012. Recognition of wave-dominated, tide-influenced shoreline systems in the rock record: Variations from a microtidal shoreline model. *Sedimentary Geology*, 279, 23-41. <https://doi.org/10.1016/j.sedgeo.2011.03.004>
- Van der Meer, J. J. M. and Menzies, J., 2011. The micromorphology of unconsolidated sediments. *Sedimentary Geology*, 238(3-4), 213-232. <https://doi.org/10.1016/j.sedgeo.2011.04.013>

- Van Morkhoven, P. F. C. M., 1963. Post Paleozoic Ostracoda, Their Morphology, Taxonomy and Economic Use, Volume II Generic Description, Elsevier Publishing Company, 478 p.
- Van Wagoner, J. C., Posamentier, H.W., Mitchum, R.M., Vail, P.R., Sarg, J.F., Loutit, T.S. and Hardenbol, J., 1988. An overview of the fundamentals of sequence stratigraphy and key definitions. In, C.K. Wilgus et al. (eds.), Sea-level changes - An integrated approach, SEPM Spec. Publ., 42, 39-45.
- Van Wagoner, J. C., Mitchum, R. M., Jr., Campion, K. M. and Rahmanian, V. D., 1990. Siliciclastic sequence stratigraphy in well logs, core and outcrops: concepts for high-resolution correlation of time and facies. Am. Assoc. Pet. Geol., Methods Explor. Ser. 7, 55 pp.
- Val, J., Bádenas, B., Aurell, M. and Rosales, I., 2017. Cyclostratigraphy and chemostratigraphy of a bioclastic storm-dominated carbonate ramp (late Pliensbachian, Iberian Basin). *Sedimentary Geology*, 355, 93–113. <https://doi.org/10.1016/j.sedgeo.2017.04.007>
- Varol, B. and Kazano, N., 1981. The litho- and biofacies properties of the Upper Jurassic-Lower Cretaceous carbonate sequence. *Bull. Geol. Soc. Turkey*, 24: 31-38.
- Wagreich, M. and Krenmayr, H. G., 2005. Upper Cretaceous oceanic red beds (CORB) in the Northern Calcareous Alps (Nierental Formation, Austria): slope topography and clastic input as primary controlling factors. *Cretaceous Research*, Vol. 26, pp. 57-64.
- Wagreich, M., Neuhuber, S., Egger, J., Wendler, I., Scott, R. W., Malata, E. and Sanders, D., 2009. Cretaceous oceanic red beds (CORBs) in the Austrian Eastern Alps: passive-margin vs. active-margin depositional settings. In: Hu, X.M., Wang, C.S., Scott, R.W., Wagreich, M., Jansa, L. (Eds.), SEPM Special Publication, Tulsa, Oklahoma, No. 91, pp. 37-91.

- Walker R. G. and Plint A. G., 1992. Wave and storm-dominated shallow marine systems. In: *Facies Models: Response to Sea-level Change* (Ed. by R.C. Walker and N.P. James), pp. 219-238. Ceol. Ass. Can., Waterloo, Ontario.
- Wanas, H. A., Sallam, E., Zobaa, M. K. and Li, X., 2015. Mid-Eocene alluvial-lacustrine succession at Gebel El-Goza El-Hamra (Shabrawet area, NE Eastern Desert, Egypt): Facies analysis, sequence stratigraphy and paleoclimatic implications. *Sedimentary Geology*, 329, 115–129. <https://doi.org/10.1016/j.sedgeo.2015.09.006>
- Wang, G., 2012. Laminae combination and genetic classification of Eocene shale in Jiyang depression. *Journal of Jilin University (Earth Science Edition)* 42 (3).
- Wang, P. and Li, Q., 2009. The South China Sea - Paleooceanography and Sedimentology. *Developments in Paleoenvironmental Research*, Springer, vol. (13), 75-278. <https://doi.org/10.1007/978-1-4020-9745-4>
- Wang, L., Zou, C., Zheng, P., Chen, Zhang, S.Q., Xu, B. and Li, H., 2009. Geochemical evidence of shale gas existed in the lower Paleozoic Sichuan Basin. *Nat. Gas. Ind.* 29 (5), 59-62, (in Chinese with English abstract).
- Wang, L., Wang, C., Li, Y., Zhu, L. and Wei, Y., 2011. Sedimentary and organic geochemical investigation of tertiary lacustrine oil-shale in the central Tibetan plateau: Palaeolimnological and palaeoclimatic significances. *International Journal of Coal Geology*, 86(2–3), 254–265. <https://doi.org/10.1016/j.coal.2011.02.011>
- Wang, P., Huang, Y., Wang, C., Feng, Z. and Huang, Q., 2013. Pyrite morphology in the first member of the Late Cretaceous Qingshankou Formation, Songliao Basin, Northeast China. *Palaeogeography, Palaeoclimatology, Palaeoecology*, 385, 125-136. <https://doi.org/10.1016/j.palaeo.2012.09.027>
- Wang, P. X., Li, Q. and Li, C. F., 2014. *Geology of the China Seas*. In *Developments in Marine Geology*, Vol. 6. Amsterdam, Netherlands: Elsevier.

- Wartes, M. A., Carroll, A. R., Greene, T.J ., Cheng, K. and Ting, H., 2000. Permian lacustrine deposits of Northwest China. In: Lake Basins Through Space and Time (Eds E.H. Gierlowski-Kordesch and K.R. Kelts), AAPG Stud. Geol., 46, 123–132.
- Wei, W., Lu, Y., Xing, F., Liu, Z., Pan, L. and Algeo, T. J., 2017. Sedimentary facies associations and sequence stratigraphy of source and reservoir rocks of the lacustrine Eocene Niubao Formation (Lunpola Basin, central Tibet). *Marine and Petroleum Geology*, 86, 1273–1290.  
<https://doi.org/10.1016/j.marpetgeo.2017.07.032>
- Weimer, P. and Posamentier, H. W., (Eds.), 1993. Siliciclastic sequence stratigraphy: Recent developments and applications. AAPG, Memoir 58, Tulsa, Oklahoma.
- Wignall, P. B. and Newton, R., 1998. Pyrite framboid diameter as a measure of oxygen deficiency in ancient mudrocks. *American Journal of Science*.  
<https://doi.org/10.2475/ajs.298.7.537>
- Wignall, P. B., Newton, R. and Brookfield, M. E., 2005. Pyrite framboid evidence for oxygen-poor deposition during the Permian-Triassic crisis in Kashmir. *Palaeogeography, Palaeoclimatology, Palaeoecology*.  
<https://doi.org/10.1016/j.palaeo.2004.10.009>
- Wilkin, R., Arthur, M. and Dean, W., 1997. History of water-column anoxia in the Black Sea indicated by pyrite framboid size distributions. *Earth and Planetary Science Letters*. [https://doi.org/10.1016/S0012-821X\(97\)00053-8](https://doi.org/10.1016/S0012-821X(97)00053-8)
- Wilkin, R. T., Barnes, H. L. and Brantley, S. L., 1996. The size distribution of framboidal pyrite in modern sediments: An indicator of redox conditions. *Geochimica et Cosmochimica Acta*.  
[https://doi.org/10.1016/00167037\(96\)00209-8](https://doi.org/10.1016/00167037(96)00209-8)
- Wilkin, R. T. and Barnes, H. L., 1997. Formation processes of framboidal pyrite. *Geochimica et Cosmochimica Acta*.  
[https://doi.org/10.1016/S00167037\(96\)00320-1](https://doi.org/10.1016/S00167037(96)00320-1)

- Wilkins, A. D., 2003. Terminology and the classification of fine grained sedimentary rocks-is there a difference between a claystone, a mudstone and a shale?, (1950), 1-12.
- Willmann, R., 1985. Responses of the plio-pleistocene freshwater gastropods of Kos (Greece, Aegean sea) to environmental changes. *Lecture Notes in Earth Sciences*, 1, 295–321.
- Witt, W., 2011. Mixed ostracod faunas, co-occurrence of marine Oligocene and nonmarine Miocene taxa at Pinarhisar, Thrace, Turkey. *Zitteliana* 51, 237–254
- Wu, H., Zhang, S., Hinnov, L. A., Jiang, G., Feng, Q., Li, H. and Yang, T., 2013. Time-calibrated Milankovitch cycles for the late Permian. *Nature communications*, 4, 2452. <https://doi.org/10.1038/ncomms3452>
- Xiafei, Z. and Zhonghua, T., 2000. Lacustrine Deposits of the Upper Permian Pingdiquan Formation in the Kelameili Area of the Junggar Basin , Xinjiang , China.
- Xu, J. J., Bechtel, A., Sachsenhofer, R. F., Liu, Z., Gratzer, R., Meng, Q. and Song, Y., 2015. High resolution geochemical analysis of organic matter accumulation in the Qingshankou Formation, Upper Cretaceous, Songliao Basin (NE China). *Int. J. Coal Geol.* 141-142, 23-32.
- Yanılmaz, E., Taka, M., Şengüler, İ. ve Sümer, A., 1980. Göynük (Bolu) bitümlü şist sahası hakkında rapor. MTA Rapor No: 6993. 25 s. Ankara
- Yang, W., Feng, Q., Liu, Y., Tabor, N., Miggins, D., Crowley, J. L., ... Thomas, S., 2010. Depositional environments and cyclo- and chronostratigraphy of uppermost Carboniferous-Lower Triassic -lacustrine deposits, southern Bogda Mountains, NW China - A terrestrialluvial paleoclimatic record of mid-latitude NE Pangea. *Global and Planetary Change*, 73(1-2), 15-113. <https://doi.org/10.1016/j.gloplacha.2010.03.008>

- Yang, P., Xie, Y., Li, X., Bai, D., Liu, Z. and Chen, H., 2012. Hydrocarbon-generating potential of the source rocks of the Sinian Doushantuo formation on the western side of Xuefeng mountain. *Geol. China* 39 (5), 1299-1309, (in Chinese with English abstract).
- Yang, T., Cao, Y., Wang, Y. and Zhang, S.. 2015. Types, sedimentary characteristics and genetic mechanisms of deep-water gravity flows: A case study of the middle submember in Member 3 of Shahejie Formation in Jiyang depression. *Acta Pet. Sin.*, 36, 1048–1059.
- Yang, Y., Qiu, L., Wan, M., Jia, X., Cao, Y. and Lei, D., 2018. Depositional model for a salinized lacustrine basin: The Permian Lucaogou Formation, Jimsar Sag, Junggar Basin, NW China. *Journal of Asian Earth Sciences*. <https://doi.org/10.1016/j.jseaes.2018.08.021>
- Ye, L., Yu, G., Liao, M., Hu, S., Wang, L. and Gao, L., 2017. Terrestrial-marine sedimentary cycles in the South Yellow Sea , China: implications for paleoenvironmental reconstruction since MIS 5, 1, 170–188. <https://doi.org/10.3906/yer-1608-18>
- Yen T. F. and Chilingarian, G. V., 1976. Oil-shale. Elsevier Scientific Publishing Company, 291 p., New York.
- Yeşiladalı-Bulkan, Ö., Yalçın, M. N. ve Mann, U., 2005. Himmetoğlu havzasındaki (Göynük-Bolu) kömür-bitümlü şeyl birlikteliğinin paleo-ortam koşulları. *İstanbul Üniv. Müh. Fak. Yerbilimleri Dergisi*, 18 (1), 81-97
- Yiğitbaş, E. and Elmas, A., 1997. Batı Pontidlerin Geç Mesozoyik - Tersiyer evrimine yaklaşım: Cide - Devrek virgasyonu'nun gelişimi.. *Geosound/Yerbilimleri Dergisi*. 23. 23-36.
- Yılmaz, O., 1971. Etude petrographique et geochronologique de la region Cacas. These, Univ. Grenoble.
- Yılmaz, İ. Ö., 2008. Cretaceous Pelagic Red Beds and Black Shales (Aptian-

Santonian), NW Turkey: Global Oceanic Anoxic and Oxidic Events. Turkish Journal of Earth Sciences, Vol. 17, pp. 263-296.

Yılmaz, İ. Ö., Altner, D., Tekin, U. K., Tüysüz, O., Ocakoğlu, F. and Acikalin, S., 2010. Cenomanian-Turonian Oceanic Anoxic Event (OAE2) in the Sakarya Zone, Northwestern Turkey: Sedimentological, cyclostratigraphic, and geochemical records. Cretaceous Research, Vol. 31, pp. 207-226.

Yılmaz, İ. Ö., Ocakoğlu, F. and Wagreich, M., 2012. The Santonian-Campanian oceanic anoxic deposits in the Mudurnu-Göynük and Haymana basins, NW Turkey: a possible paleoceanographic link. 34th International Geological Congress, Brisbane, Australia.

Yılmaz, S., Boztu, D. and Öztürk, A., 1993. Geological setting, petrographic and geochemical characteristics of the Cretaceous and Tertiary igneous rocks in the Hekimhan- Hasançelebi area, northwest Malatya, Turkey. Geological Journal, 28, 383-398.

Yılmaz, Y., 1977. Bilecik-Söğüt Dolayındaki Eski Temel Karmaşığı'nın Petrojenetik Evrimi [Petrogenetic Evolution of the Old Basement Complex in the Bilecik-Söğüt Area]. Habilitation Thesis, İstanbul University [in Turkish with English abstract, unpublished].

Yılmaz, Y., 1981. Sakarya kıtasının güney kenarının tektonik evrimi: İstanbul Üniversitesi, Yerbilimleri, Vol. 1, pp. 33-52 (in Turkish).

Yılmaz, Y., Genç, S.C., Yiğitbaş, E., Bozcu, M. and Yılmaz, K., 1995. Geological evolution of the late Mesozoic continental margin, Northwestern Anatolia. Tectonophysics 243, 155-171.

Yılmaz, Y., Tüysüz, O., Yiğitbaş, E., Genç, Ş. C. and Şengör, A. M. C., 1997. Geology and tectonic evolution of the Pontides. In: Robinson, A. G. (ed.) Regional and Petroleum Geology of the Black Sea and Surrounding Region. American Association of Petroleum Geologists Memoir, 68, 183-226.

- Yılmaz, Y., Tüysüz, O., Ustaomer, T., Robertson, A. H. F., Varentsov, I. M., Muzyliov, N. G., ... Cannon, W. F., 2016. Petrographic and petrophysical characterization of the Eagle Ford Shale in La Salle and Gonzales counties, Gulf Coast region, Texas. *Sedimentary Geology*, 34(4), 126pp. <https://doi.org/10.1016/j.palaeo.2013.12.004>
- Yi-yong, Z., Xiu, L., Heng-ren, Y. and Jian-guo, L., 2003. Tertiary Biostratigraphy of China; *Biostratigraphy of China*, 525-576.
- Young, M. J., Gawthorpe, R. L. and Ian, R., 2008. Sedimentology and sequence stratigraphy of a transfer zone coarse-grain. *Sedimentology*, 47(6), 1081–1104.
- Yu, W., Algeo, T. J., Du, Y., Maynard, B., Guo, H. and Zhou, Q., 2016. Genesis of Cryogenian Datangpo manganese deposit : Hydrothermal influence and episodic post-glacial ventilation of Nanhua Basin , *South China Palaeogeography , Palaeoclimatology , Palaeoecology* Genesis of Cryogenian Datangpo manganese deposit : Hydrotherm. *Palaeogeography, Palaeoclimatology, Palaeoecology*, 459(June), 321–337. <https://doi.org/10.1016/j.palaeo.2016.05.023>
- Zachos, J., Pagani, M., Sloan, L., Thomas, E. and Billups, K., 2001. Trends, rhythms, and aberrations in global climate 65 Ma to present. *Science* 292, 686-693.
- Zachos, J. C., Dickens, G. R. and Zeebe, R. E., 2008. An early Cenozoic perspective on greenhouse warming and carbon-cycle dynamics. *Nature* 451, 279-283
- Zeller, M., Reid, S. B., Eberli, G. P., Weger, R. J. and Massaferro, J. L., 2015. Sequence architecture and heterogeneities of a field - Scale Vaca Muerta analog (Neuquén Basin, Argentina) - From outcrop to synthetic seismic. *Marine and Petroleum Geology*, 66, 829-847. <https://doi.org/10.1016/j.marpetgeo.2015.07.021>
- Zeng, H., Ambrose, W. A. and Edgar, V., 2001. Seismic sedimentology and regional depositional systems in Mioceno Norte, Lake Maracaibo, Venezuela. *The Leading Edge*. 20. 1260-1269. <https://doi.org/10.1190/1.1487259>

- Zeng, X., Cai, J., Dong, Z., Bian, L. and Li, Y., 2018. Relationship between Mineral and Organic Matter in Shales: The Case of Shahejie Formation, Dongying Sag, China, 1-21. <https://doi.org/10.3390/min8060222>
- Zeng, S., Wang, J., Fu, X., Chen, W., Feng, X., Wang, D., Song, C. and Wang, Z., 2015, Geochemical characteristics, redox conditions, and organic matter accumulation of marine oil-shale from the Changliang Mountain area, northern Tibet, China: *Marine and Petroleum Geology*, v. 64, p. 203-221.
- Zhang, X., Li, Y., Lü, H., Yan, J., Tuo, J. and Zhang, T., 2013. Relationship between organic matter characteristics and depositional environment in the Silurian Longmaxi Formation in Sichuan Basin. *Journal of China Coal Society*. 38, 851-856.
- Zhou, C. and Jiang, S. Y., 2009. Palaeoceanographic redox environments for the lower Cambrian Hetang Formation in South China: Evidence from pyrite framboids, redox sensitive trace elements, and sponge biota occurrence. *Palaeogeography, Palaeoclimatology, Palaeoecology*. <https://doi.org/10.1016/j.palaeo.2008.10.024>
- Zhu, G., Jin, Q., Zhang, S., Dai, J., Wang, G., Zhang, L. and Li, J., 2005. Characteristics and origin of deep lake oil-shale of the Shahejie Formation of Paleogene in Dongying Sag, Jiyang Depression: *Journal of Palaeogeography*, 7, 59–69
- Zou, C. N., 2010. *Unconventional petroleum geology*. Elsevier, Amsterdam, Netherlands.
- Munsell rock color chart, Geological society of America, 2009

## APPENDICES

### APPENDIX A. Geochemical Data of the Studied Sections

Appendices A 1: Geochemical data of the Dağhacılar measured section.

Sample No.	Lithofacies	Total Weight (g)	Water Loss after 100 °C	Dry Weight (g)	Weight After HCl (g)	CaCO <sub>3</sub> (g)	Weight After H <sub>2</sub> O <sub>2</sub> (g)	Organic Matter (g)	Residues (g)	Obtained weight % of organic matter and minerals		
										Carbonate	Organic Matter	Residues
D01	Lime mudstone	10	0.15	9.85	2.62	7.23	1.30	1.33	1.30	73.38	13.47	13.15
D03	Lime Mudstone	10	0.11	9.89	1.45	8.43	1.01	0.44	1.01	85.33	4.49	10.18
D04	Wackestone	10	0.22	9.78	1.37	8.41	0.79	0.58	0.79	85.99	5.98	8.03
D06	Wackestone	10	0.14	9.86	3.10	6.76	1.75	1.35	1.75	68.52	13.73	17.74
D08	Packstone	10	0.21	9.79	2.09	7.71	1.34	0.75	1.34	78.70	7.64	13.66
D10	Oil-shale	10	0.14	9.86	3.51	6.35	2.44	1.07	2.44	64.40	10.81	24.79
D11	Packstone	10	0.24	9.76	3.75	6.01	2.55	1.20	2.55	61.55	12.35	26.11
D13	Packstone	10	0.23	9.77	1.85	7.92	1.33	0.51	1.33	81.08	5.27	13.64
D14	Wackestone	10	0.26	9.74	3.09	6.65	1.69	1.39	1.69	68.30	14.31	17.38
D17	Wackestone	10	0.16	9.84	1.08	8.76	0.24	0.83	0.24	89.03	8.49	2.48
D19	Packstone	10	0.16	9.84	1.93	7.91	1.05	0.88	1.05	80.38	9.00	10.63
D20	Marl	10	0.32	9.68	7.13	2.55	5.54	1.59	5.54	26.37	16.42	57.21
D21	Marl	10	0.20	9.80	5.38	4.42	4.06	1.32	4.06	45.10	13.45	41.45
D24	Marl	10	0.66	9.34	3.86	5.48	3.27	0.58	3.27	58.70	6.23	35.07
D25	Marl	10	0.32	9.68	3.49	6.19	2.65	0.84	2.65	63.95	8.63	27.42
D27	Wackestone	10	0.21	9.79	1.65	8.14	1.09	0.56	1.09	83.12	5.71	11.17
D28	Oil-shale	10	0.24	9.76	6.03	3.73	4.51	1.52	4.51	38.23	15.55	46.22
D29	Lime Mudstone	10	0.16	9.84	2.84	7.00	2.06	0.78	2.06	71.15	7.93	20.92
D30	Wackestone	10	0.27	9.73	3.72	6.01	2.23	1.49	2.23	61.80	15.28	22.92
D31	Lime Mudstone	10	0.24	9.76	4.45	5.31	3.82	0.63	3.82	54.37	6.47	39.16
D34	Marl	10	0.25	9.75	6.81	2.94	5.79	1.03	5.79	30.15	10.54	59.31
D35	Oil-shale	10	0.20	9.80	4.85	4.95	2.99	1.86	2.99	50.52	18.99	30.50
D36	Oil-shale	10	0.17	9.83	4.86	4.97	3.66	1.20	3.66	50.54	12.20	37.26
D37	Oil-shale	10	0.24	9.76	5.03	4.73	3.20	1.83	3.20	48.46	18.74	32.81
D38	Oil-shale	10	0.20	9.80	4.31	5.49	3.26	1.05	3.26	56.00	10.74	33.26
D40	Oil-shale	10	0.29	9.71	4.31	5.40	2.96	1.35	2.96	55.61	13.88	30.51
D41	Oil-shale	10	0.18	9.82	5.21	4.61	3.81	1.40	3.81	46.97	14.26	38.78
D43	Marl	10	0.30	9.70	5.11	4.58	4.39	0.73	4.39	47.25	7.50	45.25
D45	Marl	10	0.29	9.71	6.37	3.34	5.41	0.97	5.41	34.37	9.96	55.67
D50	Oil-shale	10	0.24	9.76	4.59	5.17	3.63	0.96	3.63	52.95	9.81	37.24
D51	Oil-shale	10	0.19	9.81	4.37	5.44	4.04	0.32	4.04	55.48	3.30	41.21
D52	Oil-shale	10	0.02	9.98	3.42	6.56	2.66	0.76	2.66	65.72	7.63	26.66
D54	Oil-shale	10	0.15	9.85	7.06	2.78	5.90	1.16	5.90	28.26	11.79	59.94
D55	Oil-shale	10	0.18	9.82	7.39	2.43	6.33	1.06	6.33	24.78	10.75	64.47
D58	Oil-shale	10	0.23	9.77	3.02	6.75	1.80	1.22	1.80	69.09	12.50	18.42
D59	Oil-shale	10	0.34	9.66	3.11	6.55	2.16	0.95	2.16	67.78	9.83	22.38
D62	Oil-shale	10	0.30	9.70	2.15	7.55	1.24	0.91	1.24	77.86	9.40	12.74
D66	Marl	10	0.26	9.74	7.13	2.62	6.33	0.80	6.33	26.86	8.20	64.95
D69	Oil-shale	10	0.19	9.81	5.34	4.47	3.88	1.46	3.88	45.55	14.85	39.59
D71	Oil-shale	10	0.06	9.94	7.21	2.74	6.18	1.03	6.18	27.52	10.35	62.13
D72	Oil-shale	10	0.29	9.71	4.20	5.51	3.16	1.04	3.16	56.74	10.69	32.57
D73	Marl	10	0.21	9.79	7.63	2.17	7.05	0.58	7.05	22.11	5.91	71.98

Appendices A 2: Organic matter and minerals component weight percent data of geochemical analysis and petrographic data of selected samples from the Dağhacılar section.

Sample No.	Lithofacies	Obtained weight % of organic matter and minerals				Source Potential	Porosity	Brittle mineral content (brittle mineral content > 40%)
		Carbonate	Organic Matter	Clay	Quartz/Feldspar			
D01	Lime mudstone	73.38	13.47	13.15	0.00			
D03	Lime Mudstone	85.33	4.49	9.18	1.00			
D04	Wackestone	85.99	5.98	8.03	0.00			
D06	Wackestone	68.52	13.73	15.74	2.00			
D08	Packstone	78.70	7.64	13.66	0.00			
D10	Oil-shale	64.40	10.81	12.38	0.00			
D11	Packstone	61.55	12.35	25.11	1.00			
D13	Packstone	81.08	5.27	13.64	0.00			
D14	Wackestone	68.30	14.31	17.38	0.00			
D17	Wackestone	89.03	8.49	2.48	0.00			
D19	Packstone	80.38	9.00	10.63	0.00			
D20	Marl	26.37	16.42	68.45	0.00			
D21	Marl	45.10	13.45	33.19	2.84			
D24	Marl	58.70	6.23	35.40	2.00			
D25	Marl	63.95	8.63	22.83	5.60			
D27	Wackestone	83.12	5.71	11.17	0.00			
D28	Oil-shale	38.23	15.55	47.60	7.13			
D29	Lime Mudstone	71.15	7.93	17.42	3.50			
D30	Wackestone	61.80	15.28	22.92	0.00			
D31	Lime Mudstone	54.37	6.47	39.16	0.00			
D34	Marl	30.15	10.54	66.30	0.00			
D35	Oil-shale	50.52	18.99	0.76	22.72			
D36	Oil-shale	50.54	12.20	0.00	37.25			
D37	Oil-shale	48.46	18.74	40.37	0.00			
D38	Oil-shale	56.00	10.74	4.11	25.23			
D40	Oil-shale	55.61	13.88	0.59	34.83			
D41	Oil-shale	46.97	14.26	22.43	21.49			
D43	Marl	47.25	7.50	44.50	4.42			
D45	Marl	34.37	9.96	38.01	18.83			
D50	Oil-shale	52.95	9.81	41.29	0.00			
D51	Oil-shale	55.48	3.30	42.62	0.00			
D52	Oil-shale	65.72	7.63	23.45	5.41			
D54	Oil-shale	28.26	11.79	60.00	7.96			
D55	Oil-shale	24.78	10.75	67.23	5.00			
D58	Oil-shale	69.09	12.50	21.05	0.00			
D59	Oil-shale	67.78	9.83	12.62	12.20			
D62	Oil-shale	77.86	9.40	14.06	0.00			
D66	Marl	26.86	8.20	10.60	60.10			
D69	Oil-shale	45.55	14.85	16.96	26.20			
D71	Oil-shale	27.52	10.35	15.74	53.57			
D72	Oil-shale	56.74	10.69	11.20	25.27			
D73	Marl	22.11	5.91	16.17	53.99			
	Average	56.42	10.55	24.04	10.47			
	Min	16.00	3.30	0.00	0.00			
	Max	89.03	18.99	68.45	60.10			

Appendices A 3: Geochemical data of the Hasanlar measured section.

Sample No.	Lithofacies	Total Weight (g)	Water Loss after 100 °C	Dry Weight (g)	Weight After HCl (g)	CaCO <sub>3</sub> (g)	Weight After H <sub>2</sub> O <sub>2</sub> (g)	Organic Matter (g)	Residues (g)	Obtained weight % of organic matter and minerals		
										Carbonate	Organic Matter	Residues
H0A	Wackestone	10	0.29	9.71	9.00	0.71	7.62	1.38	7.62	7.31	14.26	78.43
H0B	Oil-shale	10	0.43	9.57	2.25	7.32	1.75	0.51	1.75	76.45	5.31	18.24
H03	Oil-shale	10	1.00	9.00	2.65	6.35	1.85	0.80	1.85	70.56	8.89	20.56
H07	Lime Mudstone	10	0.11	9.89	5.51	4.38	4.75	0.77	4.75	44.27	7.74	47.99
H08	Oil-shale	10	0.14	9.86	4.29	5.57	2.83	1.46	2.83	56.50	14.82	28.68
H12	Wackestone	10	0.08	9.92	2.05	7.87	1.27	0.78	1.27	79.32	7.85	12.83
H13	Oil-shale	10	0.36	9.64	5.74	3.90	4.45	1.30	4.45	40.43	13.43	46.13
H14	Oil-shale	10	0.12	9.88	3.59	6.29	2.03	1.56	2.03	63.68	15.79	20.53
H15	Oil-shale	10	0.45	9.55	7.79	1.76	6.54	1.25	6.54	18.43	13.05	68.52
H18	Oil-shale	10	0.47	9.53	5.34	4.19	3.78	1.56	3.78	43.99	16.39	39.62
H20	Oil-shale	10	0.12	9.88	4.27	5.60	2.77	1.51	2.77	56.74	15.25	28.01
H21	Lime Mudstone	10	0.18	9.82	3.47	6.35	2.32	1.14	2.32	64.70	11.66	23.64

Appendices A 4: Organic matter and minerals component weight percent data of geochemical analysis and petrographic data of selected samples from the Hasanlar section.

Sample No.	Lithofacies	Obtained weight % of organic matter and minerals				Source Potential	Porosity	Brittle mineral content (brittle mineral content > 40%)
		Carbonate	Organic Matter	Clay	Quartz/Feldspar			
H0A	Wackestone	7.31	14.26	75.43	3.00			
H0B	Oil-shale	76.45	5.31	13.75	5.51			
H03	Oil-shale	70.56	8.89	4.95	6.87			
H07	Lime mudstone	44.27	7.74	47.99	0.00			
H08	Oil-shale	56.50	14.82	33.67	0.00			
H12	Wackestone	79.32	7.85	12.83	0.00			
H13	Oil-shale	40.43	13.43	30.31	19.37			
H14	Oil-shale	63.68	15.79	22.54	0.00			
H15	Oil-shale	18.43	13.05	51.87	25.57			
H18	Oil-shale	43.99	16.39	47.39	0.00			
H20	Oil-shale	56.74	15.25	11.17	7.27			
H21	Lime mudstone	64.70	11.66	21.64	2.00			
	Average	51.86	12.04	31.13	5.80			
	Min	7.31	5.31	4.95	0.00			
	Max	79.32	16.39	75.43	25.57			

Appendices A 5: Geochemical data of the Kösüre measured section.

Sample No.	Lithofacies	Total Weight (g)	Water Loss after 100 °C	Dry Weight (g)	Weight After HCl (g)	CaCO <sub>3</sub> (g)	Weight After H <sub>2</sub> O <sub>2</sub> (g)	Organic Matter (g)	Residues (g)	Obtained weight % of organic matter and minerals		
										Carbonate	Organic Matter	Residues
K01	Marl	10	0.31	9.69	5.47	4.22	3.97	1.50	3.97	43.53	15.49	40.98
K02	Marl	10	0.31	9.69	5.39	4.30	4.54	0.86	4.54	44.38	8.83	46.79
K05	Marl	10	0.21	9.79	4.28	5.51	3.37	0.91	3.37	56.30	9.29	34.41
K07	Wackestone	10	0.12	9.88	0.72	9.15	0.31	0.42	0.31	92.66	4.23	3.10
K09	Wackestone	10	0.07	9.93	1.48	8.46	0.34	1.14	0.34	85.13	11.46	3.41
K11	Packstone	10	0.06	9.94	1.53	8.40	0.70	0.84	0.70	84.57	8.42	7.01
K12	Packstone	10	0.12	9.88	0.95	8.94	0.46	0.49	0.46	90.44	4.94	4.63
K13	Oil-shale	10	0.81	9.19	6.26	2.93	6.23	0.03	6.23	31.86	0.35	67.80
K15	Marl	10	0.44	9.56	5.07	4.48	3.44	1.63	3.44	46.91	17.10	35.99
K19	Oil-shale	10	0.20	9.80	6.00	3.80	4.51	1.49	4.51	38.78	15.20	46.02
K20	Marl	10	0.22	9.78	3.47	6.31	1.99	1.48	1.99	64.48	15.18	20.34
K21	Wackestone	10	0.16	9.84	1.71	8.12	1.00	0.72	1.00	82.61	7.27	10.12
K22	Marl	10	0.42	9.58	6.41	3.17	5.70	0.71	5.70	33.11	7.37	59.51
K24	Oil-shale	10	0.50	9.50	6.81	2.70	5.91	0.89	5.91	28.40	9.41	62.18
K26	Marl	10	0.54	9.46	5.42	4.04	4.77	0.66	4.77	42.71	6.94	50.35
K28	Marl	10	0.17	9.83	3.86	5.97	2.88	0.97	2.88	60.78	9.88	29.34
K30	Wackestone	10	0.10	9.90	1.48	8.42	0.78	0.70	0.78	85.07	7.03	7.90
K31	Marl	10	0.15	9.85	4.53	5.32	3.99	0.54	3.99	53.96	5.49	40.55
K33	Wackestone	10	0.15	9.85	1.35	8.50	0.53	0.82	0.53	86.28	8.30	5.43
K34	Wackestone	10	0.15	9.85	3.02	6.83	2.78	0.24	2.78	69.35	2.43	28.22
K35	Wackestone	10	0.19	9.81	1.31	8.50	0.99	0.32	0.99	86.68	3.25	10.07
K38	Wackestone	10	0.12	9.88	5.71	4.17	4.71	1.01	4.71	42.18	10.17	47.65
K40	Oil-shale	10	0.53	9.47	4.97	4.50	4.87	0.10	4.87	47.55	1.02	51.44
K45	Oil-shale	10	0.39	9.61	7.07	2.54	5.47	1.60	5.47	26.45	16.63	56.92
K46	Oil-shale	10	0.38	9.62	7.91	1.70	6.09	1.83	6.09	17.72	18.99	63.29

Appendices A 6: Organic matter and minerals component weight percent data of geochemical analysis and petrographic data of selected samples from the Kösüre section.

Sample No.	Lithofacies	Obtained weight % of organic matter and minerals				Source Potential	Porosity	Brittle mineral content (brittle mineral content > 40%)
		Carbonate	Organic Matter	Clay	Quartz/Feldspar			
K01	Marl	43.53	15.49	40.61	6.62			
K02	Marl	44.38	8.83	37.91	11.71			
K05	Marl	56.30	9.29	33.52	4.41			
K07	Wackestone	92.66	4.23	3.10	0.00			
K09	Wackestone	85.13	11.46	3.41	0.00			
K11	Packstone	84.57	8.42	7.01	0.00			
K12	Packstone	90.44	4.94	4.63	0.00			
K13	Oil-shale	31.86	0.35	46.78	20.92			
K15	Marl	46.91	17.10	24.73	18.69			
K19	Oil-shale	38.78	15.20	39.10	14.61			
K20	Marl	64.48	15.18	21.88	1.19			
K21	Wackestone	82.61	7.27	10.12	0.00			
K22	Marl	33.11	7.37	63.86	0.00			
K24	Oil-shale	28.40	9.41	66.20	1.37			
K26	Marl	42.71	6.94	54.11	0.00			
K28	Marl	60.78	9.88	31.80	0.00			
K30	Wackestone	85.07	7.03	7.90	0.00			
K31	Marl	53.96	5.49	42.90	0.00			
K33	Wackestone	86.28	8.30	5.43	0.00			
K34	Wackestone	69.35	2.43	28.22	0.00			
K35	Wackestone	86.68	3.25	10.07	0.00			
K38	Wackestone	42.18	10.17	47.65	0.00			
K40	Oil-shale	47.55	1.02	43.28	7.64			
K45	Oil-shale	26.45	16.63	63.37	2.67			
K46	Oil-shale	17.72	18.99	75.66	2.47			
	Average	53.93	8.29	39.72	1.18			
	Min	17.72	0.35	3.10	0.00			
	Max	92.66	18.99	75.66	20.92			

Appendices A 7: Geochemical data of the Karahisar measured section.

Sample No.	Lithofacies	Total Weight (g)	Water Loss after 100 °C	Dry Weight (g)	Weight After HCl (g)	CaCO <sub>3</sub> (g)	Weight After H <sub>2</sub> O <sub>2</sub> (g)	Organic Matter (g)	Residues (g)	Obtained weight % of organic matter and minerals		
										Carbonate	Organic Matter	Residues
T01	Oil-shale	10	1.14	8.86	2.94	5.92	2.23	0.71	2.23	66.84	8.02	25.15
T03	Oil-shale	10	0.19	9.81	3.48	6.33	2.13	1.36	2.13	64.52	13.81	21.66
T04	Oil-shale	10	0.31	9.69	4.71	4.98	2.94	1.77	2.94	51.42	18.25	30.32
T05	Oil-shale	10	0.72	9.28	4.01	5.26	2.86	1.15	2.86	56.74	12.41	30.85
T06	Oil-shale	10	0.24	9.76	3.48	6.27	2.76	0.73	2.76	64.29	7.45	28.26
T08	Lime Mudstone	10	0.19	9.81	4.29	5.51	3.50	0.79	3.50	56.22	8.06	35.72
T09	Oil-shale	10	0.33	9.67	4.34	5.34	3.85	0.49	3.85	55.17	5.03	39.80
T10	Oil-shale	10	0.68	9.32	4.43	4.89	3.51	0.92	3.51	52.46	9.88	37.66
T12	Lime Mudstone	10	0.21	9.79	6.83	2.96	5.60	1.23	5.60	30.24	12.57	57.19
T13	Lime Mudstone	10	0.25	9.75	7.12	2.64	5.37	1.75	5.37	27.03	17.94	55.03
T14	Oil-shale	10	0.34	9.66	5.96	3.70	4.03	1.93	4.03	38.31	19.93	41.76
T16	Lime Mudstone	10	0.09	9.91	7.46	2.45	5.99	1.47	5.99	24.71	14.83	60.47
T17	Oil-shale	10	0.23	9.77	4.88	4.88	3.86	1.02	3.86	49.98	10.47	39.54
T18	Oil-shale	10	0.37	9.63	4.99	4.64	3.59	1.40	3.59	48.19	14.55	37.26
T20	Oil-shale	10	0.21	9.79	4.99	4.79	3.12	1.88	3.12	48.99	19.16	31.85
T21	Lime Mudstone	10	0.08	9.92	5.04	4.88	3.45	1.59	3.45	49.20	16.06	34.74
T22	Oil-shale	10	0.32	9.68	4.86	4.82	3.85	1.00	3.85	49.82	10.38	39.80
T24	Oil-shale	10	0.29	9.71	5.43	4.29	4.20	1.22	4.20	44.12	12.60	43.28
T26	Lime Mudstone	10	0.37	9.63	6.84	2.79	6.11	0.73	6.11	28.98	7.56	63.46
T28	Lime Mudstone	10	0.28	9.72	4.43	5.29	3.40	1.03	3.40	54.43	10.63	34.93
T29	Oil-shale	10	0.25	9.75	5.53	4.23	4.36	1.16	4.36	43.36	11.92	44.72

Appendices A 8: Organic matter and minerals component weight percent data of geochemical analysis and petrographic data of selected samples from the Karahisar section.

Sample No.	Lithofacies	Obtained weight % of organic matter and minerals				Source Potential	Porosity	Brittle mineral content (brittle mineral content > 40%)
		Carbonate	Organic Matter	Clay	Quartz/Feldspar			
T01	Oil-shale	66.84	8.02	8.94	18.40			
T03	Oil-shale	64.52	13.81	21.66	0.00			
T04	Oil-shale	51.42	18.25	15.63	21.46			
T05	Oil-shale	56.74	12.41	19.14	7.00			
T06	Oil-shale	64.29	7.45	28.26	0.00			
T08	Lime Mudstone	56.22	8.06	35.72	0.00			
T09	Oil-shale	55.17	5.03	3.80	38.11			
T10	Oil-shale	52.46	9.88	37.66	0.00			
T12	Lime Mudstone	30.24	12.57	57.19	0.00			
T13	Lime Mudstone	27.03	17.94	55.03	0.00			
T14	Oil-shale	38.31	19.93	41.76	0.00			
T16	Lime Mudstone	24.71	14.83	60.47	0.00			
T17	Oil-shale	49.98	10.47	24.39	17.76			
T18	Oil-shale	48.19	14.55	37.26	0.00			
T20	Oil-shale	48.99	19.16	31.85	0.00			
T21	Lime Mudstone	49.20	16.06	34.74	0.00			
T22	Oil-shale	49.82	10.38	22.67	18.34			
T24	Oil-shale	44.12	12.60	43.28	0.00			
T26	Lime Mudstone	28.98	7.56	63.46	0.00			
T28	Lime Mudstone	54.43	10.63	34.93	0.00			
T29	Oil-shale	43.36	11.92	44.72	0.00			
	Average	47.86	12.45	34.41	5.77			
	Min	24.71	5.03	3.80	0.00			
	Max	66.84	19.93	63.46	38.11			

Appendices A 9: Geochemical data of the Sünnet measured section.

Sample No.	Lithofacies	Total Weight (g)	Water Loss after 100 °C	Dry Weight (g)	Weight After HCl (g)	CaCO <sub>3</sub> (g)	Weight After H <sub>2</sub> O <sub>2</sub> (g)	Organic Matter (g)	Residues (g)	Obtained weight % of organic matter and minerals		
										Carbonate	Organic Matter	Residues
S06	Oil-shale	10	0.31	9.69	6.64	3.06	6.14	0.49	6.14	31.55	5.09	63.36
S07	Oil-shale	10	0.43	9.57	8.23	1.34	7.38	0.85	7.38	14.03	8.86	77.10
S11	Oil-shale	10	0.41	9.59	9.18	0.42	8.38	0.80	8.38	4.33	8.32	87.35
S13	Oil-shale	10	0.39	9.61	8.61	1.00	6.59	2.02	6.59	10.40	21.05	68.56
S14	Oil-shale	10	0.30	9.70	5.90	3.80	5.39	0.51	5.39	39.16	5.26	55.57
S15	Oil-shale	10	0.44	9.56	8.04	1.53	6.88	1.16	6.88	15.96	12.13	71.92
S16	Wackestone	10	0.12	9.88	2.65	7.23	0.84	1.81	0.84	73.20	18.35	8.45
S17	Packstone	10	0.29	9.71	4.43	5.28	1.53	2.90	1.53	54.35	29.91	15.74
S20	Oil-shale	10	0.41	9.59	8.04	1.55	6.78	1.26	6.78	16.15	13.17	70.69
S22	Oil-shale	10	0.00	10.00	7.39	2.61	6.29	1.10	6.29	26.08	10.99	62.93
S26	Wackestone	10	0.05	9.95	2.04	7.91	0.45	1.59	0.45	79.50	16.01	4.49
S28	Rudstone	10	0.07	9.93	4.41	5.52	3.95	0.46	3.95	55.56	4.64	39.80
S30	Oil-shale	10	0.00	10.00	7.66	2.34	7.07	0.59	7.07	23.40	5.90	70.69
S32	Rudstone	10	0.20	9.80	6.24	3.56	5.81	0.43	5.81	36.34	4.36	59.31

Appendices A 10: Organic matter and minerals component weight percent data of geochemical analysis of selected samples from the Sünnet section.

Sample No.	Lithofacies	Obtained weight % of organic matter and minerals				Source Potential	Porosity	Brittle mineral content (brittle mineral content > 40%)
		Carbonate	Organic Matter	Clay	Quartz/Feldspar			
S06	Oil-shale	31.55	5.09	1.59	64.04			
S07	Oil-shale	14.03	8.86	21.27	60.64			
S11	Oil-shale	4.33	8.32	40.00	55.23			
S13	Oil-shale	10.40	21.05	41.81	44.66			
S14	Oil-shale	39.16	5.26	3.00	52.57			
S15	Oil-shale	15.96	12.13	40.17	41.67			
S16	Wackestone	73.20	18.35	0.00	8.45			
S17	Packstone	54.35	29.91	0.00	15.74			
S20	Oil-shale	16.15	13.17	0.00	70.69			
S22	Oil-shale	26.08	10.99	17.76	63.64			
S26	Wackestone	79.50	16.01	35.35	31.64			
S28	Rudstone	55.56	4.64	0.00	39.80			
S30	Oil-shale	23.40	5.90	0.00	70.69			
S32	Rudstone	36.34	4.36	0.00	59.31			
	Average	34.28	11.72	14.35	48.48			
	Min	4.33	4.36	0.00	8.45			
	Max	79.50	29.91	41.81	70.69			

## APPENDIX B. EXTRACTED OSTRACODS AND CHAROPHYTE GYROGONITES STATISTICAL DATA

Appendices B 1: (50% Diluted) CH<sub>3</sub>COOH + (15% Diluted) H<sub>2</sub>O<sub>2</sub> extracted Ostracods and Charophyte fossils statistical data and thin section data from the Dağhacılar section.

Sample No.	Lithofacies	Solvent (1:3)	Timing (Minutes)	Extracted Microfossil %	Thin Section Studies %
D01	Lime Mudstone	(50% Diluted) CH <sub>3</sub> COOH+ (15% Diluted) H <sub>2</sub> O <sub>2</sub>	30mins	0	1
D03	Lime Mudstone	(50% Diluted) CH <sub>3</sub> COOH+ (15% Diluted) H <sub>2</sub> O <sub>2</sub>	30mins	3	3
D04	Wackestone	(50% Diluted) CH <sub>3</sub> COOH+ (15% Diluted) H <sub>2</sub> O <sub>2</sub>	20mins	1	40 (Ghost features)
D06	Wackestone	(50% Diluted) CH <sub>3</sub> COOH+ (15% Diluted) H <sub>2</sub> O <sub>2</sub>	30mins	10	20
D08	Packstone	(50% Diluted) CH <sub>3</sub> COOH+ (15% Diluted) H <sub>2</sub> O <sub>2</sub>	30mins	5	5
D10	Oil-shale	(50% Diluted) CH <sub>3</sub> COOH+ (15% Diluted) H <sub>2</sub> O <sub>2</sub>	15mins	25	49
D11	Packstone	(50% Diluted) CH <sub>3</sub> COOH+ (15% Diluted) H <sub>2</sub> O <sub>2</sub>	30mins	25	53
D13	Packstone	(50% Diluted) CH <sub>3</sub> COOH+ (15% Diluted) H <sub>2</sub> O <sub>2</sub>	30mins	0	0
D14	Wackestone	(50% Diluted) CH <sub>3</sub> COOH+ (15% Diluted) H <sub>2</sub> O <sub>2</sub>	30mins	20	35
D17	Wackestone	(50% Diluted) CH <sub>3</sub> COOH+ (15% Diluted) H <sub>2</sub> O <sub>2</sub>	30mins	5	7
D19	Packstone	(50% Diluted) CH <sub>3</sub> COOH+ (15% Diluted) H <sub>2</sub> O <sub>2</sub>	15mins	3	10
D20	Marl	(50% Diluted) CH <sub>3</sub> COOH+ (15% Diluted) H <sub>2</sub> O <sub>2</sub>	20mins	25	25
D21	Marl	(50% Diluted) CH <sub>3</sub> COOH+ (15% Diluted) H <sub>2</sub> O <sub>2</sub>	20mins	0	0
D24	Marl	(50% Diluted) CH <sub>3</sub> COOH+ (15% Diluted) H <sub>2</sub> O <sub>2</sub>	20mins	15	15
D27	Wackestone	(50% Diluted) CH <sub>3</sub> COOH+ (15% Diluted) H <sub>2</sub> O <sub>2</sub>	30mins	1	2
D28	Oil-shale	(50% Diluted) CH <sub>3</sub> COOH+ (15% Diluted) H <sub>2</sub> O <sub>2</sub>	30mins	0	0
D29	Lime Mudstone	(50% Diluted) CH <sub>3</sub> COOH+ (15% Diluted) H <sub>2</sub> O <sub>2</sub>	30mins	0	0
D30	Wackestone	(50% Diluted) CH <sub>3</sub> COOH+ (15% Diluted) H <sub>2</sub> O <sub>2</sub>	30mins	20	53
D31	Lime Mudstone	(50% Diluted) CH <sub>3</sub> COOH+ (15% Diluted) H <sub>2</sub> O <sub>2</sub>	30mins	0	0
D34	Marl	(50% Diluted) CH <sub>3</sub> COOH+ (15% Diluted) H <sub>2</sub> O <sub>2</sub>	20mins	0	0
D35	Oil-shale	(50% Diluted) CH <sub>3</sub> COOH+ (15% Diluted) H <sub>2</sub> O <sub>2</sub>	30mins	0	0
D36	Oil-shale	(50% Diluted) CH <sub>3</sub> COOH+ (15% Diluted) H <sub>2</sub> O <sub>2</sub>	30mins	0	5
D37	Oil-shale	(50% Diluted) CH <sub>3</sub> COOH+ (15% Diluted) H <sub>2</sub> O <sub>2</sub>	30mins	0	0
D38	Oil-shale	(50% Diluted) CH <sub>3</sub> COOH+ (15% Diluted) H <sub>2</sub> O <sub>2</sub>	30mins	0	0
D40	Oil-shale	(50% Diluted) CH <sub>3</sub> COOH+ (15% Diluted) H <sub>2</sub> O <sub>2</sub>	30mins	0	0
D41	Oil-shale	(50% Diluted) CH <sub>3</sub> COOH+ (15% Diluted) H <sub>2</sub> O <sub>2</sub>	30mins	0	0
D43	Marl	(50% Diluted) CH <sub>3</sub> COOH+ (15% Diluted) H <sub>2</sub> O <sub>2</sub>	20mins	0	0
D45	Oil-shale	(50% Diluted) CH <sub>3</sub> COOH+ (15% Diluted) H <sub>2</sub> O <sub>2</sub>	30mins	0	0
D50	Oil-shale	(50% Diluted) CH <sub>3</sub> COOH+ (15% Diluted) H <sub>2</sub> O <sub>2</sub>	30mins	0	0
D51	Oil-shale	(50% Diluted) CH <sub>3</sub> COOH+ (15% Diluted) H <sub>2</sub> O <sub>2</sub>	30mins	0	0
D52	Oil-shale	(50% Diluted) CH <sub>3</sub> COOH+ (15% Diluted) H <sub>2</sub> O <sub>2</sub>	30mins	0	0
D54	Oil-shale	(50% Diluted) CH <sub>3</sub> COOH+ (15% Diluted) H <sub>2</sub> O <sub>2</sub>	30mins	0	0
D55	Oil-shale	(50% Diluted) CH <sub>3</sub> COOH+ (15% Diluted) H <sub>2</sub> O <sub>2</sub>	30mins	0	0
D58	Oil-shale	(50% Diluted) CH <sub>3</sub> COOH+ (15% Diluted) H <sub>2</sub> O <sub>2</sub>	30mins	0	0
D59	Oil-shale	(50% Diluted) CH <sub>3</sub> COOH+ (15% Diluted) H <sub>2</sub> O <sub>2</sub>	30mins	0	0
D62	Oil-shale	(50% Diluted) CH <sub>3</sub> COOH+ (15% Diluted) H <sub>2</sub> O <sub>2</sub>	30mins	0	0
D66	Marl	(50% Diluted) CH <sub>3</sub> COOH+ (15% Diluted) H <sub>2</sub> O <sub>2</sub>	20mins	0	0
D69	Oil-shale	(50% Diluted) CH <sub>3</sub> COOH+ (15% Diluted) H <sub>2</sub> O <sub>2</sub>	20mins	0	0
D71	Oil-shale	(50% Diluted) CH <sub>3</sub> COOH+ (15% Diluted) H <sub>2</sub> O <sub>2</sub>	20mins	0	0
D72	Oil-shale	(50% Diluted) CH <sub>3</sub> COOH+ (15% Diluted) H <sub>2</sub> O <sub>2</sub>	20mins	0	0
D73	Marl	(50% Diluted) CH <sub>3</sub> COOH+ (15% Diluted) H <sub>2</sub> O <sub>2</sub>	20mins	0	0

Appendices B 2: (50% Diluted) CH<sub>3</sub>COOH + (15% Diluted) H<sub>2</sub>O<sub>2</sub> extracted Ostracods and Charophyte fossils statistical data and thin section data from the Hasanlar section.

Sample No.	Lithofacies	Solvent (1:3)	Timing (Minutes)	Extracted Microfossil %	Thin Section Studies %
H0a	Wackestone	(50% Diluted) CH <sub>3</sub> COOH+ (15% Diluted) H <sub>2</sub> O <sub>2</sub>	30mins	0	11
H0b	Oil-shale	(50% Diluted) CH <sub>3</sub> COOH+ (15% Diluted) H <sub>2</sub> O <sub>2</sub>	30mins	0	0
H03	Oil-shale	(50% Diluted) CH <sub>3</sub> COOH+ (15% Diluted) H <sub>2</sub> O <sub>2</sub>	15mins	0	0
H04	Lime Mudstone	(50% Diluted) CH <sub>3</sub> COOH+ (15% Diluted) H <sub>2</sub> O <sub>2</sub>	30mins	0	0
H07	Lime Mudstone	(50% Diluted) CH <sub>3</sub> COOH+ (15% Diluted) H <sub>2</sub> O <sub>2</sub>	30mins	0	0
H08	Oil-shale	(50% Diluted) CH <sub>3</sub> COOH+ (15% Diluted) H <sub>2</sub> O <sub>2</sub>	15mins	0	0
H10	Lime Mudstone	(50% Diluted) CH <sub>3</sub> COOH+ (15% Diluted) H <sub>2</sub> O <sub>2</sub>	30mins	0	0
H12	Wackestone	(50% Diluted) CH <sub>3</sub> COOH+ (15% Diluted) H <sub>2</sub> O <sub>2</sub>	30mins	0	2
H13	Oil-shale	(50% Diluted) CH <sub>3</sub> COOH+ (15% Diluted) H <sub>2</sub> O <sub>2</sub>	30mins	2	20
H15	Oil-shale	(50% Diluted) CH <sub>3</sub> COOH+ (15% Diluted) H <sub>2</sub> O <sub>2</sub>	30mins	0	0
H18	Oil-shale	(50% Diluted) CH <sub>3</sub> COOH+ (15% Diluted) H <sub>2</sub> O <sub>2</sub>	15mins	0	0
H19	Lime Mudstone	(50% Diluted) CH <sub>3</sub> COOH+ (15% Diluted) H <sub>2</sub> O <sub>2</sub>	30mins	0	5
H20	Oil-shale	(50% Diluted) CH <sub>3</sub> COOH+ (15% Diluted) H <sub>2</sub> O <sub>2</sub>	15mins	0	5
H21	Lime Mudstone	(50% Diluted) CH <sub>3</sub> COOH+ (15% Diluted) H <sub>2</sub> O <sub>2</sub>	30mins	2	2

Appendices B 3: (50% Diluted) CH<sub>3</sub>COOH + (15% Diluted) H<sub>2</sub>O<sub>2</sub> extracted Ostracods and Charophyte fossils statistical data and thin section data from the Kösüre section.

Sample No.	Lithofacies	Solvent (1:3)	Timing (Minutes)	Extracted Microfossil %	Thin Section Studies %
K01	Marl	(50% Diluted) CH <sub>3</sub> COOH+ (15% Diluted) H <sub>2</sub> O <sub>2</sub>	20mins	0	0
K02	Marl	(50% Diluted) CH <sub>3</sub> COOH+ (15% Diluted) H <sub>2</sub> O <sub>2</sub>	20mins	0	0
K05	Marl	(50% Diluted) CH <sub>3</sub> COOH+ (15% Diluted) H <sub>2</sub> O <sub>2</sub>	20mins	1	1
K07	Wackestone	(50% Diluted) CH <sub>3</sub> COOH+ (15% Diluted) H <sub>2</sub> O <sub>2</sub>	30mins	0	0
K09	Wackestone	(50% Diluted) CH <sub>3</sub> COOH+ (15% Diluted) H <sub>2</sub> O <sub>2</sub>	30mins	0	0
K11	Packstone	(50% Diluted) CH <sub>3</sub> COOH+ (15% Diluted) H <sub>2</sub> O <sub>2</sub>	30mins	1	5
K12	Packstone	(50% Diluted) CH <sub>3</sub> COOH+ (15% Diluted) H <sub>2</sub> O <sub>2</sub>	30mins	0	0
K13	Oil-shale	(50% Diluted) CH <sub>3</sub> COOH+ (15% Diluted) H <sub>2</sub> O <sub>2</sub>	30mins	1	0
K15	Marl	(50% Diluted) CH <sub>3</sub> COOH+ (15% Diluted) H <sub>2</sub> O <sub>2</sub>	30mins	2	0
K19	Oil-shale	(50% Diluted) CH <sub>3</sub> COOH+ (15% Diluted) H <sub>2</sub> O <sub>2</sub>	30mins	0	0
K20	Marl	(50% Diluted) CH <sub>3</sub> COOH+ (15% Diluted) H <sub>2</sub> O <sub>2</sub>	15mins	15	15
K21	Wackestone	(50% Diluted) CH <sub>3</sub> COOH+ (15% Diluted) H <sub>2</sub> O <sub>2</sub>	30mins	0	5
K22	Marl	(50% Diluted) CH <sub>3</sub> COOH+ (15% Diluted) H <sub>2</sub> O <sub>2</sub>	20mins	3	3
K24	Oil-shale	(50% Diluted) CH <sub>3</sub> COOH+ (15% Diluted) H <sub>2</sub> O <sub>2</sub>	30mins	0	0
K25	Wackestone	(50% Diluted) CH <sub>3</sub> COOH+ (15% Diluted) H <sub>2</sub> O <sub>2</sub>	30mins	2	11
K26	Marl	(50% Diluted) CH <sub>3</sub> COOH+ (15% Diluted) H <sub>2</sub> O <sub>2</sub>	20mins	0	0
K28	Wackestone	(50% Diluted) CH <sub>3</sub> COOH+ (15% Diluted) H <sub>2</sub> O <sub>2</sub>	30mins	10	10
K30	Wackestone	(50% Diluted) CH <sub>3</sub> COOH+ (15% Diluted) H <sub>2</sub> O <sub>2</sub>	30mins	0	0
K31	Marl	(50% Diluted) CH <sub>3</sub> COOH+ (15% Diluted) H <sub>2</sub> O <sub>2</sub>	20mins	10	10
K33	Wackestone	(50% Diluted) CH <sub>3</sub> COOH+ (15% Diluted) H <sub>2</sub> O <sub>2</sub>	30mins	15	15
K34	Wackestone	(50% Diluted) CH <sub>3</sub> COOH+ (15% Diluted) H <sub>2</sub> O <sub>2</sub>	30mins	0	0
K35	Wackestone	(50% Diluted) CH <sub>3</sub> COOH+ (15% Diluted) H <sub>2</sub> O <sub>2</sub>	30mins	0	0
K38	Wackestone	(50% Diluted) CH <sub>3</sub> COOH+ (15% Diluted) H <sub>2</sub> O <sub>2</sub>	15mins	0	0
K40	Oil-shale	(50% Diluted) CH <sub>3</sub> COOH+ (15% Diluted) H <sub>2</sub> O <sub>2</sub>	30mins	0	0
K45	Oil-shale	(50% Diluted) CH <sub>3</sub> COOH+ (15% Diluted) H <sub>2</sub> O <sub>2</sub>	30mins	0	0
K46	Oil-shale	(50% Diluted) CH <sub>3</sub> COOH+ (15% Diluted) H <sub>2</sub> O <sub>2</sub>	30mins	0	0

Appendices B 4: (50% Diluted) CH<sub>3</sub>COOH + (15% Diluted) H<sub>2</sub>O<sub>2</sub> extracted Ostracods and Charophyte fossils statistical data and thin section data from the Karahisar section.

Sample No	Lithofacies	Solvent (1:3)	Timing (Minutes)	Extracted Microfossil %	Thin Section Studies %
T01	Oil-shale	(50% Diluted) CH <sub>3</sub> COOH+ (15% Diluted) H <sub>2</sub> O <sub>2</sub>	30mins	0	0
T03	Oil-shale	(50% Diluted) CH <sub>3</sub> COOH+ (15% Diluted) H <sub>2</sub> O <sub>2</sub>	30mins	0	0
T04	Oil-shale	(50% Diluted) CH <sub>3</sub> COOH+ (15% Diluted) H <sub>2</sub> O <sub>2</sub>	30mins	0	0
T05	Oil-shale	(50% Diluted) CH <sub>3</sub> COOH+ (15% Diluted) H <sub>2</sub> O <sub>2</sub>	30mins	0	0
T06	Oil-shale	(50% Diluted) CH <sub>3</sub> COOH+ (15% Diluted) H <sub>2</sub> O <sub>2</sub>	30mins	0	0
T08	Lime Mudstone	(50% Diluted) CH <sub>3</sub> COOH+ (15% Diluted) H <sub>2</sub> O <sub>2</sub>	30mins	0	0
T09	Oil-shale	(50% Diluted) CH <sub>3</sub> COOH+ (15% Diluted) H <sub>2</sub> O <sub>2</sub>	30mins	0	0
T10	Oil-shale	(50% Diluted) CH <sub>3</sub> COOH+ (15% Diluted) H <sub>2</sub> O <sub>2</sub>	30mins	0	0
T12	Lime Mudstone	(50% Diluted) CH <sub>3</sub> COOH+ (15% Diluted) H <sub>2</sub> O <sub>2</sub>	30mins	0	1
T13	Lime Mudstone	(50% Diluted) CH <sub>3</sub> COOH+ (15% Diluted) H <sub>2</sub> O <sub>2</sub>	30mins	0	0
T14	Oil-shale	(50% Diluted) CH <sub>3</sub> COOH+ (15% Diluted) H <sub>2</sub> O <sub>2</sub>	30mins	0	0
T16	Lime Mudstone	(50% Diluted) CH <sub>3</sub> COOH+ (15% Diluted) H <sub>2</sub> O <sub>2</sub>	30mins	0	0
T17	Oil-shale	(50% Diluted) CH <sub>3</sub> COOH+ (15% Diluted) H <sub>2</sub> O <sub>2</sub>	20mins	0	0
T18	Oil-shale	(50% Diluted) CH <sub>3</sub> COOH+ (15% Diluted) H <sub>2</sub> O <sub>2</sub>	30mins	0	0
T20	Oil-shale	(50% Diluted) CH <sub>3</sub> COOH+ (15% Diluted) H <sub>2</sub> O <sub>2</sub>	30mins	0	0
T21	Oil-shale	(50% Diluted) CH <sub>3</sub> COOH+ (15% Diluted) H <sub>2</sub> O <sub>2</sub>	30mins	0	0
T22	Oil-shale	(50% Diluted) CH <sub>3</sub> COOH+ (15% Diluted) H <sub>2</sub> O <sub>2</sub>	30mins	0	0
T24	Oil-shale	(50% Diluted) CH <sub>3</sub> COOH+ (15% Diluted) H <sub>2</sub> O <sub>2</sub>	30mins	0	0
T26	Lime Mudstone	(50% Diluted) CH <sub>3</sub> COOH+ (15% Diluted) H <sub>2</sub> O <sub>2</sub>	30mins	0	0
T28	Lime Mudstone	(50% Diluted) CH <sub>3</sub> COOH+ (15% Diluted) H <sub>2</sub> O <sub>2</sub>	30mins	0	0
T29	Oil-shale	(50% Diluted) CH <sub>3</sub> COOH+ (15% Diluted) H <sub>2</sub> O <sub>2</sub>	30mins	0	0

Appendices B 5: (50% Diluted) CH<sub>3</sub>COOH + (15% Diluted) H<sub>2</sub>O<sub>2</sub> extracted Ostracods and Charophyte fossils statistical data and thin section data from the Sünnet section.

Sample No	Lithofacies	Solvent (1:3)	Timing (Minutes)	Extracted Microfossil %	Thin Section Studies %
S06	Oil-shale	(50% Diluted) CH <sub>3</sub> COOH+ (15% Diluted) H <sub>2</sub> O <sub>2</sub>	20mins	0	0
S07	Oil-shale	(50% Diluted) CH <sub>3</sub> COOH+ (15% Diluted) H <sub>2</sub> O <sub>2</sub>	20mins	0	0
S11	Oil-shale	(50% Diluted) CH <sub>3</sub> COOH+ (15% Diluted) H <sub>2</sub> O <sub>2</sub>	20mins	0	0
S12	Lime Mudstone	(50% Diluted) CH <sub>3</sub> COOH+ (15% Diluted) H <sub>2</sub> O <sub>2</sub>	30mins	0	0
S13	Oil-shale	(50% Diluted) CH <sub>3</sub> COOH+ (15% Diluted) H <sub>2</sub> O <sub>2</sub>	20mins	2	2
S14	Oil-shale	(50% Diluted) CH <sub>3</sub> COOH+ (15% Diluted) H <sub>2</sub> O <sub>2</sub>	30mins	0	0
S15	Oil-shale	(50% Diluted) CH <sub>3</sub> COOH+ (15% Diluted) H <sub>2</sub> O <sub>2</sub>	30mins	0	0
S16	Wackestone	(50% Diluted) CH <sub>3</sub> COOH+ (15% Diluted) H <sub>2</sub> O <sub>2</sub>	30mins	5	13
S17	Packstone	(50% Diluted) CH <sub>3</sub> COOH+ (15% Diluted) H <sub>2</sub> O <sub>2</sub>	10mins	37	42
S20	Oil-shale	(50% Diluted) CH <sub>3</sub> COOH+ (15% Diluted) H <sub>2</sub> O <sub>2</sub>	30mins	0	0
S22	Oil-shale	(50% Diluted) CH <sub>3</sub> COOH+ (15% Diluted) H <sub>2</sub> O <sub>2</sub>	30mins	0	0
S26	Wackestone	(50% Diluted) CH <sub>3</sub> COOH+ (15% Diluted) H <sub>2</sub> O <sub>2</sub>	30mins	11	11
S28	Rudstone	(50% Diluted) CH <sub>3</sub> COOH+ (15% Diluted) H <sub>2</sub> O <sub>2</sub>	30mins	0	0
S30	Oil-shale	(50% Diluted) CH <sub>3</sub> COOH+ (15% Diluted) H <sub>2</sub> O <sub>2</sub>	30mins	0	0
S32	Rudstone	(50% Diluted) CH <sub>3</sub> COOH+ (15% Diluted) H <sub>2</sub> O <sub>2</sub>	30mins	0	0



## CURRICULUM VITAE

### PERSONAL INFORMATION

Surname, Name : AFRIDI, BAKHT ZAMIR  
Nationality : Pakistani  
Date and Place of Birth : 12 Jan 1989, F. R Kohat, Pakistan  
Phone : +92 333 941 3914  
E-mail : [e195097@metu.edu.tr](mailto:e195097@metu.edu.tr); [bakhtafridi@gmail.com](mailto:bakhtafridi@gmail.com)

### EDUCATION

<b>Degree</b>	<b>Institution</b>	<b>Year of Graduation</b>
MS	METU, Geological Engineering	2014
BS	UOP, Peshawar, Geology Department	2011
High School	Warsak Model School and College, Peshawar	2006

### FOREIGN LANGUAGES

English

### PUBLICATIONS

1. Hanif, M., Ali., F. and Afridi, B., Z. "Depositional unit II of the Paleocene Tethyan Carbonate Platform Benthic community from the Upper Indus Basin, Pakistan". Journal of Himalayan Earth Sciences, 46, 55-65 (2013).

### HOBBIES

Cricket, Tennis, Football